EVALUATION OF THE PETROLEUM SYSTEMS BY 1D AND 2D NUMERICAL MODELING AND GEOCHEMICAL ANALYSIS IN THE AREA OF MOST RECENT EXPLORATION WELLS ON THE DEEPWATER SCOTIAN SLOPE, OFFSHORE NOVA SCOTIA

(Revised Final Report)

(Contract Number 60127404: Agreement Number 4600007900 of October 2, 2006)

Submitted to
Paul J. Harvey
Project Manager
Nova Scotia Department of Energy
5151 George Street, Suite 400
Halifax, Nova Scotia
B3J 3P7

By

Dr. P. K. Mukhopadhyay (Muki)
Global Geoenergy Research Ltd.
1657 Barrington Street, Suite 427
(P.O. Box 9469, Station A)
Halifax, Nova Scotia
B3J 2A1 (B3K 5S3)

June 26, 2006

ACKNOWLEDGMENTS

I extend my sincere gratitude to Alison Scott (Deputy Minister), Sandy MacMullin, Jack MacDonald, Paul Harvey, Kim Doane, and Kris Kendell, Resources and Royalties Division of the Nova Scotia Department of Energy for their support and help with this project. I acknowledge the help of Paul Harvey and Kris Kendell for their contribution to the 2-D seismic interpretation, early data input, and continuous encouragement during the crucial phase of this study. The author acknowledges the help of Sarah Scratch, Resources and Royalties Division of the Nova Scotia Department of Energy for digitally drafting various figures.

I would also like to extend my sincere gratitude to Brent Smith and Steve Bigelow, Resources and Rights Group of the Canada-Nova Scotia Offshore Petroleum Board (CNSOPB) for their permission to view the seismic data and provide their input in the interpretation. I would also like to acknowledge TGS-NOPEC for their permission to use the seismic data. The assistance of Carl Makrides, Brian Altheim, and Dave Brown from the Resources and Rights Group and Mary Jean Verrall, Kerry O'Kroneg, Nancy White, and Nancy Hynes from the Data Achieve, Core Storage, and Laboratory of the Canada Nova Scotia Offshore Petroleum Board is also greatly appreciated.

I would also like to acknowledge and extend my sincere thanks to Paul Harvey and Kris Kendell from the Nova Scotia Department of Energy and Saikat Mukhopadhyay from Global Geoenergy Research Limited for the review of an earlier version of the final report for this project. I also acknowledge the assistance of Saikat Mukhopadhyay and Debra Wheeler for data processing required in this project.

I would also like to acknowledge the help of John Wade, Sonya Dehler, Phil Moir, Rob Fensone, and Dave Mosher from the Geological Survey of Canada (Atlantic), Keith Louden from the Dalhousie University, and Jason Crux, Consultant, and Andrew McRae from the St. Mary's University for their fruitful discussions on various aspect of geological interpretations. I thank Michael Enachescu (Memorial University, St. John's, Newfoundland) and Pierre Jutras (St. Mary's University, Halifax, Nova Scotia) and Jennifer Young for sending me the Master's Thesis of Jennifer Young and Adam MacDonald.

Table of Contents

Table of Contents
(continued)

Table of Contents
(continued)

[1]Evaluation of the Petroleum Systems by One and Two Dimensional Numerical Modeling and Geochemical Analysis in the Area of Most Recent Exploration Wells on the Deepwater Scotian Slope, Offshore Nova Scotia

Dr. P. K. Mukhopadhyay (Muki), Global Geoenergy Research Limited, 1657 Barrington Street, Suite 427, Halifax, Nova Scotia, Canada, B3J 2A1

(Contract Number 60127404: Agreement Number 4600007900 of October 2, 2006)

A. EXECUTIVE SUMMARY

This research contract was awarded by the Nova Scotia Department of Energy to Global Geoenergy Research Limited of Halifax, Nova Scotia to re-assess the petroleum system risk after a limited success to find oil and gas within the Scotian Basin, Eastern Canada. Eleven wells were drilled on the slope, but only Marathon Oil and its partners made a gas and condensate discovery (30 meters net pay within the middle to Early Cretaceous age sands – Missisauga Formation) in the Annapolis G-24 well. The contract research covered the area between the deepwater portion of the Eastern Margin of the Sable Subbasin to the Central Margin of the Shelburne Subbasin, where the most recent deepwater wells have been drilled since 2001 (Figure A).

This petroleum system risk assessment has been achieved through a preliminary evaluation of the geological and geophysical data, the interpretation of the new and older geochemical data, one dimensional thermal and pressure modeling of twelve wells (eleven slope and shelf), and the comprehensive interpretation of two-dimensional migration and phase separation modeling of five seismic lines using the PetroMod 1D/2D/3D software (version 9.02) of IES Incorporated of Germany (Figure B).

[1] *Final Report by Global Geoenergy Research Limited on the "Evaluation of the Petroleum Systems by ..... Numerical Modeling and Geochemical Analysis……. on the Deepwater Scotian Slope, Offshore Nova Scotia (Contract Number 60127404 (Agreement Number 4600007900 of October 2, 2006)*

As a requirement of the modeling software, a complete suite of geological, geophysical, and geochemical parameters have been incorporated as input parameters. Other than basic geological (lithology, geological age, structure, etc) and geochemical (heat flow, source rock potential,

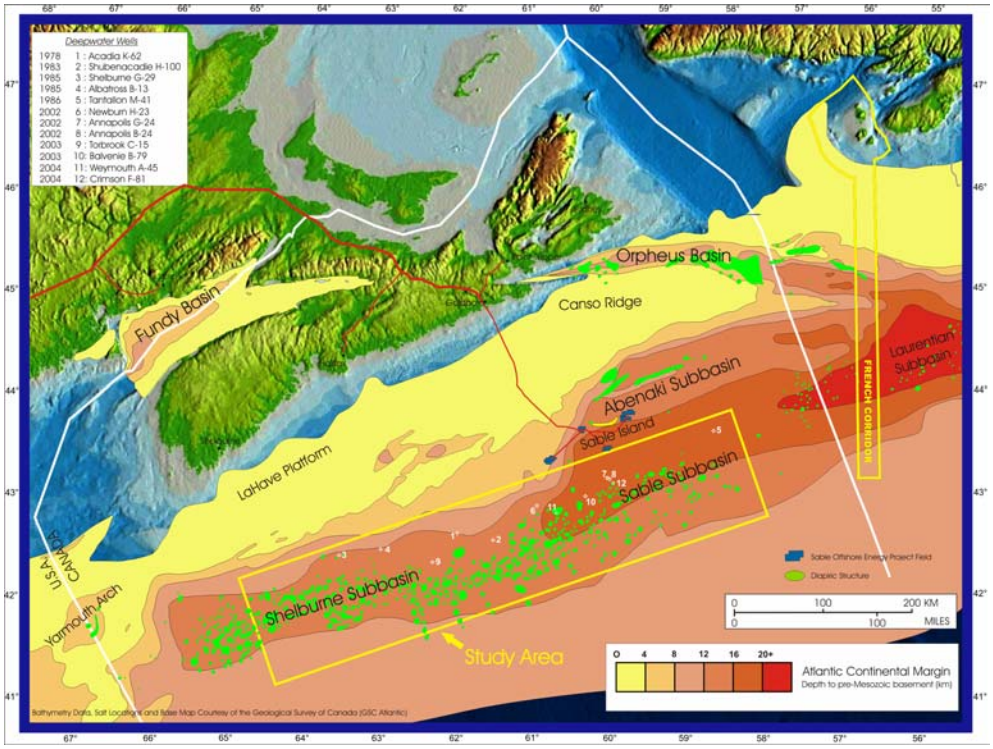

Figure A. Location of the study area showing structural elements of the Scotian Basin showing location of the salt structures and wells (modified after Wade and MacLean, 1990)

maturation, etc.) data, the software also requires some intricate geological and geochemical properties for the modeling simulation of five seismic lines. These properties included the timing of the salt movement (both diapiric and allochthonous stages), data on the individual faults (opened or closed), reservoir properties, multi-component kinetics of candidate source rocks from the Scotian Margin, and the phase behavior of the individual hydrocarbons. Thus, the hybrid simulator of the petroleum system modeling deals with the thermal evolution, three-phase (oil, gas,

and water) complex hydrocarbon migration, reservoir saturation histories through geological time in individual cells, and the eventual mass balance of expelled and accumulated hydrocarbons within the five two-dimensional seismic cross sections (A-A', B-B', C-C', D-D', E-E'; 9a, 9b, 9c, 9d, and 9e; Figure B).

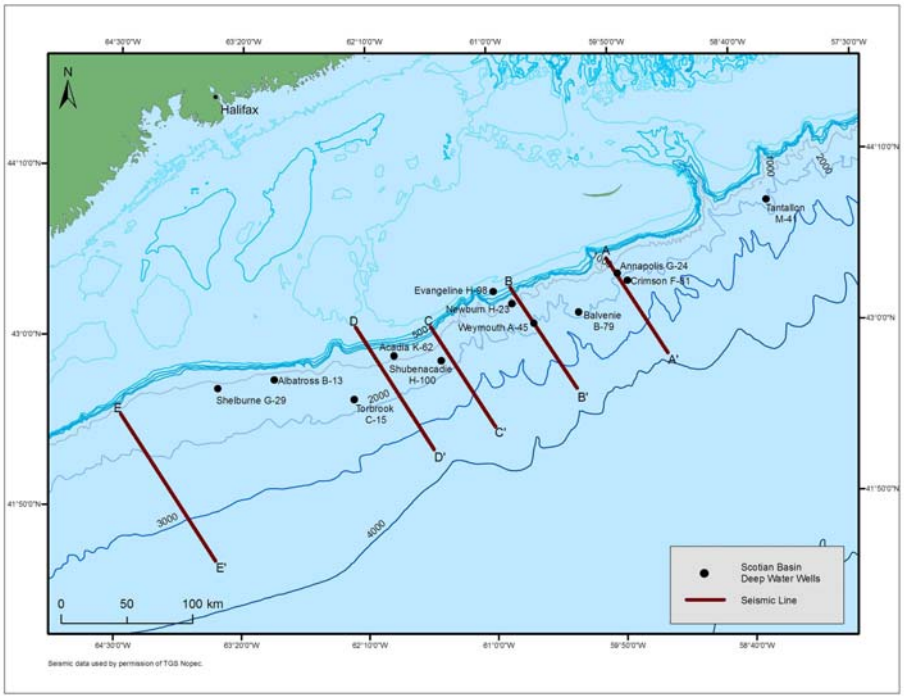

Figure B. Bathymetric map of Nova Scotia with locations of the eleven slope and one shelf wells used for the 1D modeling and five 2-D seismic lines utilized for the 2D modeling

A.1. Salt Movement and Its Relation to Play Types and Reservoir Sands

Based on earlier work of Wade and MacLean (1990) and Shimeld (2004), various phases of vertical intrusion and horizontal extrusion of salt are observed within the Triassic to recent sediments of the eastern part of the Sable Subbasin (Salt Subprovince III of Shimeld, 2004). Therefore, the timing of the salt emplacement within seismic lines A-A', B-B' and C-C', D-D', and E-E' are different. Based on previous studies on the salt emplacement (Ing et al., 2004; Jackson et al., 2004; Jackson and

Vanderville, 1994; Rowan, 1995, 2002; Young, 2005), the following five schematic conceptual stages have been identified for the A-A' and B-B' seismic lines (Mukhopadhyay et al., 2006). These five conceptual stages also include the corresponding timing of hydrocarbon emplacement within various reservoirs which will be evaluated during the two-dimensional numerical modeling (Figure C):

- **Stage 1 (Early to Middle Jurassic):** Initiates oil generation from the Early Jurassic source rock due to a high sedimentation rate and high heat flow shortly after the rifting within the Scotian Margin (170-150 Ma). The expelled oil acts as a lubricant, which will increase the fluidity of the salt. Thus, the active salt diapirism has been initiated due to the continuation of the high heat flow, the sedimentation rate, and the high fluidity of the salt during the Middle Jurassic Period,

- **Stage 2 (Late Jurassic to Early Cretaceous):** Starts the full phase of oil and gas expulsion from the Early to Middle Jurassic source rocks due to the high sedimentation rate and heat flow. The oil has increased the fluidity of the salt for its rapid growth into the main diapiric stage. At this stage, the formation of sand within the Early Cretaceous reservoirs could be hindered by the position and thickness of the diapiric structures as suggested by Waltham and Davison (2001). Reservoir quality sands could be deposited within the salt flank or salt top plays during Late Jurassic Period,

- **Stage 3 (Early to Late Cretaceous):** The major phase of oil expulsion and cracking of oil to gas from the Early Jurassic and Jurassic Verrill Canyon source rocks is closely related to the high sedimentation rate and high heat flow. The continuing high sedimentation rate, heat flow, and fluidity of the salt will mobilize the basinward leaning of the diapirs and formation of "hourglass"

salt stocks and salt tongues. At this stage, the downslope displacement of sediment by sliding on top of the salt body has created various growth faults, which will accelerate the turbidite flows. However, counter regional faults over the "hourglass" structures will create obstacles to turbidite flows (Waltham and Davison, 2001)". This period initiates major sand bypassing of the distorted mini-basins of the upper slope due to the presence of canopy-like thick and flat salt bodies. Eventually, the reservoir-quality sands will be deposited within the middle and ultra-deep slope.

- **Stage 4 (Early Tertiary):** This is the time of salt withdrawal and formation of major salt tongue and canopies. Major sediment input and possible formation of deep-water sand reservoirs within the salt withdrawal area could occur. However, by-passing of sands over the canopy area could be the major event during this time period. The oil and gas expulsion is continuing due to moderate to high heat flow and the high sedimentation rate has continued to mobilize the major movement of allochthonous salts.

- **Stage 5 (Late Tertiary):** During this stage, the secondary cracking of oil to gas or condensate occurs from all three major source rocks (*gas from Early and Late Jurassic source rocks and condensate from the Cretaceous Verrill Canyon source rock*). Major gas and condensate expulsion is initiated due to the continued high sedimentation rate and higher heat flow on top of the salt. Reservoir sands develop as turtle structure and turbidite channels. Lower heat flow within the sub-salt play types in the Early Cretaceous sands are observed, which would be saturated with hydrocarbons if the sands are indeed present within those reservoirs. However, most sands on

top of the allochthonous canopies will still continue to bypass the upper slope and deposit within the middle and lower slope.

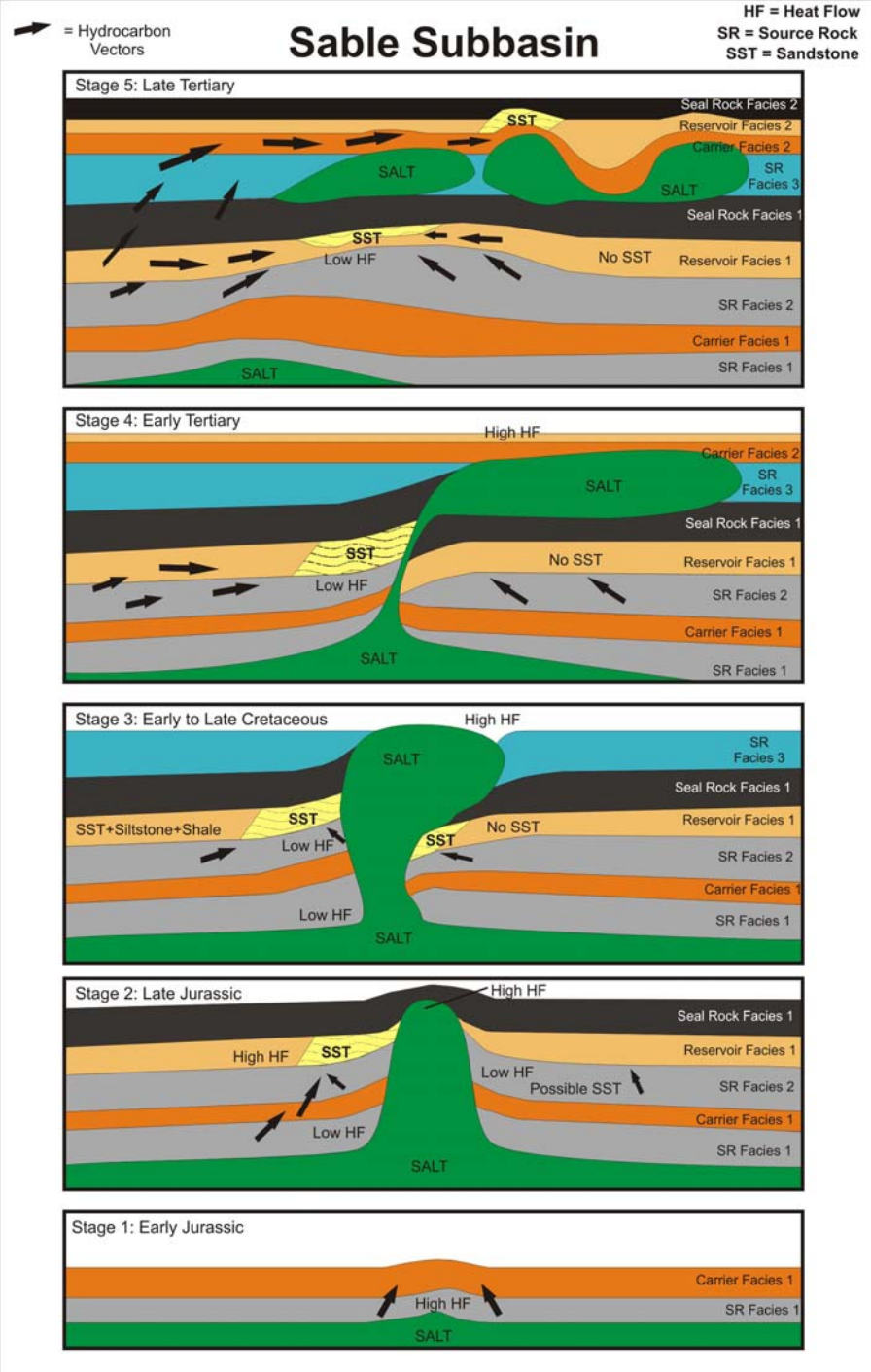

Figure C. Conceptual model of relationship between the stages of salt emplacement and various petroleum system parameters such as sand dispersal and heat flow within the source rocks of the slope region from the Sable Subbasin (after Mukhopadhyay et al., in press).

The sedimentation rate and heat flow within the area between the western part of the Sable Subbasin and the eastern part of the Shelburne Subbasin (Salt Sub-Province II of Shimeld, 2004) were possibly lower compared to the Salt Sub-Province III (eastern Sable Subbasin), especially during the Early Jurassic to Early Cretaceous Periods. The timing of the main phase of salt diapirism within the seismic lines C-C' and D-D' was considered to be late in geological time (younger than 110 Ma). This concept has also been applied to the 2D petroleum system modeling of seismic lines C-C', D-D' and E-E'. However, more work is necessary to understand the timing of salt diapirism of seismic line E-E' as the diapiric salt is located within the upper slope.

A recent sequence stratigraphic study (Brent Smith, CNSOPB Confidential report, 2006) of the Scotian Margin have identified several paleo-submarine channels within the upper slope region of the area between the Torbrook C-15 and the Shubenacadie H-100 wells and within the area east of the Tantallon M-41 well for various time periods (one in Late Jurassic to Early Cretaceous and the other in the Early Tertiary periods). No major channels could be located within the Eastern Sable Subbasin area. As the paleo-submarine channels are the sand transport avenues from the shelf to the slope region, more reservoir quality sands are expected to be deposited within the upper slope region of these areas where these paleo-submarine channels exist.

A.2. Source Rock Characterization

A.2.1. Organic Facies, Source Rock Potential and Maturation

The current geochemical work on the organic facies, source rock potential, and maturation indicates the following aspects of the source rock characterization:

- The organic petrographic charactization of the sediments from the Early Missisauga or Cretaceous Verrill Canyon Formation of the

Crimson F-81 and Annapolis G-24 wells suggests that they are derived from a **delta front depositional environment and not as deepwater turbidite derived organic matter**. Accordingly, the morphology of these sediments suggests that these sediments were deposited in a dysoxic depositional environment forming gas and condensate prone Type II-III or III source rocks. On the other hand, similar source rocks from the Weymouth A-45 well and the Tertiary Banquereau Formation sediments from the Torbrook C-15 well are organic rich and indicate that they are distinctly derived from a deepwater marine anoxic depositional environment forming mainly oil prone and condensate prone Type II and II-III source rocks.

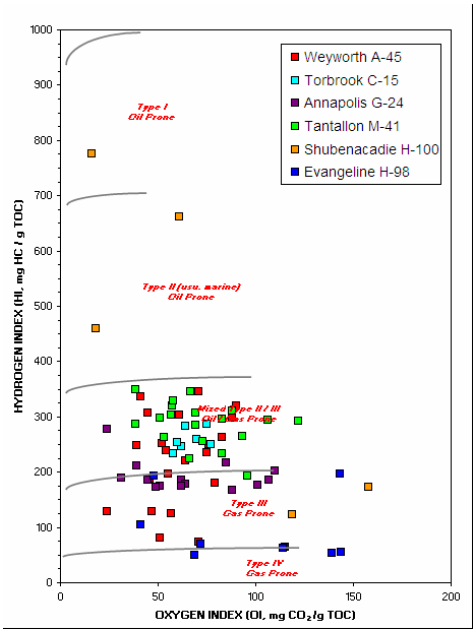

Figure D. Source rock potential (plot of S_2 and TOC) with positions of various sediments from selected Scotian Slope wells. Type I and II - oil prone; Type II-III - gas and condensate prone; Type III - mainly gas prone; Type IV - mostly non-source rock or minor gas (modified after Mukhopadhyay et al., 2000, 2003)

- Based on earlier and current research on source rock evaluation of the sediments from the Scotian shelf and slope wells and the DSDP wells of the Moroccan Margin and Blake Bahama Basin (Legs 76 and 79), the following stratigraphic units could be projected as potential source rocks within the Scotian Slope (modified from Mukhopadhyay

et al, 2000; Mukhopadhyay, 2002; Mukhopadhyay et al., 2003; Rullkotter and Mukhopadhyay, 1986, Rullkotter et al., 1984):

- **Late Triassic/Early Jurassic lacustrine** (Sinumarian-Toarcian: ***Iroquois/Mohican Formation***): organic rich, oil prone Type I to II; (analogues from other rift basins from Moroccan onshore and Newark Basin wells). This is a projected source rock as no analogues has yet been found from any deepwater wells on the Scotian Margin;
- **Middle Jurassic marine** (Callovian: ***Misaine Member***): gas/condensate prone and organic-rich mixed marine and terrestrial Type II-III and III (analogues from the DSDP well [Leg 76], Blake-Bahama Basin and Acadia K-62 well from the Scotian Slope;
- **Late Jurassic marine** (Kimmeridgian-Oxfordian: ***Jurassic Verrill Canyon Formation***), oil-prone, mainly marine Type II (analogues from the DSDP Leg 79 and various Shelf and Shelf-Margin wells from the Scotian Basin and the Grand Bank;
- **Early Cretaceous marine** (Berriasian/Valanginian: ***Lower Missisauga or Cretaceous Verrill Canyon Formation)*** (Mukhopadhyay et al., 2000, 2003); oil and gas prone Type II, II-III, and III (analogues from the Annapolis G-24 [GSC data], Tantallon M-41, and the Weymouth A-45 wells from the Scotian Slope and DSDP Leg 79);
- **Mid-Cretaceous marine** (Aptian to Cenomanian; **Shortland Shale or Logan Canyon Formation**); gas and condensate prone Type II-III or III (analogues from the Shubenacadie H-100 and well from the DSDP Leg 75 and Leg 79);
- **Early Tertiary marine** (Paleocene-Eocene; **Banquereau Formation**), oil and gas prone Type I, II or II-III (analogues from the Albatross B-13, Annapolis G-24 [GSC data]; Shubenacadie H-100, and the Torbrook C-15 wells).

- The comparable bottom-hole temperature and maturity of the Early Jurassic (the Acadia K-62 well only) to Tertiary sediments from various Scotian Slope wells suggest that (i) the Early to Middle Jurassic sediments have higher heat flow and maturity compared to the Cretaceous and Tertiary sediments within the Shelburne Subbasin and western part of the Sable Subbasin, (ii) higher heat flow within the Jurassic age sediments from the Shelburne Subbasin is similar to the Cretaceous to recent sediments from the eastern Sable Subbasin (area around the seismic lines A-A' and B-B'). Therefore, the Early and Middle Jurassic sediments from the Acadia K-62 and Albatross B-13 wells from the Shelburne Subbasin and the Early Cretaceous sediments from the Crimson F-81 and Weymouth A-45 wells from the Eastern Sable Subbasin are mature and lie within the "Principle Phase of Oil and Condensate Generation". All Tertiary sediments from the Torbrook C-15 well and the Cretaceous or Tertiary sediments from the Shubenacadie H-100, Albatross B-13, and Shelburne G-29 wells are immature for hydrocarbon generation.

A.2.2. Source Rock Kinetics

The multi-component kinetics analysis of four hydrocarbon components for two prolific source rocks (Cretaceous Verrill Canyon – Weymouth A-45 well, 6206m; and Jurassic Verrill Canyon – Alma K-85 well, 3540m) from the Scotian Margin has documented the following hydrocarbon component distributions for each source rock, which will be achieved during the catagenetic transformation of hydrocarbons from the source rock. It will also illustrate the probable temperature of cracking of each hydrocarbon components (C_1, C_2 to C_5, C_6 to C_{14}, and C_{15+}).

Volumetrically, the primary cracking of each unit of the *Jurassic and Cretaceous Verrill Canyon* source rock will generate the following percentages of hydrocarbon components:

- ✓ ***Cretaceous Verrill Canyon:*** *17% normal gravity oil (C_{15+}), 62% light oil and condensate (C_6 to C_{14}); 15% wet gas (C_2 to C_5), 6% dry gas or methane (C_1)*, and
- ✓ ***Jurassic Verrill Canyon:*** *40% normal gravity oil (C_{15+}), 47% light oil and condensate (C_6 to C_{14}); 10% wet gas (C_2 to C_5), 3% dry gas or methane (C_1).*

The computed temperature and maturity of 10%, 50%, and 90% hydrocarbon expulsion (various components) for the Cretaceous and Jurassic Verrill Canyon source rocks could be demonstrated as follows (Table A-1):

Table A-1

Components	Temperature (°C) for 10% Hydrocarbon Conversion	Temperature (°C) for 50% Hydrocarbon Conversion	Temperature (°C) for 90% Hydrocarbon Conversion	% R_o for 10% Hydrocarbon Conversion	% R_o for 50% Hydrocarbon Conversion	% R_o for 90% Hydrocarbon Conversion
Cretaceous Verrill Canyon						
C_{15+}	110	125	138	0.63	0.73	0.83
C_6 to C_{14}	136	151	165	0.81	0.99	1.22
C_2 to C_5	137	157	176	0.82	1.10	1.43
C_1	138	162	186	0.83	1.17	1.65
Jurassic Verrill Canyon						
C_{15+}	87	113	140	0.47	0.64	0.85
C_6 to C_{14}	128	144	157	0.75	0.89	1.10
C_2 to C_5	136	153	169	0.81	1.03	1.30
C_1	141	165	190	0.86	1.22	1.74

C_{15+} = normal gravity oil; C_6 to C_{14} = light oil and condensate
C_2 to C_5 = wet gas; C_1 = dry gas (methane)

The Jurassic Verrill Canyon source rock has documented an early generation of hydrocarbons (especially the normal gravity oil fraction). However, the broad spectrum of the activation energy distributions suggests that it will continue expelling the hydrocarbons much longer in

total geological time periods than the Cretaceous Verrill Canyon source rock. Therefore, the Jurassic Verrill Canyon source rock will also produce more secondary gas from the cracking of normal gravity crude oil and light oil. The overall early generation and expulsion of hydrocarbons from both source rocks (Jurassic and Cretaceous Verrill Canyon) compared to other typical Type II source rocks from the various parts of the world (Kimmeridgian Shale, Woodford Shale, etc.) may indicate the possible presence of abundant oxygen-functional group compounds within the kerogen network (derived from the terrestrial organic matter).

A.3. One Dimensional Petroleum System Modeling: Thermal and Pressure Properties

The one dimensional petroleum system modeling of twelve wells has established the following aspects of the burial or thermal histories, hydrocarbon charge, and migration histories:

- ✓ At least three different heat flow zones exist within the Scotian Slope are as follows:
  - (a) moderate to low heat flow: area east of the Shelburne G-29 and west of the Evangeline G-98 wells,
  - (b) moderate to high heat flow: area between the Evangeline H-98 and the Crimson F-81 wells, and
  - (c) low heat flow: area in proximity to the Tantallon M-41 well.
- ✓ The burial and thermal histories of all twelve wells suggest that only the Cretaceous Verrill Canyon source rock from the Annapolis G-24 and the Newburn H-23 wells (eastern Sable Subbasin) and the Early to Middle Jurassic sediments from the Acadia K-62 well (western Sable Subbasin) have attained the liquid and vapor phases of hydrocarbon generation (Figure E). As such, the expulsion of hydrocarbons from various source rocks did not attain the main

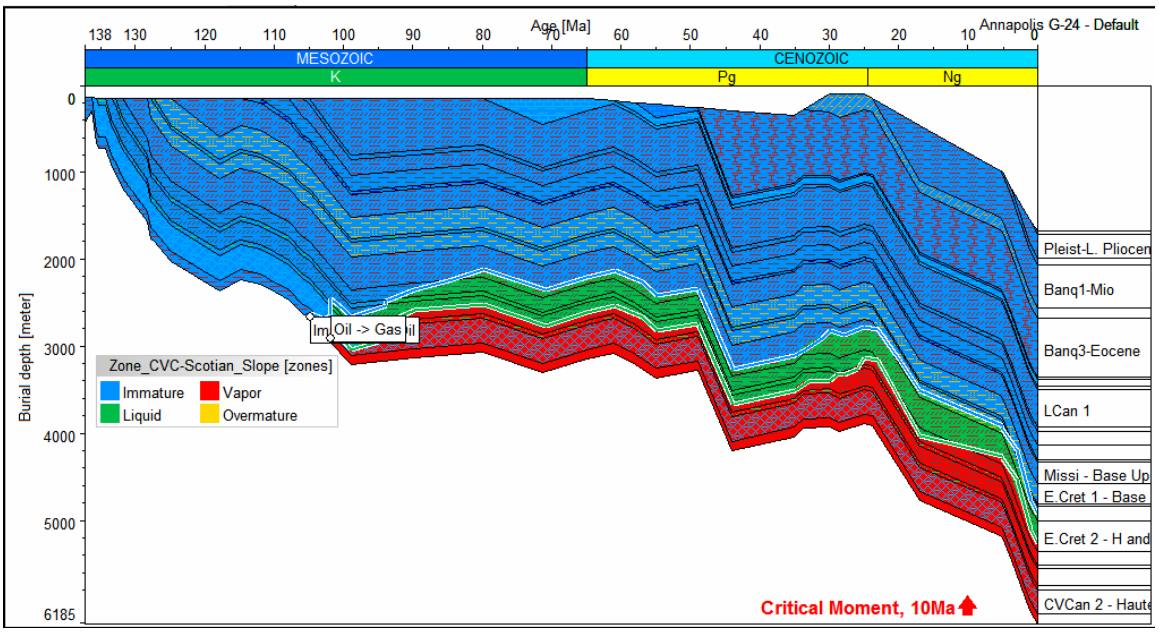

Figure E. Burial history of the Annapolis G-24 well with maturity zones (immature, liquid or oil, vapor or gas/condensate, and overmature gas)

vapor phase (R_o > 1.0%) for the optimum saturation of the Cretaceous and Tertiary reservoirs until 30 Ma. Therefore, the "critical moment" of hydrocarbon emplacement within all twelve wells has either been reached very recently (last 30-5 Ma) or has not been reached at all. This data clearly indicates that (i) deeper drilling into the Jurassic Period sediments and (ii) penetrating at least 5000 m of sediment thickness is necessary to get any significant hydrocarbon saturated reservoirs within the area surrounding these twelve wells from the Scotian Slope.

✓ The modeling pressure data indicates that the sediments below 5000 m within most of the eastern Sable Subbasin wells (Annapolis G-24, Crimson F-81, Newburn H-23, and Weymouth A-45) are within the overpressure regime. The deeper sediments within the area between the Shelburne G-29 in the eastern Shelburne Subbasin and the Shubenacadie H-100 well in the western Sable Subbasin do not lie within the overpressure regime. However, some of the younger sediments (Banquereau Formation) within the western part of the

Sable Subbasin slope are situated within an overpressure regime. This type of overpressure is usually caused by the compaction disequilibrium of these younger sediments.

A.4. Two Dimensional Petroleum System Modeling:

The review of the two dimensional petroleum system modeling of the five seismic lines (A-A', B-B', C-C', D-D', and E-E') from the Scotian Margin has documented the following salient features of the hydrocarbon migration, reservoir saturation, and reservoir properties:

A.4.1. Eastern Sable Subbasin (lines A-A' and B-B')

- The best Cretaceous to Miocene reservoir sands (derived as a result of modeling) could be located either within the northwestern side of the salt growing area or within the distal margin towards the southeastern side of these two lines. A typical example would be the Early Cretaceous sand packages (reservoir) within the Annapolis G-24 well. The lack of similar Early Cretaceous reservoir within the Crimson F-81 well could be inferred as being located within the southeastern side of the leaning diapir during the Early to Middle Cretaceous time. The slight variation in maturity between these two wells may support this concept. The sediments within the area between Annapolis G-24 and Crimson F-81 wells were situated within a salt withdrawal stage around 130-110 Ma. Accordingly, most of the turbidite sands have bypassed the upper slope (allochthonous salt affected areas) to the lower slope in a water-depth deeper than 2500m,
- Two to three phases of hydrocarbon expulsion (170 Ma, 130 Ma, and 30-0 Ma) could be documented within various parts of seismic lines A-A' and B-B',

As discussed earlier, most of the earlier generated C15+ oil was cracked to dry gas. Accordingly, a volume expansion of expelled hydrocarbons

occurred around 110 Ma within the Cretaceous sediments due to the high maturity (>1.15% Ro) of the Early Jurassic and Jurassic Verrill Canyon source rocks. This volume expansion of the fluids could have triggered the overpressure within the existing reservoirs since 55 Ma. The hydrocarbon migration vectors above the Early Cretaceous Annapolis G-24 reservoir clearly indicate a hydrocarbon leak from the top of the reservoir (Figure F). This leaking is possibly created due to the diffusion and buoyancy of low molecular weight reservoir

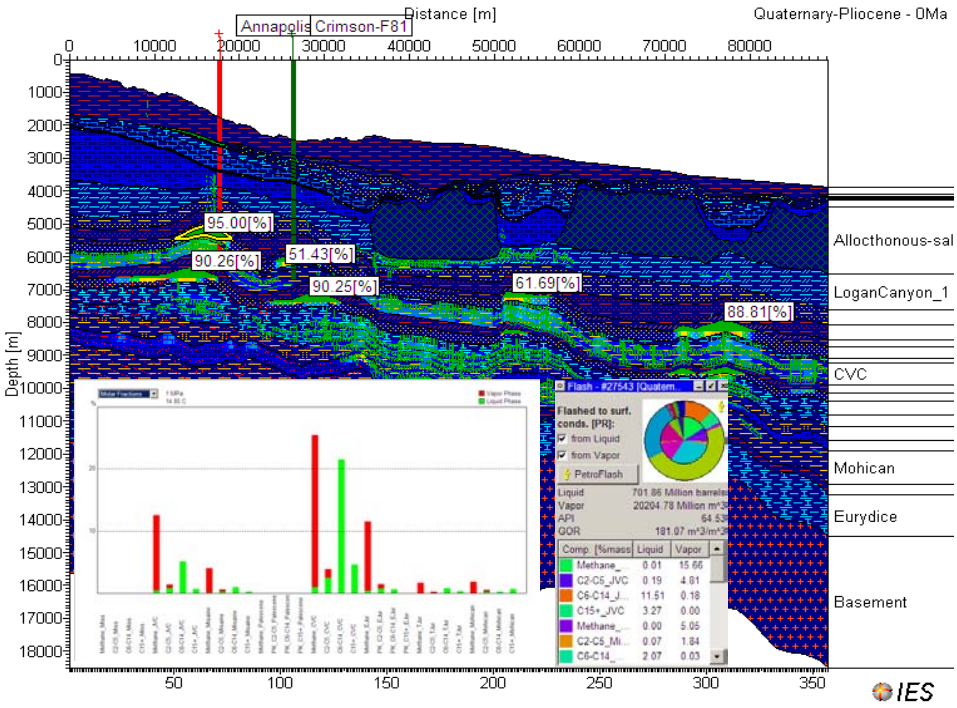

Figure F. Line A-A' – Saturation of various reservoirs with API gravity, possible GOR, and Hydrocarbon component tracking (in molar fraction) of Early Cretaceous turbidite reservoir of the Annapolis G-24 well.

hydrocarbons. However, the reservoir hydrocarbons are being replenished due to the input of the liquid phase hydrocarbon migration from the oil prone Cretaceous Verrill Canyon source rock (Figure F). Therefore, the overpressure within the Early Cretaceous reservoir of the Annapolis G-24 well is being maintained. All Jurassic and Early Cretaceous reservoirs within both seismic lines (A-A' and B-B') lie

within an overpressure regime. Most Miocene reservoirs are mostly either under normal pressure or have a mild overpressure,

- ❖ All reservoirs contain more than 85-90% dry gas with 10-15% of wet gas and condensate. The Early Cretaceous and Late Jurassic reservoirs (mostly conceptual) have an API 64.8^{o} and a GOR of 183.1 m^3/m^3 (Figure F).

A.4.2. Western Sable Subbasin – Eastern Shelburne Subbasin (seismic lines C-C', D-D', and E-E'

- ✓ Salt diapirs are located on the landward side of the seismic line E-E' and on the deeper basinward side of the other two lines (C-C' and D-D'). Accordingly, a well defined deepwater channel reservoir could be located within the basinward side of the seismic line E-E', (beyond the salt diapirs). All resulting reservoirs (derived from the modeling results within the sand-rich units) within the seismic lines C-C' and D-D' occur either as an anticlinal play type (related to the basement structures) or occur as salt-top and salt-flank play types within the upper to middle slope,
- ✓ The timing of the rapid salt diapiric growth within the seismic lines C-C', D-D' and E-E' coincides with the timing of the major expulsion of the liquid hydrocarbons from the Early Jurassic and Jurassic Verrill Canyon source rocks (around 110 Ma). The migration of C_{15+} oil from the Early Jurassic source rock has started around 130 Ma.
- ✓ Two phases of hydrocarbon migrations are documented from the Early Jurassic and Jurassic Verrill Canyon source rocks in the seismic line E-E': (i) the expulsion of the C_{15+} oil and C_6 to C_{14} light oil and condensate occurred around 130-110 Ma; and (ii) the expulsion of both primary or secondary gas expulsion happened between 75 Ma and 55 Ma due to the cracking of C_{15+} oil from both those two source rocks. The reservoirs were saturated with

hydrocarbons between 75 Ma and 55 Ma within the seismic line E-E',

- ✓ One phase of hydrocarbon expulsion (light oil, gas and condensate) could have started since 75 Ma within the seismic lines C-C' and D-D'. Within the seismic lines C-C' and D-D', the full hydrocarbon saturation of various reservoirs (derived from modeling sand-rich zones) has started comparatively later (than the line E-E') and in between 75 Ma and 5.3 Ma,
- ✓ Within all three seismic lines, the Jurassic, Cretaceous and the Tertiary reservoirs were being replenished with oil from the Cretaceous Verrill Canyon source rock and gas from the Early Jurassic and Jurassic Verrill Canyon source rocks,
- ✓ All turbidite channels (one on line D-D' and one on E-E' – identified in Figure 9e) and salt-flank or salt-crest (top) (two within line D-D', identified in Figure H) reservoirs have more than 90% hydrocarbon saturated (Figure G),
- ✓ The genetic fingerprinting on the source rock to reservoir hydrocarbon composition suggests that all reservoir hydrocarbons (Late Jurassic, Early Cretaceous, and Early Miocene) are genetically related to the Early Jurassic and Jurassic Verrill Canyon source rocks within the seismic lines E-E'. All reservoirs within seismic line E-E' show more than 95% dry gas. The reservoir hydrocarbons on this line have an API of 50^{o}-58^{o} and GOR of 343-158 m^3/m^3.
- ✓ The genetic fingerprinting on the correlation of the source rock to reservoir hydrocarbon composition within the seismic lines C-C' and D-D' suggests that all reservoir hydrocarbons have some contributions from all major source rocks (Figure G). Most of the Cretaceous and Tertiary reservoirs within these two seismic lines (C-C' and D-D') contain mixtures of 10-20% light oil (C_{10} and C_{20}), 20-30% condensate, and 50-70% dry gas. The reservoir hydrocarbons have an API of 48^{o} to 59^{o} API and GOR of 71 to 84 m^3/m^3 (Figure G)

- ✓ The Early to Middle Cretaceous and the Tertiary reservoirs of these three seismic lines within the normal or mild overpressure regime. Most Jurassic reservoir hydrocarbons are situated within an overpressure regime. The amount of overpressure in all three seismic lines within this region is much lower compared to the seismic lines A-A' and B-B'.

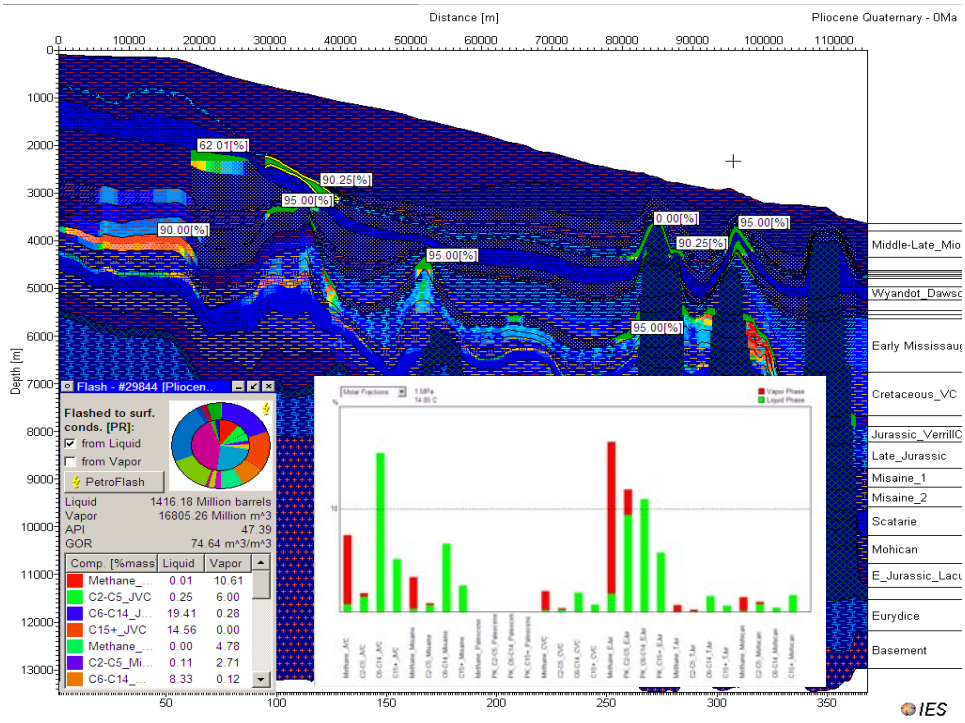

Figure G. Line D-D' – Saturation of various reservoirs with API gravity, possible GOR, and Hydrocarbon component tracking (molar fraction) of Mid-Paleocene turbidite reservoir.

A.5. Mass Balance of Reservoir Hydrocarbons

The major interest of the two-dimensional petroleum system modeling is to achieve a mass balance of hydrocarbons within the area surrounding the five major northwest-southeast seismic lines (A-A', B-B', C-C', D-D', and E-E'). This mass balance of hydrocarbons includes as follows: (i) how much mass of hydrocarbons have been generated and expelled from three major source rocks (Early Jurassic, Jurassic Verrill Canyon and Cretaceous Verrill Canyon); (ii) what volume or mass of hydrocarbons have accumulated within various reservoirs; and (ii) what volume or mass of

hydrocarbons have been lost during migration (from the source rock to the reservoir through the carrier bed) or lost due to the secondary cracking of liquid hydrocarbons to gas or the loss due to the stability of the seal rock. The mass balance data for all five seismic lines indicates that the three major source rocks (as discussed earlier) have contributed more than 90% of the total hydrocarbon masses accumulated within various reservoirs.

Lines A-A' and B-B' are from the eastern part of the Sable Subbasin slope area, which are associated with the complex salt canopy structures. Lines C-C' and D-D' are from the western section of the Shelburne Subbasin or within the western part of Sable Subbasin and are associated with salt diapiric structures. The mass balance of hydrocarbons for all five seismic lines is summarized in the following Table B-1 (masses calculated within a kilometer radius area; eg. Figure H):

Table B-1

Seismic Line	Total Mass Generated $(10)^9$ Kg (Mtons)/m^3	Total Mass Expelled $(10)^9$ Kg (Mtons)/m^3	**Total Mass Accumulated in Reservoirs $(10)^9$ Kg (Mtons)/m^3**	Total Mass Lost from Reservoirs $(10)^9$ Kg (Mtons)/m^3	Each Source Rock Contribution (%)	How the HC lost from Reservoirs	Main Reservoirs for Accumulated Hydrocarbons (%)
A-A'	6861.64	6382.1	**488.5**	5893.6	65 JVC/CVC 30 EJ	*Vertical Seal *Sec. Cracking	60% Late Jurassic
B-B'	8227.6	7292.31	**709.14**	6583.2	60 JVC/CVC 18 EJ	*Horizontal/vertical *Sec. Cracking	45% Middle Misssauga 30% Late Jurassic
C-C'	2926.12	2340.24	**508.9**	1831.26	40 JVC/CVC 30 EJ	*60% Vertical Seal *Sec. Cracking	50% Late Jurassic
D-D'	3451.1	2290.4	**888.1**	1402.3	40 JVC/CVC 30 EJ	*70% Vertical Seal & Horizontal Seal	35% Middle Paleocene 35% Late Jurassic
E-E'	9074.32	8043.48	**574.13**	7469.34	38 JVC/CVC 45 EJ	60% Sec. Cracking 30% horizontal	80% Early Miocene & Middle Cretaceous

EJ = Oil Prone Early Jurassic Lacustrine Type I and II; JVC = Oil Prone Jurassic Verrill Canyon Marine Type II; CVC = Oil Prone Cretaceous Verrill Canyon Marine Type II; HC = hydrocarbons; Sec. Cracking = Secondary cracking of oil to dry gas in reservoir or carrier bed or within source rock and related volume expansion
* Reservoirs = except the Early Cretaceous reservoir within the Annapolis G-24 well, all other reservoirs are conceptual reservoir derived from the modeling data

Using the similar basic geological, geophysical, and geochemical input parameters for all five seismic lines, the mass balance of hydrocarbon data suggests that the seismic line D-D' area would be the best

suitable exploration target area because of the ratio of the total accumulated hydrocarbons and hydrocarbon losses (Figure H).

Within line D-D', the Late Jurassic or Early Cretaceous reservoirs, which occur as salt-top or salt-flank plays and the Tertiary reservoirs as salt-top or turbidite channel plays should be the best future exploration targets (Figure H). The expected reservoir hydrocarbons within line D-D' would be 60-70% dry gas, 20-30% condensate, and 10-20% light Oil (C_{10} to C_{20} normal alkanes).

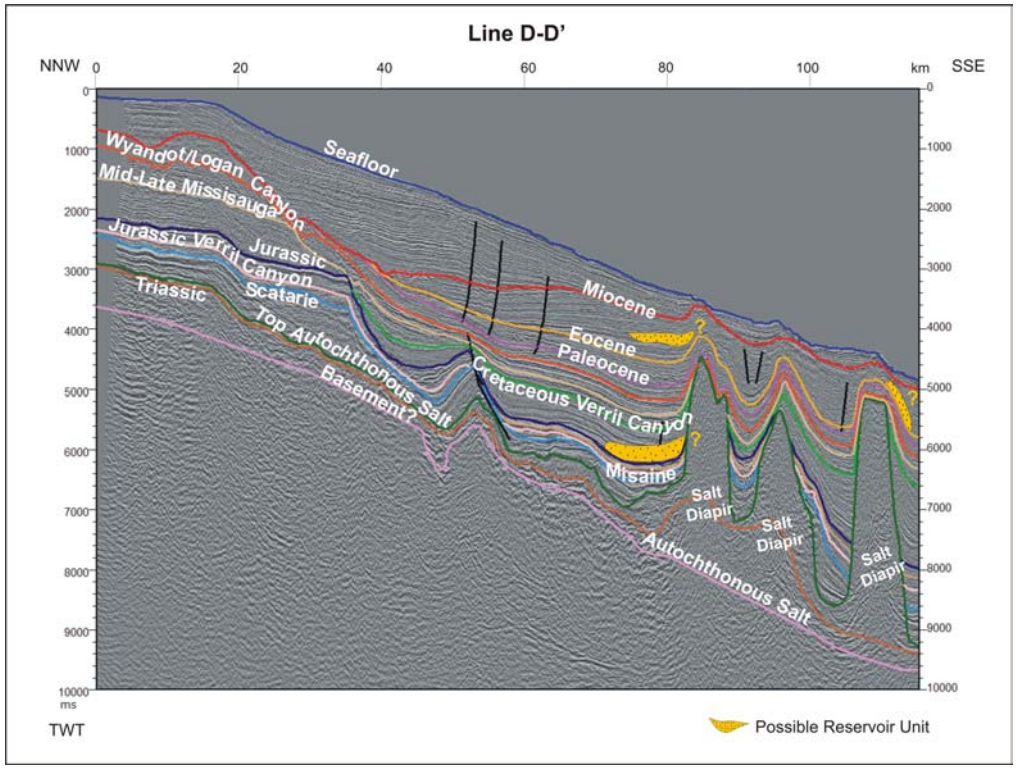

Figure H. Seismic line D-D' (Eastern Shelburne Subbasin) with selected formation boundaries, faults, salt diapirs, and possible reservoir units (depth in ms)

In spite of huge masses (or volumes) of expelled hydrocarbons within the seismic lines A-A' or B-B' and E-E', the accumulated hydrocarbons within various reservoirs are much lower than the seismic line D-D'. This is caused by the major hydrocarbon losses through the vertical or lateral seal

and the timing of secondary cracking of oil to gas, which are possibly related to the complex salt structures. The Late Jurassic deepwater sands within the seismic line C-C' could be a secondary target within the Western Sable Subbasin because of the moderate expelled and accumulated reservoir hydrocarbons. The reservoir hydrocarbon composition should be similar to the seismic line D-D' as both areas lie within the low to moderate heat flow regime.

The following three exploration targets could be recommended within the eastern part of the Sable Subbasin:

1. **The Late Jurassic channel deepwater play type within a present day water depth o 500-2500 m,**
2. **The Middle to Early Cretaceous deepwater or delta-front channel play type. This target should occur within the shelf side of the complex canopy system and be restricted to a present depth of less than 2000 m,**
3. **The Late Jurassic to Early Tertiary deepwater turbidite channel sands beyond 2500 m water depth depth.**

The expected reservoir hydrocarbons within seismic lines A-A' and B-B' could contain greater than 80-90% dry gas, 10-20% condensate, and 0-10% light oil. Sub-salt reservoirs may contain more than 30-40% condensate and light oil.

More work is necessary to predict any exploration risk within the seismic line E-E'. The expected reservoir hydrocarbons within the line E-E' would be more than 90% dry gas because of the high heat flow in this region due to its closeness to the Jurassic and Cretaceous volcanic activities.

A.6. Exploration Risk

A comprehensive petroleum system risk analysis of the 2D numerical modeling of five seismic lines identified the following risk factors:

- ✓ Viable petroleum system is dependent on the heat flow, timing of salt movement, and sand dispersal especially within the mini-basins of the Eastern Sable Subbasin,
- ✓ Least Risk for Drilling: The Middle Cretaceous to Early Tertiary turbidite fans and Late Jurassic-Early Cretaceous salt-flank or salt-crest plays (depths between 1500 - 2500 m water depth) on seismic lines D-D' and E-E' will have the lowest risk for future exploration within the Scotian Margin. Probable reservoir hydrocarbon will be as follows: 43-56^{o} API gas (>60%), condensate (10-30%), and light oil (10-20%). Late Jurassic reservoirs may contain 90% dry gas
- ✓ Moderate Risk for Drilling: The Early Cretaceous turbidite fan or delta-front plays and Late Jurassic channel sand plays on the northwestern side of allochthonous salts (within a water depth of 500 - 2000 m) on the seismic lines A-A' and B-B' will have moderate risk for future exploration within the Scotian Margin,
- ✓ High Risk for Drilling: The Miocene and Early Cretaceous turbidite fan plays within the allochthonous salt-related deepwater areas of the eastern portion of the Sable Subbasin (between 500 – 2500 m water depth) will have the highest risk for future exploration within the Scotian Margin,
- ✓ Expected Pore Pressure of Reservoir Liquid: Tertiary – Normal to mild overpressure especially within the Eastern Sable Subbasin; Late Jurassic to Early Cretaceous - overpressure

B. RECOMMENDATIONS

The Phase I petroleum system risk assessment indicates a major gap in knowledge on the relationship between the timing of the salt movement, deepwater sand dispersal, the histories of the hydrocarbon generation-migration-entrapment, and the stability of the seals. Therefore, the following future work is highly pertinent and recommended:

- Completion of a Phase II study of this project using two dimensional petroleum system modeling for another fifteen to twenty 2-D seismic lines (depth converted and interpreted). This work should be performed in conjunction with the identification of various reservoirs, play types and their relationship with the timing of the salt movement,
- Re-evaluation of the basement structures and establish a basement fracture map of the Scotian Slope,
- Analysis of the biostratigraphy of at least two to three wells from the Sable Subbasin (recent wells) or purchase already existing proprietary confidential data from a service company,
- Analysis of vitrinite reflectance of the Annapolis G-24, Newburn H-23, and the Tantallon M-61 wells after the solvent extraction of the synthetic oil-base drilling mud,
- Procurement of the interpreted seepage data from the Satellite Image analysis and the Scotian Slope surface geochemical studies. This data will be incorporated with the Phase II petroleum system risk assessment work in conjunction with the two dimensional numerical modeling of fifteen to twenty seismic lines.

Using these diversified parameters of the petroleum systems, the contract research has completed the Phase I study of the risk assessment and the evaluation of the hydrocarbon prospectivity of the study area within the Scotian Slope, Offshore Nova Scotia, Eastern Canada. *Considering the vast*

aerial extent of the target area, lack of dense grid of 2D petroleum system modeling, absence of any detailed work on the timing of the salt movement, and the lack of properly defined (based on sequence stratigraphic interpretation) defined traps and reservoir units, the conclusion of this report (Phase I) should be considered preliminary. For complete appraisal of the petroleum system risk and identification of the future drilling targets within the Scotian Margin, Phase II research is highly pertinent.

C. REFERENCES

Ings, S., Beaumont, C. and Lykke, G. 2004. Numerical Modeling of Salt Tectonics on Passive Continental Margins: Preliminary Assessment of the Effects of Sediment Loading, Buoyancy, Margin Tilt, and Isotasy. In Post, P. J., Olson, D. L., Lyons, K. T., Palmes, S. L., Harrison, P. F., and Rosen, N. C., eds., Salt-sediment interactions and hydrocarbon prospectivity: concepts, applications, and case studies for the 21st century: 24th Annual GCSSEPM Foundation Bob F. Perkins Research Conference, p. 36-68.

Jackson, M. P. A., Hudec, M. R., and Jennette, D. C., 2004, Insights from a gravity-driven linked system in deep-water lower Congo Basin, Gabon. In Post, P. J., Olson, D. L., Lyons, K. T., Palmes, S. L., Harrison, P. F., and Rosen, N. C., eds., Salt-sediment interactions and hydrocarbon prospectivity: concepts, applications, and case studies for the 21st century: 24th Annual GCSSEPM Foundation Bob F. Perkins Research Conference, p. 735–752.

Jackson, M. P. A. and Vendeville, B. C. 1994. Regional extension as a geological trigger for diapirism: GSA Bulletin, v. 106, p. 57-73.

Mukhopadhyay, P. K., Harvey, P. J. and Kendell, K. in press. Genetic Relationship between Salt Mobilization and Petroleum System Parameters: Possible Solution of finding Commercial Oil and Gas within Offshore Nova Scotia, Canada during the Next Phase of Deepwater Exploration Proceedings of the GCAGS Conference, Lafayette, New Orleans, September 2006.

Mukhopadhyay, P. K., Brown, D. E., Kidston, A. G., Bowman, T, D., Faber, J. and Harvey, P.J. 2003. Petroleum Systems of Deepwater Scotian Basin, Eastern Canada: Challenges for Finding Oil versus Gas Provinces. Proceedings 2003 Offshore Technology Conference, Paper Number 15304, p. 1-11.

Mukhopadhyay, P. K., Wade, J. A. and Kruge, M. A. 2000. Petroleum Systems of the Scotian Basin, Offshore Eastern Canada and its Implications for Future Prospects in the Shelf Break and Slope Areas. AAPG Annual Convention Extended Abstract, New Orleans, Louisiana.

Mukhopadhyay, P.K. 2002. Evaluation of Petroleum Systems for Five Dummy Wells From Various Seismic Sections of the Scotian Slope, Offshore Nova Scotia, Based on One-Dimensional Numerical Modelling and Using Geochemical Concepts. Canada-Nova Scotia Offshore Petroleum Board Confidential Internal Report.

Rowan, M. G. Practical Salt Tectonics. 2002. Short Course Note Book, CIM-Petroleum Society, Halifax Section, October 7-8, 2002, Halifax, Nova Scotia, Canada.

Rowan, M. G. 1995, Structural styles and evolution of allochthonous salt, central Louisiana outer shelf and upper slope. In. Jackson, M. P. A. et al. (Eds.) Salt Tectonics: a global perspective: AAPG Memoir 65, p. 199-228.

Rullkotter, J. and Mukhopadhyay, P. K. 1986. "Comparison of Mesozoic carbonaceous claystones in the western and eastern North Atlantic (DSDP Legs 76, 79, and 93)": In (Summerhayes, C. P. and Shackleton, N. J. (Eds.) *North Atlantic Paleoceanography*. Geological Society of London Special Publication, v. **22**, p. 377-387.

Rullkotter, J., Mukhopadhyay, P. K., Schaefer, R. G., and Welte, D. H. 1984. "Geochemistry and petrography of organic matter in sediments from Deep Sea Drilling Project Sites 545 and 547, Mazagan Escarpment", In Hinz, K. et al. (Eds) *Initial Report of DSDP Leg 79*, p. 775-806.

Shimeld, J. W. 2004. A comparison of Salt Tectonic Subprovinces beneath the Scotian Slope and Laurentian Fan. 24th Annual GCS-SEPM Foundation Bob F. Perkins Research Conference, Houston, pp 502-532, CD-ROM.

Wade, J. A. and MacLean, B.C. 1990. Aspects of the geology of the Scotian Basin from recent seismic and well data. In Keen, M. J. and Williams, G. L. (Eds.). Geology of the Continental Margin of Eastern Canada, Geology of Canada, Part 2, p. 167- 238.

Waltham, D. and Davison, I. 2001. Obstacles and sinks: Effects on Turbidite flow on Deepwater Continental Margins. 21st Annual GCS-SEPM Bob. F. Perkins Research Conference: Petroleum Systems of the Deep-Water Basins, p. 511-522 (CD-ROM)

Young, J.L., 2005, The stratigraphic and structural history of the Mesozoic and Cenozoic of the Central Nova Scotian Slope, Eastern Canada. Unpublished M. Sc thesis, Memorial University, St. John's, Newfoundland, Canada, 229 p.

Evaluation of the Petroleum Systems by One and Two Dimensional Numerical Modeling and Geochemical Analysis in the Area of Most Recent Exploration Wells on the Deepwater Scotian Slope, Offshore Nova Scotia

1. INTRODUCTION

The Scotian Basin is one of the major passive margin Triassic-Quaternary depocenters in Eastern Canada (Figure 1a). This basin, within Nova Scotia's provincial jurisdiction, extends from the Laurentian Subbasin in the east to the Yarmouth Arch on the United States-Canada border in the west. The aerial extent for the exploration areas of the deepwater Scotian Basin is approximately 150, 000 square kilometers.

The Scotian Basin has attracted petroleum exploration activity since 1959, when Mobil started its first aeromagnetic survey (Wade et al., 1989). The first offshore well Tors Cove D-52 (located in the eastern Scotian Basin) was drilled in 1966 on an anticline (top of a salt diapir). From 1966 to 1990, approximately 167 wells have been drilled in the Scotian Slope region (Figure 1b). During that time, only five wells (Acadia K-62, Albatross B-13, Shelburne G-29, Shubenacadie H-100, and Tantallon M-41; Figure 1a) were drilled in the Scotian Margin and no significant quantities of hydrocarbons could be detected in this region. Twenty-two wells have been classified as 'significant' discoveries of hydrocarbons in the Scotian Basin. Within this discovered petroleum, two wells contain light oil, two have light oil and gas, and 18 other wells have gas and condensates. All these discoveries are within the Scotian Shelf in less than 200m water depth and within a 100 kilometres of the Sable Island area (Figure 1b).

From 1990 until the present time, another phase of renewed interest has resulted in the drilling of 37 additional wells that include both exploration and production wells (current total: 204 wells; CNSOPB Website, 2006).

From 1990 to 1994, exploration and development activities were concentrated over the Cohasset and Panuke fields within the LaHave Platform of the Scotian Basin. Lasmo Oil Company and its partners (Nova Scotia Resources and PanCanadian Oil & Gas Company) developed the Cohasset and Panuke fields and the production of light crude oil started in 1992. Since 1995, ExxonMobil (Mobil Oil Canada Ltd.) and its major partners (Shell Canada and Imperial Oil) commenced the initiative for the development of the Venture, Thebaud, Alma, South Venture, and the Glenelg fields within the Scotian Shelf (Figure 1b). In 1999, a significant discovery of gas and condensate was made by PanCanadian Energy (currently EnCana) within the Jurassic carbonate bank reservoir (Abenaki Formation). This discovery was made by the Panuke J-99 well located on the eastern part of the Jurassic Carbonate Bank. The Deep Panuke Field is still currently on hold and could be under consideration for future development.

Renewed interest in hydrocarbon exploration in the deepwater offshore Nova Scotia in late 2001 resulting from successes in other global analogous deepwater areas resulted in the drilling of six wells since 2001 (Annapolis B-24/G-24, Balvenie B-79, Crimson F-81, Newburn H-23, Torbrook C-15, and Weymouth A-45; Figure 1a). However, only the Annapolis G-24 well, Marathon Oil and its partners made a gas and condensate discovery in the Mississauga sands (Middle to Early Cretaceous) (Figure 1c). Approximately 30 meters of net pay was encountered over two zones in the Missisauga sands. None of the other deepwater wells drilled in the Scotian Slope encountered any significant hydrocarbons although some of these wells (Balvenie B-79 and Newburn H-23) indicate some condensate and gas saturation in thin sandstones and carbonates (for reference, see well history reports for each well).

1.1. Administrative Aspects

The proposed project was initiated by the Resource Assessment and Royalties Division of the Nova Scotia Department of Energy in June 2005. Accordingly, a public tender for the submission of proposals to "Evaluation of the Petroleum Systems By 1D and 2D Numerical Modeling and Geochemical Analysis in the area of most recent exploration wells on the deepwater Scotian Slope, offshore Nova Scotia" was advertised at the Public Tender Office in late September 2005. Global Geoenergy Research Ltd of Halifax, Nova Scotia submitted a comprehensive research proposal in response to the "Request for Proposal" (Tender Number 60127404) from the Nova Scotia Procurement Branch of the Public Tender Office for the Nova Scotia Department of Energy.

The project was awarded to Global Geoenergy Research Limited and work commenced on November 2, 2005. The time schedule of the contract work was eventually delayed by six weeks due to a delay in securing the 1D/2D/3D petroleum system modeling license from IES Incorporated, Aachen, Germany in November 2005 and the acquisition of the five 2D seismic lines from the Canada Nova Scotia Offshore Petroleum Board (CNSOPB). The original submission date of the final report (April 15, 2006) for this project has been extended until May 31, 2006 based on an approved request (dated April 12, 2006) from Global Geoenergy Research Limited.

The total contract price is $120,000.00 + HST. However, $27,750.00 has been allotted from the contract price for various geochemical analysis (multi-component kinetics of two candidate source rocks, TOC, Rock-Eval pyrolysis, and). Global Geoenergy Research Limited has subcontracted most parts of the geochemical work (multi-component kinetics, TOC, and Rock-Eval pyrolysis) to Humble Geochemical Services (Humble Instrument

& Services Inc.) in Humble, Texas, USA. Global Geoenergy Research Limited has performed the vitrinite reflectance analysis for the project in its headquarters in Halifax, Nova Scotia.

1.2. Implications of the Project

The major geological framework of the Scotian Slope is similar to the deepwater Gulf of Mexico, offshore Morocco, and the West African margin as all these basins have been affected by salt tectonics and major growth faults. However, specific geological parameters (thickness of Pliocene-Pleistocene sediments, difference in heat flow histories, etc) of the Scotian Slope are quite dissimilar to the other deepwater basins. Compared to the deepwater GOM and the West African Margin but the Triassic to early Cretaceous sediments from the Scotian Slope are more similar to the Moroccan deepwater sediments (Figures 2a and 2b). The vast amount of geological and geophysical information and interpretations that are currently available within the public domain as publications and reports are mostly concentrated within the shelf part of the Scotian Basin (Jansa and Wade, 1975; Mukhopadhyay et al., 1995; Wade and MacLean, 1990; Wade et al., 1995; Welsink et al., 1989). Only a few publications are available on the deepwater Scotian Basin (Geological Survey of Canada Basin Database, 2006; Hogg, 2001; Kidston et al., 2002; Mukhopadhyay et al., 2000, 2002, 2003; Mukhopadhyay and Wade, 1993; Mukhopadhyay, 2000; Shimeld, 2004). In 2002, the Canada Nova Scotia Offshore Petroleum Board (CNSOPB) published an in-depth study on the resource estimation of the Scotian Slope based partially on the study of analogues from other Atlantic Margin basins and 1D petroleum system modeling (Kidston et al., 2002). The hydrocarbon reserve estimation by the CNSOPB is mainly based on the probabilistic methods.

This report will include a combination of existing and new data from geological, geophysical, and geochemical sources to help the petroleum industries highlight the risks associated with oil and gas exploration and identify various reservoir properties before drilling (including reservoir saturation, composition of the hydrocarbons, reservoir pressure, and temperature) within the deepwater Sable Subbasin and surrounding deepwater areas offshore Nova Scotia. Future companies interested in the deepwater Scotian Basin will receive valuable information to achieve their prospect evaluation based on a better understanding of the petroleum system elements before drilling very expensive and high risk wells.

1.3. Scope of the Contract

Although there has been extensive 2-D and 3-D seismic acquisition programs over the past several years, the petroleum industries have recently halted additional drilling within the Scotian Slope while they assess the new geological information acquired from the recently drilled wells and re-assess the data. Based on consultation with industry, the Nova Scotia Department of Energy initiated this contract to develop a better understanding of the geological processes to better identify prospective areas. This report examines the latest geosciences data (mostly from the well history reports and recent publications) to better understand the petroleum systems in selected areas of the Scotian Slope. However, this report could not use various biostratigraphy and geochemistry completed on recent deepwater wells by the petroleum industry as this data will not be public until 2008-2010.

The report will cover various selected areas between the eastern part of the Sable Subbasin (Tantallon M-41 well) and the central part of the Shelburne Subbasin (Shelburne G-29 well) of the Scotian Margin (Figure 1a). This type of work is very important as similar integrated studies on

petroleum system risk assessment have resulted in major discoveries for other Atlantic Margin basins (deepwater Brazil, West Africa, and Gulf of Mexico) in the recent past.

This contract report will incorporate the evaluation of the deepwater oil and gas prospects based on the petroleum system risk assessment (Magoon and Dow, 1994; Mukhopadhyay et al., 2003). A ***petroleum system*** (Magoon and Dow, 1994) is a composite geological system that includes integration of all available geological, geophysical, and geochemical elements and processes including structural reconstruction play types, reservoir and traps, hydrocarbon charge and migration, and accumulation related to existing oil and gas entrapment. The ***petroleum system model*** is a dynamic earth system model as it provides a complete record through geological time. The models are mostly comprised of merged petroleum systems.

The contract has established a comprehensive understanding of how the ambient conditions of the petroleum system within a selected area of the deepwater Sable and Shelburne subbasins have changed over geological time. The objective of the project is to evaluate a full n-component, three phase, one and two dimensional modeling of the 'petroleum system' incorporating various geological, geophysical, and geochemical data. One dimensional (1-D) modeling will be used for the initial assessment of the burial and maturation histories of the basin and timing of hydrocarbon expulsion (using multi-component kinetics) from the existing 11 slope wells and one shelf well Evangeline H-98. Two-dimensional modeling (2-D) of five seismic lines will determine the migration fairways, the relationship between phase migration with reservoir saturation and compositions, reservoir pressure/temperature conditions, seal rock stability, and risk assessment for potential reservoirs.

The proposed research has evaluated geologically macro-, micro-, and molecular levels of the petroleum system risk assessment as the target basin has major risks involving reservoir formation, timing of hydrocarbon migration, seal stability, etc. Therefore, it will also exhibit the following parameters:

- ✓ Constraints of the heat flow, temperature, hydrocarbon movement in the area where salt tectonism is pervasive.
- ✓ Geological implications of salt tectonics and its relationship to the transportation of turbidite sands and the anoxicity of the source rocks in mini-basins and other deepwater areas (a theory on the by-passing of sands surrounding the mini-basin),
- ✓ Fingerprinting of hydrocarbon migration from source to reservoir units via carrier beds, and
- ✓ Hydrocarbon seepage from the reservoir and the stability of vertical and horizontal seals along five analyzed seismic sections.

1.4. Work Schedules

The analytical part of the contract was conducted over the last five months commencing on November 2, 2005. The schematic below in Table C illustrates the major work flow and timelines:

Table C

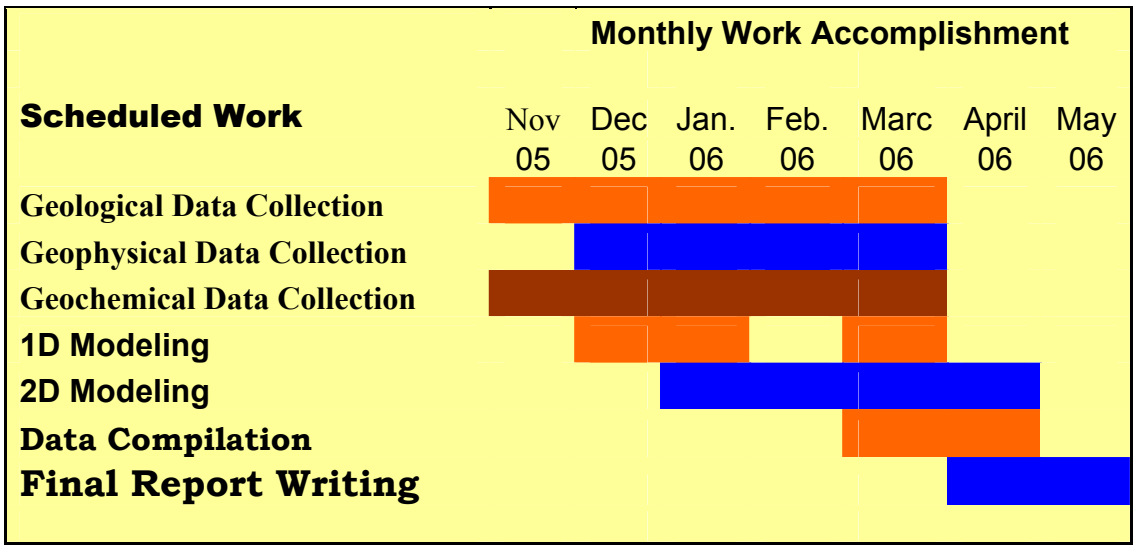

Table A. Chart shows the work flow and schedule for the project

2. GEOLOGICAL FRAMEWORK

The Scotian Basin contains Mesozoic-Cenozoic sedimentary rocks, which are up to 16 km thick. It developed during the break-up of the Supercontinent Pangaea in the Late Triassic to Early Jurassic (~230-190 Ma) Period as North America separated from Africa (Jansa and Wade, 1975; Welsink et al., 1989; Wade and MacLean, 1990; Louden 2002). In the Nova Scotia Margin, the extrusive volcanism in the southwest during the Bajocian age (example; Georges Bank) to non-volcanic margin in the northeast (example: Sable Subbasin) as seen through the East Coast Magnetic Anomaly documents the boundary between the continental and oceanic crust (Dehler et al, 2004; Funck et al., 2004; Louden et al., 2005; Wu et al., in press). Prior to rifting, the Essaoiura Basin from Morocco was juxtaposed with the Scotian Basin (CNSOPB, 2005, ONAREP, 2000) (Figure 2a). At approximately 225 Ma, a part of the Pangean Supercontinent (part of Nova Scotia and Morocco's margins), which was situated within a paleo-latitude of 10-20^{o} drifted northward. During that period of the Mesozoic era, a thermal uplift occurred within the Nova Scotia-Newfoundland area of Pangaea resulting in the development of a

rift valley system (Wade et al., 1989, Wade and MacLean, 1990). This rift valley system eventually separated North America from Africa during the early Jurassic. The subsidence history of the Scotian Basin and Labrador Shelf indicates that these regions underwent extension during rifting in the Early Jurassic and Late Cretaceous and has since subsided passively due to conductive cooling of the lithosphere (Royden and Keen, 1980). Renewed tectonism during the Sinumarian period resulted in the complex faulting and erosion of Late Triassic-Early Jurassic sediments forming Break-Up Inconformity (Wade and MacLean, 1990).

The Scotian Basin extends for a distance of 1200 km along the continental margin of Canada south of Nova Scotia and Newfoundland. Rifting of Pangaea through the Late Triassic and early Jurassic opened up a thick sequence of sedimentary strata in a series of interconnected subbasins or grabens and ridges or platforms which include the following structural elements: Abenaki Subbasin, Burin Platform, Canso Ridge, LaHave Platform, Mohican Graben, Orpheus Graben, Sable Subbasin, Shelburne Subbasin, and South Whale Subbasin (Fig. 1b). Smaller isolated basement lows (Naskapi and Mohican grabens) were also formed during the rifting.

The Scotian Slope covers an area of about 150,000 square kilometers, which includes three major subbasins within the Nova Scotia territorial region: Laurentian, Sable, and Shelburne (Wade and McLean, 1990) (Figures 1a and 1b). Most of the Jurassic-Tertiary sediments of the slope area of these three subbasins have been penetrated by the Early Jurassic Argo salt in various forms excluding diapirs, canopies, etc (Figures 1b and 2a).

The synrift facies, the Eurydice Formation is Late Triassic to Early Jurassic in age (Scythian to Sinemurian). This formation overlies the Pre-

Mesozoic basement, and contains fluvial, lacustrine, and aeolian sediments. The Eurydice Formation in the deeper grabens consists of evaporite facies, which is overlain by similar facies of the Argo Formation from Ladinian to Sinemurian age (Fig. 2a; Wade and MacLean, 1990; Wade et al., 1995). The synrift Eurydice and Argo Formations may be up to 10 km thick in the Orpheus Graben, 5 km in Abenaki Subbasin and 3 km in the Sable Subbasin (Wade et al., 1995).

The post-rift sediments begin with the clastic Mohican Formation (Sinemurian to Bajocian age) and a local dolostone facies, the Iroquois Formation from Sinemurian to Pliensbachian in age (Figures 1c and 2b). The Mohican Formation is overlain by a variety of continental to marine facies, which are Middle to Late Jurassic in age. These include the continental Mohawk Formation (sandstone and shale; Bathonian to Oxfordian age) and the shelf area, the deltaic Mic Mac Formation (sandstone, shale and limestone; Bathonian to Tithonian age), a carbonate bank facies of the Abenaki Formation (carbonate and calcareous shale: Bathonian to Kimmeridgian in age) with its four members (Artimon, Baccaro, Misaine, and Scatarie), and a basinal shale facies of the Verrill Canyon Formation (Bathonian to Kimmeridgian) within the Scotian Slope (Figures 1c and 2b). None of the recently drilled slope wells have penetrated any Jurassic aged sediment. No deepwater basinal facies sediments have been observed in the Acadia K-62 and Albatross B-13 wells as they are associated with the Jurassic Carbonate Bank.

During the Early Cretaceous, a widespread regression was initiated which resulted in a much larger fluvial-deltaic system (major sandstone and shale sequence) termed the Missisauga Formation (Berriasian to Aptian age). The rapid deposition and increased sedimentation resulted in the migration of the delta and also growth faults that stepped progressively

seaward as the delta prograded. The overall trend of marine regression and deltaic sedimentation continued until the end of Barremian. However, a high order transgressive event during the Hauterivian is easily identified by the "O" marker, an oolitic limestone unit (Wade and MacLean, 1990; Shimeld, 2004). This middle member extends from the shale unit to the base of a series of limestone beds, which is a typical lithological marker ("O" marker). The maximum thickness of the Missisauga Formation is about 2100 m in the Sable Subbasin. Locally, on the LaHave Platform, the carbonate facies of the Abenaki Formation is flanked and overlain by the typical Missisauga clastics (Wade et al., 1989). In the distal part of the delta and the slope regions, the sand and shale facies of the distal Missisauga Formation and the shale and siltstone facies of the Verrill Canyon Formation are continued. In the Annapolis G-24, Newburn H-23, and Weymouth A-45 wells, the Missisauga age equivalent sediments (Aptian and older, Wade and MacLean, 1990, Wade et al., 1995) were encountered below 4332 m, 4570 m, and 5108 m, respectively (see Chapter 3 of this manuscript).

The Missisauga Formation is overlain by the regressive and transgressive Logan Canyon Formation (sandstone and shale; Aptian to Cenomanian age). The Shortland Shale is the deeper water basinal facies of the Logan Canyon Formation and exceeds more than 2000 m in thickness along the shelf-break areas (example: Evangeline H-98) (Wade and MacLean, 1990). The thickness of the Logan Canyon Formation varies from 1600 m in the Sable Subbasin to 1000 m in the Abenaki Subbasin to 500 m on the LaHave Platform (Wade et al., 1989). The type section of the Logan canyon Formation can be seen in the Cree E-35 well. The upper part of the trangressive Logan Canyon Formation is overlain by another transgressive sequence of the Dawson Canyon Formation (Turonian to Santonian age), which consists of up to 300 m of mainly marine shale. The transgressive Dawson Canyon Formation is overlain by a limestone and chalk facies,

the Wyandot Formation (Santonian to Maastrictian age) that has an average thickness of 135 m and is overlain by the Banquereau Formation.

The deep-water shale facies of the Banquereau Formation includes strata ranging from Campanian to Maestrictian and to the Eocene age. Overlying regressive facies were formed during the erosion and reworking of the Cretaceous facies due to tectonic tilting of the Scotian Basin in the Late Tertiary. Regression and progradation in the Late Tertiary and Quaternary have formed the present day Scotian Shelf and Slope (Wade et al., 1989). The maximum thickness of the Banquereau Formation occurred in the outer shelf and slope areas, which exceeded 2000 m in places (Shubenacadie H-100 well). The Banquereau Formation sediments are overlain by unconsolidated glacial till, glaciomarine silts, and marine sediments that were deposited during the Quaternary Period.

The Scotian Basin (offshore Nova Scotia) and the Essaoiura and Tarfaya basins (offshore Morocco) have a close similarity in tectonic and stratigraphic evolution through time prior to rifting. A comparable evolution of the salt basins and the stratigraphic chart of the Nova Scotian and the Moroccan offshore successions are illustrated in Figures 2a and 2b. In the Moroccan Margin, the opening of the Atlantic was preceded by Triassic-early Jurassic rifting followed by massive regional subsidence during the Jurassic and much of the Early Cretaceous (ONAREP, 2000).

3. SOURCE ROCK EVALUATION – CURRENT CONTRACT

3.1. Introduction

The most common ingredient of a petroleum source rock is to identify its organic richness or total organic carbon (TOC) content. Organic carbon is composed basically of three components: (1) oil and gas already formed; (2)

insoluble organic matter (kerogen); and (3) dead carbon, which has no potential for hydrocarbons.

It is the organic matter type that determines the type of product that will predominate during decomposition. The variability of the organic matter type depends on the original biomass that was ultimately condensed into a macromolecule of insoluble organic matter or kerogen. Kerogen type is a function of chemical composition and structure. Basically, there are oil and gas prone components in kerogen. Type I (mainly anoxic lacustrine and marine algal remains) and II (marine biodegraded algal sometimes mixed with terrestrial or lacustriane algal/higher plant components) kerogens have predominantly oil prone kerogen, whereas Type III kerogens (mainly terrestrial humic and lipid components) have predominantly gas prone kerogen (Tissot and Welte, 1979; Hunt, 1996; Mukhopadhyay and Wade, 1990; Peters et al., 2005).

Type IV kerogens are non-source rocks or they do not generate enough hydrocarbons. However, in most basins of the world, a majority of deepwater source rocks in the world include some mixtures of Type II and Type III kerogens forming mainly light oil, condensate, and gas (Hunt, 1996; Mukhopadhyay et al., 2003).

The generation of oil and gas and the conversion of oil to gas are described by primary and secondary hydrocarbon cracking reactions, respectively. Primary products include oil and associated gas both resulting in the decomposition of kerogen (the primary macromolecular structure of organic matter). Secondary gas or non-associated gas is derived from primary products, i.e. oil. Yields are also a function of primary and secondary cracking reactions, which are dependent on thermal exposure or thermal maturity.

3.2. Samples and Source Rock Analysis

Thirty samples from four wells (Alma K-85 – one sample; Annapolis G-24 – one sample; Torbrook C-15 – 7 samples; and Weymouth A-45 – 21 samples) have been analyzed for Rock-Eval pyrolysis and total organic carbon (TOC) (Table1). The two samples from Alma K-85 (Jurassic Verrill Canyon) and Annapolis G-24 (Cretaceous Verrill Canyon) were selected for multi-component kinetics analysis [components: C_1, C_2 to C_5, C_6 to C_{14}, C_{15+}; (Table 1)]. All thirty samples were collected as unwashed cuttings. Similarly, thirty samples from three wells (Crimson F-81 – 4 samples; Torbrook C-15 – 7 samples; and Weymouth A-45 – 19 samples) have been analyzed for vitrinite reflectance measurements (Table 2). One sample from the Newburn H-23 well has also been collected from a sidewall core at 5962.8 m. This sample was not analyzed due to possible low organic matter content.

Two samples selected for multi-component kinetics analysis are organic-rich (Alma K-85: 2.43% TOC - Jurassic Verrill Canyon Formation and Annapolis G-24: 4.56% TOC - Cretaceous Verrill Canyon Formation; Table 1). Based on the hydrogen potential (S_2 and hydrogen index), only the Alma K-85 sample is considered to be a mixed oil/gas prone source rock [Figures 3a (i to iii)]. In spite of low calculated maturity (VRo for Alma sample is 0.49% and 0.60% for the Annapolis G-24 sample), both samples have already expelled a moderate amount of hydrocarbons suggesting an early generation of oil in both samples.

All seven samples from the Torbrook C-15 well are moderately organic rich (1.46 to 1.85% TOC – Table 1). Similarly, based on the S_2 and hydrogen index values, all seven organic rich shale samples (Miocene to Eocene age) from the Torbrook C-15 well have moderate to high hydrocarbon potential

(hydrogen index: 233 to 287 mg HC/g TOC). Based on various Rock-Eval pyrolysis plots, these sediments are considered to be mixed oil and gas prone kerogen Type II-III source rocks [Figures 3b (i, ii, and iii)]. The production index data suggests that all samples have low hydrocarbon expulsion suggesting an immaturity of these sediments.

With the exception of one sample (depth: 5760 m – 0.92%), all samples from the Weymouth A-45 well are moderately organic rich and show mostly 1-2% TOC (Table 1). Sediments beyond 6182m show moderately high S_2 (mostly greater than 3.5 mg HC/g of rock) and hydrogen index values (249-346 mg HC/g TOC) suggesting elevated hydrocarbon potential. Accordingly, the Cretaceous Verrill Canyon sediments (of Hautervian age) from 6206 m to 6520 m in the Weymouth A-45 well have the highest hydrocarbon potential. These sediments are considered to be mixed oil and gas prone kerogen Type II-III source rocks [Figures 3c (i to iv)].

3.3. Multicomponent Kinetics and Hydrocarbon Expulsion

The kinetics determination is the rate of conversion of hydrocarbons in geological time and temperature from the insoluble part (kerogen) of the source rock. In most of the numerical simulation models of the geological systems, the rate of conversion of kerogen in the source rock to petroleum uses a series of first order parallel, stoichiometric thermal cracking reactions (Peters et al. 2005). Therefore, in a laboratory simulation, the timing and amount of each molecular component or components of expelled hydrocarbons could be documented analyzing the distribution of activation energies and a single Arrhenius factor, which are used to calculate kerogen decomposition rates using rate equations and an assumed first order reaction (Jarvie and Lundell, 2003). As the slight variations of organic facies can bring high uncertainties for the timing and amount of hydrocarbon expulsion from a single source rock, multiple component kerogen kinetic measurements have been performed on two

source rocks to yield a more reliable evaluation of uncertainty in numerical simulations of petroleum generation. The detailed procedure for the multi-component kinetic determinations is illustrated (Appendix A-2).

As defined earlier, two prolific source rocks (Cretaceous and Jurassic Verrill Canyon) from the Scotian Margin have been selected for multi-component kinetics determination. Four groups of hydrocarbon components have been analyzed: (C_1 [dry gas]; C_2 to C_5 [wet gas]; C_6 to C_{14} [condensate – light oil]; C_{15+} [normal gravity to heavy oil].
As the Cretaceous Verrill Canyon sample from the Annapolis G-24 well has shown anomalous S_1 and S_2 in two different measurements during Rock-Eval pyrolysis, another sample from the Weymouth A-45 well was selected for multi-component kinetics analysis after scrutinizing the Rock-Eval pyrolysis data. The hydrocarbon potential and total organic carbon data from these two samples was used for the kinetic analysis from the Weymouth A-45 (6206 m – Cretaceous Verrill Canyon) and Alma K-85 (3520 m – Jurassic Verrill Canyon) has been illustrated in Table 3a and 4a. The replacement sample has a better hydrocarbon potential.

The kinetics analysis from four hydrocarbon components (C_1, C_2 to C_5, C_6 to C_{14}, and C_{15+}) of two samples suggest that both C_{15+} oil and C_6 to C_{14} condensate fractions from the Cretaceous Verrill Canyon (Weymouth A-45, 6206 m) have higher activation energy distributions and corresponding timing of hydrocarbon expulsion than the sample from the Jurassic Verrill Canyon (Alma K-85, 3520 m) (Tables 3b and 4b; Figures 4a (i) and 4a (iii) and 4b (i) and 4b (iii). The main activation energy distributions of C_{15+} oil and condensate (C_6 to C_{14}) fractions from the Cretaceous Verrill Canyon source rock are centered at 48-51 and 52-54 Kcal/mole, whereas some of these fractions in the Jurassic Verrill canyon source rock is concentrated at 43-47 and 49-52 Kcal/mole (Tables 3b and 4b). The pyrolysis-gas chromatographic compositional grouping of expelled hydrocarbons from

both samples suggest that the volumetrically primary cracking of each unit of Cretaceous Verrill Canyon source rock will generate 17% normal gravity C_{15+}oil, 62% C_6 to C_{14} condensate and light oil; 15% C_2 to C_5 wet gas, 6% methane (C_1) [Figure 4a (ii))]. On the other hand, Jurassic Verrill Canyon source rock will generate 40% normal gravity C_{15+}oil, 47% C_6 to C_{14} condensate and light oil; 10% C_2 to C_5 wet gas, 3% methane (C_1) [Figure 4b (ii))]. The normalized kinetics calculation from the primary cracking of kerogen suggests that the Cretaceous Verrill Canyon source rock has 10% inert carbon, whereas the Jurassic Verrill Canyon consists of less than 5% inert component.

The computed temperature (^{0}C) and vitrinite reflectance (% Ro) at onset (10%), 50% and 90% hydrocarbon conversion from the Cretaceous and Jurassic Verrill Canyon source rocks have been documented in Table A-2:

Table A-2

Components	Temperature (^{o}C) for 10% Hydrocarbon Conversion	Temperature (^{o}C) for 50% Hydrocarbon Conversion	Temperature (^{o}C) for 90% Hydrocarbon Conversion	% R_o for 10% Hydrocarbon Conversion	% R_o for 50% Hydrocarbon Conversion	% R_o for 90% Hydrocarbon Conversion
Cretaceous Verrill Canyon						
C_{15+}	110	125	138	0.63	0.73	0.83
C_6 to C_{14}	136	151	165	0.81	0.99	1.22
C_2 to C_5	137	157	176	0.82	1.10	1.43
C_1	138	162	186	0.83	1.17	1.65
Jurassic Verrill Canyon						
C_{15+}	87	113	140	0.47	0.64	0.85
C_6 to C_{14}	128	144	157	0.75	0.89	1.10
C_2 to C_5	136	153	169	0.81	1.03	1.30
C_1	141	165	190	0.86	1.22	1.74

C_{15+} = normal gravity oil; C_6 to C_{14} = light oil and condensate
C_2 to C_5 = wet gas; C_1 = dry gas (methane)

The kinetics modeling data suggests that the Jurassic Verrill Canyon source rock generates the oil fraction earlier than the Cretaceous Verrill Canyon source rock. On the other hand, the Cretaceous Verrill Canyon source rock generates gas fractions earlier than the Jurassic Verrill

Canyon source rock. The definition of the primary decomposition of the kerogen is strictly based on the differences in reaction kinetics resulting from inherent compositional differences in organic matter. The inherent differences in organic matter composition are possibly caused by the nature of sediment transport. These reactivity differences in the rates of kerogen decomposition can result in different levels of conversion at equivalent thermal exposure (Jarvie et al., 2003). This may affect the timing of onset and peak hydrocarbon generation for individual source rocks. This data suggests that the Cretaceous Verrill Canyon source rock has started generating oil around 110-120^{0}C and at a maturity of 0.63 and 0.73% Ro, whereas the hydrocarbon expulsion from the Jurassic Verrill Canyon source rock is at 87 to 134^{0}C and at a maturity of 0.75 and 0.89% Ro. The early generation of oil from both the Jurassic and Cretaceous Verrill Canyon source rocks compared to typical Type II source rocks (Kimmeridgian or Woodford Shale, etc.) may indicate possible abundance of an oxygen-functional group of compounds derived from the terrestrial organic matter input also visualized from the organic petrological studies (Jarvie et al., 2003, Mukhopadhyay, 2000).

3.4. Vitrinite Reflectance Analysis

Thirty organic rich sediments from the Crimson F-81, Torbrook C-15 and Weymouth A-45 were selected for vitrinite reflectance measurement. The maturity of all four Early Cretaceous sediments (6025 m to 6740 m) from the Crimson F-81 well lie between the early to late phase of oil generation and early phase of gas generation (0.65% to 0.94% VRo) (Table 2).
All seven Tertiary (Miocene to Eocene) samples from the Torbrook C-15 well are immature for hydrocarbon generation and have a low thermal gradient (slope: y =3.861.8Ln(x) + 7141; Figure 5B). The organic rich sediments from the Weymouth A-45 well (Figure 5C) up to 5501 m (Cenomanian to Barremian) are immature for hydrocarbon generation

similar to the Tertiary sediments from the Torbrook C-15 well. However, all other source rocks between 5760 m and 6520 m are mature for liquid hydrocarbon generation. The amorphous organic matter rich and oil prone Cretaceous Verrill Canyon source rocks between 6206 m and 6520 m lie within the principle phase of hydrocarbon generation.

3.5. Organic Facies and Source Rock Potential

The visual kerogen and Rock-Eval pyrolysis data from all Cretaceous (Missisauga and Cretaceous Verrill canyon formations) samples below 5750 m depth from the Weymouth A-45 well, all five Tertiary Banquereau formation samples from the Torbrook C-15 well (Eocene to Miocene age), and one Jurassic Verrill Canyon sample from the Alma K-85 well contain abundant framboidal and fine grained pyrite and marine amorphous fluffy lipid components (biodegraded algal). This organic matter is partially mixed with terrestrial components (vitrinite and inertinite) forming oil and gas prone Type II-III source rocks (Figures 5d and 5e). This data suggests that these sediments were deposited in a partially anoxic depositional environment. The autochthonous and allochthonous terrestrial ligno-cellulose components (vitrinite and inertinite) of the Type II-III source rocks from the Torbrook C-15 and Weymouth A-45 wells suggest that they were derived from turbidity induced flow from the shelf. The amorphous organic matter of the Cretaceous Verrill Canyon source rocks (Type II-III) from the Weymouth A-45 well shows distinctive features of a deepwater organic facies due to the presence of fecal pellets of zooplanktons and more well preserved vitrinite grains. Morphologically, these sediments are similar to the Cretaceous Type II and II-III source rocks from various Deep Sea Drilling Project Sites from offshore Morocco and Blake Bahama Basin (DSDP Leg 76 and Leg 79; Rullkotter et al., 1984 and 1986, Rullkotter and Mukhopadhyay, 1986). The anoxicity was developed on typical deep marine depositional settings due to a relationship between the higher

influx of terrestrial organic matter and the lower consumption of organic matter by bacteria.

Visual kerogen analysis of most organic matter within all four samples from the Crimson F-81 well and in one sample from the Annapolis G-24 well indicates that they contain low framboidal pyrite and abundant terrestrial organic matter because of the recycled and rounded grains vitrinites, semifusinite, and exinite (oxidized spores and resins). Therefore, they form mainly gas (with some condensate) prone kerogen Type III or II-III source rocks. This type of organic association is quite typical of a sedimentary setting in a deltaic front and shallow upper slope areas where deltaic organic matter usually deposits in a dysoxic deepwater environment (Tables 1 and 2; Figure 5f).

Various plots of Tmax (maturation) versus S_1 or production index values from the Rock-Eval pyrolysis have been used to define the generated hydrocarbons within the source rocks. However, all four recently drilled wells on the Scotian Slope (Annapolis G-24, Crimson F-81, Torbrook C-15, and Weymouth A-45) were drilled with synthetic oil based mud additives. Unfortunately, some of the anomalous nature of the S_1 fraction of these organic-rich sediments from these wells could be related to oil impregnation, which could be derived from the synthetic oil based mud additives. Therefore, all interpretations related to the S_1 fraction should be taken with extreme caution. Similarly, the maturity data might be partially suppressed due to the base oil contamination, in spite of using common extraction procedures.

The organic facies, hydrocarbon potential, and maturity of the five selected wells (Alma K-85, Annapolis G-24, Crimson F-81, Torbrook C-15, and Weymouth A-45) that were analyzed for the current contract can be summarized as follows:

- ❖ All sediments from the Torbrook C-15 and Weymouth A-45 wells are kerogen Type II-III source rocks and were deposited in a partially anoxic deepwater depositional environment. Early Cretaceous Verrill Canyon (Hauterivian age) sediments below 6206m from the Weymouth A-45 well are considered to be mature oil-prone source rock. All Tertiary sediments from the Torbrook C-15 well are immature for hydrocarbon generation.
- ❖ The morphology of the organic matter within the Cretaceous Verrill Canyon (Early Missisauga Formation) source rocks from the Crimson F-81 and Annapolis G-24 wells suggest that they are derived from a delta front depositional environment. On the other hand, similar source rocks from the Weymouth A-45 well indicate that they are distinctively deepwater marine organic facies.
- ❖ All four analyzed sediments from the Crimson F-81 well and sediments below 5760 m in the Weymouth A-45 well are mature for oil and gas generation.
- ❖ The S_1 and Production Index values from the Torbrook C-15 well indicate the low maturity of these sediments. On the contrary, moderately low production index values within the mature (>0.5% VRo) kerogen Type II-III (amorphous organic matter rich) source rocks from the Weymouth A-45 well suggest the possible expulsion of hydrocarbons from these sediments (Figure 3c [v]).

4. PETROLEUM SYSTEM MODELING

The space-time-continuum of generation, expulsion, migration, and accumulation of hydrocarbons involves many complex, dynamic, multivariate processes that are used in basin analysis. Moreover, the interrelated chain of processes leading to the end product 'petroleum' is highly nonlinear. Therefore, any predictive interpretation and 'hypothesis testing' concerning the formation and occurrence of petroleum makes it

absolutely necessary to retrace back to the changing ambient conditions and to reconstruct the important parameters. The 'basin simulation or basin modeling' would be the best choice for predicting the hydrocarbon phase, property and composition in a complex reservoir situation. Therefore, an accurate numerical modeling of the petroleum system is pertinent to tracing back the geological and thermal histories of various parts of the basin. The petroleum system provides a complete record of the sedimentary and hydrocarbon emplacement histories of any specific region through geological time.

The following parameters illustrate the comparable features of one, two, and three dimensional petroleum system modeling:

- The one dimensional modeling is essential for the initial assessments, calibration, and reconnaissance work in an known (using the wells already drilled) or unknown terrain (projected as a 1D dummy well),
- The two dimensional modeling is essential for the reconnaissance based on 2-D seismic and geological sections, and for semi-quantitative assessments of the reservoir hydrocarbon saturation, pressure, timing of migration, and volume,
- The three dimensional modeling is essential for all quantitative assessments of the hydrocarbon volume within the reservoirs, and
- All dimensions are essential for the petroleum system modeling and must be fully integrated. The three dimensional modeling will not replace one dimensional or two dimensional similar to as the 3-D seismic will not replace the 2-D seismic interpretations.

Petroleum systems modeling is used to provide a basic framework for integrated earth models and to calculate and predict temperature and pressure, hydrocarbon charge components, migration through geological time, the assessment of target reservoir hydrocarbon saturation, and

hydrocarbon volume assessment. It also includes the understanding of complex oil and gas properties such as hydrocarbon composition, fingerprinting of multi-component hydrocarbon distributions of various source rocks, and reservoir hydrocarbon properties (gas and oil ratios, API gravities, bubble point curves, etc.) in complex deepwater petroleum systems. A complete review of various attributes of the petroleum system modeling (especially the multi-component migration components) has been illustrated in details in Appendix C. The details of various modeling parameters have been discussed with 1-D and 2-D modeling sections of this manuscript (Chapters 5 and 6)

The report comprises an integrated study of petroleum system risk analysis within a target area between the deepwater portions of the Sable Subbasin and Shelburne Subbasin in order to identify potential hydrocarbon areas that can be targeted by future exploration. This will delineate future oil and gas exploration strategies (Figure 6). An integrated petroleum system risk assessment requires a complete appraisal of four modular elements of the petroleum system: (1) geological and geophysical; (2) geochemical; (3) hydrocarbon emplacement; and (4) hydrocarbon survival (Mukhopadhyay et al., 2003) (Figure 6). The work on the geological and geophysical component encompasses all studies related to litho- and chrono-stratigraphic boundaries, structural complexities, sequence stratigraphy, and defining traps, seals, and play type sizes. The geochemical component includes defining source rock potential, maturation, fingerprinting the timing and the amount of each individual or group of hydrocarbon components released from individual source rocks (Figure 6). The precise identification of hydrocarbon emplacement within individual traps and their compositional variations is documented by one- and two-dimensional petroleum system modeling that requires the input of geological, geophysical, and geochemical components. The hydrocarbon survival component is usually documented from a combined analysis of seal stability and seepage. This work is

accomplished through systematic studies of stability of individual reservoir hydrocarbons from the 2D numerical modeling of seal leakage. The hydrocarbon survival components analyzed by seepage through their surface and subsurface expressions by satellite imagery, the geochemistry of upper layers, and the identification of seismic anomalies could not be documented in this report. This data was either not available or had to be purchased. Therefore, no interpretation could be included in this report because it is confidential at the time of this report.

4.1. Modeling Input Database: Introduction

The rifting on the Scotia Margin during the Late Triassic to Early Jurassic Period (230 Ma to 190 Ma) may have initiated the formation of various fault-controlled half grabens including Mohican, Naskapi, Orpheus, etc., (Figure 7a). The rifting is later succeeded by three main basement subsidences during Jurassic, Cretaceous, and Tertiary Periods (Jansa and Wade, 1975; Welsink et al, 1989; Wade and MacLean, 1990). These subsidences created two major subbasins in the east (Abenaki, Sable) and one in the west (Shelburne) of the shelf-slope region in the Scotian Basin (Figure 7b).

This study will include the histories of the petroleum system development from the Late Triassic (Norian: 210 Ma) to Recent (0 Ma) deepwater sediments of the Sable Subbasin and Shelburne Subbasin. The study area for this contract is from the eastern to the western part of the Scotian Slope: from the east of the Annapolis B-24 well in the Sable Subbasin to the Shelburne G-29 well within the Shelburne Subbasin (Figure 7b). The report includes the hydrocarbon risk analysis through petroleum system numerical modeling (one dimensional modeling of 12 wells and two dimensional modeling of five seismic lines) using all geosciences related information within the study area. These wells include *Acadia K-62,*

Albatross B-13, Annapolis G-24, Balvenie B-79, Crimson F-81, Evangeline H-98 (shelf well), Newburn H-23, Shubenacadie H-100, Shelburne G-29, Tantallon M-41, Torbrook C-15, Weymouth A-45. The 2-D seismic lines are A-A', B-B', C-C', D-D', and E-E' (Figure 7c). Although the Evangeline H-98 well is not situated in the slope region of the Scotian Basin, it was analyzed because of its proximity to the Newburn H-23 well and contains some deepwater facies within the Missisauga Formation. This contract also included 1D modeling of the Tantallon M-41 well and 2D modeling of seismic line E-E' located in the western part of the Shelburne Subbasin and is not within the study area (Figures 7b, 7c, and 7d).

As a requirement to build the complete geological history for the numerical simulation, the database for integrated petroleum system modeling includes various geological, geophysical, and geochemical elements (Figure 8a). The geological and geophysical database includes the following:

- formation boundaries,
- possible lithology or lithology mixes for each stratigraphic unit,
- sequence stratigraphic boundaries (paleochannel erosion and formation of submarine fans during low sea-level, onlap, erosion etc.),
- defining the timing of erosion, paleowater depths, and paleotemperature (through time) from biostratigraphic analysis,
- defining heat flow in relation to basement fracture and oceanic crust, and
- designating the hydrocarbon reservoirs and their proper seals in relation to various play types, etc.

The geophysical database requires the following parameters:

- ✓ seismic sequence boundaries, seismic velocities of each individual stratigraphic sequence for time-depth conversion

(depth-converted seismic section preferred), and seismic stratigraphy,

- ✓ the timing of salt emplacement, play types, reservoirs, and seals, etc.

The geochemical database includes the following:

- ❖ defining source rock intervals and hydrocarbon potential,
- ❖ present day maturity profile,
- ❖ nature and timing of hydrocarbon expulsion using multi-component kinetics, and
- ❖ oil and gas properties for each individual source rock based on compositional analysis by pyrolysis-gas chromatography (Figure 8a).

4.2. Geological and Geophysical Input Data

Of the twelve wells evaluated in this study, two wells (Albatross B-13 and Shelburne G-29) lie within the Slope area of the Shelburne Subbasin; three wells (Torbrook C-15, Acadia K-62, and Shubenacadie H-100) are within the slope area between the Shelburne and Sable subbasins; six wells (Evangeline H-98, Newburn H-23, Weymouth A-45, Balvenie B-79, Annapolis G-24, and Crimson F-81) are within the slope areas of the Sable Subbasin (near Sable Island); and one well (Tantallon M-41) lies within the slope area between the Sable and the Laurentian subbasins (Figures 7b, 7c, and 8b).

For one and two dimensional modeling, the formation boundaries and age of each stratigraphic and lithological boundary have been assigned from the well history reports for individual wells. The assignment of various stratigraphic nomenclatures from each individual well has been established using earlier publications (Wade and MacLean, 1990; Wade et al., 1995) and

by the author's personal discussions with John Wade from the Geological Survey of Canada (Figure 8c). Published biostratigraphic data from the Geological Survey of Canada Basin Database and the recent data from various Open File Reports from the Geological Survey of Canada have been utilized for chronostratigraphic age definition of each stratigraphic unit. The age, paleo-waterdepths, paleo-temperature, unconformities at various intervals have been established after discussions with various biostratigraphers and geologists in Nova Scotia (Pierre Ascoli, Frank Thomas, Rob Fensone, and John Wade from the Geological Survey of Canada and Jason Crux from Crux Biostratigraphic Consulting), by utilizing Geological Survey of Canada Open File Reports, Geological Survey of Canada Basin Database, and by reviewing current or recent publications. The new geological time scale of Gradstein and Ogg (2004) has been followed to determine precise ages of each stratigraphic unit (Figure 8d).

The stratigraphic intervals and total drilling depths of 12 (11 from the Slope and one from the shelf) wells from the Scotian Basin have been illustrated in Figures 8e, 8f (i), 8f (ii), and 8f (iii) and Table 5. These figures also include the correlation of stratigraphic intervals of each well with the modified Scotian Margin lithostratigraphy. This data shows that only two wells (Acadia K-62 and Albatross B-13) that are associated with the Jurassic Carbonate Bank and consist of Jurassic age sediments [Figure 8f (ii)]. Similar to the Shelburne G-29 well and Tantallon M-41 well, four recent deepwater wells (Annapolis G-24, Crimson F-81, Newburn H-23, and Weymouth A-45) were drilled to the Early-Middle Cretaceous Missisauga equivalent sediments [Figure 8f (ii); Table 5). Two recent wells, Balvenie B-79 and Torbrook C-15, were drilled up to the Middle-Late Cretaceous and Tertiary age, respectively.

The five seismic lines (A-A' through E-E') were chosen after viewing the TGS-Nopec interpreted seismic lines within our study area. This work was

performed in collaboration with Brent Smith of Canada Nova Scotia Offshore Petroleum Board. These five lines were specifically selected based on the nature of the salt movement and the different types of plays that may be associated with the salt. The seismic lines A-A' and B-B' include large allochthonous canopies within the middle slope region. These two lines pass through two recently drilled slope wells (Annapolis G-24 and Weymouth A-45) within the Sable Subbasin (Figures 9a and 9b). Lines C-C' includes two thin and two broad salt diapirs within the middle to lower slope region and are located within the western part of the Sable Subbasin (Figure 9c). These diapirs are associated with rooted autochthonous Jurassic Argo salt. The seismic line D-D' that lies within the area between the Sable and Shelburne subbasins includes narrow salt diapirs (Figure 9d). Similar to line C-C', these diapirs associated with the autochthonous Jurassic salt. The seismic line E-E' contains one broad and one narrow salt diapirs within the upper slope (Figure 9e). This line is situated within the western part of the Shelburne Subbasin.

The details of the seismic interpretation of the seismic data used in this study have been documented earlier by Kidston et al (2002). Kidston et al. (2002) have interpreted earlier that the top of the various formations was based on the correlation of significant seismic markers documented from the Deep Sea Drilling Project wells and based on other earlier publications (Ebinger and Tucholke, 1988; Wade and MacLean, 1990, Wade et al., 1995). The following seismic markers have been identified: Seafloor; Base Pleistocene/Upper Pliocene; Mid-tertiary (Oligocene) Unconformity, Top Cretaceous or Wyandot Equivalent; Mid-Cretaceous 'O' Marker Equivalent; Top salt, Base salt, Top Jurassic, Mid Jurassic, early Jurassic Break-Up Unconformity, Rifted Triassic, Basement. The seismic markers were assigned to the five seismic lines in this study on the basis of earlier publications (Kidston et al., 2002; Wade and MacLean, 1993) and from the identification by Brent Smith of the Canada Nova Scotia Offshore Petroleum

Board as part of their evaluation of the deepwater area by Kidston et al. (2002). These markers were subdivided into various intermediate layers in collaboration with the geophysicists from the Nova Scotia Department of Energy (Paul Harvey and Kris Kendell) and through discussions with John Wade of the Geological Survey of Canada.

4.2.1. Lithology, Unconformities, and Faults

In preparation for the two dimensional modeling of the five seismic lines, the SEGY files received from the Canada Nova Scotia Offshore Petroleum Board (with permission from TGS-Nopec) and loaded into the SeisStrat module of the PetroMod 9.0 software package (IES Inc., Aachen, Germany). For each of these seismic lines, all the major formation boundaries and top and bottom of salt, and lithology were assigned (in SeisStrat). Based on measured internal velocities of different lithology units of each formation from various slope wells and available data from Tom Bowman of Abundant Investments, Denver, Colorado, each of these five seismic lines were converted from time section to depth (within the SeisStrat). The average interval velocities were also linked to the mixed lithology of each formation as shown in Table 6. The following are the average interval velocities (in m/s) that were used for the conversion:
seawater – 1500; Plio/Pleistocene – 1850; Miocene – 2100; Oligocene – 2200; Eocene – 2250; Paleocene -2300; Top Cretaceous – 2350; Petrel (Shelf Backreef) – 1900; “O” Marker – 3350; Cretaceous Verrill Canyon or Missisauga – 3750; Abenaki (Shelf backreef) – 4200; Misaine – 4700; Scatarie – 5450; Mohican – 5250; Salt -4500; Triassic – 4500; and Meguma Basement – 5000.

The lithology of each stratigraphic unit from each of the 11 slope wells and one shelf well was collected from the individual well history reports. As most of the individual stratigraphic units from various wells contain a mixed lithology, a separate table has been created to include the percentages of

mixtures for each individual lithological entity (shale, sandstone, siltstone, limestone, marl, chalk, dolomite, anhydrite, salt, etc.) (Table 6). Thus, the model will accommodate minor variations of various physical properties of mixed populations such as thermal conductivities, compaction (porosity and permeability), capillary pressure, and fracture pressure. Table 6 illustrates the proportions of individual lithology mix and their marker stratigraphic units (within the slope wells) where they are specifically located. The mixed lithology of various geological units as observed from various well history reports have also been utilized for marking the lithology variations within each stratigraphic interval from these five seismic lines.

On each seismic line, all geological input parameters have been assigned to the depth section in PetroBuilder (PetroMod 9.02; IES Inc.). The geological age, splitting of larger stratigraphic units, lithology mix, facies, unconformity age and thickness, opening and closing time of each individual fault plane, timing and replacement thickness of salt piercing and salt movement for both diapirs and allochthonous salts have been assigned for each stratigraphic interval or their sub-layers on each seismic line. The geological age of each interval was assigned based on earlier works (Wade and MacLean, 1990; Wade et al., 1995; Figure 8c).

Unconformities have been assigned based on the biostratigraphy data from various wells and earlier publications (Geological Survey of Canada Basin database; 2006; Hogg et al., 2000 [Figure 10]; Wade and MacLean, 1990, Wade et al., 1995). The following are the various geological time periods where unconformities have been assigned: 196-190 Ma (Break-UP Unconformity), 170-168 Ma; 145-141 Ma (Jurassic-Cretaceous boundary); 89-71 Ma, 68-61 Ma (Cretaceous-Tertiary boundary); 47-45 Ma (Mid-Eocene); 33.9 or 28.4-23.03 (Oligocene); and 7.2-5.3 Ma (Late Miocene Unconformity). With the exception of the Oligocene unconformity, the eroded thickness of most of the unconformities has been considered to be from 100

to 300 m. This is because most of the erosion of the younger sedimentary units (Early Cretaceous to Recent) is sub-aqueous.

None of these faults were considered as sealing faults as there is no data available on this aspect. As no data on the timing of these faults is also available for this project, these faults have been kept as open since the time of initiation as shown in the following section:

- Seismic lines A-A' and B-B' have several basement faults which could not be intersected on the other three lines. In Line A-A', the basement faults have been kept open from 170 Ma to present. The Neogene faults in this line were kept open since 7.25 or 5.33 Ma (depends on the time of intersection of various Neogene sediments),
- In line B-B', all ten basement faults were kept open from 185 or 147 Ma (depends on the time of intersection of various Jurassic sediments) to the present time. The Cretaceous faults on that seismic line were kept open since 65 Ma and the Neogene faults since 7 or 2 Ma (depends on the time of intersection of various Neogene sediments) (depends on the time of intersection of various Neogene sediments),
- In line C-C', the Cretaceous faults were kept open since 61 or 47 Ma, where the Neogene faults were kept open since 11.2 or 7.5 Ma (depends on the time of intersection of various Cretaceous and Neogene sediments)
- In line D-D', the boundary fault (between the slope and the shelf) was kept open since 162 Ma; the Cretaceous faults between 89 Ma or 68 Ma and the Neogene faults between 5.3 or 2 Ma (depends on the time of intersection of various Cretaceous and Neogene sediments).
- In line E-E', the main fault (between the Eurydice and Early Missisauga) was kept open since 102 Ma, whereas the Cretaceous faults from 89 Ma and the Neogene faults from11.2 Ma.

4.2.2. Play Types, Deepwater Well Results, Reservoirs, and Seals

4.2.2.1. Play Types

With the exception of Miocene turbidite plays, most of the plays observed in the Scotian Slope have been connected with typical passive margin salt emplacements. The most common play types with excellent sand reservoir potential in the deepwater Scotian Basin are possibly related to lowstand regressive phases of the passive margin development within the Scotian Basin. These phases occurred during: (1) the Late to Middle Missisauga Formation; (2) the Cree member of the Logan Canyon Formation; and (3) part of the Banquereau Formation (mainly the Paleocene, Oligocene, and Miocene periods) as the deepwater section of the margin is similar to other deepwater basins of the world which were also affected by salt movement (Weimer et al., 1998; Pettingill and Weimer, 2001 – Figure 11a). Various play types from the deepwater Scotian Margin are listed as follows (Kidston et al., 2002; Hogg et al., 2001; Figure 11b):

- ✓ basement uplifted anticlines,
- ✓ syn-rift structural and stratigraphic traps,
- ✓ diapir flank and diapir crest,
- ✓ inter-salt or sub-salt plus slope fans,
- ✓ salt-cored toe thrusts and supra-salt,
- ✓ compressional structures such as 'confined' and 'unconfined' mini-basin floor, (Figure 11b).

Other stratigraphic traps including turbidite fans could be associated with an unconformity possibly the Mid-Miocene, Oligocene (Chattian), Mid-Cretaceous, etc. (Figures 11c and 11d). The onlap of sediments over the unconformity surface (especially over extensional growth faults) could generate a major turbidite submarine fan play (Figures 11d and 11e). Comparable play types are documented from the Moroccan Margin (Tari, 2006; Figure 11e).

Contrary to other world analogues where the majority of the discovered oil/gas fields are in Neogene sediments, Miocene play types within the upper slope region of the Scotian Margin can have a problem with competent seal. The Plio-Pleistocene sediments are thin and not compacted enough to act as efficient vertical seal. The turbidite sands associated with the Paleocene, the mid to Early Cretaceous (similar to delta front or turbidite sands in the Annapolis G-24 and Newburn H-23 wells) and the Late Jurassic (Tithonian) salt flank traps could be better prospects for gas and condensate. Miocene, Eocene and Early Cretaceous (Wyandot Formation) fractured carbonates could also form additional play types as seen by the presence of a thin sequence of gas-charged Miocene limestone within the Balvenie B-79 well.

4.2.2.2. Well Results

The following summarizes the results of the various slope wells. The information is based on the well logs and well history reports, which also includes some physical and chemical properties:

Acadia K-62: *No discovery*; target may be Abenaki Formation (Baccaro Member) fractured carbonate reef; high porosity and permeability; TD – 5287 m; Water Depth - 866.3 m.

Albatross B-13: *No discovery*; target - fractured carbonate reef from the Abenaki Formation; moderate to high porosity and permeability; some stains; TD – 4045 m; Water Depth – 1341 m

Annapolis G-24: *Discovery of gas and condensate within various turbidite sands from the Early Cretaceous Missisauga Formation (H-Sand, L-sand, and M-Sand).* Main discovery is within the M-Sand (overall thickness - 28 meters between 5498.3 to 5527.5 m). Log porosity is about 17 to 17.5%; no core available for permeability measurement. Other thin sand-rich gas-charged zones are: H-sand: 4842-4866 m; and L-sand: 5040.5-5097.8 m. Within these two sand units, log porosity varies from 14 to 17% within thin sand units; other thin sand units with some gas shows are within 5908-5910 m; 5920-5921 m, and 5956-5961 m; TD – 1678 m; Water Depth – 1678 m.

Hydrocarbon data from the Annapolis G-24 well

- Pressure gradients for two gas-charged sandstone zones: upper sand (5501-5515m): 0.147 psia; lower sand (5520-5530m): 0.117 psia
- The gas composition shows 88.3% Methane, 5.4% Ethane, 1.96% Propane, 2.62% CO2 (in mole percent), and the remaining Butane, Pentane and C_{6+} hydrocarbons
- The C1/C2 ratio of 11.4 suggests the presence of high gravity oil; wetness and balance ratios indicate productive dry gas associated with very wet gas, condensate or high gravity oil (API>35),
- Stable carbon isotopes of C1, C2, and C3 gases are -41 to -42, -28.0 to -29.1, and -25.3 to 26.3 parts per mil suggesting that mature thermogenic gases were possibly derived around 0.9-1.0% VRo from mixture of marine and terrestrial organic matter.

Balvenie B-79: *No discovery*; the target was the turbidite sands within the Logan Canyon Formation and Missisauga Formation. Non-productive gas shows with Middle Eocene carbonate; non-productive gas shows within thin 1-2 m sand units in the following mixed sand/silt/shale lithology intervals: 3462.8-6463.2 m (mixed shale, siltstone and carbonate), 4363-4372 m, 4389-4394 m, 4493-4499 m, 4527-4532 m; TD – 4750 m (did not reach Missisauga Formation target); Water Depth – 1803 m

Crimson F-81: *No discovery*; target was similar to Annapolis G-24 discovery; Details of the sands are currently unavailable because of confidentiality until August 2006; TD – 6677 m; Water Depth – 2091.5 m

Newburn H-23: *No discovery*; target was turbidite sands at various Cretaceous intervals (Logan Canyon and Missisauga Formation equivalent); non-productive gas shows in thin turbidite sands (<5m) at 4305-4325m and 4349-4358 m (13% to 18% porosity and 0.01 to 42.4 mD permeability), 5402-5408 m (17 to 19% porosity and 0.01 to 6.43 mD permeability); other good thin sand units (less than 2 m) are at 4909.5-4949 m, 5775.5-5779 m,

5801-5803 m, 5811-5813 m, and 5957.5-5960.5 m (14% porosity and 0.01 to 0.03 mD permeability – gas charged); TD – 6070 m; Water Depth – 977 m

Shelburne G-29: *No discovery*; target was possibly Early Cretaceous (Roseway Member) and Abenaki Formation fractured carbonate and Tertiary turbidite sands. TD – 4005 m; Water Depth – 1153.5 m.

Shubenacadie H-100: *No discovery*; target was Banquereau Formation Miocene turbidite sands; several thin sands within the Banquereau and bands of 0-15m tight sands were encountered within the interval from 2639 m to 2662 m. TD – 4200 m in Mid-Cretaceous (Albian); Water Depth – 1476.5 m.

Tantallon M-41: *No discovery*; target was possibly early to Mid-Cretaceous turbidite sands; one meter thin sands across several intervals below 4000 m were encountered; TD – 5602 m in Early to Middle Missisauga Equivalent; Water Depth – 1516 m

Torbrook C-15: *No discovery*; target was Miocene turbidite sands; no sands could be detected; TD – 3600 m in Banquereau Formation (Eocene); Water Depth – 1674.5 m.

Weymouth A-45: *No Discovery*; target was sub-salt Early (Missisauga) to Mid-Cretaceous (Logan Canyon) turbidite sands; some gas and condensate shows; TD – 6520 m in Early to Middle Missisauga equivalent; Water Depth – 1689 m.

4.2.2.3. Deepwater Reservoirs and Seals

Four major factors are responsible for the deposition of reservoir systems in deep-water turbidite fans: tectonics, sedimentary characteristics, sea-level changes, and climate (Bouma et al., 2002, Stow et al., 1985). During the rising of the source areas on land and lowering of the sea-level, the sands from the shelf deltas could feed sediment supply directly into a deep-water basin (Bouma and Scott, 2004). Cummings (2004) has pointed out that Upper Missisauga incised braided sand sheets could be good candidates as

a feeder system for deep-water slope and basin floor sand reservoir bodies. Onlap onto erosional surfaces could form sites for the deposition of turbidite channel sheet sands. Booth et al (2000) has documented from the Auger Basin of the Central Gulf of Mexico Margin that the basal onlap packages with erosional basal contacts form thickly-bedded sheet sands and highly amalgamated channel-fill deposits with high net/gross sands compared to erosional downcutting by the chaotic zones and stratigraphic pinch out within onlap packages. These chaotic facies contain laterally discontinuous channel fill and low net/gross ratio. The coarse and fine grained nature of the deepwater sediments is controlled by the coastline regardless of whether the feeding sediments will be canyon-fed or delta-fed. Shelf-margin deltas typically form fine-grained sediment as they are located within wide, low-gradient shelves (Bouma and Scott, 2004). MacDonald (2006) has shown some similar features within the Miocene to recent sediments from the Scotian Slope. Kendrick (2000) has documented some of the major reservoir architecture in the Northern Gulf of Mexico.

Various deepwater reservoirs include layered amalgamated sheet sands (Auger Field), channel-levee deposits (Thoe Field), and amalgamated channel complexes (Ram/Powell Field). Usually, the turbidite sand fill deposits in two phases (1) an initial “ponded phase” accommodation (adjacent to seafloor escarpment with high net/gross sheet sands) and (2) bypass accommodation phase with established graded slopes with low net/gross sand fill. Accordingly, the sedimentary wedge on top of the salt sheet forming trench slope basins will be determined by initial extension, translation and compression.

Previous works of John Wade has produced paleogeographic maps where the progradation of sediments from various delta systems were categorized into two time periods - Late Jurassic at 150 Ma and early Cretaceous at 135 Ma (Figures 12a and 12b; Atlantic Geosciences Society, 2001; Kidston et al.,

2002). These sediments were derived from the erosion of the Devonian-Permian sediment sources around the Gulf of St. Lawrence, onshore Nova Scotia and the New Brunswick region. The sediments that built up within the unstable shelf south of the basement hinge zone initiated the subsidence and formation of major growth faults within the Scotian Basin. These structural elements had eventually initiated the deltaic and turbidite reservoir sand deposition within the shelf-break and slope region (Atlantic Geoscience Society, 2001; Kidston et al., 2002; Murphy et al., 2002).

A recent sequence stratigraphic study using three-dimensional seismic lines from the Scotian Margin has resulted in the identification of various paleo-submarine channels in the Late Jurassic-Early Cretaceous, Early Tertiary – late Cretaceous, and Middle Tertiary Periods (Brent Smith, CNSOPB unpublished confidential report). The following trends of various submarine channels have been observed:

- ✓ **Late Jurassic-Early Cretaceous**: during the Late Jurassic-Early Cretaceous Period, only one major channel could be observed southwest of the Montagnais I-94 well beyond all of the salt structures within the middle to the lower slope. Some doubtful channels exist in the middle to the lower slope region between the Acadia K-62 well and the Shubenacadie H-100 well. During this time period, a major shelf-slope boundary fault existed, which could have initiated major turbidite flow channels;
- ✓ **Early Tertiary-Late Cretaceous**: during this period several major channels exist in the following locations:
    - South of the Montagnais I-94 well towards the slope and to the left;
    - A major NE-SW fault exists at the Jurassic Carbonate Bank edge in the area between the Torbrook C-15 and Shubenacadie H-100 wells. Two to three major channels could be observed between the Acadia K-62 and Shubenacadie H-100 wells, and

- A major channel exists between the Balvenie B-79 and Weymouth A-45 wells

✓ **Middle Tertiary (Oligocene)**:

- In the area between the Shubenacadie H-100 and the Acadia K-62 wells - the same major NE-SW fault exists at the Jurassic Carbonate Bank edge and three or four major channels could be detected;
- In the area between the Balvenie B-79 and the Weymouth A-45 wells, one or two major channels could be observed;
- Several major channels exist east of the Annapolis G-24 well; and
- At least five to six channels exist in the area between the Tantallon M-41 well and the Laurentian Subbasin.

The reservoir sands from both the Annapolis G-24 and the Newburn H-23 wells show a mixture of sand, silt, and clay-sized material. The Early Cretaceous organic matter from the Annapolis G-24 and Crimson F-81 wells show some evidence of a delta front environment. Therefore, it would be possible that the clean sands from the shelf deltas might have been transported to the lower slope through feeder channels within these areas leaving the shale dominated sands behind the upper slope.

On the five selected seismic lines (Figures 9a through 9e), several possible submarine fan sand reservoirs could be detected. Two of them are marked within the seismic line D-D' (Figure 9d), which are salt-flank play types. Another submarine channel sand was detected in line E-E' (Figure 9e). The 2D petroleum system modeling of five seismic lines is considered to be the first phase of the petroleum system risk analysis as no comprehensive research was carried out on individual reservoir identification as part of the study and the timing of the salt movement. Therefore, some thin divisions

have been made of well-defined stratigraphic zones (Early-Middle Miocene, Middle Paleocene, Middle Missisauga, and late Jurassic) as reservoir units in order to observe an inflection of hydrocarbon saturation within these units.

As observed in the well history reports of the new slope wells, shale or claystone is the dominant component of most of the stratigraphic units. Therefore, most of the reservoirs analyzed in this contract are assumed to have an impermeable shale vertical seal rock. Abundant impermeable shales from the Misaine, Jurassic Verrill Canyon (slope), Missisauga or Cretaceous Verrill Canyon, Logan Canyon, Shortland Shale and Banquereau Formations (slope) are considered to be vertical seals. However, in the case of lines A-A' and B-B', reservoirs in a sub-salt situation, salt was assumed to be the vertical seal.

4.2.3. Source Rock Assignment

4.2.3.1. Oragnic facies and Source Rock Potential

Prior to this contract, both Global Geoenergy Research Limited and the Geological Survey of Canada have performed various source rock analysis on other wells from the Scotian Slope (Albatross B-13, Shelburne G-29, Shubenacadie H-100, Tantallon M-41 wells from Mukhopadhyay, 2000; Acadia K-62 and Annapolis G-24 from Geological Survey of Canada Basin Database, 2006 and Open File Report, 2003). Selected Rock-Eval and TOC data from the earlier reports and the current geochemical analysis (Weymouth A-45) indicates that the lower part of these three wells contains good quality Cretaceous Verrill Canyon source rocks (Tantallon M-41, Mukhopadhyay, 2000; Weymouth A-45, this report, Figure 3c; and Annapolis G-24, Geological Survey of Canada, 2004, Table 7). Synthesizing and comparing the earlier and current works from the Scotian Margin with various DSDP wells located within the Central Atlantic Margin, the following observations on the organic richness and source rock potential could be

established (modified from Mukhopadhyay et al., 2003; Figure 13a, 13b, and 13c):

- The Banquereau Formation shows the presence of anoxic, organic-rich oil prone immature kerogen Type I and II source rocks,
- The Shortland Shale Formation has dysoxic gas and condensate prone immature to early mature Type II-III and III source rocks, and
- The Cretaceous Verrill Canyon (Berriasian to Barremian) Formation has mature, organic-rich, some oil prone Type and gas and condensate prone Type II-III or III source rocks which were deposited on anoxic to dysoxic depositional environment.

The sequence stratigraphic interpretation of the seismic lines in this study suggests that some of the source rock units within the Jurassic and Cretaceous age could be approximately 500-1000 m thick (Mukhopadhyay, 2002; Mukhopadhyay, 2003). However, from earlier studies, organic-rich oil prone source rocks in the Scotian Slope could be thin (100-300 m) and might be developed under four types of depositional environment:

1. Anoxicity within the sediments depositional site formed by salinity gradients in freshwater lakes during the Late Triassic to Early Jurassic rifting as seen in the DSDP wells of the Moroccan Margin and the Newark Basin;
2. The development of open ocean anoxia due to marine upwelling and abundance of phytoplankton (Kimmeridgian shale from Grand Banks);
3. The rate of terrestrial organic matter dispersal within the slope region is significantly higher than the rate of organic matter decomposition by bacteria. This type of organic matter is also observed within the Early Cretaceous sediments from the Moroccan Margin (DSDP well Leg 79; Rullkotter and Mukhopadhyay, 1986; Rullkotter et al., 1986); and

4. Anoxicity developed when rooted salt diapirs flanking a mini-basin remain for a longer period of time without going into a phase of salt withdrawal and formation of allochthonous canopies (possible example: Early Cretaceous sediments in the Weymouth A-45 well). In all other cases, an open marine environment with early diapir salt structures would form oxic and dysoxic gas prone (Type III) and non-source (Type IV) rocks.

Based on earlier studies and current analysis on source rock evaluation from the Scotian shelf and slope wells from the DSDP wells of the Moroccan Margin and Blake Bahama Basin (Legs 76 and 79), the following stratigraphic units could be projected as potential source rocks within the Scotian Slope that were used in the 1D and 2D petroleum system modeling in this study (modified from Mukhopadhyay et al., 2003):

- **Late Triassic/Early Jurassic lacustrine** (Sinumarian-Toarcian: ***Iroquois/Mohican Formation***): organic rich, oil prone Type I to II; (analogues from other rift basins including the Moroccan onshore and from the Newark Basin wells);
- **Middle Jurassic marine** (Callovian: ***Misaine Member***): gas/condensate prone and organic-rich mixed marine and terrestrial Type II-III and III; (DSDP well from the Blake-Bahama Basin; Rullkotter et al., 1986, 1984);
- **Late Jurassic marine** (Kimmeridgian-Oxfordian: ***Jurassic Verrill Canyon Formation***), oil-prone, mainly marine Type II; (DSDP data and shelf wells from Scotian and various Grand Bank basins; Mukhopadhyay, 1990; Mukhopadhyay and Wade, 1993; Powell, 1985; Rullkotter et al., 1984);
- **Early Cretaceous marine** (Berriasian/Valanginian: ***Lower Missisauga or Cretaceous Verrill Canyon Formation***) oil and

gas prone Type II-III or II; (Weymouth A-45 and Tantallon M-41 wells; Mukhopadhyay et al., 2002; Rullkotter and Mukhopadhyay, 1986; Rullkotter et al, 1984);

- **Mid-Cretaceous marine** (Aptian to Cenomanian; **Shortland Shale or Logan Canyon Formation**), gas and condensate prone Type II-III or III (Shubenacadie H-100 well); and
- **Early Tertiary marine** (Paleocene-Eocene; **Banquereau Formation**), oil and gas prone Type I, II or II-III (Albatross B-13, Annapolis G-24 (GSC data), and Shubenacadie H-100 and Torbrook C-15 wells).

Similar to the Scotian Margin, the Triassic synrift lacustrine Type I source rock (TOC > 2.5%) and middle [Callovian] to late Jurassic (Oxfordian – Kimmeridgian) Type II marine source rocks (TOC: 2 to 5%) have been documented in the Doukkala Basin and the offshore Tarfaya and Essaouira basins, offshore Moroccan (ONAREP, 2000). Contrary to Early Cretaceous marine Type II source rocks in the Scotian Margin, Mid-Cretaceous marine Type II source rocks (TOC up to 20%) are dominant in the Moroccan Margin.

Figures 13b and 13c illustrate the overall source rock potential of various Slope wells. In general, the majority of the analyzed source rocks are from the Cretaceous Verrill Canyon, Shortland Shale, and Banquereau Formations from all Scotian Slope wells. These source rocks mainly show gas and condensate prone (with minor light oil) Type II-III source rocks (Figures 13b and 13c). However, these source rocks have undergone some advanced maturity. Therefore, the input data for all these source rocks (especially the Cretaceous Verrill Canyon Formation sediments) have been recalculated to convert to the original TOC and hydrogen index at their immature stages based on the method described by Peter et al (2005). The hydrocarbon potential of the recalculated source rocks indicate that they

are mostly organic-rich and oil-prone Type II source rocks in their immature stage.

As none of these slope wells have encountered typical Jurassic Verrill Canyon, Misaine and Mohican source rocks, the total organic carbon and hydrogen index values of these source rocks from the shelf or shelf-break wells have been incorporated. Similar to the source rocks from the slope wells, recalculated TOC and hydrogen index data has been included. The TOC and hydrogen index values of the Early Jurassic lacustrine source rocks were based on similar source rocks from the Newark Basin (Dr. Michael Kruge, personal communication) and data from various DSDP wells.

4.2.3.2. Source Rock Kinetics

As defined earlier, two measured multi-component kinetics (source rocks of the Jurassic Verrill Canyon Formation from the Alma K-85 well and the Cretaceous Verrill Canyon Formation from the Weymouth A-45 well) have been utilized for hydrocarbon generation and expulsion. The analytical results from the primary cracking of kerogen indicate that (1) the oil component (C_{15+}) of the organic macromolecule has shown an early generation of hydrocarbons, and (2) the condensate and light oil fraction (C_6 to C_{14}) of the expelled hydrocarbons are the highest components. However, on advanced maturation, both the C_{15+} and C_6 to C_{14} components will undergo secondary cracking to dry gas. Accordingly, default kinetics from the IES software on secondary cracking has been used for the modeling. Also some of the other Type I and Type III default kinetics for the sediments from the Mohican and Misaine formations were incorporated into the modeling. The chemical properties of various oil and gas compound classes from the default parameters were used in the calculation of API gravity, GOR and Bubble Point curve. Each of the four hydrocarbon components (C_1 and C_2 to C_5, C_6 to C_{14}, and C_{15+}) have been

identified for each of the formations in order to track the source rock in the output data.

4.2.4. Heat Flow and Maturation

Similar to the east coast basins of the USA, the heat flow and associated lithospheric thermal regimes within the rifted Scotian Margin is closely connected to the tectonic evolution and physical properties of the continental crust (Morgan and Gosnold, 1989). Main convective high heat transfers from the mid-oceanic ridge to surrounding sediments during the late Triassic-Early Jurassic period whereas both convective and conductive heat transfer in later periods continued as no volcanic rejuvenation within the younger strata has been noticed. Heat is lost through an advection during the uplift and erosion of upper crust. The heat flux and maturity of the Jurassic-Recent sediments is closely connected with the Scotian Margin structural and thickness variations of the continental crust and their transition to the oceanic crust, and major basement fractures. This conclusion is based on the relationship between the thermal gradient and thermal conductivity.

Beaumont et al (1982) has illustrated a lithospheric extension model for the rifting and its subsequent thermal and mechanical consequences on the sediments from the Scotian Margin. Based on the uniform crustal thickness model and changing various parameters, Beaumont et al (1982) predicted the temperature of the Scotian Basin at different time periods following the Early Jurassic rifting. They have predicted the following temperatures on various parts of Scotian Shelf and Slope using uniform extension, extension with melt segregation models, and depth dependent extension (changing the beta and T_R). For the uniform extension model, the predicted temperatures for the sediments at the lowermost slope region in various geological periods would be as follows: at 185 Ma – 400^{o}C and 300^{o}C; at 175 Ma – 350^{o}C and 250^{o}C; 135 Ma – 300^{o}C and 200^{o}C; 100

Ma – 300°C and 180°C; 60 Ma – 300°C and 160°C; and Present day - 300°C and 180°C. They have also compared the depth dependent extension models with or without the radiogenic heat.

Based on the gravity and magnetic data and deep seismic reflection profiles, Funck et al (2004), Louden et al (2005), and Wu et al (in press) has documented the crustal structure of the Scotian Margin. They have documented a transition from non-volcanic in the north to volcanic margin in the south. The continental crust below the Scotian Basin has a maximum thickness of 36 km with velocities of 5.5 – 6.9 km/s. According to Wu et al (in press), no evidences of magmatic underplating beneath the continental crust could be documented. Therefore, there is no additional heat source within the Jurassic-Recent sedimentary wedge of the Scotian Margin. However, they have predicted a 4-km thick layer of partially serpentinized mantle (velocity: 7.6-7.95 km/s) beneath the highly faulted continental crust which overlies a 4 to 5 km thick transition zone and initial oceanic crust which extends ~200 km seaward (Figure 14a). However, they have moved the continent-ocean boundary ~ 50 km away than what was earlier published.

The thermal history is based on: (1) rifting heat flow or (2) transient heat flow based on the calibration of measured vitrinite reflectance or present day BHT data of various drilled wells. Based on the crustal structures and landward presence of the sepentinized mantle near the Sable Island area (Wu et al., in press), the heat flow of Early Jurassic sediments is considered to be higher within the deepwater portion of the Sable Subbasin (between the Annapolis G-24 and Weymouth A-45 wells) compared to the eastern part of the Shelburne Subbasin. The present day bottom hole temperature data indicates that Early Cretaceous sediments (shale) of the Annapolis G-24 and Newburn H-23 wells around a depth of 6000 m have a temperature of 150-155°C, whereas bottom hole

temperature of the Early Cretaceous sediments (carbonates) from the Shelburne G-29 well at 4000 m is 110^{o}C.

Figure 14b illustrates the maturity profile of various wells (Acadia K-62, Albatross B-13, Crimson F-81, Shelburne G-29, Shubenacadie H-100, Tantallon M-41, Torbrook C-15, and Weymouth A-45) from the deepwater portion of the Sable and Shelburne Subbasins. This data also shows that there are maturity differences between the Sable and Shelburne Subbasin slope wells. Earlier data from Evangeline H-98 (GSC Basin database; not shown in these figures) show anomalously high maturity values possibly caused due to oxidation. Figure 14d show the maturity trend of similar sediments from the Crimson F-81, Tantallon M-41, and Weymouth A-45 wells. The data from both Figures 14c and 14d indicates lower heat flow within the Cretaceous sediments from the Tantallon M-41 well and the Acadia K-62, Albratross B-13, Shelburne G-28 wells than similar Cretaceous age sediments of two slope wells from the Sable Subbasin (Crimson F-81 and Weymouth A-45) even though most of the Cretaceous sediments within the Weymouth A-45 well were within a sub-salt stage during the Tertiary time. The Acadia K-62 well, which contains both Early Jurassic and Middle Jurassic sediments, has the highest thermal gradient (Figures 14b and 14c). The Middle to Late Jurassic sediments from the Albatross B-13 well show slightly elevated heat flow compared to the Cretaceous and Tertiary sediments. This data may indicate that heat flow during Jurassic period was higher compared to the Cretaceous and Tertiary sediments. The close similarity of the maturity trends of Shubenacadie H-100 (include Mid- to Late Cretaceous and Tertiary sediments) and the Torbrook C-15 (Tertiary sediments) wells indicate that the heat flow during the Middle Cretaceous to Tertiary time is distinctly lower compared to the Early Cretaceous and late Jurassic Periods. The present day high bottom-hole temperatures of both the Annapolis G-24 and Newburn H-23 wells indicate that a possible increase in crustal

temperature began during the Plio-Pleistocene time and especially surrounding the Sable Island area. This higher heat flow may also be caused by a high heat flux emanating through the major fractures as seen on the Basement Fracture Map of the Scotian Basin (data from the Earthfield Technology, Houston, Texas). Present day heat flow data (~35 mW/m^2) near the Torbrook C-15 well indicates a low heat flow (Keith Louden, Personal Communication). This data correlates well with the measured vitrinite reflectance trend of Torbrook C-15 and Shubenacadie H-100 wells.

Based on the maturity data, heat flow histories of the other basins from the Atlantic Margins, a transient heat flow was used since 200Ma. This transient heat assumes the highest heat at 200 Ma and a regular rate of decrease since that time. As the rifting heat flow is the main component, the highest heat flow (80-100 mW/m^2) was selected for the Early Jurassic sediments. This was systematically reduced to 40 to 60 mW/m^2 at the present day based on the maturity data. Measured vitrinite reflectance (maturation) data from eight wells were used for the calibration of heat flow in the 1D and 2D modeling. Three heat flow trends have been utilized for the petroleum system modeling of the 11 slope wells and the Evangeline H-98 well and the five 2-D seismic lines. The highest heat flow trend was used on seismic line E-E' (explained later) and areas beyond 3000 m water depths on seismic lines A-A', B-B', C-C', and D-D'.

4.2.5. Salt Tectonics and Its Relationship with Reservoir Sands and Source Rock Anoxicity

The movement of the salt is driven by buoyancy and differential loading which is based on the low density salt coupling and decoupling of other denser sedimentary overburden causing the pressure gradient (Jackson and Vendeville, 1994). This explanation is more valid as buoyancy could not be a major force of salt movement. In various deepwater salt basins of

the world that the elongate, tabular salt canopies could slide over tens of thousands of square kilometers as detached salt bodies. These canopies can also move more than 10 to 20 kilometers from their source salt. Once the salt is buried beneath 1000 m of sediment it behaves as a low density plastic material. The salt then penetrates denser overlying strata horizontally and vertically where density and differential loading play a major role in salt movement during gravity sliding, extension and contraction (Jackson and Vendeville, 1994; Rowan, 1995; Young, 2005).

Similar to other passive conjugate margin settings (offshore Morocco, Gulf of Mexico, offshore Angola, etc.), various salt tectonic structures of the Scotian Margin (diapir, canopies, salt weld, tongues, etc.) are associated with the Jurassic to Tertiary sediments (Wade and MacLean, 1990; Shimeld, 2004) (Figures 1b and 2b). The salt emplacement within the Scotian Slope developed from a seaward thinning sediment wedge resulting from landward sediment influx. The salt emplacement within the aggrading sediments in this type of passive margin setting has possibly been developed from the four main phases of salt emplacements. These four phases of salt movement are similar to what was postulated earlier by various researchers (Jackson et al., 2004; Vandeville and Jackson, 1992; Rowan, 2002; Ing, 2004) and as follows:

1) initiation of salt channel flow and formation of mini-basins associated with the diapirs (Figure 15a);
2) onset of listric growth faults and extension of overburden sediments (Figure 15a);
3) large-scale evacuation of salt, formation of rafts and distortion of mini-basins (Figures 15b and 15c); and
4) formation of a contractional allochthonous salt nappe that thrusts over the deposional limit of the salt (Figure 15b and 15c).

The distribution of salt within the target area of the Scotian Basin suggests that the Sable and Shelburne subbasins were initially the loci of

evaporite deposition with each subbasin accumulating thick sequences of redbeds and evaporites (interfingering with lacustrine source rocks of the Early Jurassic) just before and after the break-up (Wade and MacLean, 1990).

Based on recent interpretation of the 2-D TGS-Nopec multichannel seismic reflection data and earlier works by John Wade and Barry MacLean from the Geological Survey of Canada (MacLean and Wade, 1993; Wade and MacLean, 1990), Shimeld (2004) has identified the following five salt provinces within the Scotian Margin with significant differences in the morphology of the diapirs and pattern of sedimentation (Figure 15d):

- **Subprovince I** (area near the Georges Bank up to the south of Shelburne Arch) – marginal shelf synclines flank passive diapirism with seaward overhangs where the autochthonous source salt layer was depleted by the end of the Cretaceous. At that time, the salt canopy system has been moved seaward of the overhang walls. This salt canopy system has possibly been rejuvenated in the Late Paleogene to Pliocene Periods. However, the canopies became less extensive towards the east of Subprovince I;
- **Subprovince II** (includes most of the eastern part of Shelburne Subbasin up to the east of Shubenacadie H-100 well and west of Weymouth A-45 well) - this salt subprovince contains mainly vertical diapirs of varying shapes and sizes. In the westernmost part of the Subprovince II, the diapirs are mushroom-shaped and eventually merge with the tongue of salt canopies. The diapirs in the easternmost part of the subprovince II are possibly detached from its autochthonous counterpart. The association of diapirs and surrounding sediments or bathymetric relief suggests that the diapirism is quite active until the present time and has possibly been rejuvenated since the Miocene time;

- **Subprovince III** (slope region of the Eastern Sable Subbasin) - the allochthonous large canopies are the dominant salt emplacement features that cover mostly Cretaceous sediments within this salt subprovince. The younger sediments on top of the canopies are deformed by complex extensional structures forming turtles and expulsion grabens;
- **Subprovince IV** (east of Sable Subbasin from the Gully to the Laurentian Subbasin) - the main feature of this subprovince is a lack of any diapiric structures within the shelf-break within the Upper Slope region. However, some isolated diapirs could be observed within the middle and lower slope. The major compressional phase occurs during the Late Cretaceous and followed definitely until the Middle Miocene; and
- **Subprovince V** (deepwater portion of the Laurentian Subbasin) - the western edge of the Subprovince V contains coalesced allochthonous tongues. In general, diapirs beneath the upper slope of this subprovince have a post-kinematic cover over other regions in the study area. The crests of some of the diapirs are within 100 m of the seafloor.

The variabilities of salt movement as defined within these five subprovinces shows a close similarity with the five probable hydrocarbon subprovinces based on source rock maturity and potential (Mukhopadhyay and Wygrala, 2001; Mukhopadhyay et al., 2003).

The majority of the deepwater reservoirs within this study area and other Central and South Atlantic Margins are associated with salt movement. The deepwater turbidite sand deposition (Cretaceous and Tertiary) and Jurassic sliding blocks forming traps are controlled by the lateral and vertical motion of both autochthonous and allochthonous Triassic-Jurassic salt and associated listric faults. Most of the salt-related turbidite fan and fold-anticline play types are similar to analogous salt-related

basins from other Atlantic Margin basins such as the Gulf of Mexico and offshore West Africa (Pettingill and Weimer, 2001).

With the exception of the major sands in the Annapolis G-24 well and thin sands from some other wells (Newburn H-23, Crimson F-81, Shelburne G-29, Shubenacadie H-100, and Weymouth A-15), the upper to upper-middle slope from this part of the Sable Subbasin was definitely situated within the by-pass zone during the Early to Late Cretaceous period (Mukhopadhyay et al., 2006). These zones were dominated by fine grained clastics usually present in a graded slope with low net/gross ratio. The Weymouth A-45 well (located within seismic line B - B') drilled in a water depth of 1689 m was targeting the Middle to Early Cretaceous channel sands as a sub-salt play. The absence of thick sand below the salt possibly indicates contemporaneous formation of salt canopies and eventual bypassing of sands during the Early to Middle Cretaceous Periods. On the other hand, relatively thick sands within the two zones of the Annapolis G-24 well possibly indicate that these sands were derived either (a) within a ponded accommodation zone during a "salt withdrawal" phase; or (b) within the sedimentary apron on the landward side where a salt diapir forms a bathymetric obstruction to the sand movement on the seaward side during the Early to Middle Cretaceous Periods (Waltham and Davison, 2001).

Within the target area of this project, the five seismic lines were positioned at regular intervals as much as possible. Accordingly, two of these seismic lines (A-A' and B-B') were taken from the allochthonous salt canopy system of the Sable Subbasin and within the designated Subprovince III of Shimeld (2004). The other three seismic lines (C-C', D-D', and E-E') are located further west of the Sable Sabbasin and within the Shelburne Subbasin. These three lines lie within major salt diapiric areas and within the Subprovince II of Shimeld (2004 (Figure 15d). Comparing the seismic

line A-A' with B-B', it is observed that both seismic lines do not have any connection with the Early Jurassic autochthonous salt sheet at the present time. However, the morphology of the salt canopies of the seismic line B-B' suggests that some possible connections between the autochthonous Jurassic Argo salt sheet and the allochthonous salt canopies might have earlier been existed. This concept has been utilized for the 2D modeling of the seismic line B-B'. Seismic lines C-C', D-D', and E-E' show that all salt diapirs are attached to the Early Jurassic autochthonous salt. The designated reservoirs within seismic line D-D' are all salt-flank play types in water depth greater than 2000 m (Figure 9d). On the other hand, the defined reservoir within seismic line E-E' belongs to turbidite channel plays (Figure 9e).

It is assumed that the timing of the salt emplacement within the Eastern Sable Subbasin (seismic lines A-A' and B-B'; Salt Subprovince III area of Shimeld, 2004) and the Western Sable Subbasin or Eastern Shelburne Subbasin (seismic lines C-C', D-D', and E-E'; Salt Subprovince II area of Shimeld, 2004) is different. Based on the sedimentation rate, heat flow histories, and earlier data on the timing of the hydrocarbon expulsion from the Early Jurassic and Jurassic Verrill Canyon source rocks (Mukhopadhyay et al., 2003), the following five schematic conceptual stages of salt movement have been identified for the Eastern Sable Subbasin (seismic lines A-A' and B-B'; Figure 15e) which leads to the formation of the dissected salt canopies in this region:

1) **Stage 1 (Early to Middle Jurassic):** Initiates the oil generation from the Early Jurassic source rock due to a high sedimentation rate and high heat flow shortly after the rifting within Scotian Margin (170-150 Ma). The expelled oil acts as a lubricant, which will increase the fluidity of the salt. The active salt diapirism has thereby initiated due to the continuation of the high heat flow,

the sedimentation rate, and the high fluidity of the salt during the Middle Jurassic Period,

2) **Stage 2 (Late Jurassic to Early Cretaceous):** Starts the full phase of oil and gas expulsion from the Early to Middle Jurassic source rocks due to the high sedimentation rate and heat flow. The oil has increased the fluidity of the salt for its rapid growth the main diapiric stage. At this stage, the formation of sand within the Early Cretaceous reservoirs could be hindered by the position and thickness of the diapiric structures as suggested by Waltham and Davison (2001). Reservoir quality sands could be deposited within the salt flank or salt top play types during Late Jurassic Period,
3) **Stage 3 (Early to Late Cretaceous):** The major phase of oil expulsion and cracking of oil to gas from the Early Jurassic and Jurassic Verrill Canyon source rocks is closely related to the high sedimentation rate and high heat flow. The continuous high sedimentation rate, heat flow, and fluidity of the salt will mobilize the basinward leaning of the diapirs and formation of "hourglass" salt stocks, and the formation of salt tongues. The downslope displacement of sediment by sliding on top of the salt body has created various growth faults at this stage, which will accelerate the turbidite flows. However, counter regional faults over the "hourglass structures will create obstacles to turbidite flows (Waltham and Davison, 2001)". This period initiates major sand bypassing of the distorted mini-basins of the upper slope due to the presence of thick and flat salt bodies. Eventually, the reservoir-quality sands will be deposited within the middle and ultra deep slope,
4) **Stage 4 (Early Tertiary):** This is the timing of the salt withdrawal and formation of major salt tongue and canopies. At this time, development of major sediment input and possible

formation of major deep-water sand reservoirs within the salt withdrawal area could occur. However, by-passing of sands over the canopy area could be the major feature at this time period. The oil and gas expulsion has been continued due to moderate to high heat flow and the high sedimentation rate has continued to mobilize the major movement of allochthonous salts, and

5) **Stage 5 (Late Tertiary):** This stage would be the time for the secondary cracking of oil to gas or condensate from all three major source rocks (*gas from Early and Late Jurassic source rocks and condensate from the Cretaceous Verrill Canyon source rock*). A major gas and condensate expulsion will be initiated due to the continued high sedimentation rate and higher heat flow on top of the salt. Reservoir sands develop as turtle structure and turbidite channels. Lower heat flow within the sub-salt play types in the Early Cretaceous sands could be observed, which would be saturated with hydrocarbons if the sands are present within those reservoirs. However, most sands on top of the allochthonous canopies will still continue to bypass the upper slope and deposit within the middle and lower slope.

The timing of all the five conceptual salt movement stages will be incorporated as input parameters in the 2D petroleum system modeling.

The sedimentation rate and heat flow within the area between the western part of the Sable Subbasin and in the eastern part of the Shelburne Subbasin (Salt Sub-Province II of Shimeld, 2004) were considered lower compared to the Salt Sub-Province III, especially during the Early Jurassic to Early Cretaceous Periods. Therefore, the timing of the main phase of salt diapirism within the seismic lines C-C' and D-D' was considered to be late in geological time (younger than 110 Ma). This concept has been applied for the 2D petroleum system modeling of seismic lines C-C', D-D' and E-E'.

5. ONE DIMENSIONAL PETROLEUM SYSTEM MODELING

Historically, in the late 1970s, one dimensional basin modeling began the era of petroleum system modeling (Appendix C-2). Appendix C illustrates some of the salient features of the one and two dimensional petroleum modeling. The geometric framework of the model is provided by the mappable boundaries of the principle stratigraphic units. These stratigraphic units are linked to a library of relevant physical parameters and the temporal framework in geological time. This framework is defined by assigning the ages of deposition and erosion to each unit. Finally, boundary conditions such as surface temperatures and heat flow at the base of the system are defined as a function of geologic time.

Accordingly, one dimensional numerical modeling of the sedimentary units within various drilled wells within the Scotian Slope will illustrate the following:

- The thermal and maturation histories of the sediments
- The time when the source rocks begin to generate and expel hydrocarbons,
- The maximum amount of hydrocarbon transformation from all lower source rocks in each individual well
- Possible porosity and various calculated pressure data from each individual sedimentary unit
- The petroleum system events chart showing when the trap is formed to accommodate the hydrocarbons and the seal is emplaced to retain the hydrocarbons within the trap.
- Based on the above information, the *'critical moment'* of hydrocarbon emplacement within the individual area or well will be documented.

One dimensional numerical modeling (using PetroMod 1D software of IES Inc., Germany) has been performed for eleven slope wells and one shelf well to document various petroleum system elements as discussed. The basic data input structure for both one and two dimensional modeling are the same as both need the following data:

- ✓ Complete geological parameters -
  - ❖ Present well water depth;
  - ❖ Thickness of each stratigraphic units and their beginning and end depositional ages;
  - ❖ Thickness and beginning/ending ages of the unconformities; paleo- and present day water depth, temperature of the sediment-water interface, and heat flow;
- ✓ Petroleum system parameters -
  - ❖ Source Rock
  - ❖ Reservoir rock
  - ❖ Seal Rock
  - ❖ Overburden rocks
  - ❖ Timing of salt emplacement
  - ❖ Underburden rock (if any)
- ✓ Geochemical parameters
  - ❖ Source rock properties (TOC, Rock-Eval data)
  - ❖ Vitrinite Reflectance or other maturity data
  - ❖ Present day bottom-hole temperature data
  - ❖ Present day heat flow data, if any
  - ❖ Measured multi-component kinetics from the Jurassic and Cretaceous Verrill canyon source rocks and
  - ❖ Selected oil or gas physical and chemical properties

As discussed earlier, the following wells have been studied for one dimensional numerical modeling: *Acadia K-62* (water depth [WD]: 866.3m); *Albatross B-13* (WD: 1341m); *Annapolis G-24* (WD: 1678m); *Balvenie B-79*

(WD: 1803m); *Crimson F-81* (WD: 2091.5m); *Evangeline H-98* (shelf well; WD: 174m); *Newburn H-23* (WD: 977m); *Shelburne G-29* (WD: 1153.5m); *Shubenacadie H-100* (WD: 1486.5m); *Tantallon M-41* (WD: 1516m); *Torbrook C-15* (WD: 1674.5m); and Weymouth A-45 (WD: 1689.5m) (Figure 7c). Figure 16 illustrates the world co-ordinates and location of these 11 slope wells and the Evangeline H-98 well, which may contain some deepwater turbidite sediments. With the exception of the Tantallon M-41 well in east of Sable Subbasin, the interpretation of the one dimensional modeling will follow the complexities of salt movement as defined by Shimeld (2004) (Figure 15d). Accordingly, the interpretation on one dimensional modeling will start with the Shelburne G-29 well in the eastern part of the Shelburne Subbasin to the Tantallon M-41 well in the eastern portion of the Sable Subbasin. Tables 8a, 8b, 8c, and 8d illustrate some of the geological and geochemical input parameters of four Scotian Slope wells (Acadia K-62, Annapolis G-24, Newburn H-23, and Weymouth A-45).

5.1. Eastern Shelburne Subbasin and Western Sable Subbasin

As discussed earlier, the drilled wells within the eastern part of the Shelburne Subbasin and western part of the Sable Subbasin did not penetrate any allochthonous salt-related structures as they lie within the "Salt Subprovince II of Shimeld (2004; Figure 15d)". Based on one measured present day heat flow data (35-40 mW/m^2; Keith Louden, personal communication) and some earlier measured and calculated maturity data within this region (Mukhopadhyay et al., 2003), the area between the Shelburne G-29 to the Shubenacadie H-100 wells is considered to have a low to moderate heat flow regime. Five deepwater wells [*Acadia K-62, Albatross B-13, Shubenacadie H-100, Shelburne G-29,*

and Torbrook C-15; Figure 7c and Figure 8f (i)] have been drilled in this part of the Scotian Basin.

The burial history of the Shelburne G-29 well suggests that the Cretaceous to recent sediments from this well have encountered the maximum burial depth at the present time (Figure 17a). It also shows a very low sedimentation rate between 142 Ma and 15 Ma, and a slightly higher sedimentation rate between 15 Ma and to the present time. Accordingly, iso-temperature and iso-maturity lines indicate that the lowermost sedimentary unit (Cretaceous Verrill Canyon 2 of Berriasian age) has just entered the "oil window" (Figures 17a and 17b). Therefore, the transformation ratio of this source rock (Early Cretaceous) is still very low (0.15%) and suggests the presence of a minor amount of hydrocarbons (Figure 17c). The oil stains within some of the Cretaceous carbonates have possibly been derived from a deeper Jurassic Verrill Canyon Type II-III or Type III Mid-Jurassic Misaine Member source rocks. The petroleum system events chart indicates that the "Critical Moment" of hydrocarbon emplacement has not yet been achieved within the drilled depth of the Shelburne G-29 well (Figure 17d).

Although the Albatross B-13 well has penetrated sediments of the Middle Jurassic Periods (Misaine Member) at a depth similar to the Shelburne B-29 well, the iso-temperature line did not show any higher temperature for the lowermost sediments compared to the Shelburne G-29 well (Figure 18a). However, the sediments show higher maturity (Figure 18b) and higher hydrocarbon transformation ratio (about 15% for the lowermost source rock; Figure 18c) compared to the Shelburne B-29 well because of its higher heat flow for Mid-Jurassic sediments. Accordingly, the Misaine (Middle Jurassic) source rock lie within the "early oil generation zone" (Figure 18d) and has generated more than 50 mg oil/g TOC (Figure 18e). However, as the source rock has not yet generated enough C_6 to C_{14}

hydrocarbons, the threshold for hydrocarbon expulsion has not yet been achieved (Figures 18f and 18g). The drilled target for this well was the Abenaki Formation carbonate reservoir. The modeled and well porosity data indicates that the target reservoir rock achieved well developed porosity (>15%; Figure 18h). However, the hydrocarbon emplacement has not been achieved possibly due to: (a) a lack of threshold maturity of the source rock within the surrounding area (observed from the petroleum system events chart; Figure 18i); and (b) the problem of hydrocarbon migration from the deeper basinal source rocks because of the presence of a sealing growth fault (observed from previous 2D modeling experiments in this region). The modeled pressure data for both Shelburne B-29 and Albatross B-13 wells did not indicate any overpressure corroborating the well data (Figure 18h). The petroleum system events chart indicates no "critical moment" of hydrocarbon emplacement has been achieved although all other petroleum system elements have reached their early development (Figure 18i).

The Torbrook C-15 well was targeting for a Miocene turbidite fan play type and drilled only about 2000m (TD: 3600m; WD: 1674.5m) of sediments up to the Late Eocene. All sediments up to the Late Eocene show low temperatures and lie within an immature stage (Figures 19a and 19b). As such, no hydrocarbon transformation could be achieved (Figures 19c and 19d). The petroleum system events chart indicates that no "critical moment" of hydrocarbon emplacement within any sand-rich reservoirs has been achieved (Figure 19e).

The Middle to Late Jurassic sediments from the Acadia K-62 well shows the highest modeled bottom-hole temperature (~125^{o}C; Figure 20a) and maturity compared to other wells (~0.8% Modeled %R_o; Figure 20b). The lowermost source rocks from this well with an approximate transformation ratio of 41% (Figure 20c) lie within the main phase of oil generation (Figure

20d). The Mohican and Misaine source rocks generate about 180 mg/g TOC of normal gravity oil (C_{15+}) (Figure 20e) and 54 mg of light oil and condensate (C_6 to C_{14} hydrocarbons)/g TOC (Figure 20f). However, these sediments have generated low concentrations of primary dry gas (Figure 20g). Although no oil-saturated reservoir has been documented within this well, the reservoir data shows higher porosity. The petroleum system events chart indicates that the "critical moment" of the hydrocarbon emplacement started at 10 Ma (Figure 20i).

The Shubenacadie H-100 well has been drilled up to Mid-Cretaceous Shortland Shale Formation (Figure 8f[iii]). Similar to the Shelburne G-29 and Albatross B-13 wells, the sediments from the Shubenacadie H-100 well remain immature and did not reach the critical temperature and maturity (Figures 21a and 21b). Although geochemical data of the sediments from the Banquareau and Shortland Shale Formation indicate the presence of oil prone source rocks (Figure 13a), the transformation ratios (Figure 21c) of these source rocks show that they are immature for hydrocarbon expulsion. Accordingly, based on the petroleum system events chart, the "critical moment" of hydrocarbon emplacement has never been achieved within this well (Figure 21d).

5.2. Eastern Sable Subbasin

The drilled wells occur within the eastern portion of the Sable Subbasin. The sediments within this area are mainly associated with allochthonous salt-related structures as they lie within the "Salt Subprovince III of Shimeld (2004)" (Figure 15d). Based on earlier measured maturity of the sediments from the shelf and slope wells (Mukhopadhyay et al., 2003; Mukhopadhyay, 2000), the area surrounding the eastern part of the Sable Island region is considered to be moderate to high heat flow regime. Five deepwater wells (*Annapolis G-24, Balvenie B-79, Crimson F-81, Newburn B-*

23, and Weymouth A-45; Figures 7 and 8j [ii]) and one shelf well (*Evangeline H-98 – considered for this project*) have been drilled in this region of the Scotian Basin. With the exception of *Balvenie B-79* well, all wells were drilled deeper (mostly up to Early Cretaceous) as this region has thick sedimentary units mainly within the Cretaceous and Jurassic periods. The Evangeline H-98 (shelf well) and Newburn H-23 (slope well) are the westernmost wells and Crimson F-81 well is the easternmost well within this region (Figure 8f [ii] and Figure 16).

The Evangeline H-98 and Newburn H-23 wells were drilled very close to each other. Stratigraphically the Newburn H-23 well went deeper into Early Cretaceous sediments (possibly up to Berriasian age; Table 8c). The comparable burial histories of both the Evangeline H-98 and Newburn H-23 wells indicate that the deepest burial of the sediments has reached at the present time (Figures 22a and 23a). Both wells have similar present day temperature profiles at the bottom of the well (Figures 22b and 23b). The iso-maturity lines indicate that the Early Cretaceous sediments of the Newburn H-23 has reached a vitrinite reflectance of 1.25% Ro compared to less than 1.00% Ro at the bottom of the Evangeline H-98 well. The source rocks from the lower part of both wells have similar kerogen type (Type II-III and III), but show different transformation ratios (~62% in the Newburn H-23 instead of ~35% within the Evangeline H-98 well; Figures 22c and 23c). Accordingly, the Cretaceous Verrill Canyon (Early Cretaceous) source rocks from the Newburn H-23 well have generated similar amount of normal gravity oil (C_{15+}) (Figures 22e and 23e), but generated more light oil and condensate (C_6 to C_{14}), and primary methane (C_1) than the Shortland Shale source rocks from the Evangeline H-98 well (Figures 22f, 22g, 23f, and 23g). The lowermost sediments from both wells reached the vapor phase of the hydrocarbon zone (Figures 22d and 23d). The modeled porosity and pressure trends of the Early Cretaceous reservoir sands show moderately good porosity Figure 22h). The lowermost sediments from both

wells lie within an overpressure regime (Figure 23h). The expulsion of hydrocarbons from the lowermost sediments from both wells started between 90 and 70 Ma (Figures 22i and 23i). The “critical moment” of hydrocarbon emplacement is earlier within the Newburn H-23 well than the Evangeline H-98 well (20 Ma compared to 10 Ma) (Figures 22j and 23j).

As discussed earlier, the Weymouth A-45 well, which was drilled at a water depth of 1689m, was targeted for the Middle to Early Cretaceous channel sands as sub-salt play type. The burial history of the sediments indicates that maximum burial depth is reached at the present time. Accordingly, the iso-temperature and iso-maturity lines indicate the lowermost Cretaceous source rocks (Cretaceous Verrill Canyon based on organic petrology) have reached approximately 125^{o}C and 0.8% Ro (Figures 24a and 24b). The low transformation ratio (18%) of these Early Cretaceous sediments of the Weymouth A-45 well suggests that these source rocks lie within the early phase of oil generation (Figures 24c and 24d). As the source rocks are mainly oil prone Type II kerogen, they have generated and expelled about 68-71 mg oil (C_{15+})/g TOC. However, because of low percentage of the transformation ratio that is possibly related to the lower maturity of the sediments compared to the Newburn H-23 well, the amount of light oil and condensate (C_6 to C_{14}) is low (Figures 24e, 24f, 24g, and 24h). Although no sand-rich reservoir unit was reported in this well, the modeled porosity data indicates that sand-shale-silt zone of the Logan Canyon Formation has a porosity of about 20%. The lowermost sediments (Cretaceous Verrill Canyon Formation) lie within an overpressure regime (Figure 24i). The petroleum system events chart indicates that the “critical moment” of hydrocarbon emplacement has possibly started around 5 Ma (Figure 24j).

As discussed earlier, burial history, temperature, and maturity profile of the Balvenie B-79 well indicate that the lowermost sediments are still

within the very early stages of maturity and have very low hydrocarbon transformation ratios due to the low thickness of the Cretaceous sediments (Figures 25a, 25b, 25c, 25d). Accordingly, only a small amount of normal gravity oil (C_{15+}) has been generated (Figure 25e). The porosity and pore pressure data indicate that Mid-Cretaceous sands (if present) could have good porosity (~20%) and should lie within moderate pressure regime (Figure 25f). Based on the low to moderate maturity of the lowermost sediments from the Balvenie B-79 well, the "critical moment" of hydrocarbon emplacement from any of these sediments has been achieved (Figure 25g). Therefore, some selected gas shows (as discussed earlier) indicate that the hydrocarbons have possibly migrated into those zones within the well from the lowermost Cretaceous or Jurassic Verrill Canyon or Early Jurassic source rocks.

The iso-temperature and iso-maturity lines from the Annapolis G-24 well indicate that the lowermost sediments have reached the optimum temperature and maturity to generate and expel hydrocarbons (Figures 26a and 26b). Accordingly, the lowermost Cretaceous Verrill Canyon source rocks have shown a transformation ratio of more than 50%. Generation of liquid hydrocarbons has possibly started since 90 Ma and reached the main vapor phase during last 20 Ma (Figures 26c and 26d). As the Cretaceous Verrill Canyon sediments are mainly kerogen Type II-III and III (light oil, condensate, gas prone) source rocks, these sediments have generated and expelled more than 76 mg oil (C_{15+})/g TOC, 105 mg light oil and condensate (C_6 to C_{14})/g TOC, 40 mg methane/g TOC (Figures 26e, 26f, and 26g). The modeled porosity is comparatively lower than the observed log porosity (Figure 26h). Various modeled pressure data indicates a close correlation of fracture pressure and measured pressure within the well. The "critical moment" of hydrocarbon emplacement within Middle and Early Cretaceous reservoir is around 10 Ma (Figure 26j),

although most of the hydrocarbons expelled from the Cretaceous Verrill Canyon source rock migrated into the reservoir since 90 Ma (Figure 26k).

The burial history of the Crimson F-81 well indicates that the deepest burial of these sediments is achieved at the present day (Figures 27a and 27b). Although from 90 Ma the sediments are within 125^{o}C iso-temperature line, the main phase of oil phase maturity for this type of source rock (III) arrived only during the last 30 Ma (Figures 27a, 27b and 27c). As such, only 26% of the lowermost sediments from this well are within the liquid and vapor phases and the remaining 74% of those sediments have not yet generated any hydrocarbons (Figures 27c and 27d). Within that 26% of the generated hydrocarbons, only 76 mg oil (C_{15+})/g TOC, 24 mg light oil and condensate (C_6 to C_{14})/g TOC, 16 mg methane/g TOC have been generated (Figures 27e, 27f, and 27g). The pyrolysis-gas chromatography data indicates that the major component of this source rock would be condensate (C_6 to C_{14}) and dry gas, as the normal gravity oil (C_{15+}) is a minor component, which will eventually be cracked to methane in an advanced maturity (Figure 4a[ii]). However, the condensate (C_6 to C_{14}) and dry gas fractions did not reach enough saturation at this maturity level. This data corroborates the non-discovery of any condensate and gas shows within this well. If sands were present within the Early Cretaceous sediments (similar to Annapolis G-24 well), the porosity should have been more than 10% (Figure 27h). These sands would be saturated with a non-economic amount of condensate, gas, and minor oil. Based on the timing of lighter hydrocarbon generation, the "critical moment" of hydrocarbon emplacement within this well would be 5 Ma although the C_{15+} oil has started generating and expelling since 90 Ma (Figures 27i and 27j).

5.3. Eastern Part of the Laurentian Subbasin

The sediments within the western part of the Laurentian Subbasin are associated with a combination of autochthonous and allochthonous salt-related structures as they lie within the "Salt Subprovince IV of Shimeld, 2004" (Figure 15d). Based on earlier measured maturity of the sediments from the shelf and slope wells (Mukhopadhyay et al., 2003; Mukhopadhyay, 2000; Figure 13a), the sediments within the area surrounding the Tantallon M-41 well lie within a low to moderate heat flow regime (Mukhopadhyay et al., 2003). The iso-temperature, iso-maturity, and iso-hydrocarbon zone lines of the Tantallon M-41 indicate that the Cretaceous Verrill Canyon sediment (lowermost in the three units) is within the early stage of oil generation (Figures 28a, 28b, and 28c). Accordingly, only the lowermost sediments from the Tantallon M-41 well have 12% hydrocarbon transformation although these sediments have Type II oil prone kerogen. As such, from the lowermost three source rocks, a maximum amount of 56 mg of oil (C_{15+}), 1.52 mg of light oil and condensate (C_6 to C_{14}), 3 mg of methane (per gram of total organic carbon of these source rocks) has been generated (Figures 28e, 28f, and 28g). Although there are not enough hydrocarbons from these three Cretaceous Verrill Canyon source rocks to saturate any reservoir, the "critical moment" of hydrocarbon emplacement possibly started around 5 Ma (Figures 28h, and 28i).

Based on the similar measured multi-component kinetics, the timing of main hydrocarbon expulsion from the Cretaceous Verrill Canyon (Barremian to Berriasian) source rocks is different for various wells from the central and eastern part of the Sable Subbasin. In the Annapolis G-24, Newburn H-23, Crimson F-81, and Weymouth A-45 wells, the first phase of expulsion of C_{15+} oil occurs between 90-60 Ma (Fig. 18). However, the main phase of C_{15+} (oil) and C_6 to C_{14} (light oil and condensate)

hydrocarbon expulsion occur within the last 20 Ma. In the western part of the Sable Subbasin and within the Shelburne Subbasin, none of the Cretaceous Verrill Canyon source rocks from any of these wells expel any significant amount of hydrocarbons. The Early Jurassic Mohican Formation and Middle Jurassic Misaine member source rocks have expelled hydrocarbons (C_{15+} oil and C_6 to C_{14} light oil and condensate) since 110 Ma.

Based on one dimensional petroleum system numerical modeling, various aspects of hydrocarbon charge and migration histories have been identified that could be summarized as follows:

- ✓ With the exception of the Weymouth A-45 well, none of the other eleven deepwater wells have penetrated any salt. Therefore, the effect on the heat flux related to the salt movement could not be visualized from the one dimensional modeling. However, based on the earlier measured and calculated maturity data, at least three heat flow zones could be documented within the Scotian Slope. The variability in heat flow may possibly be controlled by the basement fractures (higher heat flux close to them) and thickness of the lower crust. These heat flow zones are
  - (a) Moderate to low heat flow: area east of Shelburne G-29 and west of Evangeline G-98 wells;
  - (b) Moderate to high heat flow: area between Evangeline H-98 and Crimson F-81 wells; and
  - (c) Low to moderate heat flow: area around the Tantallon M-41 well.
- ✓ In all analyzed wells, burial history suggests that the lowermost sediments have reached the maximum depth only during the last 5 Ma. With the exception of Newburn B-23 and Annapolis G-24, the other four wells did not penetrate deep enough to reach the optimum temperature and maturity to transform any of the

lowermost source rocks to generate adequate hydrocarbons. The "critical moment" of hydrocarbon emplacement within these wells has either been reached very recently (last 5 Ma) or did not happen at all.

- ✓ The thermal histories of most wells suggest that only Cretaceous Verrill Canyon source rocks within most of these wells attain the liquid or vapor phases ("oil window) of hydrocarbon generation. Although the hydrocarbons have saturated the Early Cretaceous reservoirs within the eastern and central part of the Sable Slope since 90 Ma, but the source rock could not generate enough hydrocarbons for the optimum saturation of the reservoir until the source rock reached the main vapor phase (R_o > 1.0%). This criterion has been met only in the Annapolis G-24 and the Newburn H-23 wells, where Early to Middle Cretaceous reservoirs have been charged with gas and condensate possibly since the last 30 Ma. The kinetics of hydrocarbons play a crucial role to identify the timing of the optimum reservoir saturation. Accordingly, all other upper source rocks (Middle Cretaceous, Eocene, and Miocene) are immature for hydrocarbon generation and expulsion. The older source rocks (Jurassic Verrill Canyon, Misaine, and Early Jurassic) have contributed a major part of the hydrocarbons to these reservoirs.
- ✓ Within the area between the Shelburne G-29 well and the Shubenacadie H-100 well, the lowermost source rocks from most wells did not reach the optimum temperature and maturity to reach the main vapor phase of hydrocarbon expulsion. Accordingly, the "critical moment" of hydrocarbon emplacement has not yet been reached in most wells. The Early to Middle Jurassic sediments from the Acadia K-62 indicate that sediments could charge the Late Jurassic to Miocene reservoirs. This data clearly indicates that deeper drilling within the Jurassic and possibly up to a sediment

thickness of at least 5000m is necessary to get any significantly charged hydrocarbon reservoirs in this region.

- ✓ The modeling pressure data indicates that the sediments below 3500m within most of the Eastern Sable Subbasin wells (Annapolis G-24 and surrounding areas) are in overpressure regime because of the presence of currently active vapor phase hydrocarbons. The deeper sediments within the area between the Shelburne G-29 well in the southwest and Shubenacadie H-100 well in the northeast do not lie within the overpressure regime. However, some of the younger sediments (Banquereau Formation) are in an overpressure situation, which is possibly caused due to the compaction disequilibrium of these sediments.

6. TWO DIMENSIONAL PETROLEUM SYSTEM MODELING

As discussed earlier, Appendix C illustrates a brief preview of the historical development of petroleum system modeling. It also explains various aspects of hydrocarbon migration or hydrocarbon phase properties. Two-dimensional petroleum system modeling will demonstrate the following petroleum system risk components within the five analyzed seismic lines (A-A', B-B', C-C', D-D', E-E'; Figures 9a through 9e and Figure 29):

- ➢ Establish the thermal evolution of hydrocarbons and the migration of hydrocarbons from source to reservoir rock units via carrier beds through geological time. Accordingly, it will precisely define the temperature, heat flow, maturation (vitrinite reflectance) and pressure through time in both 2-D and selected 1-D sections,
- ➢ Demonstrate various constraints of hydrocarbon movement in the area where salt tectonics is pervasive,
- ➢ Assess the hydrocarbon saturation in target reservoirs and the hydrocarbon phase behaviour,

- Establish the development of equilibrium conditions within various hydrocarbon reservoirs and seal units by precise evaluation of three-phase separation and pressure distribution within these units. Define and create PVT-controlled component behaviour in complex reservoirs.
- Track the possible oil/gas reservoir hydrocarbons to their source rock components, and
- Establish the risk assessment and the best potential target conceptual reservoirs for future drilling although 3D petroleum system modeling is best done to better define these parameters in the future.

Hydrocarbon accumulations consist of a multitude of different hydrocarbon phases (water, oil, and gas phase) and different components (single substance such as methane, etc.) or mixed components (wet gas - C2 – C4 hydrocarbons, etc.) or generalized classes (saturates, NSO's. etc). The transition from one phase to another hydrocarbon phase (liquid to vapor) is controlled by temperature and pressure whereby it has positioned itself close to the *Dew Point, Bubble Point, and Critical Point*. For each seismic line, the multi-component kinetics has been used for each simulation run. The detailed parameters of the multi-component kinetics [generation of C_1 (dry gas), C_2-C_5 (wet gas), C_6-C_{14} (condensate and light oil), and C_{15+} (normal gravity crude oil) have been assigned. Multi-component default kinetics of kerogen Type I has also been used as no kinetics for that type of kerogen from the Scotian Basin has been analyzed for this contract. This multi-component kinetics of the Type I kerogen (used for this contract) is the proprietary data of IES Incorporated of Germany. The dry gas is considered to be either primary (directly cracking from kerogen) or secondary (cracking of dry gas from earlier generated oil and wet gas). The modeling also used the default kinetics from the PetroMod database for the secondary cracking of oil to gas.

Prior to the simulation run for the 2D petroleum system modeling of each of these five seismic lines, the following input data has been included within the PetroBuilder module of the PetroMod software (version 9.02):
(a) stratigraphic intervals, faults, and projected drilled wells (Figure 30a) and geological age (Figure 30b);
(b) petroleum system events structure along with the input lithology, kinetics, and source rock properties [Figure 30c (i) and (ii)];
(c) fault properties (Figure 30d);
(d) paleo-trend surfaces [water-depth, temperature, and heat flow; Figures 30e (i), (ii), (iii)];
(e) assigned unconformities (Figure 30f);
(f) timing of salt movement (Figure 30g and 30h); and
(h) grid intervals for the 2-D seismic lines as the entire numerical calculations run through the grid structure of the model (Figure 30i). All lines contain more than 300 grid lines.

Selected wells have also been incorporated within various seismic lines (Annapolis G-24 well within seismic line A-A'). The Crimson F-81 well was also projected to line A-A' as the well is situated close to the line. The Line B-B' passes through the Weymouth A-45 well (Figure 30a). The Shubenacadie H-100 well could be projected on the seismic line C-C' although the well does not fall exactly on the line. Similarly, Acadia K-62 well could be projected on Line D-D'. No deepwater well is situated close to the seismic line E-E'. All five 2-D seismic lines are dip lines and are trending NNW-SSE.

Within the simulation run of the 2D modeling, three main options had been monitored prior to the simulation run. These were *check control*, *kinetics*, and *petroflow* parameters. The factors within '*check control*' include run control, sampling or maximum cell thickness, tools/special options including salt movement, fault properties etc., and calculation

steps (Figure 31). The factors for the '*kinetics*' include specification of the calibration parameters (details could not be shown in Figure 31). It also includes generation potential (individual kinetics of source rocks) as no biomarker study has specifically been carried out in this project. The parameters within '*petroflow*' include choice of general migration variability (Darcy Flow, Flowpath or Hybrid; Appendix C-11). The cracking of oil to gas within the carrier bed and the closeness or openness of the basin sides have to be defined within the 'Petroflow'. The other two parameters within '*petroflow*' are permeability threshold and hybrid/flowpath display options. All simulations have been run after checking all the above-mentioned parameters.

After the satisfactory input of various parameters, each individual seismic section has been assigned to run a simulation. Although four to six simulations of the same line was run after changing various input parameters, the results described in this report will include data of the final simulation that includes multi-component kinetics of two source rocks to show the API and GOR of selected reservoir hydrocarbons.

As discussed earlier, the complex salt canopies within the slope region are solely associated with the eastern sector of the deepwater portion of the Sable Subbasin. The results of the interpretation of the 2D petroleum system modeling will be described commencing with the westernmost seismic line E-E', then moving to the central part of the target area comprising seismic lines D-D' and C-C', and the finally discussing the complex salt canopy area with seismic lines B-B' and A-A'.

Basement faults no doubt exist on all seismic lines. However, more efforts was taken to interpret basement faults within seismic lines A-A' and B-B', as seems to be easier to be seen in those lines. The basement faults became more ambiguous in seismic lines C-C', D-D', and E-E'.

6.1. Seismic Line E-E'

The seismic line E-E' is located to the west of the Shelburne G-29 well within the Shelburne Subbasin (Figures 32a and 32b). The Pre- to Synrift Late Triassic to Early Jurassic Eurydice Formation sediments are the thickest unit (about 5000-6000 m in the central part of the line) (Figures 32b and 32c). The Argo salt is represented as two diapiric structures within the northwestern (shelf) side of the line and extends to the central part of the seismic line E-E' (Figure 32c). The Late Jurassic sediments (especially the Jurassic Verrill Canyon) are thin and less than 1000m (Figure 32c). Based on various features of the salt movement and scrutiny of the earlier published data (Wade and MacLean, 1990; Shimeld, 2004), the timing of early salt movement and late salt piercement has been implemented. Therefore as discussed by the simulation, 1000 m of Argo salt has been deposited at 199 Ma. The early salt movement has taken place between the period of 199 Ma and 168 Ma. Slow salt piercement structures started developing around 160 Ma and 145 Ma. However, the main rapid salt piercement structures develop between 110 Ma and 40 Ma in nine phases. Accordingly, nine sedimentary layers above 110 Ma have been replaced by salt during this time period.

6.1.1. Thermal Evolution and Hydrocarbon Transformation

The heat flow varies from 54.5 mW/m^2 (Early Jurassic sediment below the salt) to 89.7 mW/m^2 in Tertiary sediment on top of the salt [Figure 32d (i)]. The sediments which are the part of the mini-basin flanking the major salt diapir show slightly lower heat flow compared to the (a) normal sediments where heat flow is derived mainly from the basement and (b) the heat flow within the salt body. Because of general high heat flow due to the volcanic activities within the Georges Bank Dehler et al., 2004), most of the Late Jurassic to Cretaceous sediments are within the "Principal Phase of Oil

Generation" [110-180°C and 0.7% to 2.0% R_o; Figures 32d (ii) and 32d (iii)]. The modeling of pore pressure for the reservoir sediments within seismic line E-E' indicates that the Late Jurassic and Early Cretaceous reservoirs are within the overpressure regime (>60 MPa), whereas the Miocene reservoirs remain within normal pressure condition (20-30 MPa) (Figure 32e).

The hydrocarbon vectors or hydrocarbon flowpath shows the timing of hydrocarbon saturation of various reservoirs [Figures 32f (i), (ii), (iii), (iv), and (v)]. This data suggests that the Miocene salt-top reservoir has been fully saturated only at the present time [Figure 32f (v) compared to Figure 32f (iv)]. The Cretaceous Verrill Canyon reservoir has been fully saturated at 102 Ma (see the sequences of Figures from 32f (i), 32f (ii), and 32f (iii, and 32f (iv)].

6.1.2. Reservoir Hydrocarbons to Source Rock Tracking

The flash calculation of the Miocene salt top reservoir indicates that more than 95% of the reservoirs contain dry gas with about 58° API and the Gas-Oil Ratio (GOR) is 340 m^3/m^3 (Figure 32g). This dry gas is mainly derived from the Early Jurassic and Triassic lacustrine Type I or II source rocks (Figures 32h). About 10% of the gas composition is derived from the Jurassic Verrill Canyon (JVC) source rocks (Figure 32h). The bubble point curve of this reservoir hydrocarbon indicates that it would be mainly gas at the surface pressure and temperature condition (Figure 32i).

The flash calculation of the Cretaceous Verrill Canyon reservoir indicates that the hydrocarbons at the reservoir condition remain mainly as liquid phase with an API of 50.38° and a GOR of 158.5 m^3/m^3 (Figure 32j). However, flash calculation of the same source rock indicates that reservoir hydrocarbons at the atmospheric condition will show mainly dry gas (Figure 32k). Volumetrically, the reservoir contains about 90%

hydrocarbons derived from the Early Jurassic lacustrine Type I or from the marine Type II Jurassic Verrill canyon source rocks [Figure 32k (i)]. However, the analysis based on molar composition of the same hydrocarbons at atmospheric condition will give rise to 70% dry gas and 30% condensate from the Jurassic Verrill Canyon and the Early Jurassic source rocks [Figure 32 k (ii)].

6.1.3. Mass Balance of Hydrocarbons

The calculated hydrocarbon mass balance of the petroleum systems of the seismic line E-E' (masses calculated within a kilometer radius) would be as follows (Table 9a):

1) The total mass of hydrocarbons generated from all six source rocks is $(9074.32)^9$ kg(Mtons)/m^3. Out of this amount, the total mass of hydrocarbons expelled is $(8043.48)^9$ kg(Mtons)/m^3. The Late Triassic and Early Jurassic lacustrine source rocks accounts for 45% of the hydrocarbons. The Jurassic and Cretaceous Verrill Canyon source rocks contribute about 38% of the remaining hydrocarbons (Figure 32l),
2) The total amount of hydrocarbons accumulated in four reservoirs is $(574.13^9$ kg(Mtons)/m^3. Out of that accumulated hydrocarbons, 80% of the hydrocarbons have been concentrated within the Logan Canyon $(222)^9$ kg(Mtons)/m^3 and Early Miocene reservoirs $(202)^9$ kg(Mtons)/m^3. The main reservoir saturation occurs after 75 Ma. All the reservoirs were fully saturated around 55 Ma (Figure 32l).
3) The total amount of hydrocarbon losses within the stratigraphic column is $(7469.34)^9$ kg (Mtons)/m^3. The main losses of the hydrocarbons are the losses due to the absence of proper sealing on both sides (horizontal seal) and losses due to secondary cracking of hydrocarbons within the reservoirs. Both these losses account for 60% of the hydrocarbon losses.

6.2. Seismic Line D-D'

The seismic line D-D' is situated at the boundary of the Shelburne Subbasin and Sable Subbasin and lies between the Torbrook C-15 and Acadia K-62 wells (Figure 33a). The gradient of the seafloor within seismic line E-E' is steep and trending from NNW to SSE (Figure 33b). Similar to line E-E', the line D-D' also illustrates that Triassic to Recent sediments lie on top of an unknown basement. The basement in the northwestern side of the line is much thicker compared to the southeastern part of the section. The early Jurassic Argo salt occurs both as autochthonous sheets and in the form of three major diapirs in the southeastern section of the seismic line (Figure 33b). In the central part of the section an anticlinal structure developed which is possibly related to the basement structure or early salt movement or due to the sliding of bank edge carbonates. The Jurassic to Cretaceous sediments are thin in the middle part of the section and thicker on both sides. Similar to line E-E', the Early and Middle Jurassic sediments are comparatively thicker than the Late Jurassic and Cretaceous sediments especially in the central part of the section (Figures 33b and 33c). Several salt-flank and salt-top play types could be identified. These potential sediments have been designated as conceptual reservoir units (Figures 33b and 33c).

Similar to line E-E', the timing of the early salt movement and salt piercement phases have been incorporated within the input parameter of PetroBuilder. Based on the calibration of the current thickness of the autochthonous salt, 500 m of Argo salt has been deposited at 199 Ma. The timing of the early piercement of the Argo Salt has been documented in five phases between 155 Ma and 140 Ma. Concurrent to the higher sedimentation rate of the Middle Cretaceous to Tertiary sediments, the timing of rapid salt piercement between 110 Ma and 45 Ma has been

included in eight phases. Accordingly, eight sedimentary layers above 110 Ma have been replaced by salt during this time period (Figure 33c).

6.2.1. Thermal Evolution and Hydrocarbon Transformation

Figure 33d illustrates the general state of the output data after the modeling simulation. It also shows the reservoir zones where hydrocarbons have been saturated and emplaced (Figure 33d). All salt-flank or salt-top (Jurassic to Tertiary) and Miocene Turbidite sandstone reservoirs have more than 90% hydrocarbon saturation (Figure 33d). The heat flow history of this seismic line shows a higher thermal gradient in the Late Triassic to Cretaceous period compared to most parts of the Tertiary. The present day heat flow varies between 56 and 93 mW/m^2 depending on the position of the measurement in association with the salt diapir and basement structure (Figure 33e). The upper slope is not affected by the salt diapirs. Accordingly, the upper slope has much lower heat flow than the lower slope area which is connected to three salt diapirs. The heat flow close to the salt is much higher than in other lithologies. The salt provides an additional basement heat source into the system. Usually, it will act as a heat chimney which will bring the heat from the basement to the upper part of the geological section. However, sediments in the flank of a salt diapir within a mini-basin are cooler and have much lower heat flow (59.1 mW/m^2) compared to the salt-top sediments (88.9 mW/m^2) even if they are stratigraphically older (Figure 33e). Figures 33f (i) through 33f (vi) document the changes in maturity and temperature for various sedimentary units from 90 Ma to the present day. The data shows that both the temperature and maturity values within the middle to lower slope region have fluctuated depending on their closeness to a salt diapir at that time. This data also indicates that a major phase of gas and condensate migration from the Early Jurassic and Early Cretaceous source rocks might have started around 90-70 Ma as it coincides with the timing of the salt movement.

The above migration concept has also been corroborated using the timing of the hydrocarbon saturation of various reservoirs from 90 Ma to the present day [from Figure 33g (i) to Figure 33g (vii)]. This data indicates that some of the Early Missisauga and Late Jurassic salt flank or salt top reservoirs were fully saturated at 75 Ma [Figures 33g (ii) and 33g (iii)]. However, most of the younger reservoirs (especially the main Middle Paleocene one) and other Late Jurassic and Early Missisauga reservoirs became fully saturated only around 11.2 Ma. At that time, both Early Jurassic and Jurassic Verrill Canyon source rocks reached optimum temperature and maturity (>150^{o}C and 1.2% R_o) for the cracking of previously generated C_{15+} hydrocarbons to secondary gas. As the SSE part of the line has evolved into a higher heat flow regime because of salt diapirism, most of the salt flank and salt-top reservoirs in this region were fully saturated around 30 Ma.

6.2.2. Reservoir Hydrocarbons to Source Rock Tracking

The hybrid simulation of the main Middle Paleocene reservoir indicates that reservoir hydrocarbon will have 47.39^{o} API and the Gas-Oil ratio is 74.64 m^3/m^3 [Figure 33h (i)]. The main hydrocarbon components of the Middle Paleocene reservoir are light oil and condensate (C_6 and C_{14}) fraction, which are derived from the Jurassic Verrill Canyon and Early Jurassic Lacustrine source rocks. The dry (C_1) and wet gas (C_2 – C_5) fractions of the reservoir hydrocarbons were derived from the Early Jurassic source rock [Figures 33h (ii) and 33h (iii)]. About 10% of the components were originated from the Cretaceous Verrill Canyon source rock. The bubble point curve of this reservoir hydrocarbon indicates that it would be mainly composed of condensate and gas with some light oil at the surface condition [Figure 33h (iv)]. The Middle Paleocene salt-flank and salt-top reservoir, which is associated with the salt diapir shows that the hydrocarbons are still in liquid phase with a 48.84^{o} API and 70.93 m^3/m^3

GOR [Figure 33 i(i)]. The reservoir hydrocarbon to source rock tracking indicates similar hydrocarbon fractions [light oil/condensate (C_6 and C_{14}), wet and dry gas] which are mostly derived from the Jurassic Verrill Canyon and Early Jurassic Lacustrine source rocks [Figures 33i (ii)].

On the other hand, the hydrocarbon saturation of the Late Jurassic salt flank reservoir (situated in between two diapirs) indicates that this hydrocarbon has a 59.26^0 API with a GOR of 83.85 m^3/m^3 [Figure 33j (ii)]. However, the hydrocarbon to source rock tracking indicates that mainly dry gas and condensate have been derived from the Jurassic and Cretaceous Verrill Canyon source rocks [Figure 33j (2)]. The Cretaceous Verrill Canyon (CVC) source rock has a direct connection with the Jurassic salt-flank Late Jurassic reservoir.

The modeled pore pressure data suggests that Middle Paleocene reservoirs are within a normal to mild overpressure regime, whereas the Jurassic salt-flank reservoir shows a moderate to high overpressure condition.

6.2.3. One Dimensional Modeling Extraction

The burial, temperature and maturation histories of one dimensional extraction for a dummy deepwater location (top of Jurassic reservoir) in the middle of the seismic line D-D' indicate that the Jurassic Verrill Canyon source rock is still within the "main phase oil generation" [Figures 33m (i), (ii), (iii)]. Within the middle of the seismic line D-D', the Early Jurassic, Misaine, and Jurassic Verrill canyon source rocks show a hydrocarbon transformation ratio of 97%, 85%, and 36%, respectively [Figure 33m (iv)].

6.2.4. Mass Balance of Hydrocarbons

The calculated hydrocarbon mass balance of the petroleum systems of the seismic line D-D' (masses calculated within one kilometer radius) would be as follows (Table 9b):

1) The total mass of hydrocarbons generated from all six source rocks is $(3451.1)^9$ kg(Mtons)/m^3. Out of this amount, the total mass of hydrocarbons expelled is $(2290.4)^9$ kg(Mtons)/m^3. The Late Triassic and Early Jurassic lacustrine source rocks account for 30% of the hydrocarbons. The Jurassic and Cretaceous Verrill Canyon source rocks constitute about 40% of the remaining hydrocarbons,
2) The total amount of hydrocarbons accumulated in four reservoir sequences is $(888.1)^9$ kg (Mtons)/m^3. Of these hydrocarbons, 33% of the hydrocarbons have accumulated in the Middle Paleocene reservoirs $(351.3)^9$ kg (Mtons)/m^3. The main reservoir saturation occurs after 50 Ma. All the reservoirs were fully saturated around 10 Ma (Figure 33p).
3) The total amount of hydrocarbon losses within the stratigraphic column is $(1402.3)^9$ kg (Mtons)/m^3. The main losses of the hydrocarbons are losses due to the absence of proper vertical sealing from the reservoirs. This loss accounts for 70% of the hydrocarbon losses. The main loss of hydrocarbons from the Middle Paleocene reservoir has occurred between 5.3 Ma and the present day.
4) Volumetrically, the normal gravity crude oil (C_{15+} hydrocarbons), light oil and condensate fractions (C_6 and C_{14}) from the Early Jurassic, Jurassic Verrill Canyon, and Cretaceous Verrill Canyon source rocks and methane from the Early Jurassic source rock constitute the main hydrocarbon components of all reservoirs (Figure 33n). Volumetrically, in a surface condition, the liquid fraction of the reservoir will be transformed into methane, condensate, and light oil. The Paleocene reservoir may contain about 10% normal gravity oil (C_{15+}) in a surface condition.

6.3. Seismic Line C-C'

The seismic line C-C' is situated within the western part of the Sable Subbasin and lies between the Shubenacadie H-100 and Evangeline H-98 wells (Figures 34a). The line is parallel to seismic line D-D' and includes the Triassic to Recent age sediments, which are overlying the unknown basement (Figure 34b). Similar to the seismic line D-D', the line C-C' contains both autochthonous Jurassic salt and four Jurassic salt diapirs which penetrate the younger sediments from top Jurassic to the Late Tertiary (Figure 34b). The Cretaceous and the Jurassic sediments remain in uniform thickness from the upper to lower slope region (Figures 34b and 34c). The Jurassic and Cretaceous sediments have similar thicknesses. In the upper slope region, the basement has been uplifted to form anticlinal structures in four zones possibly due to an early movement of the salt (Figure 34c). Salt swells may have been formed in this area were formed due to the basement uplifts. Several salt-flank and salt-top play types could be identified. However, no definite reservoir units could be identified within these uplifted basement areas (Figure 34c).

Similar to line D-D', the timing of the early salt movement and phases of salt piercement have been documented in PetroBuilder before the simulation of the model. Based on the calibration of the current thickness of the autochthonous salt, seismic velocity, and density, about 1000 m of Argo salt has been deposited at 199 Ma. The early slow upward movement of the Jurassic Argo salt has taken place between the period of 199 Ma and 110 Ma. Concurrent to the higher sedimentation rate of the Middle Cretaceous to Tertiary sediments, eleven phases of rapid development of the salt diapiric structures have been implemented (in the model) within a geological time span of 80 Ma and 2.5 Ma. Thus, eleven sedimentary layers above 80 Ma have been replaced by salt facies during these time periods. The replaced sedimentary layers within these diapiric zones are:

Cretaceous Verrill Canyon (at 80 Ma), Early Missisauga (75 Ma), Missisauga Reservoir (65 Ma), Mid-Missisauga (60 Ma), Logan Canyon (55 Ma), Wyandot_Dawson Canyon (45 Ma), Middle Paleocene (15 Ma), Late Paleocene (10 Ma), Early-Middle Eocene (5 Ma), Middle Eocene (2.5 Ma), Late Eocene (2.5 Ma).

6.3.1. Thermal Evolution and Hydrocarbon Transformation

Figure 34d illustrates output data with possible hydrocarbon saturated reservoir zones within the seismic line C-C'. The present day heat flow data indicates that low to moderate heat flow regime within the northwestern (shelf) side of the line (54 to 62 mW/m^2), whereas the diapiric zone (southeastern side) has shown a generally high heat flow (64 to 119 mW/m^2). As discussed earlier, the flank of the diapirs has moderate to low heat flow similar to the northwestern non-diapiric are [Figure 34e (i)]. On the other hand, the temperature and maturity data suggests that the flank of the salt diapirs have higher temperatures compared to the body of the salt at the similar depth [Figures 34e (i), 34e (ii), and 34e (iii). This is possibly because salt body is acting like a chimney releasing the heat from the basement to the top of the section because of its higher thermal conductivity.

6.3.2. Reservoir Hydrocarbons to Source Rock Tracking

The main play within the line C-C' is the Late Jurassic reservoir facies. The flash simulation of the Late Jurassic reservoir indicates that the reservoir hydrocarbon will have a 55.47^o API and the Gas-Oil ratio is 195.47 m^3/m^3 [Figure 34f (i). The main volume percentages of hydrocarbon components of this reservoir would be dry gas and were derived from the Early to Middle Jurassic source rocks [Early Jurassic lacustrine, Mohican formation, and Misaine Member; Figure 34f (ii)]. The bubble point curve of the reservoir hydrocarbons indicates that gas would constitute about 95% of the hydrocarbon ingredient [Figure 34f (iii)]. On

the other hand, the hybrid simulation of the salt-top Middle Miocene reservoir (90% saturation) indicates that this reservoir will have 50.01° API and a GOR of 63.98 m^3/m^3 [Figure 34g (i)]. Dry gas (methane) and condensate (C_6 to C_{14}) would be the main hydrocarbon components of this reservoir. The hydrocarbons will mainly be derived from the Early Jurassic and Jurassic Verrill Canyon source rocks [Figure 34g (ii)]. The bubble point curve of the reservoir hydrocarbons indicates that it would be in a mixed condensate and gas phase.

6.3.3. Mass Balance of Hydrocarbons

The calculated hydrocarbon mass balance of the petroleum systems of the seismic line C-C' (masses calculated within a kilometer radius) would be as follows (Table 9c):

1) The total mass of hydrocarbons generated from all six source rocks is $(2926.12)^9$ kg (Mtons)/m^3. Out of this amount, the total mass of hydrocarbons expelled is $(2340.24)^9$ kg (Mtons)/m^3 (Table 9c). The Late Triassic and Early Jurassic lacustrine source rocks account for 30% of the hydrocarbons. The Jurassic and Cretaceous Verrill Canyon source rocks contribute about 40% of the remaining hydrocarbons,
2) Volumetrically, the dry gas (methane) from the Early Jurassic, Misaine, and Jurassic Verrill Canyon source rocks contributes the main hydrocarbon component of all important reservoirs (Figure 34h).
3) The total amount of hydrocarbons accumulated in four reservoirs is $(508.9)^9$ kg (Mtons)/m^3. Of these hydrocarbons, 50% of the hydrocarbons have accumulated in the Late Jurassic reservoir $(263.5)^9$ kg (Mtons)/m^3. The main reservoir saturation starts after 75 Ma. The Late Jurassic reservoirs were fully saturated around 55 Ma (Figure 34i). The Miocene reservoir is fully saturated around 5.3 Ma.

4) The total amount of hydrocarbon losses within the seismic line is $(1831.26)^9$ kg (Mtons)/m^3. The main losses of the hydrocarbons are a result of the absence of proper vertical sealing above these reservoirs. The vertical seal loss accounts for about 60% $(1390.6)^9$ kg (Mtons)/m^3 of the hydrocarbon losses. The main loss of hydrocarbons from the Late Jurassic reservoir has occurred between 50 Ma to the present day.

6.4. Seismic Line B-B'

The seismic line B-B' is situated within the complex salt canopy area of the deepwater portion of the Sable Subbasin (Salt Subprovince III of Shimeld, 2004) (Figure 35a). The seismic line indicates the presence of Triassic to Recent sediments, which overlies the unknown Pre-Triassic basement (Figure 35b). The gradient of the slope is gentler compared to E-E' and D-D' lines. The seismic line includes thick Jurassic and Cretaceous sediments. The autochthonous Jurassic Argo salt is thin and did not show any connection with the allochthonous salt bodies (Figure 35c). Several major basement and Cretaceous to Tertiary growth faults occur within this seismic line. No reservoir sands could be defined on this line.

Five disconnected allochthonous Jurassic Argo salt bodies occur within the central and southeastern part of the line forming various sub-salt play types (Figure 35b). Based on the presence of the allochthonous salt on this line, it was determined that 600 meter of autochthonous salt was deposited uniformly at 185 Ma which was progressively thinned out until all the allochthonous salt have been emplaced to its present shape at 60 Ma. Therefore, the autochthonous salt body has gone through sixteen different time phases of allochthonous salt movement starting at 136 Ma and ending at 60 Ma. At 60 Ma, the allochthonous salt bodies have been completely detached from their autochthonous counterpart. Between 60

Ma and 5.3 Ma, all the detached allochthonous salt canopies took their final shape through five successive time slices. During 60 Ma and 5.3 Ma, these allochthonous salt canopies became fully or partially dissociated from each other (Figure 35c).

6.4.1. Thermal Evolution and Hydrocarbon Transformation

Four time sequences (141 ma, 110 Ma, 50 Ma, and present day) of heat flow and temperature histories have illustrated how the candidate source rocks have been catagenetically altered to establish the hydrocarbon charge histories of the seismic line B-B' [Figures 35d (i), (ii), (iii), (iv) and 35e (i), (ii), (iii), (iv))]. This data shows that a high heat flow (> 80 mW/m^2) and temperature have persisted between 110 Ma and 50 Ma [Figures 35d (ii), (iii) and 35e (ii), (iii)]. During that time period, most of the target conceptual reservoirs had reached its present day maturity and received most of the saturation of hydrocarbons [Figures 35e (ii), (iii), (iv) and 35f]. Similarly, the pore pressure data suggest that an overpressure condition should have existed within the Missisauga and the Logan Canyon conceptual reservoirs since the last 50 Ma (Figure 35g).

6.4.2. Conceptual reservoir Hydrocarbons to Source Rock Tracking

Figure 35h (i) illustrates the present day conceptual reservoir zone along with hydrocarbon flow paths and the projection of Weymouth A-45 well including various picks of stratigraphic intervals. Figure 35h (ii) illustrates the possible hydrocarbon saturation within the present day conceptual reservoir units. This data also shows the hydrocarbon migration vectors and the projection of Weymouth A-45 well. The hydrocarbon migration flowpath and vectors surrounding various conceptual reservoirs indicate that most of the conceptual reservoirs are vertically leaking hydrocarbons in spite of the salt remaining as the top seal. The hybrid simulation of conceptual Logan Canyon conceptual reservoir suggests that the conceptual reservoir hydrocarbons would have an API of 60.84^o and a

GOR of 88.74 m^3/m^3, in case conceptual reservoir existed within the Weymouth A-45 well [Figure 35i (i)]. The conceptual reservoir hydrocarbon to source rock tracking data indicates that methane (dry gas) and C_6 to C_{14} components (light oil or condensate) are the main reservoir hydrocarbon components. These hydrocarbons were derived from the Early Jurassic lacustrine and the Jurassic or Cretaceous Verrill Canyon marine source rocks [Figures 35i (ii) and 35i (iii)]. The phase composition and the bubble point curve have also fingerprinted the concentration of similar type of hydrocarbons [dry gas, condensate and minor light oil; Figures 35i (iv) and 35i (v)].

6.4.3. Mass Balance of Hydrocarbons

The calculated hydrocarbon mass balance of the petroleum systems of the seismic line B-B' (masses calculated within a kilometer radius) would be as follows (Table 9d):

1) The total mass of hydrocarbons generated from all six source rocks is $(8227.6)^9$ kg(Mtons)/m^3. Out of this amount, the total mass of hydrocarbons expelled is $(7292.31)^9$ kg (Mtons)/m^3 (Table 9d). The Jurassic and Cretaceous Verrill Canyon source rocks account for 60% of the hydrocarbons. The Early Jurassic lacustrine source rock contribute about 18% of the remaining hydrocarbons,
2) The total amount of hydrocarbons accumulated in four conceptual reservoir sequences is $(709.14)^9$ kg (Mtons)/m^3. Of these hydrocarbons, 45% of the hydrocarbons have accumulated in the Middle Missisauga conceptual reservoirs $(393.9)^9$ kg(Mtons)/m^3,
3) Volumetrically, the methane (from the Early Jurassic rock) and the light oil or condensates (from the Cretaceous Verrill Canyon source rocks) compose the main hydrocarbon components of all important conceptual reservoirs (Logan

Canyon and Middle Missisauga conceptual reservoirs; Figure 35j).

4) The total amount of hydrocarbon losses within the seismic line B-B' is $(6583.2)^9$ kg (Mtons)/m^3. The main losses of hydrocarbons resulted from the absence of proper vertical sealing from the conceptual reservoirs. This loss accounts for about 80% $(4262.04)^9$ kg (Mtons)/m^3 of the hydrocarbon losses. The main loss of hydrocarbons from the Middle Missisauga conceptual reservoir occurred between 65 Ma to present day,
5) The main conceptual reservoir saturation started after 125 Ma. All the conceptual reservoirs were fully saturated around 30 Ma (Figure 35k),

6.5. Seismic Line A-A'

The seismic line A-A' is located within the eastern part of the Sable Subbasin and south of the Sable Island area (Figure 36a). Similar to the seismic line B-B', the seismic line A-A' is also situated within the complex salt canopy area of the Scotian Slope (Salt Subprovince III of Shimeld, 2004) (Figures 15d and 36a). This seismic line includes Triassic to Recent sediments, which has a gentle slope from the northwestern side of the upper slope to the southeastern side of the lower slope (Figure 36b). The seismic line also includes thick Jurassic and Cretaceous sediments (Figures 36c and 36d). Seven basement faults and two major growth faults within the Cretaceous to Tertiary sediments could be documented (Figures 36b and 36c). Similar to the four other seismic lines, seven unconformities and six source rock units have been incorporated within the line A-A' [Figures 36c (i) and 36c (ii)]. The Annapolis G-24 well lies directly on this line and the Crimson F-81 has been projected on the line as well [Figure 36c (i)]. Based on the well history report of the Annapolis G-24 well, the

Early Missisauga turbidite (deltaic?) conceptual reservoir sand unit has been included [Figure 36d (i)]. Other play types within this seismic line are several sub-salt related traps and Jurassic deepwater sands.

Three completely detached allochthonous salt bodies occur within the central and southeastern part of the line A-A' (Figure 36b). The autochthonous Jurassic Argo salt horizon is thin and does not have any connection with the three allochthonous salt bodies. It is assumed that the movements of the autochthonous and allochthonous salt bodies are discretely separate and are not related to each other. From the nature of the autochthonous salt bodies at different grid points of the seismic section, five hundred meter of autochthonous salt was deposited around 199 Ma. The thickness of the salt was later reduced to 100m at 145 Ma through various successive changes. At the present time period, no autochthonous salt could be visualized on the seismic line A-A' beyond the 3500 m water depth within the ultra-deep region of the slope. It is considered that around 115 Ma the allochthonous salt body entered the central part of the seismic line A-A' from behind possibly from the north-north-west side of the upper slope below the Annapolis G-24 well. A schematic representation of the fifteen time slices of the salt growth has been documented in Figures 36d (i) to 36d (xiv). This salt growth had possibly started as a basinward leaning diapir around 115 Ma. The leaning diapir has been systematically changed to completely detached allochthonous salt bodies at the present time through successive intermediate stages of salt withdrawal and the formation of allochthonous canopies as shown in our earlier conceptual model (Mukhopadhyay et al., 2006; Figure 15e).

Based on the sequential stages of salt emplacement, heat flow histories of this area indicate a higher heat flux between 85 Ma and 55 Ma (75 mW/m^2 to 153 mW/m^2). The higher maturity and temperature below the

Annapolis G-24 well possibly indicate the presence of the salt structures between 85 to 55 Ma [Figures 35d (iv) to 35d (viii) and Figures 35e (i) to 35 (viii)]. The higher present day bottom-hole temperature of the well represents the relics of earlier higher heat flux below this well [Figure 36f) and Figures 35e (i) to 35 (v)]].

6.5.2. Thermal Evolution and Hydrocarbon Transformation

The systematic correlation of migration flowpath or vectors, hydrocarbon saturation of various reservoir units, modeled temperature, and the maturation histories from 105 Ma to the present day have illustrated that the main saturation of the Annapolis G-24 Early Cretaceous reservoir possibly started around 95 Ma [Figures 36g (i) to 36g (vii) and especially Figure 36g (ii)]. At that time, the top of Jurassic Verrill Canyon source rock has a maturity of 1.15% R_o [Figure 36g (ii)]. The reservoir was fully saturated with liquid hydrocarbons around 65.5 Ma [Figures 36g (iv)]. The expelled oil that was already present within the reservoir and associated carrier bed may have been cracked to methane possibly after 75 Ma.

The present day modeled pore pressure of the Annapolis G-24 reservoir suggests that the Missisauga reservoir within the Annapolis G-24 well is within an overpressure regime (66.85 MPa) corroborating with the well data (Figure 36h).

6.5.2. Reservoir Hydrocarbons to Source Rock Tracking

The modeled flash calculation using the hybrid simulation suggests that the hydrocarbons within the Early Cretaceous reservoir should have an API of 64.83^o and a GOR of 181 m^3/m^3 [Figure 36i (i)]. The saturation of a similar Cretaceous conceptual reservoir within the Crimson F-81 indicates that the conceptual reservoir did not have enough hydrocarbon saturation. This data suggests that the Early Cretaceous conceptual reservoir within the Crimson F-81 well did not have enough saturation even if porous and

permeable Missisauga sands existed in that well [Figure 36i (i)]. However, the Late Jurassic conceptual reservoirs below both the Annapolis G-24 and Crimson F-81 wells should have been saturated with 90% dry gas [Figure 36i (i)].

The conceptual reservoir hydrocarbon to source rock tracking of the Early Cretaceous conceptual reservoir of the Annapolis G-24 well indicates that the methane (>80% dry gas) and C_6 to C_{14} components (10-20% light oil/condensate) from the Early Jurassic, Jurassic Verrill Canyon, and Cretaceous Verrill Canyon source rocks would have been the main components for this reservoir hydrocarbons [Figures 36i (ii) and 36i (iii)]. The Early Jurassic lacustrine source rock has contributed about 18-25% of the dry gas within this reservoir [Figure 36i (iii)]. The phase composition and the bubble point curve fingerprints similar type of hydrocarbon fractions [dry gas, condensate and minor light oil; Figures 36i (iv) and 36i (v)].

6.5.3. Mass Balance of Hydrocarbons

The calculated hydrocarbon mass balance of the petroleum systems of the seismic line A-A' (masses calculated within a kilometer radius) would be as follows (Table 9e):

1) The total mass of hydrocarbons generated from all six source rocks is $(6861.64)^9$ kg(Mtons)/m^3. Out of this generated hydrocarbons, the mass of total hydrocarbons expelled is $(6382.1)^9$ kg (Mons)/m^3. The Jurassic and Cretaceous Verrill Canyon source rocks account for 65% of the hydrocarbons. The Early Jurassic source rock contribute about 18-25% of the remaining hydrocarbons,
2) Volumetrically, the dry gas (methane) from the Early Jurassic, Misaine, and Top Jurassic source rocks composes the main hydrocarbon component of all important conceptual reservoirs

(Figure 36i). However, most conceptual reservoirs have about 10-30% light oil and condensate (C_6 to C_{14}).

3) The total mass of hydrocarbons accumulated in four conceptual reservoir sequences is (488.5) ^{9} kg (Mtons)/m^3. Of these conceptual reservoir hydrocarbons, 60% of the hydrocarbons have accumulated in the Late Jurassic conceptual reservoirs (287.3)^9 kg (Mtons)/m^3. The main conceptual reservoir saturation occurs after 95 Ma. All the conceptual reservoirs were fully saturated around 65.5 Ma (Figure 36j).
4) The total amount of hydrocarbon losses within the seismic line A-A' is (5893.6)^9 kg (Mtons)/m^3. The main losses of the hydrocarbons resulted from the absence of proper vertical and lateral seals within the conceptual reservoirs (Late Jurassic conceptual reservoir has a better seal). This loss accounts for about 50% (2936.6)^9 kg (Mtons)/m^3 of the hydrocarbon losses. The main loss of hydrocarbons from the Missisauga and Tertiary conceptual reservoirs has occurred between 30 Ma to present day.

6.5.4. One-Dimensional Extraction of Annapolis G-24 well

The one dimensional extraction of various petroleum system parameters from the Annapolis G-24 well suggests the following [Figures 36l (i), (ii)], and (iii)]:

(a) A major subsidence occurred between 120 and 144 Ma,

(b) The modeled temperature of 200^{o}C and 2% R_o would have existed around 8000 m and 7000 m, respectively,

(c) The middle part of the Jurassic Verrill Canyon source rock should have maturity of 1.74% R_o at the present time indicating an active dry gas generation,

(d) The transformation ratio of various source rocks suggest that the Early Jurassic lacustrine and Mohican Formation source rocks should have 100% conversion to hydrocarbons, while Jurassic and Cretaceous Verrill Canyon source rocks has been converted to 90-97% and 30-20% hydrocarbons, respectively (Figure 36l (iv)].

Figure 36l (v) illustrates saturation histories of various conceptual reservoir rocks through geological time. Accordingly, the Early Cretaceous reservoir rock should been fully saturated around 65.5 Ma [Figure 36l (v)]. A major expulsion of C_{15+} oil from the Early Jurassic lacustrine and Jurassic source rocks occur between 170 Ma and 130 Ma. This data corroborates the earlier concept that the liquid hydrocarbons derived from these two source rocks will act as lubricants for the gravity gliding forces of the salt movement [Figure 36l (vi), (vii), (viii)] [Mukhopadhyay et al., 2006 (in press)]. Eventually, a combination of the major expulsion of oil, high heat flow, and high sedimentation rate between 160 Ma and 110 Ma mobilized the transformation of salt diapirs in a rapid state. These parameters activated the gravity sliding of the diapiric salt after 110 Ma within the seismic line A-A'. This diapiric salt had eventually transformed into various allochthonous salt canopies through various intermediate stages of the leaning diapirs and salt withdrawal. The liquid hydrocarbon expulsion of the Cretaceous Verrill Canyon source rock (since the last 30 Ma) may have imprinted some residual effect on the separation of allochthonous salt bodies into their present form [Figure 36l (ix)].

The pore pressure and the reservoir permeability data from the one dimensional extraction of Annapolis G-24 well suggest that the reservoir hydrocarbons lie within an overpressure regime corroborating the well data. The discrepancies on the pressure prediction from the one dimensional (normal pressure) and two dimensional (overpressure) modeling may indicate that the hydrocarbon charge factor would be the

main reason. The concentration of abundant dry gas within the Early Cretaceous reservoir of the Annapolis G-24 well is mainly causing the overpressure. This dry gas is derived from the cracking of the early generated oil from the Early Jurassic and Jurassic Verrill Canyon source rocks. This dry gas expelled since 110 Ma and saturated the Early Cretaceous reservoir. Accordingly, the overpressure has possibly started since 55 Ma. In one dimensional modeling, an only Cretaceous Verrill Canyon source rock was utilized as the well did not penetrate the other two source rocks.

6.6. Summary of 2D Petroleum System Modeling

The review of the numerical modeling of the five seismic lines (A-A', B-B', C-C', D-D', and E-E') from the Scotian Margin establishes the differences in burial and thermal histories, stages of autochthonous and allochthonous salt movement, migration of hydrocarbons, reservoir saturation pore pressure histories, loss of hydrocarbon from various target reservoirs, and eventual mass balance of reservoir accumulation between seismic lines A-A, B-B' (Eastern Sable Subbasin) and C-C', D-D', E-E' (Western Sable Subbasin to Eastern Shelburne Subbasin). This data establishes the following conclusions:

6.6.1.Eastern Sable Subbasin (Seismic Lines A-A' and B-B'):

The higher maturation and temperature histories of the sediments within these two seismic lines are being controlled by the higher basement heat flux and lower thickness of the lower crust during the Early Jurassic Period. The high heat flux during Early to Middle Jurassic Periods has possibly triggered the higher sedimentation rate and the expulsion of C15+ hydrocarbons from the oil prone Early Jurassic lacustrine source rock starting at 170 Ma. As the higher heat flow continues due to the rising of the salt diapirs during the Late Jurassic and Early Cretaceous Periods,

another major expulsion of liquid hydrocarbons from the oil prone Jurassic Verrill Canyon source rock has occurred around 140 Ma within the seismic lines A-A' and B-B'. These two phases of liquid hydrocarbon expulsion coincides with the timing of the major growth of the salt diapirs and the beginning of the allochthonous salt emplacement within these two seismic lines of the eastern Sable Subbasin. The timing of oil expulsion phases and concomitant allochthonous salt movement due to high sedimentation rate and low friction from the presence of oil have possibly controlled: (a) the development of the allochthonous salt movement; (b) the formation of various Early Cretaceous to Miocene deepwater turbidite reservoir sands; (c) the hydrocarbon charge or preservation histories, and (d) the hydrocarbon losses from the various reservoirs and the carrier beds within the two seismic lines (A-A' and B-B') of the Eastern Sable Subbasin.

Based on the various risk assessment, the following conclusions on the two dimensional petroleum systems modeling within the seismic lines A-A' and B-B' could be made:

- The best Cretaceous to Miocene reservoir sands could be located either within the north-north-western side of the salt growing area or within the distal margin on the south-south-eastern side of these two lines. A typical example would be the presence of the Early Cretaceous reservoir of the Annapolis G-24 well and the lack of similar Cretaceous conceptual reservoir on the Crimson F-81 well. The lack of Early Cretaceous reservoir within the Crimson F-81 well is possibly caused due to its position on distal (basinal) side of the leaning diapir during Early Cretaceous time. The variation in maturity between these two wells also supports this concept. The Cretaceous sediments within the area between the Annapolis G-24 and Crimson F-81 wells were possibly within a salt withdrawal zone around 135-110 Ma. Accordingly, the turbidite sands during the Early to

Middle Cretaceous time have bypassed over the leaning diapir from the upper slope to a water depth deeper than 2500m.

- Because of higher maturity (>1.15% Ro) of the Early Jurassic and Jurassic Verrill Canyon source rocks around 110 Ma, most of the earlier generated C15+ oil has been cracked to condensate and dry gas creating an expansion of fluid volume. This volume expansion of the fluids could have triggered the overpressure within the existing reservoirs since 55 Ma. This phenomena could be very well documented by comparing the pressure versus depth plots of the 1D modeling of the Annapolis G-24 well and the 1D projection of the Annapolis G-24 well from the seismic line A-A'. Currently, the reservoir hydrocarbons from the Annapolis G-24 well are possibly leaking by the diffusion and the buoyancy of low molecular weight hydrocarbons. However, the reservoir hydrocarbons are being balanced and the overpressure is being maintained at the present time due to the renewed expulsion of oil from the Cretaceous Verrill source rock since last 30 Ma. However, two to three phases of hydrocarbon expulsion (170 Ma, 140 Ma, and 30-0 Ma) could be documented within various parts of seismic lines A-A' and B-B',
- All conceptual reservoirs contain more than 85% dry gas with 10-15% of wet gas and condensate. The Cretaceous and Jurassic conceptual reservoirs have an API of 64.8^{o} and a GOR of 183 m^3/m^3.
- All Jurassic and Early Cretaceous reservoirs are situated within an overpressure regime. The Miocene conceptual reservoirs lie either within a normal pressure regime or in a mild overpressure condition.

6.6.2. Western Sable Subbasin and Eastern Shelburne Subbasin (Seismic Lines C-C', D-D', and E-E')

In contrast to the two seismic lines from the Eastern Sable Subbasin, the maturation and temperature histories of these three lines (C-C', D-D', and E-E') are controlled by the heat flux derived from the basement and the variable heat flux caused by the slow growth of the salt diapirs. The areas unaffected by the salt diapirs lie on the southeastern side of the line E-E' and on the northwestern hand side of the lines D-D' and C-C'. Thus, the hydrocarbon charge, the reservoir accumulation, and the compositional variability of various reservoirs could be directly monitored by the basement heat induced maturity and expulsion. The petroleum system modeling of the seismic lines C-C', D-D', and E-E' establishes the following conclusions:

- ✓ Salt diapirs are located within the landward side of the seismic line E-E' and on the deeper basinward side of the other two lines (C-C' and D-D'). Within the seismic line E-E', well defined deepwater channel sand bodies could be located within the basinward side beyond the salt diapirs (eg. deepwater channel sand conceptual reservoir). All deepwater conceptual reservoirs within the seismic lines C-C' and D-D' are formed either as an anticlinal play type related to the basement structures (within the upper slope) or occur as salt-top and salt-flank play types,
- ✓ The timing of the rapid salt diapiric growth within seismic lines C-C', D-D' and E-E' coincides with the timing of the major expulsion of liquid hydrocarbons from the Early Jurassic and Jurassic Verrill Canyon source rocks after 110 Ma. The initial migration of C_{15+} oil from the Early Jurassic source rock has started around 130 Ma.
- ✓ Two phases of hydrocarbon migrations could be documented from the Early Jurassic and Jurassic Verrill

Canyon source rocks in the seismic line E-E': (a) the expulsion of the C_{15+} oil and C_6 to C_{14} light oil and condensate occurred around 130-110 Ma and (ii) the expulsion of both primary or secondary gas and condensate expulsion started between 75 Ma and 0 Ma possibly from the cracking of C_{15+} oil from both those two source rocks; and (c) the reservoirs have been fully saturated with hydrocarbons between 75 Ma and 55 Ma.

- ✓ One phase of hydrocarbon expulsion (light oil, gas and condensate) could be observed within the seismic lines C-C' and D-D', which has started since 75 Ma. The conceptual reservoirs have been fully saturated with hydrocarbons between 75 Ma and 5.3 Ma, which is comparatively later than the line E-E'.
- ✓ From the genetic fingerprinting on the source rock reservoir hydrocarbon composition suggest that from all conceptual reservoir hydrocarbons (Late Jurassic, Early Cretaceous, and Early Miocene) are genetically related to the Early Jurassic and Jurassic Verrill Canyon source rocks. All conceptual reservoirs within the seismic line E-E' contain more than 95% dry gas and have an API of 50-58^o and GOR of 343-158 m^3/m^3. On the other hand, because of the low heat flow and lower sedimentation rate during the Late Jurassic and Early Cretaceous Periods, most of the Cretaceous and Tertiary conceptual reservoirs within the seismic lines C-C' and D-D' contain mixtures of hydrocarbons [10-20% light oil (C_{10} and C_{20}), 20-30% condensate, and 50-70% dry gas]. The conceptual reservoir hydrocarbons within lines C-C' and D-D' have an API of 48^o to 59^o API and GOR of 71 to 84 m^3/m^3,

- ✓ The Early to Middle Cretaceous and the Tertiary conceptual reservoirs of these three seismic lines lie within a normal or mild overpressure regime. Most Jurassic conceptual reservoir hydrocarbons occur within an overpressure condition. However, the amount of overpressure is much lower compared to the seismic lines A-A' and B-B'.

6.6.3. Mass Balance of Hydrocarbons of All Five Seismic Lines – A Comparison

The calculated hydrocarbon mass balance of the petroleum systems of the five seismic lines (masses calculated within a kilometer radius; Tables 9a, 9b, 9c, 9d, and 9e) could be summarized in Table B-2:

Table B-2

Seismic Line	Total Mass Generated $(10)^9$ Kg (Mtons)/m^3	Total Mass Expelled $(10)^9$ Kg (Mtons)/m^3	**Total Mass Accumulated in Reservoirs $(10)^9$ Kg (Mtons)/m^3**	Total Mass Lost from Reservoirs $(10)^9$ Kg (Mtons)/m^3	Each Source Rock Contribution (%)	How the HC lost from Reservoirs	Main Reservoirs for Accumulated Hydrocarbons (%)
A-A'	6861.64	6382.1	**488.5**	5893.6	65 JVC/CVC 30 EJ	*Vertical Seal *Sec. Cracking	60% Late Jurassic
B-B'	8227.6	7292.31	**709.14**	6583.2	60 JVC/CVC 18 EJ	*Horizontal/vertical *Sec. Cracking	45% Middle Misssauga 30% Late Jurassic
C-C'	2926.12	2340.24	**508.9**	1831.26	40 JVC/CVC 30 EJ	*60% Vertical Seal *Sec. Cracking	50% Late Jurassic
D-D'	3451.1	2290.4	**888.1**	1402.3	40 JVC/CVC 30 EJ	*70% Vertical Seal & Horizontal Seal	35% Middle Paleocene 35% Late Jurassic/Early Cretaceous
E-E'	9074.32	8043.48	**574.13**	7469.34	38 JVC/CVC 45 EJ	60% Sec. Cracking 30% horizontal	80% Early Miocene & Middle Cretaceous

EJ = Oil Prone Early Jurassic Lacustrine Type I and II; JVC = Oil Prone Jurassic Verrill Canyon Marine Type II;
CVC = Oil Prone Cretaceous Verrill Canyon Marine Type II
Sec. Cracking = Secondary cracking of oil to dry gas in reservoir or carrier bed or within source rock and related volume expansion
* Reservoirs = except the Early Cretaceous reservoir within the Annapolis G-24 well, all other reservoirs are conceptual reservoir derived from the modeling data

The mass balance of hydrocarbons suggests that in spite of the huge masses of expelled hydrocarbons within the seismic lines A-A', B-B', and E-E' area, seismic line D-D' area would be the best suitable for the future

exploration drilling because of masses of the preserved hydrocarbons within various conceptual reservoirs. With the exception of the seismic line E-E', the Late Jurassic, a few Early Cretaceous and the Tertiary conceptual reservoirs should be the best future exploration targets.

7. CONCLUSIONS

The following conclusions of the research contract pertaining to the **Phase I** of the petroleum system risk assessment of the selected area within the Scotian Margin is based on: (i) the conceptual relationship between hydrocarbon expulsion, sedimentation rate, salt movement, and conceptual reservoir formation; (ii) the source rock potential, maturation, and multi-component reaction kinetics of selected source rocks; (iii) one dimensional modeling of eleven deepwater wells and one shelf well; (iv) two-dimensional petroleum system modeling of five seismic lines; and (v) mass balance of conceptual reservoir hydrocarbons within these five seismic lines.

7.1. Conceptual Model for Salt Emplacement and Sand Dispersal

A comparatively thinner lower crust, the presence of serpentinized mantle, and the presence of major basement fractures generated a higher heat flux within the eastern part of the Sable Subbasin (Sable Island area – seismic lines A-A' and B-B'; Salt Subprovince III of Shimeld, 2004). Major expulsion of C_{15+} oil from the Early Jurassic lacustrine and Jurassic Jurassic Verrill Canyon marine source rocks occurred during 170 and 130 Ma. The oil acts as a solvent or lubricant for the initial salt movement in this region. During 170-130 Ma, the high sedimentation rate in the Middle to Late Jurassic and Early Cretaceous Periods mobilized the autochthonous Jurassic Argo salt into an early active diapiric stage. The volume expansion of the fluids from the cracking of early oil to gas,

continued higher heat flow (surrounding the diapirs), and the second phase of high sedimentation rate in the Late Cretaceous and the Early Tertiary period accelerated the sliding of the diapiric salt to allochthonous canopies through an intermediate state of leaning diapirs and salt withdrawal. Thus, the movement of sand is restricted surrounding the active salt movement area forming only rare turbidite channels or delta margin channel reservoir facies (eg. Early Cretaceous reservoirs in the Annapolis G-24 well) or salt-related play types (salt-top or sub-salt) within the upper slope of the seismic line A-A', which may contain shale-dominated reservoirs.

A slow sedimentation rate and the persistence of moderate to low heat flow during the Middle Jurassic to Late Cretaceous Periods (Western Sable Sabbasin/Central Shelburne Subbasin - seismic lines C-C', D-D', and E-E'; Salt Subprovince II of Shimeld, 2004), the autochthonous Jurassic Argo salt only mobilized to a diapiric stage. During the slow active diapirism, the sands could have possibly accumulated as turbidite channels (line E-E') and salt-flank or salt-top (line D-D') play types during the Early Cretaceous and Early Tertiary Periods.

7.2. Source Rock Characterization and Kinetics

- The morphology of the organic-rich sediments from the Cretaceous Verrill Canyon (Early Missisauga Formation) from the Crimson F-81 and Annapolis G-24 wells suggest that they were possibly derived from a *dysoxic delta front depositional environment and not as deepwater turbidite derived organic matter* as previously thought forming gas and condensate prone Type II-III and III source rocks. The organic-rich Early Cretaceous sediments from the Weymouth A-45 well and the Tertiary Banquereau Formation sediments from the Torbrook C-15 well were distinctively derived from the deepwater

anoxic marine organic facies forming mainly oil and condensate prone Type II and II-III source rocks.

- The following stratigraphic units could be projected as potential source rocks within the Scotian Slope (Mukhopadhyay, 2000; Mukhopadhyay et al., 2003): (i) Late Triassic/Early Jurassic lacustrine (Sinumarian-Toarcian: *Iroquois/Mohican Formation*) – oil prone Type I; (ii) Middle Jurassic marine (Callovian: *Misaine Member*): gas/condensate prone Type II-III and III; (iii) Late Jurassic marine (Kimmeridgian-Oxfordian: *Jurassic Verrill Canyon Formation*), oil-prone, Type II; (iii) Early Cretaceous marine (Berriasian/Valanginian: *Lower Missisauga or Cretaceous Verrill Canyon Formation*): oil and gas prone Type II, II-III, and III; (iv) Mid-Cretaceous marine (Aptian to Cenomanian; Shortland Shale or Logan Canyon Formation): gas and condensate prone Type II-III or III; (v) Early Tertiary marine (Paleocene-Eocene; Banquereau Formation): oil and gas prone Type I, II or II-III.
- The correlation of heat flow and maturation indicates that (i) Early to Middle Jurassic sediments have a higher heat flow and maturity compared to the Cretaceous and Tertiary sediments within the Shelburne Subbasin and the western part of the Sable Subbasin, (ii) higher heat flow within the Jurassic age sediments of the Shelburne Subbasin is similar to heat flow histories of the Cretaceous to Recent sediments from the Eastern Sable Subbasin (area around the Shelburne Subbasin). Therefore, the Early and Middle Jurassic sediments from the Acadia K-62 and Albatross B-13 wells in the Shelburne Subbasin and the Early Cretaceous sediments from the Crimson F-81 and Weymouth A-45 wells of the Eastern Sable Subbasin are mature and lie within the “Principle Phase of Oil and Condensate Generation”. All Tertiary sediments from the Torbrook C-15 well and the Cretaceous or Tertiary sediments from the

Shubenacadie H-100, Albatross B-13, Shelburne G-29 wells are immature for hydrocarbon generation.

- ❖ The multi-component kinetics analysis of four hydrocarbon components for two prolific source rocks (Cretaceous Verrill Canyon and Jurassic Verrill Canyon) from the Scotian Margin has indicated that volumetrically primary cracking of the Cretaceous Verrill Canyon (CVC) and Jurassic Verrill Canyon source rocks will generate 17% and 40% normal gravity oil (C_{15+}), 62% and 47% light oil and condensate (C_6 to C_{14}); 15% and 10% wet gas (C_2 to C_5), 6% and 3% dry gas or methane (C_1), respectively,
- ❖ The computed temperature and maturity for 90% hydrocarbon conversion from two major source rocks would be: **Cretaceous Verrill Canyon (CVC) source rock** - normal gravity crude oil (C_{15+}) – 138^{0}C and 0.83% R_o; light oil and condensate (C_6 to C_{14}) - 165^{0}C and 1.22% R_o; wet gas (C_2 to C_5) - 176^{0}C and 1.43% R_o; and dry gas or methane (C_1)– 186^{0}C and 1.65% R_o. **Jurassic Verrill Canyon (JVC) source rock** - normal gravity crude oil (C_{15+}) -140^0 C and 0.85%; light oil and condensate (C_6 to C_{14}) - 157^{0}C and 1.10% ; wet gas (C_2 to C_5) - 169^{0}C and 1.30% ; dry gas or methane (C_1) - 190^{0}C and 1.74%. However, the JVC will start generating hydrocarbons much earlier than the CVC. The overall early generation and expulsion of hydrocarbons from both source rocks (Jurassic and Cretaceous Verrill Canyon) compared to other typical Type II source rocks from various parts of the world (Kimmeridgian Shale, Woodford Shale, etc.) may indicate the possible presence of abundant oxygen-functional group compounds within the kerogen network derived from the terrestrial organic matter.

7.3. One Dimensional Petroleum System Modeling

- ✓ At least three different heat flow zones exist within the Scotian Slope

(a) Moderate to low heat flow: area east of the Shelburne G-29 and west of Evangeline G-98 wells,

(b) Moderate to high heat flow: area between the Evangeline H-98 and Crimson F-81 wells, and

(c) Low heat flow: area around the Tantallon M-41 well.

- ✓ The burial and thermal histories of most wells suggest that only the Cretaceous Verrill Canyon source rock from the Annapolis G-24 and the Newburn H-23 wells (eastern Sable Subbasin) and the Early to Middle Jurassic sediments from the Acadia K-62 well (western Sable Subbasin) have attained the liquid and vapor phases of hydrocarbon generation ("oil window). Therefore, the "critical moment" of hydrocarbon emplacement has either been reached very recently in geological time (last 10 Ma) or did not reach it at all.
- ✓ The modeling pressure data indicates that the sediments below 5000m within most of the eastern Sable Subbasin wells (Annapolis G-24, Crimson F-81, Newburn H-23, and Weymouth A-45) are in overpressure regime. The deeper sediments within the area between the Shelburne G-29 well in the southwest and Shubenacadie H-100 well in the northeast do not lie within the overpressure regime.

7.4. Two Dimensional Petroleum System Modeling

7.4.1. Eastern Sable Subbasin (Seismic Lines A-A' and B-B')

- ❖ The sediments between the Annapolis G-24 and Crimson F-81 wells were possibly situated within a salt withdrawal area around 130-110 Ma. Thus, most of the Cretaceous to Miocene turbidite sands within the seismic lines A-A' and B-B' have bypassed the upper slope (allochthonous salt affected areas) to a water depth deeper than 2500 m. The Early Cretaceous 30 m thick porous sand reservoir within the Annapolis G-24 well is the only example of sand dispersal within this region,

- ❖ Two to three phases of hydrocarbon expulsion (170 Ma, 140 Ma, and 30-0 Ma) could be documented within various parts of seismic lines A-A' and B-B',
- ❖ Most of the earlier generated C15+ oil from the Early Jurassic and Jurassic Verrill Canyon source rocks have been cracked to condensate and dry gas due to the high maturity (>1.15% Ro) of the source rocks beyond 110 Ma. Thus, a volume expansion of hydrocarbons has occurred which could have triggered the overpressure within the existing reservoirs at least since 55 Ma. Currently, the hydrocarbons above the Annapolis G-24 reservoir are leaking. However, the reservoir hydrocarbons are being balanced by the liquid hydrocarbon charge within this reservoir from the oil prone Cretaceous Verrill source rock. Therefore, the overpressure is still being maintained.
- ❖ All Jurassic and Early Cretaceous reservoirs within both seismic lines lie within an overpressure regime. The Miocene conceptual reservoirs are mostly normal pressure or mild overpressure,
- ❖ All reservoirs contain more than 85% dry gas with 10-15% of wet gas and condensate. The Cretaceous and Jurassic reservoirs have an API of 64.8^{o} and a GOR of 183.1 m^3/m^3.

7.4.2. Western Sable Subbasin or Eastern Shelburne Subbasin (Seismic Lines C-C', D-D', and E-E')

- ✓ The timing of the rapid salt diapiric growth within the seismic lines C-C', D-D' and E-E' (western part of the Sable Subbasin and Eastern Shelburne Subbasin) coincides with the timing of the major expulsion of liquid hydrocarbons from early Jurassic and Jurassic Verrill Canyon source rocks after 110 Ma. The migration of C_{15+} oil from the Early Jurassic source rock began around 130 Ma.
- ✓ Two phases of hydrocarbon migrations could be documented from the Early Jurassic and Jurassic Verrill Canyon source rocks in the

seismic line E-E': the expulsion of the C_{15+} oil and C_6 to C_{14} light oil and condensate occurred around 130-110 Ma and the expulsion of both primary or secondary gas and condensate expulsion occurred between 75 Ma and 55 Ma from the cracking of C_{15+} oil from both those two source rocks (Early Jurassic and Jurassic Verrill Canyon). One phase of hydrocarbon expulsion (light oil, gas and condensate) could be observed within the seismic lines C-C' and D-D', which began around since 75 Ma. All three seismic lines, the Jurassic, Cretaceous and the Tertiary reservoirs were replenished with oil (Cretaceous Verrill Canyon source rock) and gas,

- ✓ The reservoirs were saturated with hydrocarbons between 75 Ma and 55 Ma on the seismic line E-E'. For seismic lines C-C' and D-D', the full hydrocarbon saturation within various conceptual reservoirs began comparatively later than line E-E' (between 75 Ma and 5.3 Ma),
- ✓ All properly identified turbidite channels (line E-E') and salt-flank or salt-top (line D-D') conceptual reservoirs have shown more than 90% hydrocarbon saturation,
- ✓ The genetic fingerprinting on the source rock to conceptual reservoir hydrocarbon composition suggests that all conceptual reservoir hydrocarbons (Late Jurassic, Early Cretaceous, and Early Miocene) are genetically related to the Early Jurassic and Jurassic Verrill Canyon source rocks.
- ✓ All conceptual reservoirs within the seismic line E-E' show more than 95% dry gas. Most of the Cretaceous and Tertiary conceptual reservoirs within the seismic lines C-C' and D-D' contain mixtures of 10-20% light oil (C_{10} and C_{20}), 20-30% condensate, and 50-70% dry gas,
- ✓ The conceptual reservoir hydrocarbons on line E-E' have an API of 50^o-58^o and a GOR of 343-158 m^3/m^3. The conceptual reservoir

hydrocarbons on lines C-C' and D-D' have an API of 48° to 59° API and GOR of 71 to 84 m^3/m^3

- ✓ The Early to Middle Cretaceous and Tertiary conceptual reservoirs of the three seismic lines lie within normal or mild overpressure regime. Most Jurassic conceptual reservoir hydrocarbons lie within an overpressure condition. The amount of overpressure in three seismic lines within this region is much lower compared to seismic lines A-A' and B-B'.

7.5 Mass Balance of Conceptual reservoir Hydrocarbons

The mass balance of conceptual reservoir hydrocarbons has established that three major source rocks (Early Jurassic, Jurassic Verrill Canyon, and Cretaceous Verrill Canyon) have contributed more than 90% of the total hydrocarbon masses accumulated within various conceptual reservoirs within the five seismic lines. The mass balance of hydrocarbons indicate that the Late Jurassic or Early Cretaceous conceptual reservoirs which occur as salt-top or salt-flank play types and the Tertiary conceptual reservoirs as salt-top or turbidite channel play types should be the best future exploration targets within this area between the Shubenacadie H-100 and the Shelburne G-29 wells. The expected conceptual reservoir hydrocarbons would be 60-70% dry gas, 20-30% condensate, and 10-20% light oil (C_{10} to C_{20} normal alkanes). In the eastern Sable Subbasin, the Late Jurassic conceptual reservoirs, which were formed as a deepwater channel play type or marine delta margin channel play type will not be affected by the salt movement. On the other hand, the Middle to Early Cretaceous turbidite play type on the northeastern side (shelf side) of the complex canopy system will be restricted to a water depth of less than 2000m. The Late Cretaceous to Early Tertiary deepwater turbidite channels could only occur beyond 2500 m water depth. The expected conceptual reservoir hydrocarbons will

contain 80-90% dry gas, 10-20% condensate, and 0-10% light oil. Sub-salt conceptual reservoirs may contain more than 20-30% condensate and light oil.

8. REFERENCES CITED

American Association of Testing and Materials (ASTM), 1991. Annual Book of Standards, Section 5, volume 5.05: gaseous fuels, coals, and coke, ASTM, Philadelphia, PA, 910 p.

Atlantic Geoscience Society. 2001. The Last Billion Years. Nimbus Publishing, Halifax, Nova Scotia, Canada, 212p.

Behar, F., M. Vandenbroucke, Y. Tang, F. Marquis, and J. Espitalie, 1997, Thermal cracking of kerogen in open and closed systems: determination of kinetic parameters and stoichiometric coefficients for oil and gas generation, *Org. Geochem.*, Vol. 26, No. 5/6, pp. 321-339.

Beaumont, C. Keen, C. E. and Boutillier, R. 1982. On the evolution of rifted continental margin: comparison of models and observations for the Nova Scotia margin. Gephys. J. R. Astr. Soc. V. 70, p. 667-715

Booth, J. R., DuVernay III, Pfeifer, D. S. and Styzen, M. J. 2000. Sequence statigraphic framework, depositional models and stacking pattern of ponded and slope fan systems in the Auger Basin, Central Gulf of Mexico. GCSSEPM Foundation 20th Annual Bob F. Perkins Research Conference, "Deep-water reservoirs of the world", December 3-6, 2000, Houston, Texas (CD-ROM), 82-103.

Bouma, A. R. and Scott, Erik, D. 2004. Source to Sink: The Importance of the Updip Coastal area in Defining Deep-Water sand Characteristics. 23rd Annual GCSSEPM Foundation Bob F. Perkins Research Conference "Shelf Margin Deltas and Linked Down Slope Petroleum Systems: Global Significance and Future Exploration Potential", p. 597-617

Bouma, A.H., Sprague, R.A. and Khan, A.M. 2002. Geological reservoir characteristics of fine-grained turbidite systems. GCAGS Transactions, v. 52, p. 59-64 (CD-ROM).

Braun, R.L., A.K. Burnham, J.G. Reynolds, and J.E. Clarkson, 1991, Pyrolysis Kinetics for Lacustrine and Marine Source Rocks by Programmed Micropyrolysis, *Energy & Fuels*, 5, pp. 192-204.

Burnham, A.K., R.L. Braun, H.R. Gregg, and A.M. Samoun, 1987, Comparison of methods for measuring kerogen pyrolysis rates and fitting kinetic parameters, *Energy & Fuels*, 1, pp. 452-458.

Burnham, A.K., R.L. Braun, and A.M. Samoun, 1988, Further comparison of methods for measuring kerogen pyrolysis rates and fitting kinetic parameters, In *Adv. Org. Geochem. 1987, Part II,* L. Nattavelli and L. Novelli, *eds.*, Pergamon Press, Oxford, pp. 839-846.

Burnham, *A. K.,* R. L. Braun, T.T. Coburn, E.I. Sandvik, B.J. Schmidt, R.A. Noble, 1996, An Appropriate Kinetic Model for Well-Preserved Algal Kerogens, *Energy Fuels*, No. 10, pp. 49-59.

Burnham, A. K. and Robert L. Braun, 1999, Global Kinetic Analysis of Complex Materials, Energy & Fuels, Vol. 13, No. 1, pp. 1-22.

Cummings, D. I. 2004. Sedimentology and Stratigraphy of an ancient progradational terrigenous clastic Shelf Margin, Missisauga Formation (Upper Jurassic-Lower Cretaceous), Offshore Nova Scotia, Canada. Unpublished PhD Thesis, University of Ottawa, Ottawa, Ontario, 201p.

Dehler, S.A. Keen, C.E., Funck, T., Jackson, H. R., and Louden K. E. 2004. The limit of volcanic rifting: A structural model across the volcanic and non-volcanic transition off Nova Scotia. EOS Tans. AGU, 85 (178), Jt. Assem. Suppl. Abstract T31D-04

Dow, W. G. 1977. Kerogen studies and geological interpretations. Jour. Geochem. Expl. V. 7, p. 133-157

Durand, B. 1980. Kerogen. Insoluble Organic Matter from Sedimentary Rocks. Technip Publication, Paris, 519p.

Ebinger, C.A. and Tucholke, B.E. 1988. Marine Geology of the Sohn Basin, Canadian Atlantic Margin. AAPG Bulletin, v. 72, no. 12, p.1450-1468.

Espitalie, J., Deroo, Cr., and Marquis, F. 1985. Rock-Eval pyrolysis and its applications. *Rep. Inst. Fr. Petrol.* 33878, 72p.

Espitalie, J. F. Marquis, and S. Drouet, 1993, Critical study of kinetic modeling parameters, in *Basin Modeling: Advances and Applications*, A.G. Dore *et al.*, *eds.*, Elsevier, Amsterdam.

Enachescu, M., 2005. Atlantic Canada's progress report, Atlantic Canada Business Magazine, 16(2), 13 pp.

Funck, T., Jackson, R.H., Louden, K.E., Dehler, S.A. and Wu, Y. 2004. Crustal structure of northern Nova Scotia rifted continental margin (eastern Canada). Jour. Geophy. Res.., v. 109, B09102-1 to 19.

Gradstein, F. M., Ogg, J. G. et al. 2004. A Geological Time Scale 2004. Cambridge University Press, 500 p.

Hogg, J. R., Dolph, D. A., MacKidd, D. and Michael, K. 2001. 2001. Petroleum Systems of the Deep Water Scotian salt Province, Offshore Nova Scotia, Canada. In "Petroleum Systems of the Deep-Water Basins", GCSSEPM Foundation 21st Annual Perkins Research Conference, Houston, Texas, p. 23-34.

Hunt, J.M. 1995. *Petroleum Geochemistry and Geology*. W. H. Freeman and Company, New York, 743p.

Ings, S., Beaumont, C. and Lykke, G. 2004. Numerical Modeling of Salt Tectonics on Passive Continental Margins: Preliminary Assessment of the Effects of Sediment Loading, Buoyancy, Margin Tilt, and Isotasy. In Post, P. J., Olson, D. L., Lyons, K. T., Palmes, S. L., Harrison, P. F., and Rosen, N. C., eds., Salt-sediment interactions and hydrocarbon prospectivity: concepts, applications, and case studies for the 21st century: 24th Annual GCSSEPM Foundation Bob F. Perkins Research Conference, p. 36-68.

Jackson, M. P. A., Hudec, M. R., and Jennette, D. C., 2004, Insights from a gravity-driven linked system in deep-water lower Congo Basin, Gabon. In Post, P. J., Olson, D. L., Lyons, K. T., Palmes, S. L., Harrison, P. F., and Rosen, N. C., eds., Salt-sediment interactions and hydrocarbon prospectivity: concepts, applications, and case studies for the 21st century: 24th Annual GCSSEPM Foundation Bob F. Perkins Research Conference, p. 735–752.

Jackson, M. P. A. and Vendeville, B. C. 1994. Regional extension as a geological trigger for diapirism: GSA Bulletin, v. 106, p. 57-73.

Jansa, L. F. and Wade, J. A. 1975. Geology of the continental margin off Nova Scotia and Newfoundland: offshore geology of Eastern Canada, Volume 2 – Regional Geology, Geological Survey of Canada Paper 74-30, p. 51-106.

Jarvie, D.M. 1998. Factors affecting Rock-Eval derived kinetic parameters, Chemical Geology, Vol. 93, p. 79-99.

Jarvie, D. M. and D. Wavrek. 1996. Comparison of the timing of hydrocarbon generation for major petroleum source rocks in North and South America, 1996 II AAPG/SVG International Meeting, Caracas, Venezuela, September 6, 1996, *poster presentation*.

Jarvie, Daniel M., P. R. Walker, W. D. Weldon, and B. Leroux. 1998 Evaluation of Decomposition Reaction Mechanisms and Pathways using Quantitative Closed System Pyrolysis and High Resolution Gas Chromatography, Pittsburgh Conference on Analytical Chemistry and Applied Spectroscopy, paper 2160P, New Orleans, La.

Jarvie, D. M., B. Leroux, P.R. Walker, and W.D. Weldon, 1998. Experimentally-derived gas and oil generation yields and kinetics on source rocks, Williston Basin, 8th International Williston Basin Symposium, Regina, Saskatchewan, *oral presentation*.

Jarvie, D. M., B. Leroux, W. D. Weldon, P. R. Walker, and D. A. Wavrek. 1999. Compositional Kinetic Parameters and Yields from Oil and Gas Prone Source Rocks and Oil Asphaltene Fractions, 19th International Meeting on Organic Geochemistry, Istanbul, Turkey, *poster presentation.*

Jarvie, D. M. and L. L. Lundell, 2000. Amount, type, and kinetics of thermal transformation of organic matter in the Miocene Monterey Formation, *in* The Monterey Formation: From Rocks to Molecules, Caroline M. Isaacs and Jurgen Rullkotter, *eds.*, Chapter 15: Columbia University Press.

Kendrick, J.W. 2000. Turbidite reservoir architecture in the northern Gulf of Mexico deepwater: Insights from the development of Auger, Tahoe, and Ram/Powell Fields. GCSSEPM Foundation 20th Annual Bob F. Perkins Research Conference, “Deep-water reservoirs of the world”, December 3-6, 2000, Houston, Texas (CD-ROM), 450-468.

Kidston, A.G., Brown, D. E., Smith, B.M. and Altheim, B. 2005. The Upper Jurassic Abenaki Formation Offshore Nova Scotia: A Seismic and geologic Perspective. Canada Nova Scotia Offshore Petroleum Board Resource Assessment Report (CD-ROM), 168p.

Kidston, A.G., Brown, D. E., Altheim, B. and Smith, B.M. 2002, Hydrocarbon Potential of the Deepwater Scotian Slope. Canada Nova Scotia Offshore Petroleum Board Resource Assessment Report (CD-ROM), 111p.

Louden, K., Helen, L, Funck, T. and Wu, J. 2005. Large-scale structural variations across the eastern Canadian Continental Margins: Documenting

the Rift-to-Drift Transition. 25th Annual Annual GCS-SEPM Bob. F. Perkins Research Conference: Petroleum Systems of the Divergent Continental Margin Basins, p. 1-12 (CD-ROM)
.
Louden, K. 2002. Tectonic evolution of the east coast of Canada CSEG Recorder, February, 2002, p. 37-48.

MacDonald, A. W. 2006. Cenozoic seismic stratigraphy of the central Nova Scotian Margin: the interplay of erosion, deposition, and salt tectonics. Unpublished M. Sc thesis, St. Mary's University, Halifax, Nova Scotia, Canada, 152 p.

Morgan, P. and Gosnold, W. D. 1989. Heat flow and thermal regimes in the continental United States. In Pakiser, L. C. and Mooney, W. D., Geophysical Framework of the continental United States: Boulder, Colorado, Geological Society of America Memoir 172, p. 493-521.

Mukhopadhyay, P. K., Harvey, P. J. and Kendell, K. in press. Genetic Relationship between Salt Mobilization and Petroleum System Parameters: Possible Solution of finding Commercial Oil and Gas within Offshore Nova Scotia, Canada during the Next Phase of Deepwater Exploration Proceedings of the GCAGS Conference, Lafayette, New Orleans, September 2006.

Mukhopadhyay, P. K. Harvey, P. J. and Brown, D. E. 2005. Re-evaluation of the Petroleum Systems of the Scotian Slope, Eastern Canada Based on Recent Drilling within Deepwater Nova Scotia. Annual Convention of AAPG Abstract, Calgary, Alberta.

Mukhopadhyay, P. K., Brown, D. E., Kidston, A. G., Bowman, T, D., Faber, J. and Harvey, P.J. 2003. Petroleum Systems of Deepwater Scotian Basin, Eastern Canada: Challenges for Finding Oil versus Gas Provinces. Proceedings 2003 Offshore Technology Conference, Paper Number 15304, p. 1-11.

Mukhopadhyay, P. K., Wade, J. A., Kruge, M. A.,, Samoun, A. and Harvey, P. J. 2002. Deepwater petroleum system of Jurassic-Tertiary sediments of the Scotian Basin, offshore Nova Scotia, eastern Canada. AAPG Annual Meeting Abstract, March 10-13, 2002, Houston, Texas.

Mukhopadhyay, P. K. (Muki) and Wygrala, B. 2001. How to avoid dry holes in deepwater Scotian Basin? Implications of Geochemical Interpretations and Petroleum Systems Modeling. Abstract CIM Research Talks at the Nova Scotia Oil & Gas Conference (Core Conference).

Mukhopadhyay, P. K., Wade, J. A. and Kruge, M. A. 2000. Petroleum Systems of the Scotian Basin, Offshore Eastern Canada and its Implications for Future Prospects in the Shelf Break and Slope Areas. AAPG Annual Convention Extended Abstract, New Orleans, Louisiana

Mukhopadhyay, P. K., Wade, J. A. and Kruge, M. A. 1995. Organic facies and maturation of Jurassic/Cretaceous rocks, possible oil-source rock correlation based on pyrolysis of asphaltenes, Scotian Basin, Canada. *Org. Geochem.* 22 (1), p. 85-104.

Mukhopadhyay, P.K. and Wade, J.A. 1993. A review of the organic matter type, maturity and hydrocarbon source potential of deep ocean basin sediments from central North Atlantic". Geological Survey of Canada Open File Report No. 3156.

Mukhopadhyay, P. K. and Wade, J. A. 1990. Organic facies and maturation of sediments from the three Scotian Shelf Wells. *Bull. Can. Petrol. Geol.* 38 (4), 407-424.

Mukhopadhyay, P. K. 2000. Petroleum Systems of the Scotian Basin – A Review. Confidential Report of Global Geoenergy Research Limited for various North American oil companies. 305 p.

Mukhopadhyay, P.K. 2002. Evaluation of Petroleum Systems for Five Dummy Wells From Various Seismic Sections of the Scotian Slope, Offshore Nova Scotia, Based on One-Dimensional Numerical Modeling and Using Geochemical Concepts. Canada-Nova Scotia Offshore Petroleum Board Confidential Internal Report.

Mukhopadhyay, P. K. 1994. Vitrinite Reflectance as Maturity Parameter: Petrographic and Molecular Characterization and its Applications to Basin Modeling. In P. K. Mukhopadhyay and W. G. Dow (Editors), Vitrinite Reflectance as a Maturity Parameter: Applications and Limitations. American Chemical Society Symposium series 570, p. 1-25. Washington, D. C.

Mukhopadhyay, P. K. 1992. Maturation of organic matter as revealed by microscopic methods: applications and limitations of vitrinite reflectance, continuous spectral and laser fluorescence spectroscopy. In *Diagenesis III, Developments in Sedimentology 47* (K. H. Wolf, and G. V. Chilingar Editors), Elsevier Publication, Amsterdam, Chapter 9, Pp. 435-510.

Mukhopadhyay, P. K. 1990. Evaluation of organic facies of the Verrill Canyon Formation, Sable Subbasin, Scotian Shelf. Geological Survey of Canada Open File Report 2435.

Murphy, R. K., McPherson, S., Segall, M. P., Nemcok, M., Allen, R. B. and Abrams, M. A. 2002. "Sediment Distribution and Dispersal in the Deepwater Scotian Margin: Key Controls for Sediment Influx to the Deep Basin". Abstract of the CIM Petroleum Society - Halifax Section Sixth Annual Petroleum Technical Seminars. Brown, D.E., (ed.), Halifax, Nova Scotia, Canada, 82p.

ONAREP, 2000. Hydrocarbon Exploration opportunities in Morocco. Kingdom of Morocco, Office National des Recherches et d'Exploitations Petrolieres (ONAREP); CD-ROM.

Rullkotter, J., Mukhopadhyay, P. K., Disko, U., Schaefer, R. G., and Welte, D. H. 1986. „Facies and diagenesis of organic matter in deep sea sediments from Blake Outer Ridge and Blake Bahama Basin, western North Atlatic": In Degens, E. T. et al. (Eds), *Biogeochemistry of Black Shales,* University of Hamburg Special Publication, v. **60**, p. 179-203.

Peters, K.E., Walters, C.C. and Moldowan, J.M. 2005. The Biomarkers Volume I. Biomarkers and Isotopes in the Environment and Human History. Cambridge University Press, 471p.

Peters, K. 1986. Guidelines for evaluating petroleum source rock using programmed pyrolysis. Bull. Amer. Assoc. Pet. Geol. V. 70, p. 318-329.

Pettingill, H. S. and Weimer, P. 2001. Worldwide Deep-water Exploration and Production: Past, Present, and Future. In. Fillion et al. (Eds.). Petroleum Systems of Deepwater Basins: Global and Gulf of Mexico Experience. Gulf Coast Society of Economic paleontologists and Mineralogists Foundation, 21st Annual Bob F. Perkins Research Conference, December 2-5, 2001, Houston, Texas (CD-ROM).

Powell, T. G.1985. "Paleogeographic implications for the distribution of upper Jurassic source beds: Offshore Eastern Canada". *Bull. Can. Pet. Geol.* **33 (1)**, 116-119.

Royden, L. and Keen, C. E. 1980. Rifting process and thermal evolution of the continental margin of eastern Canada determined from subsidence curves. Earth and Planetary Sc. Lett. v. 51, p. 343-361.

Rowan, M. G. Practical Salt Tectonics. 2002. Short Course Note Book, CIM-Petroleum Society, Halifax Section, October 7-8, 2002, Halifax, Nova Scotia, Canada.

Rowan, M. G. 1995, Structural styles and evolution of allochthonous salt, central Louisiana outer shelf and upper slope. In. Jackson, M. P. A. et al. (Eds.) Salt Tectonics: a global perspective: AAPG Memoir 65, p. 199-228.

Rullkotter, J. and Mukhopadhyay, P. K. 1986. "Comparison of Mesozoic carbonaceous claystones in the western and eastern North Atlantic (DSDP Legs 76, 79, and 93)": In (Summerhayes, C. P. and Shackleton, N. J. (Eds.) *North Atlantic Paleoceanography*. Geological Society of London Special Publication, v. **22**, p. 377-387.

Rullkotter, J., Mukhopadhyay, P. K., Schaefer, R. G., and Welte, D. H. 1984. "Geochemistry and petrography of organic matter in sediments from Deep Sea Drilling Project Sites 545 and 547, Mazagan Escarpment", In Hinz, K. et al. (Eds) *Initial Report of DSDP Leg 79*, p. 775-806.

Shimeld, J. W. 2004. A comparison of Salt Tectonic Subprovinces beneath the Scotian Slope and Laurentian Fan. 24th Annual GCS-SEPM Foundation Bob F. Perkins Research Conference, Houston, pp 502-532, CD-ROM.

Shimeld, J. W. 2004, A comparison of Salt Tectonic Subprovinces beneath the Scotian Slope and Laurentian Fan. 24th Annual GCS-SEPM Foundation Bob F. Perkins Research Conference, Houston, pp 502-532, CD-ROM.

Stach, E., Mackowsky, M. Th., Teichmuller, M., Taylor, G. H., Chandra, D., and Teichmuller, R. (1982) *Textbook of Coal Petrology*. 3rd Ed. 536 p. Borntraeger, Stuttgart.

Sundararaman, P., P.H. Merz, and R.G. Mann, 1992, Determination of kerogen activation energy distribution, *Energy & Fuels*, Vol. 6, p. 793-803.

Tang, Y. and M. Stauffer, 1994, Multiple Cold Trap Pyrolysis Gas Chromatography: a new technique for modeling hydrocarbon generation, in *Advances in Organic Geochemistry 1993*, *Org. Geochem.* Vol. 22, No. 3-5, p. 863-872.

Tang, Y. and M. Stauffer, 1994, Development of Multiple Cold Trap Pyrolysis, *J. Appl. Anal. Pyrolysis*, Vol. 28, pp. 167-174.

Tari, G., Coterill, K, Kaminski, M., Molnar, J. and Valasek, D. 2006. Deep-water exploration in Morocco: What did not work so far and what may work in the near future? Abstract at the Nova Scotia Energy Forum 2006, Antigonish, Nova Scotia.

Tari, G.C. Molner, J. and Thompson, P. 2005. Salt tectonics in the Ras Tafelney-Safi segment of the Moroccan Atlantic margin. Abstract, Halifax 2005, GAC-MAC-CSPG-CSSS Conference and Exhibition Technical Program.

Tegelaar, Erik. and R. A. Noble, 1994, Kinetics of hydrocarbon generation as a function of the molecular structure of kerogen as revealed by pyrolysis-gas chromatography, in *Adv. Org. Geochem. 1993*, Nils Telnaes, Ger van Graas, and Kjell Oygard, eds., pp. 543-574.

Tissot, B. and Welte, D. H. (1984) *Petroleum Formation and Occurrence*. Springer-Verlag, Berlin, 699 p.

Ungerer, P. and R. Pelet, 1987, Extrapolation of the kinetics of oil and gas formation from laboratory experiments to sedimentary basins, *Nature*, 27, pp. 52-54.

Wade, J. A., MacLean, B.C. and Williams, G.L. 1995. Mesozoic and Cenozoic stratigraphy, eastern Scotian Shelf: new interpretation. Can. Jour. Earth Sc. v. 32, p. 1462-1473.

Wade, J. A. and MacLean, B.C. 1990. Aspects of the geology of the Scotian Basin from recent seismic and well data. In Keen, M. J. and Williams, G. L. (Eds.). Geology of the Continental Margin of Eastern Canada, Geology of Canada, Part 2, p. 167- 238.

Wade, J. A., Campbell, G.R., Procter, R.M., and Taylor, G.C. 1989. Petroleum Resources of the Scotian Shelf. Geological Survey of Canada Paper 88-10, 26p, English version.

Waltham, D. and Davison, I. 2001. Obstacles and sinks: Effects on Turbidite flow on Deepwater Continental Margins. 21st Annual GCS-SEPM Bob. F. Perkins Research Conference: Petroleum Systems of the Deep-Water Basins, p. 511-522 (CD-ROM)

Waples, D.W., 2000. The kinetics of in-reservoir oil destruction and gas formation: constraints from experimental and empirical data, and from thermodynamics, *Org. Geochem.*, Vol. 31, No. 6, p. 553-575.

Wels ink, N. J., J. D. Dwyer, and R. J. Knight, 1989. Tectono-stratigraphy of the Passive margin, Offshore Nova Scotia", In Extensional Tectonics and Stratigraphy of the North Atlantic Margin. *Amer. Assoc. Pet. Geol. Memoir* 46, p. 215-231.

Wu, Y., Louden, K.E., Funck, T., Jackson, H.R., and Dehler, S.A., Crustal structure of the central Nova Scotia margin off Eastern Canada, Geophy. J. Int., in press.

Young, J.L., 2005. The stratigraphic and structural history of the Mesozoic and Cenozoic of the Central Nova Scotian Slope, Eastern Canada. Unpublished M. Sc thesis, Memorial University, 229 p.

Young, J. L., Enachescu, M. E., Calon. T. J. and Pulham, A. J, 2005, Mesozoic through Cenozoic evolution of the central Scotian Slope Basin, offshore Eastern Canada, Abstract, Halifax 2005, GAC-MAC-CSPG-CSSS Conference and Exhibition Technical Program, p. 214-215.

Tables

Table 1. Rock-Eval Pyrolysis and TOC Data of Five Wells

(Wells: Alma K-85, Annapolis G-24, Torbrook C-15, and Weymouth A-45)

Well Name	Median Depth	LECO TOC	S1	S2	S3	Tmax	Hydrogen Index	Oxygen Index	Production Index
Annapolis G-24	4550	4.56	33.13	5.76	0.93	431	126	20	0.85
Alma K-85	3520	2.43	11.38	6.62	0.64	425	272	26	0.64
Torbrook C-15	2665	1.64	0.21	4.25	1.15	355	259	70	0.05
Torbrook C-15	2955	1.85	0.33	5.31	1.39	353	287	75	0.06
Torbrook C-15	3135	1.46	0.18	3.65	1.13	350	250	77	0.05
Torbrook C-15	3245	1.50	0.17	3.69	0.93	360	246	62	0.04
Torbrook C-15	3495	1.59	0.22	4.03	0.96	362	253	60	0.05
Torbrook C-15	3535	1.51	0.20	3.52	0.88	359	233	58	0.05
Torbrook C-15	3600	1.71	0.31	4.86	1.10	429	284	64	0.06
Weymouth A-45	4415	1.06	0.19	1.92	0.84	427	181	79	0.09
Weymouth A-45	4505	1.38	0.10	1.11	0.70	433	80	51	0.08
Weymouth A-45	4750	1.11	0.09	0.82	0.79	431	74	71	0.10
Weymouth A-45	5110	1.42	0.16	1.77	0.81	435	125	57	0.08
Weymouth A-45	5383	2.02	0.20	2.59	0.48	435	128	24	0.07
Weymouth A-45	5501	1.79	0.20	2.30	0.84	432	128	47	0.08
Weymouth A-45	5760	0.92	0.19	2.17	0.69	430	236	75	0.08
Weymouth A-45	5915	1.37	0.24	2.68	0.76	434	196	55	0.08
Weymouth A-45	6182	1.30	0.27	4.38	0.53	449	337	41	0.06
Weymouth A-45	6380	1.85	0.32	4.09	1.19	426	221	64	0.07
Weymouth A-45	6450	1.26	0.25	3.16	0.66	446	251	52	0.07
Weymouth A-45	6520	1.45	0.26	3.46	0.78	444	239	54	0.07
Weymouth A-45	6080	0.76	0.14	1.43	0.35	445	188	46	0.09
Weymouth A-45	6134	1.50	0.25	3.95	1.24	426	263	83	0.06
Weymouth A-45	6156	1.19	0.24	2.98	0.91	440	250	76	0.07
Weymouth A-45	6206	1.55	0.24	4.76	0.70	440	307	45	0.05
Weymouth A-45	6306	1.18	0.28	3.52	1.04	441	298	88	0.07
Weymouth A-45	6410	1.32	0.27	4.00	0.80	446	303	61	0.06
Weymouth A-45	6482	1.37	0.24	3.41	0.53	440	249	39	0.07
Weymouth A-45	6504	1.27	0.28	4.40	0.90	444	346	71	0.06
Weymouth A-45	6512	1.30	0.32	4.15	1.17	445	319	90	0.07

Table 2: Vitrinite Reflectance Data: 30 samples, Scotian Slope, Offshore Nova Scotia

Well Name	Depth	% Ro	Std.	Number of Vitrinite Grains Measured and Types					
	(m)	(mean Vit Ro)	Dev.	Total No.	Supp. Vit	Auto. Vit.	Allo. Vit.	Maturity	Comments
Crimson F-81	6025	0.65	0.09	21	1	10	10	Mature	Abundant recycled or corroded vitrinite grains
(4 samples)	6225	0.79	0.07	50	0	14	36	Mature	Abundant recycled or corroded vitrinite grains
	6670	0.9	0.09	50	6	21	23	Mature	Abundant recycled or corroded vitrinite grains
	6740	0.94	0.08	50	24	25	1	Mature	Abundant suppressed vitrinite grains
Torbrook C-15	2665	0.29	0.06	50	0	6	46	Immature	Abundant recycled or corroded vitrinite grains
(7 samples)	2955	0.32	0.05	50	0	15	35	Immature	Abundant recycled or corroded vitrinite grains
	3125	0.34	0.04	50	2	12	36	Immature	Abundant recycled or corroded vitrinite grains
	3245	0.35	0.05	50	0	16	34	Immature	Abundant recycled or corroded vitrinite grains
	3495	0.37	0.08	23	1	16	6	Immature	Low amount of vitrinite grains
	3535	0.36	0.06	21	1	12	8	Immature	Low amount of vitrinite grains
	3600	0.36	0.05	50	7	18	25	Immature	Abundant recycled or corroded vitrinite grains
Weymouth A-15	4415	0.3	0.03	50	0	26	24	Immature	Abundant recycled or corroded vitrinite grains
(19 samples)	4505	0.32	0.04	50	0	36	14	Immature	Vitrinite grains are well preserved
	4750	0.37	0.04	51	1	26	25	Immature	Abundant recycled or corroded vitrinite grains
	5110	0.42	0.04	50	0	29	21	Immature	Vitrinite grains are well preserved; AOM 2 abundant
	5383	0.45	0.03	50	0	34	16	Immature	Vitrinite grains are well preserved; AOM 2 abundant
	5501	0.39	0.03	51	0	19	33	Immature	Abundant recycled or corroded vitrinite grains
	5760	0.52	0.05	50	1	17	32	Mature	Abundant recycled or corroded vitrinite grains
	5915	0.56	0.05	50	0	25	25	Mature	Abundant recycled or corroded vitrinite grains
	6080	0.58	0.09	50	0	38	12	Mature	Vitrinite grains are well preserved; AOM 2 abundant
	6156	0.65	0.11	50	0	19	31	Mature	Abundant recycled or corroded vitrinite grains
	6182	0.62	0.06	50	5	14	31	Mature	Abundant recycled or corroded vitrinite grains
	6206	0.67	0.08	50	3	27	20	Mature	Vitrinite grains are well preserved; AOM 2 abundant
	6306	0.72	0.07	50	5	15	30	Mature	Abundant recycled or corroded vitrinite grains
	6380	0.73	0.05	50	2	11	37	Mature	Abundant recycled or corroded vitrinite grains
	6410	0.73	0.03	42	13	10	19	Mature	Less recycled or corroded vitrinite grains
	6450	0.76	0.08	50	1	21	28	Mature	Abundant recycled or corroded vitrinite grains
	6504	0.78	0.09	50	1	15	34	Mature	Abundant recycled or corroded vitrinite grains
	6512	0.79	0.1	50	8	16	26	Mature	Abundant recycled or corroded vitrinite grains
	6520	0.8	0.07	50	9	31	10	Mature	Vitrinite grains are well preserved; AOM 2 abundant

% Ro = Mean random vitrinite reflectance; Std. Dev. - Standard Deviation									
Total No. = Total number of vitrinite grains measured; Supp. Vit. = Suppressed vitrinite or solid bitumen									
Auto. Vit. = Autochthonous or 1st cycle vitrinite; Allo. Vit. = Allochthonous Vitrinite or Recycled Vitrinite									

Weymouth A-45 6206 m.											
	Basic Geochemical Data										
	TOC	**S1**	**S2**	**S3**	**Tmax**	**Cal. VRo**	**HI**	**OI**	**S2 / S3**	**PI**	**S1/TOC**
	1.55	0.24	4.76	0.70	440	0.76	307	45	7	0.05	15

TOC in weight percent
S1 volatile hydrocarbons in milligrams of hydrocarbons per gram of rock
S2 pyrolysis hydrocarbons in milligrams of hydrocarbons per gram of rock
S3 in milligrams carbon dioxide per gram of rock
Tmax of S2 peak in ^{o}C
Cal. VRo is based on Tmax using the equation of Jarvie et al. (2001)
HI (hydrogen index) in milligrams of hydrocarbon per gram of TOC
OI (oxygen index) in milligrams of carbon dioxide per gram of TOC
PI (production index) (unitless)
S1/TOC (x 100) in milligrams of volatile hydrocarbons per gram of TOC

Weymouth A-45 6206 m.										
Fraction:	**Total**		**C_{15}+**		**C_6-C_{14}**		**C_2-C_5**		**C_1**	
Arrhenius factor :	1.05E+14 /sec		7.50E+12 /sec		2.10E+13 /sec		2.30E+14 /sec		1.10E+15 /sec	
Reactant No.	**%**	**Activation Energy (cal/mole)**	**%**	**Activation Energy (cal/mole)**	**%**	**Activation Energy (cal/mole)**	**%**	**Activation Energy (cal/mole)**	**%**	**Activation Energy (cal/mole)**
1	0.11	44000	0.22	46060	0.22	49914	0.22	50869	0.15	50952
2	0.79	45000	0.88	46550	0.88	50445	0.88	51708	0.38	51724
3	0.71	46000	2.70	47040	2.70	50976	2.70	52546	0.87	52496
4	1.93	47000	6.48	47530	6.48	51507	6.48	53385	1.80	53268
5	0.85	48000	12.10	48020	12.10	52038	12.10	54223	3.32	54040
6	4.31	49000	17.60	48510	17.60	52569	17.60	55062	5.47	54812
7	2.26	50000	20.05	49000	20.05	53100	20.05	55900	8.07	55584
8	6.54	51000	17.60	49490	17.60	53631	17.60	56739	10.65	56356
9	3.80	52000	12.10	49980	12.10	54162	12.10	57577	12.58	57128
10	11.48	53000	6.48	50470	6.48	54693	6.48	58416	13.45	57900
11	12.27	54000	2.70	50960	2.70	55224	2.70	59254	12.58	58672
12	28.28	55000	0.88	51450	0.88	55755	0.88	60093	10.65	59444
13	15.69	56000	0.22	51940	0.22	56286	0.22	60931	8.07	60216
14	8.10	57000							5.47	60988
15	1.05	58000							3.32	61760
16	1.28	60000							1.80	62532
17	0.55	64000							0.87	63304
18									0.38	64076
19									0.15	64848
20										
21										
22										
23										
24										
25										
Total:	100.00		100.00		100.00		100.00		100.00	

Note : Each Fraction equals to 100%

CONSTANT HEATING RATE MODEL RESULTS

1°C/my using Gaussian kinetic results

Weymouth A-45 6206 m.										
	TOTAL		C_{15}+		C_6-C_{14}		C_2-C_5		C_1	
Conversion	Computed Temperature (°C)	Computed Vitrinite Reflectance (%R_o)	Computed Temperature (°C)	Computed Vitrinite Reflectance (%R_o)	Computed Temperature (°C)	Computed Vitrinite Reflectance (%R_o)	Computed Temperature (°C)	Computed Vitrinite Reflectance (%R_o)	Computed Temperature (°C)	Computed Vitrinite Reflectance (%R_o)
10% TR	116	0.66	110	0.63	136	0.81	137	0.82	138	0.83
50% TR	151	0.99	125	0.73	151	0.99	157	1.10	162	1.17
90% TR	170	1.32	138	0.83	165	1.22	176	1.43	186	1.65

TR = transformation ratio computed from Gaussian kinetic model results by fraction

Alma K-85 3520 m. (cuttings)											
	Basic Geochemical Data										
	TOC	**S1**	**S2**	**S3**	**Tmax**	**Cal. VRo**	**HI**	**OI**	**S2 / S3**	**PI**	**S1/TOC**
	2.43	11.38	6.62	0.64	425	0.49	272	26	10	0.63	468

TOC in weight percent
S1 volatile hydrocarbons in milligrams of hydrocarbons per gram of rock
S2 pyrolysis hydrocarbons in milligrams of hydrocarbons per gram of rock
S3 in milligrams carbon dioxide per gram of rock
Tmax of S2 peak in ^{o}C
Cal. VRo is based on Tmax using the equation of Jarvie et al. (2001)
HI (hydrogen index) in milligrams of hydrocarbon per gram of TOC
OI (oxygen index) in milligrams of carbon dioxide per gram of TOC
PI (production index) (unitless)
S1/TOC (x 100) in milligrams of volatile hydrocarbons per gram of TOC

GAUSSIAN COMPOSITIONAL KINETIC RESULTS

Well: Alma K-85
Depth: 3520 m

Alma K-85 3520 m. (cuttings)										
Fraction:	**Total**		**C_{15}+**		**C_6-C_{14}**		**C_2-C_5**		**C_1**	
Arrhenius factor :	2.85E+13 /sec		8.00E+11 /sec		8.50E+12 /sec		8.60E+14 /sec		9.00E+14 /sec	
Reactant No.	**%**	**Activation Energy (cal/mole)**	**%**	**Activation Energy (cal/mole)**	**%**	**Activation Energy (cal/mole)**	**%**	**Activation Energy (cal/mole)**	**%**	**Activation Energy (cal/mole)**
1	2.02	44000	0.15	39015	0.22	48316	0.22	52263	0.15	51216
2	3.25	45000	0.38	39780	0.88	48830	0.88	52969	0.38	51992
3	4.40	46000	0.87	40545	2.70	49344	2.70	53675	0.87	52768
4	6.68	47000	1.80	41310	6.48	49858	6.48	54381	1.80	53544
5	4.31	48000	3.32	42075	12.10	50372	12.10	55088	3.32	54320
6	11.48	49000	5.47	42840	17.60	50886	17.60	55794	5.47	55096
7	5.76	50000	8.07	43605	20.05	51400	20.05	56500	8.07	55872
8	20.67	51000	10.65	44370	17.60	51914	17.60	57206	10.65	56648
9	12.11	52000	12.58	45135	12.10	52428	12.10	57913	12.58	57424
10	28.93	53000	13.45	45900	6.48	52942	6.48	58619	13.45	58200
11	0.39	56000	12.58	46665	2.70	53456	2.70	59325	12.58	58976
12			10.65	47430	0.88	53970	0.88	60031	10.65	59752
13			8.07	48195	0.22	54484	0.22	60738	8.07	60528
14			5.47	48960					5.47	61304
15			3.32	49725					3.32	62080
16			1.80	50490					1.80	62856
17			0.87	51255					0.87	63632
18			0.38	52020					0.38	64408
19			0.15	52785					0.15	65184
20										
21										
22										
23										
24										
25										
Total:	100.00		100.00		100.00		100.00		100.00	

Table 4b

Note: Each fraction equals 100%

CONSTANT HEATING RATE MODEL RESULTS

1°C/my using Gaussian kinetic results

Alma K-85 3520 m. (cuttings)										
	TOTAL		C_{15}+		C_6-C_{14}		C_2-C_5		C_1	
Conversion	Computed Temperature (°C)	Computed Vitrinite Reflectance (%R_o)	Computed Temperature (°C)	Computed Vitrinite Reflectance (%R_o)	Computed Temperature (°C)	Computed Vitrinite Reflectance (%R_o)	Computed Temperature (°C)	Computed Vitrinite Reflectance (%R_o)	Computed Temperature (°C)	Computed Vitrinite Reflectance (%R_o)
10% TR	96	0.52	87	0.47	128	0.75	136	0.81	141	0.86
50% TR	132	0.77	113	0.64	144	0.89	153	1.03	165	1.22
90% TR	152	1.01	140	0.85	157	1.10	169	1.30	190	1.74

TR = transformation ratio computed from Gaussian kinetic model results by fraction

Table 5. Scotian Slope Wells: Formation Tops														
Well Name	UW1	X World Axis	Y World Axis	Water Depth	End	Top Mio.	Top Eoc.	Top Cret.	Top L.Can	Top Miss.	Top Jura	Mid Jura	Mid-Early Jura	
				(m)	Depth (m)									
Acadia K-62	300 K62 43000 6145(	588443	4745870	866.3	5287	1410	2094	2508	2784	2878	3306	4086	4950	
Albatross B-13	300 B13 42500 6300(	497000	4727620	1341	4045	1900	1990	2373	2420	2468	2570	3855		
Annapolis G-24	300 G24 43300 5945(	758528	4808830	1678.5	6182	2060	2682	3457	3490	4332				
Balvenie B-79	300 B79 43100 6000(	729167	4779300	1803	4750	2920	3000	3565	3820					
Crimson F-81	300 F81 43202 5942[5]	766224	4803550	2091	6676		3298	3560	3880	4901				
Evangeline H-98	300 H98 43200 6045(	663816	4794870	174	5048	995	1500	1665	2824					
Newburn H-23	300 H23 43200 6045(	678253	4785650	977	6070	1890	2519	2850	3340	4570				
Shelburne G-29	300 G29 42400 6330(	454146	4720860	1153.5	4005	2040	2340	2670	3210	3750				
Shubenacadie H-1(	300 H00 42500 6115(	624366	4742240	1476.5	4200	2580	3060	3485	3990					
Tantallon M-41	300 M41 44000 5815	800000	4855790	1516	5602	2350	2550	3130	3210	4155				
Torbrook C-15	300 C15 42340 6217[3]	558004	4712810	1674.5	3600									
Weymouth A-45	300 A45 43040 6036[1]	695036	4770820	1690.3	6520									
Top Mio. = Top Miocene; Top Eoc. = Top Eocene; Top Cret. = Top Cretaceous; Top L.Can. = Top Logan Canyon Formation; Top Miss. = Top Missisauga Formation; Top Jura. = Top Jurassic														
Mid Jura = Middle Jurassic period; Mid-Early Jura = early to middle Jurassic period														

Table 6. Proportions of various lithologies forming various *Lithology Mix*											
(used as the input parameter within the PetroBuilder Module of the Petroleum System Modeling)											
Mix Name	**Sandstone**	**Shale**	**Siltstone**	**Limestone**	**Marl**	**Chalk**	**Dolomite**	**Anhydrite**	**Salt**	**Type Well**	**Formation**
	(%)	**(%)**	**(%)**	**(%)**	**(%)**	**(%)**	**(%)**	**(%)**	**(%)**	**(%)**	**(%)**
Lithology Mix 1	**10**	**50**	**20**	**10**	**10**					**Tantallon M-41**	**Banquereau-L.Paleocene**
Lithology Mix 2	**20**	**45**	**5**	**25**		**5**				**Annapolis G-24**	**Naskapi-Base Target**
Lithology Mix 3		**60**	**15**	**5**			**15**	**5**		**Annapolis G-24**	**CVC 2 - Hauterivian**
Lithology Mix 4	**20**	**80**								**Balvenie B-79**	**Logan Canyon-M.Albian**
Lithology Mix 5	**2**	**80**	**10**		**8**					**Annapolis G-24**	**Barremian-K40**
Lithology Mix 6	**10**	**75**	**15**							**Acadia K-62**	**Mid-Late Eocene**
Lithology Mix 7		**90**	**10**							**Crimson F-81**	**Logan Canyon-K30**
Lithology Mix 8	**20**	**40**	**40**							**Annapolis G-24**	**CVCRes-Hauterivian**
Lithology Mix 9		**90**	**5**		**5**					**Newburn H-23**	**Plio-Pleistocene**
Lithology Mix 10		**90**			**10**					**Newburn H-23**	**Banquereau-E_M.Miocene**
Lithology Mix 11	**10**	**50**	**40**							**Crimson F-81**	**Missisauga - L. Sand**
Lithology Mix 12	**40**	**50**	**10**							**Annapolis G-24**	**E.Cret.-M.Sand**
Lithology Mix 14	**10**	**50**	**30**	**10**						**Balvenie B-79**	**Logan Canyon - E.Cenoman.**
Lithology Mix 14_1	**10**	**50**	**30**		**10**					**Annapolis G-24**	**E. Cret.-Base Up. Target**
Lithology Mix 15		**50**		**25**	**25**					**Newburn H-23**	**Wyandot-Dawson Canyon**
Lithology Mix 17		**80**		**10**	**10**					**Newburn H-23**	**L.Cretaceous_E.Mastrict.**
Lithology Mix 18		**50**	**35**	**10**	**5**					**Shubenacadie H-100**	**Wyandot-Dawson Canyon**
Lithology Mix 19		**50**	**10**			**40**				**Acadia K-62**	**Wyandot**
Lithology Mix 20	**5**	**65**	**30**							**Acadia K-62**	**Late Miocene**
Lithology Mix 21	**5**	**75**	**15**		**5**					**Crimson F-81**	**Missisauga - H. Sand**
Lithology Mix 22	**10**	**70**	**20**							**Crimson F-81**	**Missisauga - M. Sand**
Lithology Mix 23	**25**	**50**	**15**	**10**						**Acadia K-62**	**Misaine**
Lithology Mix 24		**80**		**20**						**Balvenie B-79**	**Petrel**
Lithology Mix 25	**15**	**75**	**10**							**Balvenie B-79**	**Logan Canyon-L.Albian**
Lithology Mix 25_1	**10**	**80**			**10**					**Tantallon M-41**	**Banquereau_M.Eocene**
Lithology Mix 26	**5**	**70**	**10**	**5**	**10**					**Tantallon M-41**	**Logan Canyon-L.M. Albian**
Lithology Mix 27		**20**		**20**	**50**		**10**			**Acadia K-62**	**Mohican/Iroquis**
Lithology Mix 28				**50**			**50**			**Acadia K-62**	**Abenaki(Baccaro)**
(*) mixed lithologies were ascertained from the lithological descriptions of the well history report of various individual well											

Table 6. Proportions of various lithologies forming various *Lithology Mix*											
(used as the input parameter within the PetroBuilder Module of the Petroleum System Modeling)											
Mix Name	**Sandstone**	**Shale**	**Siltstone**	**Limestone**	**Marl**	**Chalk**	**Dolomite**	**Anhydrite**	**Salt**	**Type Well**	**Formation**
Lithology Mix 29				70	10		20			**Albatross B-13**	**Abenaki1-Tithonian**
Lithology Mix 30		20		30			50			**Acadia K-62**	**Scatarie**
Lithology Mix 31		20	10		70					**Line 504**	**Wyandot-Dawson Canyon**
Lithology Mix 32		20		20		60				**Tantallon M-41**	**Wyandot 1**
Lithology Mix 35		80	10			5	5			**Tantallon M-41**	**CVC1-E.Barre._L.Hauteri.**
Lithology Mix 36		10		90						**Albatross B-13**	**CVC-Valanginian**
Lithology Mix 37		20		80						**Albatross B-13**	**Dawson Canyon-Campanian**
Lithology Mix 38		10						10	80	**Weymouth A-45**	**Logan Canyon-Breciated zone**
Lithology Mix 39		80	10	10						**Weymouth A-45**	**Logan Canyon 6**
Lithology Mix 40		90	5	5						**Weymouth A-45**	**L.Missisauga Equivalent 1**
SHALEsilt		75	25							**Shubenacadie H-100**	**Quarternary-L.Pliocene**
LIMEdolomite				75			25			**Acadia K-62**	**Roseway Equivalent 2**
LIMEshaly			25	75						**Balvenie B-79**	**Wyandot**
SANDshaly	75	25								**Shubenacadie H-100**	**Turbidite Fan1-Paleocene**
SHALE+SILT		50	50							**Annapolis G-24**	**Quarternary**
SILTShaly		25	75							**Annapolis G-24**	**Banquereau-Miocene**
SHALEcalc		90		10						**Annapolis G-24**	**Dawson Canyon-Petrel**
LIMEmarly				90	10					**Albatross B-13**	**Abenaki-Oxfordian**
(*) mixed lithologies were ascertained from the lithological descriptions of the well history report of various individual well											

Well: Annapolis G-24 - Rock-Eval Pyrolysis and TOC data

Depth	TOC	S1	S2	S3	Tmax	HI	OI	PI
2555	5.82	37.06	21.31	4.51	446	366	77	0.63
2580	4.51	34.32	9.66	0.68	442	214	15	0.78
2630	3.84	26.64	6.99	2.17	441	182	57	0.79
2755	2.90	16.74	4.28	4.31	392	148	149	0.80
2780	1.71	8.09	2.64	3.71	388	154	217	0.75
2980	2.53	13.30	4.67	4.42	399	185	175	0.74
3005	2.96	13.92	5.54	4.54	394	188	153	0.71
3105	2.55	12.50	7.50	2.80	410	295	110	0.62
3180	2.29	12.96	4.17	2.08	409	182	91	0.76
3255	2.46	16.81	4.61	1.87	419	187	76	0.78
3280	2.94	20.78	5.38	1.51	440	183	51	0.79
3330	2.35	16.90	4.70	2.13	433	200	91	0.78
3355	2.81	22.81	6.79	1.13	458	242	40	0.77
3405	2.38	18.46	4.27	1.60	445	180	67	0.81
3430	3.09	19.61	4.82	1.53	435	156	50	0.80
3555	2.21	11.09	3.64	0.21	406	165	10	0.75
3580	2.20	10.75	3.47	3.88	390	158	176	0.76
3655	1.70	8.27	2.50	3.84	378	147	226	0.77
3680	1.56	7.07	2.30	4.04	384	147	259	0.75
3780	1.43	7.62	2.47	0.22	388	173	15	0.75
3805	1.66	9.53	2.62	3.19	392	158	192	0.78
3855	1.97	10.44	3.37	3.84	388	172	195	0.76
3880	2.27	13.19	3.62	3.34	392	160	147	0.78
3905	2.70	15.18	3.77	2.90	401	140	107	0.80
3930	2.73	13.05	3.92	3.39	394	144	124	0.77
3955	3.11	16.81	3.88	1.41	419	125	45	0.81
3980	3.00	16.44	4.60	2.58	401	154	86	0.78
3980	3.00	16.44	4.60	2.58	401	154	86	0.78
4005	2.11	11.00	3.60	3.14	392	171	149	0.75
4030	2.98	12.75	4.20	2.49	398	141	84	0.75
4055	3.82	20.66	4.95	1.13	417	130	30	0.81
4080	4.12	17.05	5.61	2.24	414	137	54	0.75
4105	3.56	16.01	4.74	2.85	408	133	80	0.77
4130	3.49	15.77	4.60	2.87	405	132	82	0.77
4155	3.59	14.79	4.40	2.32	411	123	65	0.77

Well: Annapolis G-24 - Rock-Eval Pyrolysis and TOC data

Depth	TOC	S1	S2	S3	Tmax	HI	OI	PI
4180	3.44	14.75	4.49	2.36	410	131	69	0.77
4205	4.88	21.51	5.85	1.71	419	120	35	0.79
4230	5.43	23.62	6.99	1.45	425	129	27	0.77
4255	2.41	14.60	5.88	2.26	416	245	94	0.71
4280	4.15	20.20	4.89	1.66	419	118	40	0.80
4305	3.98	20.01	4.89	1.60	420	123	40	0.80
4330	3.85	15.73	5.77	1.74	422	150	45	0.73
4355	3.33	15.91	4.99	3.31	401	150	99	0.76
4380	4.14	20.95	5.21	1.66	421	126	40	0.80
4430	3.74	21.25	5.20	1.77	407	139	47	0.80
4455	2.42	13.20	9.36	1.90	437	388	79	0.58
4480	3.67	19.19	5.07	1.72	422	139	47	0.79
4505	3.23	18.55	4.92	2.93	405	153	91	0.79
4530	2.99	16.90	4.99	0.53	402	167	18	0.77
4580	3.08	19.56	4.22	2.60	399	137	84	0.82
4630	4.01	27.93	6.16	2.19	405	154	55	0.82
4680	3.07	20.90	5.01	2.56	400	164	83	0.81
4705	3.20	19.82	5.17	3.57	393	162	112	0.79
4730	3.04	20.08	5.28	2.96	392	174	97	0.79
4780	2.88	18.13	4.64	3.68	396	161	128	0.80
4805	2.54	15.58	4.00	1.87	394	158	74	0.80
4855	3.37	21.05	5.84	2.44	393	174	72	0.78
4880	3.12	21.57	4.40	2.79	392	141	89	0.83
4905	3.29	21.87	4.75	2.61	389	145	79	0.82
4930	3.31	19.32	5.70	3.07	390	173	93	0.77
4980	2.23	12.13	3.70	3.31	389	166	148	0.77
5005	2.34	11.99	5.60	1.88	399	240	80	0.68
5055	2.60	16.40	4.74	2.25	392	183	87	0.78
5080	3.28	20.53	7.54	2.03	413	230	62	0.73
5105	2.83	16.94	5.69	2.55	394	201	90	0.75
5155	4.26	24.79	8.00	2.90	398	188	68	0.76
5180	4.24	26.66	7.72	2.63	400	182	62	0.78
5205	3.55	20.31	7.39	2.36	397	208	66	0.73
5255	3.76	21.45	8.16	2.18	407	218	58	0.72
5280	4.13	25.31	9.03	2.35	403	219	57	0.74

Well: Annapolis G-24 - Rock-Eval Pyrolysis and TOC data

Depth	TOC	S1	S2	S3	Tmax	HI	OI	PI
5330	3.72	23.33	6.92	3.04	393	186	82	0.77
5355	3.63	21.87	6.71	2.24	405	185	62	0.77
5380	4.05	23.62	7.18	2.59	394	178	64	0.77
5430	3.76	26.58	6.00	4.46	390	160	119	0.82
5455	4.28	28.68	7.55	4.34	392	177	101	0.79
5480	1.91	11.06	4.14	1.63	412	217	85	0.73
5505	4.05	25.19	11.18	0.98	439	277	24	0.69
5530	3.11	17.62	6.22	3.67	407	200	118	0.74
5555	3.25	19.64	5.99	3.49	403	185	107	0.77
5605	3.57	22.35	6.58	1.62	393	185	45	0.77
5630	3.50	22.50	5.83	3.07	396	167	88	0.79
5680	2.11	10.79	3.99	2.78	394	190	132	0.73
5730	3.35	19.12	6.79	3.70	393	203	110	0.74
5780	3.04	19.37	5.78	3.75	398	190	123	0.77
5830	3.23	19.29	5.51	0.08	393	171	2	0.78
5880	5.09	34.41	8.90	3.14	397	175	62	0.79
5930	5.87	39.29	10.85	2.65	412	185	45	0.78
5980	3.68	21.29	6.38	1.88	400	174	51	0.77
6030	3.54	23.74	6.70	1.11	410	190	31	0.78
6080	3.95	20.23	8.36	1.54	406	212	39	0.71
6130	4.81	29.73	8.29	2.35	404	173	49	0.78
6180	5.44	38.98	10.25	1.68	413	189	31	0.79

Acadia K-62: PetroMod 1d Modelling Input Data										
Stratigraphy (Well)	**Top**	**Base**	**Present**	**Eroded**	**Deposition**	**Deposition**	**Erosion**	**Erosion**	**Lithology**	**Petroleum**
	(m)	**(m)**	**Thickn**	**Thickness**	**From (Ma)**	**To (Ma)**	**From (Ma)**	**To (Ma)**		**System**
			(m)	**(m)**						**Elements**
Water Depth	0	866.3								
Plio-Pleistocene-Banq1	866.3	1410	543.7		5.33	0			SHALEsilt	Overburden Rock
L.Miocene-Banq 2	1410	2064	654		7.1	5.3			Lithology Mix 20	Overburden Rock
M-E. Miocene-Banq 3	2064	2094	30	200	23.03	12.8	12.8	7.1	Lithology Mix 7	Source Rock
M-L. Eocene-Banq 4	2094	2214	120	300	38	33.9	33.9	23.03	Lithology Mix 6	Source Rock
M.Eocene-Banq 5	2214	2334	120		48.6	38			SHALEcalc	Overburden Rock
E.Eocene-Banq 6	2334	2394	60		55.8	48.6			Lithology Mix 19	Overburden Rock
Paleocene-Banq 7	2394	2508	114		65.5	55.8			Lithology Mix 21	Overburden Rock
Maastrictian	2508	2550	42	200	70.6	68	68	65.5	Lithology Mix 24	Overburden Rock
Camp-Maastrict	2550	2593	43		75	70.6			Lithology Mix 5	Overburden Rock
Wyandot	2593	2620	27	100	83.5	78	78	75	Lithology Mix 19	Overburden Rock
Dawson Canyon/Petrel	2620	2784	164	200	120	105	105	83.5	SHALEcalc	Seal Rock
Roseway Eq. 1 - E. Aptian	2784	2878	94		125	120			Lithology Mix 27	Reservoir Rock
Roseway Eq. 2 - Haut_Valang	2878	3067	189	100	132	127	127	125	LIMEdolom	Reservoir Rock
Roseway Eq. 3 - Berriasian	3067	3306	239	100	142	135	135	132	LIMEdolom	Reservoir Rock
Baccaro, Abenaki Oxford_Kimm	3306	4086	780	200	159	150.8	150.8	142	Lithology Mix 28	Reservoir Rock
Misaine Eq. - Callovian	4086	4304	218		162	159			Lithology Mix 23	Reservoir Rock
Scatarie Eq. -Bajo_Callov	4304	4950	646		167.7	162			Lithology Mix 30	Source Rock
Mohican/Iroquois Equiv.	4950	5287	337		187	167.7			Lithology Mix 27	Source Rock

Well: Annapolis G-24 - Selected input data										
Formation	**Start Depth**	**End Depth**	**Thickness**	**Erosion**	**Deposition**	**Deposition**	**Erosion**	**Erosion**	**Lithology**	**Petroleum System**
	(m)	**(m)**	**(m)**	**Thickness**	**Start (age)**	**End (age)**	**Start (age)**	**End (age)**		**Elements**
Quarternary	1678	1714	36		2	0			SHALE&SILT	Overburden Rock
Pleist-L. Pliocene	1714	1985	271		3.6	2			SHALEsilt	Overburden Rock
Early Pliocene	1985	2060	75		5.3	3.6			SHALE&SILT	Overburden Rock
Banq1-Mio	2060	2555	495	200	23.8	17	17	5.3	SHALEsilt	Overburden Rock
Banq2-Mio	2555	2682	127	200	33.7	28.5	28.5	23.8	SILTshaly	Overburden Rock
Banq3-Eocene	2682	3310	628	500	49	44	44	33.7	Lithology Mix 15	Overburden Rock
Banq4-Paleocene	3310	3400	90	500	57.9	55	55	49	LIMEshaly	Overburden Rock
Paleo - K10 Map Horizon	3400	3457	57		61	57.9			Lithology Mix 14	Overburden Rock
Wyandot	3457	3490	33	500	80	71.3	71.3	61	Lithology Mix 14	Overburden Rock
Wyandot-Missi 1	3490	3930	440	200	105	99	99	80	Lithology Mix 7	Seal Rock
Top Upper Target	3930	3975	45		106	105			Lithology Mix 8	Reservoir Rock
Missi 2 - Top Upper Target	3975	4130	155		112	106			Lithology Mix 7	Reservoir Rock
Missi 3 - K30 Map Horizon	4130	4296	166		116	112			Lithology Mix 8	Overburden Rock
Missi4-Base Up.Target	4296	4332	36		118	116			Lithology Mix 22	Reservoir Rock
Missi 5 - Base Up. Target	4332	4575	243	200	121	120	120	118	Lithology Mix 7	Reservoir Rock
E.Cret 1 - Base Up. Target	4575	4804	229	200	123.5	123	123	121	Lithology Mix 14	Reservoir Rock
Base Up.Target	4804	4840	36		124.5	123.5			Lithology Mix 10	Reservoir Rock
Early Cret 3 - Top Lr. Target	4840	5000	160		127	124.5			Lithology Mix 14	Reservoir Rock
E.Cret 4 - Top Lr.Target	5000	5350	350		129	127			Lithology Mix 7	Reservoir Rock
E.Cret 5 - K40 Map Horizon	5350	5508	158		130	129			Lithology Mix 3	Overburden Rock
E.Cret.Sand - K40 Map Hori	5508	5555	47		130.5	130			Lithology Mix 7	Reservoir Rock
CVCan 1 - Base Lr. Target	5555	5750	195		131	130.5			Lithology Mix 11	Reservoir Rock
CVCan Res - Base Lr.Target	5750	5800	50		131.5	131			Lithology Mix 10	Reservoir Rock
CVCan 2 - Base Lr.Target	5800	6175	375		133	131.5			Lithology Mix 1	Source Rock
CVCan 3 - Base Lr.Target	6175	6182	7	200	137	135	135	133	SHALE	Source Rock
	6182									

Newburn H-23 : PetroMod 1d Modelling Input Data										
Stratigraphy	**Top**	**Base**	**Present**	**Eroded**	**Deposition**	**Deposition**	**Erosion**	**Erosion**	**Lithology**	**Petroleum**
	(m)	**(m)**	**Thickn**	**Thickness**	**From (Ma)**	**To (Ma)**	**From (Ma)**	**To (Ma)**		**System**
			(m)	**(m)**						**Elements**
Sediment Surface			977		0	0	0	0		
Plio-Pleistocene	977	1890	913		5.3	0			Lithology Mix 9	Source Rock
Banquareau 1	1890	1920	30		11.2	5.3			Lithology Mix 11	Source Rock
Banquareau 2	1920	2269.5	349.5		14.6	11.2			SHALEsilt	Source Rock
Banquareau 3	2269.5	2370	100.5		20.5	14.6			Lithology Mix 10	Source Rock
Banquereau 4	2370	2519	149		23.8	20.5			Lithology Mix 14	Overburden Rock
Banquareau 5	2519	2677	158	500	41.3	33.7	33.7	23.8	Lithology Mix 19	Overburden Rock
Banquareau 6	2677	2850	173		49	41.3			Lithology Mix 14	Seal Rock
Late Cretaceous	2850	2855	5	500	73	65	65	49	Lithology Mix 17	Reservoir Rock
Dawson Canyon-Wyandot	2855	3010	155	200	93.5	90	90	73	Lithology Mix 15	Overburden Rock
Logan Canyon 1	3010	3340	330	200	99.6	95	95	87	Lithology Mix 6	Overburden Rock
Logan Canyon 2	3340	3481	141		103	100			Lithology Mix 20	Overburden Rock
Prodelta 1	3481	3820	339		107	103			Lithology Mix 9	Overburden Rock
Prodelta 2	3820	4099	279		112	107			Lithology Mix 11	Seal Rock
Sequence C	4099	4112	13		115	112			Lithology Mix 14	Reservoir Rock
Top Turbidite	4112	4380	268		125	115			Lithology Mix 6	Overburden Rock
Naskapi_Missisauga	4380	4570	190		127	125			Lithology Mix 4	Reservoir Rock
Sequence B	4570	4825	255		129	127			Lithology Mix 21	Overburden Rock
Cretaceous Verrill Canyon 1	4825	5025	200		130	129			Lithology Mix 6	Source Rock
Sequence A 1	5025	5400	375		132	130			Lithology Mix 14	Overburden Rock
Sequence A 2	5400	5820	420		136.4	132			Lithology Mix 4	Reservoir Rock
Cretaceous Verrill Canyon 2	5820	6070	250	200	140.2	138	138	136.4	SHALE	Source Rock
	6070									

Weymouth A-45: PetroMod 1d Modelling Input Data										
Name	**Top**	**Base**	**Present**	**Eroded**	**Deposition**	**Deposition**	**Erosion**	**Erosion**	**Lithology**	**Petroleum**
	(m)	**(m)**	**Thickn**	**Thickness**	**From (Ma)**	**To (Ma)**	**From (Ma)**	**To (Ma)**		**System**
			(m)	**(m)**						**Elements**
Sediment Surface			1689		0	0	0	0		
Plio-Pleistocene	1689	2085	396		5.33	0			Lithology Mix 14	Overburden Rock
Banquareau 1	2085	2366	281		11.61	5.33			Lithology Mix 9	Overburden Rock
Banquareau 2	2366	2703	337		15.97	11.61			Lithology Mix 5	Overburden Rock
Banquareau 3	2703	2825	122		21	15.97			Lithology Mix 7	Overburden Rock
Banquareau 4 - Brecciated Zone	2825	2855	30	300	50	33.9	33.9	21	Lithology Mix 38	Overburden Rock
Argo Salt	2855	4284.5	1429.5		75	50			SALT	Seal Rock
Logan Canyon 1- Brecciated Zone	4284.5	4380	95.5	200	97	95	95	75	Lithology Mix 38	Seal Rock
Logan Canyon 2	4380	4461	81	300	102.5	97			Lithology Mix 12	Reservoir Rock
Logan Canyon 3	4461	4592	131		108	102.5			Lithology Mix 6	Overburden Rock
Naskapi Equivalent	4592	4758	166		112	108			Lithology Mix 7	Overburden Rock
Late Missisauga Eq. 1	4758	4889	131		116	112			Lithology Mix 10	Overburden Rock
Late Missisauga Eq. 2	4889	5108	219		120	116			Lithology Mix 40	Overburden Rock
Late Missisauga Eq. 3	5108	5250	142		123	120			Lithology Mix 39	Overburden Rock
Late Missisauga Eq. 4	5250	5487	237		125	123			Lithology Mix 9	Overburden Rock
Late Missisauga Eq. 5	5487	5671	184		128	125			Lithology Mix 10	Overburden Rock
Late Missisauga Eq. 6	5671	5705	34		129	128			Lithology Mix 21	Overburden Rock
Cretaceous Verrill Canyon 1	5705	5945	240		132	129			Lithology Mix 21	Source Rock
Cretaceous Verrill Canyon 2	5945	6255	310		135	132			SHALE	Source Rock
Cretaceous Verrill Canyon 3	6255	6520	265		139	135			Lithology Mix 9	Source Rock
	6520									

Mass Balance of Hydrocarbons

mass in $(10)^9$ kg(Mtons)/m$^{3)}$

	Methane_Trias	C2-C5_Trias	C6-C14_Trias	C15+_Trias	Methane_Miss	C2-C5_Miss	C6-C14_Miss	C15+_Miss
Late_Paleocene	0	0	0	0	0.00E+00	0.00E+00	0.00E+00	0.00E+00
Middle_Paleocene	4.49E-12	4.53E-12	5.18E-12	-2.10E-11	6.15E-19	8.02E-19	8.67E-19	-3.31E-18
MidMississauga	2.97E-11	2.99E-11	3.45E-11	-1.39E-10	0.000248251	0.000838801	0.0090469	0.055592
CretaceousVerrillCanyon	1.05E-05	9.51E-06	1.08E-05	-4.61E-05	5.19E-20	6.64E-20	4.92E-20	-2.49E-19
Upp_Jurassic_Res	0.0425305	0.0308778	0.0364468	-0.167668	6.33E-19	8.32E-19	8.98E-19	-3.42E-18
Jurassic_VerrillCanyon	0.0603453	0.036936	0.0373599	-0.211714	1.59E-21	2.09E-21	2.30E-21	-8.63E-21
Late_Jurassic	0.29171	0.16649	0.13101	-0.94832	8.05E-22	1.06E-21	1.15E-21	-4.36E-21
Misaine_1	0.936546	0.428994	0.171388	-2.5973	2.78E-22	3.65E-22	3.97E-22	-1.50E-21
Scatarie	1.87E+01	-9.53E-01	-5.49E+00	-2.81E+01	1.85E-21	2.41E-21	2.68E-21	-1.00E-20
Mohican	146.516	-1.9045	-22.2349	-245.231	3.20E-21	3.19E-21	2.83E-21	-1.38E-20
Early_Jur_Lacustrine_SR	7.24E+01	6.97E+00	-1.07E+01	-1.28E+02	1.32E-23	5.19E-24	-2.02E-25	-2.93E-23
Triassic _Lacustrine_SR	181.918	166.635	205.768	1552.17	3.46E-25	6.22E-26	-3.74E-26	-6.41E-25
Sum Generated	**420.934**	**171.409**	**167.74**	**1146.67**	**0.000248251**	**0.000838801**	**0.0090469**	**0.055592**
Late_Paleocene	0.036005	0.015809	0.010805	0.021448	3.99E-09	1.35E-08	1.46E-07	8.96E-07
Middle_Paleocene	0.32841	0.23777	0.15961	0.4171	1.30E-08	4.53E-08	5.15E-07	3.09E-06
MidMississauga	0.00723757	0.00200663	0.00136301	0.00182403	2.46E-04	8.33E-04	8.98E-03	5.52E-02
CretaceousVerrillCanyon	0.0114007	0.0037908	0.00301181	0.00220817	2.25E-17	5.18E-16	3.39E-14	2.69E-13
Upp_Jurassic_Res	5.15E+00	6.83E-01	4.76E-01	9.34E-01	5.91E-19	8.29E-17	7.61E-15	4.37E-14
Jurassic_VerrillCanyon	3.52E+00	3.25E-01	0.222533	0.124633	7.34E-22	2.96E-20	2.80E-18	1.62E-17
Late_Jurassic	4.20E+00	3.11E-01	2.04E-01	1.05E-01	5.19E-22	1.25E-20	1.16E-18	6.69E-18
Misaine_1	2.68046	0.188352	0.120865	0.0600702	1.54E-22	1.39E-21	1.17E-19	6.75E-19
Scatarie	46.9432	2.4415	1.26893	0.354696	1.30E-21	1.85E-21	3.80E-20	2.19E-19
Mohican	3.24806	0.0348003	0.0155155	0.00309808	4.78E-23	5.41E-23	1.88E-22	6.63E-22
Early_Jur_Lacustrine_SR	0.61071	0.000108659	8.49E-05	2.66E-05	5.82E-26	2.34E-26	2.16E-26	3.73E-26
Triassic _Lacustrine_SR	105.176	0.00710712	3.93E-05	4.80E-06	1.86E-28	1.78E-28	2.32E-28	7.34E-29
Sum Accumulated in Source	**1.72E+02**	**4.25E+00**	**2.48312**	**2.02431**	**0.000246407**	**0.000832579**	**0.00897796**	**0.055175**
Late_Paleocene	-3.60E-02	-1.58E-02	-1.08E-02	-2.14E-02	-3.99E-09	-1.35E-08	-1.46E-07	-8.96E-07
Middle_Paleocene	-3.28E-01	-2.38E-01	-1.60E-01	-4.17E-01	-1.30E-08	-4.53E-08	-5.15E-07	-3.09E-06
MidMississauga	-7.24E-03	-2.01E-03	-1.36E-03	-1.82E-03	1.86E-06	6.28E-06	6.96E-05	0.000421
CretaceousVerrillCanyon	-1.14E-02	-3.78E-03	-3.00E-03	-2.25E-03	-2.24E-17	-5.18E-16	-3.39E-14	-2.69E-13
Upp_Jurassic_Res	-5.10944	-0.65183	-0.439988	-1.10215	4.24E-20	-8.21E-17	-7.61E-15	-4.37E-14
Jurassic_VerrillCanyon	-3.46E+00	-2.88E-01	-1.85E-01	-3.36E-01	8.55E-22	-2.75E-20	-2.80E-18	-1.62E-17
Late_Jurassic	-3.91E+00	-1.44E-01	-7.29E-02	-1.05303	2.85E-22	-1.14E-20	-1.16E-18	-6.70E-18
Misaine_1	-1.74E+00	2.41E-01	5.05E-02	-2.66E+00	1.23E-22	-1.02E-21	-1.17E-19	-6.77E-19
Scatarie	-2.82E+01	-3.39E+00	-6.76E+00	-2.85E+01	5.50E-22	5.61E-22	-3.54E-20	-2.29E-19
Mohican	143.268	-1.9393	-22.2504	-245.234	3.15E-21	3.13E-21	2.64E-21	-1.44E-20
Early_Jur_Lacustrine_SR	71.8293	6.96789	-10.6821	-128.2	1.31E-23	5.16E-24	-2.24E-25	-2.93E-23
Triassic _Lacustrine_SR	7.67E+01	1.67E+02	2.06E+02	1.55E+03	3.46E-25	6.20E-26	-3.76E-26	-6.41E-25
Sum Expelled	**249.025**	**167.159**	**165.257**	**1144.65**	**1.84E-06**	**6.22E-06**	**6.89E-05**	**0.00041702**
Middle-LateMioceneReservoi	2.05E+00	1.83E-01	1.99E-02	2.38E-03	1.31E-09	3.38E-09	1.78E-08	1.15E-08
Early_MiocReservoir	2.46E+01	4.83E+00	2.64E+00	4.57E+00	9.42E-07	3.17E-06	3.40E-05	0.000208078
LoganCanyon	7.97E+00	3.80E+00	2.61E+00	5.66E+00	1.80E-07	6.15E-07	6.92E-06	4.15E-05
MississaugaReservoir	5.80823	1.25834	0.913195	0.867986	7.08E-10	2.45E-09	3.44E-08	1.84E-07

Mass Balance of Hydrocarbons

mass in $(10)^9$ kg(Mtons)/$m^{3)}$

	Methane_JVC	C2-C5_JVC	C6-C14_JVC	C15+_JVC	Methane_Misaine	C2-C5_Misaine
Late_Paleocene	0.00E+00	0.00E+00	0.00E+00	0.00E+00	0	0
Middle_Paleocene	1.62E-11	1.88E-11	-6.26E-13	-5.67E-11	2.22E-12	2.65E-12
MidMississauga	1.03E-10	1.21E-10	3.59E-12	-3.71E-10	1.47E-11	1.76E-11
CretaceousVerrillCanyon	3.42E-05	3.84E-05	-3.11E-06	-0.000115561	1.45E-05	1.67E-05
Upp_Jurassic_Res	0.129356	0.137435	-0.0507652	-0.381618	0.0262939	0.0295851
Jurassic_VerrillCanyon	141.207	50.3385	843.436	772.732	0.0901484	0.0899588
Late_Jurassic	0.35581	0.342888	-0.04116	-1.1138	0.78954	0.64594
Misaine_1	0.609591	0.535793	0.213323	-2.15974	5.34E+01	17.7809
Scatarie	7.18E+00	3.60E+00	-3.50E+00	-1.45E+01	1.31E+01	6.50E+00
Mohican	46.795	8.633	-8.227	-87.552	3.77E+01	8.25E+00
Early_Jur_Lacustrine_SR	15.741	1.9098	-2.9426	-26.044	7.2274	1.0696
Triassic _Lacustrine_SR	2.0439	0.24264	-0.43673	-3.2251	1.0397	0.1385
Sum Generated	**214.062**	**65.7418**	**828.448**	**637.707**	**113.383**	**34.5036**
Late_Paleocene	0.018444	0.0099956	0.16182	0.10617	0.0048465	0.0030145
Middle_Paleocene	0.26056	0.1596	2.6914	1.704	0.05775	0.041189
MidMississauga	9.24E-04	4.75E-04	8.03E-03	4.90E-03	0.000489046	0.000180975
CretaceousVerrillCanyon	0.0483459	0.0062028	0.0450666	0.015487	1.24E-02	4.88E-03
Upp_Jurassic_Res	5.30E+00	1.93E+00	3.26E+01	2.40E+01	1.81E+00	6.03E-01
Jurassic_VerrillCanyon	5.38429	1.50804	14.7483	3.50423	1.97E+00	8.30E-01
Late_Jurassic	0.85331	0.272218	0.64471	0.968371	2.43315	1.02423
Misaine_1	0.448431	0.119357	0.128447	0.207933	1.91338	0.532011
Scatarie	6.47352	0.235386	0.30414	0.040737	4.28283	0.30885
Mohican	0.252365	0.00129243	0.00121783	0.000267423	0.290969	0.00559738
Early_Jur_Lacustrine_SR	0.0248187	5.39E-05	6.07E-05	1.87E-05	0.0128921	2.69E-05
Triassic _Lacustrine_SR	0.00368714	4.12E-05	3.18E-05	3.65E-06	0.00193335	1.41E-05
Sum Accumulated in Source	**19.0655**	**4.24749**	**51.3602**	**30.5228**	**1.28E+01**	**3.35E+00**
Late_Paleocene	-0.018444	-0.0099956	-0.16182	-0.10617	-4.85E-03	-3.01E-03
Middle_Paleocene	-0.26056	-0.1596	-2.69E+00	-1.70E+00	-5.78E-02	-4.12E-02
MidMississauga	-0.000923754	-0.000474845	-0.00802611	-0.00490353	-4.89E-04	-1.81E-04
CretaceousVerrillCanyon	-0.0483117	-0.00616445	-0.0450697	-0.0156026	-0.0123662	-0.00486005
Upp_Jurassic_Res	-5.16741	-1.7974	-32.6778	-24.3523	-1.78822	-0.573226
Jurassic_VerrillCanyon	135.823	48.8305	828.688	769.228	-1.88E+00	-7.40E-01
Late_Jurassic	-0.4975	0.07067	-0.68587	-2.08217	-1.64E+00	-3.78E-01
Misaine_1	0.16116	0.416436	0.084876	-2.36767	5.15E+01	1.72E+01
Scatarie	0.70718	3.36631	-3.80684	-14.5897	8.84E+00	6.19E+00
Mohican	46.5426	8.63171	-8.22822	-87.5523	3.74E+01	8.24E+00
Early_Jur_Lacustrine_SR	15.7162	1.90975	-2.94266	-26.044	7.21E+00	1.07E+00
Triassic _Lacustrine_SR	2.04E+00	2.43E-01	-4.37E-01	-3.23E+00	1.04E+00	1.38E-01
Sum Expelled	**1.95E+02**	**6.15E+01**	**7.77E+02**	**607.184**	**1.01E+02**	**3.12E+01**
Middle-LateMioceneReservoi	0.200964	0.0159673	0.030282	0.00324374	0.12701	0.0143144
Early_MiocReservoir	2.8959	0.95252	16.2486	11.5349	1.57885	0.382138
LoganCanyon	2.18447	1.2669	23.659	16.315	0.697369	0.360536
MississaugaReservoir	0.798624	0.231345	3.46581	2.12932	0.428307	0.126119

Mass Balance of Hydrocarbons

mass in $(10)^{9}$ kg(Mtons)/$m^{3)}$

	C6-C14_Misaine	C15+_Misaine	Methane_Paleocene	PK_C2-C5_Paleo	PK_C6-C14_Paleo	PK_C15+_Paleo
Late_Paleocene	0	0	4.18E-02	1.86E-01	4.86E-01	8.11E-01
Middle_Paleocene	8.18E-13	-8.91E-12	0.00023112	0.001022	0.0026728	0.0044662
MidMississauga	5.78E-12	-5.94E-11	0	0	0	0
CretaceousVerrillCanyor	3.02E-06	-5.46E-05	0	0	0	0
Upp_Jurassic_Res	0.00364694	-0.0960582	2.24E-41	2.24E-41	-6.40E-41	-2.00E-45
Jurassic_VerrillCanyon	-0.0204896	-0.275212	2.94E-44	2.89E-44	-8.32E-44	-5.11E-46
Late_Jurassic	-0.44386	-1.906	5.61E-45	5.51E-45	-1.75E-44	-6.51E-47
Misaine_1	247.44	206.323	2.80E-45	2.77E-45	-6.12E-45	-4.56E-47
Scatarie	-12.1474	-19.589	4.06E-44	3.90E-44	-1.11E-43	-3.03E-45
Mohican	-2.78E+01	-4.85E+01	1.47E-43	9.89E-44	-3.52E-43	-1.26E-44
Early_Jur_Lacustrine_SR	-4.0618	-9.501	1.40E-45	-2.64E-46	-1.81E-45	-3.58E-47
Triassic _Lacustrine_SR	-0.55798	-1.3288	0	-1.55E-47	-5.88E-47	-1.28E-48
Sum Generated	**202.459**	**125.097**	**0.0420261**	**0.187252**	**0.489103**	**0.815026**
Late_Paleocene	0.038172	0.02986	0.041032	0.18298	0.47811	0.79669
Middle_Paleocene	0.54158	0.42591	0.000233537	0.00104071	0.00272866	0.00455929
MidMississauga	0.0017519	0.00122341	1.59E-27	7.30E-27	2.99E-26	9.75E-27
CretaceousVerrillCanyor	0.0289473	0.0154769	0	0	0	0
Upp_Jurassic_Res	9.53E+00	7.96E+00	0.00E+00	0.00E+00	0.00E+00	0.00E+00
Jurassic_VerrillCanyon	5.01E+00	2.63E+00	8.41E-45	1.96E-44	3.85E-41	1.40E-45
Late_Jurassic	5.20338	2.36852	7.01E-45	1.26E-44	1.03E-41	1.40E-45
Misaine_1	3.46309	1.48168	4.20E-45	7.01E-45	3.54E-42	0
Scatarie	0.90359	0.492665	5.18E-44	9.11E-44	8.33E-42	2.80E-45
Mohican	0.0171716	0.00656008	1.40E-45	1.40E-45	3.08E-44	0
Early_Jur_Lacustrine_SR	3.62E-05	7.27E-06	0	0	0	0
Triassic _Lacustrine_SR	1.20E-05	1.20E-06	0	0	0	0
Sum Accumulated in Source	**2.47E+01**	**1.54E+01**	**0.0412655**	**0.184021**	**0.480839**	**0.801249**
Late_Paleocene	-3.82E-02	-2.99E-02	0.000763	0.00325	0.00831999	0.01387
Middle_Paleocene	-5.42E-01	-4.26E-01	-2.42E-06	-1.87E-05	-5.59E-05	-9.31E-05
MidMississauga	-1.75E-03	-1.22E-03	-1.59E-27	-7.30E-27	-2.99E-26	-9.75E-27
CretaceousVerrillCanyor	-0.0289443	-0.0155315	0	0	0	0
Upp_Jurassic_Res	-9.52585	-8.06098	2.24E-41	2.24E-41	-6.40E-41	-1.40E-45
Jurassic_VerrillCanyon	-5.03E+00	-2.91E+00	2.10E-44	9.81E-45	-3.85E-41	-1.40E-45
Late_Jurassic	-5.65E+00	-4.27E+00	-1.40E-45	-7.01E-45	-1.03E-41	-1.40E-45
Misaine_1	2.44E+02	2.05E+02	-1.40E-45	-4.20E-45	-3.54E-42	0
Scatarie	-1.31E+01	-2.01E+01	-1.12E-44	-5.18E-44	-8.44E-42	-5.61E-45
Mohican	-2.78E+01	-4.85E+01	1.46E-43	9.81E-44	-3.83E-43	-1.26E-44
Early_Jur_Lacustrine_SR	-4.06E+00	-9.50E+00	1.40E-45	0	-1.40E-45	0
Triassic _Lacustrine_SR	-5.58E-01	-1.33E+00	0.00E+00	0.00E+00	0.00E+00	0.00E+00
Sum Expelled	**1.78E+02**	**1.10E+02**	**7.61E-04**	**0.00323129**	**0.00826413**	**0.0137769**
Middle-LateMioceneReservoi	0.0117602	0.00108948	9.14E-07	3.14E-06	2.97E-06	1.08E-07
Early_MiocReservoi	3.13188	2.23089	0.000293157	0.00121536	0.00299271	0.00497903
LoganCanyon	4.22652	3.1981	1.36E-21	6.51E-21	1.74E-20	1.81E-21
MississaugaReservoi	1.13047	0.737515	1.04E-31	7.16E-31	5.83E-29	5.90E-28

Mass Balance of Hydrocarbons

mass in $(10)^9$ kg(Mtons)/$m^{3)}$

	Methane_CVC	C2-C5_CVC	C6-C14_CVC	C15+_CVC	Methane_EJur	PK_C2-C5_EJur	PK_C6-C14_EJur
Late_Paleocene	0.00E+00	0.00E+00	0.00E+00	0.00E+00	0	0	0
Middle_Paleocene	7.37E-12	8.49E-12	-3.91E-14	-2.60E-11	7.58E-12	7.65E-12	4.85E-12
MidMississauga	4.37E-11	5.04E-11	1.89E-12	-1.57E-10	5.05E-11	5.08E-11	3.30E-11
CretaceousVerrillCanyon	192.657	93.6849	1195.4	429.249	5.43E-05	4.79E-05	2.38E-05
Upp_Jurassic_Res	0.0967148	0.0950513	-0.100575	-0.201997	0.0870743	0.0708262	0.0348017
Jurassic_VerrillCanyon	0.0168451	0.0182494	-0.00405217	-0.0531328	0.24723	0.170182	-0.0120439
Late_Jurassic	0.023978	0.0263437	0.003177	-0.086452	1.8251	0.91776	-0.755
Misaine_1	0.0262021	0.0279965	0.00969514	-0.100366	4.77495	2.35706	-1.84356
Scatarie	4.53E-01	3.14E-01	-1.37E-01	-1.13E+00	7.55E+01	1.26E+01	-4.84E+01
Mohican	0.89142	0.30116	-0.59386	-1.3728	426.974	42.1009	-235.418
Early_Jur_Lacustrine_SR	0.078489	0.011171	-0.043196	-0.10337	356.72	343.879	797.078
Triassic _Lacustrine_SR	0.01651	0.0049835	-0.0054713	-0.029769	58.901	14.791	-22.597
Sum Generated	**194.26**	**94.4842**	**1194.53**	**426.167**	**925.005**	**416.875**	**488.076**
Late_Paleocene	0.053593	0.03307	0.47591	0.20037	0.052382	0.047666	0.090889
Middle_Paleocene	0.59955	0.40206	5.8669	2.3617	5.13E-01	6.46E-01	1.2643
MidMississauga	0.0153474	0.00774291	0.10319	0.0326651	8.53E-03	4.01E-03	6.16E-03
CretaceousVerrillCanyon	33.8333	15.9482	176.873	45.4691	0.0556817	0.0432455	0.0702176
Upp_Jurassic_Res	1.62E+00	7.07E-01	7.82E+00	3.05E+00	1.21E+01	8.28E+00	1.79E+01
Jurassic_VerrillCanyon	0.048483	0.0274534	0.318662	0.151822	8.50996	4.52622	8.35913
Late_Jurassic	0.0110619	0.0057116	0.0413872	0.0084751	8.4445	3.64245	6.82341
Misaine_1	0.00337791	0.00158027	0.00836658	0.00199662	4.82409	1.93461	3.85242
Scatarie	0.195847	0.066028	0.132086	0.0187715	69.16	9.4326	13.342
Mohican	0.0149929	0.000731853	0.000899204	0.00016679	5.44411	1.87928	3.1031
Early_Jur_Lacustrine_SR	0.00200291	5.83E-05	7.64E-05	1.88E-05	7.63E-01	3.46E-01	0.69148
Triassic _Lacustrine_SR	0.00034326	4.35E-05	3.85E-05	4.34E-06	8.86E-02	1.96E-04	1.65E-04
Sum Accumulated in Source	**36.3976**	**17.1999**	**191.645**	**51.2982**	**109.953**	**30.7824**	**55.5471**
Late_Paleocene	-0.053593	-0.03307	-0.47591	-0.20037	-0.052382	-0.047666	-0.090889
Middle_Paleocene	-0.59955	-0.40206	-5.87E+00	-2.36E+00	-0.5127	-0.6455	-1.26E+00
MidMississauga	-0.0153474	-0.00774291	-0.10319	-0.0326651	-0.00852642	-0.00400638	-0.00616193
CretaceousVerrillCanyon	158.824	77.7367	1018.53	383.78	-0.0556274	-0.0431976	-0.0701938
Upp_Jurassic_Res	-1.52297	-0.612139	-7.92479	-3.25511	-12.0024	-8.21019	-17.909
Jurassic_VerrillCanyon	-0.0316379	-0.009204	-0.322714	-0.204955	-8.26273	-4.35604	-8.37117
Late_Jurassic	0.0129161	0.0206321	-0.0382102	-0.0949271	-6.6194	-2.72469	-7.57841
Misaine_1	0.0228242	0.0264162	0.00132856	-0.102363	-0.04914	0.42245	-5.69598
Scatarie	0.256723	0.248292	-0.269226	-1.15327	6.315	3.1554	-61.753
Mohican	0.876427	0.300428	-0.594759	-1.37297	421.53	40.2216	-238.521
Early_Jur_Lacustrine_SR	0.0764861	0.0111127	-0.0432724	-0.103389	355.957	343.533	796.387
Triassic _Lacustrine_SR	1.62E-02	4.94E-03	-5.51E-03	-2.98E-02	5.88E+01	1.48E+01	-2.26E+01
Sum Expelled	**1.58E+02**	**7.73E+01**	**1.00E+03**	**374.868**	**8.15E+02**	**3.86E+02**	**4.33E+02**
Middle-LateMioceneReservoi	0.165725	0.0438887	0.077385	0.0075501	2.37786	0.355222	0.05559
Early_MiocReservoir	5.4273	2.6779	34.6466	14.1084	28.161	8.725	10.7025
LoganCanyon	7.42161	4.15345	60.6014	24.043	9.22506	7.16154	12.723
MississaugaReservoir	8.90543	4.57427	64.7734	24.7111	6.96203	2.71792	4.32122

Mass Balance of Hydrocarbons

mass in $(10)^9$ kg(Mtons)/$m^{3)}$

	PK_C15+_EJur	Methane_TJur	C2-C5_TJur	C6-C14_TJur	C15+_TJur	Methane_Mohican	C2-C5_Mohican
Late_Paleocene	0	0	0	0	0	0	0
Middle_Paleocene	-3.09E-11	0	0	0	0	0	0
MidMississauga	-2.06E-10	0	0	0	0	0	0
CretaceousVerrillCanyor	-0.000199239	0	0	0	0	0	0
Upp_Jurassic_Res	-0.307389	0.16881	0.06359	1.0109	0.86031	0	0
Jurassic_VerrillCanyon	-0.70142	0.057918	0.019227	0.30162	0.2567	0	0
Late_Jurassic	-3.9359	30.744	10.179	162.94	139.52	0	0
Misaine_1	-10.353	0.08542	0.025878	0.40542	0.34504	0	0
Scatarie	-1.06E+02	0.00E+00	0.00E+00	0.00E+00	0.00E+00	0.0093251	0.011845
Mohican	-586.521	0	0	0	0	43.104	41.443
Early_Jur_Lacustrine_SR	1314.38	0	0	0	0	0	0
Triassic _Lacustrine_SR	-100.39	0	0	0	0	0	0
Sum Generated	**506.441**	**31.0561**	**10.2877**	**164.658**	**140.982**	**43.1133**	**41.4548**
Late_Paleocene	0.094256	0.0021868	0.0013758	0.0275	0.022733	0.0024946	0.0043457
Middle_Paleocene	1.3607	0.031311	0.020608	0.40518	0.31546	0.028604	0.056205
MidMississauga	5.25E-03	0.000108205	6.20E-05	0.00132655	0.00123456	0.000304481	0.000370279
CretaceousVerrillCanyor	0.054199	0.00733745	0.00121289	0.0146431	0.00925882	0.00514936	0.00518443
Upp_Jurassic_Res	2.63E+01	9.32E-01	3.66E-01	6.28E+00	5.39E+00	0.729545	0.843787
Jurassic_VerrillCanyon	7.39288	1.43615	0.360028	4.00922	3.0849	0.574328	0.593085
Late_Jurassic	5.70923	1.98433	0.387	4.09661	3.83176	0.473224	0.500663
Misaine_1	4.37177	0.0546873	0.0125363	0.487162	1.77137	0.28564	0.327256
Scatarie	13.125	0.049435	0.0237096	1.34116	6.6818	2.93025	2.37352
Mohican	3.13311	0.000828684	0.000700315	0.126929	2.20478	0.906472	0.663035
Early_Jur_Lacustrine_SR	0.838094	0.000162925	0.000111253	0.0132754	0.230668	0.00955809	0.0103706
Triassic _Lacustrine_SR	2.93E-05	7.27E-06	8.84E-06	0.00159141	0.0176904	0.00052797	0.00101228
Sum Accumulated in Source	**62.3981**	**4.49856**	**1.17385**	**16.8053**	**23.562**	**5.9461**	**5.37883**
Late_Paleocene	-0.094256	-0.0021868	-0.0013758	-0.0275	-0.022733	-0.0024946	-0.0043457
Middle_Paleocene	-1.36E+00	-0.031311	-0.020608	-4.05E-01	-3.15E-01	-0.028604	-0.056205
MidMississauga	-0.00525017	-0.000108205	-6.20E-05	-0.00132655	-0.00123456	-0.000304481	-0.000370279
CretaceousVerrillCanyor	-0.0543982	-0.00733745	-0.00121289	-0.0146431	-0.00925882	-0.00514936	-0.00518443
Upp_Jurassic_Res	-26.621	-0.763204	-0.302905	-5.26975	-4.53006	-0.729545	-0.843787
Jurassic_VerrillCanyon	-8.0943	-1.37823	-0.340801	-3.7076	-2.8282	-0.574328	-0.593085
Late_Jurassic	-9.64513	28.7597	9.792	158.843	135.688	-0.473224	-0.500663
Misaine_1	-14.7248	0.0307327	0.0133417	-0.081742	-1.42633	-0.28564	-0.327256
Scatarie	-118.855	-0.049435	-0.0237096	-1.34116	-6.6818	-2.92092	-2.36167
Mohican	-589.654	-0.000828684	-0.000700315	-0.126929	-2.20478	4.22E+01	40.78
Early_Jur_Lacustrine_SR	1313.54	-0.000162925	-0.000111253	-0.0132754	-0.230668	-9.56E-03	-0.0103706
Triassic _Lacustrine_SR	-1.00E+02	-7.27E-06	-8.84E-06	-1.59E-03	-1.77E-02	-5.28E-04	-0.00101228
Sum Expelled	**444.043**	**2.66E+01**	**9.11E+00**	**1.48E+02**	**117.42**	**3.72E+01**	**36.076**
Middle-LateMioceneReservoi	0.00340599	0.00833695	0.00195105	0.0173001	0.0362263	0.0658961	0.0494668
Early_MiocReservoir	8.68101	0.205046	0.117898	2.56692	2.52262	0.8265	0.91254
LoganCanyon	12.51	0.266749	0.16017	3.4109	2.8075	0.354444	0.593274
MississaugaReservoir	3.49274	0.0895103	0.0372321	0.788017	0.827042	0.233171	0.285614

Mass Balance of Hydrocarbons

mass in $(10)^9$ kg(Mtons)/$m^{3)}$

	C6-C14_Mohican	C15+_Mohican	Sum
Late_Paleocene	0	0	1.52501
Middle_Paleocene	0	0	0.00839212
MidMississauga	0	0	0.065726
CretaceousVerrillCanyon	0	0	1910.99
Upp_Jurassic_Res	0	0	1.61818
Jurassic_VerrillCanyon	0	0	1807.84
Late_Jurassic	0	0	339.672
Misaine_1	0	0	518.874
Scatarie	0.0091014	0.073949	-101.715
Mohican	29.161	237.93	-195.585
Early_Jur_Lacustrine_SR	0	0	2735.92
Triassic _Lacustrine_SR	0	0	2055.1
Sum Generated	**29.1701**	**238.004**	**9074.32**
Late_Paleocene	0.0039106	0.034275	3.10216
Middle_Paleocene	0.049243	0.405	21.3585
MidMississauga	0.000327883	0.00316191	0.285418
CretaceousVerrillCanyon	0.00417254	0.039763	272.631
Upp_Jurassic_Res	0.720343	6.70398	190.786
Jurassic_VerrillCanyon	0.583692	5.92018	85.671
Late_Jurassic	0.570421	6.04881	61.1635
Misaine_1	0.381907	4.49184	34.1547
Scatarie	2.25429	32.59	217.767
Mohican	0.494141	11.3686	33.2188
Early_Jur_Lacustrine_SR	0.0216584	1.55937	5.13456
Triassic _Lacustrine_SR	0.00298764	0.25724	105.559
Sum Accumulated in Source	**5.08709**	**69.4222**	**1030.83**
Late_Paleocene	-0.0039106	-0.034275	-1.57715
Middle_Paleocene	-0.049243	-0.405	-21.3501
MidMississauga	-0.000327883	-0.00316191	-0.219692
CretaceousVerrillCanyon	-0.00417254	-0.039763	1638.36
Upp_Jurassic_Res	-0.720343	-6.70398	-189.168
Jurassic_VerrillCanyon	-0.583692	-5.92018	1722.17
Late_Jurassic	-0.570421	-6.04881	278.508
Misaine_1	-0.381907	-4.49184	484.719
Scatarie	-2.24519	-32.5161	-319.481
Mohican	28.6669	226.561	-228.804
Early_Jur_Lacustrine_SR	-0.0216584	-1.55937	2730.79
Triassic _Lacustrine_SR	-0.00298764	-0.25724	1949.54
Sum Expelled	**24.083**	**168.582**	**8043.48**
Middle-LateMioceneReservoi	0.0210951	0.171322	6.11783
Early_MiocReservoi	0.69396	5.55967	202.101
LoganCanyon	0.531003	4.31054	222.218
MississaugaReservoi	0.27216	2.81176	143.698

Mass Balance of Hydrocarbons

mass in $(10)^{9}$ kg(Mtons)/$m^{3)}$

Sum Accumulated in Reservoir	**40.3816**	**10.0703**	**6.18052**	**11.1072**	**1.12E-06**	**3.79E-06**	**4.10E-05**	**0.00024981**
Migration Losses	**194.231**	**0.0788356**	**0.0567975**	**0.140013**	**3.10E-09**	**1.11E-08**	**1.32E-07**	**7.81E-07**
Sec. Cracking Losses	**-174.954**	**94.6859**	**128.697**	**1054.95**	**1.22E-08**	**5.98E-10**	**-3.30E-09**	**9.45E-08**
Middle-LateMioceneReservoi	0	0	0	0	3.08E-15	2.95E-15	2.58E-16	2.81E-19
Early_MiocReservoi	0.0031489	0.00031875	3.31E-06	2.54E-09	3.91E-09	1.53E-08	2.11E-07	1.16E-06
Late_Eocene	11.071	8.0952	5.496	14.126	1.38E-07	4.45E-07	5.14E-06	3.01E-05
Middle_Eocene	5.3589	3.3368	1.9717	5.4267	2.24E-08	7.63E-08	8.76E-07	5.14E-06
Ealy-Middle_Eocene	0.17398	0.031563	0.003935	0.00038879	1.60E-10	2.46E-10	2.37E-10	8.55E-12
Late_Paleocene	1.80E+00	4.08E-01	1.19E-01	1.46E-02	7.24E-10	8.97E-10	5.20E-10	7.13E-12
Middle_Paleocene	5.36E-01	9.21E-02	1.25E-02	1.07E-03	4.69E-10	4.12E-10	1.34E-10	8.12E-13
WyandotDawsonCanyor	1.05E+01	6.57E+00	3.70E+00	1.37E+01	9.68E-09	3.07E-08	3.83E-07	2.16E-06
LoganCanyon	2.04E+01	3.58E+00	0.27381	0.0261	0.00E+00	0.00E+00	8.32E-12	1.76E-11
MidMississauga	2.10E+01	3.92E+00	2.02E-01	6.03E-04	0	0	0	0
MississaugaReservoi	2.76E+01	7.23E+00	3.25E+00	8.8651	0	0	0	0
EarlyMississauga	7.9368	2.0066	0.063948	1.40E-05	0	0	0	0
CretaceousVerrillCanyor	0	0	0	0	0	0	0	0
Upp_Jurassic_Res	0	0	0	0	0	0	0	0
Jurassic_VerrillCanyor	0	0	0	0	0	0	0	0
Late_Jurassic	0	0	0	0	0	0	0	0
Misaine_1	8.92E-20	3.65E-21	1.13E-26	3.36E-44	0	0.00E+00	0	0
Scatarie	0.0013423	0.0016645	5.62E-06	3.52E-10	0.00E+00	0.00E+00	0.00E+00	0.00E+00
Mohican	0.099517	0.13272	0.0039082	4.12E-05	0	0.00E+00	0.00E+00	0.00E+00
Early_Jur_Lacustrine_SR	4.58E-11	2.04E-11	7.98E-14	2.09E-18	0.00E+00	0.00E+00	0.00E+00	0.00E+00
Triassic _Lacustrine_SR	1.95E-10	1.19E-10	4.49E-13	6.19E-18	0.00E+00	0.00E+00	0.00E+00	0.00E+00
Sum Outflow Top	**111.62**	**39.272**	**17.8**	**48.871**	**2.24E-07**	**7.37E-07**	**8.65E-06**	**5.03E-05**
Middle-LateMioceneReservoi	4.04E+00	1.37E+00	0.89638	1.761	3.52E-07	1.20E-06	1.31E-05	8.13E-05
Early_MiocReservoi	7.83E+00	4.06E+00	2.9576	5.4001	1.03E-07	3.77E-07	4.60E-06	2.67E-05
Late_Eocene	2.73E-07	2.69E-08	5.75E-10	1.47E-14	2.18E-15	1.52E-15	5.31E-16	5.70E-20
Middle_Eocene	6.65E-06	6.70E-07	2.10E-08	6.93E-12	5.28E-14	3.74E-14	1.90E-14	2.41E-17
Ealy-Middle_Eocene	2.42E-07	2.32E-08	9.93E-10	1.37E-11	2.52E-15	1.89E-15	1.49E-15	6.22E-17
Late_Paleocene	3.08E-21	2.45E-22	9.18E-24	1.51E-25	3.20E-29	1.96E-29	1.28E-29	6.46E-31
Middle_Paleocene	0	0	0	0	5.77E-35	1.73E-33	3.53E-34	1.06E-37
WyandotDawsonCanyor	1.61E-27	2.44E-28	1.35E-29	1.31E-32	1.28E-34	6.43E-35	2.86E-35	5.65E-38
LoganCanyon	1.11E-19	1.72E-20	1.18E-21	3.51E-23	2.63E-08	1.02E-07	1.44E-06	7.84E-06
MidMississauga	2.55E-10	3.69E-11	2.48E-12	6.52E-14	2.06E-17	1.72E-17	1.92E-17	1.25E-18
MississaugaReservoi	1.94E-13	1.57E-13	1.83E-14	1.17E-15	5.33E-10	1.85E-09	2.74E-08	1.43E-07
EarlyMississauga	0.00014899	0.00012677	7.92E-05	0.00030585	4.87E-18	6.52E-16	6.45E-14	3.81E-13
CretaceousVerrillCanyor	63.533	16.701	7.9419	19.696	2.93E-32	3.81E-32	4.83E-32	1.60E-30
Upp_Jurassic_Res	0.00092906	0.00076416	0.00058471	0.00087612	4.47E-36	4.20E-35	7.79E-35	8.70E-35
Jurassic_VerrillCanyor	0.17191	0.13051	0.087167	0.21829	1.96E-44	3.64E-44	4.79E-42	2.97E-41
Late_Jurassic	0.16212	0.14095	0.11017	0.29733	3.57E-43	4.75E-43	6.50E-43	3.76E-41
Misaine_1	0.023324	0.01944	0.015243	0.033425	0	0	0	0
Scatarie	0	0	0	0	0	0	0	0
Mohican	0.10996	0.11556	0.10416	0.4297	4.54E-41	5.34E-41	6.38E-41	7.13E-40

Mass Balance of Hydrocarbons

mass in $(10)^9$ kg(Mtons)/$m^{3)}$

Sum Accumulated in Reservoir	**6.07996**	**2.46673**	**43.4037**	**29.9825**	**2.83154**	**0.883108**
Migration Losses	**7.87E-01**	**4.96E-02**	**7.60E-01**	**0.464847**	**0.353972**	**0.0182678**
Sec. Cracking Losses	**8.63E+01**	**1.73E+01**	**6.36E+01**	**8.95668**	**37.2127**	**7.90442**
Middle-LateMioceneReservoi	2.39E-07	7.81E-09	4.67E-10	1.25E-13	6.29E-08	5.91E-09
Early_MiocReservoir	3.48E-01	9.74E-02	1.14E+00	5.98E-01	0.063641	0.039043
Late_Eocene	4.9056	3.4057	64.872	46.022	1.1687	0.78001
Middle_Eocene	2.6528	1.6687	28.702	19.072	0.62428	0.3706
Ealy-Middle_Eocene	0.48599	0.045128	0.058124	0.0077066	0.10075	0.015753
Late_Paleocene	0.94848	0.1319	0.21804	0.025058	2.88E-01	4.99E-02
Middle_Paleocene	0.15592	0.024067	0.034829	0.0018927	4.05E-02	7.01E-03
WyandotDawsonCanyor	9.76E+00	4.20E+00	6.76E+01	3.71E+01	1.23E+00	5.15E-01
LoganCanyon	8.57E+00	2.94E+00	3.48E+01	2.32E+01	4.14E+00	1.22E+00
MidMississauga	0.14058	0.034593	0.4938	0.072148	1.48E-01	4.81E-02
MississaugaReservoir	0.04522	0.010777	0.34231	5.2718	0.067453	0.018934
EarlyMississauga	0.0064755	0.0013014	0.038107	0.050782	0.012465	0.0026429
CretaceousVerrillCanyor	0	0	0	0	0	0
Upp_Jurassic_Res	1.21E-06	5.79E-08	2.05E-07	5.59E-07	0.00031395	1.53E-05
Jurassic_VerrillCanyor	3.85E-17	3.65E-18	1.32E-17	7.63E-17	4.66E-10	1.14E-10
Late_Jurassic	0	0	0	0	0	0
Misaine_1	0	0	0	0	5.05E-17	5.88E-18
Scatarie	0	0	0	0	0	0
Mohican	0	0	0	0	0	0
Early_Jur_Lacustrine_SR	0	0	0	0	0	0
Triassic _Lacustrine_SR	0	0	0	0.00E+00	0	0
Sum Outflow Top	**3.14E+01**	**1.45E+01**	**2.33E+02**	**1.56E+02**	**8.6148**	**3.5584**
Middle-LateMioceneReservoi	0.53777	0.31521	6.1108	4.4902	2.67E-01	1.09E-01
Early_MiocReservoir	2.5654	1.3954	25.596	18.56	7.66E-01	4.53E-01
Late_Eocene	5.52E-08	7.62E-09	4.36E-09	4.57E-14	2.01E-08	2.27E-09
Middle_Eocene	1.36E-06	1.92E-07	1.62E-07	2.11E-11	4.91E-07	5.63E-08
Ealy-Middle_Eocene	4.91E-08	6.57E-09	8.02E-09	4.39E-11	1.80E-08	2.00E-09
Late_Paleocene	6.24E-22	6.90E-23	7.22E-23	4.78E-25	2.29E-22	2.11E-23
Middle_Paleocene	5.15E-27	1.06E-26	1.81E-27	5.20E-32	8.97E-28	3.92E-27
WyandotDawsonCanyor	3.72E-28	7.72E-29	1.27E-28	4.20E-32	1.22E-28	2.05E-29
LoganCanyon	5.6102	1.6083	14.853	8.7974	1.0506	0.43586
MidMississauga	5.68E-11	1.10E-11	2.17E-11	2.17E-13	1.94E-11	3.16E-12
MississaugaReservoir	0.69678	0.2102	1.6472	1.5875	0.3296	0.16354
EarlyMississauga	0.00011431	4.96E-05	0.0009044	0.00072427	1.58E-05	9.74E-06
CretaceousVerrillCanyor	18.501	4.893	57.451	45.359	6.0199	1.4193
Upp_Jurassic_Res	41.731	18.384	321.01	325.18	42.212	15.777
Jurassic_VerrillCanyor	0.7589	0.38642	9.6587	7.8533	0.32003	0.15777
Late_Jurassic	0.01956	0.0086215	0.10233	0.063783	0.29569	0.12863
Misaine_1	0.0048988	0.003614	0.0065697	0.016166	0.26746	0.1162
Scatarie	3.52E-19	1.52E-19	1.19E-19	2.76E-19	0.044157	0.024633
Mohican	8.82E-05	2.42E-06	2.93E-06	9.63E-07	0.0042489	0.0022582

Mass Balance of Hydrocarbons

mass in $(10)^9$ kg(Mtons)/$m^{3)}$

Sum Accumulated in Reservoir	**8.50063**	**6.1676**	**2.94E-04**	**1.22E-03**	**3.00E-03**	**4.98E-03**
Migration Losses	**0.180356**	**0.125983**	**2.21E-07**	**9.98E-07**	**2.75E-06**	**4.70E-06**
Sec. Cracking Losses	**21.695**	**2.43442**	**-6.69E-07**	**-8.04E-06**	**4.40E-06**	**1.36E-06**
Middle-LateMioceneReservoi	2.28E-10	6.66E-14	1.11E-09	3.15E-09	7.99E-10	3.51E-13
Early_MiocReservoi	0.40822	0.29618	8.84E-06	5.20E-05	0.000156	0.00025924
Late_Eocene	10.294	8.1873	0.00017734	0.00075099	0.0019459	0.0032365
Middle_Eocene	4.6537	3.71	2.95E-06	1.39E-05	3.65E-05	6.09E-05
Ealy-Middle_Eocene	0.028029	0.0061145	5.50E-07	3.19E-07	1.06E-07	4.56E-13
Late_Paleocene	8.91E-02	6.04E-03	2.31E-07	8.26E-08	2.28E-10	3.32E-16
Middle_Paleocene	1.09E-02	5.36E-04	1.27E-09	4.60E-10	1.81E-12	3.42E-18
WyandotDawsonCanyor	7.03E+00	5.83E+00	0.00E+00	0.00E+00	0.00E+00	0.00E+00
LoganCanyon	8.36E+00	4.77E+00	0.00E+00	0.00E+00	0.00E+00	0
MidMississauga	4.05E-01	8.18E-04	0	0	0	0
MississaugaReservoi	0.2463	0.69586	0	0	0	0
EarlyMississauga	0.028169	0.00011456	0	0	0	0
CretaceousVerrillCanyor	0	0	0.00E+00	0.00E+00	0.00E+00	0.00E+00
Upp_Jurassic_Res	7.59E-06	6.83E-07	0	0	0	0
Jurassic_VerrillCanyon	5.67E-11	7.48E-12	0	0	0	0
Late_Jurassic	1.09E-43	6.59E-39	0	0	0	0
Misaine_1	2.24E-16	1.32E-15	0	0	0	0
Scatarie	0	0	0	0	0	0
Mohican	0	0	0	0	0	0
Early_Jur_Lacustrine_SR	0	0	0	0	0	0
Triassic _Lacustrine_SR	0	0	0	0	0	0
Sum Outflow Top	**37.944**	**28.55**	**0.00024433**	**0.001033**	**0.0026274**	**0.0043558**
Middle-LateMioceneReservoi	1.14E+00	8.66E-01	9.31E-05	0.000413	0.0011166	0.0019086
Early_MiocReservoi	5.48E+00	4.08E+00	0.00012939	0.00057338	0.0015173	0.0025273
Late_Eocene	8.19E-10	8.85E-15	5.75E-09	1.26E-08	8.32E-10	5.42E-15
Middle_Eocene	2.99E-08	4.07E-12	1.63E-07	3.95E-07	4.16E-08	3.88E-12
Ealy-Middle_Eocene	1.52E-09	8.31E-12	1.80E-08	4.18E-08	8.08E-09	1.20E-11
Late_Paleocene	1.38E-23	9.17E-26	6.82E-15	2.27E-15	4.43E-18	2.49E-24
Middle_Paleocene	6.38E-28	2.59E-32	2.13E-13	7.00E-14	1.60E-16	6.80E-23
WyandotDawsonCanyor	2.11E-29	7.07E-33	2.36E-32	1.11E-31	2.79E-31	8.73E-35
LoganCanyon	4.0872	2.973	4.82E-40	2.05E-39	5.81E-39	8.66E-42
MidMississauga	3.90E-12	3.78E-14	5.06E-30	2.44E-29	7.60E-29	1.17E-31
MississaugaReservoi	0.62756	0.34511	1.15E-38	5.60E-38	9.23E-38	6.64E-39
EarlyMississauga	0.0001594	0.0001387	8.09E-31	6.20E-30	6.92E-28	2.15E-26
CretaceousVerrillCanyor	12.882	10.31	0	0	0	0
Upp_Jurassic_Res	81.457	51.218	0	0	0	0
Jurassic_VerrillCanyon	1.2342	0.77141	0	0	0	0
Late_Jurassic	1.3723	1.1156	0	0	0	0
Misaine_1	0.97464	0.65162	0	0	0	0
Scatarie	0.14423	0.074398	0	0	0	0
Mohican	0.0041302	0.00073475	0	0	0	0

Mass Balance of Hydrocarbons

mass in $(10)^9$ kg(Mtons)/$m^{3)}$

Sum Accumulated in Reservoir	**21.9201**	**11.4495**	**160.099**	**62.8701**	**46.7259**	**18.9597**	**27.8023**
Migration Losses	**50.8527**	**25.6578**	**348.736**	**121.951**	**2.63E+01**	**2.36E-01**	**4.44E-01**
Sec. Cracking Losses	**30.4332**	**10.535**	**83.4346**	**11.0997**	**3.79E+02**	**1.53E+02**	**1.49E+02**
Middle-LateMioceneReservoi	6.26E-07	7.66E-08	6.88E-09	6.20E-13	5.42E-07	4.65E-08	1.61E-10
Early_MiocReservoir	0.58459	0.37964	5.407	1.9853	0.31792	0.36783	0.78534
Late_Eocene	7.4747	4.6616	69.063	28.967	12.735	15.312	28.411
Middle_Eocene	2.4486	1.7629	25.541	11.148	6.8961	6.8025	11.461
Ealy-Middle_Eocene	4.46E-01	7.96E-02	1.80E-01	9.05E-03	0.90502	0.30259	0.12286
Late_Paleocene	0.85739	0.1131	0.32132	0.050788	3.1196	0.97544	0.39539
Middle_Paleocene	0.11437	0.017679	0.073187	0.0080743	0.49048	0.17284	0.039743
WyandotDawsonCanyon	4.86E+00	2.24E+00	3.01E+01	1.70E+01	9.98E+00	1.07E+01	1.66E+01
LoganCanyon	1.42E+00	6.99E-01	9.72E+00	4.6591	4.95E+01	2.46E+01	2.25E+01
MidMississauga	4.22E-06	4.95E-07	2.24E-08	6.29E-10	10.986	5.9559	0.58711
MississaugaReservoir	3.48E-06	6.92E-07	7.84E-06	0.00025598	9.7903	7.9257	9.5541
EarlyMississauga	6.76E-16	1.32E-16	0	0	4.9883	3.1957	0.14834
CretaceousVerrillCanyon	2.79E-16	5.42E-17	-4.86E-35	-3.84E-33	0	0	0
Upp_Jurassic_Res	0	0	0	0	0.0015781	0.0001813	3.27E-06
Jurassic_VerrillCanyon	0	0	0	0	3.77E-09	1.37E-09	2.46E-11
Late_Jurassic	0	0	0	0	1.70E-28	7.53E-29	2.57E-31
Misaine_1	0	0	0	0	0.00066821	0.00038257	1.51E-06
Scatarie	0	0	0	0	0.088836	0.046973	0.00019046
Mohican	0	0	0	0	1.1436	0.45444	0.020662
Early_Jur_Lacustrine_SR	0	0	0	0	5.79E-04	2.74E-04	9.17E-07
Triassic _Lacustrine_SR	0	0	0	0	0.00E+00	0.00E+00	0.00E+00
Sum Outflow Top	**24.179**	**13.654**	**195.07**	**86.828**	**1.18E+02**	**8.54E+01**	**1.07E+02**
Middle-LateMioceneReservoi	1.6784	0.91257	12.967	5.4853	4.6001	2.4523	3.7935
Early_MiocReservoir	11.699	6.6643	99.101	41.382	9.2851	8.5214	16.156
Late_Eocene	2.90E-07	3.20E-08	1.41E-08	9.45E-14	2.92E-07	5.86E-08	1.02E-09
Middle_Eocene	6.90E-06	7.71E-07	5.00E-07	4.17E-11	7.12E-06	1.45E-06	4.57E-08
Ealy-Middle_Eocene	2.99E-07	3.12E-08	2.73E-08	8.63E-11	2.58E-07	5.15E-08	2.79E-09
Late_Paleocene	3.81E-21	3.29E-22	2.53E-22	9.74E-25	3.28E-21	5.54E-22	2.52E-23
Middle_Paleocene	9.59E-27	4.35E-26	9.03E-27	1.81E-31	4.46E-27	4.17E-26	4.61E-28
WyandotDawsonCanyon	1.43E-27	1.92E-28	2.09E-28	3.81E-32	1.67E-27	5.09E-28	4.00E-29
LoganCanyon	7.9112	4.1975	56.274	22.714	6.2937	4.5075	7.8264
MidMississauga	2.37E-10	3.36E-11	4.57E-11	2.49E-13	2.68E-10	7.87E-11	8.24E-12
MississaugaReservoir	0.14557	0.06304	0.85899	1.664	1.0155	0.66401	1.1713
EarlyMississauga	0.26089	0.13093	1.8326	0.74361	7.67E-05	0.00017403	0.00035996
CretaceousVerrillCanyon	7.0703	3.2305	33.149	8.2652	57.652	20.032	26.243
Upp_Jurassic_Res	1.7071	0.78686	11.317	11.853	163.53	89.856	86.765
Jurassic_VerrillCanyon	0.0032773	0.0020969	0.030108	0.0082289	0.51089	0.3936	0.69538
Late_Jurassic	0.00079481	0.00060551	0.011059	0.0039133	0.4255	0.40018	0.75363
Misaine_1	5.59E-06	4.70E-06	9.21E-05	4.15E-05	0.21473	0.12361	0.18214
Scatarie	0	0	0	0	0.17501	0.078594	0.077915
Mohican	1.06E-05	2.26E-06	2.84E-06	5.07E-07	0.94142	1.087	2.6223

Mass Balance of Hydrocarbons

mass in $(10)^{9}$ kg(Mtons)/$m^{3)}$

Sum Accumulated in Reservoir	**24.6872**	**0.569642**	**0.317252**	**6.78314**	**6.19339**	**1.48E+00**	**1.84089**
Migration Losses	**0.421768**	**0.0198251**	**0.00752648**	**0.230634**	**2.27453**	**0.0759174**	**0.171863**
Sec. Cracking Losses	**185.334**	**8.06953**	**1.90217**	**22.9742**	**14.5051**	**18.5993**	**16.9838**
Middle-LateMioceneReservoi	7.04E-15	3.21E-08	1.35E-09	1.33E-10	4.12E-14	8.69E-08	1.35E-08
Early_MiocReservoi	0.79816	3.93E-02	1.44E-02	0.2487	0.18955	0.032233	0.041395
Late_Eocene	30.678	0.60768	0.41757	8.7806	6.6398	0.53861	1.1289
Middle_Eocene	12.408	3.01E-01	2.02E-01	3.8849	2.8806	0.33934	0.52098
Ealy-Middle_Eocene	0.020899	0.055801	0.0049914	0.014739	0.0054556	5.98E-02	0.030926
Late_Paleocene	0.0091596	0.13175	0.015885	0.076769	0.024403	0.16044	0.081811
Middle_Paleocene	0.00050158	0.020335	0.0029211	0.01052	0.0012648	0.019558	0.011018
WyandotDawsonCanyon	2.02E+01	8.94E-01	3.65E-01	6.32E+00	4.65E+00	4.77E-01	0.68203
LoganCanyon	1.34E+01	2.19E+00	5.48E-01	6.12E+00	3.84E+00	2.75E+00	2.2133
MidMississauga	1.47E-05	0.045893	0.012772	0.1768	0.0033642	0.22274	0.19355
MississaugaReservoi	16.41	0.019491	0.0049192	0.096844	0.32682	0.13565	0.16583
EarlyMississauga	9.99E-08	0.0032749	0.0006572	0.012798	0.0017928	0.048957	0.044249
CretaceousVerrillCanyon	0	0	0	0	0	0.00E+00	0
Upp_Jurassic_Res	5.67E-08	1.08E-05	4.99E-07	1.29E-06	2.64E-07	7.53E-05	1.01E-05
Jurassic_VerrillCanyon	2.20E-12	2.57E-13	2.21E-14	1.52E-13	8.55E-14	2.08E-10	1.42E-10
Late_Jurassic	3.22E-44	1.70E-18	1.41E-19	0	0	8.95E-35	3.94E-35
Misaine_1	1.03E-15	5.76E-21	5.68E-22	0	0	9.47E-08	2.54E-07
Scatarie	1.91E-12	0	0	0	0	1.46E-06	3.44E-06
Mohican	2.19E-06	0	0	0	0	1.79E-05	1.32E-05
Early_Jur_Lacustrine_SR	2.99E-12	0	0	0	0	0	0
Triassic _Lacustrine_SR	0.00E+00	0	0	0	0	0	0
Sum Outflow Top	**1.12E+02**	**4.7046**	**1.8348**	**30.839**	**22.494**	**5.116**	**5.7864**
Middle-LateMioceneReservoi	3.3704	0.056844	0.039293	0.91745	0.87398	0.14901	0.21626
Early_MiocReservoi	16.197	0.32867	0.18904	4.1707	3.4261	0.40499	0.69459
Late_Eocene	1.32E-15	7.36E-09	9.88E-10	6.61E-10	7.85E-15	1.07E-08	3.85E-09
Middle_Eocene	9.19E-13	1.80E-07	2.48E-08	2.42E-08	3.63E-12	2.59E-07	9.52E-08
Ealy-Middle_Eocene	2.17E-12	6.70E-09	8.65E-10	1.22E-09	7.24E-12	9.52E-09	3.30E-09
Late_Paleocene	2.75E-26	8.52E-23	9.09E-24	1.11E-23	8.06E-26	1.21E-22	3.49E-23
Middle_Paleocene	3.79E-34	5.52E-28	1.54E-27	3.89E-28	1.65E-32	4.24E-28	4.39E-27
WyandotDawsonCanyon	3.03E-34	4.97E-29	9.90E-30	1.81E-29	6.08E-33	5.94E-29	3.15E-29
LoganCanyon	7.1576	0.65605	0.18462	2.7477	2.152	0.52777	0.50344
MidMississauga	1.71E-14	7.65E-12	1.46E-12	3.25E-12	3.28E-14	9.51E-12	4.93E-12
MississaugaReservoi	0.65537	0.14111	0.025705	0.43633	0.5483	0.10678	0.059877
EarlyMississauga	0.00046749	1.91E-05	9.73E-06	0.00017695	0.00012146	4.90E-06	1.09E-05
CretaceousVerrillCanyon	27.745	2.2199	0.6778	10.548	10.055	2.7473	2.64
Upp_Jurassic_Res	58.432	9.003	3.633	63.563	51.287	7.7535	6.9294
Jurassic_VerrillCanyon	0.55239	0.39413	0.15907	2.4672	1.8048	0.040597	0.048675
Late_Jurassic	0.85679	0.36347	0.13362	1.9999	1.6259	0.03439	0.044733
Misaine_1	0.12571	0.030989	0.0099149	0.1756	0.17682	0.014691	0.017286
Scatarie	0.021368	1.37E-09	5.25E-10	3.74E-08	1.19E-06	0.014725	0.016711
Mohican	4.1773	1.46E-06	4.93E-07	2.29E-05	0.00012721	0.10013	0.11924

Mass Balance of Hydrocarbons

mass in $(10)^9$ kg(Mtons)/$m^{3)}$			
Sum Accumulated in Reservoir	**1.51822**	**12.8533**	**574.135**
Migration Losses	**0.384576**	**16.2503**	**791.221**
Sec. Cracking Losses	**10.9238**	**62.9384**	**2507.8**
Middle-LateMioceneReservoi	4.61E-11	9.54E-14	1.75E-06
Early_MiocReservoir	0.038186	0.38939	14.6149
Late_Eocene	0.9745	5.9299	400.75
Middle_Eocene	0.38189	2.273	166.8
Ealy-Middle_Eocene	0.01188	0.1178	3.32481
Late_Paleocene	0.033635	0.10976	10.5789
Middle_Paleocene	0.0027494	0.0040828	1.90682
WyandotDawsonCanyor	0.39144	1.8011	294.906
LoganCanyon	1.2053	7.569	265.152
MidMississauga	0.020717	0.00012368	44.6518
MississaugaReservoir	0.10815	1.2646	99.4146
EarlyMississauga	0.0027058	1.42E-06	18.5942
CretaceousVerrillCanyor	0	0	3.34E-16
Upp_Jurassic_Res	2.19E-07	4.53E-07	0.00220117
Jurassic_VerrillCanyon	3.09E-12	4.78E-12	6.17E-09
Late_Jurassic	5.53E-35	2.19E-36	1.84E-18
Misaine_1	4.38E-07	7.73E-10	0.00105307
Scatarie	3.74E-06	3.47E-11	0.139021
Mohican	1.80E-05	9.91E-07	1.85494
Early_Jur_Lacustrine_SR	0	0	0.000853797
Triassic _Lacustrine_SR	0	0	3.15E-10
Sum Outflow Top	**3.782**	**23.793**	**1571.43**
Middle-LateMioceneReservoi	0.19126	1.6353	61.2535
Early_MiocReservoir	0.65861	5.2238	303.241
Late_Eocene	1.07E-10	1.11E-14	1.12E-06
Middle_Eocene	3.89E-09	5.23E-12	2.76E-05
Ealy-Middle_Eocene	1.81E-10	9.14E-12	1.11E-06
Late_Paleocene	1.69E-24	1.08E-25	9.09E-15
Middle_Paleocene	5.96E-29	3.41E-32	2.84E-13
WyandotDawsonCanyor	2.27E-30	5.98E-33	6.83E-27
LoganCanyon	0.39547	3.5867	167.051
MidMississauga	4.37E-13	3.54E-14	1.11E-09
MississaugaReservoir	0.06443	0.86157	14.0894
EarlyMississauga	7.63E-06	3.91E-05	2.97228
CretaceousVerrillCanyor	1.7776	12.87	491.63
Upp_Jurassic_Res	4.1735	26.802	1494.36
Jurassic_VerrillCanyon	0.048954	0.34268	29.2507
Late_Jurassic	0.038676	0.31826	10.8285
Misaine_1	0.016059	0.14682	3.36711
Scatarie	0.01245	0.10548	0.789672
Mohican	0.094727	0.80301	10.7161

Mass Balance of Hydrocarbons

mass in $(10)^9$ kg(Mtons)/$m^{3)}$								
Early_Jur_Lacustrine_SR	0.0019936	0.010442	0.012762	0.097611	2.80E-45	2.80E-45	4.20E-45	2.38E-44
Triassic _Lacustrine_SR	0.83284	0.17041	0.12169	0.47081	7.01E-45	7.01E-45	8.41E-45	3.64E-44
Eurydice_1	1.0389	0.33128	0.2754	1.1758	3.89E-40	4.03E-40	4.37E-40	2.13E-39
Sum Outflow Side	**77.746**	**23.052**	**12.523**	**29.581**	**4.81E-07**	**1.68E-06**	**1.92E-05**	**0.00011601**
Sum HC Losses	**208.643**	**157.089**	**159.076**	**1133.54**	**7.21E-07**	**2.43E-06**	**2.80E-05**	**0.00016721**

Mass Balance of Hydrocarbons

mass in $(10)^9$ kg(Mtons)/m$^{3)}$						
Early_Jur_Lacustrine_SR	7.55E-09	1.62E-10	1.25E-10	2.00E-11	9.25E-09	3.09E-09
Triassic _Lacustrine_SR	1.54E-08	3.02E-10	2.12E-10	2.29E-11	6.62E-09	1.16E-10
Eurydice_1	0.0016942	3.79E-05	3.33E-05	5.74E-06	0.00077212	1.87E-05
Sum Outflow Side	**70.427**	**27.205**	**436.43**	**411.91**	**51.577**	**18.787**
Sum HC Losses	**188.917**	**59.0276**	**733.684**	**577.202**	**97.7585**	**30.2681**

Mass Balance of Hydrocarbons

mass in $(10)^9$ kg(Mtons)/$m^{3)}$						
Early_Jur_Lacustrine_SR	4.99E-09	1.58E-09	0	0	0	0
Triassic _Lacustrine_SR	1.05E-10	1.16E-11	0	0	0	0
Eurydice_1	2.21E-05	2.75E-06	0	0	0	0
Sum Outflow Side	**109.4**	**72.401**	**0.00022263**	**0.00098683**	**0.0026339**	**0.0044359**
Sum HC Losses	**169.219**	**103.511**	**0.000466512**	**0.00201279**	**0.00526845**	**0.00879776**

Mass Balance of Hydrocarbons

mass in $(10)^9$ kg(Mtons)/$m^{3)}$							
Early_Jur_Lacustrine_SR	8.92E-10	1.87E-10	1.69E-10	1.27E-11	0.42132	0.53781	1.388
Triassic _Lacustrine_SR	1.82E-09	3.77E-10	3.24E-10	1.63E-11	1.83E-05	1.73E-05	2.14E-05
Eurydice_1	0.00020041	4.10E-05	4.26E-05	4.21E-06	0.049941	0.0098398	0.0067149
Sum Outflow Side	**30.477**	**15.988**	**215.54**	**92.119**	**245.11**	**128.66**	**147.68**
Sum HC Losses	**135.942**	**65.8348**	**842.781**	**311.998**	**768.325**	**367.132**	**404.727**

Mass Balance of Hydrocarbons

mass in $(10)^9$ kg(Mtons)/$m^{3)}$							
Early_Jur_Lacustrine_SR	2.3447	4.24E-11	2.09E-11	1.72E-09	1.24E-08	0.00088126	0.0012209
Triassic _Lacustrine_SR	2.46E-06	4.40E-11	3.12E-11	3.25E-09	2.34E-08	4.26E-09	6.83E-09
Eurydice_1	0.00026346	5.98E-06	3.91E-06	0.00036775	0.0025384	0.0011227	0.0016926
Sum Outflow Side	**121.64**	**13.194**	**5.0521**	**87.026**	**71.953**	**11.896**	**11.293**
Sum HC Losses	**419.356**	**25.988**	**8.7966**	**141.07**	**111.227**	**35.6872**	**34.2351**

Mass Balance of Hydrocarbons

mass in $(10)^9$ kg(Mtons)/$m^{3)}$			
Early_Jur_Lacustrine_SR	0.00086326	0.0053249	4.82293
Triassic _Lacustrine_SR	9.88E-09	3.59E-07	1.59581
Eurydice_1	0.0017808	0.045751	2.94428
Sum Outflow Side	**7.4744**	**52.747**	**2598.9**
Sum HC Losses	**22.5648**	**155.729**	**7469.34**

Table 9b. Mass Balance of Hydrocarbons

mass in $(10)^9$ kg(Mtons)/m^3

	Methane_JVC	C2-C5_JVC	C6-C14_JVC	C15+_JVC	Methane_Misaine	C2-C5_Misaine	C6-C14_Misaine	C15+_Misaine
Late_Paleocene	1.12E-30	1.14E-30	-2.72E-30	-5.83E-31	2.46E-30	2.41E-30	-6.88E-30	-9.39E-32
Cretaceous_VC	1.30E-03	1.51E-03	2.97E-04	-4.95E-03	1.78E-05	1.89E-05	-1.36E-06	-5.90E-05
Mic Mac	7.73E+00	3.30E+00	5.74E+01	5.84E+01	0.022048	0.025393	0.003594	-0.081973
Jurassic_VerrillCanyon	3.53E+01	1.68E+01	3.74E+02	4.33E+02	4.67E-03	4.67E-03	-1.47E-03	-1.38E-02
Late_Jurassic	0.00161075	0.00130428	-0.00135896	-0.00333566	8.71E-02	6.01E-02	-8.94E-02	-1.48E-01
Misaine_1	0.00224551	0.00230527	-0.00160654	-0.0056697	1.31E+01	5.31E+00	9.48E+01	8.93E+01
Misaine_2	0.00349758	0.00329789	-0.004045	-0.00663028	1.53E+01	5.78E+00	9.65E+01	8.55E+01
Scatarie	0.0479115	0.0419468	-0.0648479	-0.0751641	3.76E-01	2.94E-01	-2.80E-01	-7.99E-01
Mohican	8.52E-03	3.89E-03	-1.18E-02	-8.01E-03	4.22E-02	2.46E-02	-2.28E-02	-8.79E-02
E_Jurassic_Lacustrine_SR	0.0002055	9.01E-05	-0.000249773	-0.00021418	2.36E-03	1.13E-03	-8.14E-04	-5.01E-03
Sum Generated	**4.31E+01**	**2.02E+01**	**4.32E+02**	**4.92E+02**	**2.89E+01**	**1.15E+01**	**1.91E+02**	**1.74E+02**
Late_Paleocene	0.0013179	0.001043	0.023517	0.017616	5.94E-04	4.71E-04	1.01E-02	8.66E-03
Cretaceous_VC	0.221544	0.0615892	0.851818	0.738383	0.00731246	0.00275339	0.0309387	0.0520896
Mic Mac	2.7467	1.1316	16.718	12.715	4.25E+00	1.39E+00	1.91E+01	1.53E+01
Jurassic_VerrillCanyon	6.60729	2.92811	55.235	41.647	1.66E+00	7.24E-01	1.44E+01	1.57E+01
Late_Jurassic	0.037434	0.0184965	0.546973	0.401254	2.45E+00	9.86E-01	1.44E+01	9.07E+00
Misaine_1	0.0559572	0.0221553	0.223745	0.132737	3.39E+00	1.23E+00	1.55E+01	8.73E+00
Misaine_2	1.63E-02	8.30E-03	6.72E-02	6.37E-02	1.72E+00	5.10E-01	5.16E+00	2.77E+00
Scatarie	5.64E-02	3.66E-02	0.27999	0.188419	8.83E-01	3.92E-01	4.05E+00	3.53E+00
Mohican	4.32E-04	2.62E-04	7.52E-04	1.08E-03	6.80E-03	5.28E-03	1.22E-02	3.02E-02
E_Jurassic_Lacustrine_SR	2.28E-07	9.69E-08	1.74E-07	4.54E-07	3.25E-04	1.21E-04	2.78E-04	9.81E-04
Sum Accumulated in Source	**9.74339**	**4.20813**	**73.947**	**55.9052**	**1.44E+01**	**5.24E+00**	**7.27E+01**	**5.52E+01**
Late_Paleocene	-0.0013179	-0.001043	-0.023517	-0.017616	-5.94E-04	-4.71E-04	-1.01E-02	-8.66E-03
Cretaceous_VC	-0.220241	-0.0600837	-8.52E-01	-7.43E-01	-7.29E-03	-2.73E-03	-3.09E-02	-5.21E-02
Mic Mac	4.98027	2.16363	4.07E+01	4.57E+01	-4.23E+00	-1.37E+00	-1.91E+01	-1.54E+01
Jurassic_VerrillCanyon	2.87E+01	1.39E+01	318.973	391.626	-1.65484	-0.719368	-14.4085	-15.7018
Late_Jurassic	-3.58E-02	-1.72E-02	-5.48E-01	-4.05E-01	-2.36E+00	-9.26E-01	-1.45E+01	-9.21E+00
Misaine_1	-5.37E-02	-1.99E-02	-2.25E-01	-1.38E-01	9.69E+00	4.08E+00	7.93E+01	8.06E+01
Misaine_2	-1.28E-02	-5.01E-03	-7.12E-02	-7.03E-02	1.36E+01	5.27E+00	9.14E+01	82.6933
Scatarie	-8.54E-03	5.38E-03	-3.45E-01	-2.64E-01	-5.07E-01	-9.83E-02	-4.33E+00	-4.33E+00
Mohican	0.00808645	0.00362855	-0.012533	-0.00908746	3.54E-02	1.94E-02	-3.50E-02	-1.18E-01
E_Jurassic_Lacustrine_SR	2.05E-04	9.00E-05	-2.50E-04	-2.15E-04	2.03E-03	1.01E-03	-1.09E-03	-5.99E-03
Sum Expelled	**3.33E+01**	**1.60E+01**	**3.58E+02**	**435.632**	**1.46E+01**	**6.25E+00**	**1.18E+02**	**1.18E+02**
Early-Middle_Miocene	7.12E-09	9.91E-09	2.46E-07	2.29E-07	4.01E-09	5.15E-09	1.17E-07	1.07E-07
Middle_Eocene	8.85E-11	4.35E-12	6.50E-13	2.30E-17	2.98E-11	1.40E-12	1.48E-13	4.14E-18
Middle_Paleocene	4.48475	2.8042	63.7166	58.5133	1.30E+00	9.23E-01	2.00E+01	1.84E+01
Logan_Canyon	1.80308	1.07125	23.517	24.7164	5.06E-01	4.16E-01	8.79E+00	7.54E+00
Mississauga_Reservoir	1.30E+00	6.40E-01	1.22E+01	1.14E+01	7.18E-01	3.54E-01	6.67E+00	5.68E+00
Upper_Jurassic_Reservoir	4.36452	1.97335	35.9975	40.5868	8.30E-01	3.68E-01	7.06E+00	6.65527
Baccaro	5.97E-01	2.80E-01	5.12E+00	4.65E+00	8.93E-01	3.61E-01	6.37E+00	5.70E+00
Sum Accumulated in Reservoir	**1.25E+01**	**6.77E+00**	**1.41E+02**	**1.40E+02**	**4.25E+00**	**2.42E+00**	**4.89E+01**	**44.0205**
Migration Losses	**6.87E-01**	**4.16E-01**	**9.84E+00**	**1.14E+01**	**8.35E-01**	**4.59E-01**	**9.48E+00**	**8.91E+00**

Table 9b. Mass Balance of Hydrocarbons

mass in $(10)^9$ kg(Mtons)/m^3

	Methane_Paleocene	PK_C2-C5_Paleocene	PK_C6-C14_Paleocene	PK_C15+_Paleocene	Methane_CVC	C2-C5_CVC
Late_Paleocene	8.28E-03	3.59E-02	9.42E-02	1.58E-01	1.29E-32	1.58E-32
Cretaceous_VC	0.00E+00	0.00E+00	0.00E+00	0.00E+00	2.27E+01	1.06E+01
Mic Mac	0.00E+00	0.00E+00	0.00E+00	0.00E+00	1.19E-15	1.37E-15
Jurassic_VerrillCanyon	0.00E+00	0.00E+00	0.00E+00	0	4.26E-03	4.42E-03
Late_Jurassic	0	0	0	0	2.60E-05	2.36E-05
Misaine_1	0	0	0	0	3.48E-07	3.12E-07
Misaine_2	0	0	0	0	4.13E-07	3.42E-07
Scatarie	0	0	0	0	1.20E-08	4.20E-09
Mohican	0.00E+00	0.00E+00	0.00E+00	0.00E+00	1.83E-09	-9.54E-11
E_Jurassic_Lacustrine_SR	0	0	0	0	4.31E-17	-2.67E-17
Sum Generated	**0.0082844**	**0.035909**	**0.094223**	**0.15842**	**22.7451**	**10.5575**
Late_Paleocene	0.0081793	0.035474	0.093093	0.15653	0.00034722	0.00018638
Cretaceous_VC	0	0	0	0	7.00537	3.15498
Mic Mac	0	0	0	0	2.47E-10	1.10E-10
Jurassic_VerrillCanyon	0	0	0	0	0.029048	0.016561
Late_Jurassic	0.00E+00	0.00E+00	0.00E+00	0.00E+00	0.00014071	9.70E-05
Misaine_1	0	0	0	0	5.98E-07	4.76E-07
Misaine_2	0.00E+00	0.00E+00	0.00E+00	0.00E+00	5.47E-07	4.78E-07
Scatarie	0	0	0	0	1.27E-08	4.93E-09
Mohican	0	0	0	0	1.42E-09	2.95E-10
E_Jurassic_Lacustrine_SR	0	0	0	0	3.54E-18	1.43E-19
Sum Accumulated in Source	**0.0081793**	**0.035474**	**0.093093**	**0.15653**	**7.03491**	**3.17183**
Late_Paleocene	0.0001051	0.000435001	0.00113	0.00189	-0.00034722	-0.00018638
Cretaceous_VC	0	0.00E+00	0.00E+00	0.00E+00	15.7355	7.40E+00
Mic Mac	0	0.00E+00	0.00E+00	0.00E+00	-2.47E-10	-1.10E-10
Jurassic_VerrillCanyon	0	0	0	0	-2.48E-02	-1.21E-02
Late_Jurassic	0	0	0	0	-1.15E-04	-7.34E-05
Misaine_1	0	0	0.00E+00	0.00E+00	-2.50E-07	-1.64E-07
Misaine_2	0	0	0	0	-1.34E-07	-1.36E-07
Scatarie	0	0	0	0	-7.52E-10	-7.30E-10
Mohican	0	0	0	0	4.10E-10	-3.90E-10
E_Jurassic_Lacustrine_SR	0	0	0	0	3.96E-17	-2.69E-17
Sum Expelled	**0.0001051**	**0.000435001**	**0.00113**	**0.00189**	**1.57E+01**	**7.39E+00**
Early-Middle_Miocene	3.69E-05	0.00016438	0.00042951	0.00071598	6.50E-10	5.28E-10
Middle_Eocene	7.77E-09	2.73E-09	3.11E-11	1.96E-12	2.64E-10	1.83E-11
Middle_Paleocene	4.33E-06	1.88E-06	7.75E-07	1.29E-06	2.17E+00	1.04E+00
Logan_Canyon	3.54E-12	2.45E-11	4.21E-10	3.06E-09	7.34E-01	3.53E-01
Mississauga_Reservoir	5.17E-18	7.09E-17	1.25E-15	1.50E-16	4.52E-01	2.20E-01
Upper_Jurassic_Reservoir	0.00E+00	0.00E+00	0.00E+00	0	1.26E+00	6.77E-01
Baccaro	0	0	0	0	2.64E-38	5.43E-38
Sum Accumulated in Reservoir	**4.12E-05**	**0.000166262**	**0.000430285**	**0.000717271**	**4.62088**	**2.29396**
Migration Losses	**6.03E-05**	**0.000266181**	**0.000696431**	**0.0011644**	**4.47139**	**2.07285**

Table 9b. Mass Balance of Hydrocarbons

mass in $(10)^9$ kg(Mtons)/m^3

	C6-C14_CVC	C15+_CVC	Methane_EJur	PK_C2-C5_EJur	PK_C6-C14_EJur	PK_C15+_EJur
Late_Paleocene	6.23E-33	-5.41E-32	5.67E-29	3.91E-29	-1.41E-28	-2.06E-31
Cretaceous_VC	1.40E+02	1.11E+02	2.34E-05	1.38E-05	1.71E-06	-6.65E-05
Mic Mac	4.18E-17	-4.25E-15	0.078942	0.079706	0.050936	-0.32243
Jurassic_VerrillCanyon	-2.86E-03	-1.10E-02	0.0074223	0.00506348	0.000645288	-0.02216
Late_Jurassic	-2.83E-05	-4.98E-05	1.55E-01	3.11E-02	-8.38E-02	-2.46E-01
Misaine_1	-3.53E-07	-6.88E-07	3.01E-01	2.29E-01	3.29E-02	-9.38E-01
Misaine_2	-4.54E-07	-7.38E-07	3.06E+00	3.94E-01	-1.40E+00	-4.85E+00
Scatarie	-1.70E-08	-9.10E-09	8.50E+00	5.20E+00	2.74E-01	-2.39E+01
Mohican	-2.70E-09	-2.85E-10	3.30E+01	1.09E+01	-9.93E+00	-6.70E+01
E_Jurassic_Lacustrine_SR	-4.05E-17	-1.07E-19	1.61E+02	1.83E+02	4.42E+02	7.09E+02
Sum Generated	**139.73**	**111.14**	**2.06E+02**	**2.00E+02**	**4.31E+02**	**6.11E+02**
Late_Paleocene	0.0028054	0.0022983	0.0029377	6.46E-03	1.67E-02	2.69E-02
Cretaceous_VC	41.38	40.3437	0.0241937	0.0292232	0.0710299	0.110861
Mic Mac	1.65E-09	9.69E-10	25.11	26.299	51.613	62.111
Jurassic_VerrillCanyon	0.17525	0.039608	5.11866	7.92878	21.312	35.79
Late_Jurassic	0.00097146	0.00024222	3.83E+00	4.67E+00	1.13E+01	1.76E+01
Misaine_1	4.35E-06	1.28E-06	6.23046	6.9841	15.5079	20.1328
Misaine_2	2.30E-06	3.25E-07	8.11E+00	6.18E+00	1.21E+01	1.44E+01
Scatarie	4.71E-09	6.44E-12	2.75E+01	2.65E+01	5.38E+01	6.20E+01
Mohican	9.86E-11	8.12E-17	1.26E+01	5.84E+00	1.09E+01	1.09E+01
E_Jurassic_Lacustrine_SR	1.86E-20	8.98E-26	1.55E+01	3.79E+00	7.55E+00	8.5324
Sum Accumulated in Source	**41.5591**	**40.3859**	**1.04E+02**	**8.82E+01**	**1.84E+02**	**2.32E+02**
Late_Paleocene	-0.0028054	-0.0022983	-2.94E-03	-6.46E-03	-1.67E-02	-0.026891
Cretaceous_VC	9.84E+01	7.08E+01	-0.0241703	-0.0292094	-0.0710282	-0.110928
Mic Mac	-1.65E-09	-9.69E-10	-25.0311	-26.2193	-51.5621	-62.4334
Jurassic_VerrillCanyon	-1.78E-01	-5.06E-02	-5.11124	-7.92372	-21.3114	-35.8122
Late_Jurassic	-1.00E-03	-2.92E-04	-3.67584	-4.64307	-11.4158	-17.8863
Misaine_1	-4.70E-06	-1.97E-06	-5.93E+00	-6.76E+00	-1.55E+01	-2.11E+01
Misaine_2	-2.75E-06	-1.06E-06	-5.05E+00	-5.78E+00	-1.35E+01	-1.92E+01
Scatarie	-2.17E-08	-9.11E-09	-19.036	-21.3099	-53.5626	-85.895
Mohican	-2.80E-09	-2.85E-10	2.05E+01	5.05E+00	-2.08E+01	-7.80E+01
E_Jurassic_Lacustrine_SR	-4.05E-17	-1.07E-19	1.45E+02	1.79E+02	4.35E+02	7.00E+02
Sum Expelled	**9.82E+01**	**7.08E+01**	**1.02E+02**	**1.12E+02**	**2.47E+02**	**3.80E+02**
Early-Middle_Miocene	7.45E-09	1.54E-08	2.27E-08	7.62E-08	2.02E-07	3.24E-07
Middle_Eocene	1.07E-12	5.20E-18	1.94E-10	3.71E-11	1.27E-13	1.88E-19
Middle_Paleocene	1.47E+01	1.40E+01	6.62E+00	1.38E+01	3.69E+01	6.11E+01
Logan_Canyon	4.89E+00	3.88E+00	6.23E+00	12.6162	3.22E+01	46.7776
Mississauga_Reservoir	3.00E+00	1.70E+00	5.87E+00	8.52E+00	2.07E+01	2.79E+01
Upper_Jurassic_Reservoir	8.30E+00	3.87E+00	3.08E+00	4.81109	13.0753	22.5036
Baccaro	2.18E-36	0	3.90E+00	4.34E+00	8.95E+00	1.24E+01
Sum Accumulated in Reservoir	**30.8303**	**23.4305**	**25.707**	**44.0515**	**111.817**	**170.684**
Migration Losses	**27.768**	**24.717**	**3.83E+00**	**6.14E+00**	**1.49E+01**	**2.26E+01**

Table 9b. Mass Balance of Hydrocarbons

mass in $(10)^9$ kg(Mtons)/m^3

	Methane_TJur	C2-C5_TJur	C6-C14_TJur	C15+_TJur	Methane_Mohican	C2-C5_Mohican	C6-C14_Mohican
Late_Paleocene	0.00E+00	0.00E+00	0.00E+00	0.00E+00	0	0	0
Cretaceous_VC	0.00E+00	0.00E+00	0.00E+00	0.00E+00	0.00E+00	0.00E+00	0.00E+00
Mic Mac	0.00E+00	0.00E+00	0.00E+00	0.00E+00	0.00E+00	0.00E+00	0.00E+00
Jurassic_VerrillCanyon	0	0	0	0	0.00E+00	0.00E+00	0.00E+00
Late_Jurassic	4.8743	2.0399	39.255	37.965	0	0	0
Misaine_1	0	0	0	0	0	0	0
Misaine_2	0	0	0	0	0	0	0
Scatarie	0	0	0	0	0.078541	0.067108	0.04489
Mohican	0.00E+00	0.00E+00	0.00E+00	0.00E+00	1.94E+01	2.50E+01	2.10E+01
E_Jurassic_Lacustrine_SR	0	0	0	0	0	0	0
Sum Generated	**4.8743**	**2.0399**	**39.255**	**37.965**	**19.4465**	**25.0411**	**21.0549**
Late_Paleocene	0.00010485	8.66E-05	0.0022619	0.0019904	0.0002515	0.00055098	0.00056224
Cretaceous_VC	0.0147529	0.00522452	0.0904394	0.0891542	0.00282857	0.00293479	0.00219624
Mic Mac	5.42E-39	3.18E-39	1.66E-37	7.89E-37	2.3741	3.2452	2.6967
Jurassic_VerrillCanyon	0.539532	0.24075	4.6802	6.5259	4.84E-01	7.11E-01	0.70657
Late_Jurassic	1.593	0.63163	10.107	6.58573	7.38E-01	8.59E-01	6.94E-01
Misaine_1	0.020118	0.0082738	0.13183	0.0588525	1.04061	1.33232	1.10099
Misaine_2	2.48E-04	8.48E-05	1.38E-03	2.76E-03	8.58E-01	1.08E+00	8.79E-01
Scatarie	0.000307507	7.61E-05	0.00125274	0.00686975	4.90161	5.97281	4.70952
Mohican	1.44E-06	4.79E-07	8.06E-06	0.000251106	1.58155	2.07195	1.50588
E_Jurassic_Lacustrine_SR	2.11E-13	8.13E-14	1.08E-12	1.92E-09	0.0229945	0.0274548	0.0170369
Sum Accumulated in Source	**2.16806**	**0.886126**	**15.0144**	**13.2715**	**12.0046**	**15.3066**	**12.3127**
Late_Paleocene	-0.00010485	-8.66E-05	-0.0022619	-0.0019904	-0.0002515	-0.00055098	-0.00056224
Cretaceous_VC	-0.0147529	-5.22E-03	-9.04E-02	-8.92E-02	-2.83E-03	-2.93E-03	-0.00219624
Mic Mac	-5.42E-39	-3.18E-39	-1.66E-37	-7.89E-37	-2.37E+00	-3.25E+00	-2.70E+00
Jurassic_VerrillCanyon	-0.539532	-0.24075	-4.6802	-6.5259	-0.48448	-0.71091	-0.70657
Late_Jurassic	3.2813	1.40827	29.148	31.3793	-0.73769	-0.8587	-0.69394
Misaine_1	-0.020118	-0.0082738	-1.32E-01	-5.89E-02	-1.04061	-1.33232	-1.10E+00
Misaine_2	-0.00024829	-8.48E-05	-0.00138057	-0.0027568	-0.858491	-1.0838	-0.879331
Scatarie	-0.000307507	-7.61E-05	-0.00125274	-0.00686975	-4.82307	-5.9057	-4.66463
Mohican	-1.44E-06	-4.79E-07	-8.06E-06	-0.000251106	17.7865	22.9021	19.5041
E_Jurassic_Lacustrine_SR	-2.11E-13	-8.13E-14	-1.08E-12	-1.92E-09	-0.0229945	-0.0274548	-0.0170369
Sum Expelled	**2.70624**	**1.15377**	**24.2406**	**24.6935**	**7.44194**	**9.73448**	**8.74216**
Early-Middle_Miocene	5.54E-10	8.13E-10	2.36E-08	2.20E-08	1.58E-09	5.55E-09	5.75E-09
Middle_Eocene	1.60E-11	7.43E-13	9.71E-14	3.64E-18	1.57E-11	2.84E-12	1.72E-14
Middle_Paleocene	0.3972	0.26159	6.7508	6.942	0.565671	1.22315	1.34325
Logan_Canyon	0.0741088	0.0366404	0.756626	0.995624	0.645579	1.43073	1.36052
Mississauga_Reservoir	8.08E-02	3.69E-02	6.68E-01	6.85E-01	6.11E-01	1.09E+00	9.95E-01
Upper_Jurassic_Reservoir	3.01E-01	1.39E-01	2.78E+00	3.20186	2.45E-01	3.69E-01	3.83E-01
Baccaro	0	0	0	0	0.33225	0.44186	0.36961
Sum Accumulated in Reservoir	**0.853566**	**0.474063**	**10.9543**	**11.8249**	**2.39947**	**4.55251**	**4.45125**
Migration Losses	**0.014356**	**0.00846574**	**0.207832**	**0.254976**	**0.283782**	**0.540615**	**0.511968**

Table 9b. Mass Balance of Hydrocarbons

mass in $(10)^9$ kg(Mtons)/m^3

	C15+_Mohican	Sum
Late_Paleocene	0	0.296836
Cretaceous_VC	0.00E+00	284.176
Mic Mac	0.00E+00	126.634
Jurassic_VerrillCanyon	0	859.541
Late_Jurassic	0	83.8978
Misaine_1	0	202.095
Misaine_2	0	200.287
Scatarie	0.36473	-9.83167
Mohican	1.77E+02	2.09E+02
E_Jurassic_Lacustrine_SR	0	1494.64
Sum Generated	**177.465**	**3451.1**
Late_Paleocene	0.0055561	0.426625
Cretaceous_VC	0.0187549	94.3121
Mic Mac	21.988	268.792
Jurassic_VerrillCanyon	6.5547	229.749
Late_Jurassic	5.91E+00	92.5142
Misaine_1	9.05361	90.8997
Misaine_2	7.16E+00	6.11E+01
Scatarie	36.8425	231.731
Mohican	9.90952	55.3684
E_Jurassic_Lacustrine_SR	0.34699	35.827
Sum Accumulated in Source	**97.7922**	**1160.73**
Late_Paleocene	-0.0055561	-0.129789
Cretaceous_VC	-0.0187549	189.864
Mic Mac	-2.20E+01	-1.42E+02
Jurassic_VerrillCanyon	-6.5547	629.792
Late_Jurassic	-5.9144	-8.61639
Misaine_1	-9.05E+00	111.195
Misaine_2	-7.15816	139.177
Scatarie	-36.4778	-241.563
Mohican	167.19	153.994
E_Jurassic_Lacustrine_SR	-0.34699	1458.82
Sum Expelled	**79.6725**	**2290.37**
Early-Middle_Miocene	5.79E-08	0.00134824
Middle_Eocene	6.08E-18	1.12E-08
Middle_Paleocene	13.3904	351.322
Logan_Canyon	11.4835	192.819
Mississauga_Reservoir	8.23E+00	1.20E+02
Upper_Jurassic_Reservoir	3.69388	1.67E+02
Baccaro	3.0473	57.7304
Sum Accumulated in Reservoir	**39.8471**	**888.098**
Migration Losses	**4.50715**	**154.867**

Table 9b. Mass Balance of Hydrocarbons

mass in $(10)^9$ kg(Mtons)/m^3

Sec. Cracking Losses	**2.72045**	**0.121287**	**0.32882**	**0.48534**	**1.66E+00**	**1.14E-01**	**3.89E-02**	**1.35E-02**
Pliocene Quaternary	2.668	2.3377	54.296	43.538	1.33E+00	1.13E+00	2.45E+01	21.491
Middle-Late_Miocene	1.97E-14	1.23E-15	7.97E-17	2.49E-24	2.90E-16	1.89E-17	5.65E-19	4.32E-26
Early-Middle_Miocene	1.00E-16	5.58E-18	3.05E-19	4.59E-24	5.64E-17	2.90E-18	1.45E-19	2.15E-24
Late_Eocene	7.90E-09	3.85E-10	3.34E-11	1.38E-13	7.35E-09	4.08E-10	3.51E-11	7.26E-14
Early-Middle_Eocene	0.0011036	6.27E-05	6.14E-06	1.23E-10	1.02E-03	6.41E-05	6.28E-06	6.95E-11
Late_Paleocene	0.6537	0.046239	0.0059506	0.00021091	3.78E-01	2.49E-02	4.15E-03	3.46E-04
Middle_Paleocene	1.5608	0.80347	20.898	23.579	3.21E-01	1.34E-01	3.11E+00	4.24E+00
Wyandot_Dawson_Canyon	8.2688	4.0813	109.67	195.08	1.62E+00	5.94E-01	1.32E+01	2.17E+01
Logan_Canyon	6.11E-01	2.05E-01	4.38E+00	6.45E+00	1.15E+00	3.14E-01	4.85E+00	5.99E+00
Mid_Mississauga	9.47E-21	3.66E-21	6.88E-21	1.69E-22	1.21E-16	1.91E-17	1.83E-17	4.31E-19
Mississauga_Reservoir	2.81E-05	4.85E-06	3.28E-05	8.14E-03	3.48E-04	5.55E-05	1.44E-04	3.20E-02
Cretaceous_VC	1.61E-23	2.84E-26	5.37E-27	2.64E-28	8.90E-24	1.59E-27	5.81E-31	1.31E-37
Upper_Jurassic_Reservoir	6.60E-07	1.21E-08	1.30E-07	7.59E-06	8.98E-07	3.41E-08	1.47E-07	9.49E-07
Baccaro	3.09E-05	4.37E-06	1.76E-05	1.18E-05	0.00080791	0.00012053	0.00092573	0.00013129
Jurassic_VerrillCanyon	3.59E-09	3.11E-10	6.78E-09	9.69E-09	9.37E-07	6.06E-08	6.41E-07	1.23E-09
Late_Jurassic	0	0	0	0	2.14E-08	2.31E-09	3.58E-08	2.00E-09
Misaine_1	0	0	0	0	1.29E-07	4.04E-09	1.41E-08	8.56E-09
Misaine_2	0	0	0	0	1.22E-10	1.72E-11	4.41E-10	4.00E-10
Scatarie	0	0	0	0	0	0	0	0
Mohican	0.00E+00	0.00E+00	0.00E+00	0.00E+00	0	0.00E+00	0	0
E_Jurassic_Lacustrine_SR	0	0	0.00E+00	0.00E+00	0.00E+00	0.00E+00	0.00E+00	0.00E+00
Sum Outflow Top	**13.764**	**7.4737**	**189.25**	**2.69E+02**	**4.7981**	**2.20E+00**	**4.57E+01**	**5.35E+01**
Middle-Late_Miocene	2.76E-28	1.86E-29	1.55E-30	6.93E-39	4.07E-30	2.86E-31	1.10E-32	1.45E-40
Early-Middle_Miocene	2.01E-27	1.24E-28	8.72E-30	1.98E-37	2.95E-29	1.90E-30	6.17E-32	3.59E-39
Late_Eocene	6.15E-24	3.98E-25	3.09E-26	4.95E-34	9.06E-26	6.10E-27	2.19E-28	9.08E-36
Middle_Eocene	2.97E-25	1.94E-26	1.53E-27	1.93E-35	4.38E-27	2.98E-28	1.08E-29	3.59E-37
Early-Middle_Eocene	9.55E-23	6.23E-24	4.90E-25	4.87E-33	1.41E-24	9.57E-26	3.47E-27	9.20E-35
Late_Paleocene	3.33E-21	1.04E-22	1.57E-24	1.34E-32	4.81E-23	1.56E-24	1.09E-26	2.38E-34
Middle_Paleocene	2.67E-21	1.85E-22	1.75E-23	4.35E-31	3.93E-23	2.83E-24	1.24E-25	7.92E-33
Wyandot_Dawson_Canyon	3.34E-02	3.56E-03	6.31E-03	1.04E-04	2.07E-02	2.27E-03	3.33E-03	4.22E-05
Logan_Canyon	2.62E-17	1.86E-18	6.20E-19	1.46E-23	3.82E-19	2.81E-20	4.31E-21	3.13E-25
Mid_Mississauga	5.05E-12	2.82E-13	9.52E-14	3.72E-19	6.70E-14	3.65E-15	6.21E-16	4.11E-21
Mississauga_Reservoir	2.16E-24	2.08E-25	9.22E-26	3.47E-27	7.93E-26	8.56E-27	2.47E-27	6.92E-29
Early Mississauga	4.25E-02	1.37E-02	2.23E-01	2.20E-01	8.18E-04	2.50E-04	1.94E-03	1.25E-03
Cretaceous_VC	7.00E-01	1.76E-01	2.39E+00	2.29E+00	2.02E-02	6.21E-03	3.51E-02	1.74E-02
Upper_Jurassic_Reservoir	3.01E-01	8.45E-02	1.29E+00	1.41E+00	9.47E-03	3.17E-03	1.82E-02	9.38E-03
Mic Mac	0.54725	0.25118	4.41E+00	3.9489	7.09E-01	2.75E-01	4.43E+00	3.80E+00
Jurassic_VerrillCanyon	1.9491	0.64665	9.2511	7.3761	7.61E-02	2.67E-02	2.20E-01	1.53E-01
Late_Jurassic	0.018496	0.0032908	0.01949	0.0071076	5.02E-01	1.69E-01	1.47E+00	1.11E+00
Misaine_1	0.00011735	3.28E-05	0.00018823	5.61E-05	1.03E+00	3.54E-01	4.95E+00	4.48E+00
Misaine_2	4.57E-06	1.52E-06	3.86E-06	6.97E-07	6.20E-01	2.09E-01	2.67E+00	2.08E+00
Scatarie	1.01E-10	7.13E-11	3.96E-10	1.52E-10	0.047921	0.0177	0.32017	0.38747
Mohican	2.32E-09	8.25E-11	2.89E-11	3.25E-16	0.000116	6.55E-06	1.82E-05	1.80E-05
E_Jurassic_Lacustrine_SR	2.62E-16	2.07E-17	3.62E-18	8.92E-20	4.52E-09	1.88E-09	8.73E-09	7.76E-09

Table 9b. Mass Balance of Hydrocarbons

mass in $(10)^9$ kg(Mtons)/m^3

Sec. Cracking Losses	**1.18E-06**	**5.13E-07**	**1.13E-07**	**3.09E-06**	**0.0813306**	**-0.0838297**
Pliocene Quaternary	1.53E-06	1.69E-06	3.16E-06	5.24E-06	0.72475	0.39131
Middle-Late_Miocene	1.26E-11	4.55E-12	4.01E-13	3.53E-14	3.69E-12	2.62E-13
Early-Middle_Miocene	4.85E-09	1.62E-09	2.28E-12	8.89E-20	7.06E-18	2.91E-19
Late_Eocene	5.75E-09	2.04E-09	1.12E-11	3.83E-15	9.13E-28	2.70E-29
Early-Middle_Eocene	3.52E-08	2.42E-08	1.30E-08	1.38E-14	6.70E-14	1.95E-15
Late_Paleocene	8.35E-07	3.31E-07	7.40E-10	3.40E-16	0.035479	0.0019431
Middle_Paleocene	0	0	0	0	0.088664	0.033236
Wyandot_Dawson_Canyon	0	0	0	0	0.56957	0.20976
Logan_Canyon	0	0	0	0	3.74E-05	7.18E-07
Mid_Mississauga	0	0	0	0	1.34E-40	5.84E-41
Mississauga_Reservoir	0.00E+00	0.00E+00	0.00E+00	0.00E+00	4.11E-13	3.20E-15
Cretaceous_VC	0.00E+00	0.00E+00	0.00E+00	0.00E+00	5.09E-11	3.85E-13
Upper_Jurassic_Reservoir	0	0	0	0	0.00E+00	0.00E+00
Baccaro	0	0	0	0	7.50E-14	5.98E-16
Jurassic_VerrillCanyon	0	0	0	0	0	0
Late_Jurassic	0	0	0	0	0	0
Misaine_1	0.00E+00	0.00E+00	0.00E+00	0.00E+00	0	0.00E+00
Misaine_2	0.00E+00	0.00E+00	0.00E+00	0.00E+00	0.00E+00	0.00E+00
Scatarie	0	0	0	0	0	0
Mohican	0	0	0	0	0.00E+00	0.00E+00
E_Jurassic_Lacustrine_SR	0	0	0	0	0	0
Sum Outflow Top	**2.41E-06**	**2.05E-06**	**3.17E-06**	**5.24E-06**	**1.4185**	**0.63624**
Middle-Late_Miocene	1.92E-24	6.43E-25	3.45E-27	9.32E-29	5.09E-26	3.92E-27
Early-Middle_Miocene	1.25E-17	4.20E-18	5.32E-21	8.51E-27	3.78E-25	2.66E-26
Late_Eocene	2.41E-17	8.05E-18	1.04E-20	1.98E-23	1.14E-21	8.43E-23
Middle_Eocene	1.34E-18	4.47E-19	5.72E-22	7.16E-25	5.51E-23	4.10E-24
Early-Middle_Eocene	5.54E-15	1.86E-15	2.35E-18	1.65E-22	1.78E-20	1.32E-21
Late_Paleocene	2.54E-15	8.61E-16	1.29E-18	2.68E-22	7.28E-19	2.62E-20
Middle_Paleocene	5.00E-21	1.91E-20	3.06E-20	6.11E-21	5.01E-19	3.94E-20
Wyandot_Dawson_Canyon	7.48E-19	3.84E-18	9.78E-18	3.61E-18	2.63E-03	2.31E-04
Logan_Canyon	5.94E-20	6.07E-19	5.35E-18	9.96E-18	5.24E-15	4.28E-16
Mid_Mississauga	1.73E-18	2.43E-17	5.75E-16	6.62E-15	1.76E-09	1.30E-10
Mississauga_Reservoir	0.00E+00	0.00E+00	0.00E+00	0.00E+00	6.46E-26	1.46E-26
Early Mississauga	0	0	0	0	1.3257	0.65616
Cretaceous_VC	0.00E+00	0.00E+00	0.00E+00	0.00E+00	3.76E+00	1.80E+00
Upper_Jurassic_Reservoir	0	0	0	0	0.019515	0.0090978
Mic Mac	0	0.00E+00	0	0	0.00E+00	0.00E+00
Jurassic_VerrillCanyon	0	0	0	0	0.0057177	0.0030986
Late_Jurassic	0	0	0	0	0.00014365	9.28E-05
Misaine_1	0	0	0	0	6.06E-07	3.96E-07
Misaine_2	0	0	0	0	2.13E-09	1.21E-09
Scatarie	0	0	0	0	5.50E-19	8.59E-21
Mohican	0.00E+00	0.00E+00	0.00E+00	0.00E+00	5.66E-15	7.25E-17
E_Jurassic_Lacustrine_SR	0.00E+00	0.00E+00	0.00E+00	0.00E+00	7.97E-42	6.92E-43

Table 9b. Mass Balance of Hydrocarbons

mass in $(10)^9$ kg(Mtons)/m^3

Sec. Cracking Losses	**0.0567023**	**0.23773**	**1.23E+01**	**2.99E+00**	**1.05E-01**	**2.39E-02**
Pliocene Quaternary	5.847	5.073	7.50E+00	1.66E+01	4.29E+01	6.89E+01
Middle-Late_Miocene	1.38E-14	1.07E-22	7.67E-16	1.35E-16	9.74E-20	1.57E-28
Early-Middle_Miocene	9.26E-21	3.08E-25	3.26E-16	6.14E-17	9.35E-20	2.91E-26
Late_Eocene	3.38E-31	9.81E-45	5.90E-08	1.29E-08	4.80E-11	4.17E-15
Early-Middle_Eocene	6.23E-17	5.21E-21	8.10E-03	1.93E-03	6.03E-06	1.79E-12
Late_Paleocene	7.23E-05	5.37E-09	2.8399	0.66125	0.011171	0.00056558
Middle_Paleocene	0.41048	1.2013	1.73E+00	1.94E+00	5.05E+00	9.02E+00
Wyandot_Dawson_Canyon	2.6325	6.3996	1.21E+01	1.35E+01	3.27E+01	5.46E+01
Logan_Canyon	3.12E-08	1.30E-11	1.41E+01	7.53E+00	1.11E+01	1.64E+01
Mid_Mississauga	4.91E-41	1.36E-41	2.70E-16	1.04E-16	1.38E-17	6.87E-19
Mississauga_Reservoir	4.61E-20	3.16E-42	9.93E-01	4.25E-01	1.13E-01	2.04E-01
Cretaceous_VC	5.56E-15	1.52E-18	3.53E-21	1.10E-23	4.27E-29	5.11E-39
Upper_Jurassic_Reservoir	0.00E+00	0.00E+00	0.025589	0.014955	0.00031291	3.75E-06
Baccaro	5.66E-19	1.18E-23	1.4649	0.61336	0.021141	4.40E-06
Jurassic_VerrillCanyon	0	0	0.31478	0.21084	0.00088489	2.25E-13
Late_Jurassic	0	0	1.24E-01	7.68E-02	2.44E-04	1.46E-15
Misaine_1	0.00E+00	0.00E+00	0.067617	0.037257	0.00012726	3.32E-14
Misaine_2	0.00E+00	0.00E+00	0.1795	0.094218	0.00036076	3.69E-14
Scatarie	0.00E+00	0.00E+00	2.1588	1.127	0.008425	1.34E-10
Mohican	0.00E+00	0.00E+00	3.9832	2.8465	2.9781	5.2214
E_Jurassic_Lacustrine_SR	0	0	0.00027269	0.00012184	8.02E-07	1.16E-11
Sum Outflow Top	**8.8901**	**12.674**	**47.573**	**45.638**	**94.829**	**154.37**
Middle-Late_Miocene	2.64E-28	5.13E-38	1.08E-29	2.03E-30	2.02E-33	3.83E-43
Early-Middle_Miocene	1.52E-27	6.98E-36	7.81E-29	1.36E-29	1.08E-32	9.82E-42
Late_Eocene	5.32E-24	1.61E-32	2.40E-25	4.35E-26	3.90E-29	2.61E-38
Middle_Eocene	2.63E-25	5.84E-34	1.16E-26	2.12E-27	1.95E-30	1.03E-39
Early-Middle_Eocene	8.39E-23	1.33E-31	3.73E-24	6.81E-25	6.26E-28	2.66E-37
Late_Paleocene	3.67E-22	5.16E-31	1.27E-22	1.24E-23	1.60E-27	4.52E-37
Middle_Paleocene	3.02E-21	1.47E-29	1.04E-22	2.00E-23	2.37E-26	2.57E-35
Wyandot_Dawson_Canyon	2.94E-04	3.98E-06	4.60E-01	1.28E-01	9.89E-03	3.41E-05
Logan_Canyon	1.15E-16	2.24E-23	1.01E-18	1.97E-19	1.71E-21	8.33E-27
Mid_Mississauga	3.58E-11	3.93E-17	1.78E-13	2.66E-14	2.50E-16	1.40E-22
Mississauga_Reservoir	1.43E-26	2.05E-28	2.06E-25	5.44E-26	1.47E-27	2.49E-29
Early Mississauga	8.8043	3.2999	2.12E-03	1.38E-03	1.68E-03	1.22E-03
Cretaceous_VC	2.17E+01	6.38E+00	5.22E-02	3.10E-02	3.27E-02	1.77E-02
Upper_Jurassic_Reservoir	0.092945	0.011604	2.40E-02	1.49E-02	1.67E-02	9.19E-03
Mic Mac	0	0	2.56E+00	3.10E+00	6.39E+00	8.14E+00
Jurassic_VerrillCanyon	0.035002	0.0063888	0.17959	0.12353	0.16974	0.1373
Late_Jurassic	0.0010619	0.00024998	1.0578	0.68876	0.9264	0.75488
Misaine_1	4.21E-06	9.11E-07	1.3105	0.99226	1.574	1.6708
Misaine_2	4.22E-09	3.59E-10	0.79893	0.76304	1.4358	1.754
Scatarie	4.49E-21	8.31E-26	3.3844	3.7653	6.9537	7.3381
Mohican	3.92E-17	1.27E-23	1.117	1.2998	2.7252	3.5539
E_Jurassic_Lacustrine_SR	8.41E-44	0	1.2893	1.9817	5.1856	8.5189

Table 9b. Mass Balance of Hydrocarbons

mass in $(10)^9$ kg(Mtons)/m^3

Sec. Cracking Losses	**0.182068**	**0.0133712**	**0.00176838**	**0.000424631**	**0.950488**	**0.209655**	**0.00764198**
Pliocene Quaternary	0.25992	0.21719	5.7083	5.0235	0.61518	1.3754	1.4097
Middle-Late_Miocene	8.68E-16	6.15E-17	3.54E-18	3.09E-25	1.43E-16	2.57E-17	4.56E-20
Early-Middle_Miocene	7.70E-18	4.57E-19	2.92E-20	4.41E-25	2.27E-17	3.14E-18	7.14E-21
Late_Eocene	7.22E-28	2.00E-30	9.46E-35	9.81E-45	3.32E-09	5.79E-10	2.16E-12
Early-Middle_Eocene	3.48E-14	1.48E-15	1.21E-16	2.98E-21	0.00045595	8.69E-05	3.55E-07
Late_Paleocene	0.040614	0.0031534	0.00021957	4.43E-09	0.21838	0.04558	0.00092804
Middle_Paleocene	0.047406	0.026908	0.78419	0.94252	0.077214	0.094436	0.12044
Wyandot_Dawson_Canyon	2.72E-02	1.08E-02	3.43E-01	1.33E+00	0.57284	0.65391	0.65979
Logan_Canyon	0.00038093	1.08E-05	2.68E-06	8.55E-10	0.65685	0.47905	0.22832
Mid_Mississauga	3.08E-17	6.01E-18	1.43E-17	6.83E-19	5.83E-17	2.81E-17	2.46E-18
Mississauga_Reservoir	3.16E-18	6.20E-19	1.38E-18	1.91E-19	2.02E-02	1.47E-02	9.16E-04
Cretaceous_VC	4.02E-24	6.53E-28	4.90E-30	1.98E-32	3.51E-23	6.36E-26	1.37E-30
Upper_Jurassic_Reservoir	9.66E-07	6.07E-08	4.77E-07	1.99E-05	9.53E-06	6.18E-06	3.54E-07
Baccaro	0.00E+00	0.00E+00	0.00E+00	0	0.037425	0.033113	0.0020456
Jurassic_VerrillCanyon	3.71E-08	3.35E-09	4.64E-08	2.48E-08	1.06E-05	9.22E-06	8.85E-07
Late_Jurassic	2.16E-10	2.34E-11	3.97E-10	4.19E-10	4.18E-07	6.44E-07	5.55E-07
Misaine_1	1.20E-22	6.96E-24	3.37E-22	2.26E-22	9.98E-08	1.15E-07	2.56E-08
Misaine_2	0	0	0	0	2.30E-07	3.30E-07	7.32E-08
Scatarie	0	0	0	0	6.11E-06	1.13E-05	5.74E-06
Mohican	0	0	0	0	0.00078292	0.00074914	1.38E-03
E_Jurassic_Lacustrine_SR	0	0	0	0	0	0	0
Sum Outflow Top	**0.37555**	**0.25804**	**6.8362**	**7.294**	**2.1994**	**2.6971**	**2.4235**
Middle-Late_Miocene	1.22E-29	9.33E-31	6.90E-32	1.02E-39	2.01E-30	3.90E-31	8.87E-34
Early-Middle_Miocene	8.84E-29	6.21E-30	3.87E-31	2.56E-38	1.46E-29	2.60E-30	4.97E-33
Late_Eocene	2.71E-25	1.99E-26	1.37E-27	6.48E-35	4.47E-26	8.32E-27	1.76E-29
Middle_Eocene	1.31E-26	9.72E-28	6.80E-29	2.56E-36	2.16E-27	4.06E-28	8.74E-31
Early-Middle_Eocene	4.22E-24	3.12E-25	2.18E-26	6.55E-34	6.95E-25	1.31E-25	2.80E-28
Late_Paleocene	1.45E-22	5.14E-24	6.88E-26	1.70E-33	2.37E-23	2.13E-24	8.75E-28
Middle_Paleocene	1.18E-22	9.24E-24	7.76E-25	5.65E-32	1.94E-23	3.86E-24	9.96E-27
Wyandot_Dawson_Canyon	4.39E-18	3.59E-19	3.37E-20	1.52E-25	5.23E-02	1.41E-02	8.31E-04
Logan_Canyon	1.15E-18	9.21E-20	2.72E-20	2.21E-24	1.89E-19	3.83E-20	3.46E-22
Mid_Mississauga	2.06E-13	1.26E-14	4.06E-15	3.03E-20	3.29E-14	4.95E-15	5.01E-17
Mississauga_Reservoir	1.94E-25	2.12E-26	1.24E-26	4.70E-28	4.18E-26	1.16E-26	2.31E-28
Early Mississauga	0.0022537	0.00072655	0.011194	0.0091143	0.00039714	0.00031509	0.00015509
Cretaceous_VC	4.80E-02	1.33E-02	1.84E-01	1.33E-01	1.00E-02	7.37E-03	3.37E-03
Upper_Jurassic_Reservoir	0.021391	0.0061176	0.090342	0.069363	0.0046522	0.0035889	0.0017577
Mic Mac	0	0	0	0	2.22E-01	0.35761	0.34401
Jurassic_VerrillCanyon	0.19807	0.066579	1.0827	0.92546	0.035083	0.028847	0.016255
Late_Jurassic	0.9433	0.29274	4.6069	4.0376	0.23303	0.17065	0.096141
Misaine_1	0.064051	0.01931	0.25107	0.1365	0.2769	0.22129	0.15182
Misaine_2	0.0036101	0.0010985	0.014363	0.0079617	0.13565	0.13809	0.11786
Scatarie	3.99E-08	1.26E-08	1.75E-07	1.14E-07	0.39206	0.52221	0.40522
Mohican	9.77E-07	2.93E-07	4.38E-06	3.38E-06	0.2446	0.26787	0.20867
E_Jurassic_Lacustrine_SR	1.59E-13	6.46E-14	8.91E-13	5.52E-13	0.0020524	0.0026856	0.001672

Table 9b. Mass Balance of Hydrocarbons

mass in $(10)^9$ kg(Mtons)/m^3

Sec. Cracking Losses	**0.0152511**	**22.5435**
Pliocene Quaternary	14.038	327.865
Middle-Late_Miocene	4.47E-26	2.16E-11
Early-Middle_Miocene	1.16E-24	6.47E-09
Late_Eocene	3.70E-14	9.97E-08
Early-Middle_Eocene	2.84E-11	1.28E-02
Late_Paleocene	0.0011807	4.97362
Middle_Paleocene	1.4147	7.76E+01
Wyandot_Dawson_Canyon	7.1076	487.662
Logan_Canyon	1.5704	75.9386
Mid_Mississauga	1.54E-18	6.90E-16
Mississauga_Reservoir	1.25E-02	1.82E+00
Cretaceous_VC	2.38E-37	5.13E-11
Upper_Jurassic_Reservoir	8.01E-08	0.0409086
Baccaro	1.53E-05	2.17405
Jurassic_VerrillCanyon	2.56E-14	0.526527
Late_Jurassic	1.01E-13	0.201226
Misaine_1	1.37E-13	1.05E-01
Misaine_2	5.09E-13	2.74E-01
Scatarie	2.34E-09	3.29E+00
Mohican	1.03E-02	1.50E+01
E_Jurassic_Lacustrine_SR	0.00E+00	0.000395332
Sum Outflow Top	**2.42E+01**	**997.569**
Middle-Late_Miocene	1.52E-40	2.62E-24
Early-Middle_Miocene	3.73E-39	1.67E-17
Late_Eocene	9.45E-36	3.21E-17
Middle_Eocene	3.74E-37	1.78E-18
Early-Middle_Eocene	9.60E-35	7.40E-15
Late_Paleocene	2.47E-34	3.41E-15
Middle_Paleocene	8.23E-33	6.08E-19
Wyandot_Dawson_Canyon	1.29E-04	7.38E-01
Logan_Canyon	3.29E-25	5.84E-15
Mid_Mississauga	4.03E-21	1.93E-09
Mississauga_Reservoir	7.01E-29	3.19E-24
Early Mississauga	0.00092793	14.6205
Cretaceous_VC	1.86E-02	3.98E+01
Upper_Jurassic_Reservoir	0.010382	3.53575
Mic Mac	2.988	4.25E+01
Jurassic_VerrillCanyon	0.11565	22.8279
Late_Jurassic	0.70727	17.8161
Misaine_1	1.2414	18.7199
Misaine_2	1.0407	11.7867
Scatarie	3.2528	26.787
Mohican	1.7649	1.12E+01
E_Jurassic_Lacustrine_SR	0.0086568	1.70E+01

Table 9b. Mass Balance of Hydrocarbons

mass in $(10)^9$ kg(Mtons)/m^3								
Sum Outflow Side	**3.592**	**1.1786**	**17.595**	**15.257**	**3.04E+00**	**1.06E+00**	**1.41E+01**	**1.20E+01**
Sum HC Losses	**20.763**	**9.18924**	**217.011**	**295.782**	**1.03E+01**	**3.83E+00**	**6.93E+01**	**7.44E+01**

Table 9b. Mass Balance of Hydrocarbons

mass in $(10)^9$ kg(Mtons)/m^3						
Sum Outflow Side	**8.13E-15**	**2.76E-15**	**5.94E-16**	**6.63E-15**	**5.12E+00**	**2.47E+00**
Sum HC Losses	**6.39E-05**	**2.69E-04**	**7.00E-04**	**1.17E-03**	**1.11E+01**	**5.09E+00**

Table 9b. Mass Balance of Hydrocarbons

mass in $(10)^9$ kg(Mtons)/m^3						
Sum Outflow Side	**3.06E+01**	**9.69E+00**	**12.239**	**12.887**	**25.423**	**31.894**
Sum HC Losses	**6.73E+01**	**4.73E+01**	**75.914**	**67.6535**	**135.291**	**208.883**

Table 9b. Mass Balance of Hydrocarbons

mass in $(10)^9$ kg(Mtons)/m^3

Sum Outflow Side	**1.28E+00**	**4.00E-01**	**6.24E+00**	**5.32E+00**	**1.6088**	**1.7346**	**1.3478**
Sum HC Losses	**1.85E+00**	**6.80E-01**	**1.33E+01**	**1.29E+01**	**5.04E+00**	**5.18E+00**	**4.29E+00**

Table 9b. Mass Balance of Hydrocarbons

mass in $(10)^9$ kg(Mtons)/m^3		
Sum Outflow Side	**11.149**	**2.27E+02**
Sum HC Losses	**3.98E+01**	**1.40E+03**

Table 9c. Mass Balance of Hydrocarbons

mass in $(10)^9$ kg(Mtons)/m^3

	Methane_JVC	C2-C5_JVC	C6-C14_JVC	C15+_JVC	Methane_Misaine	C2-C5_Misaine	C6-C14_Misaine	C15+_Misaine
Middle_Paleocene	0.00E+00	0.00E+00	0.00E+00	0.00E+00	0.00E+00	0.00E+00	0.00E+00	0.00E+00
Mid_Mississauga	2.22E-11	2.34E-11	-1.74E-11	-5.53E-11	1.07E-11	1.20E-11	2.73E-13	-3.76E-11
Early_Mississauga	1.25E-09	1.34E-09	-7.97E-10	-3.35E-09	8.32E-10	9.37E-10	5.43E-11	-2.97E-09
Cretaceous_VC	3.91E-07	5.12E-07	5.63E-07	-2.12E-06	4.84E-08	5.93E-08	3.70E-08	-2.19E-07
Jurassic_VerrillCanyon	37.4846	19.1267	413.975	444.301	1.36E-03	1.61E-03	4.18E-04	-5.35E-03
Late _Jurassic	1.72E-05	1.65E-05	-1.76E-05	-3.58E-05	9.69E-02	1.04E-01	-1.78E-02	-3.10E-01
Misaine	9.60E-07	1.12E-06	4.59E-07	-3.95E-06	3.74E+01	1.35E+01	2.01E+02	1.72E+02
Mohican	2.52E-08	1.88E-08	-3.45E-08	-3.45E-08	1.81E-01	1.06E-01	-1.54E-01	-3.11E-01
Early_Jur_Lac_SR	4.67E-09	1.92E-09	-7.22E-09	-3.25E-09	6.33E-03	1.82E-03	-5.99E-03	-7.31E-03
Sum Generated	**37.4846**	**1.91E+01**	**413.975**	**444.301**	**3.77E+01**	**1.37E+01**	**2.01E+02**	**1.71E+02**
Middle_Paleocene	1.03E+00	2.13E-01	1.90E+00	5.84E-01	8.58E-01	9.93E-02	6.64E-01	4.36E-01
Mid_Mississauga	0.0693961	0.033859	0.629357	0.515743	1.34E-02	5.87E-03	1.07E-01	9.79E-02
Early_Mississauga	0.0216042	0.0107155	0.219169	0.439332	0.0171688	0.00646864	0.077857	0.054879
Cretaceous_VC	0.0532028	0.0257789	0.727509	2.50505	2.06E-02	8.28E-03	1.20E-01	8.76E-02
Jurassic_VerrillCanyon	4.6386	1.9059	25.432	9.30876	1.26E+00	4.88E-01	5.78E+00	3.86E+00
Late _Jurassic	0.01676	0.0083339	0.075734	0.014026	4.68E+00	1.73E+00	1.73E+01	1.02E+01
Misaine	8.22E-06	5.98E-06	9.57E-05	0.000100251	9.09E+00	2.81E+00	2.14E+01	8.92E+00
Mohican	9.05E-09	5.59E-09	1.89E-08	1.41E-09	2.66E-02	1.35E-02	4.90E-02	2.31E-02
Early_Jur_Lac_SR	1.36E-09	4.64E-10	8.28E-10	2.90E-11	9.84E-04	6.01E-04	1.63E-03	4.25E-04
Sum Accumulated in Source	**5.83E+00**	**2.20E+00**	**2.90E+01**	**1.34E+01**	**1.60E+01**	**5.16E+00**	**4.54E+01**	**2.37E+01**
Middle_Paleocene	-1.03E+00	-2.13E-01	-1.90E+00	-5.84E-01	-8.58E-01	-9.93E-02	-6.64E-01	-4.36E-01
Mid_Mississauga	-0.0693961	-0.033859	-0.629357	-0.515743	-1.34E-02	-5.87E-03	-1.07E-01	-9.79E-02
Early_Mississauga	-0.0216042	-0.0107155	-0.219169	-0.439332	-1.72E-02	-6.47E-03	-7.79E-02	-5.49E-02
Cretaceous_VC	-0.0532024	-0.0257784	-7.28E-01	-2.51E+00	-2.06E-02	-8.28E-03	-1.20E-01	-8.76E-02
Jurassic_VerrillCanyon	32.846	17.2208	3.89E+02	4.35E+02	-1.26E+00	-4.87E-01	-5.77E+00	-3.87E+00
Late _Jurassic	-1.67E-02	-8.32E-03	-0.0757516	-0.0140618	-4.58452	-1.62207	-17.2738	-10.5491
Misaine	-7.26E-06	-4.86E-06	-9.52E-05	-1.04E-04	2.83E+01	1.07E+01	1.80E+02	1.63E+02
Mohican	1.62E-08	1.32E-08	-5.34E-08	-3.59E-08	1.55E-01	9.22E-02	-2.03E-01	-3.34E-01
Early_Jur_Lac_SR	3.32E-09	1.45E-09	-8.05E-09	-3.28E-09	5.34E-03	1.22E-03	-7.62E-03	-0.0077303
Sum Expelled	**3.17E+01**	**1.69E+01**	**3.85E+02**	**4.31E+02**	**2.17E+01**	**8.54E+00**	**1.55E+02**	**1.48E+02**
Early-Middle_Miocene	0.847246	0.477476	13.5651	21.6676	7.60E-01	3.59E-01	7.44E+00	8.44E+00
Middle_Eocene	5.61E-01	3.01E-01	6.86E+00	6.94E+00	4.95E-01	2.10E-01	3.46E+00	3.18E+00
Logan_Canyon	1.28E+00	5.22E-01	1.02E+01	8.4551	7.99E-01	2.46E-01	3.39E+00	2.81E+00
Mississauga_Reservoir	5.70E-01	2.72E-01	5.61E+00	4.75E+00	7.35E-01	2.68E-01	3.65E+00	2.97E+00
Late Jurassic_Reservoir	3.14E+00	1.57E+00	3.19E+01	3.75E+01	4.01E+00	1.54E+00	1.87E+01	1.41E+01
Sum Accumulated in Reservoir	**6.40148**	**3.14294**	**68.1038**	**79.3285**	**6.80E+00**	**2.63E+00**	**3.67E+01**	**3.15E+01**
Migration Losses	**0.77066**	**0.417978**	**8.31969**	**9.16699**	**1.55E+00**	**6.82E-01**	**5.41E+00**	**3.99E+00**
Sec. Cracking Losses	**9.85E-01**	**6.17E-02**	**3.52E-03**	**6.50E-03**	**-1.05E+00**	**-1.32E+00**	**1.29E+00**	**3.92E+00**
Pliocene_Quaternary	1.0327	0.86452	21.469	24.901	9.55E-01	6.32E-01	1.15E+01	11.237
Middle-Late_Miocene	2.39E+00	1.55E+00	3.97E+01	5.44E+01	2.11E+00	1.13E+00	1.97E+01	1.90E+01
Early-Middle_Miocene	1.51E-01	9.33E-03	6.40E-04	2.59E-08	1.26E-01	5.96E-03	3.03E-04	1.43E-08
Late_Eocene	3.92E-01	2.55E-02	1.07E-03	4.95E-09	3.08E-01	1.58E-02	5.20E-04	5.54E-09

Table 9c. Mass Balance of Hydrocarbons

mass in $(10)^9$ kg(Mtons)/m^3

	Methane_Paleocene	PK_C2-C5_Paleocene	PK_C6-C14_Paleocene	PK_C15+_Paleocene	Methane_CVC	C2-C5_CVC
Middle_Paleocene	4.28E-03	1.91E-02	4.98E-02	8.30E-02	0.00E+00	0.00E+00
Mid_Mississauga	0.00E+00	0.00E+00	0.00E+00	0.00E+00	2.18E-02	4.72E-03
Early_Mississauga	0.00E+00	0.00E+00	0.00E+00	0.00E+00	2.50E-01	7.45E-02
Cretaceous_VC	0.00E+00	0.00E+00	0.00E+00	0	2.36E+01	1.03E+01
Jurassic_VerrillCanyon	0	0	0	0	1.58E-06	1.93E-06
Late _Jurassic	0	0	0	0	7.60E-07	9.37E-07
Misaine	0	0	0	0	1.40E-09	1.75E-09
Mohican	0	0	0	0	1.29E-11	1.34E-11
Early_Jur_Lac_SR	0.00E+00	0.00E+00	0.00E+00	0.00E+00	2.14E-12	1.15E-12
Sum Generated	**0.0042823**	**0.01908**	**0.049836**	**0.083034**	**2.38E+01**	**1.04E+01**
Middle_Paleocene	0.00427961	0.019071	0.0498121	0.0829945	0.883417	0.327962
Mid_Mississauga	6.79E-20	1.09E-18	1.03E-17	2.25E-17	0.041042	0.0142605
Early_Mississauga	0	0	0	0	0.899141	0.320748
Cretaceous_VC	0	0	0	0	1.00E+01	4.22E+00
Jurassic_VerrillCanyon	0	0	0	0	0.0013806	0.00074301
Late _Jurassic	0.00E+00	0.00E+00	0.00E+00	0.00E+00	0.00011241	7.18E-05
Misaine	0	0	0	0	2.01E-08	2.09E-08
Mohican	0.00E+00	0.00E+00	0.00E+00	0.00E+00	5.08E-12	4.65E-12
Early_Jur_Lac_SR	0	0	0	0	8.40E-13	3.92E-13
Sum Accumulated in Source	**0.00427961**	**0.019071**	**0.0498121**	**0.0829945**	**1.19E+01**	**4.88E+00**
Middle_Paleocene	2.69E-06	9.00E-06	2.39E-05	3.95E-05	-8.83E-01	-3.28E-01
Mid_Mississauga	-6.79E-20	-1.09E-18	-1.03E-17	-2.25E-17	-0.019209	-0.0095374
Early_Mississauga	0	0	0	0	-0.64933	-0.246207
Cretaceous_VC	0	0.00E+00	0.00E+00	0.00E+00	13.5261	6.13E+00
Jurassic_VerrillCanyon	0	0.00E+00	0.00E+00	0.00E+00	-1.38E-03	-7.41E-04
Late _Jurassic	0	0	0	0	-1.12E-04	-7.09E-05
Misaine	0	0	0	0	-1.87E-08	-1.92E-08
Mohican	0	0	0.00E+00	0.00E+00	7.79E-12	8.72E-12
Early_Jur_Lac_SR	0	0	0	0	1.30E-12	7.63E-13
Sum Expelled	**2.69E-06**	**9.00E-06**	**2.39E-05**	**3.95E-05**	**1.20E+01**	**5.54E+00**
Early-Middle_Miocene	7.57E-08	4.27E-07	1.26E-06	2.09E-06	3.23E-01	1.35E-01
Middle_Eocene	2.49E-07	9.43E-07	2.68E-06	4.42E-06	2.00E-01	9.05E-02
Logan_Canyon	9.33E-09	7.59E-08	5.14E-07	1.05E-06	4.15E-01	1.57E-01
Mississauga_Reservoir	2.81E-42	2.23E-41	9.97E-41	0	2.04E-01	8.79E-02
Late Jurassic_Reservoir	0.00E+00	0.00E+00	0.00E+00	0.00E+00	2.61E+00	1.32E+00
Sum Accumulated in Reservoir	**3.34E-07**	**1.45E-06**	**4.45E-06**	**7.56E-06**	**3.76E+00**	**1.80E+00**
Migration Losses	**1.44E-07**	**5.08E-07**	**1.38E-06**	**2.31E-06**	**5.36E-01**	**2.80E-01**
Sec. Cracking Losses	**6.25E-07**	**1.05E-06**	**3.15E-07**	**2.42E-07**	**3.53E-01**	**2.16E-02**
Pliocene_Quaternary	3.32E-07	2.37E-06	7.72E-06	1.27E-05	3.57E-01	2.45E-01
Middle-Late_Miocene	3.81E-07	2.65E-06	9.05E-06	1.52E-05	1.24E+00	6.51E-01
Early-Middle_Miocene	1.74E-07	9.90E-08	2.37E-10	4.80E-16	0.052743	0.0029177
Late_Eocene	2.44E-07	3.01E-07	8.88E-10	9.65E-16	0.14135	0.0085227

Table 9c. Mass Balance of Hydrocarbons

mass in $(10)^9$ kg(Mtons)/m^3

	C6-C14_CVC	C15+_CVC	Methane_EJur	PK_C2-C5_EJur	PK_C6-C14_EJur	PK_C15+_EJur
Middle_Paleocene	0.00E+00	0.00E+00	0.00E+00	0.00E+00	0.00E+00	0.00E+00
Mid_Mississauga	4.92E-02	8.89E-01	1.05E-11	1.15E-11	8.66E-12	-4.63E-11
Early_Mississauga	8.35E-01	6.06E+00	8.69E-10	9.14E-10	6.55E-10	-3.71E-09
Cretaceous_VC	1.48E+02	2.18E+02	6.38E-08	7.04E-08	5.38E-08	-2.83E-07
Jurassic_VerrillCanyon	9.13E-07	-6.78E-06	1.92E-03	2.07E-03	1.51E-03	-8.33E-03
Late _Jurassic	5.07E-07	-3.36E-06	1.80E-01	1.62E-01	8.34E-02	-6.70E-01
Misaine	1.19E-09	-6.50E-09	8.61E-01	5.06E-01	-7.91E-02	-2.28E+00
Mohican	5.41E-12	-4.95E-11	6.20E+00	3.00E+00	-1.70E+00	-1.42E+01
Early_Jur_Lac_SR	-8.50E-13	-4.71E-12	4.06E+01	5.99E+01	1.56E+02	2.61E+02
Sum Generated	**1.49E+02**	**2.25E+02**	**4.78E+01**	**6.36E+01**	**1.54E+02**	**2.44E+02**
Middle_Paleocene	4.84398	2.957	1.00E+00	4.35E-01	4.84E-01	5.14E-01
Mid_Mississauga	0.197061	0.969051	0.0185259	2.63E-02	6.67E-02	1.07E-01
Early_Mississauga	3.97982	15.2257	0.0232445	0.0259613	0.0543945	0.0770594
Cretaceous_VC	5.86E+01	1.11E+02	0.0252116	0.029895	0.0666831	0.0992849
Jurassic_VerrillCanyon	0.013003	0.013607	1.7306	1.8409	3.6676	4.5727
Late _Jurassic	0.0014867	0.0016691	6.01E+00	5.56E+00	9.65E+00	1.01E+01
Misaine	5.67E-07	7.58E-07	3.62643	3.54303	6.36043	6.97978
Mohican	1.06E-11	4.65E-12	1.92E+00	1.92E+00	3.06E+00	2.18E+00
Early_Jur_Lac_SR	4.97E-13	9.73E-14	1.27E+00	1.33E+00	2.11E+00	1.29E+00
Sum Accumulated in Source	**6.76E+01**	**1.30E+02**	**1.56E+01**	**1.47E+01**	**2.55E+01**	**2.59E+01**
Middle_Paleocene	-4.84E+00	-2.96E+00	-1.00E+00	-4.35E-01	-4.84E-01	-0.513798
Mid_Mississauga	-0.147882	-0.080141	-1.85E-02	-2.63E-02	-6.67E-02	-1.07E-01
Early_Mississauga	-3.14459	-9.16921	-2.32E-02	-2.60E-02	-5.44E-02	-0.0770594
Cretaceous_VC	8.91E+01	1.07E+02	-0.0252115	-0.0298949	-0.066683	-0.0992852
Jurassic_VerrillCanyon	-1.30E-02	-1.36E-02	-1.72868	-1.83883	-3.66609	-4.58103
Late _Jurassic	-1.49E-03	-1.67E-03	-5.83157	-5.39966	-9.56288	-10.7718
Misaine	-5.65E-07	-7.65E-07	-2.76541	-3.03699	-6.43952	-9.25821
Mohican	-5.20E-12	-5.41E-11	4.28E+00	1.09E+00	-4.76E+00	-1.63E+01
Early_Jur_Lac_SR	-1.35E-12	-4.81E-12	3.93E+01	5.86E+01	1.54E+02	2.59E+02
Sum Expelled	**8.10E+01**	**9.50E+01**	**32.1852**	**48.8676**	**128.719**	**217.583**
Early-Middle_Miocene	1.87E+00	3.59E+00	1.76E+00	2.98E+00	8.37E+00	1.45E+01
Middle_Eocene	1.33E+00	1.84E+00	7.82E-01	1.14E+00	2.96E+00	4.86E+00
Logan_Canyon	2.27E+00	2.33E+00	9.89E-01	9.68E-01	2.17E+00	3.39E+00
Mississauga_Reservoir	1.29E+00	1.32E+00	1.03E+00	1.23E+00	2.84E+00	4.39E+00
Late Jurassic_Reservoir	2.06E+01	1.08E+01	5.86E+00	7.06E+00	1.59E+01	2.39E+01
Sum Accumulated in Reservoir	**2.73E+01**	**1.99E+01**	**1.04E+01**	**1.34E+01**	**3.22E+01**	**5.11E+01**
Migration Losses	**4.31E+00**	**2.35E+00**	**5.15E+00**	**5.51333**	**1.09E+01**	**13.2566**
Sec. Cracking Losses	**3.56E-03**	**3.46E-04**	**-6.29E+00**	**-2.62E+00**	**4.46E+00**	**2.16E+01**
Pliocene_Quaternary	3.70E+00	6.18E+00	1.86E+00	3.7118	10.195	16.977
Middle-Late_Miocene	9.81E+00	13.518	3.47E+00	6.32E+00	1.74E+01	2.95E+01
Early-Middle_Miocene	0.00014944	1.07E-08	0.1577	0.032418	8.29E-05	2.08E-10
Late_Eocene	0.00031085	5.42E-09	3.85E-01	8.42E-02	1.24E-04	8.45E-11

Table 9c. Mass Balance of Hydrocarbons

mass in $(10)^9$ kg(Mtons)/m^3

	Methane_TJur	C2-C5_TJur	C6-C14_TJur	C15+_TJur	Methane_Mohican	C2-C5_Mohican	C6-C14_Mohican
Middle_Paleocene	0.00E+00	0.00E+00	0.00E+00	0.00E+00	0	0	0
Mid_Mississauga	0.00E+00	0.00E+00	0.00E+00	0.00E+00	0.00E+00	0.00E+00	0.00E+00
Early_Mississauga	0.00E+00	0.00E+00	0.00E+00	0.00E+00	0.00E+00	0.00E+00	0.00E+00
Cretaceous_VC	0	0	0	0	0.00E+00	0.00E+00	0.00E+00
Jurassic_VerrillCanyon	0	0	0	0	0	0	0
Late _Jurassic	25.897	10.61	188.16	169.33	0	0	0
Misaine	0	0	0	0	0	0	0
Mohican	0	0	0	0	24.167	29.86	24.003
Early_Jur_Lac_SR	0.00E+00	0.00E+00	0.00E+00	0.00E+00	0.00E+00	0.00E+00	0.00E+00
Sum Generated	**25.897**	**10.61**	**188.16**	**169.33**	**24.167**	**29.86**	**24.003**
Middle_Paleocene	0.611905	0.0840032	0.825501	0.651987	0.535227	0.206447	0.0789255
Mid_Mississauga	0.020925	8.53E-03	0.151381	0.144973	0.00552846	0.0086797	0.008781
Early_Mississauga	0.0116141	0.0051102	0.099933	0.108258	0.0125517	0.0147183	0.0111699
Cretaceous_VC	3.27E-02	1.61E-02	3.87E-01	4.91E-01	0.0128166	0.0155454	0.0124896
Jurassic_VerrillCanyon	2.0271	0.81857	13.322	9.7752	8.37E-01	1.02E+00	0.76681
Late _Jurassic	7.7112	2.4164	30.514	18.12	2.72E+00	3.09E+00	2.19E+00
Misaine	0.0744451	0.015985	0.17538	0.108562	1.79385	2.04635	1.43926
Mohican	1.09E-05	2.93E-06	3.89E-05	3.12E-05	1.66E+00	1.84E+00	9.85E-01
Early_Jur_Lac_SR	3.76E-07	5.18E-08	4.72E-07	2.98E-07	0.101526	0.116329	0.0612433
Sum Accumulated in Source	**1.05E+01**	**3.36E+00**	**4.55E+01**	**29.3996**	**7.67682**	**8.36545**	**5.54867**
Middle_Paleocene	-6.12E-01	-8.40E-02	-8.26E-01	-6.52E-01	-0.535227	-0.206447	-0.0789255
Mid_Mississauga	-0.020925	-0.00852817	-0.151381	-0.144973	-0.00552846	-0.0086797	-0.008781
Early_Mississauga	-0.0116141	-5.11E-03	-0.099933	-0.108258	-0.0125517	-0.0147183	-0.0111699
Cretaceous_VC	-0.0327248	-1.61E-02	-3.87E-01	-4.91E-01	-1.28E-02	-1.55E-02	-0.0124896
Jurassic_VerrillCanyon	-2.03E+00	-8.19E-01	-1.33E+01	-9.78E+00	-8.37E-01	-1.02E+00	-7.67E-01
Late _Jurassic	18.1858	8.1936	157.646	151.21	-2.7161	-3.0933	-2.185
Misaine	-0.0744451	-0.015985	-0.17538	-0.108562	-1.79385	-2.04635	-1.43926
Mohican	-1.09E-05	-2.93E-06	-3.89E-05	-3.12E-05	22.5046	28.0165	2.30E+01
Early_Jur_Lac_SR	-3.76E-07	-5.18E-08	-4.72E-07	-2.98E-07	-0.101526	-0.116329	-0.0612433
Sum Expelled	**15.4071**	**7.25E+00**	**142.685**	**139.93**	**16.4902**	**21.4945**	**18.4543**
Early-Middle_Miocene	3.25E-01	1.76E-01	4.30E+00	5.70352	0.426027	0.696305	0.726968
Middle_Eocene	2.79E-01	1.30E-01	2.50E+00	2.30E+00	0.307405	0.443558	0.403869
Logan_Canyon	0.5006	0.175834	3.0201	2.5655	0.571432	0.565803	0.438247
Mississauga_Reservoir	3.50E-01	1.42E-01	2.39E+00	2.02E+00	5.34E-01	6.12E-01	4.95E-01
Late Jurassic_Reservoir	2.08E+00	9.03E-01	1.60E+01	1.43E+01	2.81E+00	3.37E+00	2.64E+00
Sum Accumulated in Reservoir	**3.53786**	**1.527**	**28.1919**	**26.8779**	**4.64901**	**5.68678**	**4.70045**
Migration Losses	**0.192085**	**0.100417**	**2.09691**	**2.35485**	**3.37963**	**3.93157**	**2.76987**
Sec. Cracking Losses	**5.14E-01**	**3.01E-02**	**2.18E-03**	**-3.75E-03**	**5.08E-01**	**8.75E-02**	**1.48E-03**
Pliocene_Quaternary	4.87E-01	3.76E-01	7.91E+00	7.9866	5.49E-01	1.28E+00	1.26E+00
Middle-Late_Miocene	1.1737	0.71742	15.115	15.684	1.1229	2.0796	1.9658
Early-Middle_Miocene	0.081072	0.0042823	0.00025308	1.09E-08	0.08218	0.013309	4.05E-05
Late_Eocene	0.20234	0.01188	0.00046864	4.45E-09	0.19844	0.034595	7.05E-05

Table 9c. Mass Balance of Hydrocarbons

mass in $(10)^9$ kg(Mtons)/m^3

	C15+_Mohican	Sum
Middle_Paleocene	0	0.156232
Mid_Mississauga	0.00E+00	0.964645
Early_Mississauga	0.00E+00	7.21607
Cretaceous_VC	0	400.035
Jurassic_VerrillCanyon	0	914.882
Late _Jurassic	0	393.625
Misaine	0	422.692
Mohican	198.35	269.558
Early_Jur_Lac_SR	0.00E+00	5.17E+02
Sum Generated	**198.35**	**2926.12**
Middle_Paleocene	0.596157	20.972
Mid_Mississauga	0.0838328	3.34489
Early_Mississauga	0.0851649	21.8018
Cretaceous_VC	0.100103	188.885
Jurassic_VerrillCanyon	5.689	98.7649
Late _Jurassic	1.62E+01	148.283
Misaine	10.5517	78.8932
Mohican	4.72E+00	1.84E+01
Early_Jur_Lac_SR	0.263801	6.54087
Sum Accumulated in Source	**38.2752**	**585.879**
Middle_Paleocene	-0.596157	-20.8158
Mid_Mississauga	-0.0838328	-2.38025
Early_Mississauga	-0.0851649	-14.5857
Cretaceous_VC	-0.100103	211.15
Jurassic_VerrillCanyon	-5.69E+00	8.16E+02
Late _Jurassic	-16.186	245.341
Misaine	-10.5517	343.799
Mohican	1.94E+02	251.166
Early_Jur_Lac_SR	-0.263801	510.454
Sum Expelled	**160.075**	**2340.24**
Early-Middle_Miocene	7.27675	106.727
Middle_Eocene	3.57619	45.1512
Logan_Canyon	3.5603	51.7727
Mississauga_Reservoir	4.07E+00	41.8368
Late Jurassic_Reservoir	2.09E+01	2.63E+02
Sum Accumulated in Reservoir	**39.3557**	**508.984**
Migration Losses	**19.0777**	**106.475**
Sec. Cracking Losses	**1.16E-02**	**2.26E+01**
Pliocene_Quaternary	11.452	1.47E+02
Middle-Late_Miocene	17.758	277.476
Early-Middle_Miocene	1.99E-08	0.720116
Late_Eocene	1.04E-08	1.81008

Table 9c. Mass Balance of Hydrocarbons

mass in $(10)^9$ kg(Mtons)/m^3

Middle_Eocene	0.79527	0.67693	14.98	12.206	5.45E-01	3.23E-01	5.38E+00	4.86E+00
Early-Middle_Eocene	4.6891	2.7914	59.996	54.809	2.37E+00	1.24E+00	2.19E+01	20.112
Late_Paleocene	2.72E-03	1.45E-04	1.68E-05	3.44E-10	6.95E-03	4.26E-04	3.09E-05	1.43E-09
Middle_Paleocene	9.15E+00	5.01E+00	1.23E+02	1.26E+02	3.35E+00	1.60E+00	3.40E+01	3.74E+01
Wyandot_Dawson_Canyon	1.07E-01	4.81E-02	2.06E+00	6.93E+00	6.22E-02	3.16E-02	7.89E-01	9.75E-01
Logan_Canyon	2.43E-20	3.20E-21	4.73E-23	9.13E-29	4.25E-12	2.50E-13	8.69E-15	4.77E-20
Mississauga_Reservoir	1.23E-09	8.48E-11	2.58E-10	7.81E-12	7.06E-08	1.89E-09	4.59E-12	5.79E-16
Early_Mississauga	0	0	0	0	0.00E+00	0.00E+00	0.00E+00	0.00E+00
Cretaceous_VC	0	0	0	0	0.00E+00	0.00E+00	0.00E+00	0.00E+00
Late Jurassic_Reservoir	1.29E-10	9.90E-12	1.53E-11	2.18E-11	1.71E-09	4.48E-11	1.96E-10	6.56E-13
Jurassic_VerrillCanyon	1.68E-12	1.29E-13	1.65E-12	2.65E-12	1.11E-09	1.08E-10	1.14E-10	2.20E-10
Late _Jurassic	0.00E+00	0.00E+00	0.00E+00	0.00E+00	1.01E-09	2.27E-11	9.22E-11	1.41E-10
Misaine	0.00E+00	0.00E+00	0.00E+00	0.00E+00	3.20E-11	2.98E-12	7.90E-11	6.75E-09
Scatarie	0.00E+00	0.00E+00	0.00E+00	0.00E+00	0.00E+00	0.00E+00	0.00E+00	0.00E+00
Mohican	0.00E+00	0.00E+00	0.00E+00	0.00E+00	0	0	0	0
Early_Jur_Lac_SR	0.00E+00	0.00E+00	0.00E+00	0.00E+00	0.00E+00	0.00E+00	0.00E+00	0.00E+00
Sum Outflow Top	**18.714**	**10.974**	**261.07**	**279.6**	**9.84E+00**	**4.98E+00**	**9.33E+01**	**9.36E+01**
Pliocene_Quaternary	7.29E-15	1.96E-16	9.12E-17	1.24E-19	1.85E-15	4.74E-17	1.87E-17	1.73E-20
Middle-Late_Miocene	2.47E-11	6.66E-13	3.24E-13	6.48E-16	6.26E-12	1.61E-13	6.64E-14	9.03E-17
Early-Middle_Miocene	3.68E-09	8.68E-11	6.16E-12	3.83E-16	1.19E-09	3.29E-11	1.76E-12	5.36E-17
Late_Eocene	1.37E-39	2.65E-41	2.53E-42	0.00E+00	7.54E-40	1.63E-41	9.19E-43	0
Late_Paleocene	4.97E-06	1.53E-07	3.75E-07	6.99E-09	2.41E-03	3.20E-04	2.42E-04	9.03E-05
Middle_Paleocene	8.71E-07	2.08E-08	1.47E-09	2.25E-14	2.89E-07	7.92E-09	4.07E-10	3.15E-15
Wyandot_Dawson_Canyon	2.16E-01	1.07E-01	2.62E+00	3.65E+00	4.04E-02	1.94E-02	4.44E-01	5.09E-01
Logan_Canyon	1.13E+00	5.73E-01	1.27E+01	1.47E+01	1.88E-01	8.83E-02	1.89E+00	2.06E+00
Mid_Mississauga	4.33E-01	2.20E-01	4.79E+00	5.45E+00	7.26E-02	3.38E-02	7.12E-01	7.65E-01
Mississauga_Reservoir	3.56E-01	1.80E-01	3.93E+00	4.44E+00	5.92E-02	2.76E-02	5.81E-01	6.25E-01
Early_Mississauga	2.27E+00	1.08E+00	1.57E+01	7.87E+00	1.70E+00	5.30E-01	6.08E+00	3.97E+00
Cretaceous_VC	3.37E-15	3.52E-15	3.36E-14	5.70E-16	4.25E-13	4.27E-14	1.31E-14	2.11E-16
Late Jurassic_Reservoir	1.84E-02	7.48E-03	3.50E-01	2.29E+00	1.98E-03	9.08E-04	1.67E-02	1.27E-02
Jurassic_VerrillCanyon	3.65E-01	1.66E-01	7.40E+00	2.45E+01	5.68E-02	2.48E-02	4.19E-01	3.04E-01
Late _Jurassic	1.37E-07	6.25E-08	2.75E-06	1.02E-05	6.75E-01	2.51E-01	3.22E+00	2.39E+00
Misaine	5.37E-14	3.46E-14	2.13E-13	3.91E-14	1.16E+00	3.60E-01	3.93E+00	2.95E+00
Scatarie	3.91E-08	2.60E-08	1.35E-07	1.92E-08	5.89E-01	2.37E-01	1.34E+00	9.81E-01
Mohican	4.95E-17	9.99E-18	6.90E-18	7.21E-20	1.80E-03	1.05E-03	3.71E-03	1.69E-03
Early_Jur_Lac_SR	9.62E-20	2.00E-20	1.46E-20	1.67E-22	1.80E-05	1.16E-05	3.20E-05	1.17E-05
Sum Outflow Side	**4.79E+00**	**2.33E+00**	**4.75E+01**	**6.28E+01**	**4.55E+00**	**1.57E+00**	**1.86E+01**	**1.46E+01**
Sum HC Losses	**25.2565**	**13.7861**	**3.17E+02**	**351.605**	**1.49E+01**	**5.91E+00**	**1.19E+02**	**1.16E+02**

Table 9c. Mass Balance of Hydrocarbons

mass in $(10)^9$ kg(Mtons)/m^3

Middle_Eocene	5.93E-08	7.00E-08	7.79E-08	1.28E-07	0.21853	0.14468
Early-Middle_Eocene	2.15E-07	4.20E-07	8.59E-07	1.24E-06	1.4013	0.67665
Late_Paleocene	6.62E-08	3.74E-08	1.92E-08	2.46E-14	4.63E-04	1.75E-05
Middle_Paleocene	2.36E-08	1.61E-08	2.13E-08	3.53E-08	2.26E+00	9.02E-01
Wyandot_Dawson_Canyon	0.00E+00	0.00E+00	0.00E+00	0.00E+00	9.86E-06	3.14E-06
Logan_Canyon	0.00E+00	0.00E+00	0.00E+00	0.00E+00	5.84E-14	6.78E-15
Mississauga_Reservoir	0.00E+00	0.00E+00	0.00E+00	0.00E+00	5.24E-10	6.64E-11
Early_Mississauga	0	0	0	0	9.06E-18	1.71E-18
Cretaceous_VC	0	0	0	0	6.59E-14	4.70E-16
Late Jurassic_Reservoir	0	0	0	0	0.00E+00	0.00E+00
Jurassic_VerrillCanyon	0	0	0	0	0.00E+00	0.00E+00
Late _Jurassic	0.00E+00	0.00E+00	0.00E+00	0.00E+00	0.00E+00	0.00E+00
Misaine	0.00E+00	0.00E+00	0.00E+00	0.00E+00	0.00E+00	0.00E+00
Scatarie	0	0	0	0	0.00E+00	0.00E+00
Mohican	0	0	0	0	0.00E+00	0.00E+00
Early_Jur_Lac_SR	0	0	0	0	0	0
Sum Outflow Top	**1.49E-06**	**5.97E-06**	**1.77E-05**	**2.94E-05**	**5.6721**	**2.6294**
Pliocene_Quaternary	2.39E-32	9.19E-32	1.86E-31	1.15E-39	6.90E-16	1.33E-17
Middle-Late_Miocene	8.50E-29	3.10E-28	5.90E-28	3.56E-36	2.34E-12	4.52E-14
Early-Middle_Miocene	1.40E-29	4.38E-29	6.08E-29	2.92E-37	2.65E-10	3.72E-12
Late_Eocene	0	0	0	0	3.14E-43	4.20E-45
Late_Paleocene	9.30E-08	3.26E-08	1.28E-10	9.31E-12	4.67E-07	1.04E-08
Middle_Paleocene	2.04E-42	8.14E-42	2.84E-42	0.00E+00	6.05E-08	8.84E-10
Wyandot_Dawson_Canyon	2.25E-31	5.97E-31	1.91E-31	5.17E-43	2.42E-02	9.55E-03
Logan_Canyon	0.00E+00	0.00E+00	0.00E+00	0.00E+00	1.41E-01	6.13E-02
Mid_Mississauga	0.00E+00	0.00E+00	0.00E+00	0.00E+00	5.58E-02	2.47E-02
Mississauga_Reservoir	0.00E+00	0.00E+00	0.00E+00	0.00E+00	4.58E-02	2.02E-02
Early_Mississauga	0.00E+00	0.00E+00	0.00E+00	0.00E+00	1.39E+00	6.99E-01
Cretaceous_VC	0.00E+00	0.00E+00	0.00E+00	0.00E+00	6.49E-17	2.34E-16
Late Jurassic_Reservoir	0.00E+00	0.00E+00	0.00E+00	0.00E+00	4.48E-13	7.58E-12
Jurassic_VerrillCanyon	0.00E+00	0.00E+00	0.00E+00	0.00E+00	1.30E-17	6.98E-17
Late _Jurassic	0.00E+00	0.00E+00	0.00E+00	0.00E+00	5.61E-18	6.17E-18
Misaine	0.00E+00	0.00E+00	0.00E+00	0.00E+00	1.94E-17	2.13E-17
Scatarie	0.00E+00	0.00E+00	0.00E+00	0.00E+00	1.69E-11	1.89E-11
Mohican	0	0	0	0	2.99E-20	7.54E-21
Early_Jur_Lac_SR	0.00E+00	0.00E+00	0.00E+00	0.00E+00	5.92E-23	1.54E-23
Sum Outflow Side	**9.30E-08**	**3.26E-08**	**1.28E-10**	**9.31E-12**	**1.6556**	**0.81476**
Sum HC Losses	**2.36E-06**	**7.55E-06**	**1.94E-05**	**3.19E-05**	**8.22E+00**	**3.75E+00**

Table 9c. Mass Balance of Hydrocarbons

mass in $(10)^9$ kg(Mtons)/m^3

Middle_Eocene	2.0824	2.8289	6.76E-01	1.37E+00	3.58E+00	5.89E+00
Early-Middle_Eocene	9.3993	15.716	3.00E+00	4.94E+00	1.30E+01	2.14E+01
Late_Paleocene	1.11E-06	2.30E-10	8.41E-03	2.24E-03	9.77E-06	3.38E-11
Middle_Paleocene	1.17E+01	2.60E+01	5.74E+00	9.24E+00	2.55E+01	4.46E+01
Wyandot_Dawson_Canyon	3.61E-05	2.28E-04	6.07E-02	1.03E-01	2.96E-01	5.30E-01
Logan_Canyon	1.17E-15	8.61E-18	7.57E-16	2.91E-16	5.66E-19	1.01E-24
Mississauga_Reservoi	5.58E-10	5.88E-10	3.61E-05	4.36E-06	6.25E-10	2.99E-18
Early_Mississauga	-1.42E-38	-1.64E-36	0.00E+00	0.00E+00	0.00E+00	0.00E+00
Cretaceous_VC	8.04E-18	2.09E-21	0.00E+00	0.00E+00	0.00E+00	0.00E+00
Late Jurassic_Reservoi	0.00E+00	0.00E+00	4.21E-05	3.56E-06	8.50E-09	2.87E-16
Jurassic_VerrillCanyon	0.00E+00	0.00E+00	1.62E-04	4.03E-05	1.09E-11	6.98E-22
Late _Jurassic	0.00E+00	0.00E+00	2.38E-04	9.12E-05	2.27E-09	4.92E-18
Misaine	0.00E+00	0.00E+00	2.99E-03	1.25E-03	5.26E-06	1.07E-09
Scatarie	0.00E+00	0.00E+00	0.3019	0.12629	0.00046503	1.98E-14
Mohican	0.00E+00	0.00E+00	0.79089	0.40764	0.020326	2.75E-05
Early_Jur_Lac_SR	0	0	1.36E-05	8.41E-06	1.35E-08	4.76E-15
Sum Outflow Top	**36.652**	**64.217**	**1.64E+01**	**2.63E+01**	**7.00E+01**	**1.19E+02**
Pliocene_Quaternary	2.62E-18	5.30E-21	1.74E-15	1.98E-16	2.77E-18	1.19E-21
Middle-Late_Miocene	9.31E-15	2.78E-17	5.91E-12	6.74E-13	1.02E-14	6.04E-18
Early-Middle_Miocene	8.71E-14	1.08E-17	1.14E-09	1.50E-10	2.59E-13	1.82E-18
Late_Eocene	0.00E+00	0.00E+00	7.33E-40	7.71E-41	1.70E-43	0
Late_Paleocene	1.13E-08	3.47E-10	4.07E-06	2.16E-06	2.06E-06	3.63E-07
Middle_Paleocene	2.31E-11	4.05E-16	2.76E-07	3.61E-08	5.91E-11	1.35E-17
Wyandot_Dawson_Canyon	1.29E-01	2.49E-01	3.85E-02	6.17E-02	1.72E-01	3.02E-01
Logan_Canyon	8.74E-01	1.32E+00	1.86E-01	2.85E-01	7.69E-01	1.31E+00
Mid_Mississauga	3.57E-01	5.07E-01	7.28E-02	1.10E-01	2.94E-01	4.98E-01
Mississauga_Reservoi	2.92E-01	4.17E-01	5.92E-02	8.98E-02	2.40E-01	4.06E-01
Early_Mississauga	1.11E+01	5.98E+00	2.47E+00	2.24E+00	3.84E+00	4.51E+00
Cretaceous_VC	1.19E-15	3.92E-17	3.91E-13	1.62E-13	6.09E-15	1.85E-16
Late Jurassic_Reservoi	7.69E-10	3.00E-09	3.67E-04	5.62E-04	1.49E-03	2.50E-03
Jurassic_VerrillCanyon	1.06E-14	5.14E-14	1.24E-02	1.71E-02	4.25E-02	6.78E-02
Late _Jurassic	3.45E-17	4.48E-17	1.68E-01	1.55E-01	2.60E-01	2.74E-01
Misaine	1.22E-16	1.61E-16	3.67E-01	3.20E-01	4.85E-01	4.10E-01
Scatarie	7.26E-11	6.74E-11	2.49E+00	2.18E+00	3.30E+00	2.63E+00
Mohican	4.14E-21	2.37E-22	2.94E-01	3.65E-01	7.51E-01	8.83E-01
Early_Jur_Lac_SR	8.81E-24	5.51E-25	2.97E-01	4.30E-01	1.04E+00	1.54E+00
Sum Outflow Side	**12.704**	**8.4704**	**6.46E+00**	**6.26E+00**	**1.12E+01**	**1.28E+01**
Sum HC Losses	**53.6719**	**75.0382**	**2.18E+01**	**3.55E+01**	**9.65E+01**	**1.67E+02**

Table 9c. Mass Balance of Hydrocarbons

mass in $(10)^9$ kg(Mtons)/m^3

Middle_Eocene	0.39266	0.2559	4.7352	4.018	0.30435	0.59551	0.55048
Early-Middle_Eocene	1.8584	1.1049	21.385	18.64	1.0381	1.8954	1.9204
Late_Paleocene	2.63E-03	1.62E-04	1.55E-05	4.87E-10	6.25E-03	1.27E-03	5.87E-06
Middle_Paleocene	2.32E+00	1.23E+00	3.00E+01	3.39E+01	1.49E+00	2.56E+00	2.94E+00
Wyandot_Dawson_Canyon	6.96E-02	3.68E-02	1.04E+00	1.56E+00	9.21E-03	2.03E-02	2.89E-02
Logan_Canyon	1.36E-18	1.38E-19	3.57E-22	6.45E-27	3.51E-16	1.38E-16	4.97E-19
Mississauga_Reservoir	4.25E-09	1.69E-10	5.27E-11	4.99E-14	7.73E-08	1.02E-08	6.05E-12
Early_Mississauga	0	0	0	0	0	0	0
Cretaceous_VC	0.00E+00	0.00E+00	0.00E+00	0.00E+00	0	0	0
Late Jurassic_Reservoir	2.48E-10	9.55E-12	1.09E-12	1.55E-12	1.16E-08	2.16E-08	1.75E-08
Jurassic_VerrillCanyon	4.07E-11	3.80E-12	1.43E-11	2.91E-11	5.45E-10	4.06E-10	5.76E-11
Late _Jurassic	5.57E-13	4.82E-14	9.66E-13	2.17E-12	7.28E-10	3.89E-10	3.50E-12
Misaine	0.00E+00	0.00E+00	0.00E+00	0.00E+00	3.22E-08	6.87E-08	4.77E-08
Scatarie	0.00E+00	0.00E+00	0.00E+00	0.00E+00	2.50E-06	3.75E-06	7.37E-07
Mohican	0.00E+00	0.00E+00	0.00E+00	0	2.84E-05	5.32E-05	0.00020659
Early_Jur_Lac_SR	0.00E+00	0.00E+00	0.00E+00	0.00E+00	0.00E+00	0.00E+00	0.00E+00
Sum Outflow Top	**6.59E+00**	**3.74E+00**	**8.01E+01**	**8.17E+01**	**4.80E+00**	**8.49E+00**	**8.66E+00**
Pliocene_Quaternary	2.16E-15	5.76E-17	2.52E-17	2.74E-20	2.82E-16	3.13E-17	7.15E-19
Middle-Late_Miocene	7.32E-12	1.96E-13	8.96E-14	1.43E-16	9.58E-13	1.06E-13	2.54E-15
Early-Middle_Miocene	1.37E-09	3.90E-11	2.34E-12	8.52E-17	1.80E-10	2.14E-11	6.56E-14
Late_Eocene	8.42E-40	1.90E-41	1.21E-42	0	1.12E-40	1.05E-41	3.36E-44
Late_Paleocene	0.0019625	0.00042505	0.00065774	0.00015071	6.92E-05	3.02E-05	2.41E-06
Middle_Paleocene	3.32E-07	9.38E-09	5.43E-10	5.02E-15	4.36E-08	5.14E-09	1.52E-11
Wyandot_Dawson_Canyon	5.50E-02	2.63E-02	6.33E-01	8.19E-01	7.16E-03	1.41E-02	1.86E-02
Logan_Canyon	2.92E-01	1.33E-01	2.88E+00	3.39E+00	3.96E-02	7.34E-02	8.97E-02
Mid_Mississauga	1.16E-01	5.22E-02	1.10E+00	1.27E+00	1.61E-02	2.91E-02	3.49E-02
Mississauga_Reservoir	9.43E-02	4.25E-02	8.97E-01	1.03E+00	1.30E-02	2.37E-02	2.85E-02
Early_Mississauga	1.37E+00	4.74E-01	5.97E+00	3.81E+00	1.16E+00	1.32E+00	9.51E-01
Cretaceous_VC	1.28E-14	2.02E-15	8.59E-15	1.67E-16	1.89E-13	1.04E-13	3.29E-15
Late Jurassic_Reservoir	1.36E-02	7.11E-03	1.92E-01	2.75E-01	1.29E-04	2.29E-04	2.61E-04
Jurassic_VerrillCanyon	4.09E-01	2.07E-01	4.91E+00	5.47E+00	5.02E-03	7.72E-03	7.93E-03
Late _Jurassic	2.20E+00	8.97E-01	1.56E+01	1.29E+01	8.24E-02	9.31E-02	6.88E-02
Misaine	2.35E-02	6.13E-03	6.45E-02	2.98E-02	1.66E-01	1.86E-01	1.34E-01
Scatarie	7.86E-03	1.30E-03	1.18E-02	3.90E-03	1.54E+00	1.41E+00	8.74E-01
Mohican	4.98E-07	1.48E-07	1.67E-06	6.73E-07	0.10977	0.14305	0.11066
Early_Jur_Lac_SR	1.36E-09	4.22E-10	4.81E-09	1.90E-09	5.23E-03	6.43E-03	3.66E-03
Sum Outflow Side	**4.577**	**1.8472**	**32.248**	**28.961**	**3.1498**	**3.3033**	**2.3219**
Sum HC Losses	**11.8692**	**5.71826**	**114.493**	**113.052**	**1.18E+01**	**15.8077**	**13.7538**

Table 9c. Mass Balance of Hydrocarbons

mass in $(10)^9$ kg(Mtons)/m^3		
Middle_Eocene	5.1338	72.5507
Early-Middle_Eocene	18.375	303.605
Late_Paleocene	3.08E-09	3.18E-02
Middle_Paleocene	3.06E+01	5.71E+02
Wyandot_Dawson_Canyon	3.62E-01	1.51E+01
Logan_Canyon	8.93E-23	4.58E-12
Mississauga_Reservoir	1.18E-16	4.06E-05
Early_Mississauga	0	1.08E-17
Cretaceous_VC	0	6.64E-14
Late Jurassic_Reservoir	2.54E-13	4.57E-05
Jurassic_VerrillCanyon	1.77E-19	2.02E-04
Late _Jurassic	1.15E-13	3.29E-04
Misaine	2.24E-08	4.25E-03
Scatarie	1.45E-13	0.428662
Mohican	1.55E-05	1.21919
Early_Jur_Lac_SR	0.00E+00	2.20E-05
Sum Outflow Top	**8.36E+01**	**1390.63**
Pliocene_Quaternary	6.78E-21	1.47E-14
Middle-Late_Miocene	3.55E-17	4.99E-11
Early-Middle_Miocene	2.07E-17	8.16E-09
Late_Eocene	0.00E+00	3.96E-39
Late_Paleocene	1.09E-05	0.00638965
Middle_Paleocene	1.20E-15	1.95E-06
Wyandot_Dawson_Canyon	2.20E-01	1.04E+01
Logan_Canyon	1.01E+00	4.61E+01
Mid_Mississauga	3.87E-01	1.74E+01
Mississauga_Reservoir	3.16E-01	1.42E+01
Early_Mississauga	6.73E+00	9.32E+01
Cretaceous_VC	2.60E-15	1.41E-12
Late Jurassic_Reservoir	2.68E-03	3.19E+00
Jurassic_VerrillCanyon	7.75E-02	4.44E+01
Late _Jurassic	5.59E-01	3.97E+01
Misaine	1.06E+00	1.16E+01
Scatarie	6.74E+00	2.43E+01
Mohican	0.86086	3.52544
Early_Jur_Lac_SR	2.04E-02	3.34E+00
Sum Outflow Side	**17.987**	**311.555**
Sum HC Losses	**120.719**	**1.83E+03**

Table 9d. Mass Balance of Hydrocarbons

Mass in $(10)^9$ kg(Mtons)/m^3

	Methane_Miss	C2-C5_Miss	C6-C14_Miss	C15+_Miss	Methane_JVC	C2-C5_JVC	C6-C14_JVC	C15+_JVC
Middle Mississauga	4.57E+00	1.05E+01	1.67E+01	2.07E+02	1.07E-06	6.34E-07	-8.75E-07	-1.94E-06
Early Mississauga	7.16E-02	7.45E-02	7.79E-02	-3.32E-01	1.57E-05	4.88E-06	-1.90E-05	-1.52E-05
Cretaceous_VC	4.14E-01	1.62E-01	6.24E-02	-1.04E+00	3.46E-02	-4.68E-03	-3.94E-02	-1.53E-02
Jurassic_VC	2.46E-07	3.23E-07	3.85E-07	-1.37E-06	3.48E+02	1.15E+02	1.68E+03	1.43E+03
Late_Jurassic	4.96E-07	6.39E-07	7.54E-07	-2.72E-06	1.94E+00	6.47E-01	-2.59E+00	-1.58E+00
Missaine	1.31E-05	1.50E-05	1.60E-05	-6.47E-05	2.13E-01	1.16E-01	-2.54E-01	-2.69E-01
Mohican	2.26E-04	2.94E-06	-1.78E-05	-3.77E-04	5.10E-02	7.57E-03	-5.60E-02	-3.86E-02
Early_Jur_SR	6.08E-20	1.51E-20	-1.32E-20	-1.07E-19	2.39E-03	5.33E-04	-3.72E-03	-8.73E-04
Sum Generated	**5.06E+00**	**1.07E+01**	**1.69E+01**	**2.05E+02**	**3.50E+02**	**1.16E+02**	**1.68E+03**	**1.42E+03**
Middle Mississauga	2.32955	5.05E+00	7.30972	83.352	8.29E-01	3.42E-01	5.71E+00	5.08E+00
Early Mississauga	1.13E-01	1.48E-01	1.40E-01	5.66E-01	2.65E-01	1.05E-01	1.82E+00	1.68E+00
Cretaceous_VC	0.043124	0.041138	0.048308	0.35657	8.01E-01	2.59E-01	3.75E+00	3.42E+00
Jurassic_VC	1.00E-05	3.79E-06	1.36E-05	0.00018952	10.8282	2.28345	15.6273	3.60613
Late_Jurassic	9.34E-06	3.29E-06	6.24E-06	6.01E-05	2.66E-01	1.40E-01	1.81E+00	1.85E+00
Missaine	2.83E-05	1.13E-05	1.44E-05	4.24E-05	9.34E-02	7.02E-02	3.80E-01	2.28E-01
Mohican	8.40E-05	3.65E-10	1.52E-10	1.50E-13	1.57E-02	6.96E-04	9.90E-05	7.34E-11
Early_Jur_SR	1.78E-29	4.02E-41	4.29E-42	0	3.30E-10	5.05E-11	1.47E-11	1.14E-21
Sum Accumulated in Source	**2.49E+00**	**5.23E+00**	**7.50E+00**	**8.43E+01**	**1.31E+01**	**3.20E+00**	**2.91E+01**	**1.59E+01**
Middle Mississauga	2.24E+00	5.42E+00	9.40E+00	1.23E+02	-8.29E-01	-3.42E-01	-5.71E+00	-5.08E+00
Early Mississauga	-4.11E-02	-7.37E-02	-6.19E-02	-8.97E-01	-2.65E-01	-1.05E-01	-1.82E+00	-1.68E+00
Cretaceous_VC	3.71E-01	1.20E-01	1.41E-02	-1.40E+00	-7.66E-01	-2.64E-01	-3.79E+00	-3.44E+00
Jurassic_VC	-9.78E-06	-3.46E-06	-1.32E-05	-0.000190889	3.37E+02	1.13E+02	1.66E+03	1.42E+03
Late_Jurassic	-8.84E-06	-2.65E-06	-5.49E-06	-6.28E-05	1.67E+00	5.07E-01	-4.41E+00	-3.44E+00
Missaine	-1.51E-05	3.71E-06	1.61E-06	-1.07E-04	1.20E-01	4.58E-02	-6.33E-01	-4.97E-01
Mohican	0.000141554	2.94E-06	-1.78E-05	-3.77E-04	3.54E-02	6.88E-03	-5.61E-02	-3.86E-02
Early_Jur_SR	6.08E-20	1.51E-20	-1.32E-20	-1.07E-19	0.00239399	0.000532562	-0.00372028	-0.000872793
Sum Expelled	**2.57E+00**	**5.46E+00**	**9.35E+00**	**1.21E+02**	**3.37E+02**	**1.12E+02**	**1.65E+03**	**1.41E+03**
Early_Middle_Miocene_Res	2.26E-02	8.63E-02	1.63E-01	2.48E+00	8.27E-01	4.14E-01	5.97E+00	4.60E+00
Logan_Canyon_Reser	3.37E-02	1.42E-01	2.72E-01	3.95E+00	3.62E+00	1.84E+00	2.81E+01	23.3123
Late Mississauga_Reser	1.12E-01	3.97E-01	8.95E-01	1.18E+01	1.64E+01	5.37E+00	6.82E+01	5.14E+01
Upper_Jurassic_Res	2.24E-05	9.24E-06	0.000128933	0.00170839	2.53E+01	5.27E+00	3.94E+01	1.48E+01
Sum Accumulated in Reservoir	**1.69E-01**	**6.25E-01**	**1.33E+00**	**1.82E+01**	**4.62E+01**	**1.29E+01**	**1.42E+02**	**9.41E+01**
Migration Losses	**3.11E-01**	**1.00E+00**	**2.04E+00**	**29.0189**	**8.53E+00**	**4.46E+00**	**6.96E+01**	**5.42E+01**
Sec. Cracking Losses	**3.09E-03**	**2.61E-03**	**2.49E-04**	**3.07E-03**	**1.66E+01**	**1.45E+00**	**3.41E+00**	**2.71E+00**
Quaternary-Pliocene	1.28E-03	4.74E-03	1.87E-02	2.11E-01	3.05E+00	1.34E+00	1.75E+01	1.23E+01
Middle_Late_Miocene	3.89E-06	1.56E-05	0.00011106	0.00089732	9.81E-01	5.17E-01	9.35E+00	8.27E+00
Early_Middle_Miocene_Res	7.74E-05	2.98E-05	1.92E-07	8.06E-11	2.27E-02	9.69E-04	4.19E-05	6.29E-10
Early_Middle_Miocene	1.10E-09	6.89E-10	8.56E-12	4.84E-15	4.19E-04	2.60E-05	2.02E-06	2.44E-10
Eocene	0.0039653	0.018642	0.075025	0.88138	1.45E+01	8.43E+00	1.05E+02	66.708
Paleocene	6.14E-06	1.67E-04	7.09E-04	8.73E-03	1.95E+00	1.32E+00	1.74E+01	1.05E+01
Wyandot Dawson Canyon	2.89E-01	6.20E-01	1.21E+00	1.75E+01	3.43E+01	8.63E+00	7.40E+01	3.29E+01
Logan_Canyon_Reser	2.55E-04	5.98E-04	2.11E-03	1.78E-02	4.58E+00	1.82E+00	2.86E+01	2.27E+01

Table 9d. Mass Balance of Hydrocarbons

Mass in $(10)^9$ kg(Mtons)/m^3

	Methane_Misaine	C2-C5_Misaine	C6-C14_Misaine	C15+_Misaine	Methane_CVC	C2-C5_CVC
Middle Mississauga	8.55E-06	9.91E-06	2.67E-06	-3.34E-05	1.56E-02	1.22E-02
Early Mississauga	2.22E-05	2.37E-05	5.83E-06	-8.27E-05	3.34E+01	1.55E+01
Cretaceous_VC	5.97E-03	-2.99E-03	-3.68E-03	-3.29E-03	2.67E+02	1.17E+02
Jurassic_VC	2.03E+00	-5.05E-03	-1.76E+00	-1.86678	1.88E-01	6.70E-02
Late_Jurassic	22.7454	5.19224	-21.6437	-25.5112	1.66E-02	5.24E-03
Missaine	58.2547	22.386	183.144	140.643	3.33E-02	3.47E-02
Mohican	6.65239	0.644758	-5.96778	-5.9908	5.81E-01	7.61E-03
Early_Jur_SR	0.303692	0.0803915	-0.372638	-0.235988	2.84E-08	-3.75E-08
Sum Generated	**9.00E+01**	**2.83E+01**	**1.53E+02**	**1.07E+02**	**3.01E+02**	**1.33E+02**
Middle Mississauga	0.59446	0.248584	2.919	2.50967	3.71E+01	1.68E+01
Early Mississauga	0.191689	0.0771958	0.884531	0.752125	14.2525	6.41094
Cretaceous_VC	6.58E-01	2.44E-01	2.92E+00	2.58E+00	44.5484	19.98
Jurassic_VC	1.46824	0.238189	2.36095	2.0825	0.112535	0.0492857
Late_Jurassic	2.79959	1.19718	4.86366	2.43705	3.49E-02	1.56E-02
Missaine	4.75911	1.65316	4.79778	1.54262	0.0718501	0.0301681
Mohican	1.98E+00	1.08E-01	1.48E-02	4.21E-08	0.18111	5.62E-07
Early_Jur_SR	3.52E-08	5.69E-09	1.55E-09	6.74E-19	1.55E-16	2.67E-17
Sum Accumulated in Source	**1.25E+01**	**3.77E+00**	**1.88E+01**	**1.19E+01**	**9.63E+01**	**4.33E+01**
Middle Mississauga	-0.594451	-0.248574	-2.919	-2.5097	-3.71E+01	-1.68E+01
Early Mississauga	-0.191667	-0.0771721	-0.884525	-0.752208	1.92E+01	9.07E+00
Cretaceous_VC	-6.52E-01	-2.47E-01	-2.92E+00	-2.58E+00	2.22E+02	9.69E+01
Jurassic_VC	5.58E-01	-2.43E-01	-4.12E+00	-3.95E+00	0.074997	0.0176707
Late_Jurassic	19.9458	3.99506	-26.5074	-27.9482	-0.0183364	-0.010348
Missaine	53.4956	2.07E+01	1.78E+02	1.39E+02	-0.0385283	4.51E-03
Mohican	4.66914	5.37E-01	-5.98E+00	-5.99E+00	4.00E-01	7.61E-03
Early_Jur_SR	0.303692	0.0803915	-0.372638	-0.235988	2.84E-08	-3.75E-08
Sum Expelled	**77.5336**	**24.529**	**134.632**	**95.1314**	**2.05E+02**	**8.92E+01**
Early_Middle_Miocene_Res	0.068524	0.055521	2.56E-01	1.66E-01	1.47E+00	8.88E-01
Logan_Canyon_Reser	0.365783	0.258276	1.32825	0.90222	3.81E+00	2.37E+00
Late Mississauga_Reser	1.12E+00	5.27E-01	2.86E+00	2.03E+00	2.01E+01	1.06E+01
Upper_Jurassic_Res	2.69E+00	4.65E-01	3.10E+00	2.56E+00	7.49E+00	3.10E+00
Sum Accumulated in Reservoir	**4.24E+00**	**1.31E+00**	**7.55E+00**	**5.66E+00**	**3.28E+01**	**1.69E+01**
Migration Losses	**2.64E+00**	**1.37E+00**	**7.39E+00**	**4.97E+00**	**2.03E+01**	**1.13E+01**
Sec. Cracking Losses	**-2.86E+00**	**-2.11E+00**	**5.34E+00**	**8.27417**	**6.95E+00**	**7.79E-01**
Quaternary-Pliocene	2.20E-01	1.61E-01	7.85E-01	5.04E-01	2.13E+00	1.20E+00
Middle_Late_Miocene	1.31E-01	7.62E-02	5.02E-01	3.75E-01	1.09E-01	6.47E-02
Early_Middle_Miocene_Res	1.39E-03	9.69E-05	1.04E-06	1.19E-11	8.94E-03	6.18E-04
Early_Middle_Miocene	2.57E-05	2.89E-06	4.86E-08	3.75E-12	4.50E-05	4.14E-06
Eocene	1.05E+00	8.97E-01	3.42E+00	1.94E+00	5.86E+00	4.61E+00
Paleocene	1.38E-01	1.64E-01	4.50E-01	1.76E-01	1.82E-01	1.85E-01
Wyandot Dawson Canyon	3.64E+00	8.47E-01	1.69E+00	6.64E-01	38.988	17.341
Logan_Canyon_Reser	6.68E-01	3.35E-01	1.28E+00	7.74E-01	0.41464	0.19296

Table 9d. Mass Balance of Hydrocarbons

Mass in $(10)^9$ kg(Mtons)/m^3

	C6-C14_CVC	C15+_CVC	Methane_EJur	PK_C2-C5_EJur	PK_C6-C14_EJur	PK_C15+_EJur
Middle Mississauga	-2.22E-02	-2.14E-02	1.64E-06	6.51E-07	-5.59E-07	-3.44E-06
Early Mississauga	1.86E+02	7.81E+01	4.89E-06	9.45E-07	-1.72E-06	-8.86E-06
Cretaceous_VC	1.21E+03	4.03E+02	3.76E-03	-3.68E-03	-1.67E-03	-3.74E-04
Jurassic_VC	-3.39E-01	-6.05E-02	1.13E+00	-4.39E-01	-6.98E-01	-7.79E-01
Late_Jurassic	-2.22E-02	-1.32E-02	5.07E+00	-9.32E-01	-3.10E+00	-4.88E+00
Missaine	2.14E-02	-1.37E-01	4.57E+00	-6.56E-01	-2.65E+00	-4.79E+00
Mohican	-1.11E-01	-8.95E-01	1.49E+02	-1.56E+01	-8.21E+01	-1.69E+02
Early_Jur_SR	-3.36E-09	-1.74E-10	8.36E+01	1.28E+02	3.53E+02	6.22E+02
Sum Generated	**1.39E+03**	**4.80E+02**	**2.43E+02**	**1.11E+02**	**2.64E+02**	**4.42E+02**
Middle Mississauga	1.54E+02	5.70E+01	2.50E+00	3.99E-01	6.11E-01	3.73E-01
Early Mississauga	67.9012	19.4046	8.32E-01	1.23E-01	2.02E-01	1.26E-01
Cretaceous_VC	191.058	33.9582	3.1042	3.76E-01	6.89E-01	3.88E-01
Jurassic_VC	0.482675	0.328951	1.98447	0.181844	0.289601	0.233184
Late_Jurassic	1.22E-01	1.51E-01	1.20727	0.293683	0.464857	0.420252
Missaine	0.0727059	0.0747407	1.55268	0.220692	0.307401	0.204688
Mohican	2.67E-07	2.16E-10	4.82E+00	5.68E-02	6.87E-03	1.40E-05
Early_Jur_SR	7.89E-18	4.25E-29	0.0027754	0.001116	0.00072758	3.54E-05
Sum Accumulated in Source	**4.14E+02**	**1.11E+02**	**1.60E+01**	**1.65E+00**	**2.57E+00**	**1.74E+00**
Middle Mississauga	-1.54E+02	-5.70E+01	-2.50E+00	-3.99E-01	-6.11E-01	-3.73E-01
Early Mississauga	1.18E+02	5.87E+01	-8.32E-01	-1.23E-01	-2.02E-01	-1.26E-01
Cretaceous_VC	1.01E+03	3.69E+02	-3.10E+00	-3.79E-01	-6.91E-01	-0.387914
Jurassic_VC	-0.821663	-0.389419	-8.56E-01	-6.21E-01	-9.87E-01	-1.01E+00
Late_Jurassic	-0.144051	-0.16394	3.86E+00	-1.23E+00	-3.56E+00	-5.29685
Missaine	-5.13E-02	-2.12E-01	3.02061	-0.876848	-2.95516	-4.9954
Mohican	-1.11E-01	-8.95E-01	143.925	-15.676	-82.0941	-169.238
Early_Jur_SR	-3.36E-09	-1.74E-10	83.5935	128.424	352.916	621.887
Sum Expelled	**9.77E+02**	**3.69E+02**	**227.113**	**109.124**	**261.812**	**440.457**
Early_Middle_Miocene_Res	8.50E+00	2.41E+00	7.41E-02	7.39E-02	1.42E-01	1.75E-01
Logan_Canyon_Reser	2.64E+01	9.89E+00	1.13E+00	4.03E-01	7.98E-01	1.00E+00
Late Mississauga_Reser	1.26E+02	5.36E+01	2.20896	0.83289	1.57124	1.96283
Upper_Jurassic_Res	3.10E+01	4.92E+00	1.23E+01	4.64E-01	7.90E-01	4.35E-01
Sum Accumulated in Reservoir	**1.92E+02**	**7.08E+01**	**1.57E+01**	**1.77E+00**	**3.30E+00**	**3.57E+00**
Migration Losses	**1.30E+02**	**5.23E+01**	**4.28E+00**	**1.40E+00**	**2.18E+00**	**2.12E+00**
Sec. Cracking Losses	**3.10E+00**	**1.27E+00**	**-1.59E+01**	**-2.47E+00**	**9.44E+00**	**3.35E+01**
Quaternary-Pliocene	1.58E+01	8.17E+00	2.87E-01	2.04E-01	3.74E-01	4.35E-01
Middle_Late_Miocene	9.29E-01	7.27E-01	1.42E-01	1.02E-01	1.94E-01	2.48E-01
Early_Middle_Miocene_Res	3.01E-05	4.26E-10	1.19E-03	0.00011736	1.83E-07	1.35E-13
Early_Middle_Miocene	3.79E-07	6.95E-11	1.88E-05	3.06E-06	1.11E-08	1.12E-13
Eocene	6.21E+01	2.64E+01	1.08E+00	1.0131	1.8378	2.1124
Paleocene	2.60E+00	1.7321	1.02E-01	1.39E-01	2.52E-01	2.71E-01
Wyandot Dawson Canyor	187.62	6.04E+01	10.818	1.0058	6.84E-01	5.65E-01
Logan_Canyon_Reser	2.1432	1.22E+00	1.45E+00	4.61E-01	6.97E-01	8.29E-01

Table 9d. Mass Balance of Hydrocarbons

Mass in $(10)^9$ kg(Mtons)/m^3

	Methane_TJur	C2-C5_TJur	C6-C14_TJur	C15+_TJur	Methane_Mohican	C2-C5_Mohican	C6-C14_Mohican
Middle Mississauga	0.00E+00	0.00E+00	0.00E+00	0.00E+00	0	0	0
Early Mississauga	0.00E+00	0.00E+00	0.00E+00	0.00E+00	0.00E+00	0.00E+00	0.00E+00
Cretaceous_VC	0.00E+00	0.00E+00	0.00E+00	0.00E+00	0.00E+00	0.00E+00	0.00E+00
Jurassic_VC	0	0	0	0	0.00E+00	0.00E+00	0.00E+00
Late_Jurassic	31.013	9.4959	149.02	126.8	0	0	0
Missaine	0	0	0	0	0	0	0
Mohican	0	0	0	0	52.116	43.55	29.262
Early_Jur_SR	0	0	0	0	0	0	0
Sum Generated	**3.10E+01**	**9.50E+00**	**1.49E+02**	**1.27E+02**	**5.21E+01**	**4.36E+01**	**2.93E+01**
Middle Mississauga	0.0923521	0.0319824	0.521426	0.425005	0.295456	0.282515	0.190784
Early Mississauga	0.034404	0.0116282	0.188826	0.153612	0.0964207	0.0911889	0.0627014
Cretaceous_VC	0.093369	3.02E-02	0.484585	0.40159	0.338274	0.328924	0.243543
Jurassic_VC	0.354902	0.113276	1.73469	1.3712	0.282939	0.254023	0.200596
Late_Jurassic	2.21E+00	4.56E-01	4.81E+00	3.18E+00	0.208196	0.203159	0.165201
Missaine	0.414394	0.122864	1.9218	1.43669	1.87E-01	1.84E-01	0.170551
Mohican	0.0965775	0.0272599	0.431772	0.367619	1.40E+00	6.38E-01	2.66E-01
Early_Jur_SR	2.41E-09	6.70E-10	1.07E-08	9.00E-09	2.94E-09	1.71E-09	3.61E-10
Sum Accumulated in Source	**3.30E+00**	**7.93E-01**	**1.01E+01**	**7.34E+00**	**2.81E+00**	**1.98E+00**	**1.30E+00**
Middle Mississauga	-9.24E-02	-3.20E-02	-5.21E-01	-4.25E-01	-0.295456	-0.282515	-0.190784
Early Mississauga	-3.44E-02	-1.16E-02	-1.89E-01	-0.153612	-0.0964207	-0.0911889	-0.0627014
Cretaceous_VC	-9.34E-02	-3.02E-02	-4.85E-01	-4.02E-01	-0.338274	-0.328924	-0.243543
Jurassic_VC	-0.354902	-0.113276	-1.73469	-1.3712	-0.282939	-0.254023	-0.200596
Late_Jurassic	28.8011	9.04E+00	144.214	123.616	-0.208196	-0.203159	-0.165201
Missaine	-0.414394	-1.23E-01	-1.92E+00	-1.44E+00	-1.87E-01	-1.84E-01	-0.170551
Mohican	-9.66E-02	-2.73E-02	-4.32E-01	-3.68E-01	5.07E+01	4.29E+01	2.90E+01
Early_Jur_SR	-2.41E-09	-6.70E-10	-1.07E-08	-9.00E-09	-2.94E-09	-1.71E-09	-3.61E-10
Sum Expelled	**27.7151**	**8.70256**	**138.931**	**119.46**	**49.3039**	**41.5686**	**27.9621**
Early_Middle_Miocene_Res	3.15E-02	2.14E-02	3.89E-01	3.26E-01	0.033683	0.057723	3.78E-02
Logan_Canyon_Reser	1.75E-01	1.13E-01	2.01E+00	1.68E+00	0.260612	0.381043	0.232966
Late Mississauga_Reser	0.529688	2.52E-01	4.50526	3.76817	0.598187	0.778198	0.632655
Upper_Jurassic_Res	5.03E-01	1.45E-01	2.20E+00	1.82836	1.4479	1.16176	0.815237
Sum Accumulated in Reservoir	**1.24E+00**	**5.31E-01**	**9.10E+00**	**7.60E+00**	**2.34038**	**2.37872**	**1.71867**
Migration Losses	**0.592509**	**0.297174**	**5.20264**	**4.30213**	**0.734243**	**0.987257**	**0.660579**
Sec. Cracking Losses	**1.36E+00**	**1.96E-01**	**1.74E+00**	**1.40E+00**	**1.14E+00**	**3.43E-01**	**1.27E-01**
Quaternary-Pliocene	9.54E-02	5.96E-02	1.08E+00	8.98E-01	1.02E-01	1.58E-01	1.02E-01
Middle_Late_Miocene	0.079035	0.036091	0.60873	0.49789	0.056225	0.072379	0.046341
Early_Middle_Miocene_Res	0.00043793	2.78E-05	2.02E-06	4.66E-11	0.00066302	8.00E-05	1.89E-07
Early_Middle_Miocene	6.63E-06	6.02E-07	7.60E-08	1.39E-11	1.22E-05	2.24E-06	9.20E-09
Eocene	4.44E-01	3.29E-01	6.19E+00	5.1787	5.01E-01	8.39E-01	5.42E-01
Paleocene	0.035367	0.035974	0.72003	0.61922	0.065839	0.13354	0.087601
Wyandot Dawson Canyon	0.98337	0.29874	4.7611	3.90E+00	1.9584	0.8197	3.15E-01
Logan_Canyon_Reser	0.16484	0.10073	1.7909	1.51E+00	0.32372	0.34873	2.00E-01

Table 9d. Mass Balance of Hydrocarbons

Mass in $(10)^9$ kg(Mtons)/m^3

	C15+_Mohican	Sum
Middle Mississauga	0	238.25
Early Mississauga	0.00E+00	312.472
Cretaceous_VC	0.00E+00	1991.75
Jurassic_VC	0	3566.82
Late_Jurassic	0	291.671
Missaine	0	400.665
Mohican	237.76	239.377
Early_Jur_SR	0	1186.6
Sum Generated	**2.38E+02**	**8.23E+03**
Middle Mississauga	1.15313	388.148
Early Mississauga	0.380429	117.013
Cretaceous_VC	1.57627	312.725
Jurassic_VC	2.37837	48.8477
Late_Jurassic	2.07842	31.3923
Missaine	2.85311	23.349
Mohican	3.39E+00	13.8152
Early_Jur_SR	2.20E-09	0.00465443
Sum Accumulated in Source	**1.38E+01**	**9.35E+02**
Middle Mississauga	-1.15313	-149.898
Early Mississauga	-0.380429	195.458
Cretaceous_VC	-1.57627	1679.03
Jurassic_VC	-2.37837	3517.97
Late_Jurassic	-2.07842	260.278
Missaine	-2.85311	377.315
Mohican	2.34E+02	2.26E+02
Early_Jur_SR	-2.20E-09	1186.59
Sum Expelled	**223.947**	**7292.31**
Early_Middle_Miocene_Res	2.62E-01	30.0155
Logan_Canyon_Reser	1.61765	116.491
Late Mississauga_Reser	4.81543	393.859
Upper_Jurassic_Res	6.61108	168.779
Sum Accumulated in Reservoir	**13.3061**	**709.144**
Migration Losses	**4.50617**	**426.571**
Sec. Cracking Losses	**1.05E+00**	**76.7631**
Quaternary-Pliocene	7.01E-01	6.79E+01
Middle_Late_Miocene	0.32163	24.4415
Early_Middle_Miocene_Res	3.58E-11	0.0374563
Early_Middle_Miocene	1.30E-11	5.69E-04
Eocene	3.8173	3.26E+02
Paleocene	0.58815	39.9457
Wyandot Dawson Canyor	2.33E+00	509.015
Logan_Canyon_Reser	1.35E+00	74.0262

Table 9d. Mass Balance of Hydrocarbons

Mass in $(10)^9$ kg(Mtons)/m^3

Logan_Canyon	0.42204	0.47804	0.59235	7.4315	3.06E+01	9.14E+00	1.36E+02	1.06E+02
Naskapi	5.43E-09	9.06E-09	7.63E-08	3.69E-07	9.31E+01	3.42E+01	6.16E+02	620.67
Late Mississauga_Reser	8.66E-12	3.16E-11	6.01E-10	2.84E-09	5.31E+00	2.57E+00	6.53E+01	1.18E+02
Middle Mississauga	1.08E-15	3.70E-15	-3.39E-36	-1.06E-35	0.00E+00	0.00E+00	0.00E+00	0.00E+00
Early Mississauga	0.00E+00	0.00E+00	0.00E+00	0.00E+00	0.00E+00	0.00E+00	0.00E+00	0.00E+00
Cretaceous_VC	0.00E+00	0.00E+00	0.00E+00	0.00E+00	3.77E-29	6.07E-31	1.22E-31	7.36E-39
Upper_Jurassic_Res	0.00E+00	0.00E+00	0.00E+00	0.00E+00	6.91E-03	2.04E-03	1.06E-01	5.27E+00
Jurassic_VC	0	0	0	0	7.71E-07	6.84E-08	5.60E-06	6.50E-02
Late_Jurassic	0	0	0	0	0.00E+00	0.00E+00	0.00E+00	0.00E+00
Missaine	0.00E+00	0.00E+00	0.00E+00	0.00E+00	0.00E+00	0.00E+00	0.00E+00	0.00E+00
Mohican	0.00E+00	0.00E+00	0.00E+00	0.00E+00	0.00E+00	0.00E+00	0.00E+00	0.00E+00
Early_Jur_SR	0.00E+00	0.00E+00	0.00E+00	0.00E+00	0.00E+00	0.00E+00	0.00E+00	0.00E+00
Sum Outflow Top	**7.16E-01**	**1.12E+00**	**1.90E+00**	**2.61E+01**	**1.88E+02**	**6.80E+01**	**1.07E+03**	**1.00E+03**
Quaternary-Pliocene	4.20E-21	1.22E-21	1.32E-23	4.87E-27	6.47E-18	2.50E-19	1.57E-20	3.05E-25
Middle_Late_Miocene	1.30E-18	3.79E-19	3.55E-21	4.94E-25	2.01E-15	7.76E-17	4.23E-18	3.10E-23
Early_Middle_Miocene_Res	2.23E-03	7.52E-03	2.79E-02	3.59E-01	4.38E+00	2.21E+00	4.25E+01	3.37E+01
Early_Middle_Miocene	3.83E-10	1.12E-10	1.21E-12	6.14E-16	5.91E-07	2.29E-08	1.44E-09	3.85E-14
Wyandot Dawson Canyon	4.36E-02	7.78E-02	1.15E-01	1.57E+00	6.33E+00	3.31E+00	4.67E+01	3.30E+01
Logan_Canyon_Reser	2.23E-02	1.58E-01	4.73E-01	6.11E+00	4.29E+00	2.64E+00	5.52E+01	4.49E+01
Naskapi	1.70E-01	2.92E-01	4.46E-01	5.85E+00	4.10E+01	1.07E+01	1.28E+02	6.08E+01
Late Mississauga_Reser	8.08E-01	1.41E+00	1.83E+00	1.86E+01	5.93E-02	1.43E-02	7.87E-02	0.015119
Late Mississauga	2.49E-03	6.59E-03	1.28E-02	1.85E-01	3.08E-06	7.09E-07	3.52E-06	5.02E-07
Middle Mississauga	3.25E-01	7.64E-01	1.18E+00	1.49E+01	5.51E-04	1.38E-04	6.48E-04	9.29E-05
Early Mississauga	8.40E-04	1.29E-03	1.22E-03	3.02E-03	1.64E-04	4.24E-05	1.93E-04	2.79E-05
Cretaceous_VC	8.67E-05	1.31E-04	1.25E-04	3.72E-04	1.45E-03	3.78E-04	1.68E-03	2.41E-04
Upper_Jurassic_Res	2.59E-08	3.03E-08	6.67E-08	3.15E-06	1.79E+01	5.88E+00	8.13E+01	7.01E+01
Jurassic_VC	2.74E-11	1.33E-11	1.03E-11	7.86E-12	1.93E+00	6.61E-01	9.75E+00	1.13E+01
Late_Jurassic	2.34E-12	8.73E-13	7.72E-13	8.57E-13	5.27E-01	1.38E-02	4.52E-02	3.16E-02
Missaine	2.64E-14	2.89E-14	3.19E-14	6.06E-14	3.27E-04	1.00E-04	1.25E-04	5.40E-08
Scatarie	2.22E-14	2.43E-14	2.67E-14	4.37E-14	1.67E-08	4.36E-09	4.86E-09	1.11E-10
Mohican	5.93E-08	2.75E-10	1.05E-10	1.33E-11	1.05E-04	9.01E-11	5.30E-12	5.65E-16
Early_Jur_SR	2.93E-24	1.59E-24	8.00E-25	2.46E-27	1.26E-24	3.72E-26	1.24E-26	2.22E-30
Eurydice	5.58E-21	2.00E-21	5.72E-22	5.80E-25	6.60E-01	1.67E-01	2.99E-01	1.42E-02
Sum Outflow Side	**1.38E+00**	**2.71E+00**	**4.09E+00**	**4.75E+01**	**7.70E+01**	**2.56E+01**	**3.64E+02**	**2.54E+02**
Sum HC Losses	**2.41E+00**	**4.84E+00**	**8.02E+00**	**1.03E+02**	**2.91E+02**	**9.95E+01**	**1.51E+03**	**1.31E+03**

Table 9d. Mass Balance of Hydrocarbons

Mass in $(10)^9$ kg(Mtons)/m^3

Logan_Canyon	9.51E+00	3.12E+00	1.09E+01	5.70E+00	27.483	6.3845
Naskapi	2.23E+01	6.28E+00	2.90E+01	2.12E+01	9.9954	3.6512
Late Mississauga_Reser	1.37E+00	5.98E-01	7.79E+00	7.35E+00	5.89E-01	2.70E-01
Middle Mississauga	0.00E+00	0.00E+00	0.00E+00	0.00E+00	0.00E+00	0.00E+00
Early Mississauga	0.00E+00	0.00E+00	0.00E+00	0.00E+00	4.44E-11	2.75E-13
Cretaceous_VC	4.32E-27	1.73E-28	9.78E-30	3.34E-39	4.64E-12	2.43E-14
Upper_Jurassic_Res	2.51E-01	1.20E-01	2.73E+00	3.10E+00	0.00E+00	0.00E+00
Jurassic_VC	0.0030097	0.00057932	0.028964	1.0573	0.00E+00	0.00E+00
Late_Jurassic	1.66E-07	4.40E-09	8.66E-09	3.78E-08	0.00E+00	0.00E+00
Missaine	6.20E-19	4.57E-20	0	0	0.00E+00	0.00E+00
Mohican	0	0	0	0	0.00E+00	0.00E+00
Early_Jur_SR	0.00E+00	0.00E+00	0.00E+00	0.00E+00	0.00E+00	0.00E+00
Sum Outflow Top	**3.92E+01**	**1.26E+01**	**5.85E+01**	**4.28E+01**	**8.58E+01**	**3.39E+01**
Quaternary-Pliocene	4.78E-19	3.12E-20	5.67E-22	9.06E-27	1.72E-18	8.83E-20
Middle_Late_Miocene	1.48E-16	9.68E-18	1.53E-19	9.19E-25	5.34E-16	2.73E-17
Early_Middle_Miocene_Res	1.7352	0.75024	6.9559	4.9487	1.0711	0.59591
Early_Middle_Miocene	4.37E-08	2.86E-09	5.19E-11	1.14E-15	1.57E-07	8.07E-09
Wyandot Dawson Canyor	3.57E+00	9.81E-01	5.24E+00	3.27E+00	5.59E+00	2.13E+00
Logan_Canyon_Reser	3.02E+00	1.93E+00	2.04E+01	1.30E+01	3.56E+00	3.94E+00
Naskapi	3.69E+00	1.03E+00	5.97E+00	4.05E+00	1.54E+01	6.21E+00
Late Mississauga_Reser	0.17294	0.063332	0.87722	0.73705	1.06E+01	3.53E+00
Late Mississauga	3.25E-07	1.35E-07	1.48E-06	1.19E-06	6.33E-02	3.02E-02
Middle Mississauga	5.35E-05	2.26E-05	2.00E-04	1.52E-04	6.47E+00	2.90E+00
Early Mississauga	2.08E-05	8.29E-06	7.35E-05	5.63E-05	1.30E+00	5.83E-01
Cretaceous_VC	2.48E-04	8.55E-05	7.49E-04	5.75E-04	7.44E+00	3.23E+00
Upper_Jurassic_Res	2.82E+00	9.30E-01	5.81E+00	4.18E+00	7.26E+00	3.10E+00
Jurassic_VC	5.90E-01	1.96E-01	7.09E-01	4.07E-01	3.53E-03	1.44E-03
Late_Jurassic	3.97E+00	2.83E-01	1.33E+00	8.30E-01	8.48E-04	8.76E-06
Missaine	5.30E-01	2.08E-01	2.52E+00	1.98E+00	3.69E-06	2.62E-06
Scatarie	1.01E-02	4.34E-03	1.74E-02	5.39E-03	1.52E-06	1.14E-06
Mohican	8.18E-01	4.73E-02	3.20E-02	2.69E-03	4.20E-02	4.82E-03
Early_Jur_SR	3.99E-12	7.85E-13	3.36E-13	6.70E-17	6.60E-16	4.41E-17
Eurydice	1.34E+01	4.94E+00	5.99E+00	4.61E-02	2.78E-03	3.20E-04
Sum Outflow Side	**3.43E+01**	**1.14E+01**	**5.59E+01**	**3.34E+01**	**5.88E+01**	**2.63E+01**
Sum HC Losses	**73.2897**	**23.2228**	**127.081**	**89.4725**	**1.72E+02**	**7.23E+01**

Table 9d. Mass Balance of Hydrocarbons

Mass in $(10)^9$ kg(Mtons)/m^3						
Logan_Canyon	51.119	19.876	2.97E+01	5.64E+00	5.13E+00	4.84E+00
Naskapi	37.694	18.901	4.24E+01	1.73E+01	2.86E+01	3.74E+01
Late Mississauga_Reser	3.47E+00	2.40E+00	1.11E+01	7.18E+00	1.49E+01	2.22E+01
Middle Mississauga	0.00E+00	0.00E+00	0.00E+00	0.00E+00	0.00E+00	0.00E+00
Early Mississauga	4.43E-15	1.39E-18	0.00E+00	0.00E+00	0.00E+00	0.00E+00
Cretaceous_VC	4.64E-16	1.59E-18	7.91E-27	1.28E-27	1.91E-30	8.24E-43
Upper_Jurassic_Res	0.00E+00	0.00E+00	1.05E+01	1.76E+01	4.96E+01	8.73E+01
Jurassic_VC	0.00E+00	0.00E+00	1.87E+01	3.18E+01	9.18E+01	1.67E+02
Late_Jurassic	0.00E+00	0.00E+00	3.07E-02	1.06E-02	2.37E-04	4.06E-08
Missaine	0.00E+00	0.00E+00	0.00E+00	0.00E+00	0.00E+00	0.00E+00
Mohican	0.00E+00	0.00E+00	3.37E-04	1.16E-04	6.44E-07	2.80E-15
Early_Jur_SR	0.00E+00	0.00E+00	8.74E-06	4.74E-06	6.95E-09	2.32E-15
Sum Outflow Top	**3.64E+02**	**1.40E+02**	**1.26E+02**	**8.24E+01**	**1.94E+02**	**3.23E+02**
Quaternary-Pliocene	5.57E-21	1.24E-25	4.82E-19	5.12E-20	1.04E-22	1.24E-28
Middle_Late_Miocene	1.50E-18	1.26E-23	1.49E-16	1.59E-17	2.39E-20	1.26E-26
Early_Middle_Miocene_Res	9.4245	5.4068	5.12E+00	1.09E+00	1.64E+00	1.42E+00
Early_Middle_Miocene	5.10E-10	1.57E-14	4.40E-08	4.68E-09	9.54E-12	1.57E-17
Wyandot Dawson Canyor	2.21E+01	1.22E+01	1.51E+01	1.59E+00	1.43E+00	1.25E+00
Logan_Canyon_Reser	6.41E+01	3.22E+01	1.24E+01	3.34E+00	4.30E+00	2.53E+00
Naskapi	6.59E+01	1.90E+01	7.52E+00	1.12E+00	1.48E+00	1.51E+00
Late Mississauga_Reser	1.84E+01	2.89E+00	1.16E+00	1.17E-01	1.68E-01	0.06806
Late Mississauga	3.70E-01	9.08E-02	4.20E-07	1.58E-07	1.62E-07	7.09E-08
Middle Mississauga	3.20E+01	8.51E+00	7.22E-05	2.33E-05	2.31E-05	9.47E-06
Early Mississauga	6.63E+00	2.51E+00	3.45E-05	8.56E-06	8.45E-06	3.48E-06
Cretaceous_VC	3.51E+01	1.24E+01	6.08E-04	8.67E-05	8.49E-05	3.48E-05
Upper_Jurassic_Res	3.39E+01	1.02E+01	7.75E+00	8.72E-01	7.25E-01	2.35E-01
Jurassic_VC	4.92E-03	4.49E-05	2.24E+00	1.79E-01	1.06E-01	1.23E-02
Late_Jurassic	4.52E-05	3.31E-05	6.90E+00	2.82E-01	2.29E-01	6.97E-02
Missaine	1.50E-05	1.34E-05	3.31E-01	1.59E-01	1.81E-01	9.63E-02
Scatarie	4.68E-06	3.04E-06	8.09E-02	4.38E-02	5.31E-02	3.40E-02
Mohican	3.14E-03	2.04E-04	2.35E+01	1.62E+01	4.20E+01	7.13E+01
Early_Jur_SR	3.77E-17	7.36E-20	1.43E-03	2.20E-03	5.91E-03	1.01E-02
Eurydice	5.26E-04	7.73E-06	1.48E+01	9.67E-01	5.71E-01	4.27E-03
Sum Outflow Side	**2.88E+02**	**1.05E+02**	**9.68E+01**	**2.60E+01**	**5.28E+01**	**7.86E+01**
Sum HC Losses	**7.85E+02**	**2.99E+02**	**2.11E+02**	**1.07E+02**	**2.59E+02**	**4.37E+02**

Table 9d. Mass Balance of Hydrocarbons

Mass in $(10)^9$ kg(Mtons)/m^3							
Logan_Canyon	1.8123	0.63023	10.078	8.3767	5.5746	4.0741	2.1012
Naskapi	12.249	3.3399	50.815	42.946	16.134	11.569	6.5653
Late Mississauga_Reser	1.63E+00	6.36E-01	1.20E+01	1.19E+01	3.59E+00	3.14E+00	2.03E+00
Middle Mississauga	0.00E+00	0.00E+00	0.00E+00	0.00E+00	0.00E+00	0.00E+00	0.00E+00
Early Mississauga	0.00E+00	0.00E+00	0.00E+00	0.00E+00	0.00E+00	0.00E+00	0.00E+00
Cretaceous_VC	7.98E-28	3.12E-29	2.94E-30	2.01E-39	5.46E-27	7.22E-28	2.02E-30
Upper_Jurassic_Res	7.00E-02	3.44E-02	8.78E-01	2.45E+00	1.57E+00	3.04E+00	3.69E+00
Jurassic_VC	0.00011137	1.42E-05	0.00085638	0.32698	0.21055	0.52007	1.082
Late_Jurassic	1.38E-09	5.92E-11	3.24E-10	5.22E-09	5.66E-06	2.53E-06	4.63E-07
Missaine	0.00E+00	0.00E+00	0.00E+00	0.00E+00	0.00E+00	0.00E+00	0.00E+00
Mohican	0.00E+00	0.00E+00	0.00E+00	0.00E+00	1.19E-11	1.21E-11	5.29E-10
Early_Jur_SR	0.00E+00	0.00E+00	0.00E+00	0.00E+00	0.00E+00	0.00E+00	0.00E+00
Sum Outflow Top	**1.76E+01**	**5.50E+00**	**8.89E+01**	**7.86E+01**	**3.01E+01**	**2.47E+01**	**1.68E+01**
Quaternary-Pliocene	1.86E-19	1.03E-20	8.93E-22	2.07E-26	2.45E-19	3.12E-20	9.46E-23
Middle_Late_Miocene	5.77E-17	3.18E-18	2.41E-19	2.10E-24	7.60E-17	9.66E-18	2.55E-20
Early_Middle_Miocene_Res	5.50E-01	2.09E-01	3.43E+00	2.72E+00	7.31E-01	6.76E-01	4.17E-01
Early_Middle_Miocene	1.70E-08	9.39E-10	8.18E-11	2.61E-15	2.24E-08	2.85E-09	8.66E-12
Wyandot Dawson Canyor	4.75E-01	1.93E-01	3.14E+00	2.57E+00	1.74E+00	9.71E-01	4.10E-01
Logan_Canyon_Reser	5.51E-01	2.73E-01	4.93E+00	3.92E+00	1.49E+00	2.16E+00	1.30E+00
Naskapi	1.54E+00	4.13E-01	5.76E+00	4.32E+00	1.77E+00	1.01E+00	4.98E-01
Late Mississauga_Reser	1.57E-02	5.58E-03	1.20E-01	0.10502	1.48E-01	1.51E-01	1.23E-01
Late Mississauga	1.03E-07	3.06E-08	4.61E-07	3.83E-07	3.90E-08	4.12E-08	2.82E-08
Middle Mississauga	2.66E-05	8.03E-06	1.23E-04	1.06E-04	6.72E-06	7.09E-06	5.33E-06
Early Mississauga	9.88E-06	3.02E-06	4.80E-05	4.55E-05	3.47E-06	3.74E-06	3.24E-06
Cretaceous_VC	1.10E-04	3.46E-05	5.99E-04	6.81E-04	6.79E-05	7.53E-05	7.52E-05
Upper_Jurassic_Res	8.93E-01	2.65E-01	4.09E+00	3.43E+00	8.74E-01	7.24E-01	4.89E-01
Jurassic_VC	1.61E-01	5.30E-02	8.89E-01	7.93E-01	2.55E-01	2.01E-01	1.35E-01
Late_Jurassic	3.92E-01	1.44E-01	2.52E+00	2.27E+00	3.60E-01	2.82E-01	2.07E-01
Missaine	2.21E-03	5.47E-04	8.53E-03	7.77E-03	2.68E-02	2.81E-02	2.15E-02
Scatarie	2.26E-05	5.72E-06	8.96E-05	8.19E-05	6.59E-03	7.26E-03	5.75E-03
Mohican	2.27E-03	5.67E-04	7.94E-03	6.33E-03	4.82E+00	4.82E+00	3.80E+00
Early_Jur_SR	4.94E-31	1.34E-29	1.60E-26	3.05E-25	7.62E-05	7.81E-05	2.95E-05
Eurydice	2.37E+00	6.20E-01	9.07E+00	7.43E+00	2.79E+00	2.11E+00	1.29E+00
Sum Outflow Side	**6.96E+00**	**2.18E+00**	**3.40E+01**	**2.76E+01**	**1.50E+01**	**1.31E+01**	**8.70E+00**
Sum HC Losses	**2.65E+01**	**8.17E+00**	**1.30E+02**	**1.12E+02**	**46.9635**	**39.1899**	**26.2434**

Table 9d. Mass Balance of Hydrocarbons

Mass in $(10)^9$ kg(Mtons)/m^3

Logan_Canyon	13.603	516.407
Naskapi	45.644	1828.28
Late Mississauga_Reser	1.53E+01	3.20E+02
Middle Mississauga	0.00E+00	4.78E-15
Early Mississauga	0.00E+00	4.46E-11
Cretaceous_VC	5.62E-39	4.66E-12
Upper_Jurassic_Res	4.01E+01	2.28E+02
Jurassic_VC	15.218	3.27E+02
Late_Jurassic	4.25E-09	4.15E-02
Missaine	0.00E+00	6.65E-19
Mohican	5.22E-12	4.53E-04
Early_Jur_SR	0.00E+00	1.35E-05
Sum Outflow Top	**1.39E+02**	**4.26E+03**
Quaternary-Pliocene	1.78E-26	1.01E-17
Middle_Late_Miocene	1.81E-24	3.12E-15
Early_Middle_Miocene_Res	2.48E+00	1.35E+02
Early_Middle_Miocene	2.25E-15	9.21E-07
Wyandot Dawson Canyon	2.40E+00	1.77E+02
Logan_Canyon_Reser	6.79E+00	3.00E+02
Naskapi	3.29E+00	3.99E+02
Late Mississauga_Reser	8.51E-01	6.31E+01
Late Mississauga	2.14E-07	0.760716
Middle Mississauga	5.22E-05	6.70E+01
Early Mississauga	4.28E-05	1.10E+01
Cretaceous_VC	1.23E-03	5.82E+01
Upper_Jurassic_Res	3.94E+00	2.68E+02
Jurassic_VC	1.15E+00	3.17E+01
Late_Jurassic	1.91E+00	2.26E+01
Missaine	1.95E-01	6.30E+00
Scatarie	5.51E-02	3.24E-01
Mohican	3.37E+01	2.01E+02
Early_Jur_SR	1.31E-04	2.00E-02
Eurydice	9.40E+00	7.69E+01
Sum Outflow Side	**6.62E+01**	**1.82E+03**
Sum HC Losses	**210.641**	**6583.17**

Table 9e. Mass Balance of Hydrocarbons

mass in$(10)^9$ kg(Mtons)/m^3

Horizons	Methane_Miss	C2-C5_Miss	C6-C14_Miss	C15+_Miss	Methane_JVC	C2-C5_JVC	C6-C14_JVC	C15+_JVC
Late_Paleocene	0	0	0	0	0	0	0	0
Naskapi	0.00774847	0.0251798	0.122542	1.26379	1.82E-09	2.25E-09	1.37E-09	-8.22E-09
CVC	1.51E-43	-7.35E-44	-1.59E-43	-8.93E-45	3.28E-06	3.39E-06	-2.15E-06	-8.54E-06
JVC	0	0	0	0	222.953	78.2811	1262.6	1076.29
late_Jur	0	0	0	0	0.046754	0.0380795	-0.01053	-0.13112
Misaine	0	0	0	0	0.10991	0.092899	0.036971	-0.38444
Mohican	0	0	0	0	4.0981	1.7491	1.083	-10.937
Early_Jur_Lac_SR	0	0	0	0	0.010323	0.0013733	-0.00102279	-0.017464
Sum Generated	**0.00774847**	**0.0251798**	**0.122542**	**1.26379**	**227.218**	**80.1625**	**1263.7**	**1064.82**
Late_Paleocene	1.51E-20	3.76E-19	6.47E-18	8.12E-18	1.27E-10	2.23E-10	2.90E-09	4.29E-10
Naskapi	0.0077441	0.025165	0.12237	1.2628	0.157415	0.0662979	0.944916	0.750123
CVC	4.88E-37	4.23E-37	2.34E-37	1.59E-39	0.202907	0.0629121	0.747335	0.395099
JVC	0	0	0	0	11.4881	2.17806	7.58365	1.32457
late_Jur	0	0	0	0	0.254347	0.0586887	0.184383	0.0417982
Misaine	0	0	0	0	0.0317336	0.0102224	0.0215616	0.00385246
Mohican	0	0	0	0	0.000847202	0.000136462	9.57E-05	8.17E-06
Early_Jur_Lac_SR	0	0	0	0	1.87E-09	5.55E-12	1.33E-13	7.40E-22
Sum Accumulated in Source	**0.0077441**	**0.025165**	**0.12237**	**1.2628**	**12.1353**	**2.37632**	**9.48194**	**2.51545**
Late_Paleocene	-1.51E-20	-3.76E-19	-6.47E-18	-8.12E-18	-1.27E-10	-2.23E-10	-2.90E-09	-4.29E-10
Naskapi	4.37E-06	1.48E-05	0.000172001	0.000990011	-0.157415	-0.0662979	-0.944916	-0.750123
CVC	-4.88E-37	-4.23E-37	-2.34E-37	-1.59E-39	-0.202904	-0.0629087	-0.747337	-0.395108
JVC	0	0	0	0	211.465	76.103	1255.02	1074.97
late_Jur	0	0	0	0	-0.207593	-0.0206092	-0.194913	-0.172918
Misaine	0	0	0	0	0.0781764	0.0826766	0.0154094	-0.388292
Mohican	0	0	0	0	4.09725	1.74896	1.0829	-10.937
Early_Jur_Lac_SR	0	0	0	0	0.010323	0.0013733	-0.00102279	-0.017464
Sum Expelled	**4.37E-06**	**1.48E-05**	**0.000172001**	**0.00099001**	**215.083**	**77.7862**	**1254.23**	**1062.3**
MidLate_Miocene_Res	1.58E-07	5.38E-07	6.45E-06	3.74E-05	0.54196	0.16829	2.0573	0.73778
Early_Miocene_Res	1.09E-10	1.19E-10	1.57E-11	6.07E-15	0.062039	0.0037181	0.00028953	6.29E-09
Mid_Paleocene	2.81E-10	9.51E-10	1.15E-08	6.60E-08	0.009185	0.0039905	0.060206	0.028104
Missi_Res	1.79E-13	6.19E-13	8.85E-12	4.70E-11	7.03271	2.23778	23.6981	6.98824
Up_Jur-Res	0	0	0	0	22.32	4.8992	38.144	8.7324
Sum Accumulated in Reservoir	**1.59E-07**	**5.39E-07**	**6.46E-06**	**3.74E-05**	**29.9659**	**7.31298**	**63.9599**	**16.4865**
Migration Losses	**1.25E-06**	**4.25E-06**	**4.72E-05**	**0.00028594**	**2.26915**	**0.68023**	**8.91315**	**4.02807**

Table 9e. Mass Balance of Hydrocarbons

mass in$(10)^9$ kg(Mtons)/m^3

Horizons	Methane_Misaine	C2-C5_Misaine	C6-C14_Misaine	C15+_Misaine	Methane_Paleocene	PK_C2-C5_Paleocene
Late_Paleocene	0	0	0	0	2.51E-05	0.00011321
Naskapi	2.68E-10	3.15E-10	9.45E-11	-1.06E-09	0	0
CVC	2.63E-06	2.89E-06	2.95E-07	-9.44E-06	0	0
JVC	0.1293	0.120673	-0.03102	-0.38152	0	0
late_Jur	1.3763	0.99227	-0.88586	-3.0139	0	0
Misaine	52.3643	18.0092	226.903	185.78	0	0
Mohican	8.9323	3.7448	-4.984	-15.855	0	0
Early_Jur_Lac_SR	0.021983	0.0032143	-0.0136852	-0.026307	0	0
Sum Generated	**62.8242**	**22.8702**	**220.988**	**166.504**	**2.51E-05**	**0.00011321**
Late_Paleocene	2.73E-11	1.12E-10	7.25E-10	1.60E-10	2.17E-05	9.81E-05
Naskapi	0.0498501	0.0229529	0.178882	0.125498	3.68E-19	5.36E-17
CVC	0.0486902	0.0200076	0.16191	0.112866	0	0
JVC	1.51799	0.567123	3.03162	1.65951	0	0
late_Jur	4.08552	1.4886	6.24747	2.87855	0	0
Misaine	5.10213	1.13755	4.26963	1.50415	0	0
Mohican	0.0830657	0.0322002	0.0449093	0.00206684	0	0
Early_Jur_Lac_SR	2.01E-07	1.44E-09	1.30E-10	1.15E-18	0	0
Sum Accumulated in Source	**10.8872**	**3.26843**	**13.9344**	**6.28264**	**2.17E-05**	**9.81E-05**
Late_Paleocene	-2.73E-11	-1.12E-10	-7.25E-10	-1.60E-10	3.40E-06	1.51E-05
Naskapi	-0.0498501	-0.0229529	-0.178882	-0.125498	-3.68E-19	-5.36E-17
CVC	-0.0486876	-0.0200047	-0.16191	-0.112875	0	0
JVC	-1.38869	-0.44645	-3.06264	-2.04103	0	0
late_Jur	-2.70922	-0.49633	-7.13333	-5.89245	0	0
Misaine	47.2622	16.8716	222.633	184.276	0	0
Mohican	8.84923	3.7126	-5.02891	-15.8571	0	0
Early_Jur_Lac_SR	0.0219828	0.0032143	-0.0136852	-0.026307	0	0
Sum Expelled	**51.9369**	**19.6017**	**207.054**	**160.221**	**3.40E-06**	**1.51E-05**
MidLate_Miocene_Res	0.11676	0.04903	0.44166	0.30965	7.78E-07	3.51E-06
Early_Miocene_Res	0.020082	0.0021092	6.60E-05	2.02E-09	9.46E-08	4.26E-07
Mid_Paleocene	0.0030588	0.0019233	0.015722	0.010651	9.31E-09	2.90E-09
Missi_Res	1.75696	0.737571	4.85473	3.00293	0	0
Up_Jur-Res	5.089	2.0569	11.116	6.4666	0	0
Sum Accumulated in Reservoir	**6.98586**	**2.84753**	**16.4282**	**9.78984**	**8.82E-07**	**3.93E-06**
Migration Losses	**3.30846**	**0.936205**	**3.71378**	**1.80811**	**7.64E-10**	**3.73E-09**

Table 9e. Mass Balance of Hydrocarbons

mass in$(10)^9$ kg(Mtons)/m^3

Horizons	PK_C6-C14_Paleocene	PK_C15+_Paleocene	Methane_CVC	C2-C5_CVC	C6-C14_CVC	C15+_CVC
Late_Paleocene	0.00029514	0.00048962	0	0	0	0
Naskapi	0	0	2.29E-09	2.53E-09	-7.98E-10	-7.01E-09
CVC	0	0	132.926	64.5728	825.666	333.293
JVC	0	0	0	0	0	0
late_Jur	0	0	0	0	0	0
Misaine	0	0	0	0	0	0
Mohican	0	0	0	0	0	0
Early_Jur_Lac_SR	0	0	0	0	0	0
Sum Generated	**0.00029514**	**0.00048962**	**132.926**	**64.5728**	**825.666**	**333.293**
Late_Paleocene	0.0002557	0.00042421	5.38E-12	1.75E-11	5.17E-10	2.92E-10
Naskapi	9.16E-19	3.29E-25	0.210399	0.105534	1.49198	0.717569
CVC	0	0	39.4026	18.0954	199.465	69.4621
JVC	0	0	0	0	0	0
late_Jur	0	0	0	0	0	0
Misaine	0	0	0	0	0	0
Mohican	0	0	0	0	0	0
Early_Jur_Lac_SR	0	0	0	0	0	0
Sum Accumulated in Source	**0.0002557**	**0.00042421**	**39.613**	**18.2009**	**200.957**	**70.1797**
Late_Paleocene	3.94E-05	6.54E-05	-5.38E-12	-1.75E-11	-5.17E-10	-2.92E-10
Naskapi	-9.16E-19	-3.29E-25	-0.210399	-0.105534	-1.49198	-0.717569
CVC	0	0	93.5234	46.4774	626.201	263.831
JVC	0	0	0	0	0	0
late_Jur	0	0	0	0	0	0
Misaine	0	0	0	0	0	0
Mohican	0	0	0	0	0	0
Early_Jur_Lac_SR	0	0	0	0	0	0
Sum Expelled	**3.94E-05**	**6.54E-05**	**93.313**	**46.3719**	**624.709**	**263.113**
MidLate_Miocene_Res	9.14E-06	1.52E-05	2.7922	1.3827	17.322	6.2858
Early_Miocene_Res	1.11E-06	1.84E-06	0.017269	0.0023015	0.00028478	1.47E-08
Mid_Paleocene	5.72E-12	3.52E-18	0.0046163	0.0027744	0.040829	0.03045
Missi_Res	0	0	21.5488	10.7297	136.473	37.329
Up_Jur-Res	0	0	0	0	0	0
Sum Accumulated in Reservoir	**1.02E-05**	**1.70E-05**	**24.3629**	**12.1175**	**153.836**	**43.6452**
Migration Losses	**9.85E-09**	**1.63E-08**	**12.4161**	**6.23621**	**81.6468**	**26.9274**

Table 9e. Mass Balance of Hydrocarbons

mass in$(10)^9$ kg(Mtons)/m^3

Horizons	Methane_EJur	PK_C2-C5_EJur	PK_C6-C14_EJur	PK_C15+_EJur	Methane_TJur	C2-C5_TJur	C6-C14_TJur
Late_Paleocene	0	0	0	0	0	0	0
Naskapi	6.52E-10	5.99E-10	3.41E-10	-2.49E-09	0	0	0
CVC	2.21E-06	1.61E-06	5.33E-07	-7.14E-06	0	0	0
JVC	0.078969	0.036725	-0.00968	-0.19323	0	0	0
late_Jur	0.71648	0.12325	-0.34206	-1.17	36.818	11.729	184.27
Misaine	2.7181	0.7436	-1.1641	-4.9652	0	0	0
Mohican	193.44	28.36	-88.971	-305.37	0	0	0
Early_Jur_Lac_SR	213.95	219.281	515.29	823.93	0	0	0
Sum Generated	**410.904**	**248.545**	**424.803**	**512.232**	**36.818**	**11.729**	**184.27**
Late_Paleocene	8.24E-11	2.53E-10	5.58E-10	1.73E-10	1.01E-11	1.94E-11	4.93E-10
Naskapi	0.254375	0.152807	0.230972	0.211044	0.0232545	0.00903379	0.144014
CVC	0.229037	0.12262	0.172033	0.144465	0.0253163	0.00820363	0.118772
JVC	3.42633	1.7003	2.05765	1.1561	1.48461	0.328452	2.94721
late_Jur	5.47347	2.47835	2.77259	1.33066	5.32446	0.838479	6.32615
Misaine	3.94716	1.93627	2.15597	0.879782	0.0745003	0.0131007	0.164292
Mohican	2.16243	0.367893	0.181532	0.00304881	7.84E-05	2.46E-05	0.000953617
Early_Jur_Lac_SR	0.00630405	0.0015102	0.00108003	0.00020215	1.22E-10	7.20E-11	3.66E-09
Sum Accumulated in Source	**15.4991**	**6.75975**	**7.57183**	**3.7253**	**6.93222**	**1.19729**	**9.7014**
Late_Paleocene	-8.24E-11	-2.53E-10	-5.58E-10	-1.73E-10	-1.01E-11	-1.94E-11	-4.93E-10
Naskapi	-0.254375	-0.152807	-0.230972	-0.211044	-0.0232545	-0.00903379	-0.144014
CVC	-0.229035	-0.122618	-0.172032	-0.144472	-0.0253163	-0.00820363	-0.118772
JVC	-3.34736	-1.66358	-2.06733	-1.34933	-1.48461	-0.328452	-2.94721
late_Jur	-4.75699	-2.3551	-3.11465	-2.50066	31.4935	10.8905	177.944
Misaine	-1.22906	-1.19267	-3.32007	-5.84498	-0.0745003	-0.0131007	-0.164292
Mohican	191.278	27.9921	-89.1525	-305.373	-7.84E-05	-2.46E-05	-0.000953617
Early_Jur_Lac_SR	213.944	219.279	515.289	823.93	-1.22E-10	-7.20E-11	-3.66E-09
Sum Expelled	**395.404**	**241.785**	**417.231**	**508.506**	**29.8858**	**10.5317**	**174.569**
MidLate_Miocene_Res	0.53509	0.27375	0.37197	0.2807	0.065549	0.022773	0.33466
Early_Miocene_Res	0.055541	0.0065939	1.79E-05	1.86E-11	0.0084778	0.00044845	4.77E-05
Mid_Paleocene	0.009418	0.010138	0.017148	0.012415	0.0013256	0.00071535	0.012549
Missi_Res	6.17864	2.76848	3.49088	2.11241	0.860499	0.276222	3.78869
Up_Jur-Res	12.251	5.7775	7.0628	4.6508	2.399	0.60183	7.2438
Sum Accumulated in Reservoir	**19.0297**	**8.83647**	**10.9428**	**7.05633**	**3.33485**	**0.901989**	**11.3798**
Migration Losses	**11.5223**	**4.27275**	**4.46397**	**1.9565**	**0.327199**	**0.112188**	**1.73601**

Table 9e. Mass Balance of Hydrocarbons

mass in$(10)^9$ kg(Mtons)/m^3

Horizons	C15+_TJur	Methane_Mohican	C2-C5_Mohican	C6-C14_Mohican	C15+_Mohican	Sum
Late_Paleocene	0	0	0	0	0	0.0009
Naskapi	0	0	0	0	0	1.4193
CVC	0	0	0	0	0	1356.5
JVC	0	0	0	0	0	2639.9
late_Jur	156.82	0	0	0	0	387.38
Misaine	0	0	0	0	0	480.24
Mohican	0	54.175	48.903	33.478	272.01	223.86
Early_Jur_Lac_SR	0	0	0	0	0	1772.4
Sum Generated	**156.82**	**54.175**	**48.903**	**33.478**	**272.01**	**6862**
Late_Paleocene	1.51E-10	1.71E-11	1.34E-10	1.44E-10	3.24E-10	0.0008
Naskapi	0.122895	0.032785	0.0357263	0.0272885	0.229682	7.7134
CVC	0.0928665	0.0348427	0.0332417	0.0232689	0.192231	329.37
JVC	1.78429	0.757153	0.664763	0.432591	3.64017	49.73
late_Jur	3.75127	1.07747	0.916046	0.607079	5.38741	51.523
Misaine	0.169076	0.855531	0.718683	0.466296	4.17972	27.641
Mohican	0.00355422	2.53672	1.62435	0.747935	5.76955	13.561
Early_Jur_Lac_SR	1.07E-08	0.00103196	0.000667053	0.000321959	0.00242108	0.0135
Sum Accumulated in Source	**5.92395**	**5.29553**	**3.99348**	**2.30478**	**19.4012**	**479.6**
Late_Paleocene	-1.51E-10	-1.71E-11	-1.34E-10	-1.44E-10	-3.24E-10	0.0001
Naskapi	-0.122895	-0.032785	-0.0357263	-0.0272885	-0.229682	-6.2941
CVC	-0.0928665	-0.0348427	-0.0332417	-0.0232689	-0.192231	1027.1
JVC	-1.78429	-0.757153	-0.664763	-0.432591	-3.64017	2590.2
late_Jur	153.069	-1.07747	-0.916046	-0.607079	-5.38741	335.85
Misaine	-0.169076	-0.855531	-0.718683	-0.466296	-4.17972	452.6
Mohican	-0.00355422	51.6383	47.2786	32.7301	266.24	210.3
Early_Jur_Lac_SR	-1.07E-08	-0.00103196	-0.000667053	-0.000321959	-0.00242108	1772.4
Sum Expelled	**150.896**	**48.8795**	**44.9095**	**31.1732**	**252.609**	**6382**
MidLate_Miocene_Res	0.25276	0.08505	0.083839	0.058159	0.47612	35.046
Early_Miocene_Res	2.81E-09	0.010011	0.0021767	1.35E-05	8.66E-09	0.1915
Mid_Paleocene	0.0097393	0.0016128	0.0030286	0.0025389	0.021622	0.3138
Missi_Res	2.88892	1.02161	0.963857	0.692548	5.87483	287.31
Up_Jur-Res	5.0573	3.2421	2.6715	1.7295	14.124	165.64
Sum Accumulated in Reservoir	**8.20872**	**4.36038**	**3.7244**	**2.48276**	**20.4966**	**488.5**
Migration Losses	**1.45106**	**5.23582**	**3.14699**	**1.62965**	**13.8502**	**202.6**

Table 9e. Mass Balance of Hydrocarbons

mass in$(10)^9$ kg(Mtons)/m^3

Horizons	Methane_Miss	C2-C5_Miss	C6-C14_Miss	C15+_Miss	Methane_JVC	C2-C5_JVC	C6-C14_JVC	C15+_JVC
Sec. Cracking Losses	**-1.04E-08**	**1.09E-09**	**8.90E-06**	**1.89E-06**	**-0.830061**	**-0.787008**	**2.56692**	**5.68553**
Quaternary-Pliocene	1.70E-07	5.80E-07	7.29E-06	4.12E-05	6.3244	2.1343	25.601	8.4895
Late_Eocene	0	0	0	0	0	0	0	0
Mid_Eocene	0	0	0	0	0	0	0	0
EarlyMid_Eocene	8.41E-31	8.01E-31	2.94E-32	8.40E-37	8.38E-21	8.06E-22	1.69E-23	3.28E-29
Late_Paleocene	0	0	0	0	1.30E-39	1.04E-40	5.42E-41	0
Mid_Paleocene	2.66E-10	3.99E-10	3.79E-09	1.85E-08	1.1362	0.4455	4.751	1.5723
Wyandot-DawsonCanyon	7.84E-10	2.69E-09	3.94E-08	2.07E-07	10.086	6.0139	99.816	47.842
LoganCanyon_1	1.43E-10	1.94E-10	2.32E-09	1.08E-08	69.694	30.213	590.25	591.17
Logan_Canyon_2	0	0	0	0	0.81575	0.080956	0.092725	0.0018116
CVC	0	0	0	0	0	0	0	0
Up_Jur-Res	0	0	0	0	6.58E-09	1.04E-09	1.88E-07	0.0047905
JVC	0	0	0	0	2.75E-10	1.93E-11	2.67E-09	0.00010136
late_Jur	0	0	0	0	0	0	0	0
Misaine	0	0	0	0	0	0	0	0
Scatarie	0	0	0	0	0	0	0	0
Mohican	0	0	0	0	0	0	0	0
Early_Jur_Lac_SR	0	0	0	0	0	0	0	0
Sum Outflow Top	**1.71E-07**	**5.84E-07**	**7.33E-06**	**4.14E-05**	**88.056**	**38.888**	**720.51**	**649.09**
Mid_Eocene	3.55E-09	4.27E-09	3.30E-10	2.03E-13	2.3969	0.15355	0.041723	0.0093133
EarlyMid_Eocene	1.83E-35	3.02E-35	3.50E-36	1.12E-39	9.70E-26	4.80E-27	2.19E-28	4.11E-33
Late_Paleocene	4.76E-44	3.08E-44	0	0	6.21E-34	5.63E-35	1.29E-36	8.41E-45
Mid_Paleocene	3.11E-07	1.07E-06	1.40E-05	7.78E-05	28.215	8.5012	91.303	29.041
LoganCanyon_1	2.49E-06	8.35E-06	8.82E-05	0.00054549	18.397	7.6725	117.87	48.553
Missi_Res	0	0	0	0	0	0	0	0
Early_Missi	0	0	0	0	0	0	0	0
CVC	0	0	0	0	0	0	0	0
Up_Jur-Res	0	0	0	0	45.645	15.024	243.76	305.09
JVC	0	0	0	0	0.96819	0.3409	5.2988	4.3168
late_Jur	0	0	0	0	0.00021924	4.29E-05	0.00075418	0.0044686
Misaine	0	0	0	0	3.19E-05	1.38E-06	3.71E-06	1.80E-05
Scatarie	0	0	0	0	0.00018755	9.87E-06	9.03E-06	1.04E-05
Mohican	0	0	0	0	2.54E-05	2.18E-07	1.29E-08	4.32E-09
Early_Jur_Lac_SR	0	0	0	0	1.16E-05	3.20E-06	1.14E-06	1.32E-07

Table 9e. Mass Balance of Hydrocarbons

mass in$(10)^9$ kg(Mtons)/m^3

Horizons	Methane_Misaine	C2-C5_Misaine	C6-C14_Misaine	C15+_Misaine	Methane_Paleocene	PK_C2-C5_Paleocene
Sec. Cracking Losses	**-8.89042**	**-5.27533**	**6.81402**	**18.382**	**2.38E-06**	**1.08E-05**
Quaternary-Pliocene	1.2512	0.48434	4.663	3.3299	8.51E-08	3.86E-07
Late_Eocene	0	0	0	0	5.58E-20	1.61E-20
Mid_Eocene	0	0	0	0	7.26E-20	2.10E-20
EarlyMid_Eocene	1.95E-21	3.13E-22	3.63E-24	1.25E-29	2.01E-09	6.55E-10
Late_Paleocene	4.56E-40	3.48E-41	9.58E-42	0	1.96E-09	8.48E-10
Mid_Paleocene	0.36503	0.17366	0.84259	0.43855	0	0
Wyandot-DawsonCanyon	4.1986	2.3132	21.094	14.742	0	0
LoganCanyon_1	17.928	6.8306	72.794	59.058	0	0
Logan_Canyon_2	0.4697	0.044525	0.025197	0.00041359	0	0
CVC	0	0	0	0	0	0
Up_Jur-Res	2.35E-06	4.73E-07	4.27E-05	0.06221	0	0
JVC	3.84E-07	2.84E-08	2.05E-06	0.0066947	0	0
late_Jur	5.64E-12	5.28E-13	4.46E-12	1.93E-10	0	0
Misaine	2.92E-11	4.18E-13	1.17E-12	5.11E-11	0	0
Scatarie	0	0	0	0	0	0
Mohican	0	0	0	0	0	0
Early_Jur_Lac_SR	0	0	0	0	0	0
Sum Outflow Top	**24.213**	**9.8463**	**99.419**	**77.638**	**8.91E-08**	**3.87E-07**
Mid_Eocene	0.7188	0.12565	0.070118	0.011995	3.32E-08	9.48E-09
EarlyMid_Eocene	8.38E-27	1.69E-27	4.92E-29	1.36E-33	1.35E-21	4.00E-22
Late_Paleocene	6.72E-35	1.50E-35	5.22E-37	4.20E-45	8.35E-22	3.61E-22
Mid_Paleocene	7.2927	3.2119	17.497	9.8583	1.39E-08	4.64E-09
LoganCanyon_1	6.6639	3.0221	28.652	20.672	0	0
Missi_Res	0	0	0	0	0	0
Early_Missi	0	0	0	0	0	0
CVC	0	0	0	0	0	0
Up_Jur-Res	10.181	4.3178	29.184	18.094	0	0
JVC	0.057861	0.023045	0.25018	0.17909	0	0
late_Jur	0.18249	0.070607	0.808	0.58891	0	0
Misaine	0.65929	0.22385	2.4561	1.8108	0	0
Scatarie	0.53826	0.23713	1.7057	1.3524	0	0
Mohican	0.02566	0.014302	0.055115	0.035605	0	0
Early_Jur_Lac_SR	0.00042254	0.00010411	0.00011341	1.24E-06	0	0

Table 9e. Mass Balance of Hydrocarbons

mass in$(10)^9$ kg(Mtons)/m^3

Horizons	PK_C6-C14_Paleocene	PK_C15+_Paleocene	Methane_CVC	C2-C5_CVC	C6-C14_CVC	C15+_CVC
Sec. Cracking Losses	**2.82E-05**	**4.67E-05**	**0.126034**	**0.150486**	**3.01122**	**2.12145**
Quaternary-Pliocene	1.01E-06	1.67E-06	11.743	5.8335	76.268	25.886
Late_Eocene	3.40E-23	1.92E-29	0	0	0	0
Mid_Eocene	4.43E-23	2.50E-29	0	0	0	0
EarlyMid_Eocene	7.89E-13	1.37E-19	9.26E-23	9.68E-24	3.70E-25	5.04E-30
Late_Paleocene	6.82E-13	4.90E-20	8.41E-45	0	0	0
Mid_Paleocene	0	0	0.0073355	0.002533	0.031679	0.10184
Wyandot-DawsonCanyon	0	0	1.6748	0.86262	12.758	13.656
LoganCanyon_1	0	0	1.1723	0.37501	4.7675	5.9743
Logan_Canyon_2	0	0	4.50E-06	2.03E-07	6.59E-08	3.49E-09
CVC	0	0	3.58E-17	6.86E-18	-5.28E-37	-4.30E-35
Up_Jur-Res	0	0	0	0	0	0
JVC	0	0	0	0	0	0
late_Jur	0	0	0	0	0	0
Misaine	0	0	0	0	0	0
Scatarie	0	0	0	0	0	0
Mohican	0	0	0	0	0	0
Early_Jur_Lac_SR	0	0	0	0	0	0
Sum Outflow Top	**1.01E-06**	**1.67E-06**	**14.598**	**7.0737**	**93.825**	**45.619**
Mid_Eocene	1.23E-11	7.07E-19	0.39254	0.053955	0.0041593	3.97E-07
EarlyMid_Eocene	1.13E-24	1.35E-30	3.88E-27	8.37E-28	1.01E-28	6.40E-33
Late_Paleocene	2.96E-25	2.76E-32	1.01E-35	8.71E-37	3.32E-39	0
Mid_Paleocene	1.29E-11	1.52E-17	12.889	6.4639	92.478	50.643
LoganCanyon_1	0	0	21.281	10.714	154.11	76.278
Missi_Res	0	0	4.1467	2.0317	25.955	11.069
Early_Missi	0	0	9.88E-08	4.72E-08	6.52E-07	4.87E-07
CVC	0	0	3.1012	1.5299	19.845	6.808
Up_Jur-Res	0	0	0	0	0	0
JVC	0	0	0	0	0	0
late_Jur	0	0	0	0	0	0
Misaine	0	0	0	0	0	0
Scatarie	0	0	0	0	0	0
Mohican	0	0	0	0	0	0
Early_Jur_Lac_SR	0	0	0	0	0	0

Table 9e. Mass Balance of Hydrocarbons

mass in$(10)^9$ kg(Mtons)/m^3

Horizons	Methane_EJur	PK_C2-C5_EJur	PK_C6-C14_EJur	PK_C15+_EJur	Methane_TJur	C2-C5_TJur	C6-C14_TJur
Sec. Cracking Losses	**-95.6381**	**-1.40421**	**58.1842**	**123.203**	**0.0867498**	**0.0360229**	**0.522188**
Quaternary-Pliocene	6.1905	2.9798	4.0129	2.9373	0.74948	0.26243	3.7615
Late_Eocene	0	0	0	0	0	0	0
Mid_Eocene	0	0	0	0	0	0	0
EarlyMid_Eocene	6.90E-21	1.31E-21	9.43E-25	2.31E-32	7.40E-22	7.16E-23	2.49E-24
Late_Paleocene	9.24E-39	1.27E-39	5.18E-42	0	1.88E-40	1.56E-41	6.30E-42
Mid_Paleocene	1.3773	0.61463	0.69985	0.23172	0.12715	0.046282	0.65041
Wyandot-DawsonCanyon	21.431	14.762	22.517	16.588	2.2011	1.0916	18.458
LoganCanyon_1	174.23	91.279	134.3	138.35	9.9211	3.6979	68.206
Logan_Canyon_2	11.528	2.1476	0.050329	0.00032406	0.14999	0.015976	0.013016
CVC	0	0	0	0	0	0	0
Up_Jur-Res	0.60829	0.86596	2.4126	3.8935	4.69E-08	8.99E-09	1.30E-06
JVC	0.86529	0.40641	0.37436	0.5067	8.68E-09	6.84E-10	5.69E-08
late_Jur	1.1211	0.36755	0.12506	0.00070928	7.01E-19	5.54E-20	0
Misaine	1.0052	0.91956	1.9833	3.3529	0	0	0
Scatarie	2.0308	3.3231	9.4142	16.849	0	0	0
Mohican	0.74527	0.80364	1.8599	3.3453	0	0	0
Early_Jur_Lac_SR	3.78E-05	1.46E-05	5.83E-08	2.86E-13	0	0	0
Sum Outflow Top	**221.14**	**118.47**	**177.75**	**186.06**	**13.149**	**5.1142**	**91.089**
Mid_Eocene	1.9574	0.34418	0.056745	0.0052926	0.29976	0.018609	0.021627
EarlyMid_Eocene	2.39E-26	5.01E-27	1.23E-29	3.58E-36	3.50E-27	3.41E-28	3.37E-29
Late_Paleocene	1.51E-34	2.98E-35	7.49E-38	0	3.00E-35	2.95E-36	3.13E-37
Mid_Paleocene	25.761	11.066	13.326	6.4502	3.2631	0.99099	13.794
LoganCanyon_1	42.603	23.46	33.441	24.965	3.5046	1.4065	22.58
Missi_Res	0	0	0	0	0	0	0
Early_Missi	0	0	0	0	0	0	0
CVC	0	0	0	0	0	0	0
Up_Jur-Res	43.118	16.507	13.794	6.9825	5.4026	1.7813	30.728
JVC	0.2018	0.12769	0.1536	0.092001	0.13755	0.045393	0.70107
late_Jur	0.66515	0.41454	0.48734	0.27776	0.36194	0.11989	1.9034
Misaine	1.6262	1.0187	1.2119	0.62526	0.016018	0.0038872	0.098333
Scatarie	12.398	12.097	24.937	34.723	0.0027797	0.0006487	0.015085
Mohican	4.9782	4.3556	8.8579	11.991	1.33E-05	6.01E-06	0.00020828
Early_Jur_Lac_SR	88.054	35.903	66.149	103.81	1.35E-07	1.33E-07	1.19E-05

Table 9e. Mass Balance of Hydrocarbons

mass in$(10)^9$ kg(Mtons)/m^3

Horizons	C15+_TJur	Methane_Mohican	C2-C5_Mohican	C6-C14_Mohican	C15+_Mohican	Sum
Sec. Cracking Losses	**0.402212**	**0.252305**	**0.214105**	**0.147786**	**1.25118**	**110.3**
Quaternary-Pliocene	2.7926	0.89884	0.82907	0.56325	4.6317	202.62
Late_Eocene	0	0	0	0	0	######
Mid_Eocene	0	0	0	0	0	######
EarlyMid_Eocene	1.22E-29	1.29E-21	4.14E-22	7.96E-25	5.32E-29	######
Late_Paleocene	0	6.37E-40	1.19E-40	1.44E-42	0	######
Mid_Paleocene	0.51942	0.25583	0.235	0.17321	1.5013	16.3
Wyandot-DawsonCanyon	14.406	2.9848	3.9463	3.1754	26.923	383.54
LoganCanyon_1	64.626	15.347	15.103	10.889	84.113	2260.3
Logan_Canyon_2	0.00029552	0.75542	0.17607	0.0040314	0.00040878	16.373
CVC	0	0	0	0	0	######
Up_Jur-Res	0.011437	0.0016253	0.0043312	0.0087303	0.13156	8.0051
JVC	0.0008714	0.0030426	0.0021022	0.00082509	0.0055337	2.1719
late_Jur	0	2.45E-05	1.49E-05	2.80E-06	3.55E-07	1.6145
Misaine	0	6.33E-05	6.17E-05	0.00023972	0.0021377	7.2635
Scatarie	0	0.00021578	0.00048698	0.0022263	0.023182	31.643
Mohican	0	3.90E-05	6.47E-05	0.00037065	0.0025584	6.7571
Early_Jur_Lac_SR	0	0	0	0	0	######
Sum Outflow Top	**82.357**	**20.247**	**20.297**	**14.818**	**117.33**	**2937**
Mid_Eocene	0.017074	0.37203	0.13065	0.023197	0.19852	7.4238
EarlyMid_Eocene	1.62E-33	4.80E-27	1.89E-27	9.46E-30	4.85E-33	######
Late_Paleocene	7.01E-45	2.76E-35	1.14E-35	7.16E-38	1.54E-44	######
Mid_Paleocene	10.8	4.2685	3.9596	2.9226	25.595	479.59
LoganCanyon_1	17.134	5.8717	6.2383	4.5471	36.856	736.49
Missi_Res	0	0	0	0	0	43.202
Early_Missi	0	0	0	0	0	######
CVC	0	0	0	0	0	31.284
Up_Jur-Res	28.175	5.8223	5.1727	3.1499	24.537	856.47
JVC	0.58263	0.018073	0.020869	0.015182	0.11066	13.641
late_Jur	1.591	0.062139	0.067864	0.047025	0.33519	7.9887
Misaine	0.15238	0.17773	0.18188	0.12268	0.90849	11.294
Scatarie	0.024605	1.1875	0.89624	0.65125	6.0245	96.791
Mohican	0.00043162	0.75361	0.57026	0.42126	3.7865	35.846
Early_Jur_Lac_SR	4.53E-05	0.20933	0.22981	0.15013	1.0321	295.54

Table 9e. Mass Balance of Hydrocarbons

mass in$(10)^9$ kg(Mtons)/m^3

Horizons	Methane_Miss	C2-C5_Miss	C6-C14_Miss	C15+_Miss	Methane_JVC	C2-C5_JVC	C6-C14_JVC	C15+_JVC
Eurydice	0	0	0	0	1.42E-06	6.22E-07	1.49E-07	-1.22E-22
Sum Outflow Side	**2.80E-06**	**9.43E-06**	**0.00010211**	**0.00062332**	**95.622**	**31.692**	**458.28**	**387.01**
Sum HC Losses	**4.21E-06**	**1.43E-05**	**0.000165539**	**0.00095258**	**185.117**	**70.4732**	**1190.27**	**1045.81**

Table 9e. Mass Balance of Hydrocarbons

mass in$(10)^9$ kg(Mtons)/m^3

Horizons	Methane_Misaine	C2-C5_Misaine	C6-C14_Misaine	C15+_Misaine	Methane_Paleocene	PK_C2-C5_Paleocene
Eurydice	3.31E-05	8.11E-06	4.52E-06	1.68E-15	0	0
Sum Outflow Side	**26.32**	**11.247**	**80.679**	**52.603**	**4.71E-08**	**1.41E-08**
Sum HC Losses	**44.951**	**16.7542**	**190.626**	**150.431**	**2.51E-06**	**1.12E-05**

Table 9e. Mass Balance of Hydrocarbons

mass in$(10)^9$ kg(Mtons)/m^3

Horizons	PK_C6-C14_Paleocene	PK_C15+_Paleocene	Methane_CVC	C2-C5_CVC	C6-C14_CVC	C15+_CVC
Eurydice	0	0	0	0	0	0
Sum Outflow Side	**2.53E-11**	**1.59E-17**	**41.81**	**20.794**	**292.39**	**144.8**
Sum HC Losses	**2.92E-05**	**4.84E-05**	**68.9501**	**34.2544**	**470.873**	**219.468**

Table 9e. Mass Balance of Hydrocarbons

mass in$(10)^9$ kg(Mtons)/m^3

Horizons	Methane_EJur	PK_C2-C5_EJur	PK_C6-C14_EJur	PK_C15+_EJur	Methane_TJur	C2-C5_TJur	C6-C14_TJur
Eurydice	17.984	6.3165	3.4781	0.31212	1.05E-09	6.67E-10	9.00E-08
Sum Outflow Side	**239.35**	**111.61**	**165.89**	**190.23**	**12.988**	**4.3673**	**69.842**
Sum HC Losses	**376.374**	**232.949**	**406.288**	**501.45**	**26.5509**	**9.62971**	**163.189**

Table 9e. Mass Balance of Hydrocarbons

mass in$(10)^9$ kg(Mtons)/m^3

Horizons	C15+_TJur	Methane_Mohican	C2-C5_Mohican	C6-C14_Mohican	C15+_Mohican	Sum
Eurydice	8.30E-06	0.040647	0.058495	0.044349	0.29677	28.531
Sum Outflow Side	**58.477**	**18.784**	**17.527**	**12.095**	**99.681**	**2644**
Sum HC Losses	**142.687**	**44.5191**	**41.1851**	**28.6904**	**232.112**	**5894**

Figures

(General Figures)

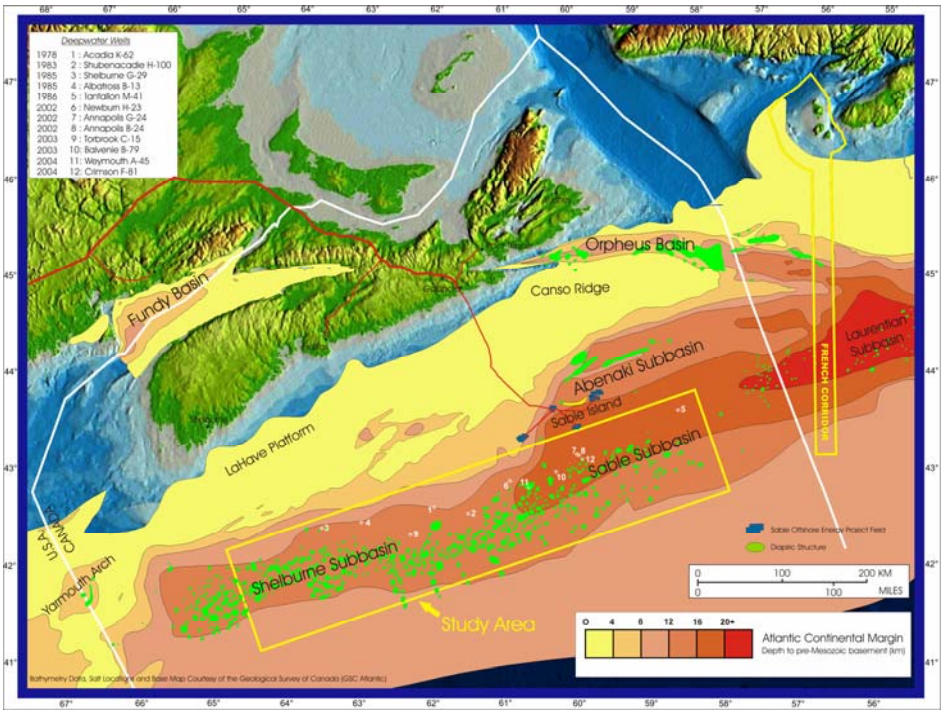

Figure 1a. Structural Elements of the Scotian Basin showing location of the study area (modified after Wade and MacLean, 1990)

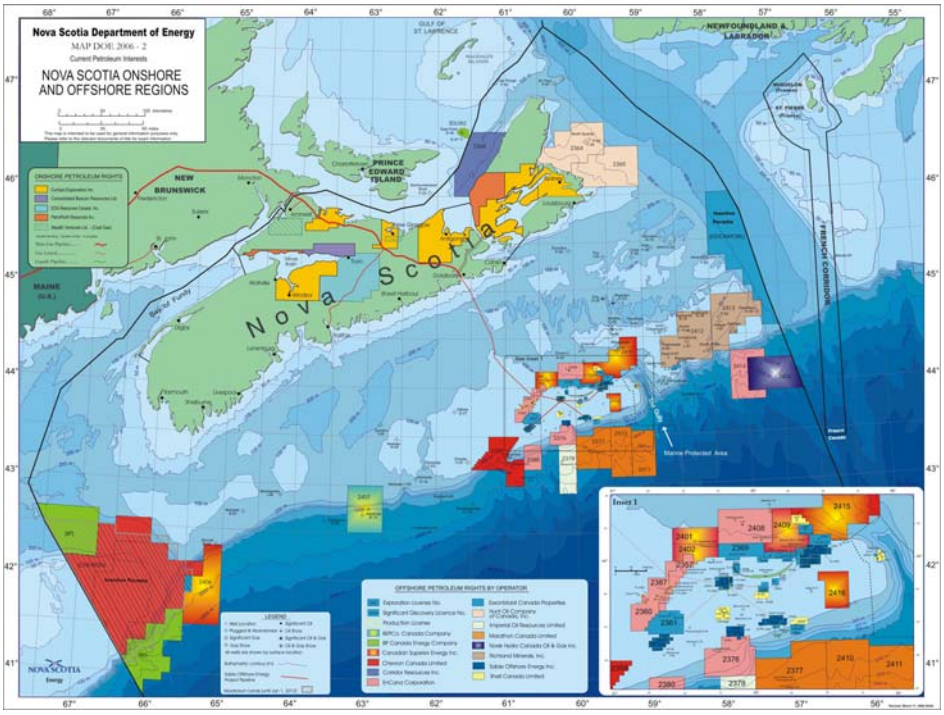

Figure 1b. Bathymetric map of Nova Scotia offshore and onshore showing the current exploration licences, various wells, significant oil and gas discoveries, and gas pipe line.

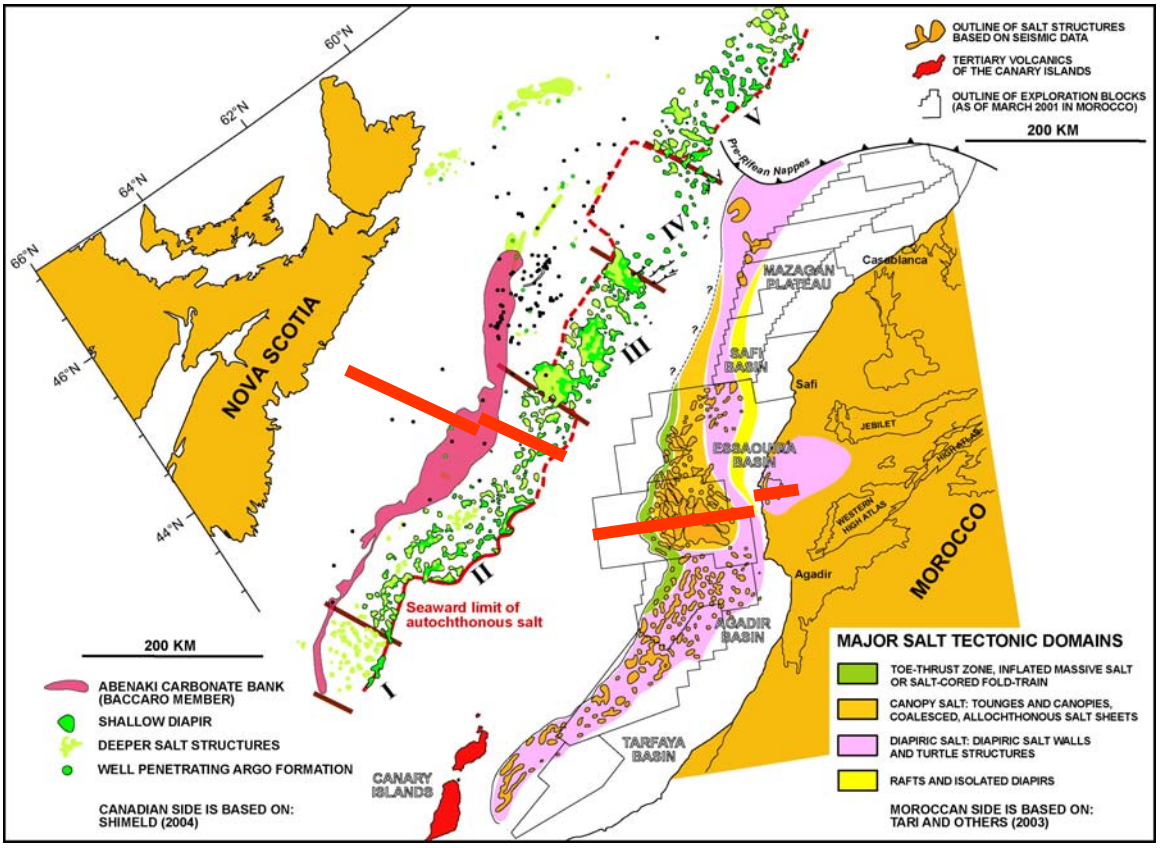

Figure 1c. Comparison of Triassic-Recent sediments from Offshore Nova Scotia and Morocco (after Tari, 2006)

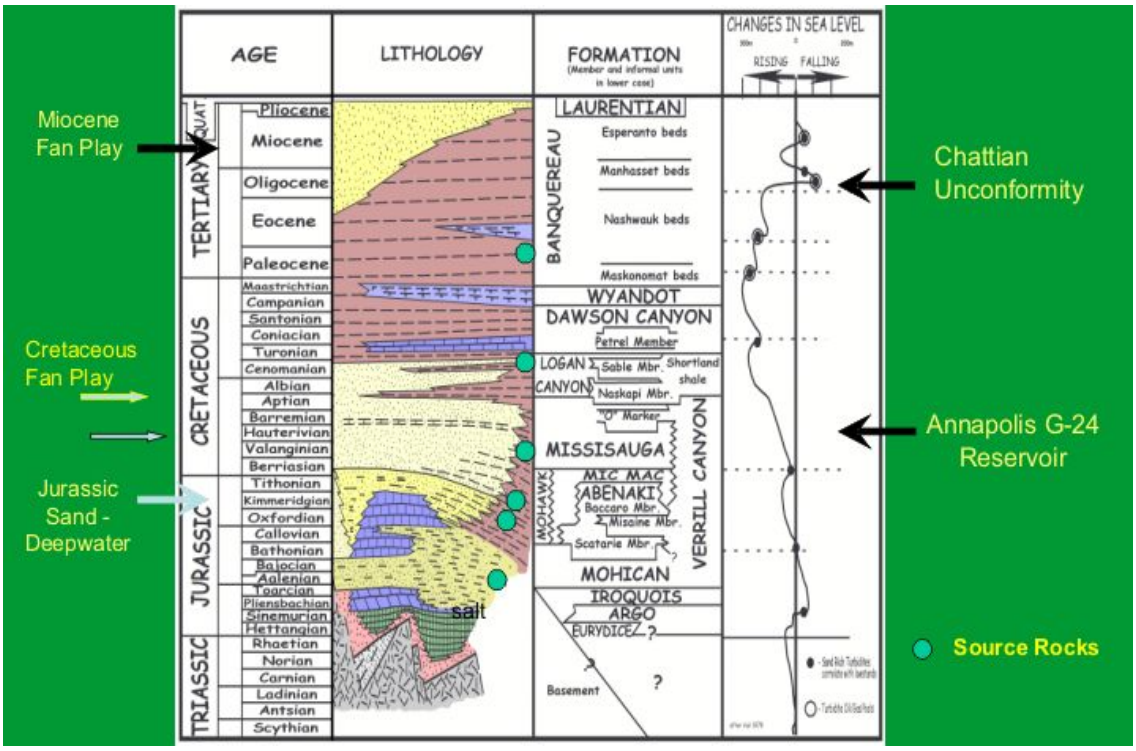

Figure 2a. Generalized stratigraphy from eastern Scotian Basin (modified after Wade et al. 1995; courtesy and permission from Jeff Faber and Tom Bowman, 2005)

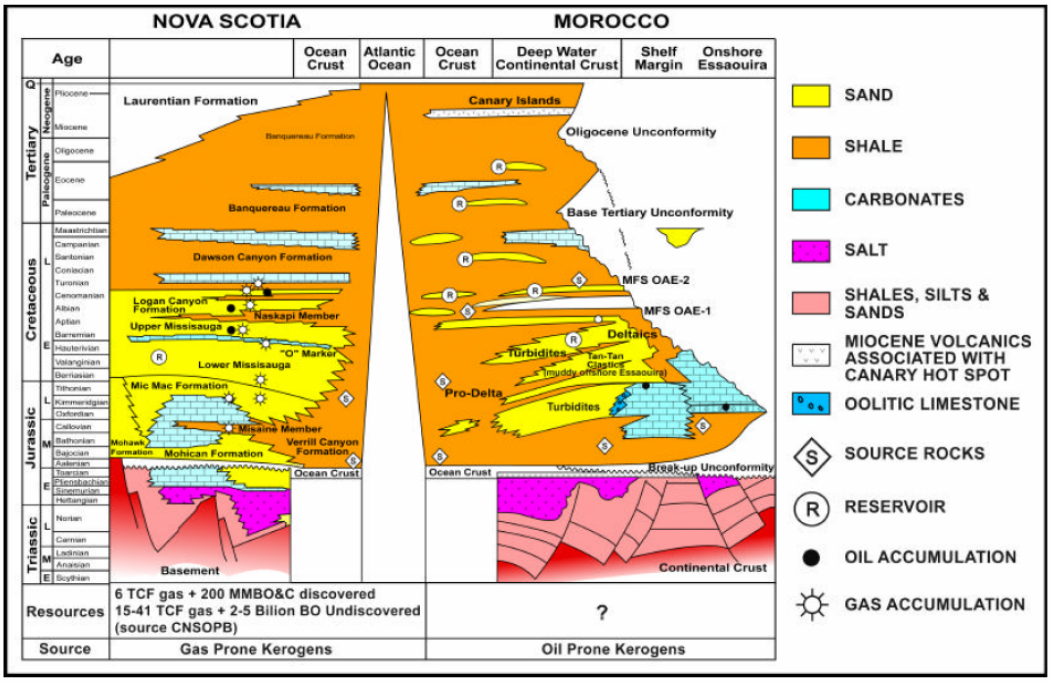

Figure 2b. Comparative stratigraphic chart for the Nova Scotia and Moroccan offshore successions (from Gabor Tari, 2005 as cited in CNSOPB, 2005)

Figures (Source Rock Analysis – Chapter 2)

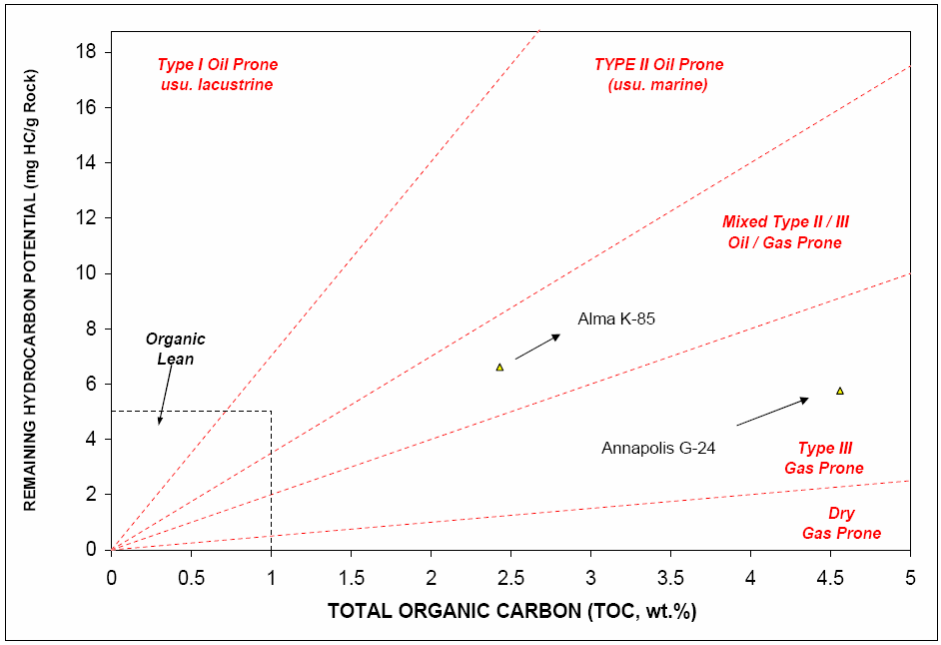

Figure 3a (i): A plot of S2 and total organic carbon showing the source rock potential of two samples selected for kinetics analysis. The sample selected from the Annapolis G-24 well for kinetics analysis was later replaced by a similar sample from the Weymouth A-45 well

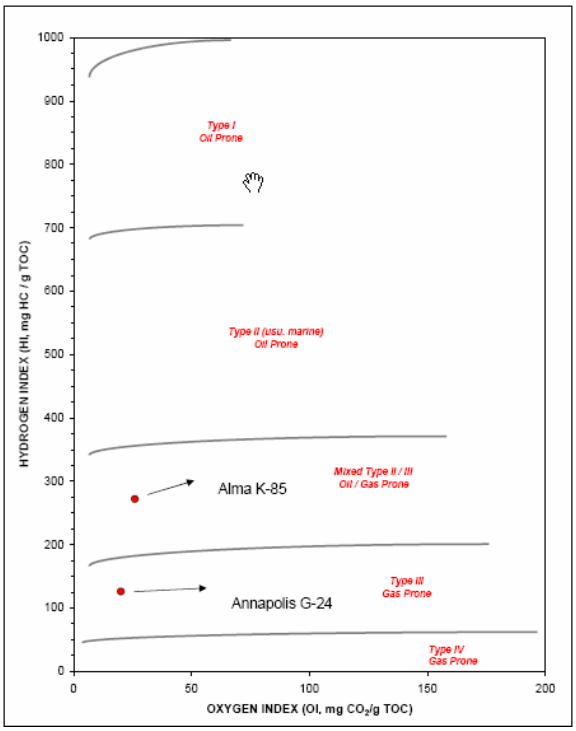

Figure 3a (ii): A plot of hydrogen index and oxygen index (pseudo-van Krevelen diagram) showing the source rock potential of two samples selected for kinetics analysis

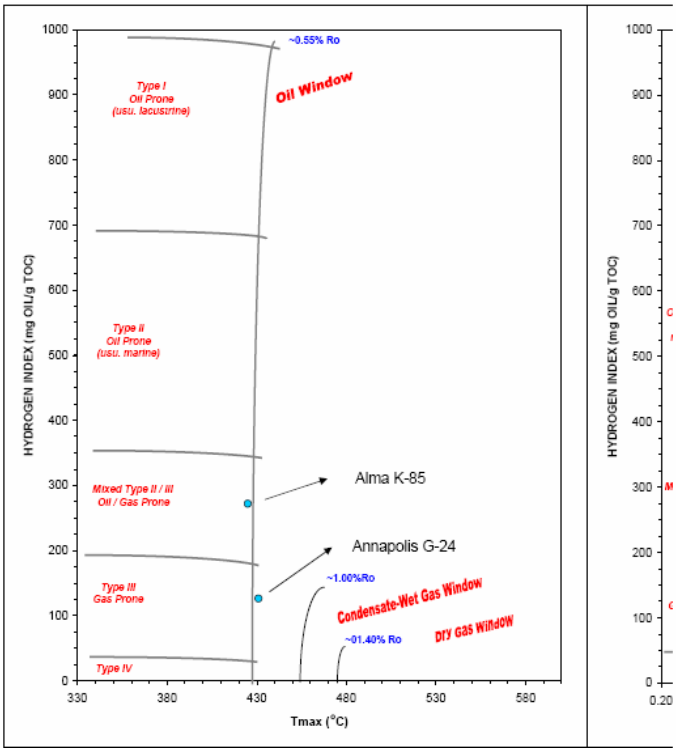

Figure 3a (iii): A plot of hydrogen index and Tmax(^{o}C) showing the source rock potential of two samples selected for kinetics analysis

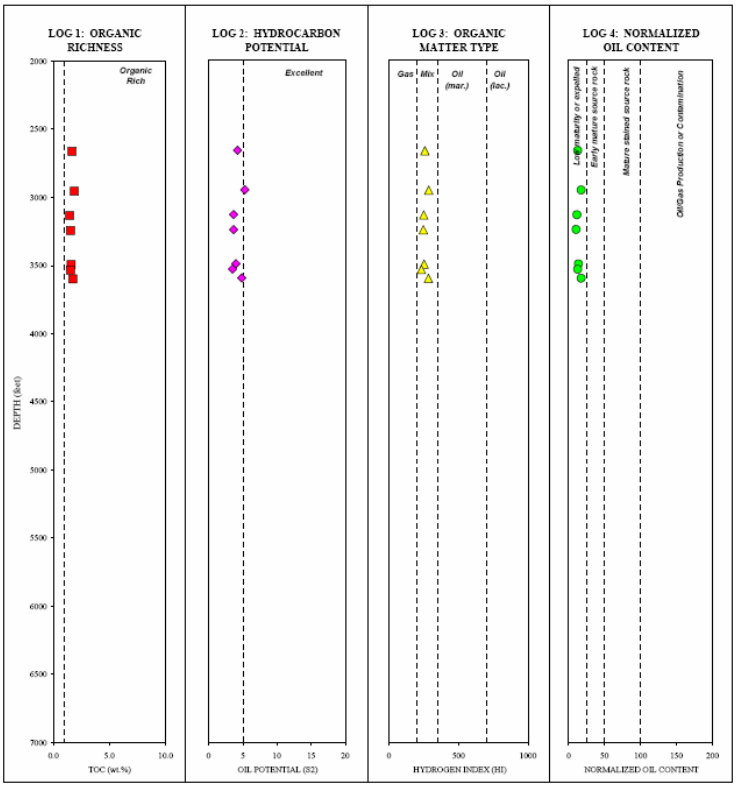

Figure 3b(i): Geochemical log of selected Tertiary samples from the Torbrook C-15 well

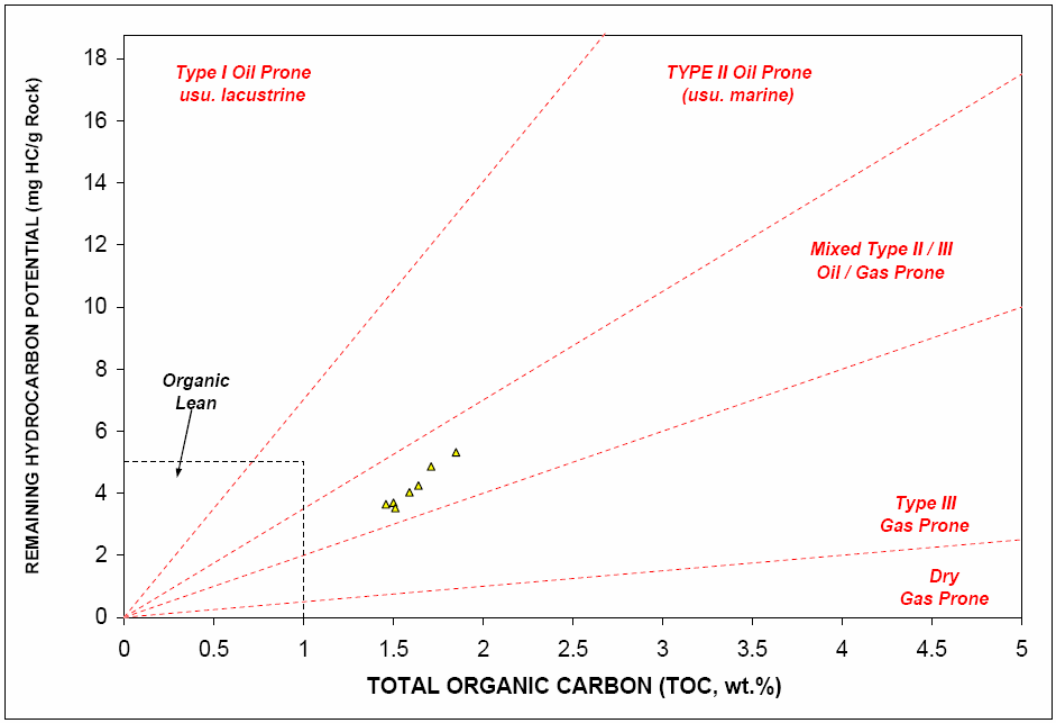

Figure 3b (ii): A plot of S2 and total organic carbon showing the source rock potential of Tertiary samples from the Torbrook C-15 well

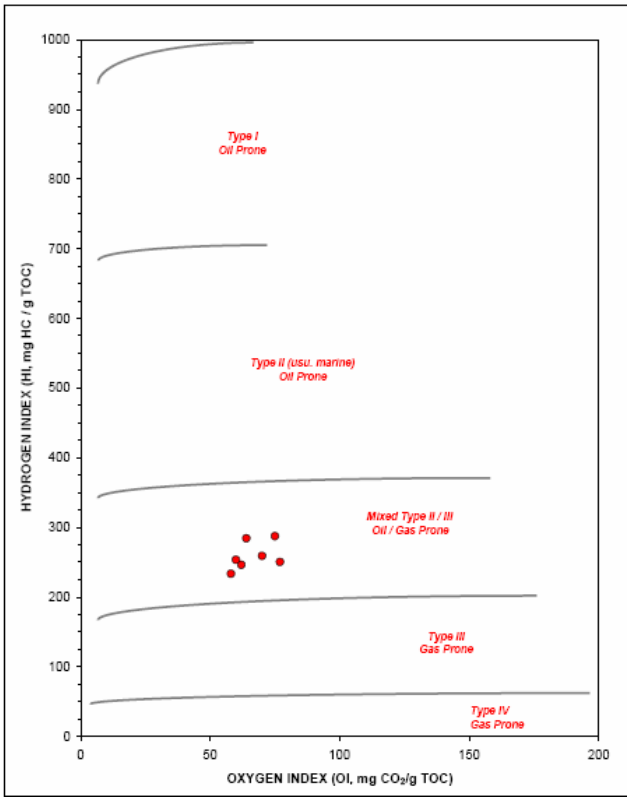

Figure 3b(iii): A plot of hydrogen index and oxygen index (pseudo-van Krevelen Diagram) showing the source rock potential of Tertiary samples from the Torbrook C-15 well

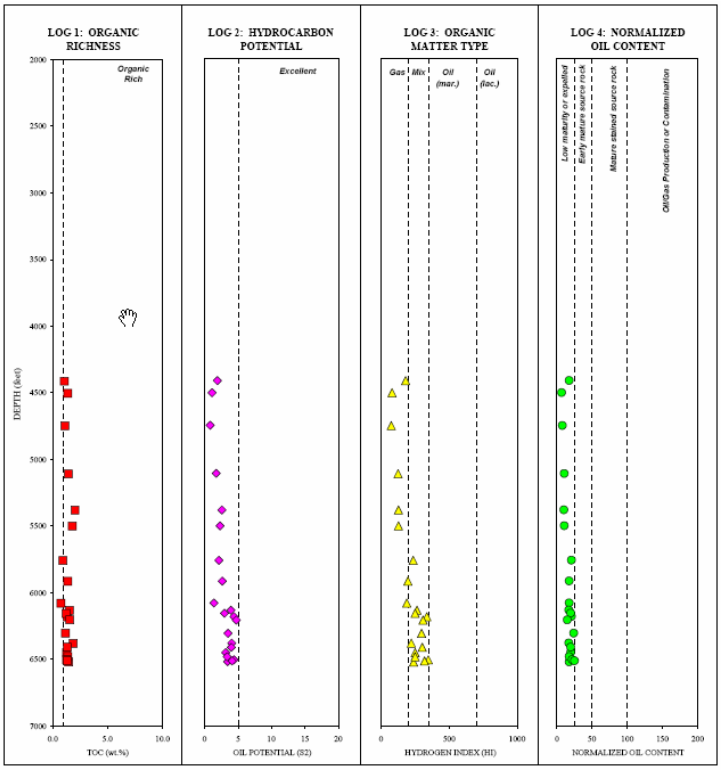

Figure 3c(i): Geochemical log of selected Cretaceous samples from the Weymouth A-45 well

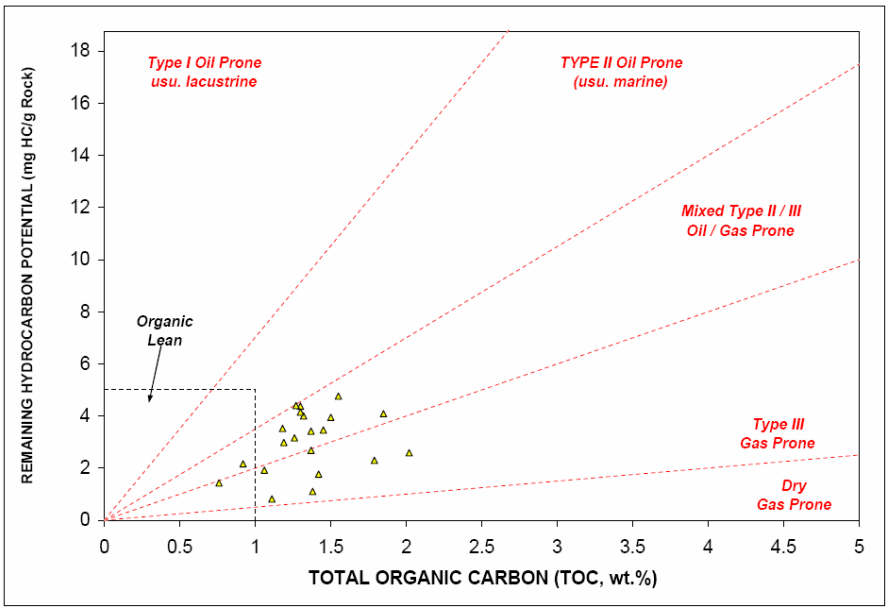

Figure 3c (ii): A plot of S2 and total organic carbon showing the source rock potential of Cretaceous sediments from the Weymouth A-45 well

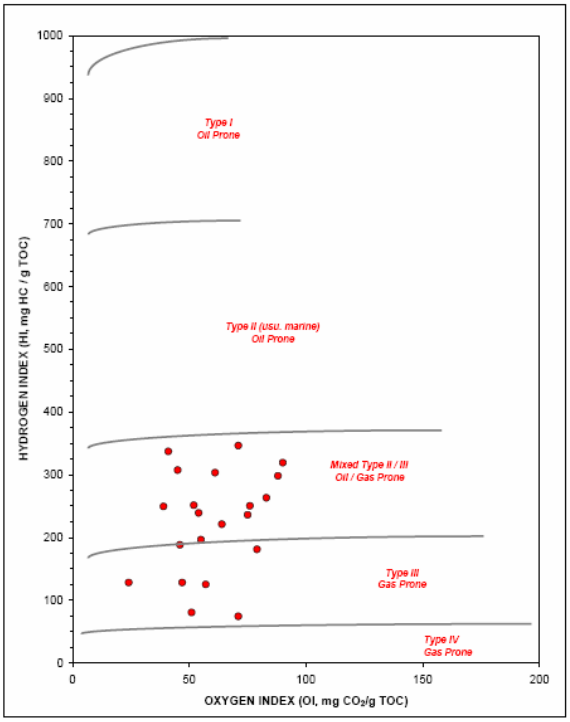

Figure 3c (iii): A plot of hydrogen index and oxygen index (pseudo-van Krevelen Diagram) showing the source rock potential of Cretaceous sediments from the Weymouth A-45 well

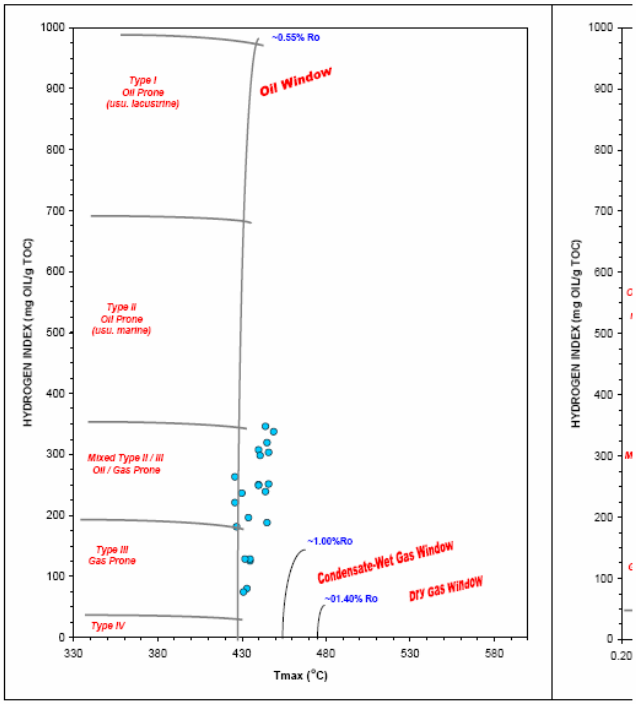

Figure 3c (iv): A plot of hydrogen index and Tmax(°C) showing the source rock potential of Cretaceous sediments from the Weymouth A-45 well

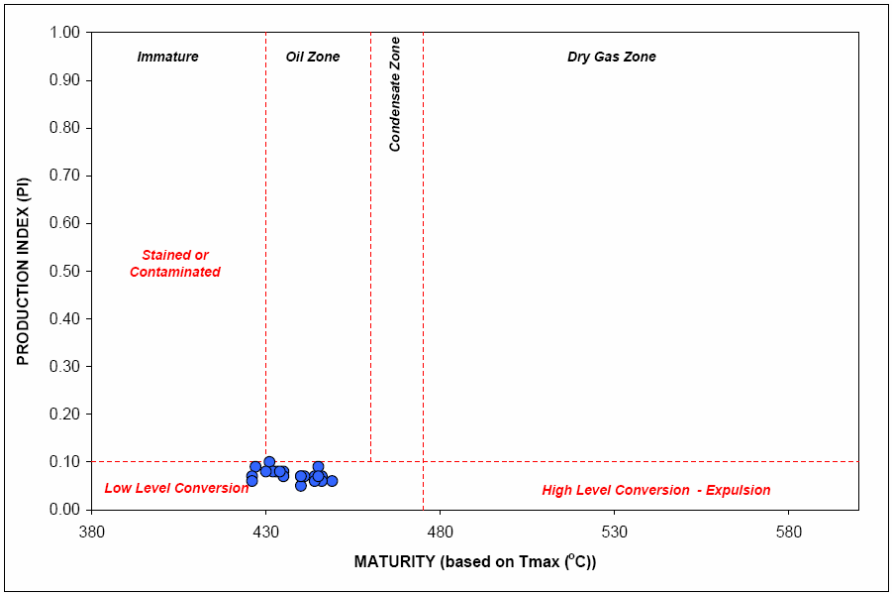

Figure 3c(v): A plot of production index ($S_1/S_1 + S_2$) and Tmax(^oC) showing the hydrocarbon transformation of Cretaceous source rocks from the Weymouth A-45 well

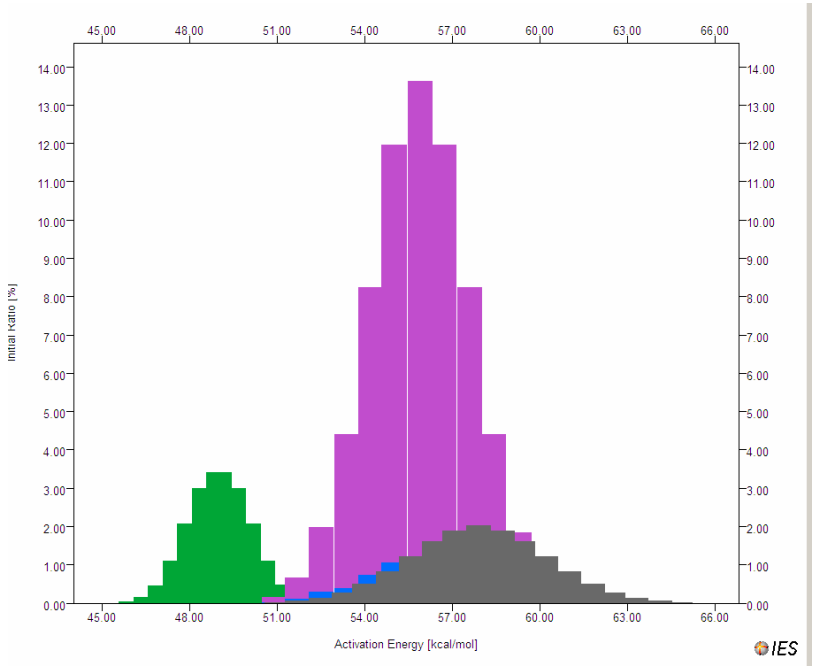

Figure 4a (i). Compositional (C1, C2-C5, C6-C14, and C15+) kinetic distribution of Cretaceous Verrill Canyon source rock from Weymouth A-45 well; light green is C15+, dark grayish green is C1.

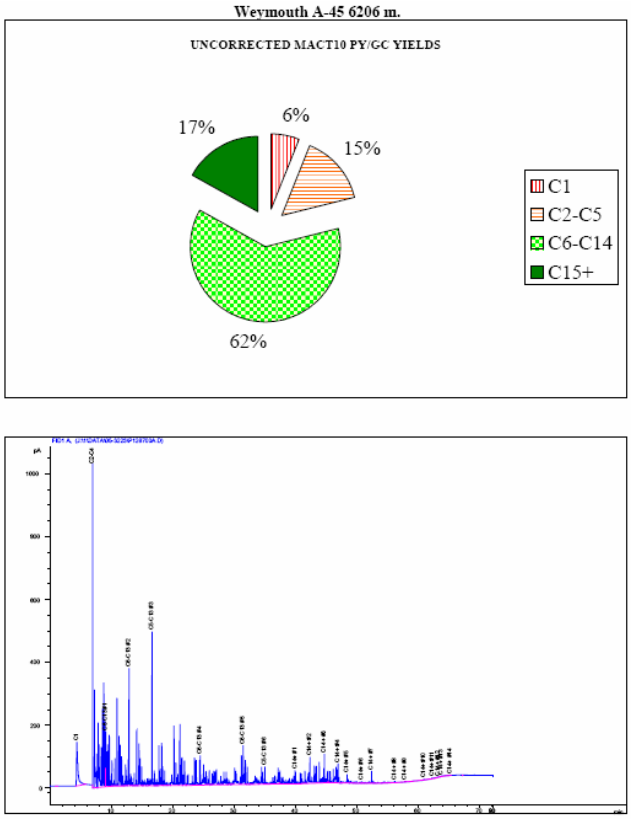

Figure 4a (ii): Pyrolysis gas chromatography of Cretaceous Verrill Canyon sediment (depth: 6206 m; lower graph) from the Weymouth A-45 well and the percentage of various hydrocarbon fractions as released during pyrolysis at various temperatures

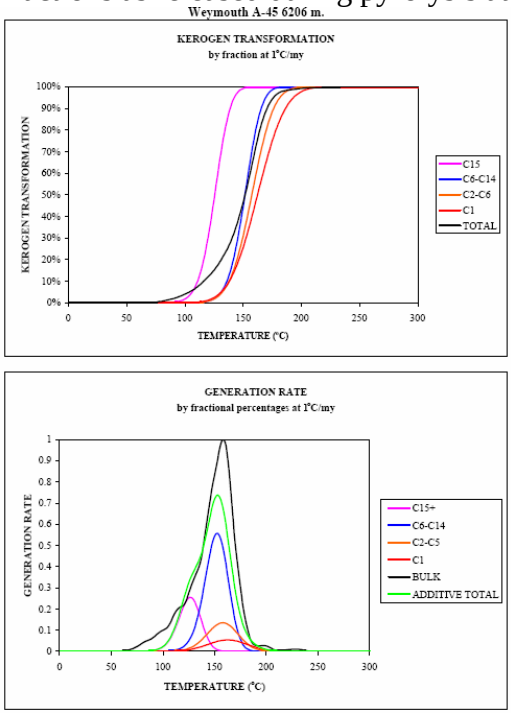

Figure 4a (iii). Temperature and timing of expulsion of each hydrocarbon fraction from the Cretaceous Verrill Canyon source rock (6206 m) from the Weymouth A-45 well

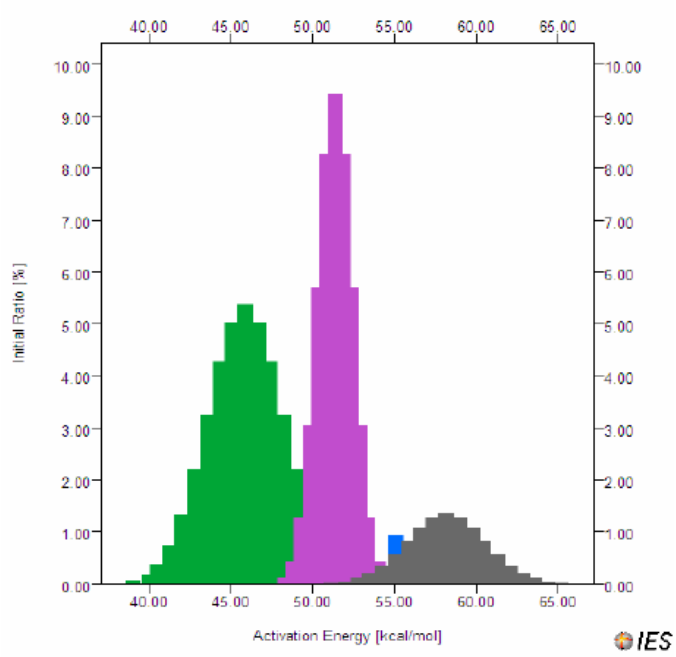

Figure 4b (i). Compositional (C1, C2-C5, C6-C14, and C15+) kinetic distribution of Jurassic Verrill Canyon source rock (depth: 3520 m) from Alma K-85 well; light green is C15+, dark grayish green is C1.

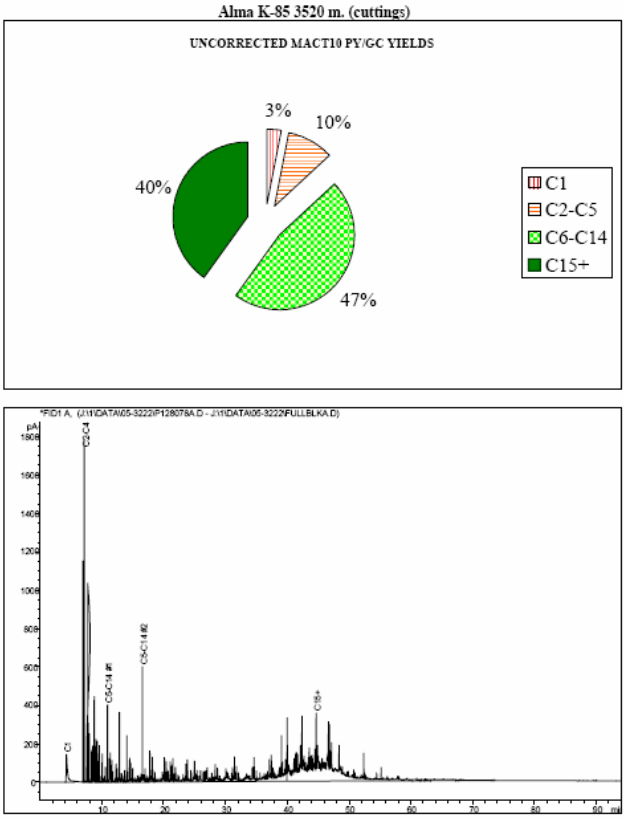

Figure 4b (ii): Pyrolysis gas chromatography of Jurassic Verrill Canyon sediment (depth: 3520 m) from the Alma K-85 well and the percentage of various hydrocarbon fractions as released during pyrolysis at various temperatures

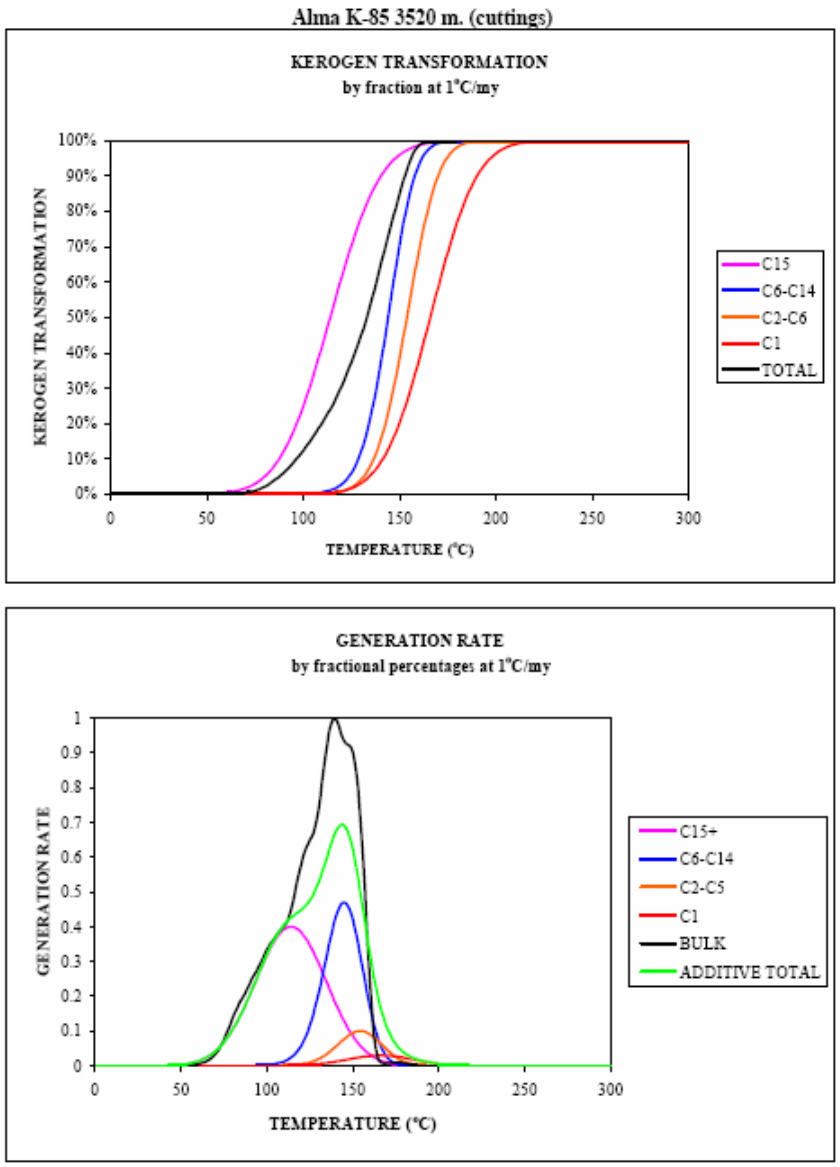

Figure 4b (iii): Temperature and timing of expulsion of each hydrocarbon fraction from the Jurassic Verrill Canyon source rock (3520 m) from the Alma K-85 well

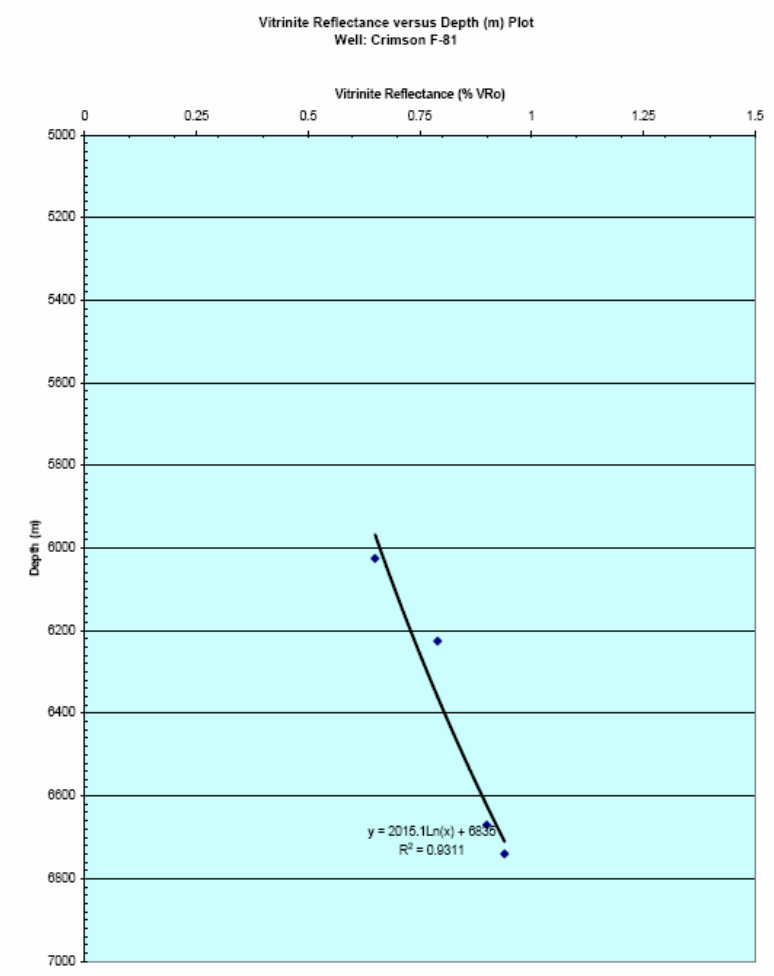

Figure 5a. A plot of vitrinite reflectance versus depth (m) from the Crimson F-81 well with trend analysis and R^2 value

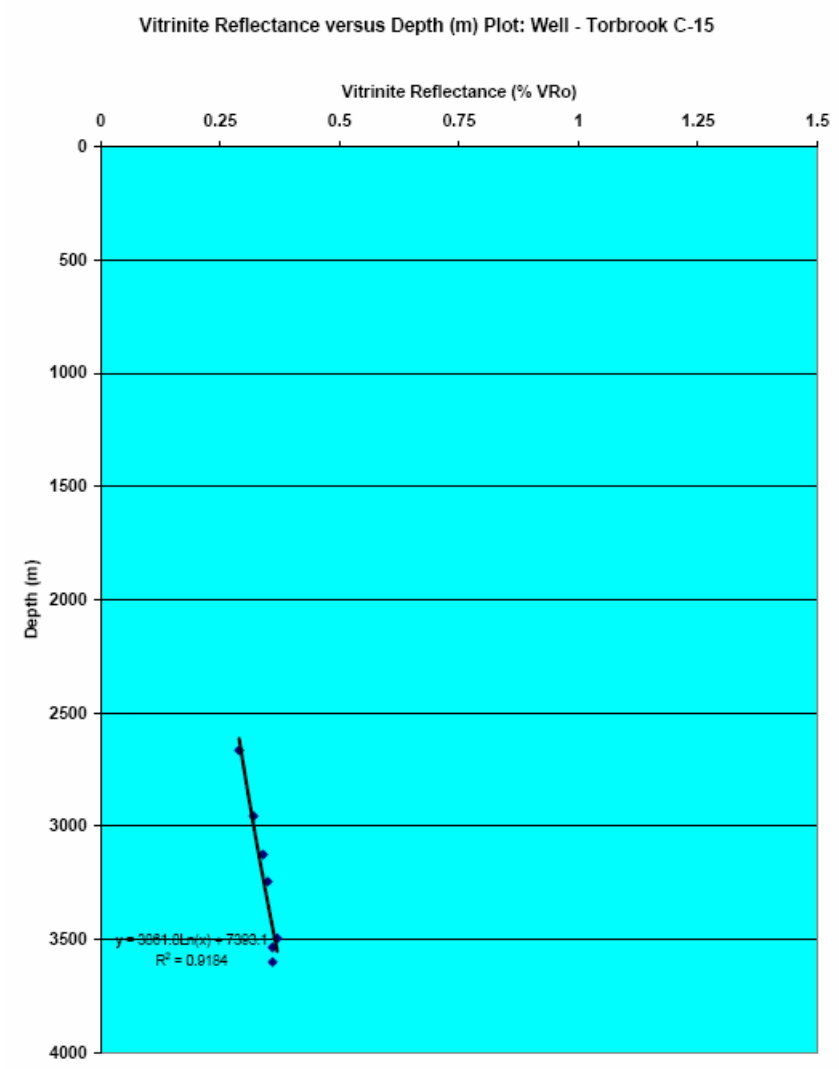

Figure 5b. A plot of vitrinite reflectance versus depth (m) from the Torbrook C-15 well with trend analysis and R^2 value

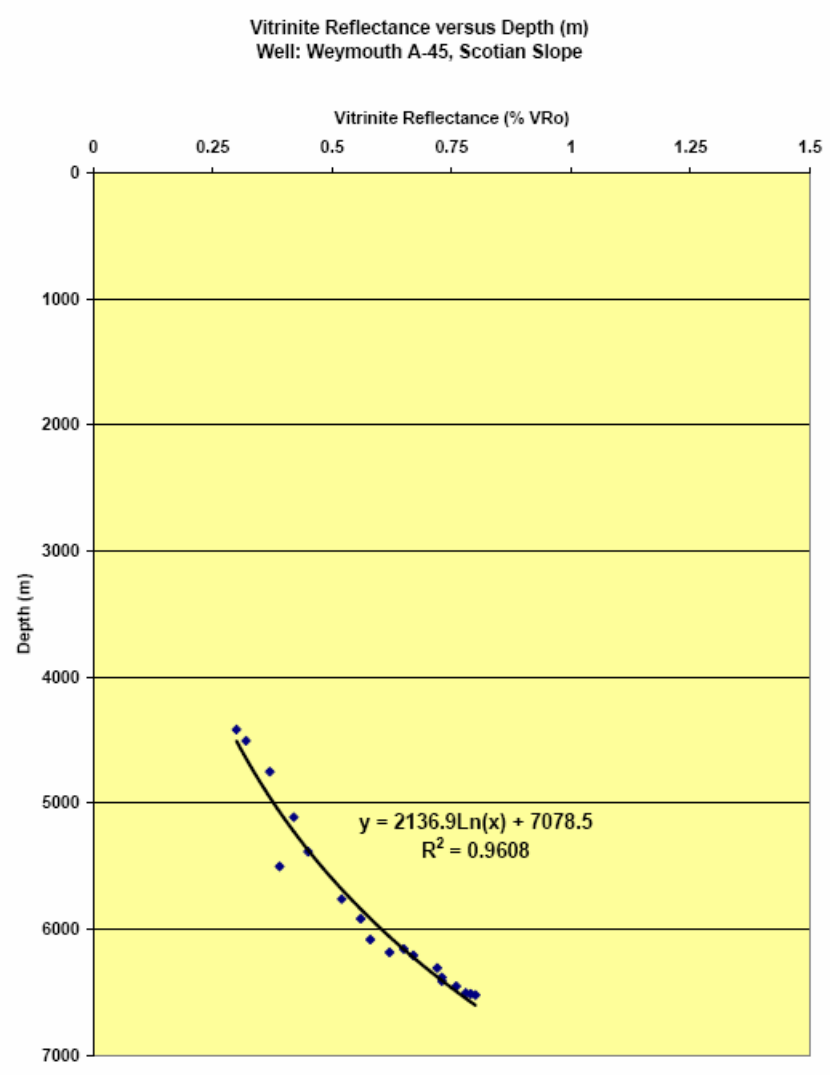

Figure 5c. A plot of vitrinite reflectance versus depth (m) from the Weymouth A-45 well with trend analysis and R^2 value

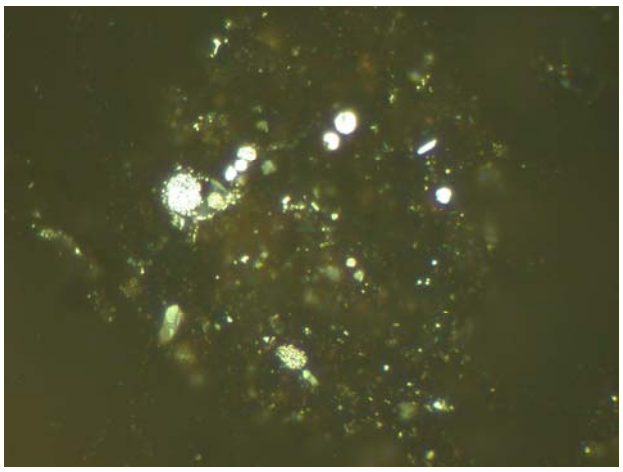

Figure 5d. Photomicrograph of amorphous liptinite 2 from Cretaceous Verrill Canyon source rock (Weymouth A-45 well, 6206 m) (incident white light excitation; X500)

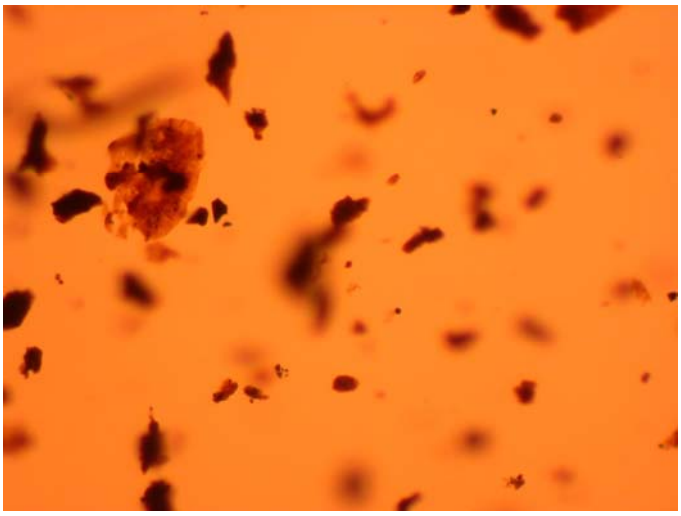

Figure 5e. Photomicrograph of amorphous liptinite 2 (possibly biodegraded algal remains) from Cretaceous Verrill Canyon source rock ((Weymouth A-45 well, 6206 m) (incident blue light [fluorescence] excitation; X500)

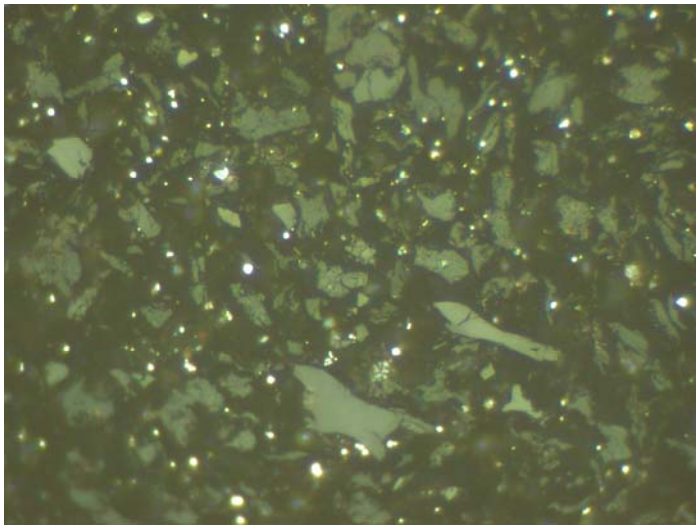

Figure 5f. Photomicrograph of abundant recycled vitrinites from the Annapolis G-24 well (incident white light; X500)

Chapter 3
Petroleum System Modeling
Data Acquisition

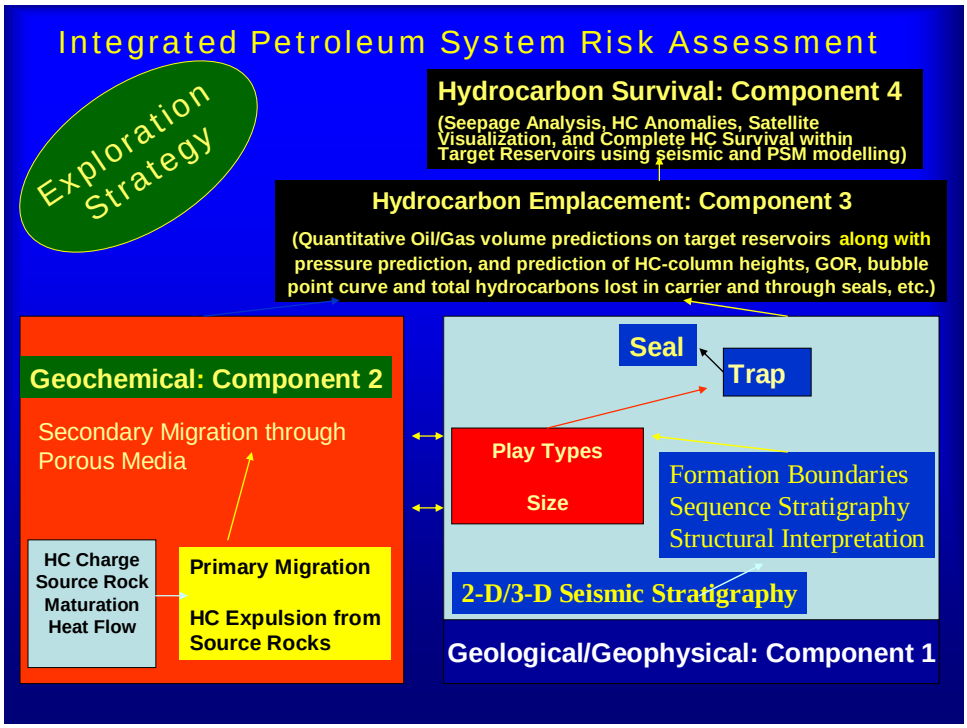

Figure 6. Schematic diagram of various petroleum system elements for hydrocarbon risk assessment (modified after Mukhopadhyay et al., 2003)

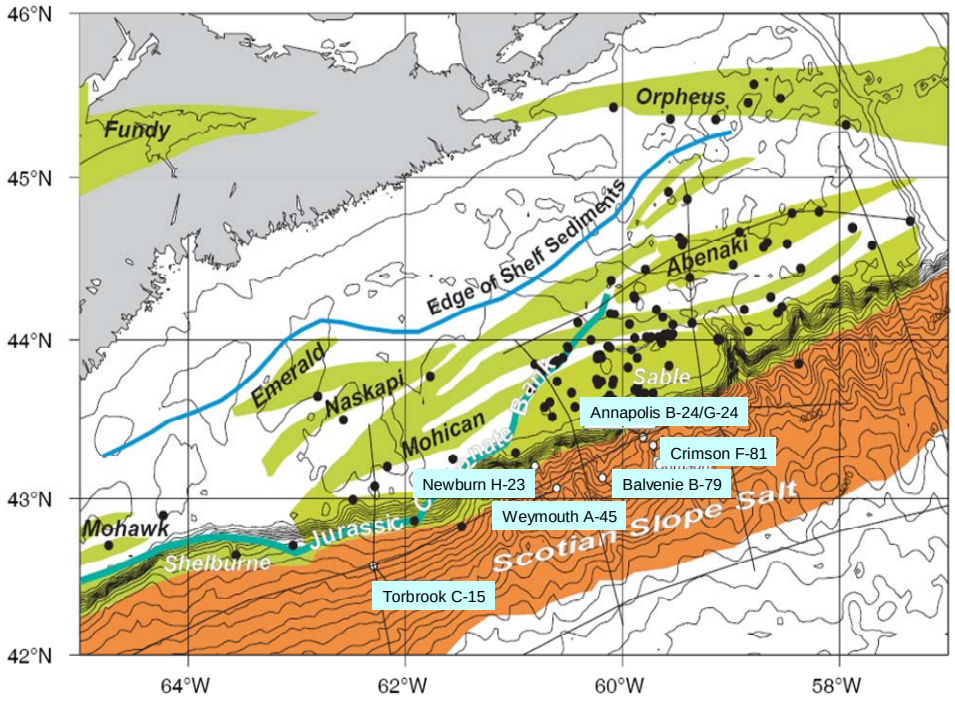

Figure 7a. Geological elements of the Scotian Basin with locations of six recently drilled deepwater wells

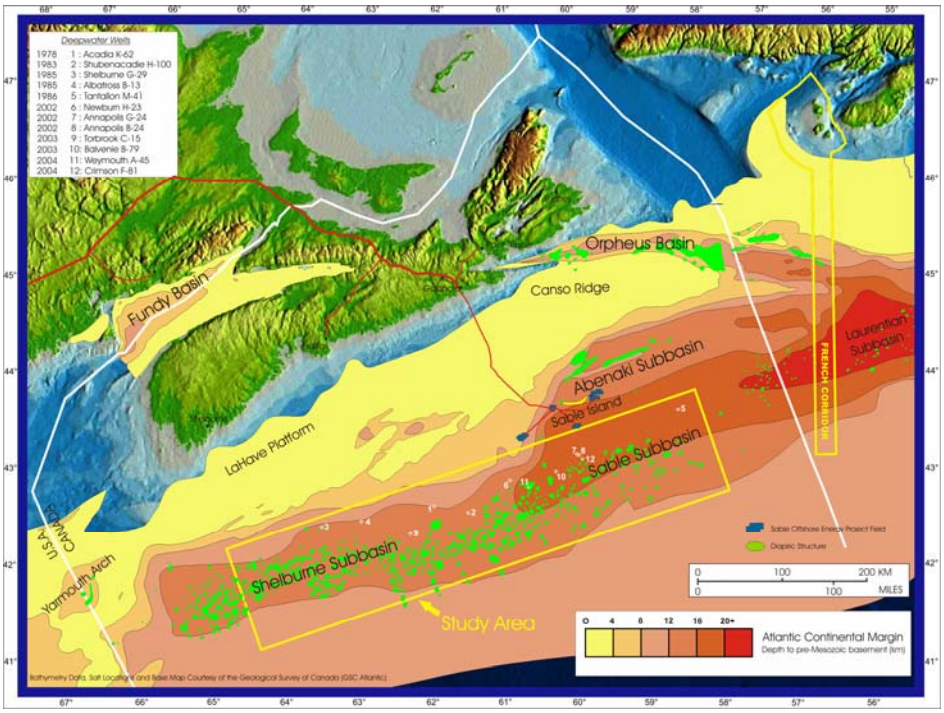

Figure 7b. Structural elements of the Scotian Basin including the target area of this contract work and the location of the 12 deepwater wells

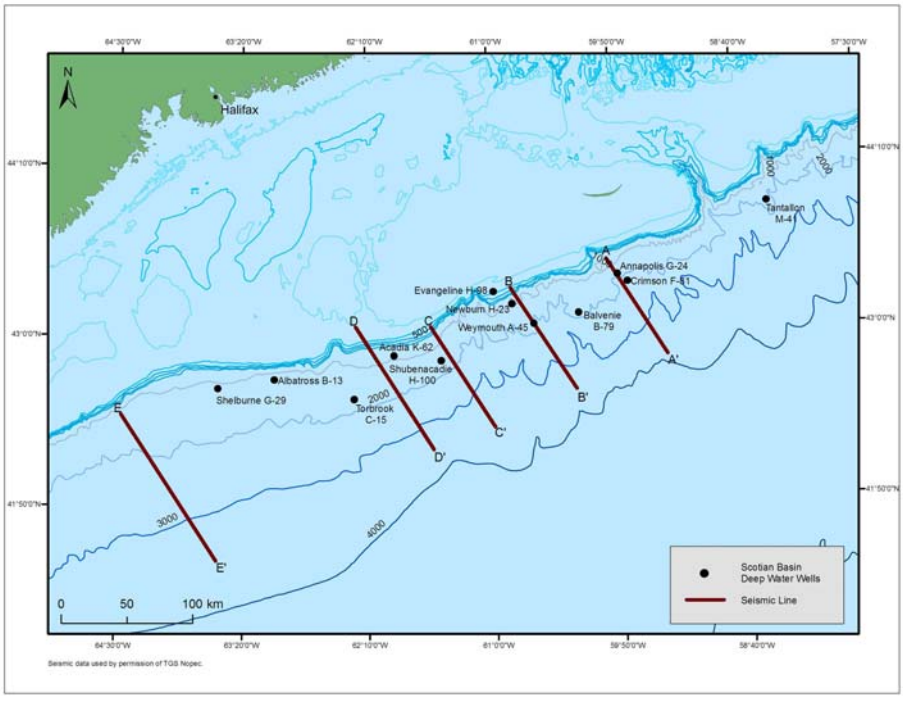

Figure 7c. Bathymetric map of Nova Scotia with locations of the 11 deepwater and one shelf wells used for the 1D modeling and five 2-D seismic lines utilized for the 2D modeling

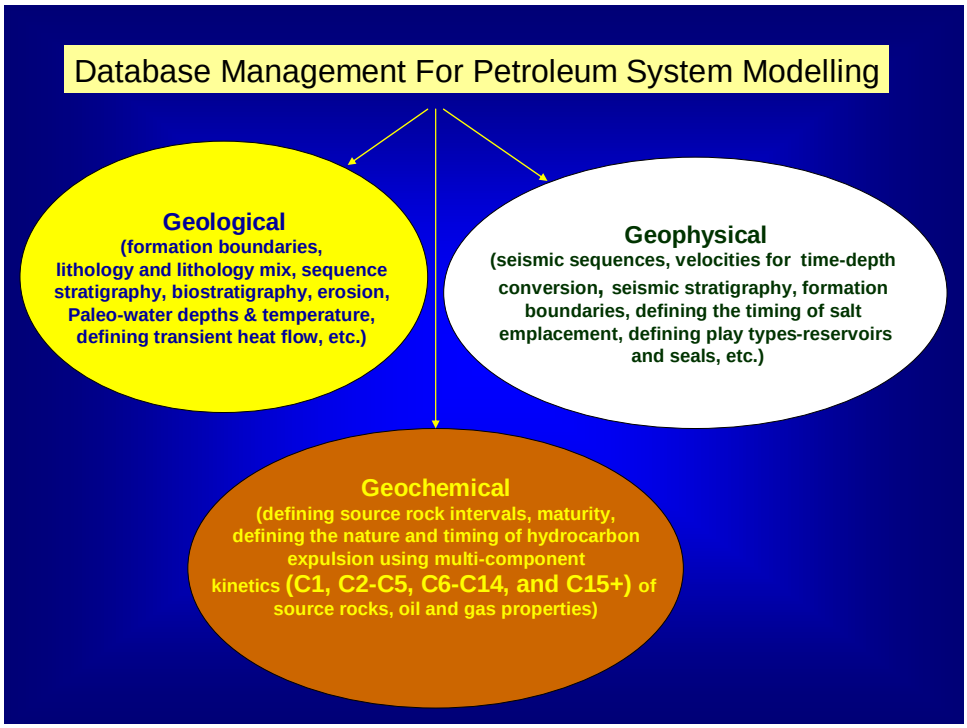

Figure 8a. Parameters of the database required for the simulation of petroleum system modeling

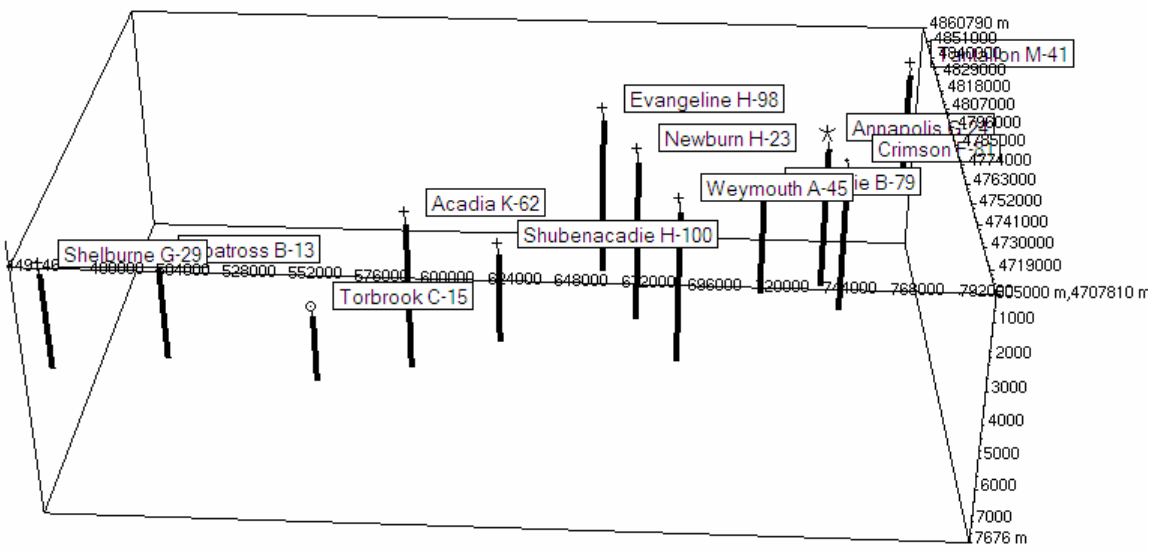

Figure 8b. Well location within the world co-ordinates of the Scotian Margin

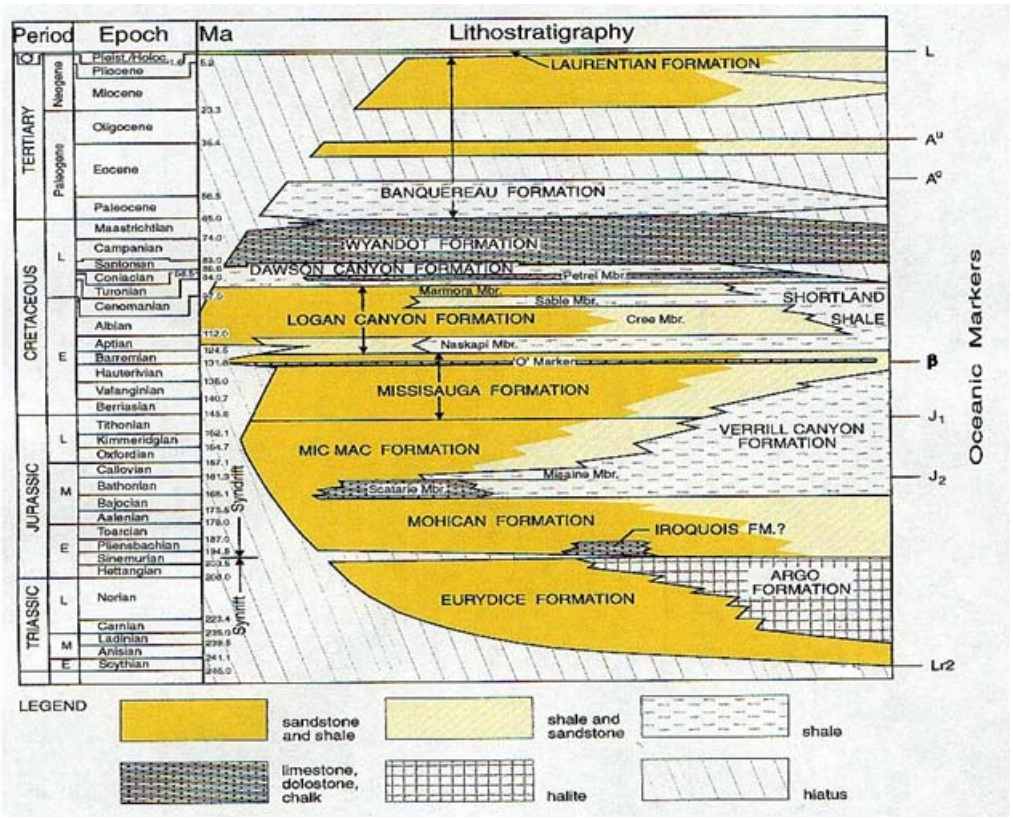

Figure 8c: Generalized Litho-and Chronostratigraphy of the Scotian Basin (After Wade et al., 1995)

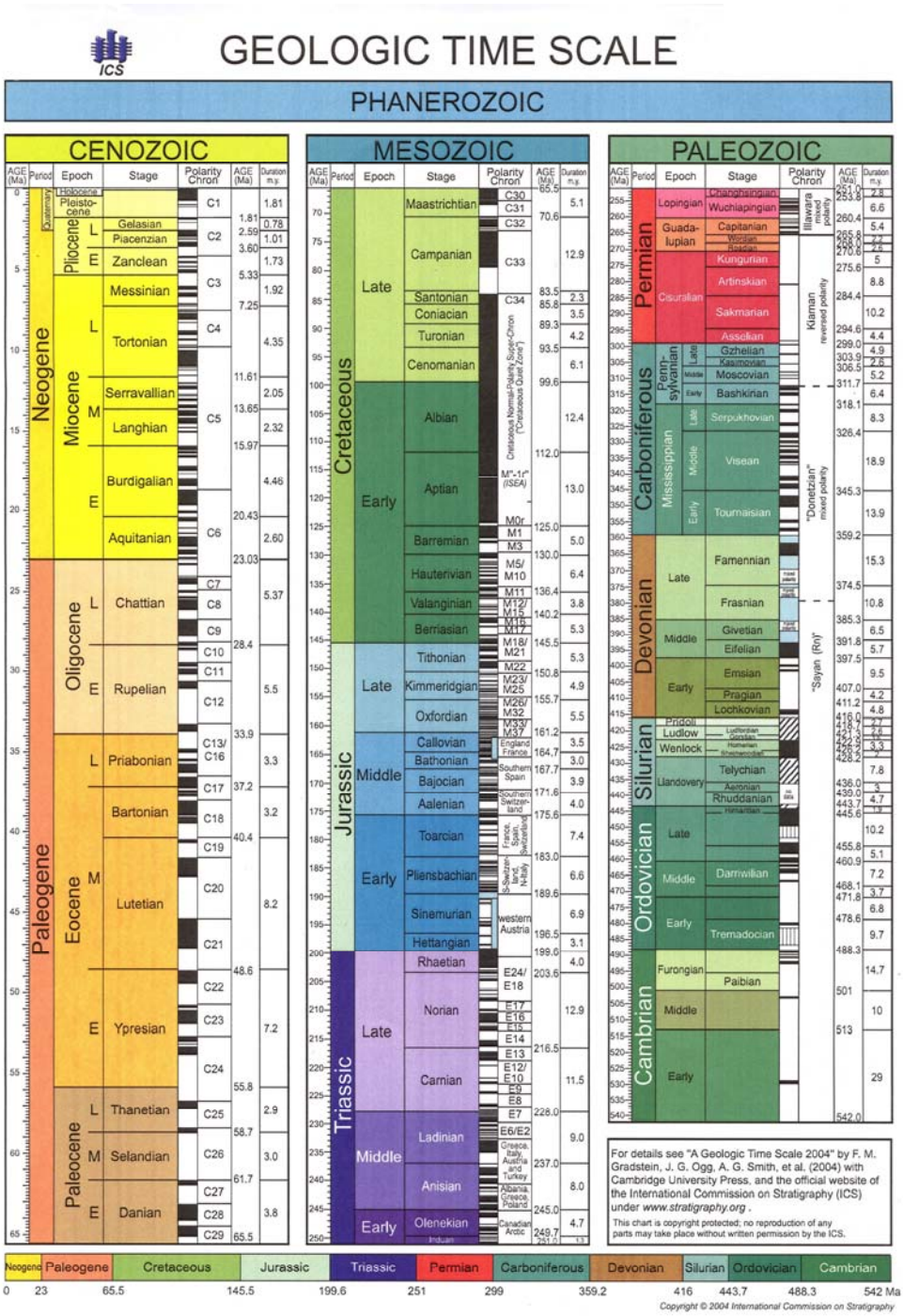

Figure 8d. Geological Time Scale (after Gradstein and Ogg, 2004) used for 1D and 2D modeling

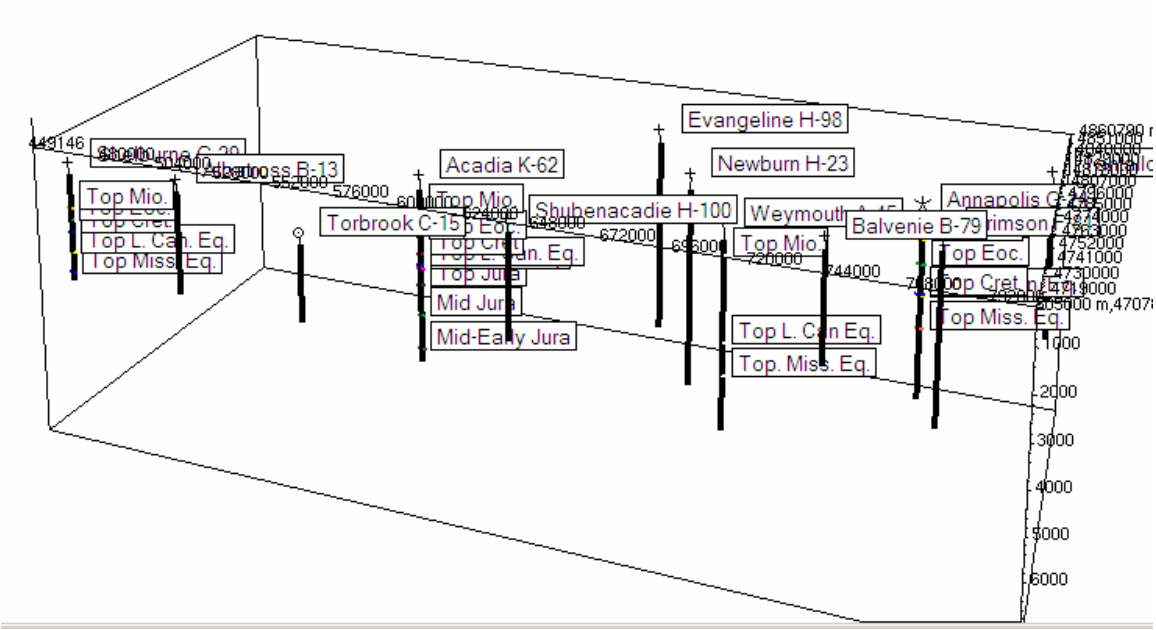

Figure 8e. Location of 12 wells (11 slope and 1 shelf) and stratigraphic tops from the selected wells

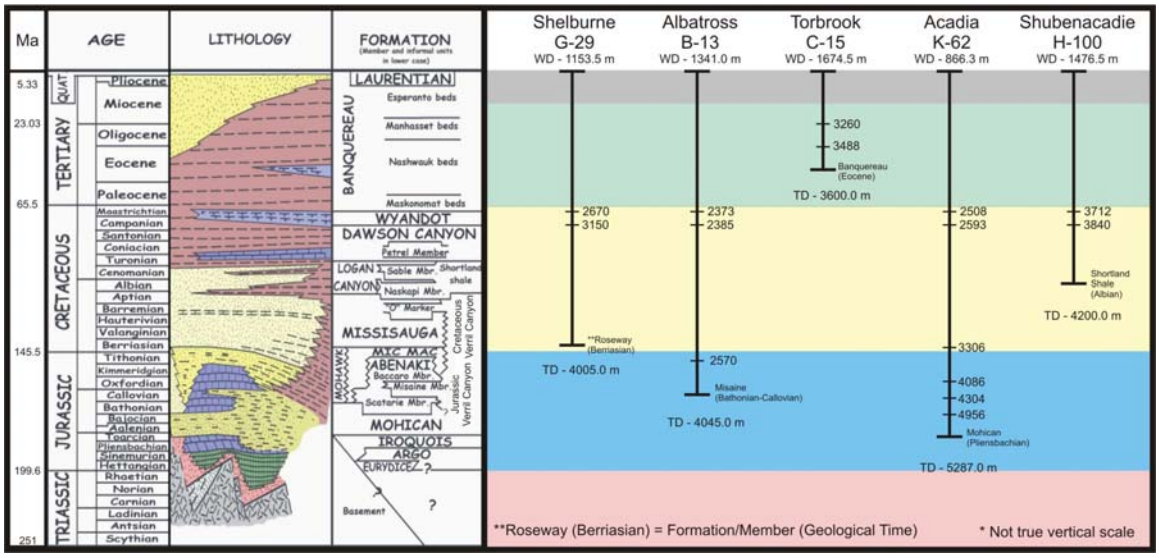

Figure 8f(i). Litho- and chronostratigraphy of the deepwater Scotian Basin showing the stratigraphic top of various intervals and TD for five slope wells from the Shelburne Subbasin and western part of the Sable Subbasin

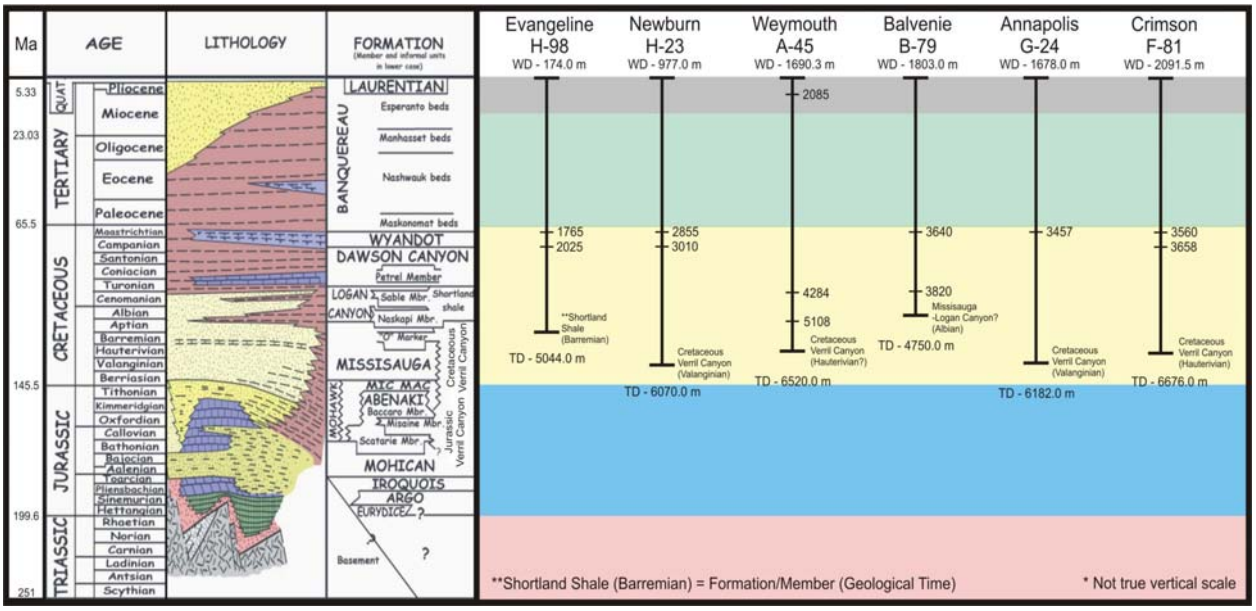

Figure 8f(ii). Litho- and chronostratigraphy of the deepwater Scotian Basin showing the stratigraphic top of various intervals and TD for five recently drilled slope wells and the Evangeline H-98 well from the Sable Subbasin

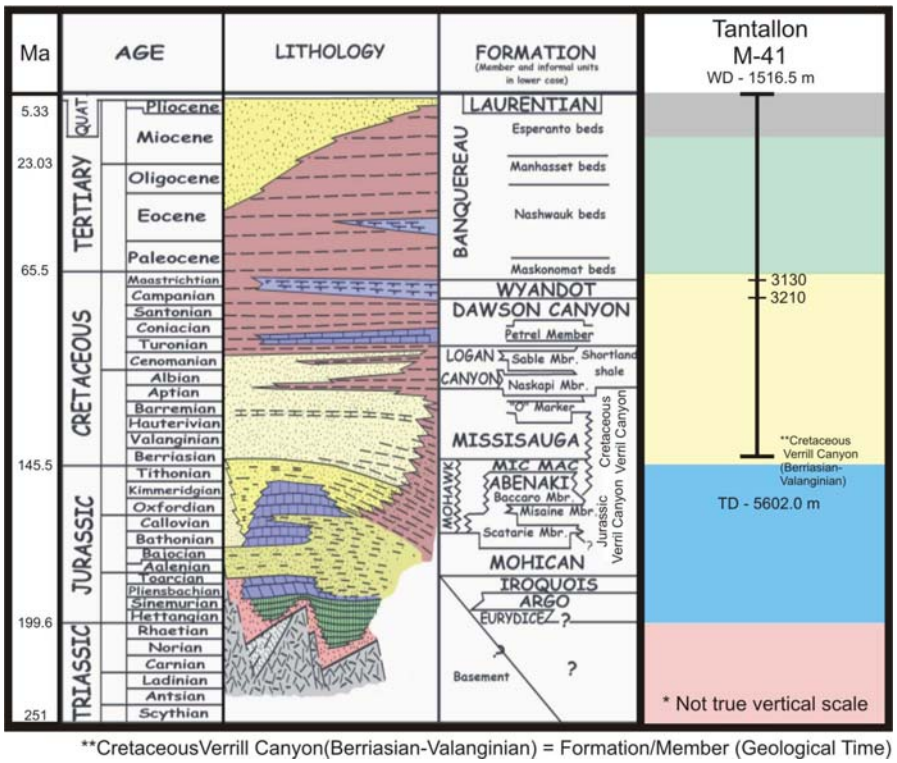

Figure 8f (iii). Litho- and chronostratigraphy of the deepwater Scotian Basin showing the stratigraphic top of various intervals and TD for the Tantallon M-41 well

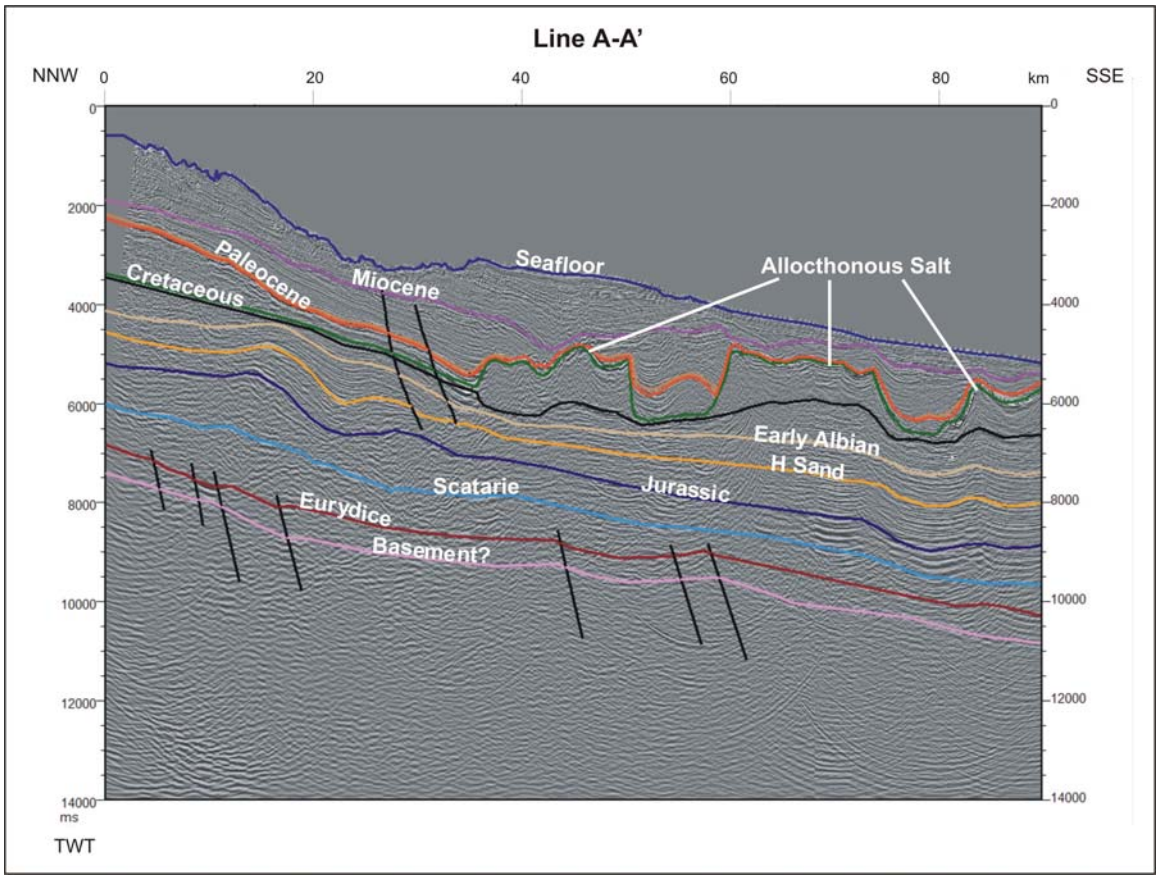

Figure 9a. Seismic line A-A' (for position on the Scotian Slope see Figure 7c)

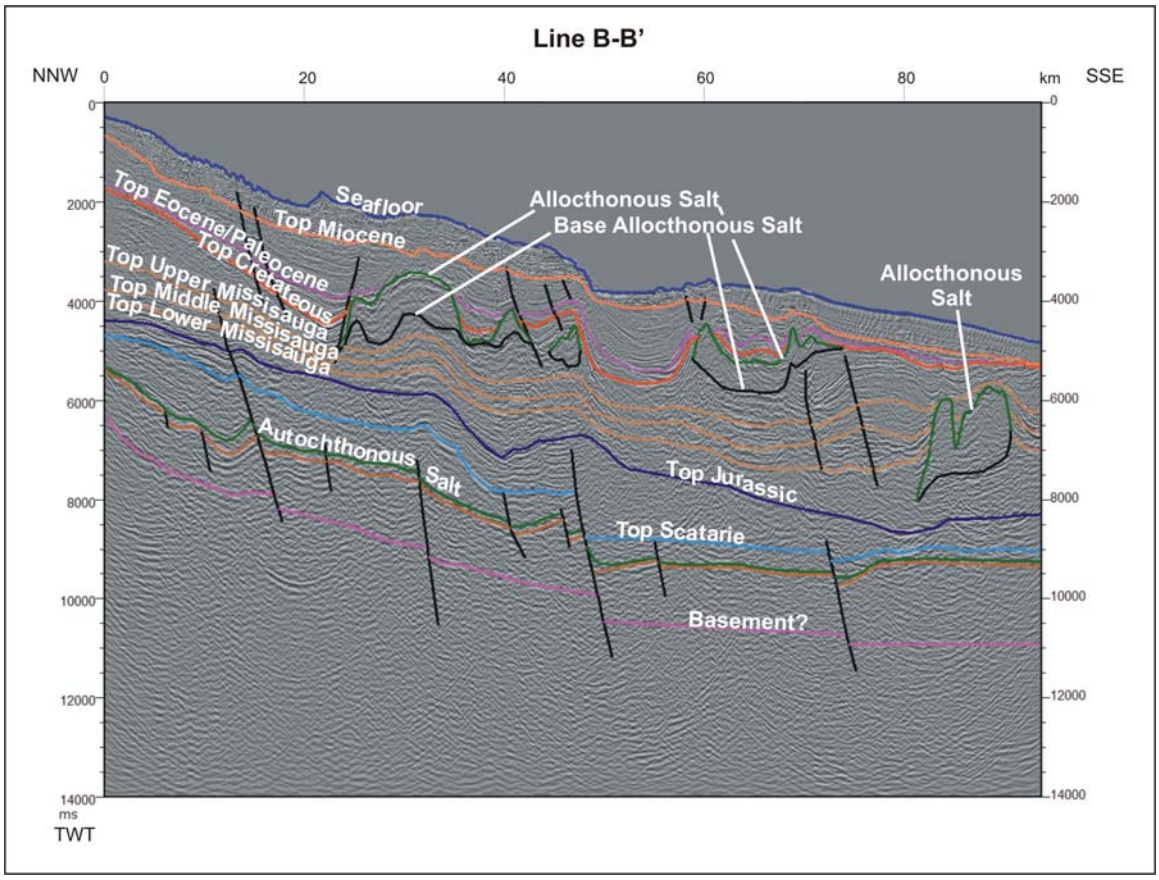

Figure 9b. Seismic line B-B' (for position on the Scotian Slope see Figure 7c)

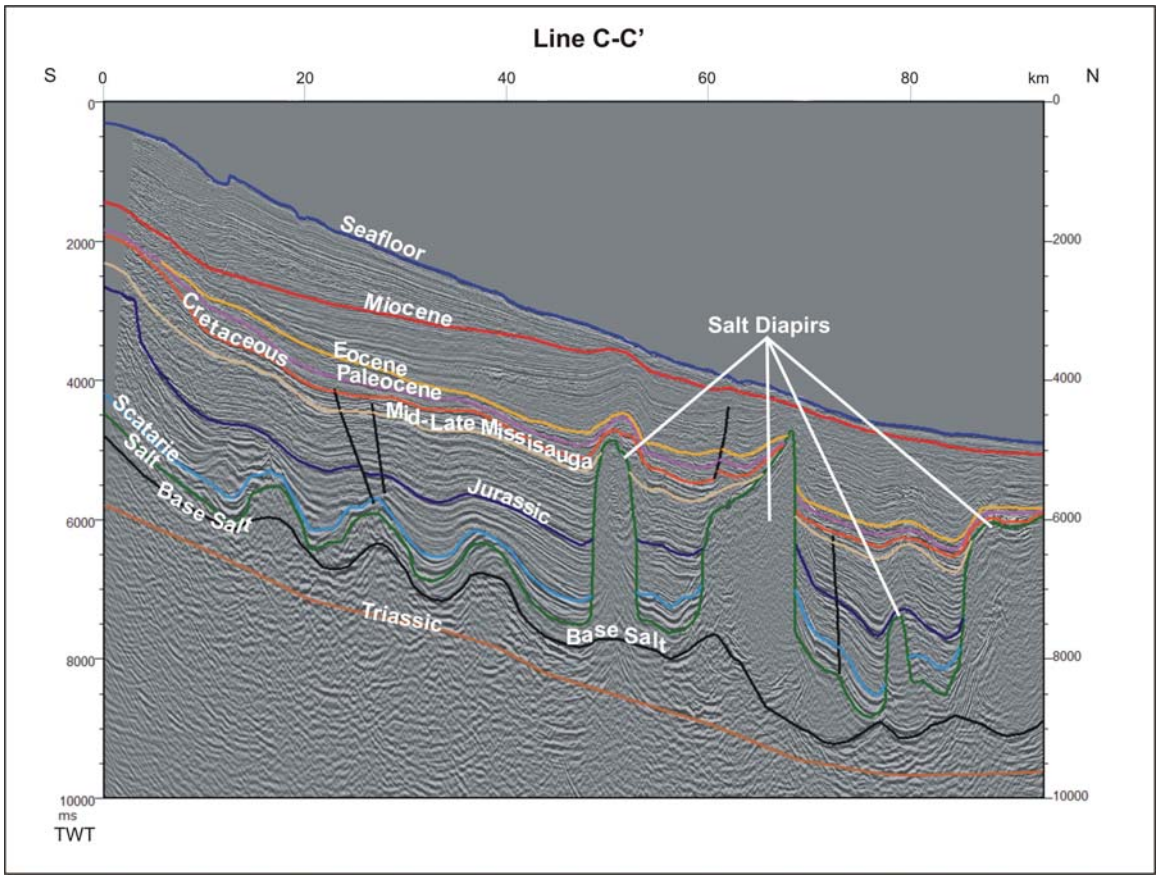

Figure 9c. Seismic line C-C' (for position on the Scotian Slope see Figure 7c)

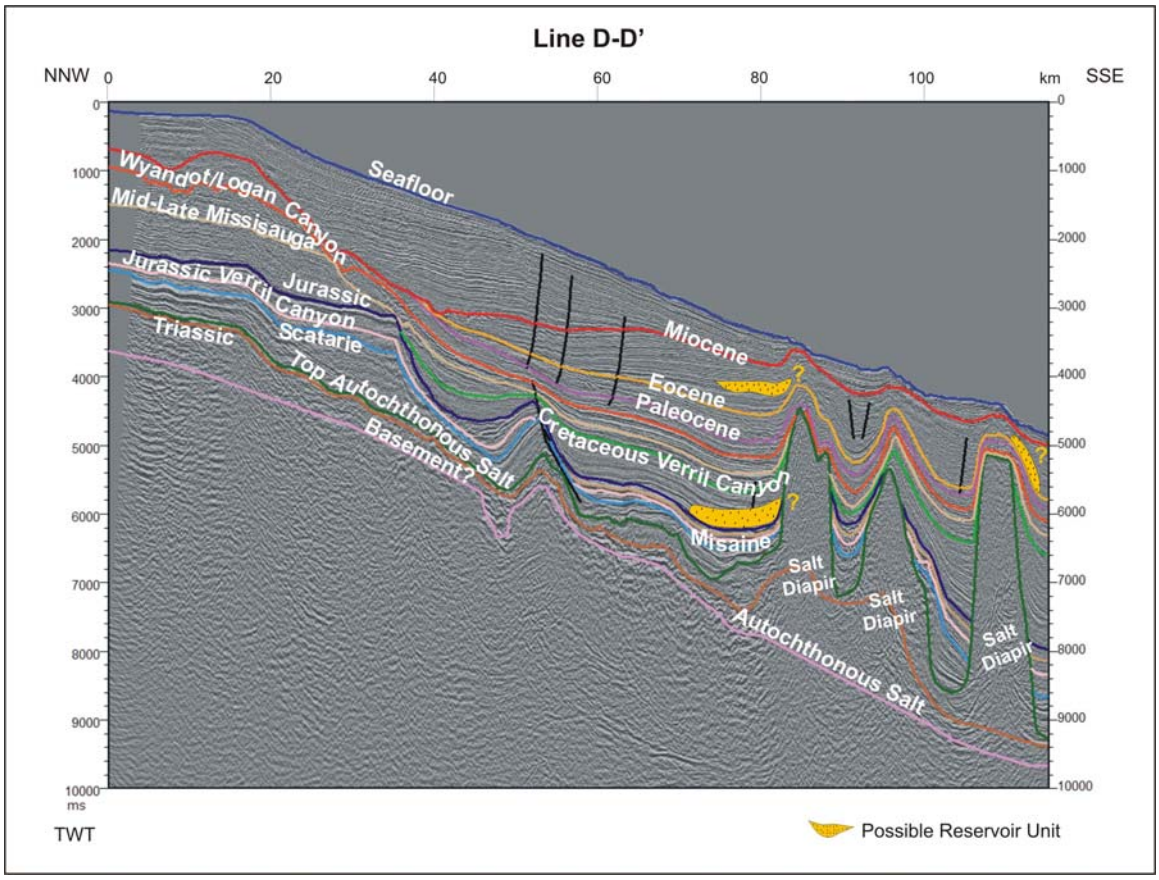

Figure 9d. Seismic line D-D' (for position on the Scotian Slope see Figure 7c)

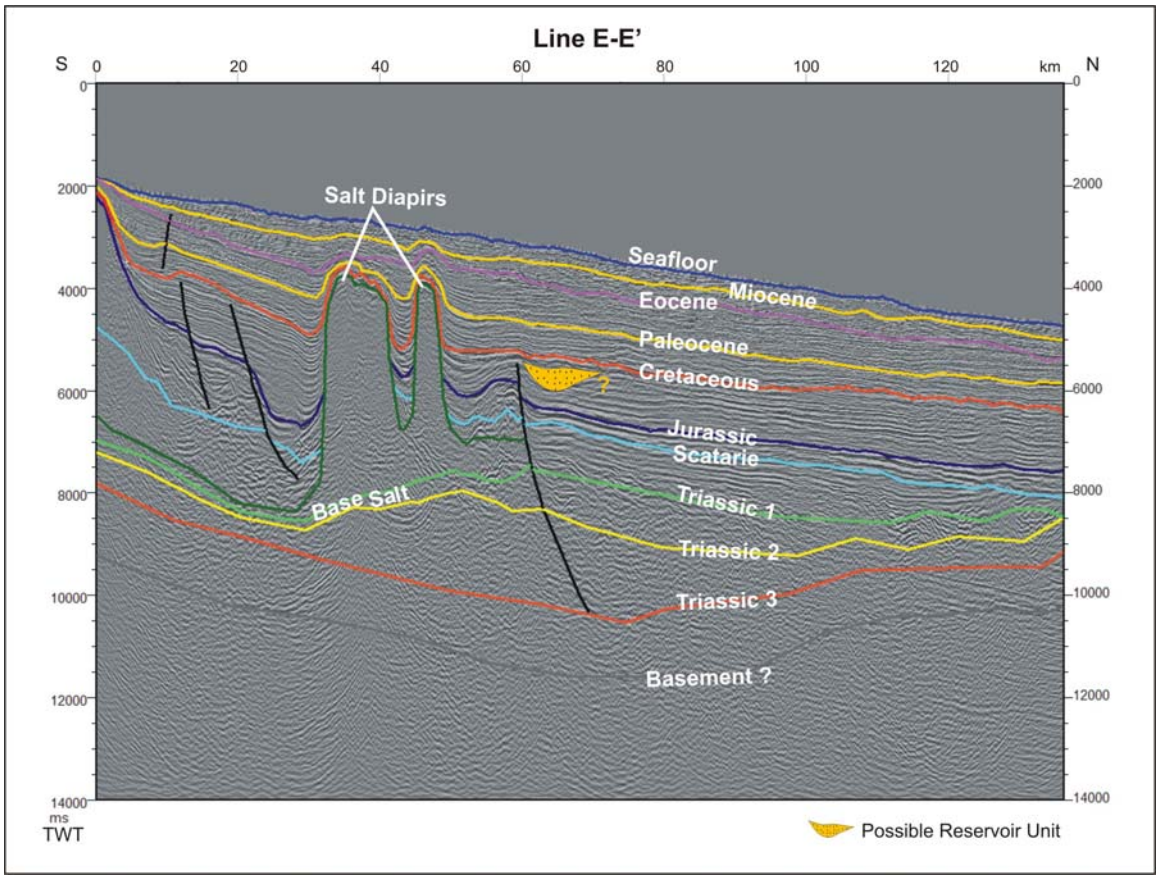

Figure 9e. Seismic line E-E' (for a location on the Scotian Slope see Figure 7c)

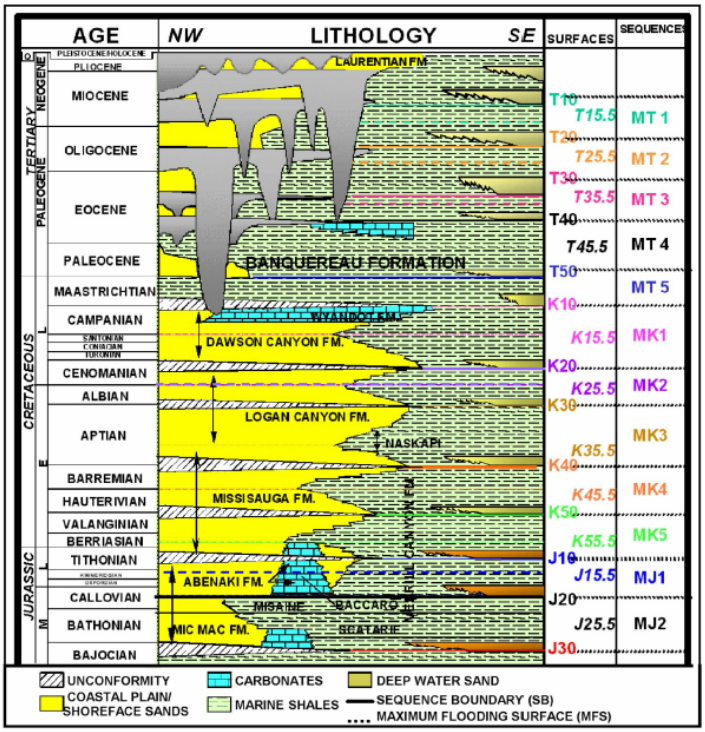

Figure 10. Stratigraphic correlation of deepwater sediments from the Scotian Basin showing various unconformities (after Hogg et al., 2001)

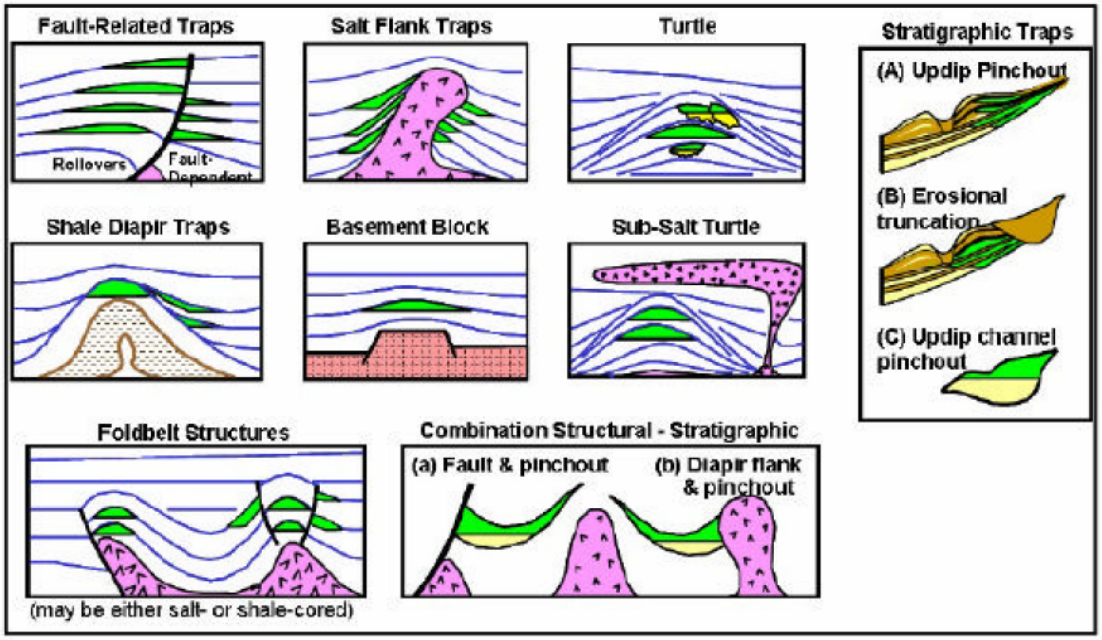

Figure 11a . Various play types as seen in different deepwater basins in the world (after Pettingill and Weimer, 2001; with permission from the authors)

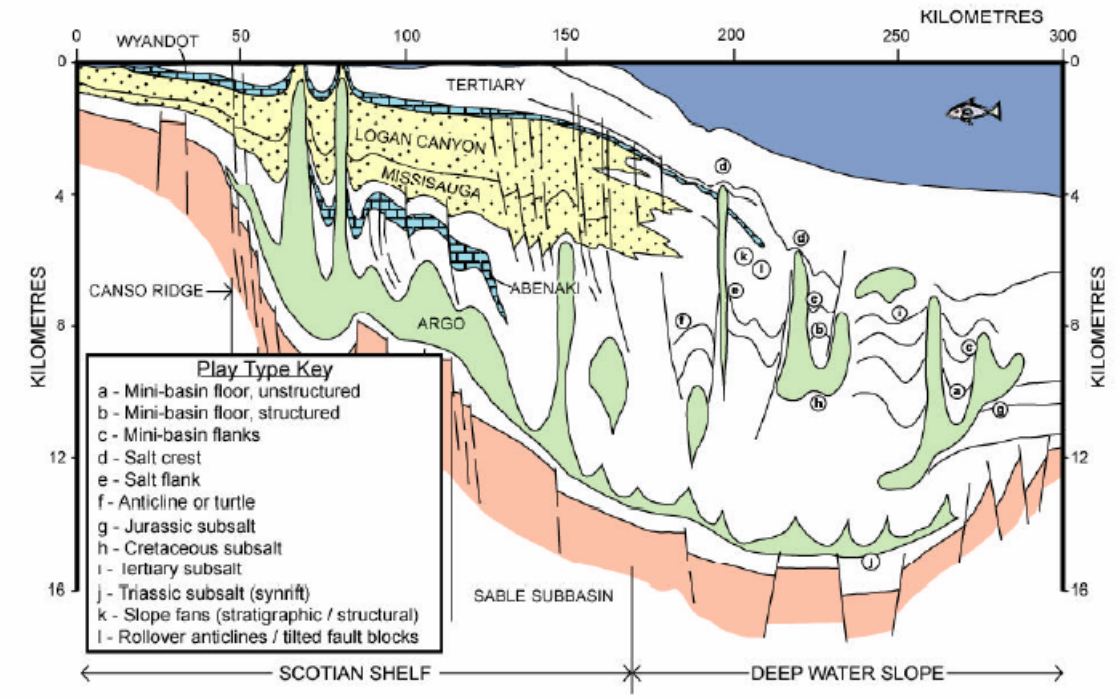

11b. Schematic diagram of conceptual play types seen from seismic stratigraphy of the Scotian Slope (from Kidston et al., 2002)

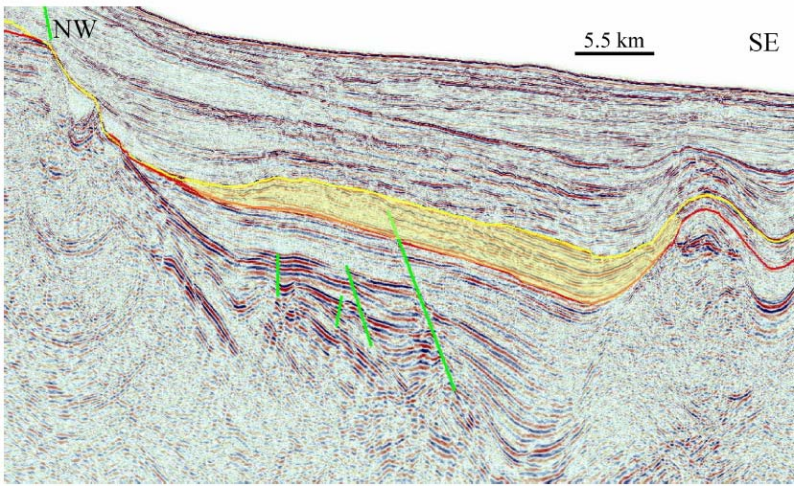

Figure 11c. Oligocene stratigraphic trap in SW Scotian Margin (from Hogg et al., 2001; courtesy of TGS-Nopec)

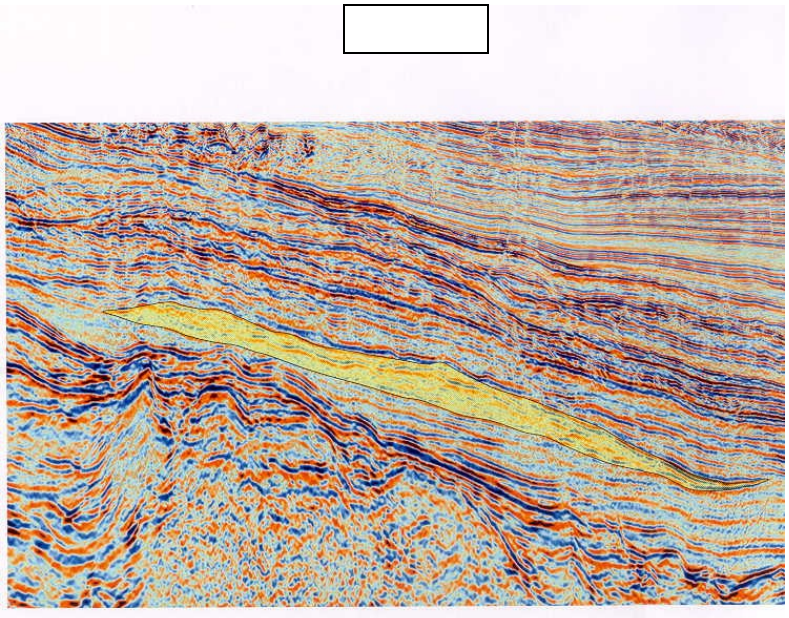

11d. Sable Subbasin: Possible early Cretaceous Turbidite Play Type
(courtesy of TGS-Nopec)

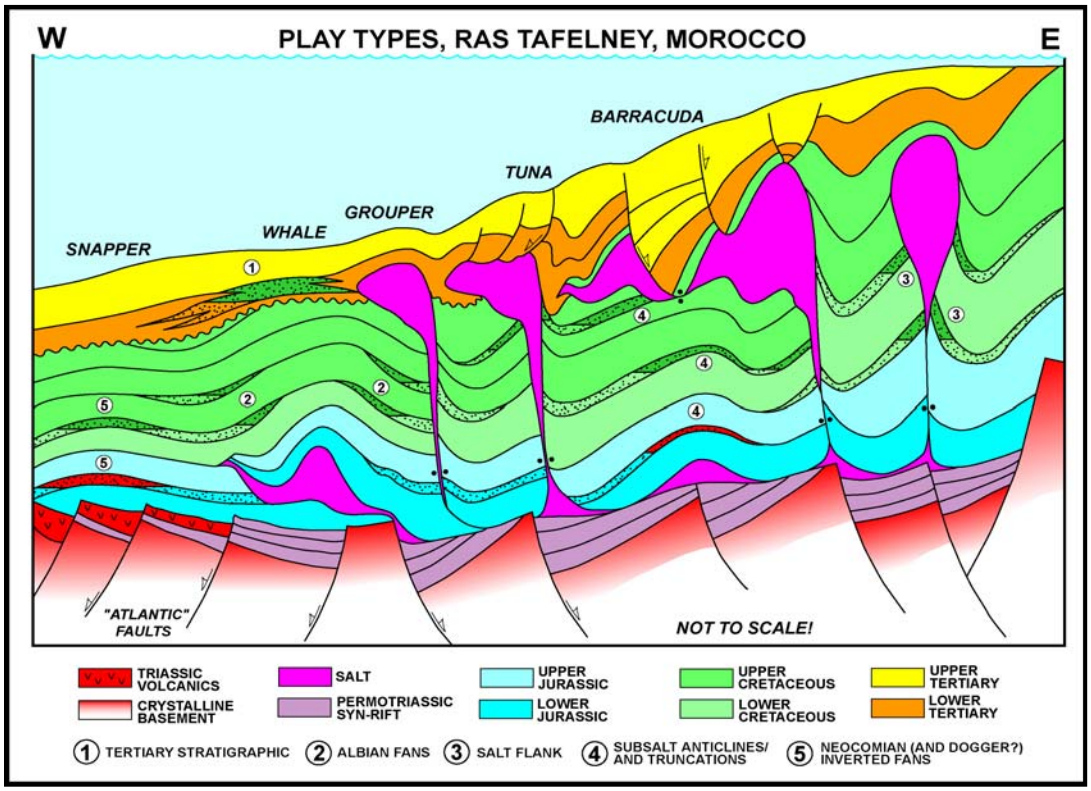

Figure 11e. Various Play Types from Ras Tafalney, Morocco
(after Tari, 2006; permission from the author)

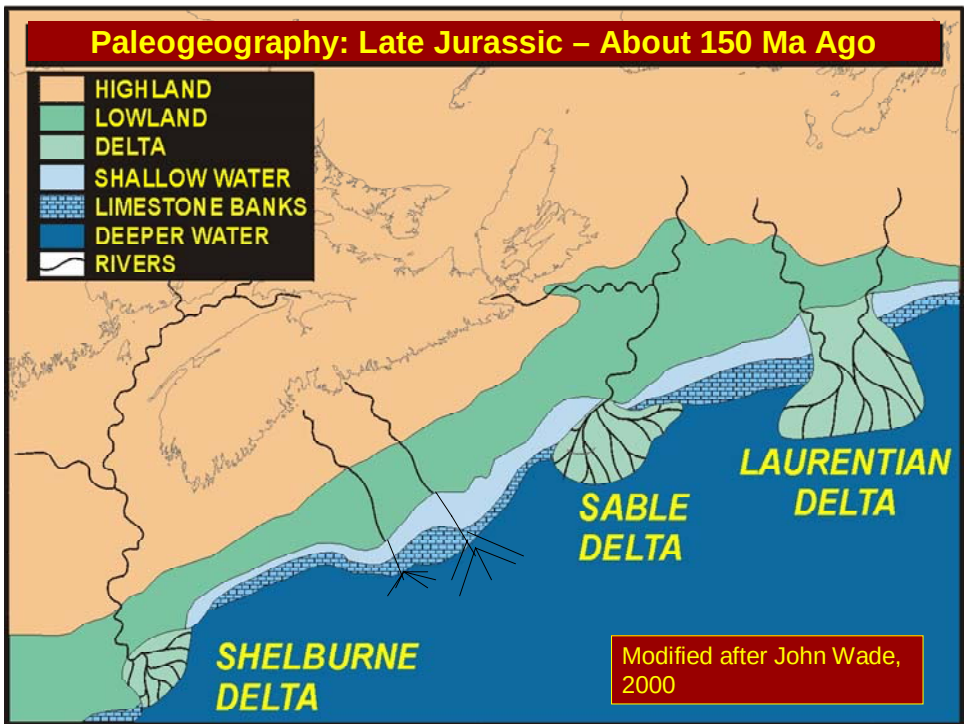

Figure 12a. Paleogeographic map of Late Jurassic Period (150 Ma) (after Wade, 2000 from Atlantic Geoscience Society, 2001)

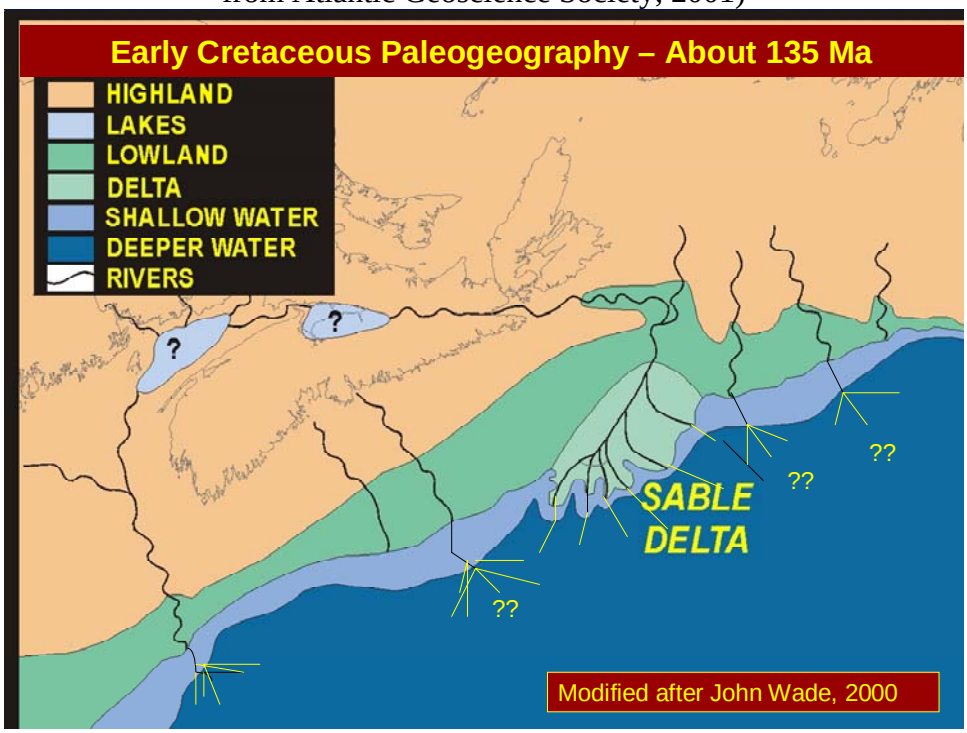

Figure 12b. Paleogeographic map of Early Cretaceous Period (135 Ma) (after Wade, 2000 from Atlantic Geoscience Society, 2001)

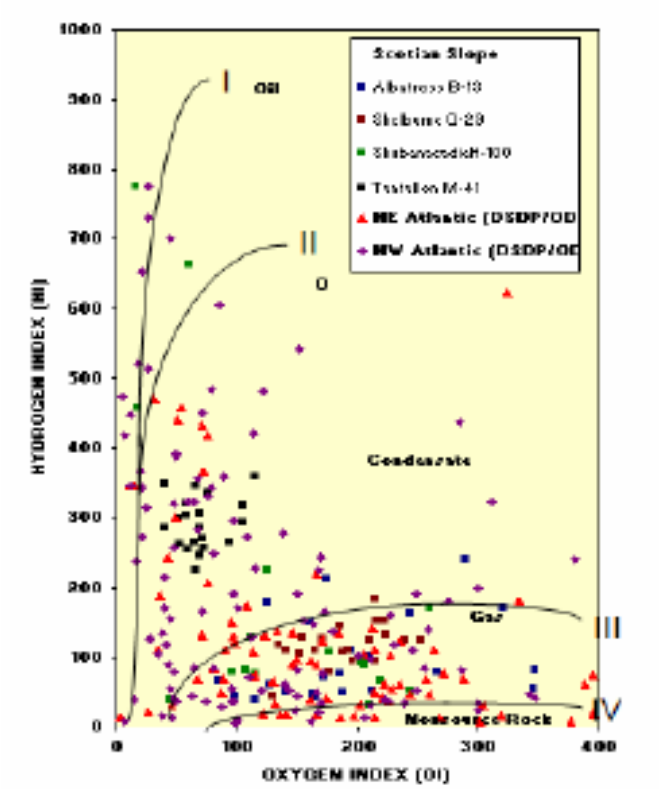

Figure 13a. Source rock potential with positions of various sediments from the Scotian Slope (drilled prior to 2000) and the DSDP wells from the Northeast and Northwest Atlantic Region. Type I and II - oil prone; Type II-III - gas and condensate prone; Type III - mainly gas prone; Type IV - mostly non-source rock

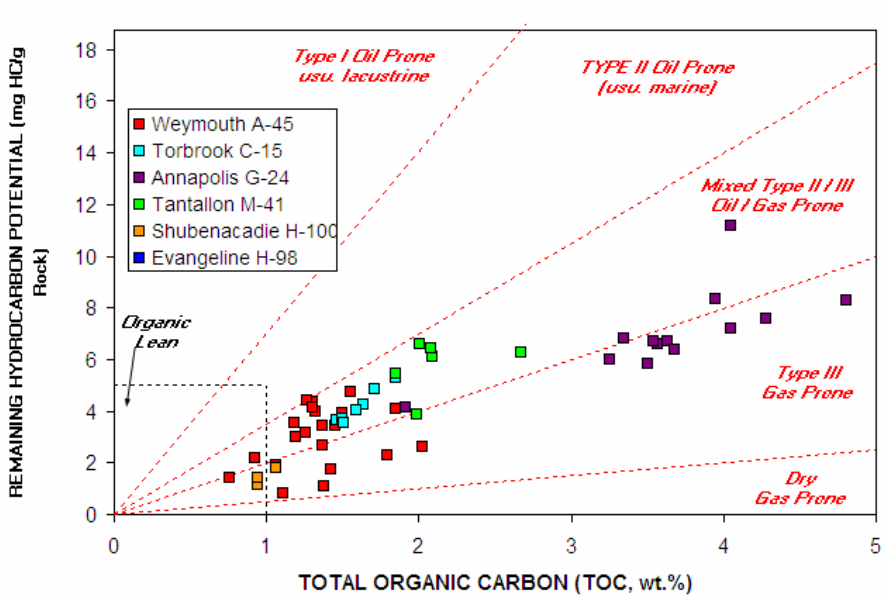

Figure 13b. Source rock potential (plot of S_2 and TOC) with positions of various sediments from selected Scotian Slope wells. Type I and II - oil prone; Type II-III - gas and condensate prone; Type III - mainly gas prone; Type IV - mostly non-source rock or minor gas

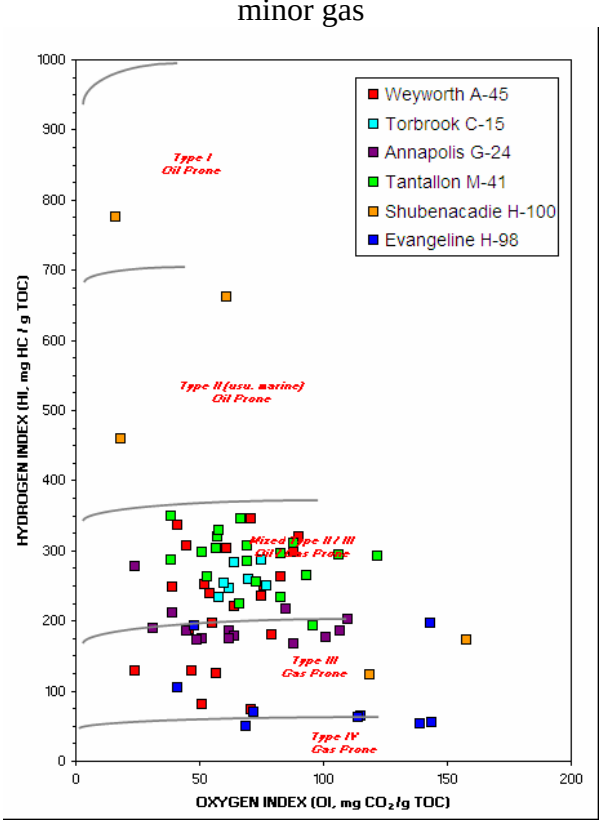

Figure 13c. Source rock potential (plot of S_2 and TOC) with positions of various sediments from selected Scotian Slope wells. Type I and II - oil prone; Type II-III - gas and condensate prone; Type III - mainly gas prone; Type IV - mostly non-source rock or minor gas

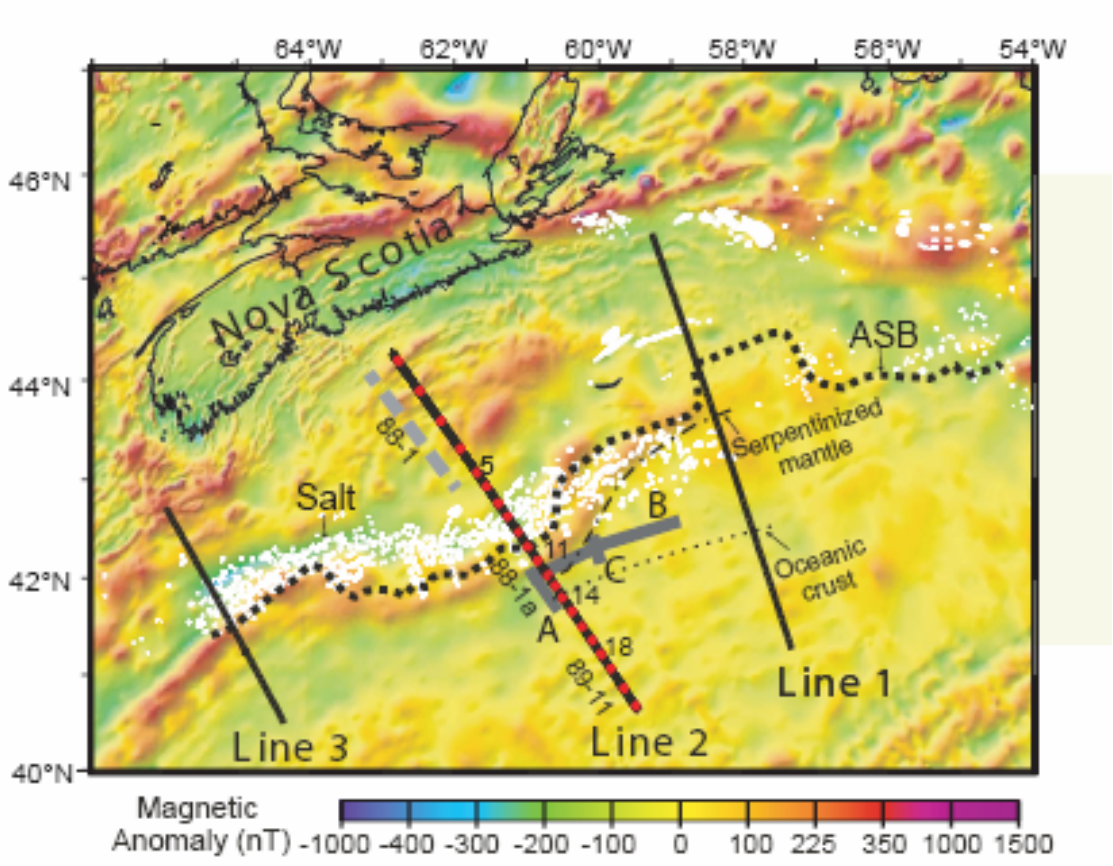

Figure 14a. Magnetic anomaly map for the Nova Scotia margin and surrounding areas (Wu et al., in press; revised from Louden et al., 2005).

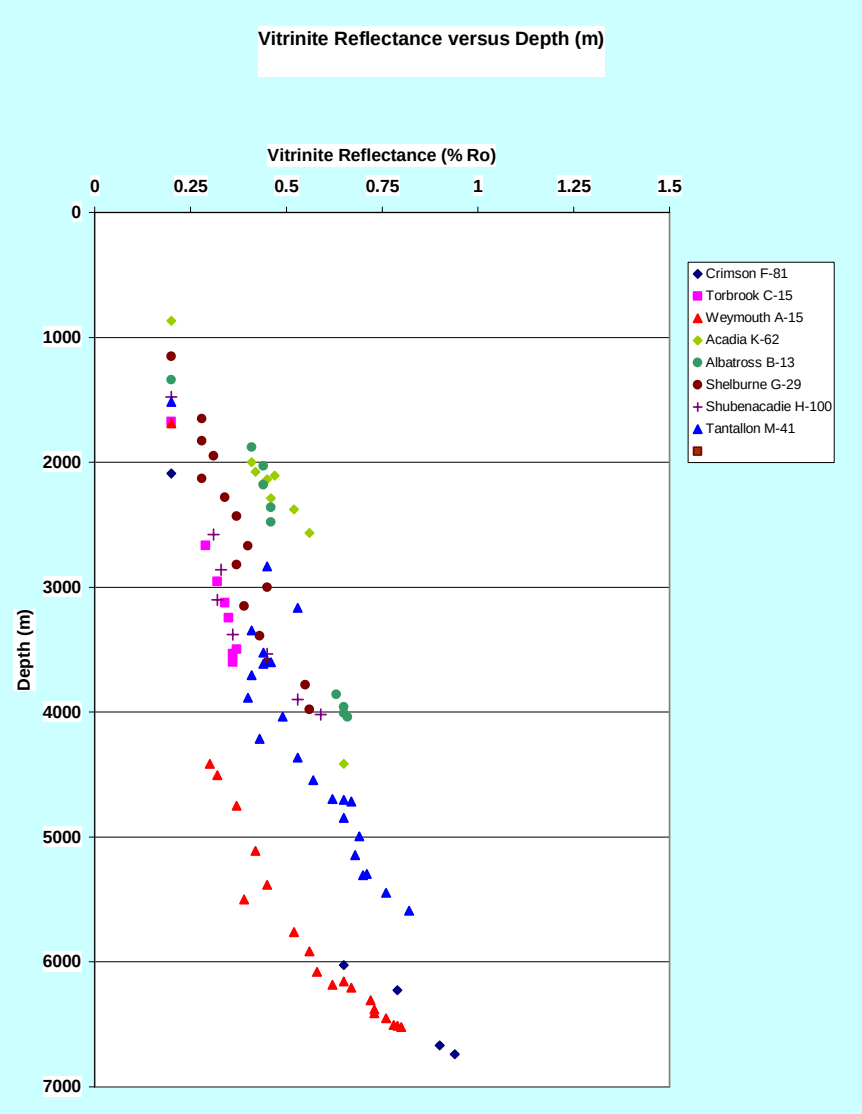

Figure 14b. Comparison of the maturation trend of selected wells from the Scotian Slope

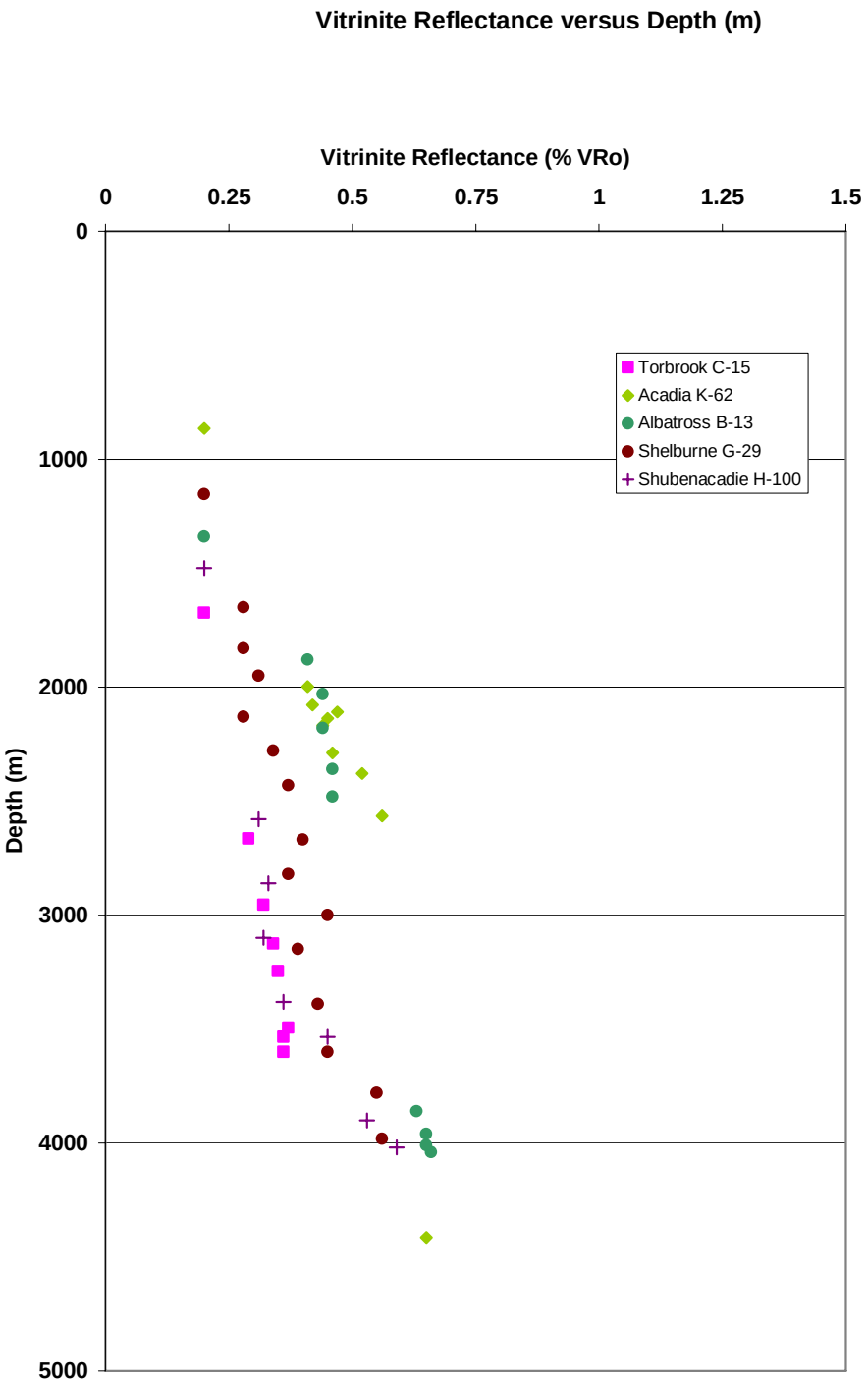

Figure 14c. Comparison of maturation trend of selected wells from the slope region from the Shelburne Subbasin and western part of the Sable subbasins

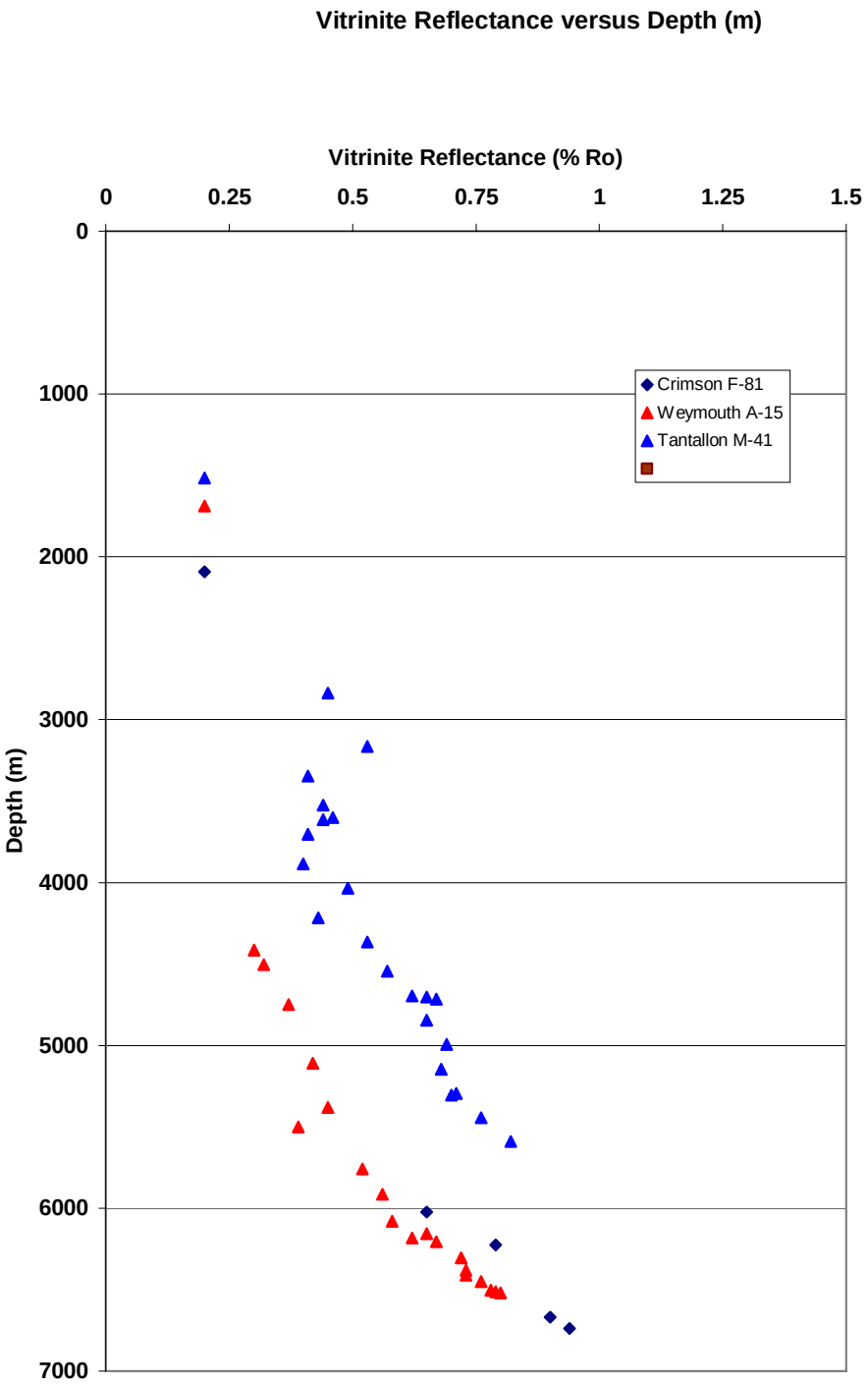

Figure 14d. Comparison of maturation trend of three wells from the slope region from the eastern and western part of the Sable Subbasin

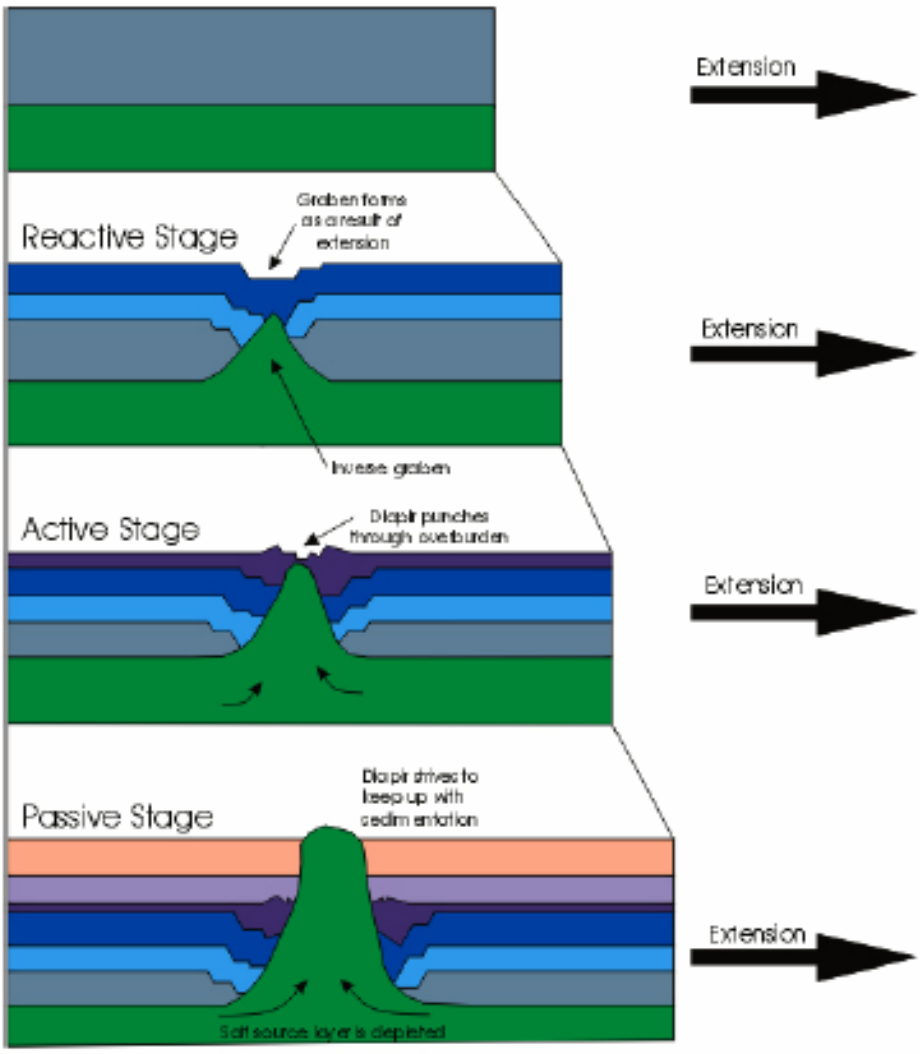

Figure 15a. Stages of salt diapirism and growth during extension (after Vandeville and Jackson, 1992)

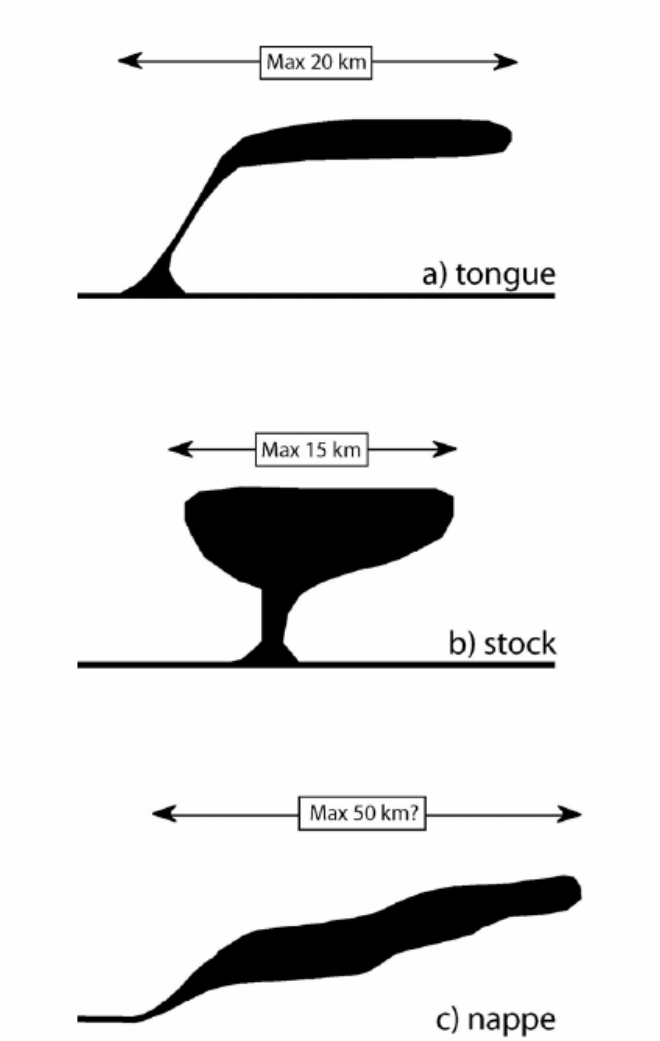

Figure 15b. End member geometries of allochthonous salt systems: top – asymmetric salt tongues; middle – radial bulb-shaped salt stocks; and bottom – salt nappe (from Young, 2004 - modified version from Rowan, 2002).

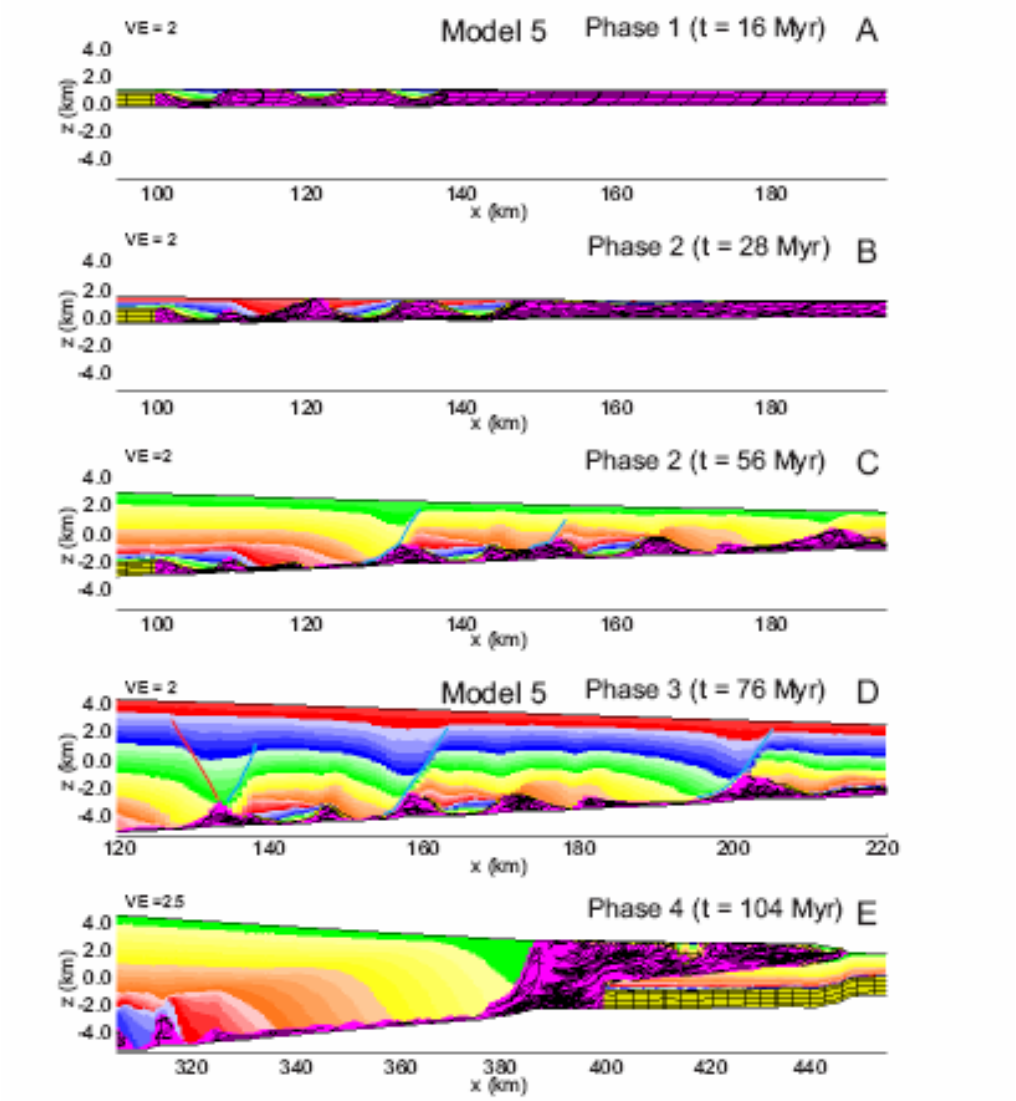

Figure 15c. Modeling of salt progradation showing effect of isostatic compensation: A. Phase I – development of mini-basins and associated diapirs; B. Phase II – onset of extensional normal faulting during sediment progradation; C: Phase III – landward tilting of salt and development of counter-regional normal faults; D: Phase IV – diachronous evolution to graben faulting augmenting counter-regional faults; and E: Phase V – formation of salt tongue and progressively climbs above the isostatically adjusting sediments during over-thrusting (after Ing et al. 2004)

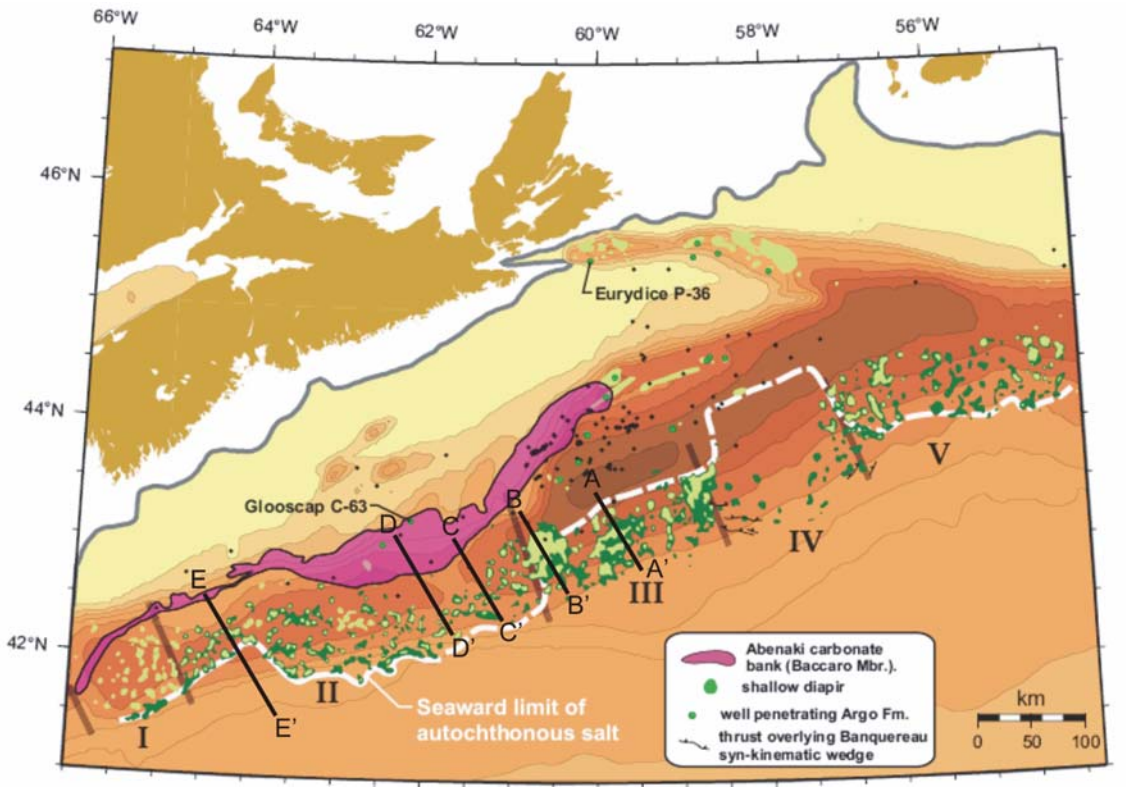

Figure 15d. Five tectono-stratigraphic sub-provinces with salt emplacement within Scotian Basin Diapiric Provinces (from Shimeld, 2004). Shallow salt bodies are indicated by light green polygons and deeper structures are dark green. The autochthonous salt bodies that are penetrated by wells are also indicated.

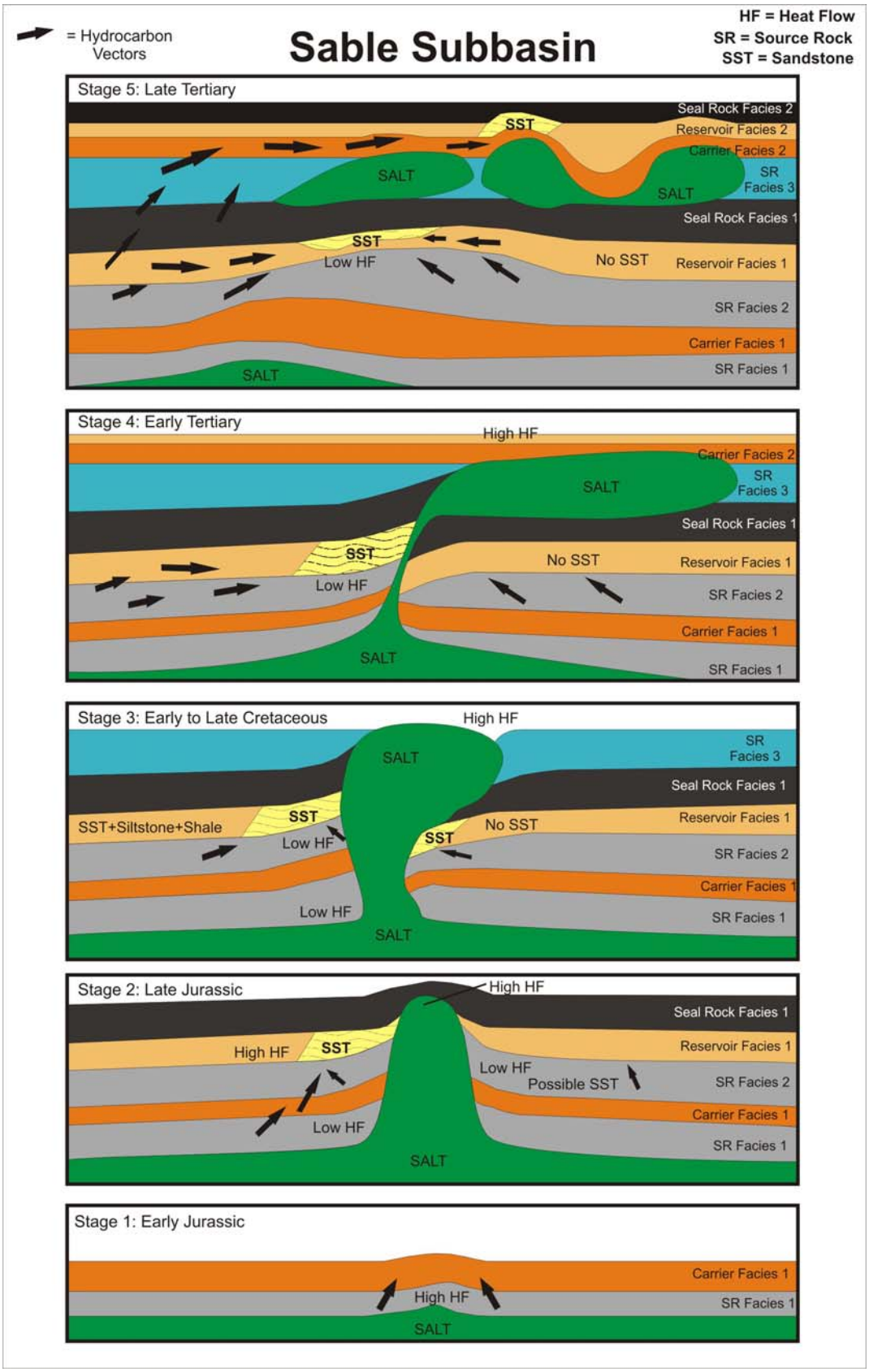
= Hydrocarbon Vectors
Sable Subbasin
HF = Heat Flow
SR = Source Rock
SST = Sandstone
Stage 5: Late Tertiary
Seal Rock Facies 2
SST
Reservoir Facies 2
Carrier Facies 2
SALT
SR Facies 3
SALT
Seal Rock Facies 1
SST
Low HF
No SST
Reservoir Facies 1
SR Facies 2
Carrier Facies 1
SALT
SR Facies 1
Stage 4: Early Tertiary
High HF
Carrier Facies 2
SR Facies 3
SALT
Seal Rock Facies 1
SST
No SST
Reservoir Facies 1
Low HF
SR Facies 2
Carrier Facies 1
SALT
SR Facies 1
Stage 3: Early to Late Cretaceous
High HF
SALT
SR Facies 3
Seal Rock Facies 1
SST+Siltstone+Shale
SST
No SST
Reservoir Facies 1
Low HF
SST
SR Facies 2
Carrier Facies 1
Low HF
SR Facies 1
SALT
Stage 2: Late Jurassic
High HF
Seal Rock Facies 1
High HF
SST
Reservoir Facies 1
Low HF
Possible SST
SR Facies 2
Carrier Facies 1
Low HF
SR Facies 1
SALT
Stage 1: Early Jurassic
Carrier Facies 1
High HF
SR Facies 1
SALT

Figure 15e. Conceptual model of relationship between the stages of salt emplacement and various petroleum system parameters such as sand dispersal and heat flow within the source rocks of the slope region from the Sable Subbasin (after Mukhopadhyay et al., in press). **Stage 1** (Early Jurassic) - oil generation from Early Jurassic source rock due to high heat flow just after rifting and overburden sedimentation initiate salt diapirism; **Stage 2** (Late Jurassic) - oil and gas expulsion from the Early and Middle Jurassic source rocks, sedimentation rate, and high heat flow mobilized the salt diapirism; **Stage 3** (Early to Late Cretaceous) - oil expulsion from Jurassic Verrill canyon source rock, sedimentation rate, and high heat flow mobilized the basinward leaning diapir and formation of "hourglass" salt stocks (starting of sand bypassing to deeper slope); **Stage 4** (Early Tertiary) - oil expulsion from Jurassic and Cretaceous Verrill canyon source rocks, sedimentation rate, and moderate to high heat flow mobilized autochthonous salt body with allochthonous salt tongue canopy (complete sand bypassing to deeper slope); **Stage 5** (Late Teriary) - oil to gas cracking and expulsion, sedimentation rate, and moderate to low heat flow mobilized allochthonous salt tongues (sand bypassing to deeper slope still continues)

Figures
(one dimensional petroleum system modeling)

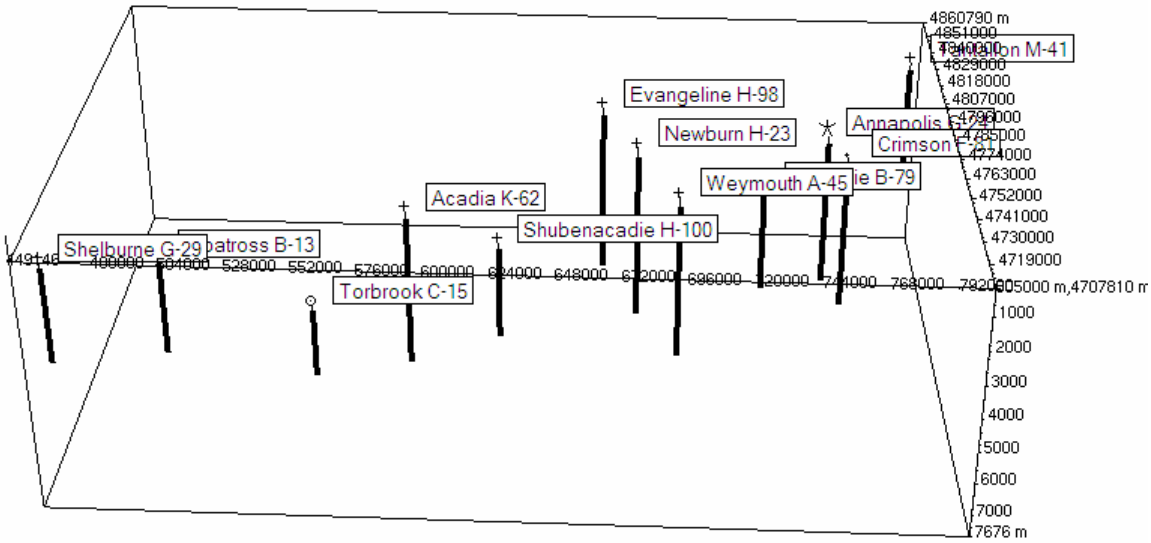

Figure 16. Well location of 12 wells (11 slope and one shelf) within the world co-ordinates of the Scotian Margin

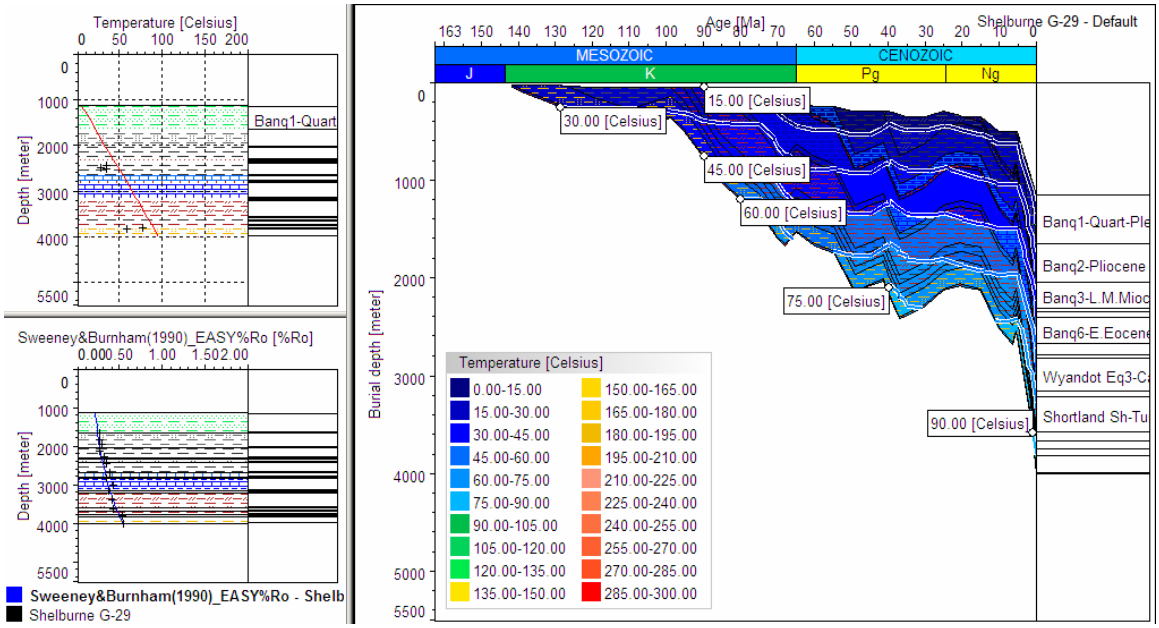

Figure 17a. Burial history of the Shelburne G-29 well with iso-temperature line and vitrinite reflectance and temperature versus depth plots

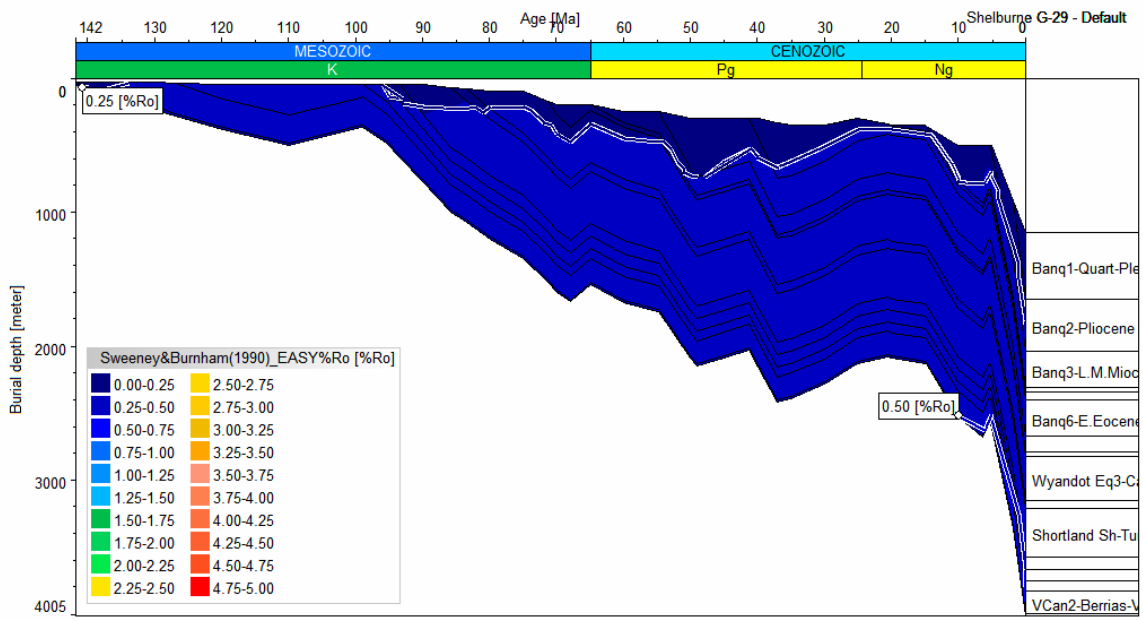

Figure 17b. Burial history of the Shelburne G-29 well with iso-maturity line

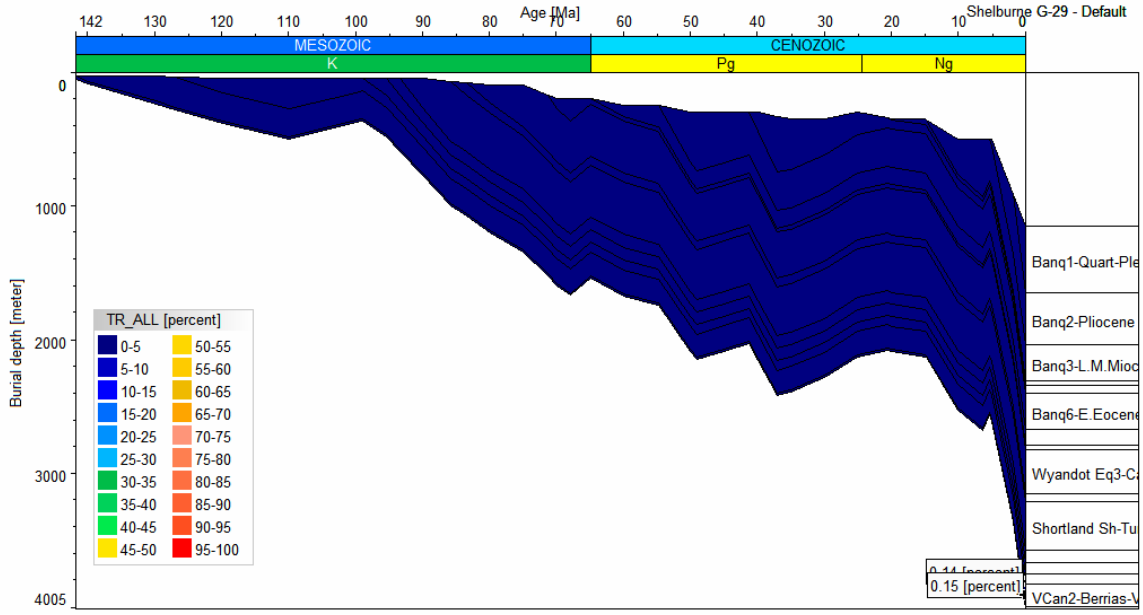

Figure 17c. Burial history of the Shelburne G-29 well with transformation ratio of oldest sedimentary unit (Roseway Member).

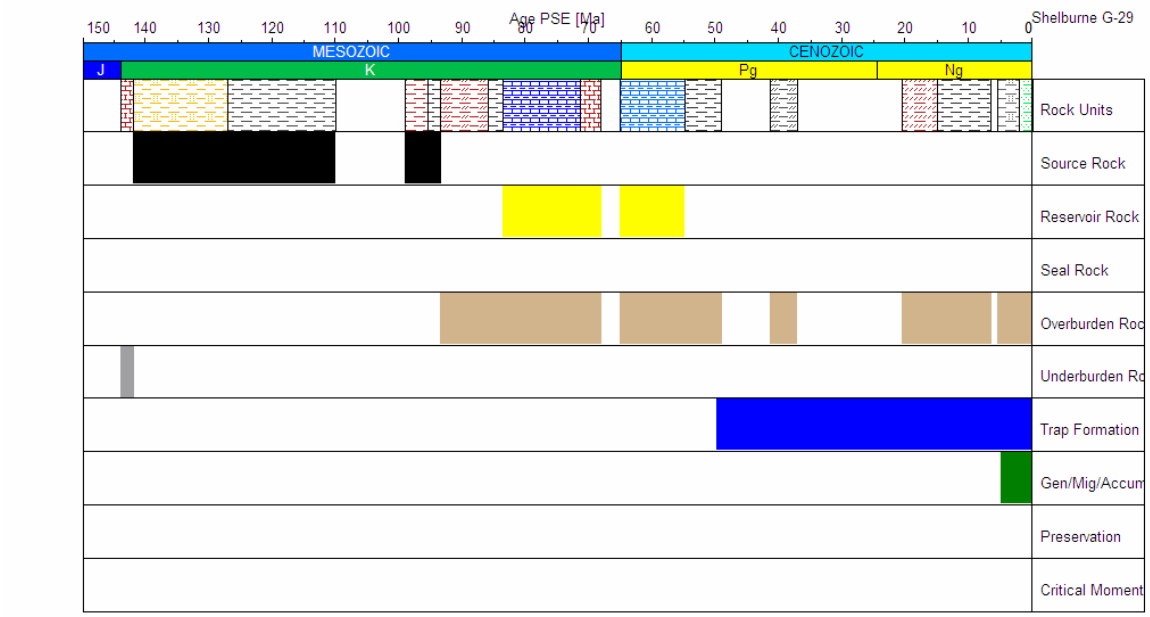

Figure 17d. Petroleum system events chart of the Shelburne G-29 well. Note that the "Critical Moment" has not yet been reached in this well.

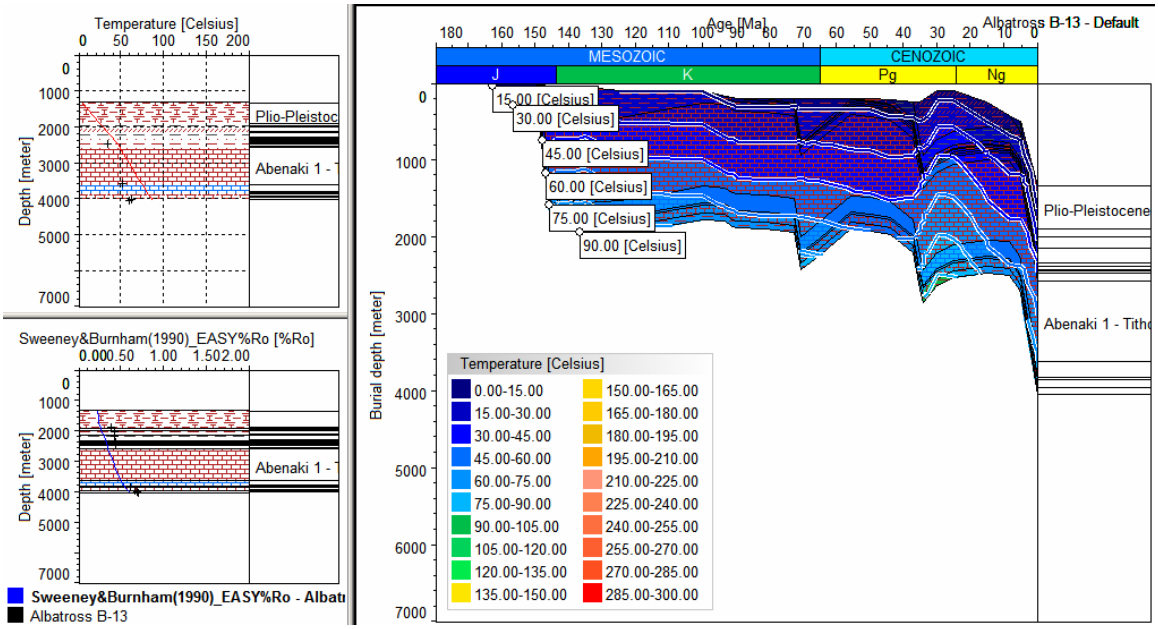

Figure 18a. Burial history of the Albatross B-13 well with iso-temperature line on the right hand side and vitrinite reflectance and temperature versus depth plots on the left hand side

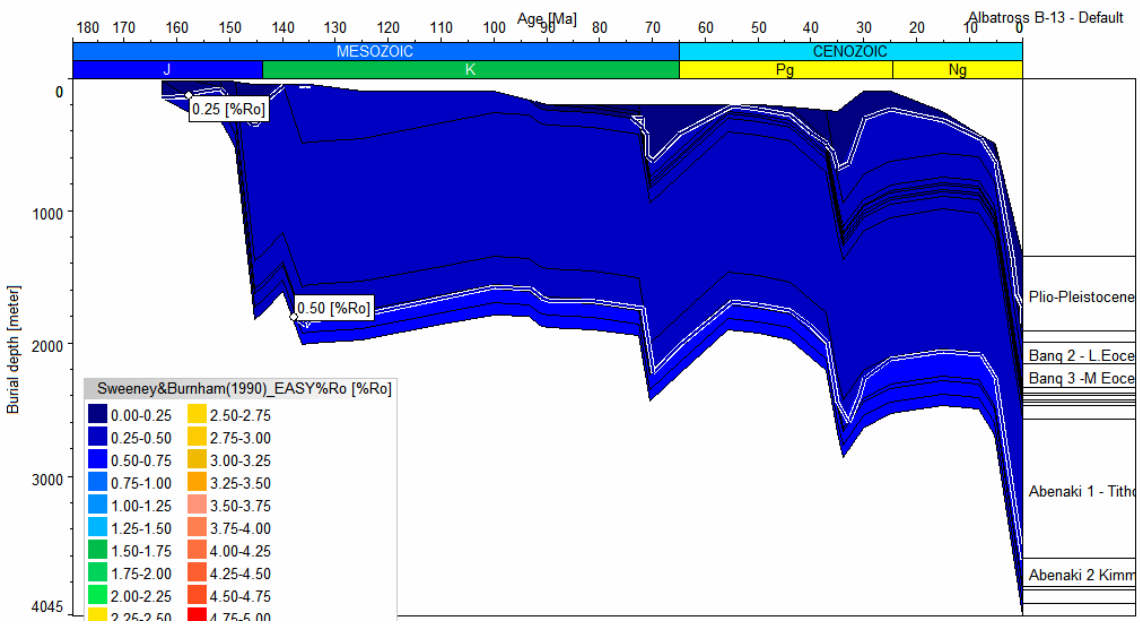

Figure 18b. Burial history of the Albatross B-13 well with iso-maturity line

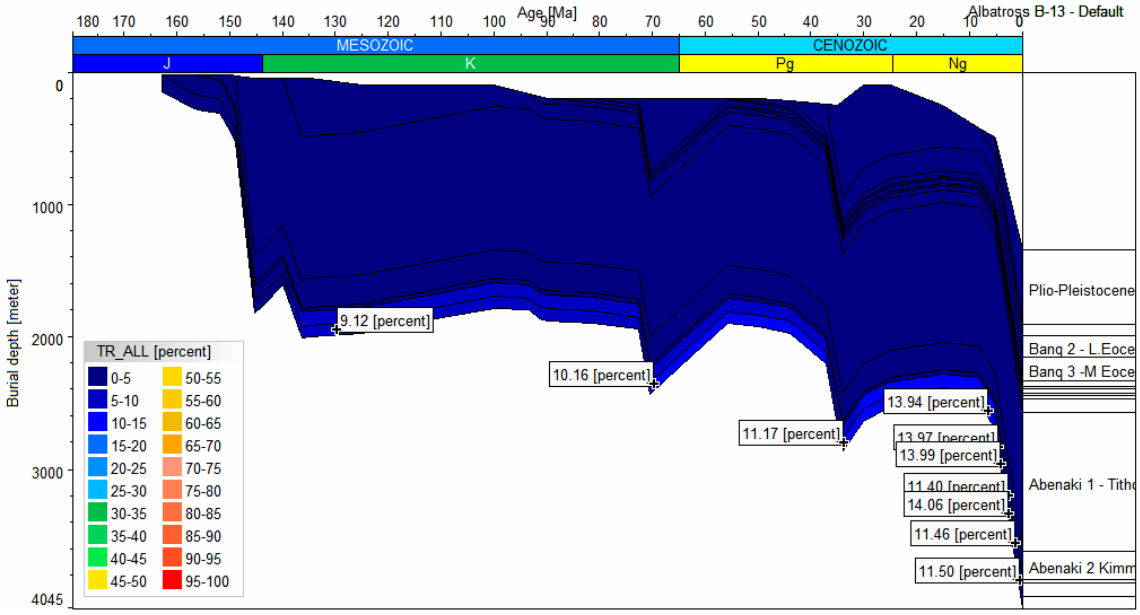

Figure 18c. Burial history of the Albatross B-13 well with hydrocarbon transformation ratios

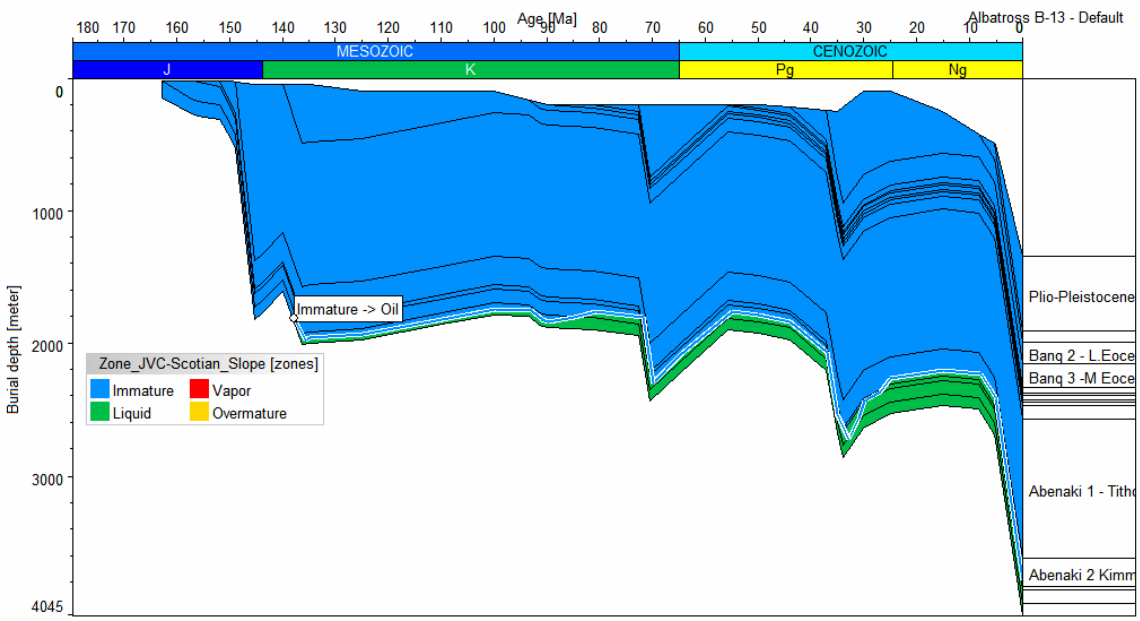

Figure 18d. Burial history of the Albatross B-13 well with iso-hydrocarbon zone line

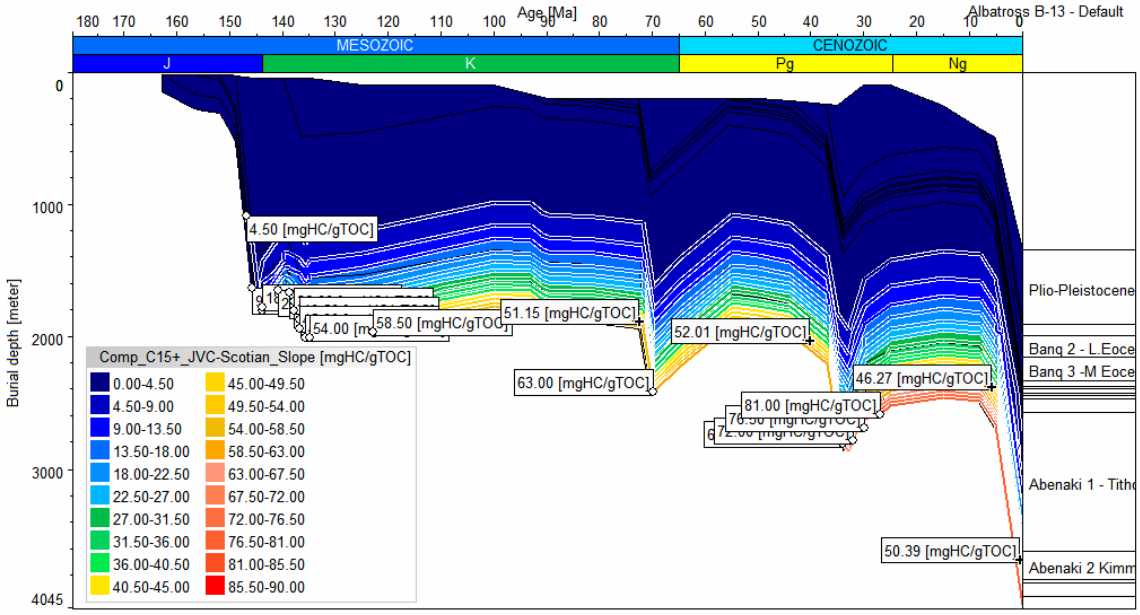

Figure 18e. Burial history of the Albatross B-13 well with amounts of oil (C15+) generation isolines

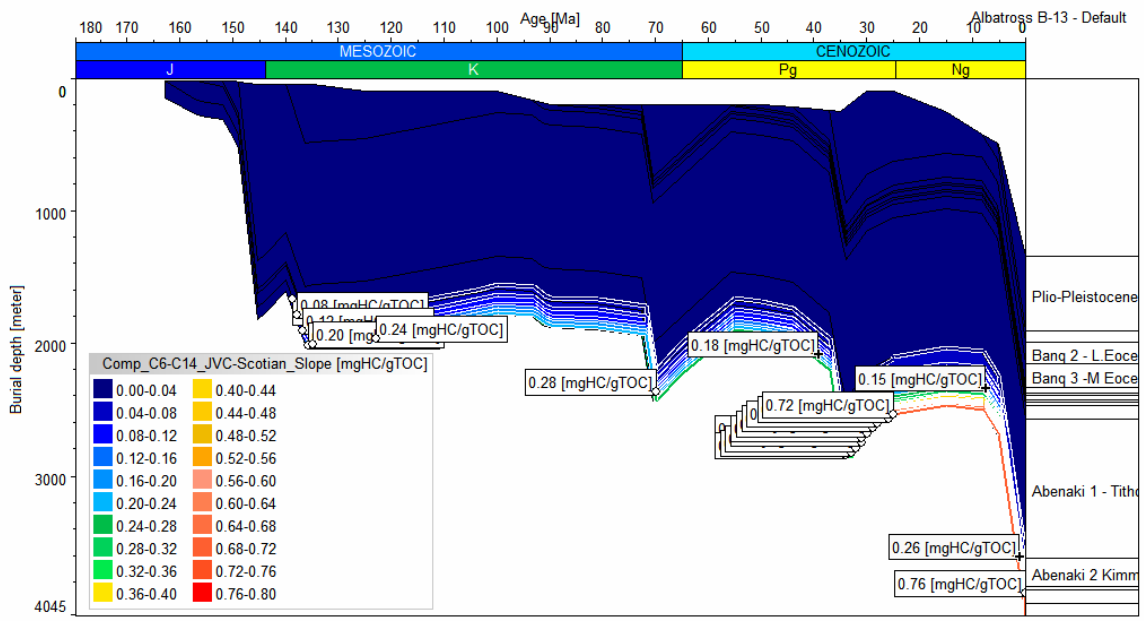

Figure 18f. Burial history of the Albatross B-13 well with light oil and condensate (C6-C14) generation isolines

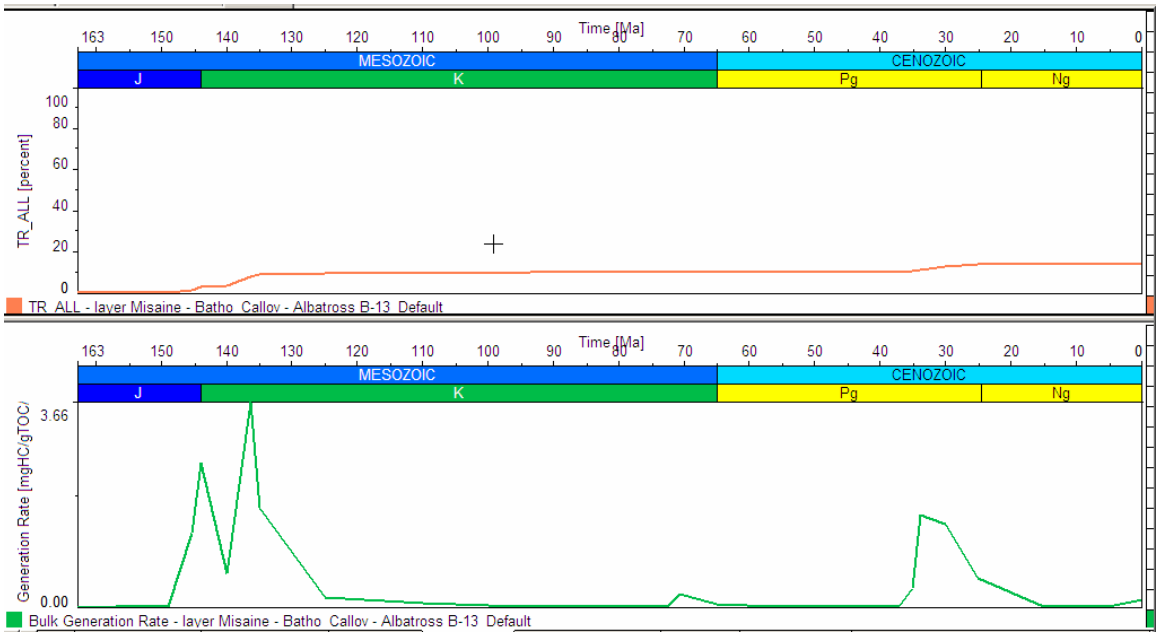

Figure 18g. Transformation ratio and bulk generation rate of the Misaine Member from the Albatross B-14 well

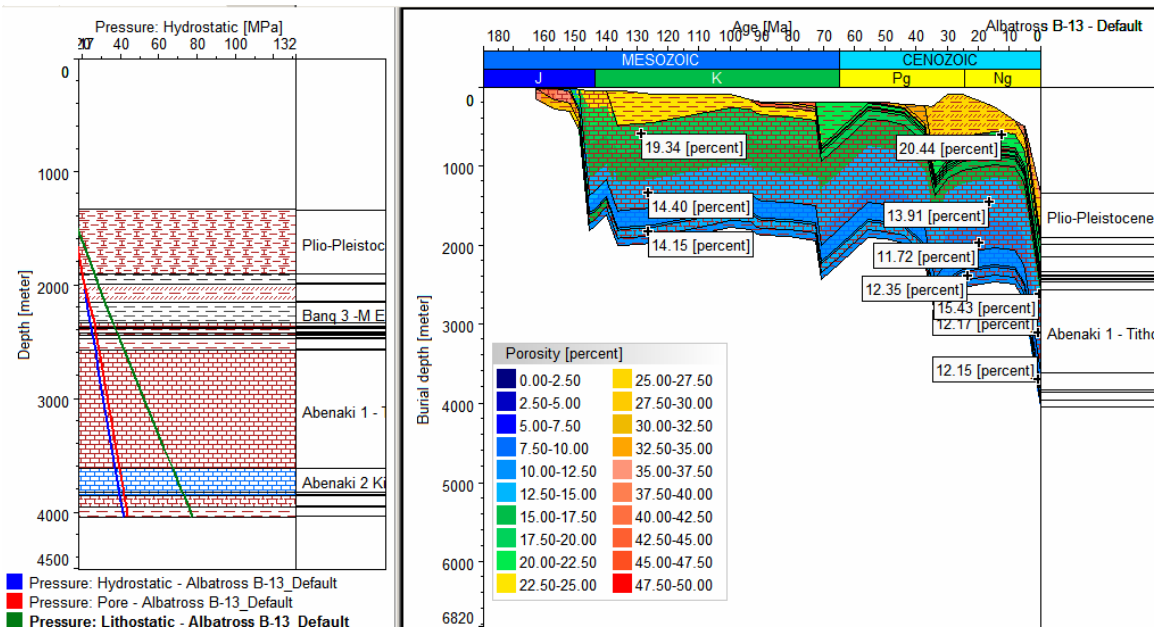

Figure 18h. Burial history of the Albatross B-13 well with porosity data on the right and various pressure versus depth plot on the left side of the figure.

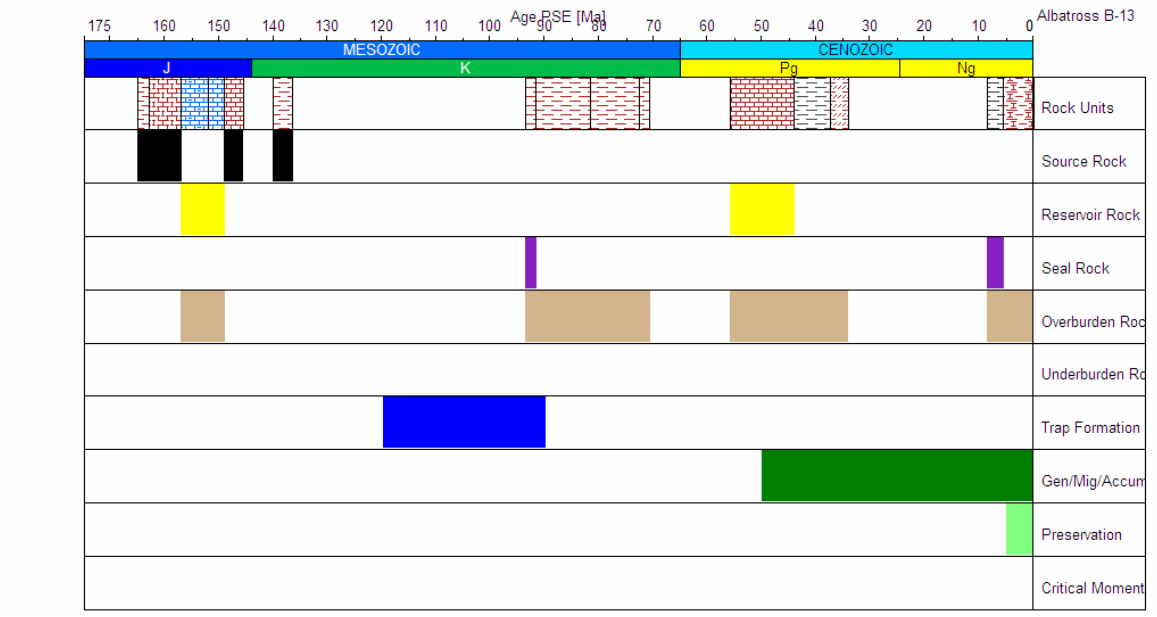

Figure 18i. Petroleum system events chart of the Albatross B-13 well. Note that the "Critical Moment" has not yet been reached in this well.

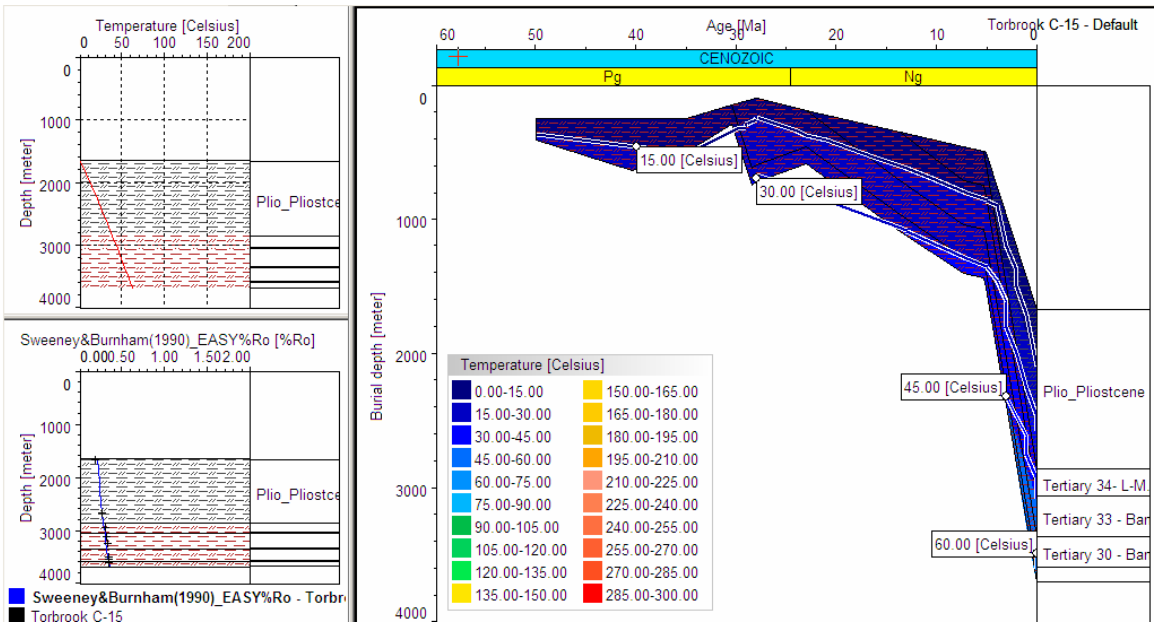

Figure 19a. Burial history of the Torbrook C-15 well with iso-temperature line on the right and vitrinite reflectance and temperature versus depth plots on the left side of the figure

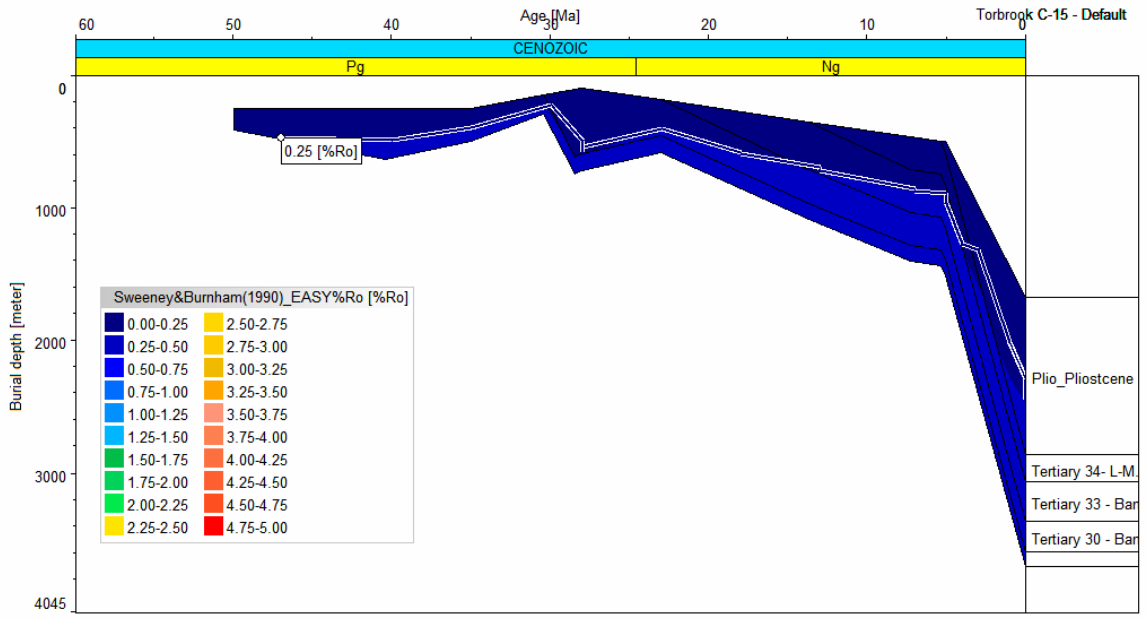

Figure 19b. Burial history of the Torbrook C-15 well with iso-maturity line

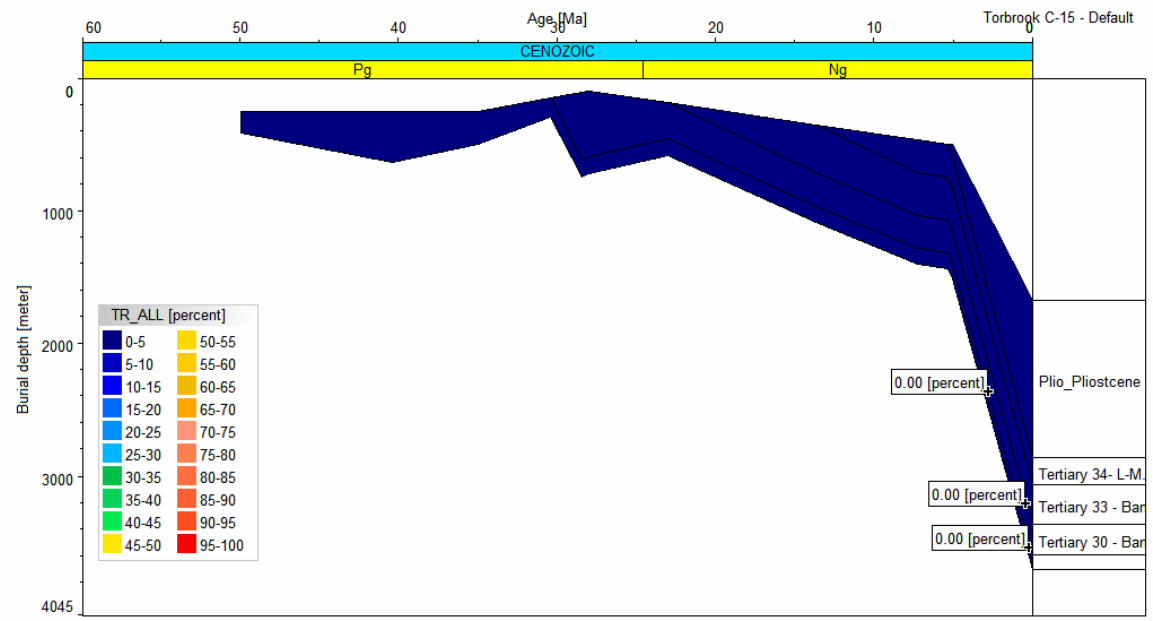

Figure 19c. Burial history of the Torbrook C-15 well with transformation ratio for lower source rock

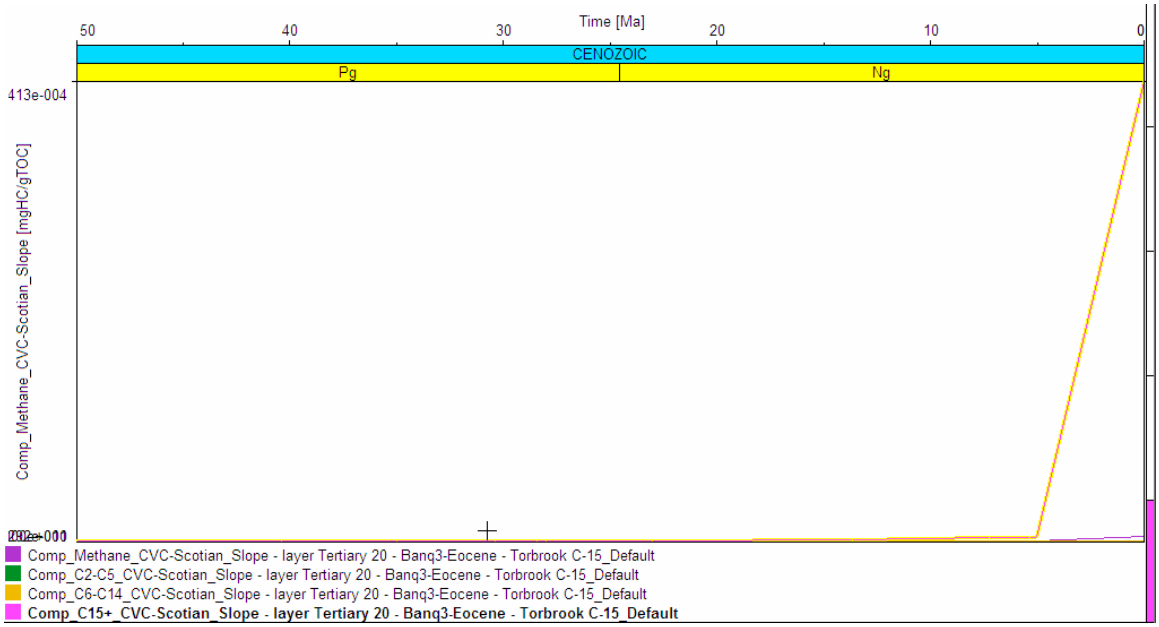

Figure 19d. Hydrocarbon (C15+) generation for lower source rock (Tertiary 20 layer of the Banquereau Formation)

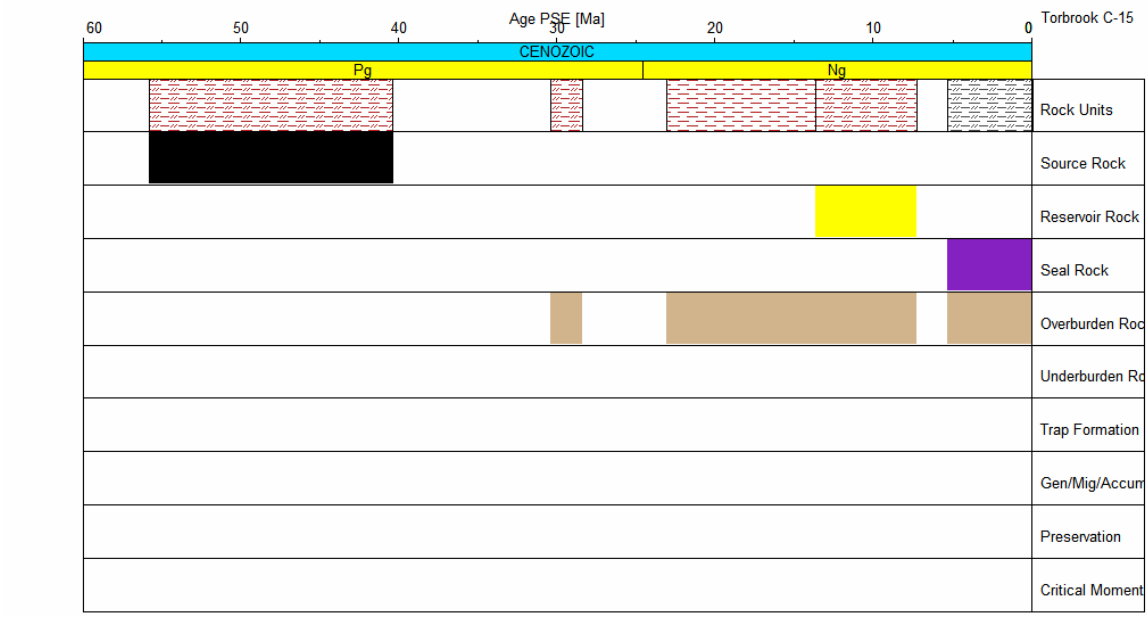

Figure 19e. Petroleum system events chart of the Torbrook C-15 well. Note that the "Critical Moment" has not yet been reached in this well.

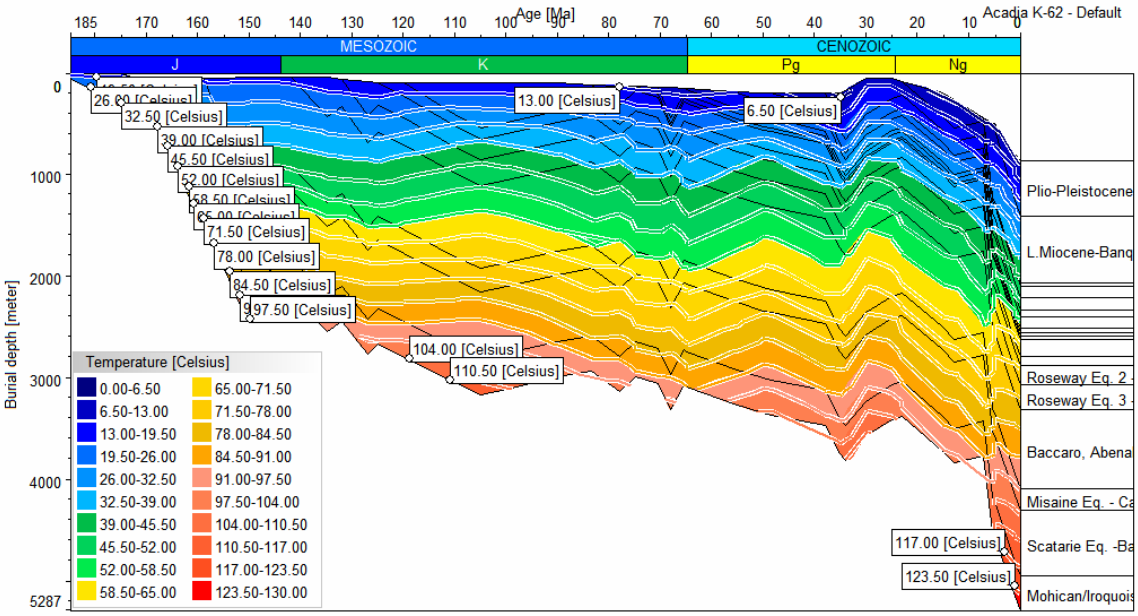

Figure 20a. Burial history of the Acadia K-62 well with iso-temperature line

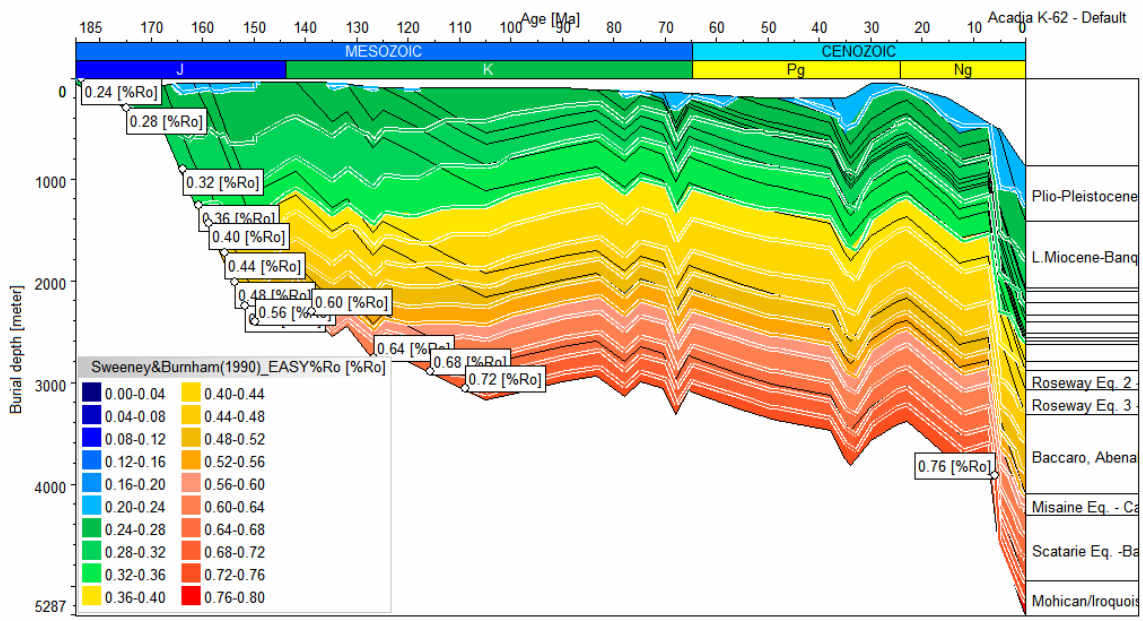

Figure 20b. Burial history of the Acadia K-62 well with iso-maturity line

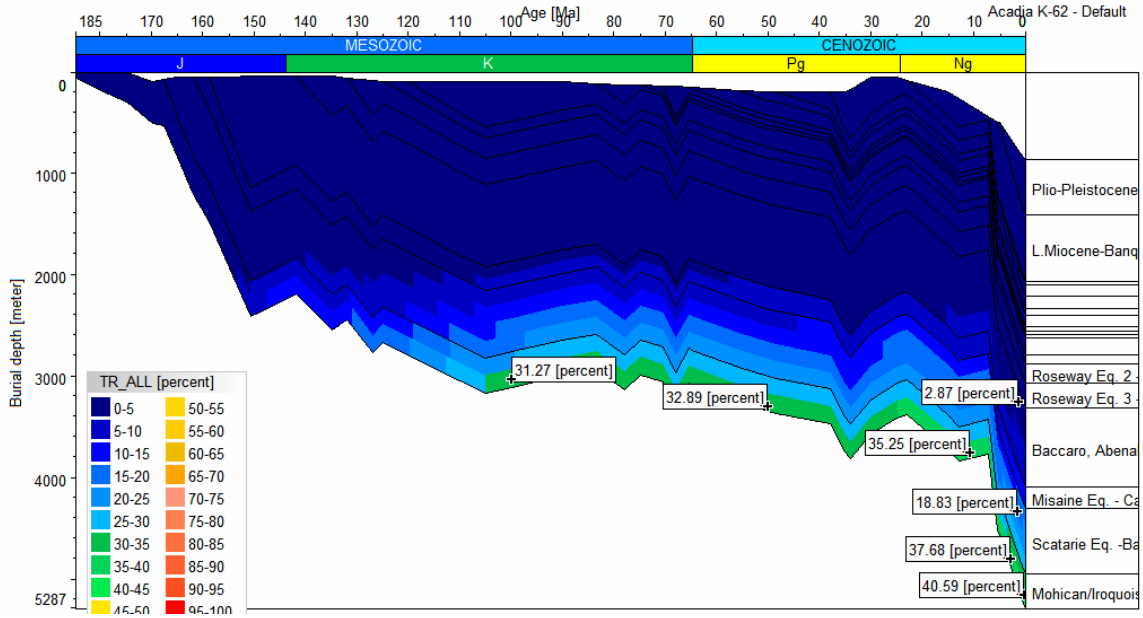

Figure 20c. Burial history of the Acadia K-62 well with transformation ratio of the source rocks from the Mohican Formation and Misaine Member)

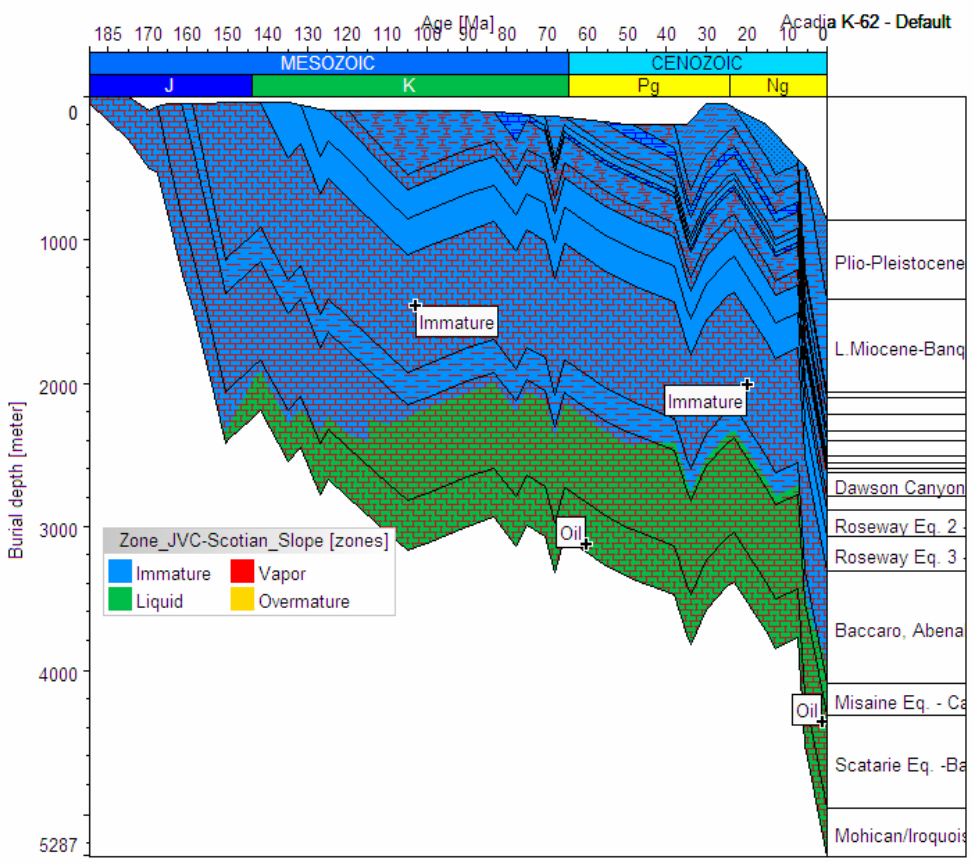

Figure 20d. Burial history of the Acadia K-62 well with iso-hydrocarbon zone lines.

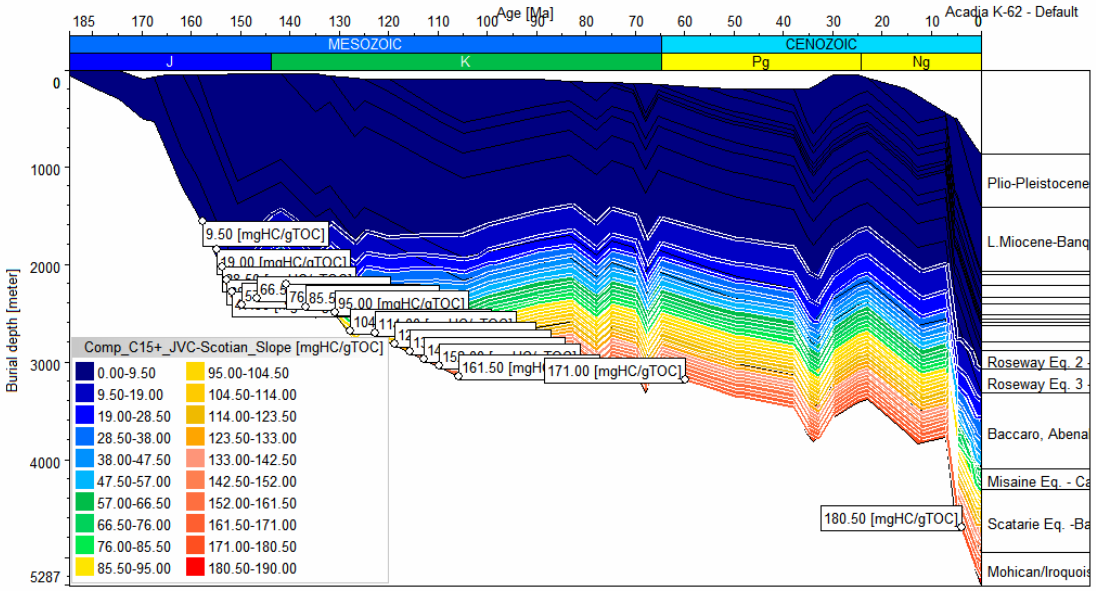

Figure 20e. Burial history of the Acadia K-62 well with C15 + (oil) hydrocarbon generation iso-lines from the Mohican Formation source rock using Jurassic Verrill Canyon multi-component kinetics.

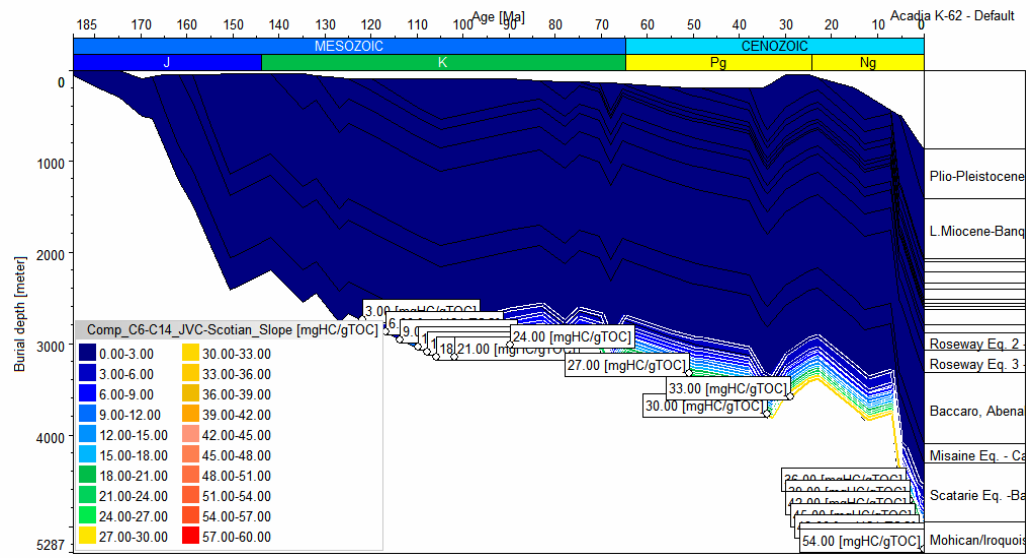

Figure 20f. Burial history of the Acadia K-62 well with C6-C14 (light oil and condensate) hydrocarbon generation isolines from the Mohican Formation and Misaine/Roseway Member source rocks using Jurassic Verrill Canyon multi-component kinetics.

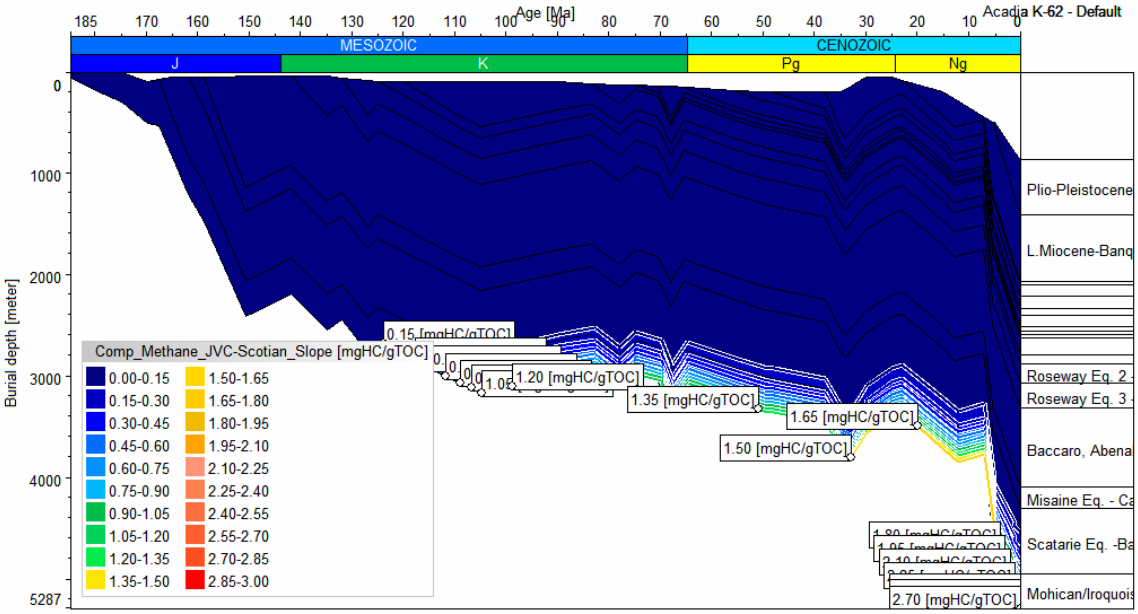

Figure 20g. Burial history of the Acadia K-62 well with methane generation from the Mohican Formation and Misaine Member source rocks using Jurassic Verrill Canyon multi-component kinetics.

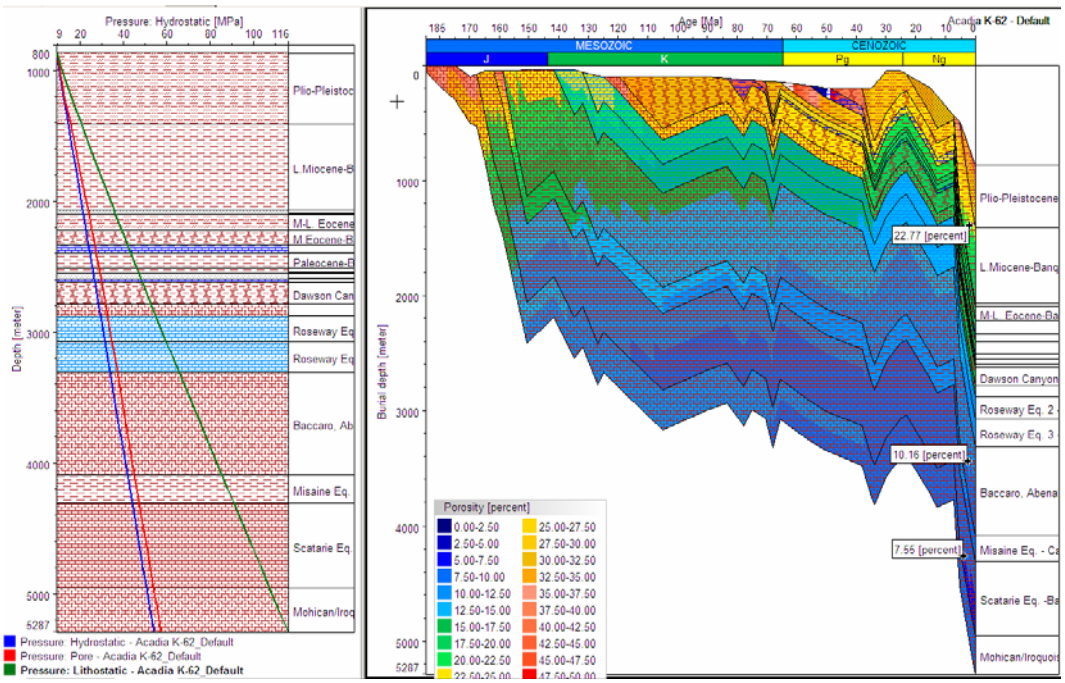

Figure 20h. Burial history of the Acadia K-15 well with porosity values on the right and various pressures versus depth plot on the left.

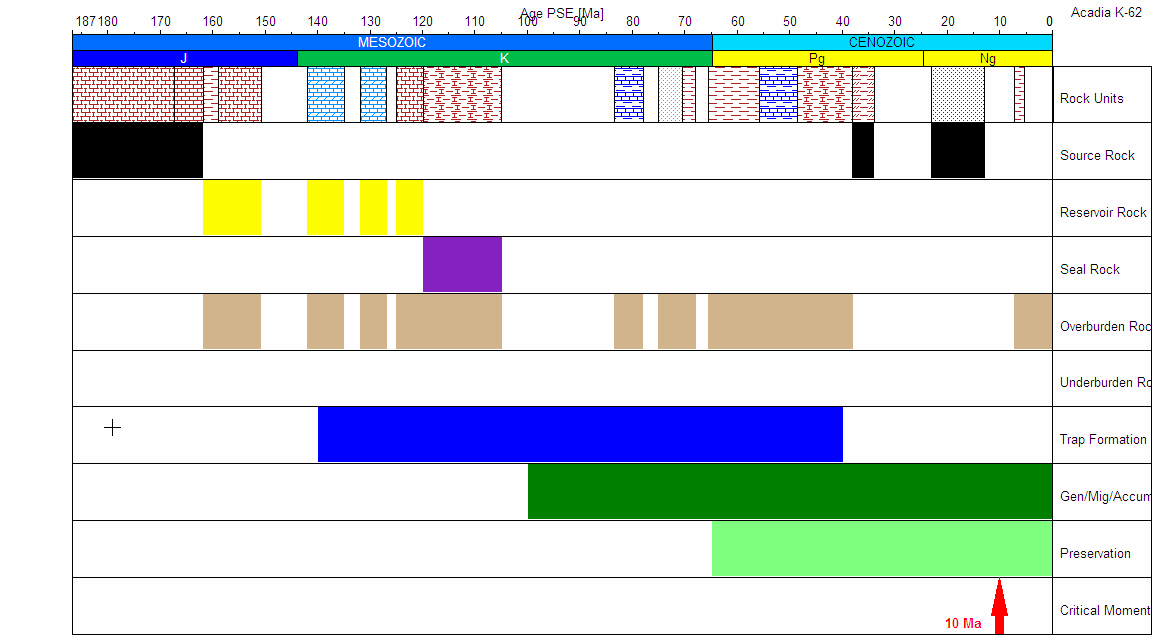

Figure 20i. Petroleum system events chart of the Acadia K-62 well with “Critical Moment” of hydrocarbon emplacement

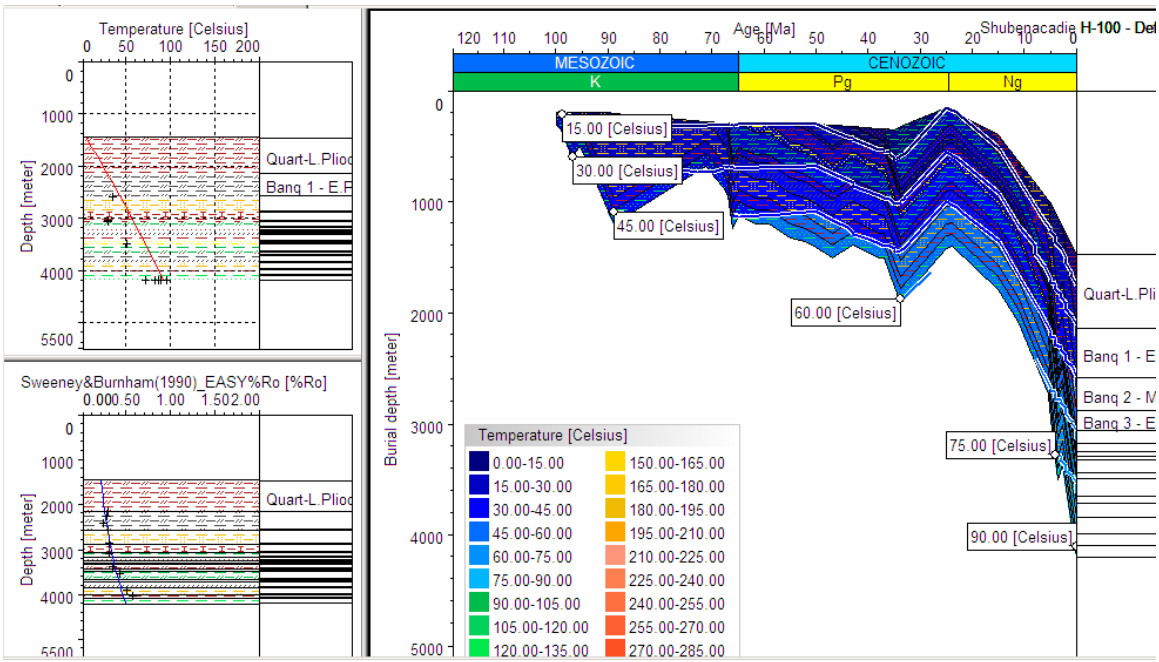

Figure 21a. Burial history of the Shubenacadie H-100 well with iso-temperature lines on the right and temperature or reflectance versus depth plots on the right

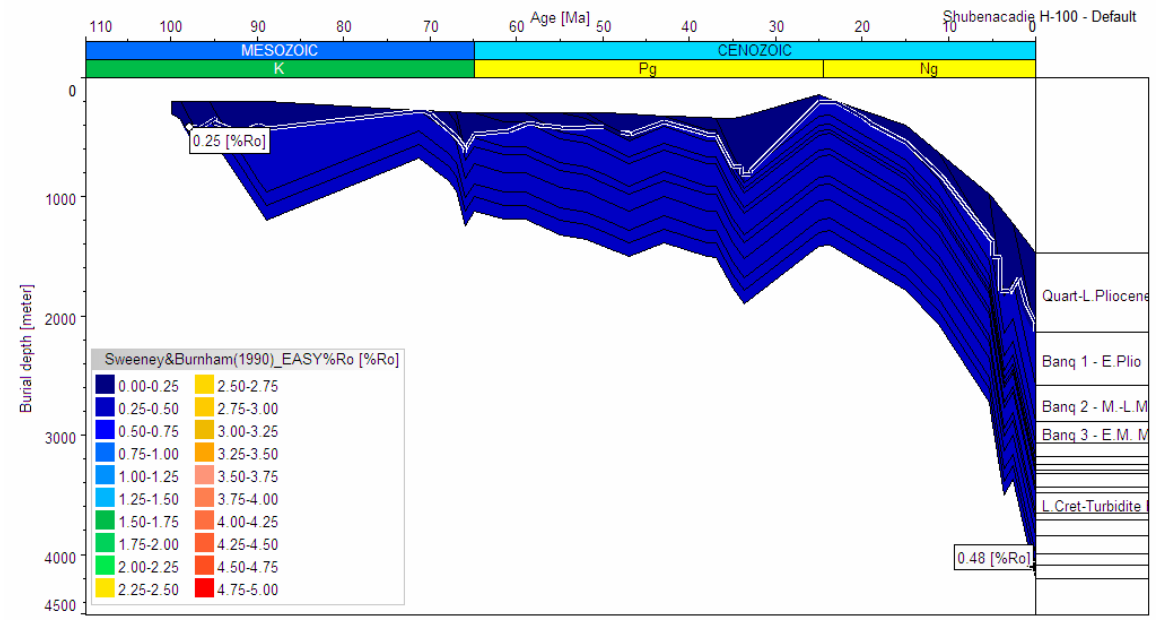

Figure 21b. Burial history of the Shubenacadie H-100 well with iso-maturity lines

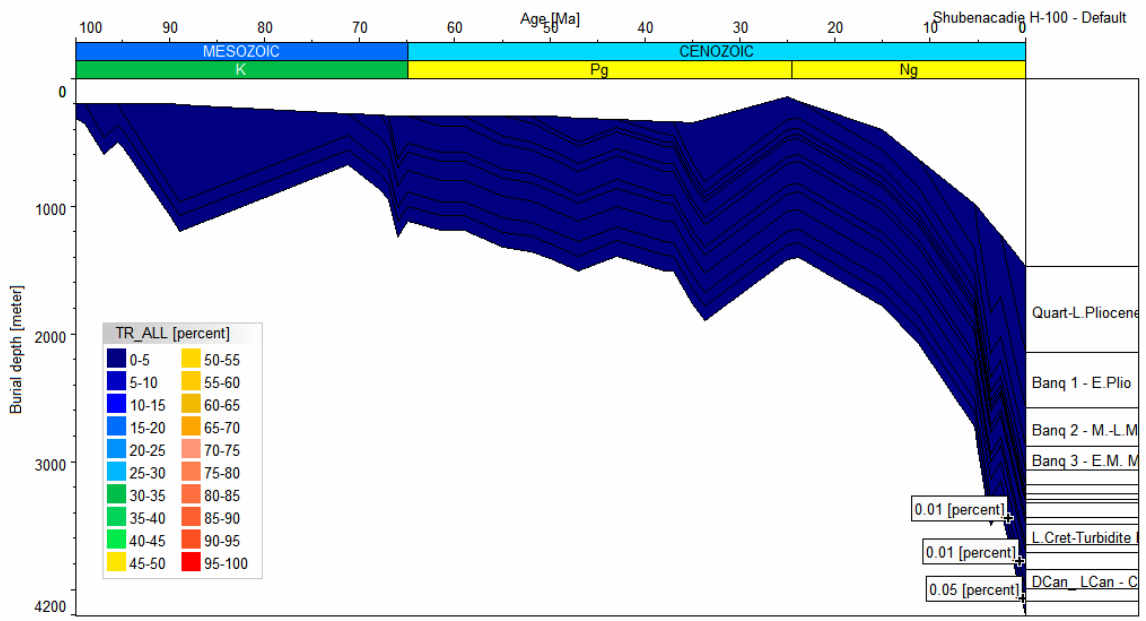

Figure 21c. Burial history of the Shubenacadie H-100 well with iso-tranformation ratio lines

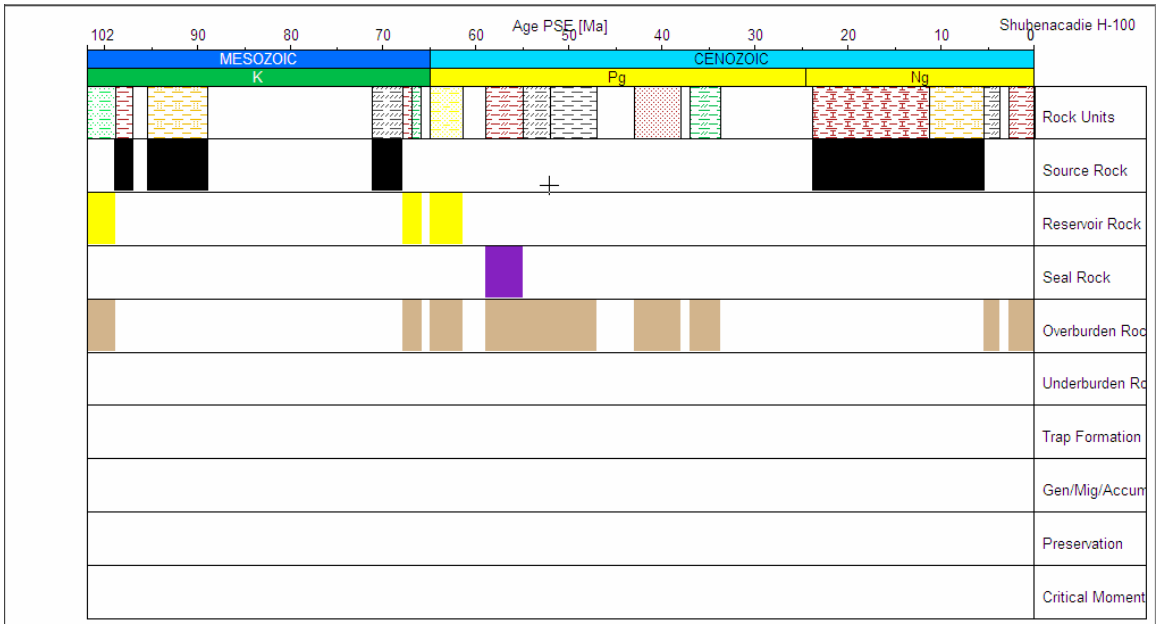

Figure 21d. Petroleum system events chart of the Shubenacadie H-100 well. Note that the "Critical Moment" has not yet been reached in this well.

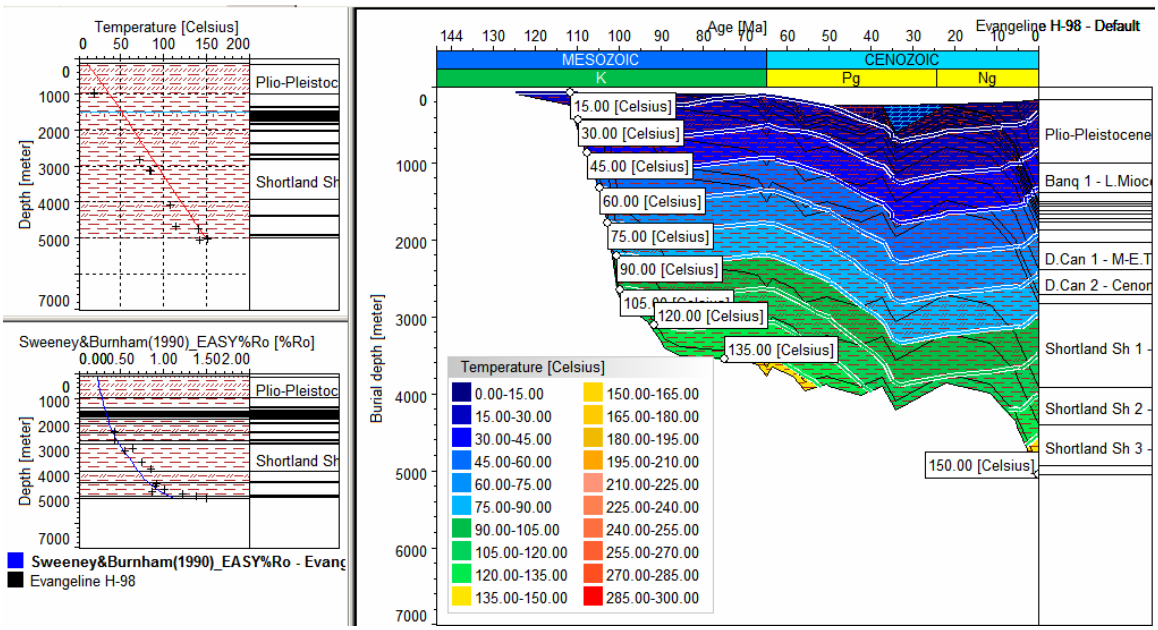

Figure 22a. Burial history of the Evangeline H-98 well with iso-temperature lines on the right and temperature or reflectance versus depth plots on the right

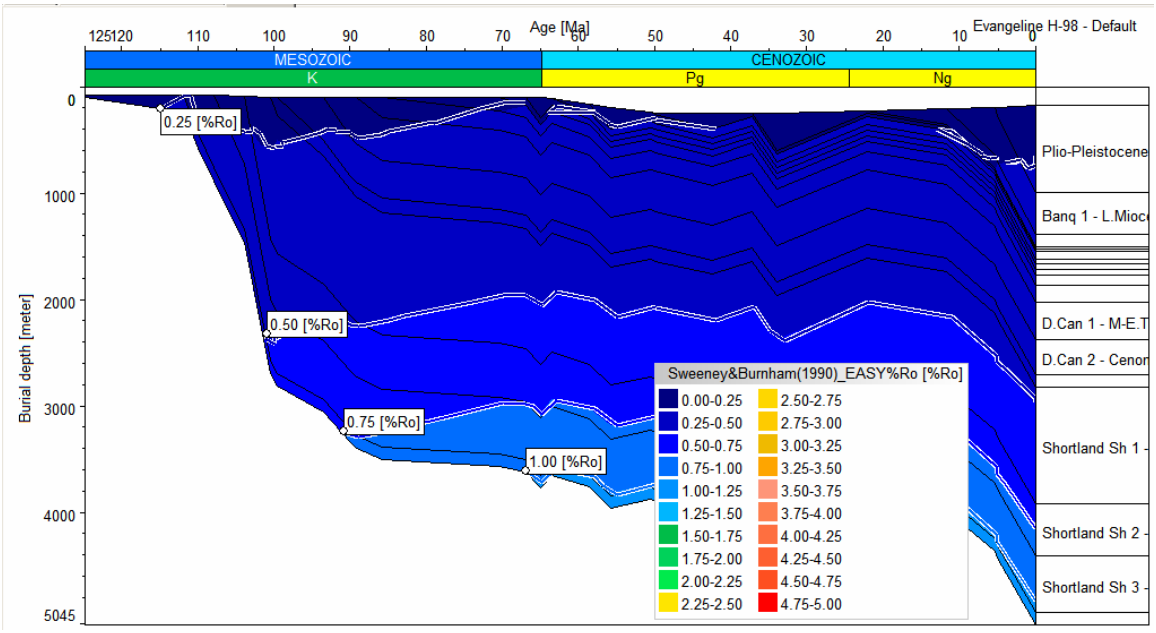

Figure 22b. Burial history of the Evangeline H-98 well with iso-maturity lines

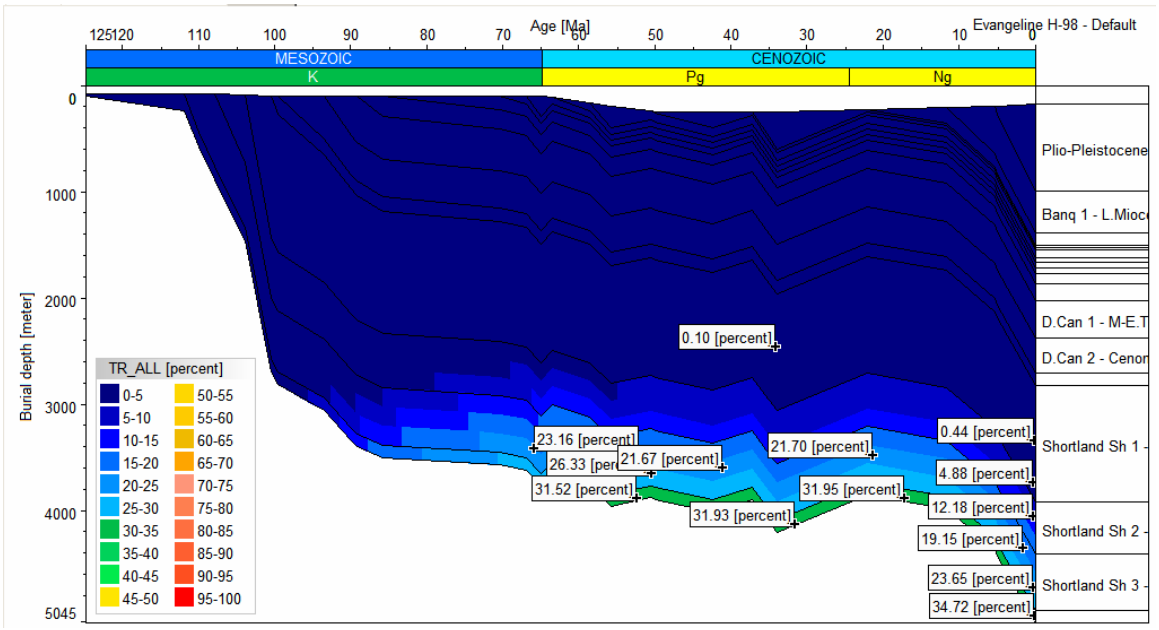

Figure 22c. Burial history of the Evangeline H-98 well with hydrocarbon iso-transformation ratio lines and values from various source rocks

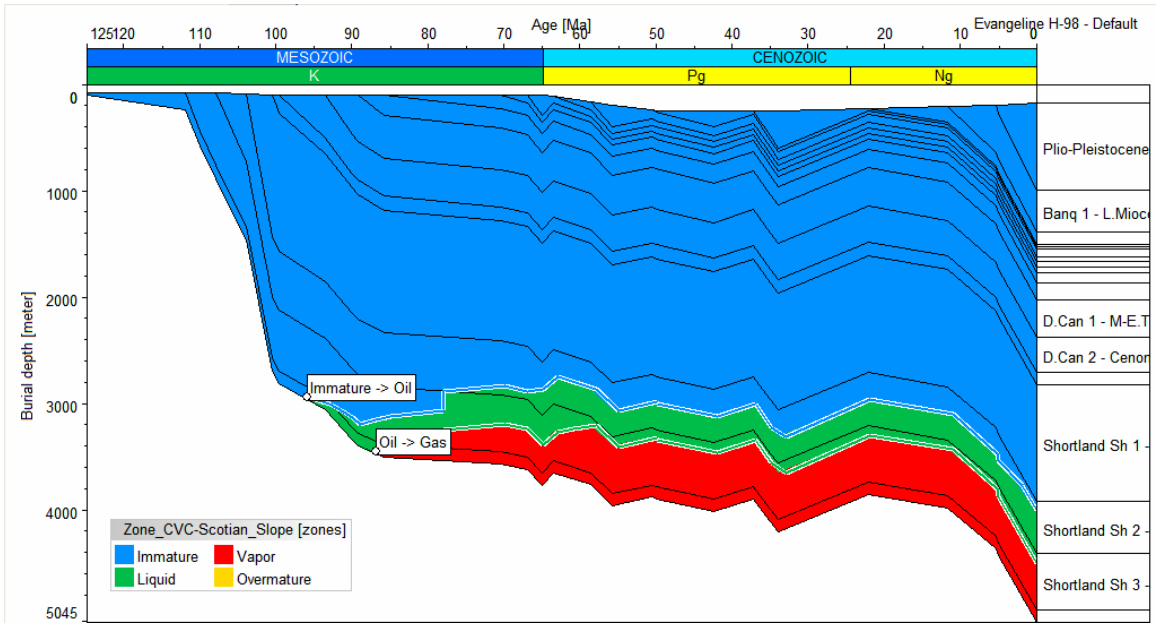

Figure 22d. Burial history of the Evangeline H-98 well with iso-hydrocarbon generation lines (immature, liquid, vapour, and overmature)

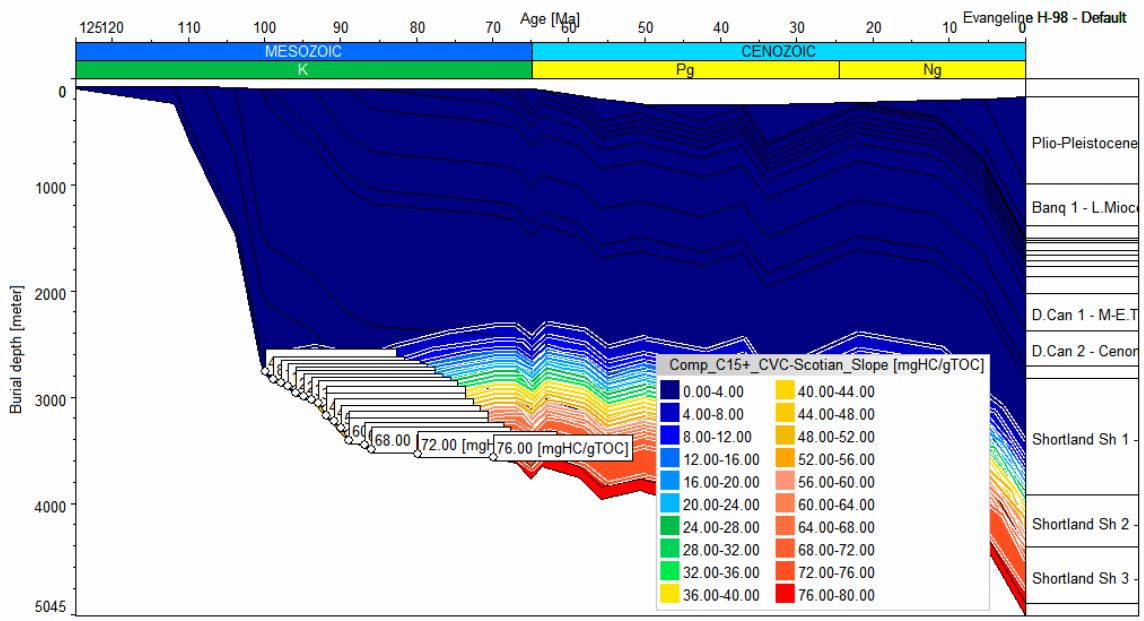

Figure 22e. Burial history of the Evangeline H-98 well with iso-oil generation lines for various Shortland Shale source rocks

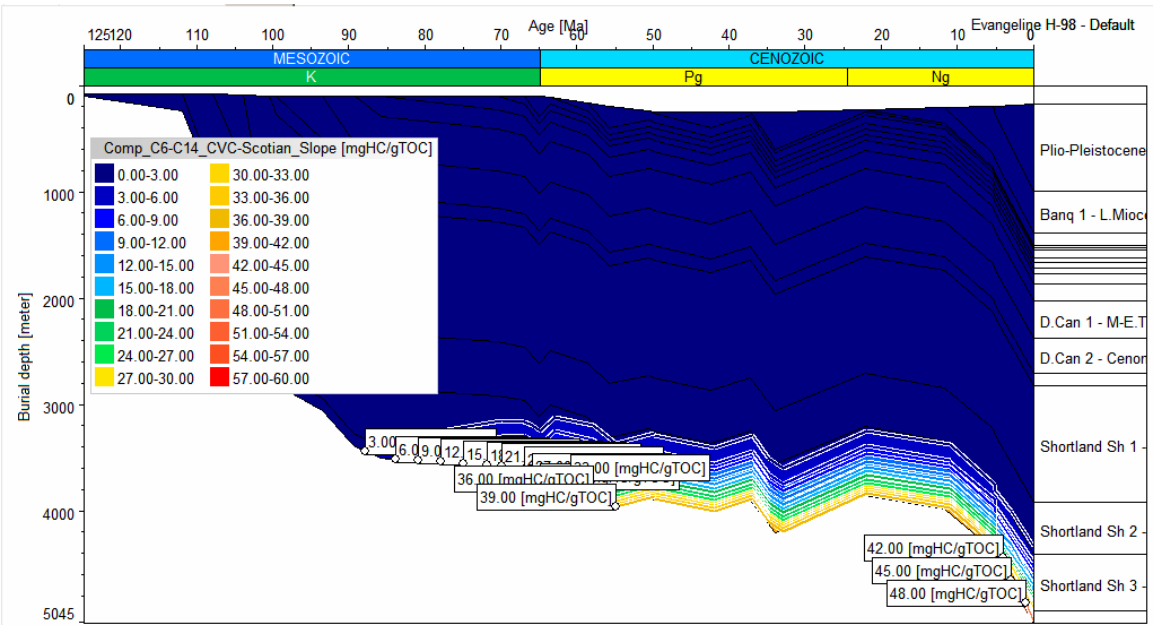

Figure 22f. Burial history of the Evangeline H-98 well with iso-light oil and condensate generation lines for various Shortland Shale source rocks

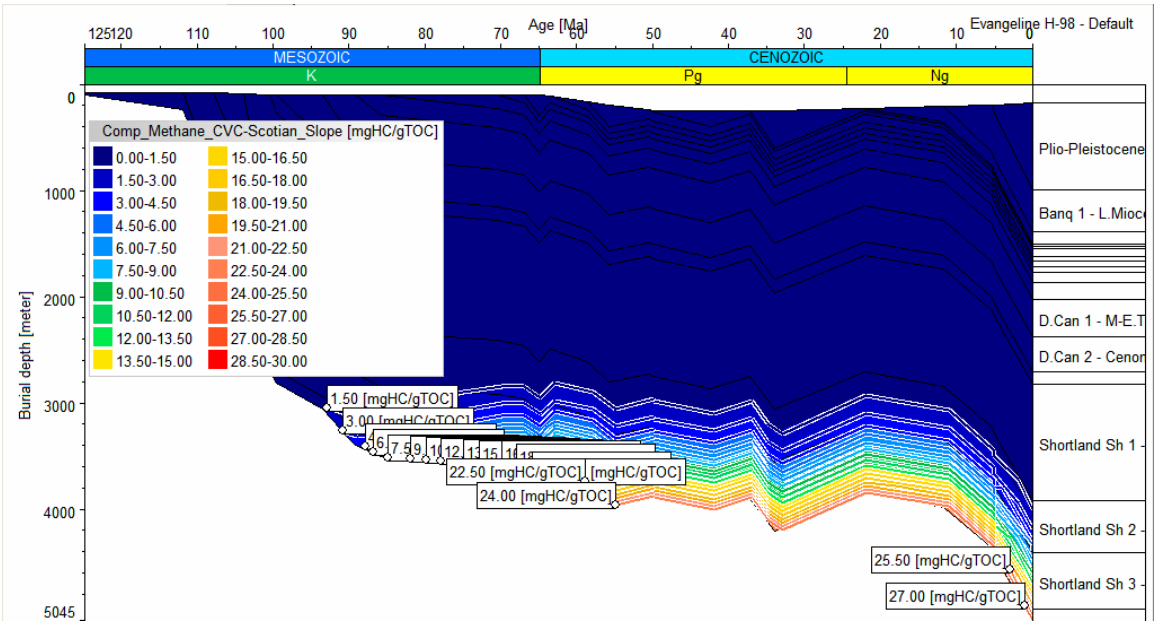

Figure 22g. Burial history of the Evangeline H-98 well with iso-methane generation lines for various Shortland Shale source rocks from primary cracking

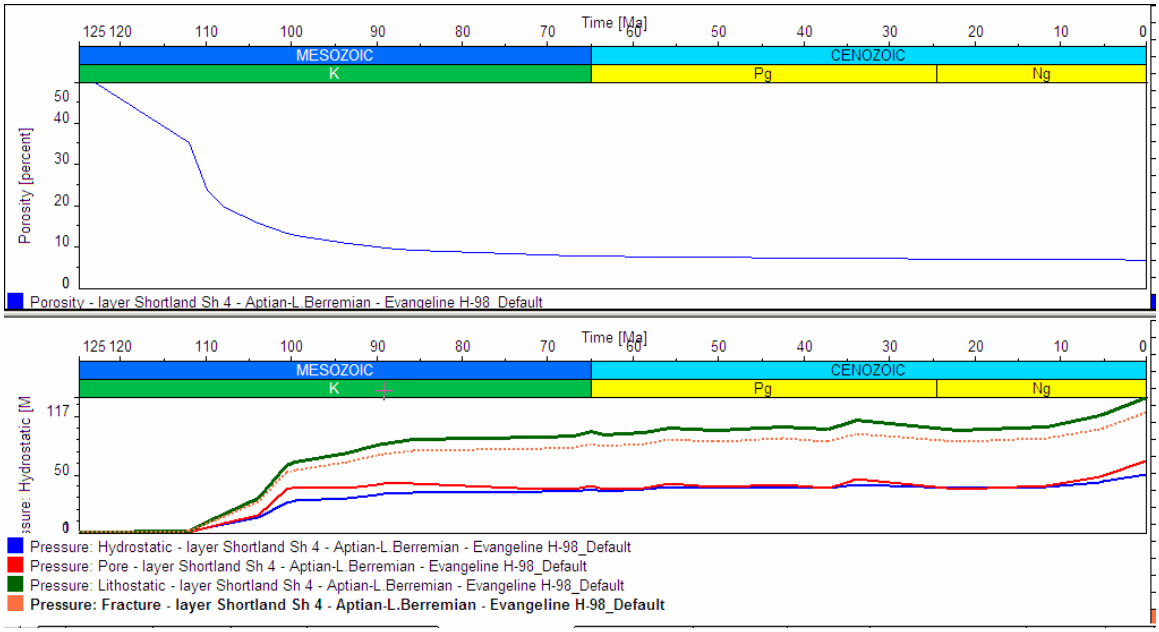

Figure 22h. Porosity and pressure trends of various Shortland Shale source rocks from the Evangeline H-98 well through geological time

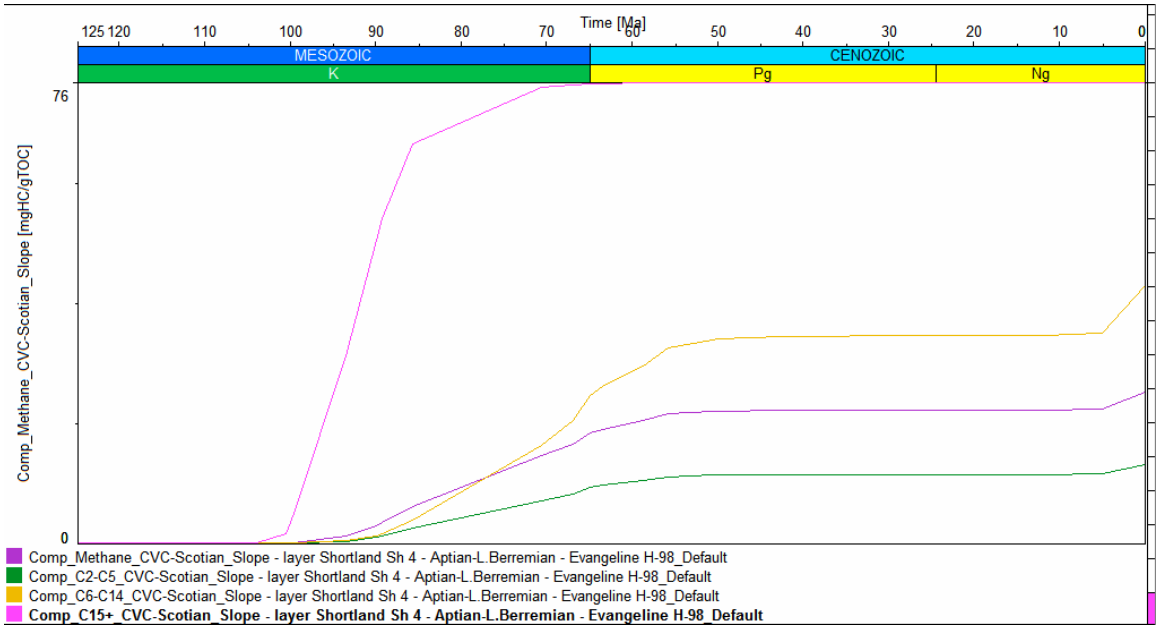

Figure 22i. Various hydrocarbon component expulsion trends through geological time of various Shortland Shale 4 source rock from the Evageline H-98 well

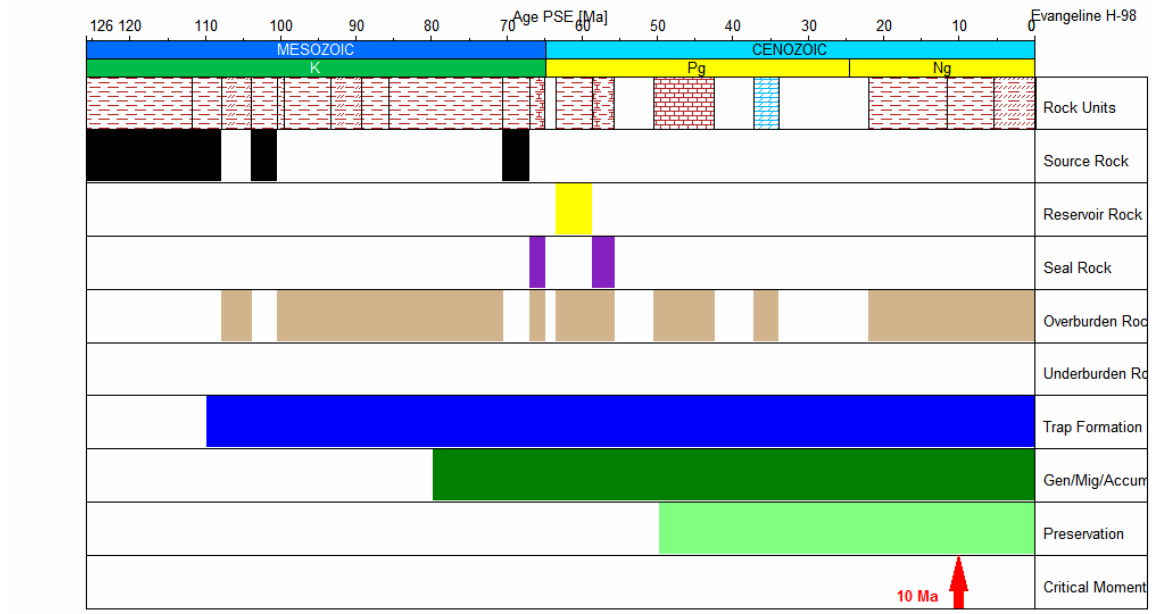

Figure 22j. Petroleum system events chart of the Evangeline H-98 well with “Critical Moment” of hydrocarbon emplacement

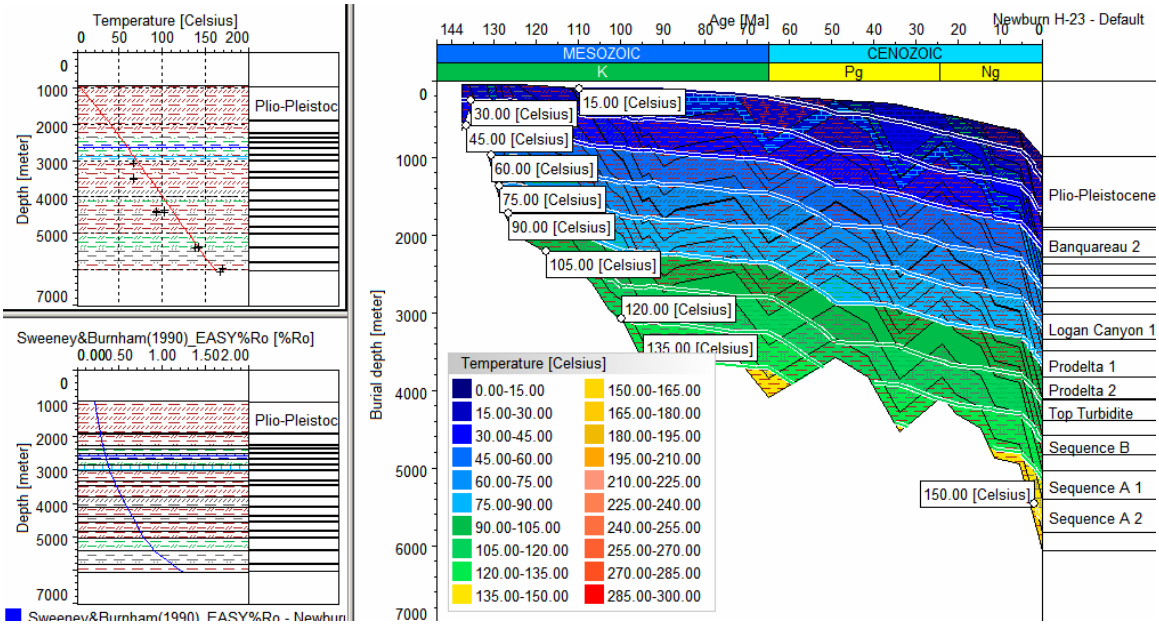

Figure 23a. Burial history of the Newburn H-23 well with iso-temperature lines on the right and temperature or reflectance versus depth plots on the right

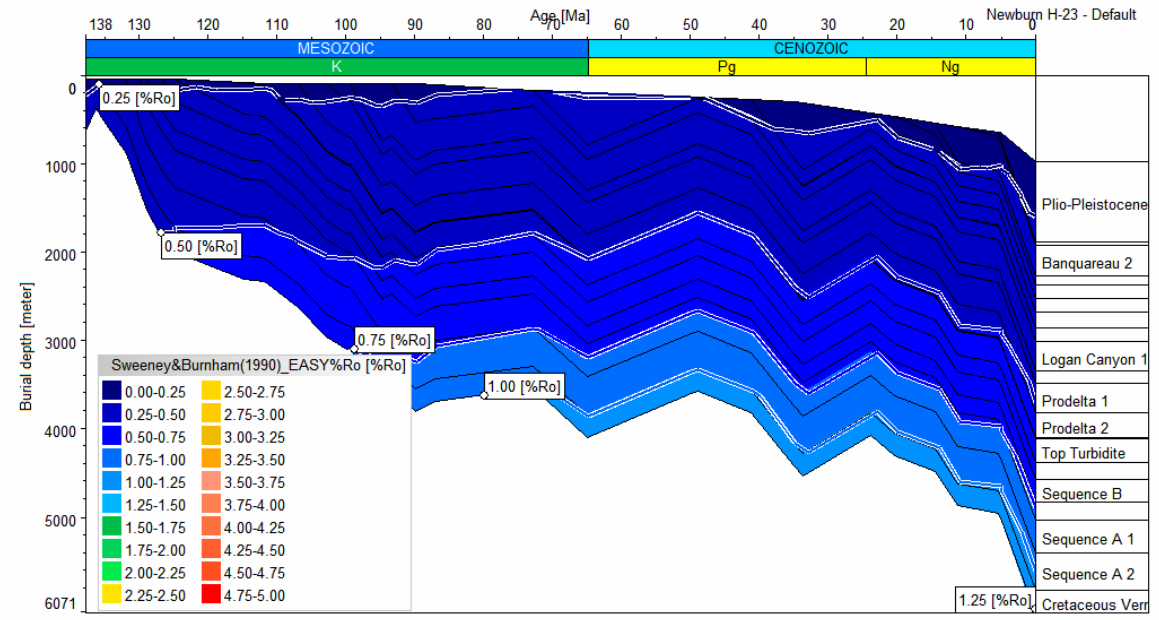

Figure 23b. Burial history of the Newburn H-23 well with iso-maturity lines

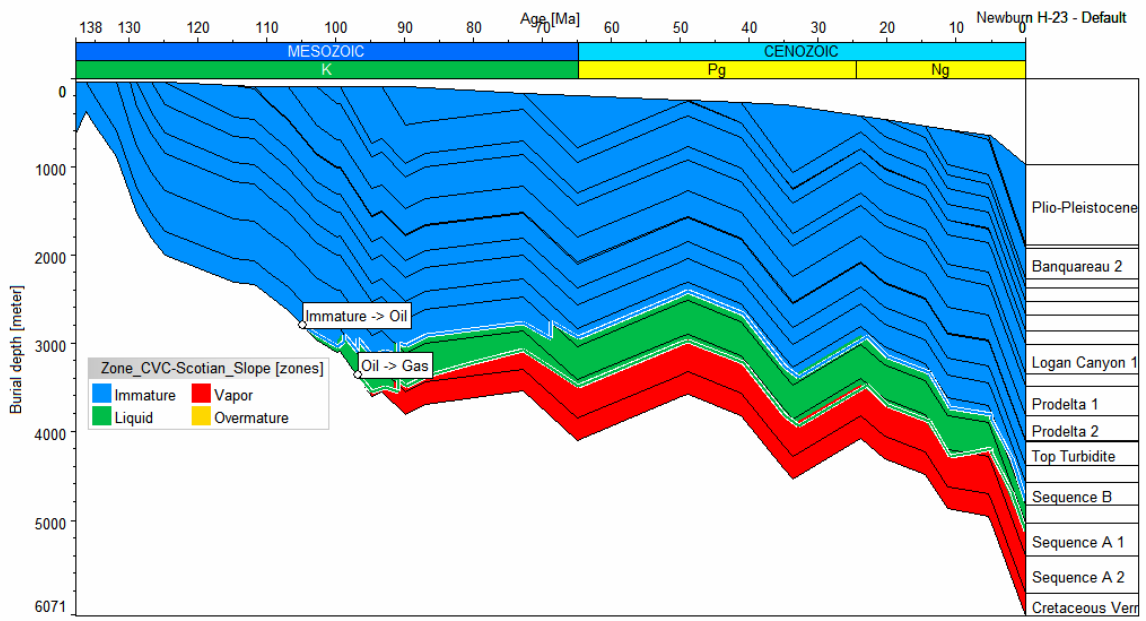

Figure 23c. Burial history with iso-hydrocarbon zones (immature, liquid, vapor, and overmature) for the Newburn H-23 well

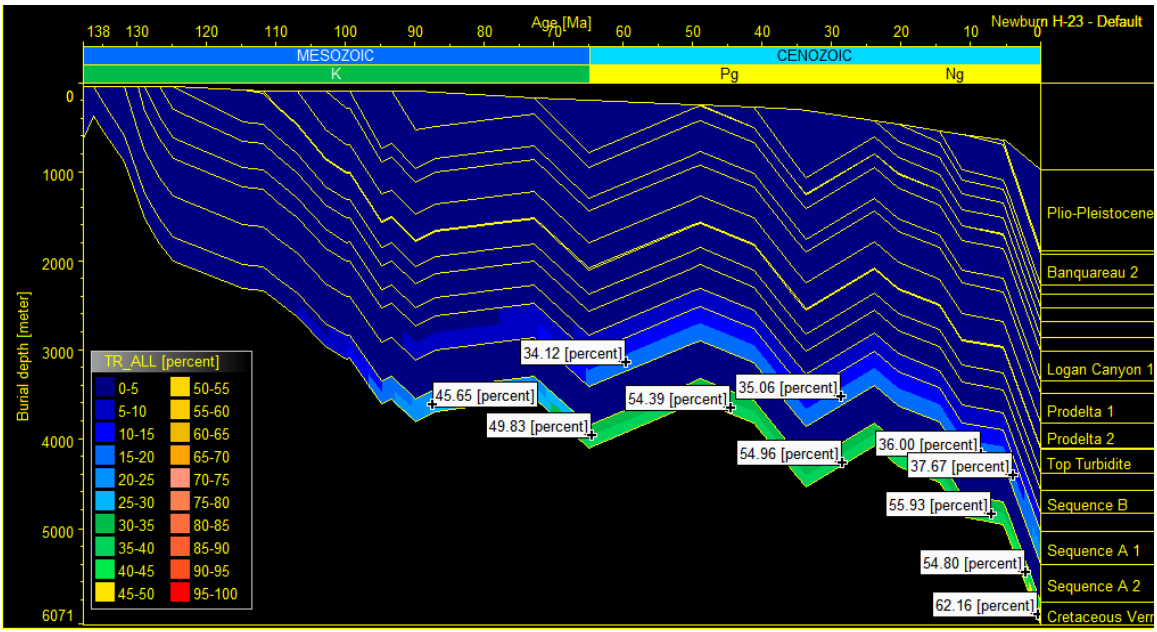

Figure 23d. Burial history of the Newburn H-23 well with iso-hydrocarbon transformation ratio trend lines from various Cretaceous Verrill Canyon source rock

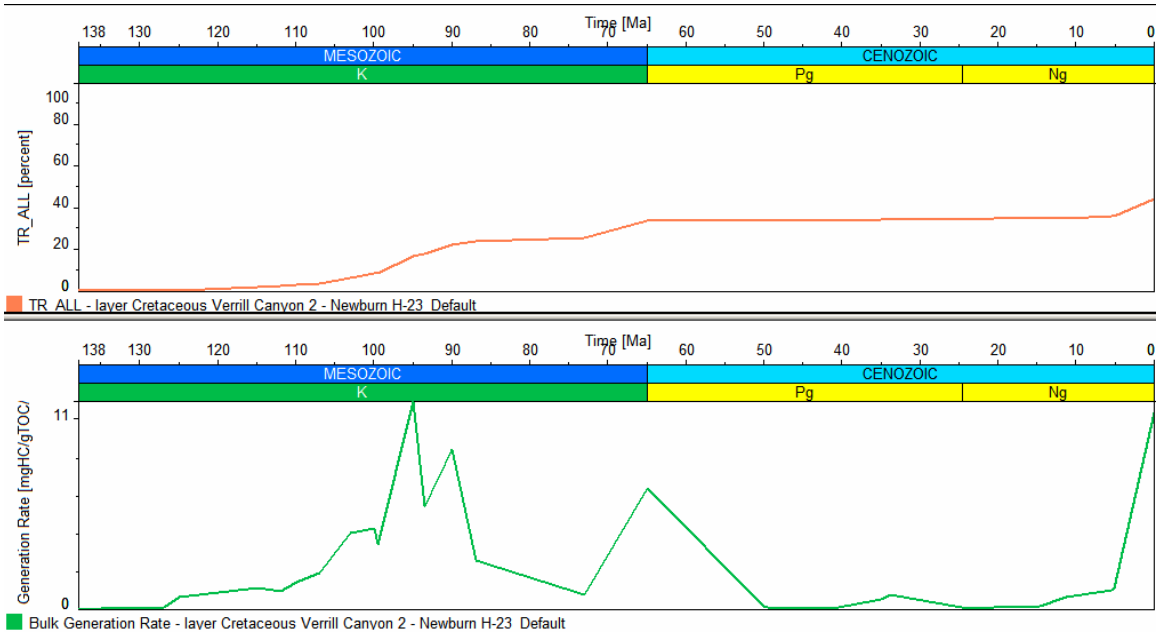

Figure 23e. Transformation ratios and bulk generation rate of various Cretaceous Verrill Canyon source rocks from the Newburn H-23 well through geological time

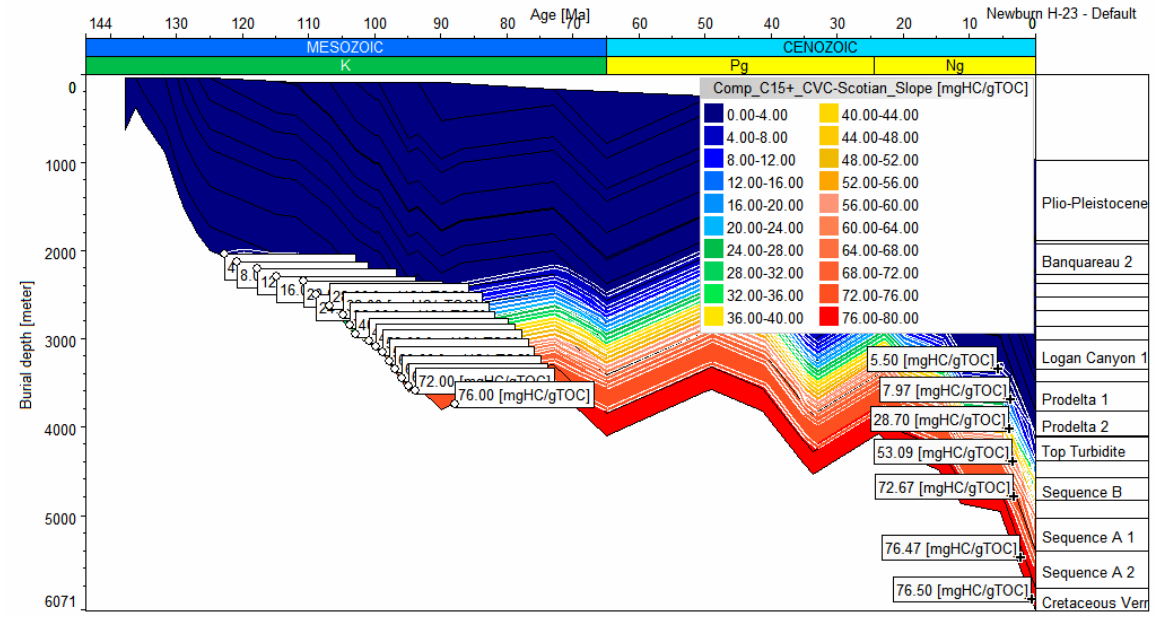

Figure 23f. Burial history of the Newburn H-23 well with iso-oil generation rate of various lower source rocks through geological time

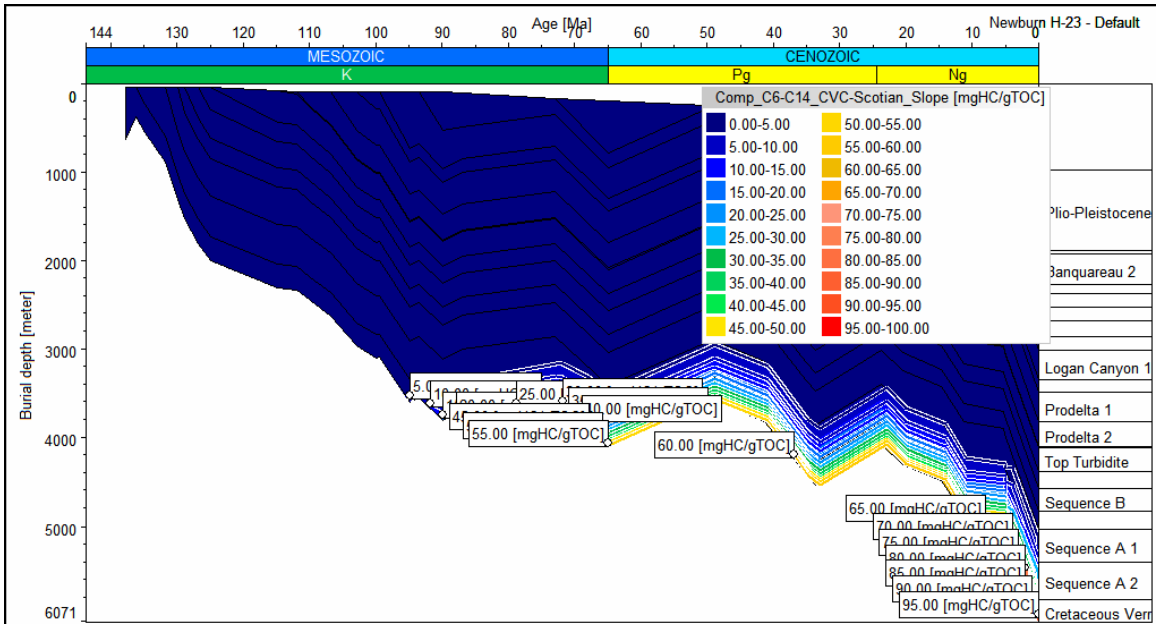

Figure 23g. Burial history of the Newburn H-23 well with iso-light oil/condensate generation rate of various lower source rocks through geological time

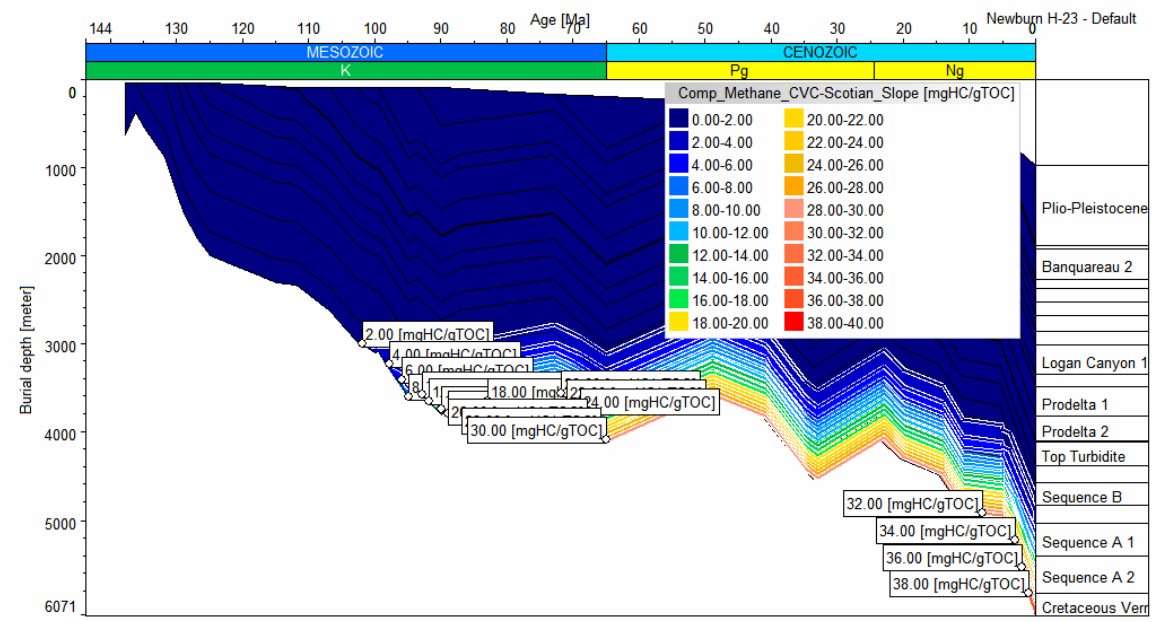

Figure 23h. Burial history of the Newburn H-23 well with iso-methane generation rate of various lower source rocks (from primary cracking) through geological time

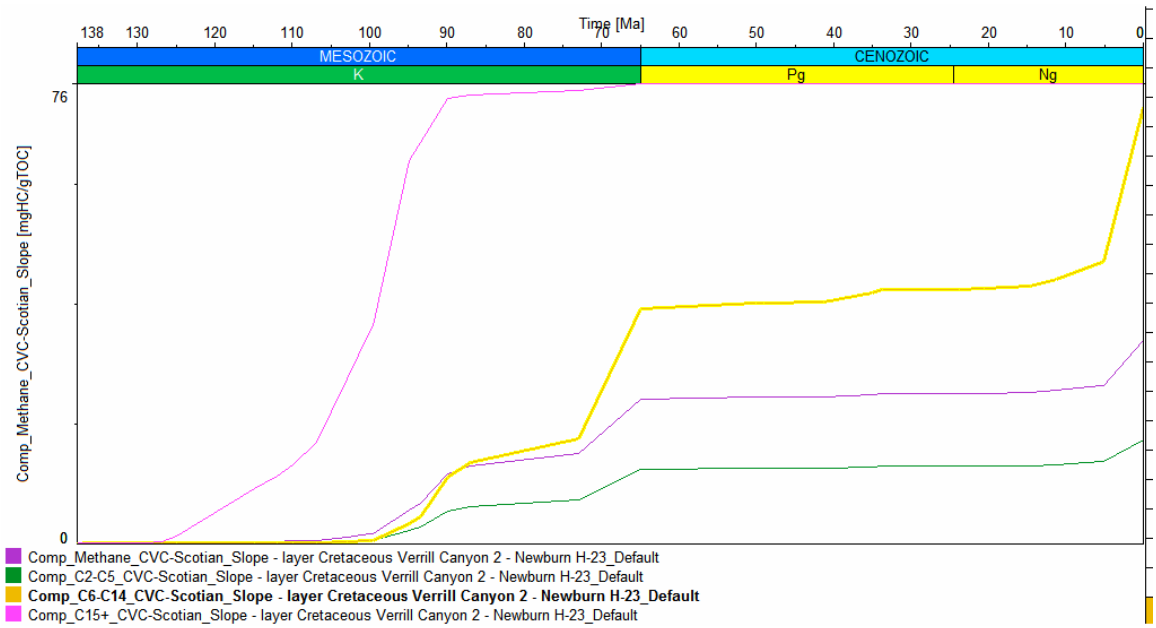

Figure 23i. Various hydrocarbon component expulsion trends through geological time of various lower source rocks from the Newburn H-23 well

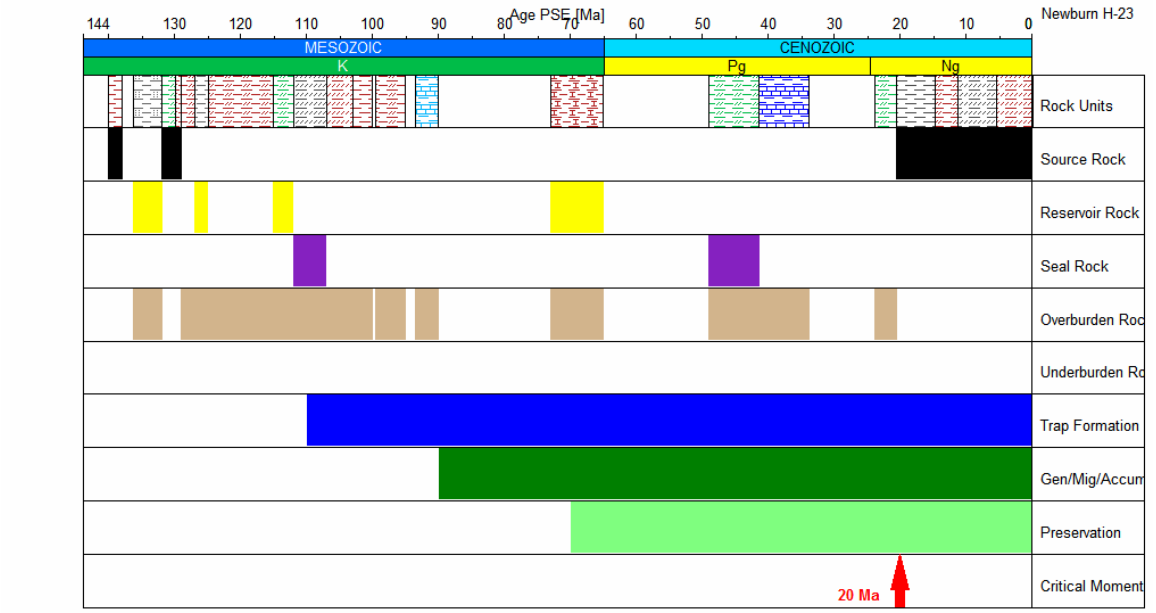

Figure 23j. Petroleum system events chart of the Newburn H-23 well with “Critical Moment” of hydrocarbon emplacement

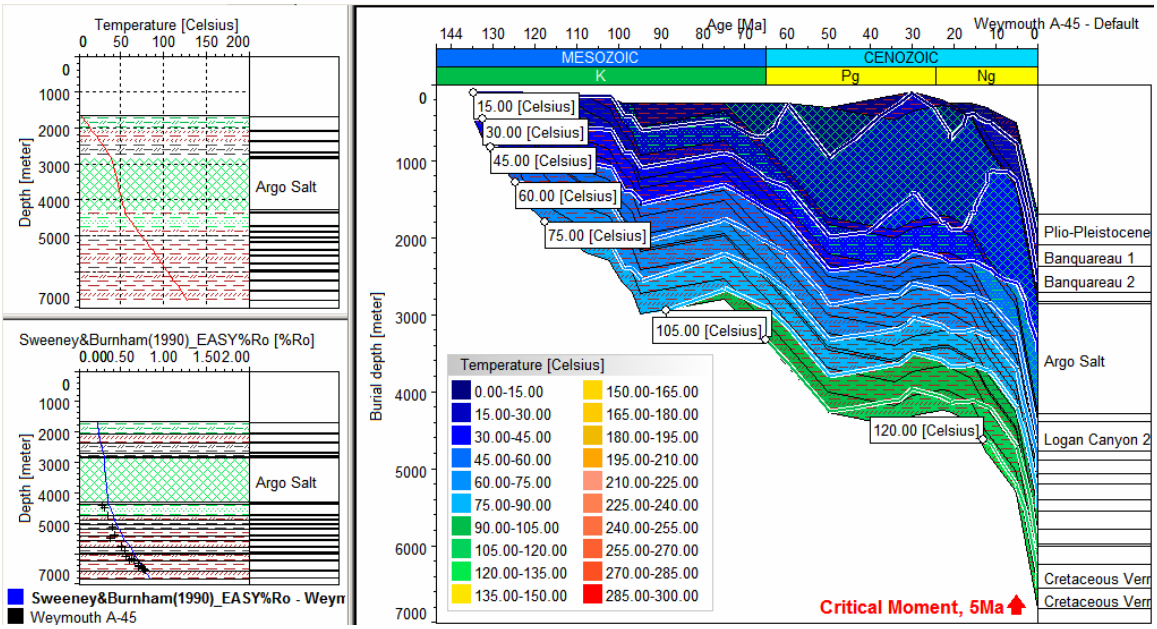

Figure 24a. Burial history of the Weymouth A-45 well with iso-temperature lines on the right and temperature or reflectance versus depth plots on the left

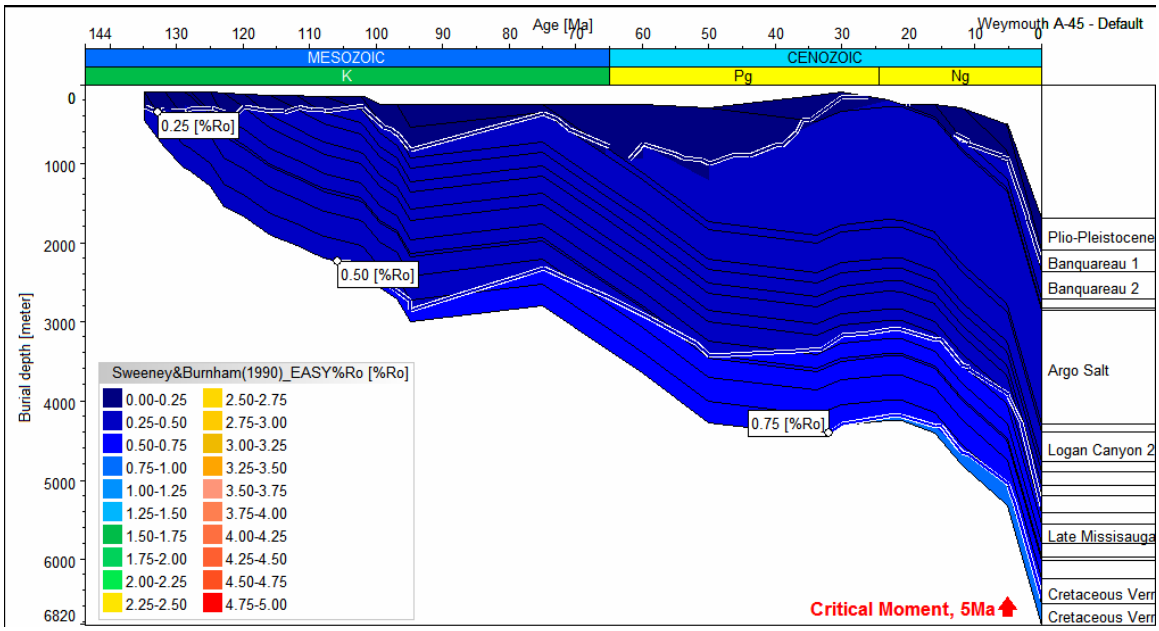

Figure 24b. Burial history of the Weymouth A-45 well with iso-maturity lines

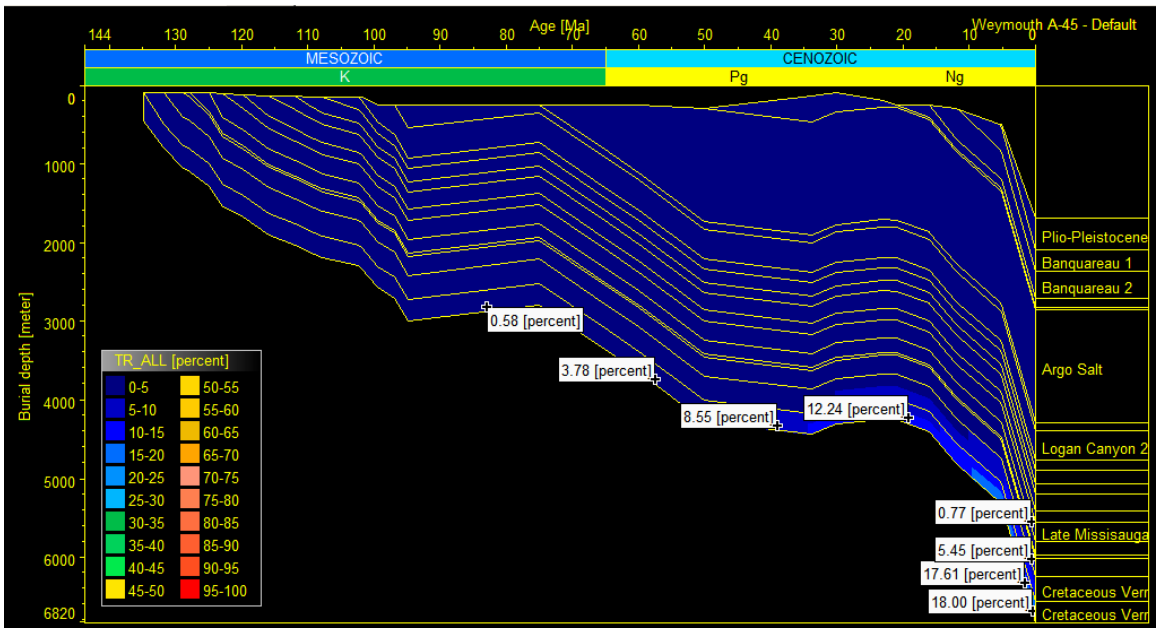

Figure 24c. Burial history of the Weymouth A-45 well with iso-transformation ratio of Middle Missisauga (Cretaceous Verrill Canyon) source rock

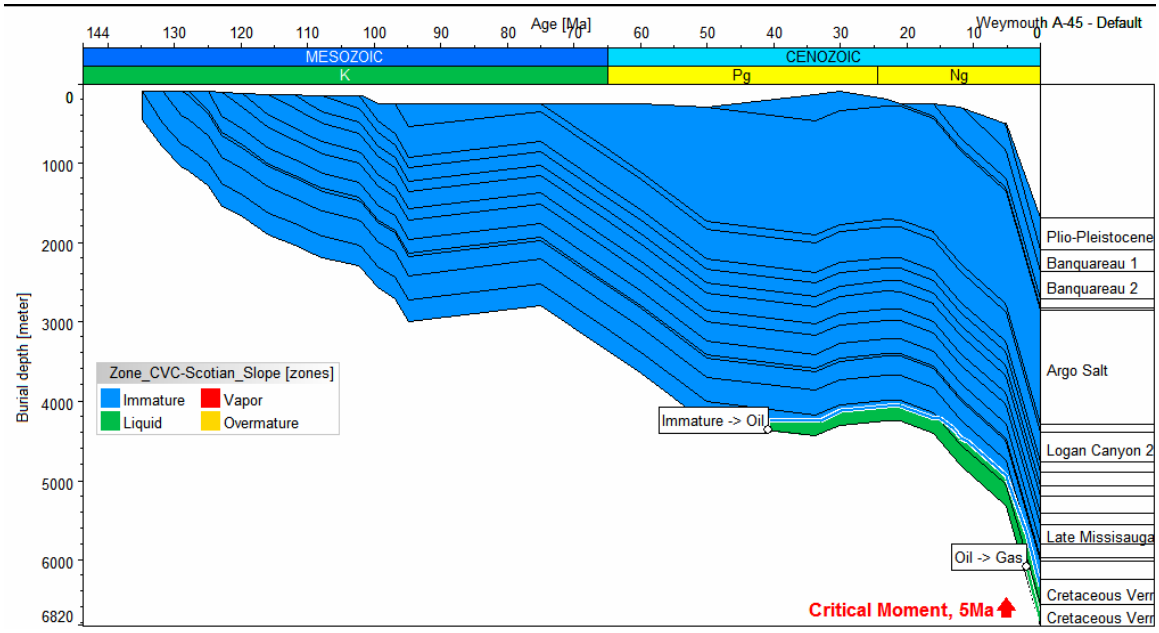

Figure 24d. Burial history of the Weymouth A-45 well with iso-hydrocarbon zones

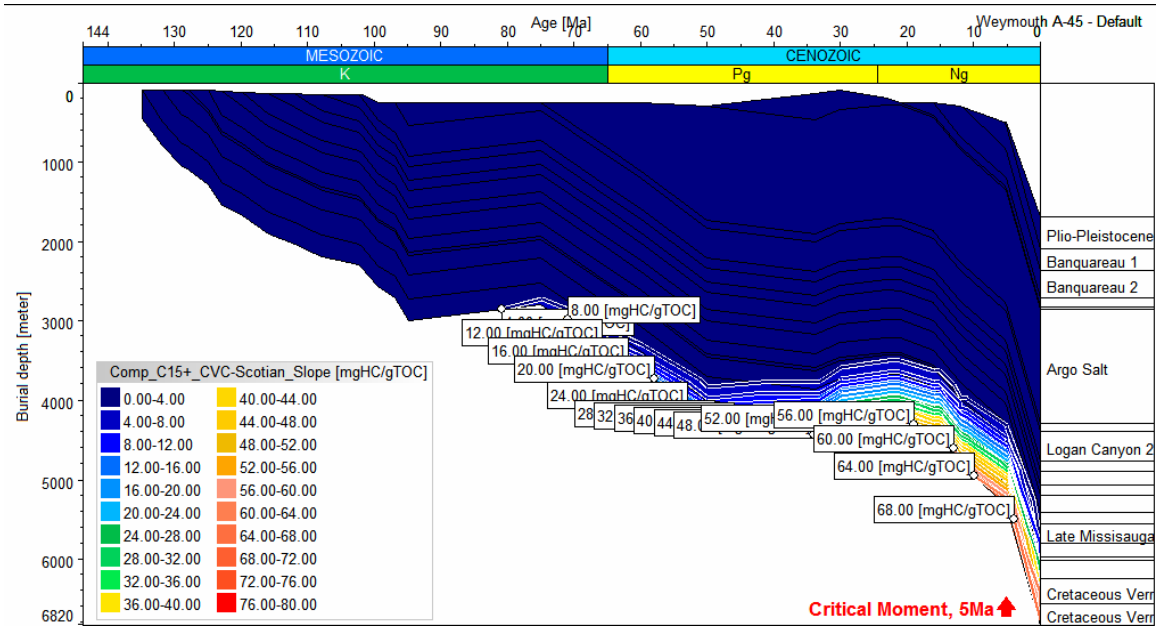

Figure 24e. Burial history of the Weymouth A-45 well with iso-oil generation lines from Late to Early Missisauga source rocks

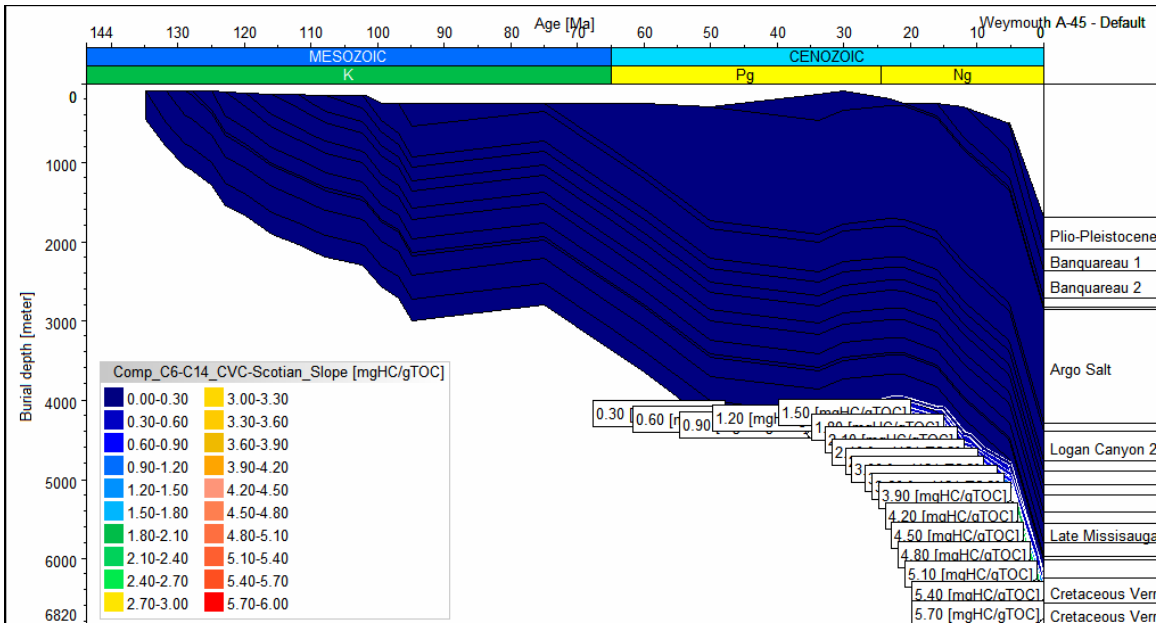

Figure 24f. Burial history of the Weymouth A-45 well with iso-light oil and condensate generation lines from Late to Early Missisauga source rocks

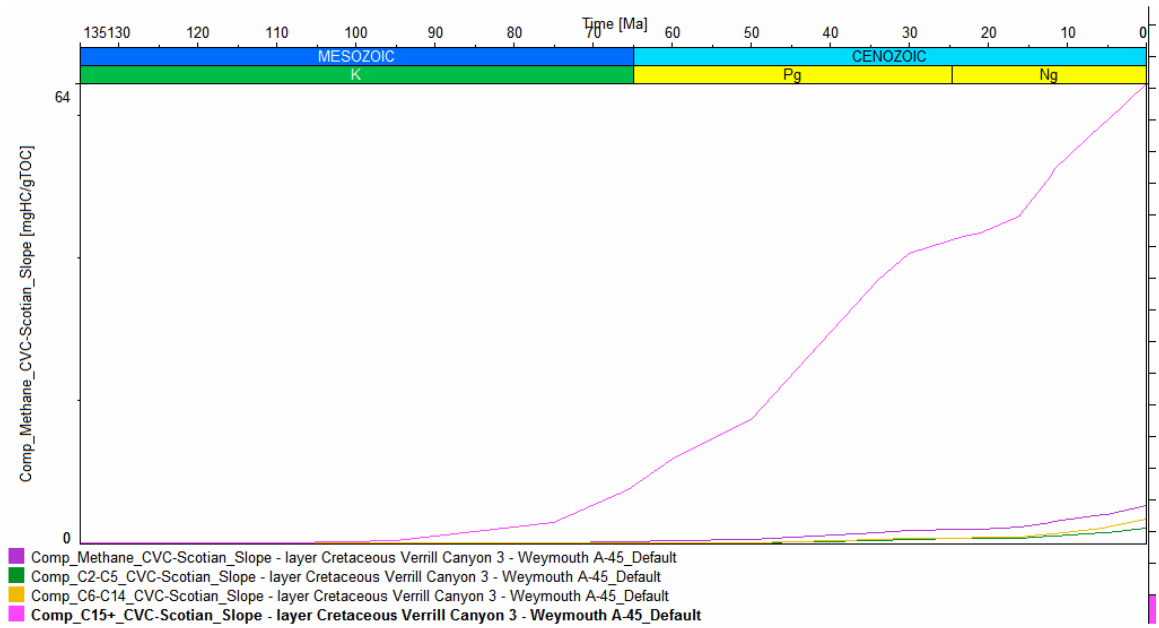

Figure 24g. Various hydrocarbon component expulsion trends through geological time of Layer Cretaceous Verrill Canyon 3 source rock from the Weymouth A-45 well

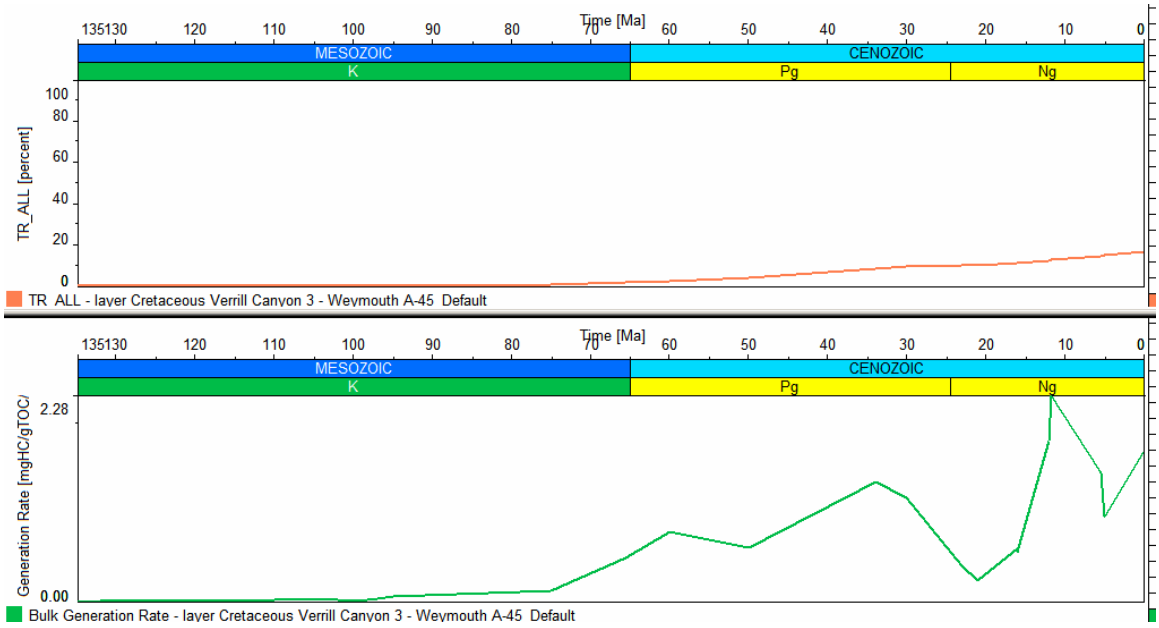

Figure 24h. Transformation ratios and bulk generation rate of Layer M, Middle Missisauga source rock from the Weymouth A-45 well through geological time

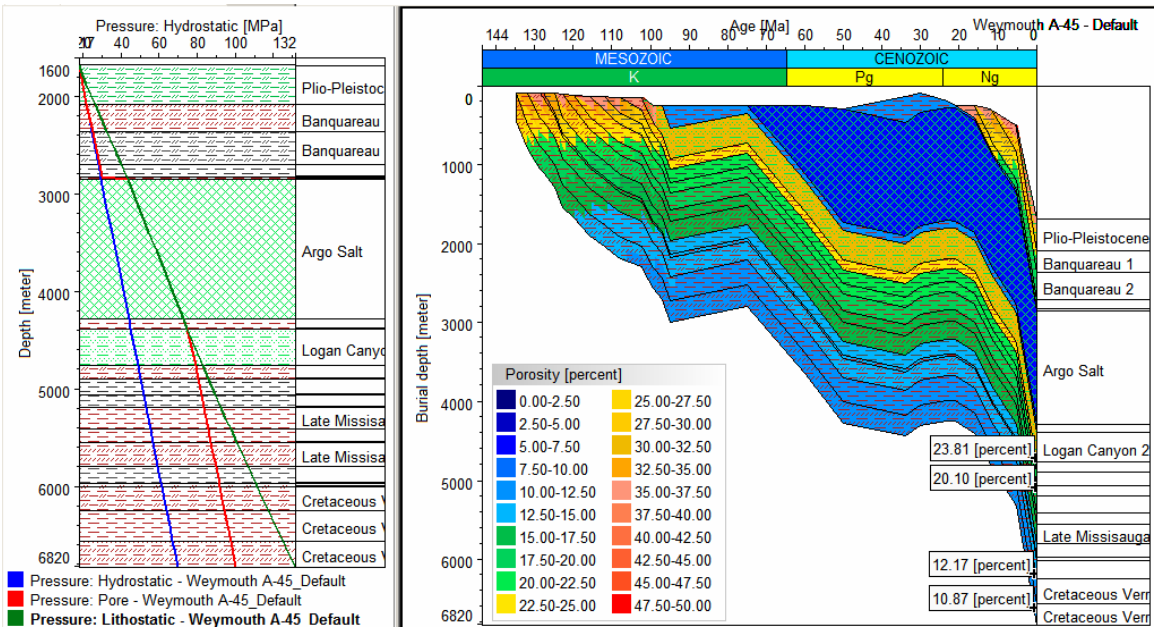

Figure 24i. Burial history of the Weymouth A-45 well with porosity lines and values on the right and various pressures versus depth plot on the left.

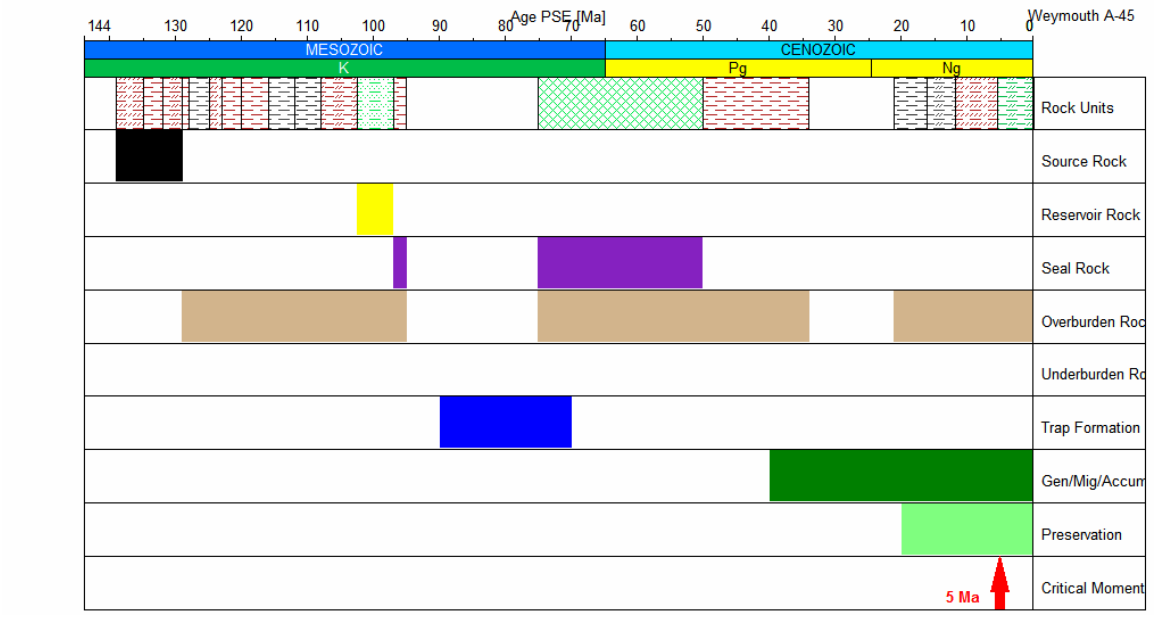

Figure 24j. Petroleum system events chart of the Weymouth A-45 well with “Critical Moment” of hydrocarbon emplacement

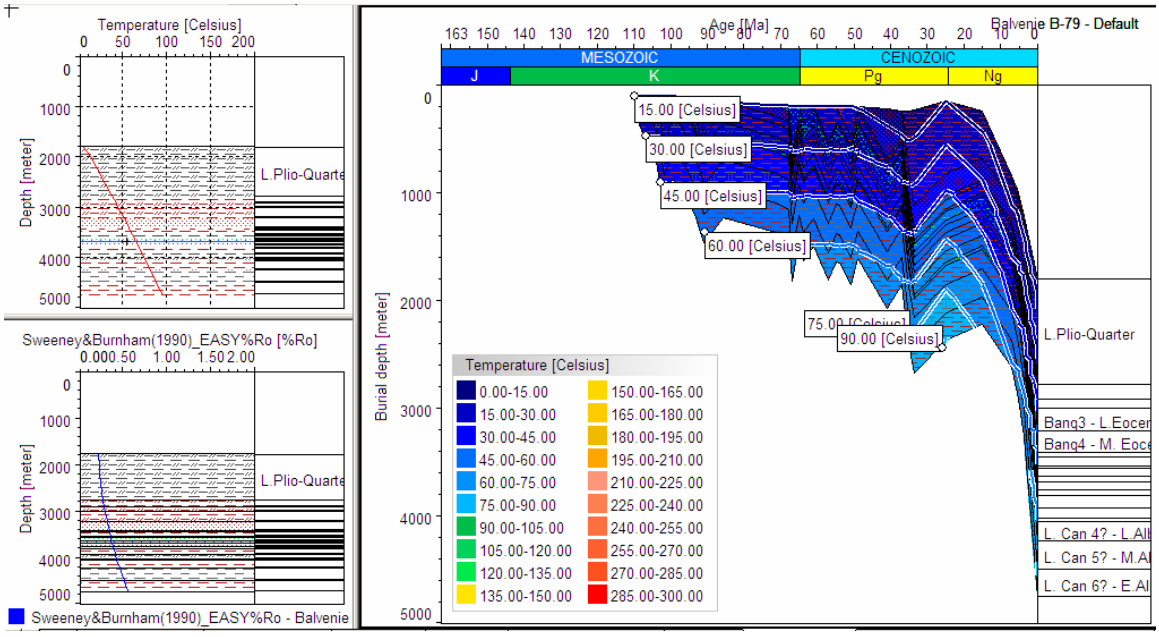

Figure 25a. Burial history of the Balvenie B-79 well with iso-temperature lines on the right and temperature or reflectance versus depth plots on the left

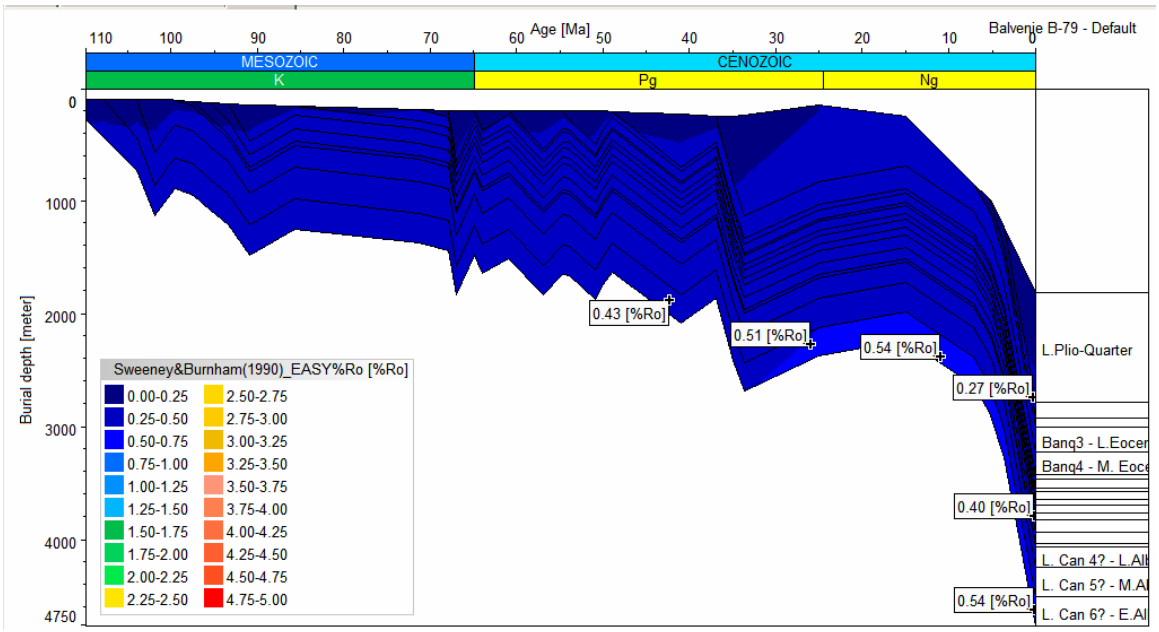

Figure 25b. Burial history of the Balvenie B-79 well with iso-maturity lines

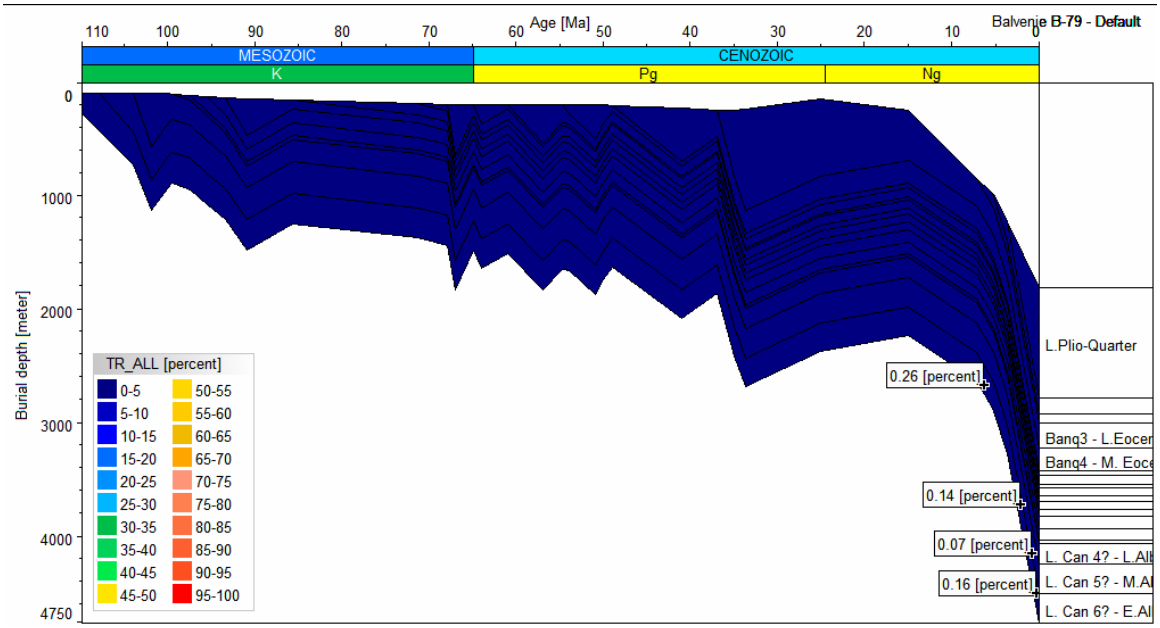

Figure 25c. Burial history of the Balvenie B-79 well with iso-hydrocarbon transformation ratio lines for various source rocks and values for the lowermost source rock

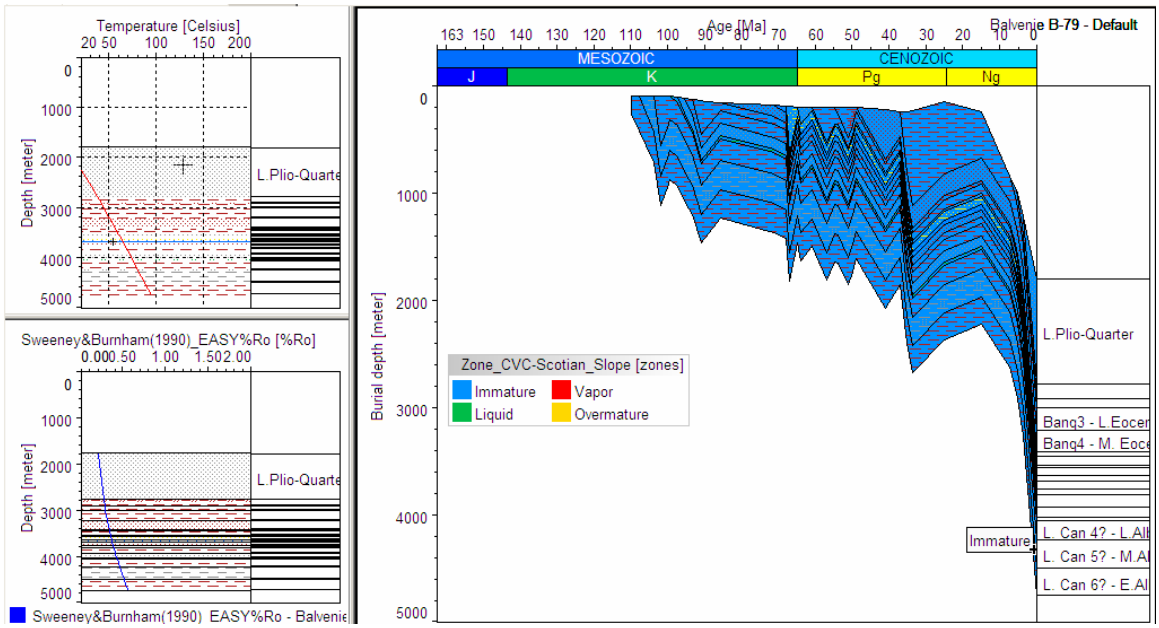

Figure 25d. Burial history of the Balvenie B-79 well with iso-hydrocarbon zone lines (immature, liquid, vapour, and overmature) on the right and temperature or maturity versus depth plots on the left

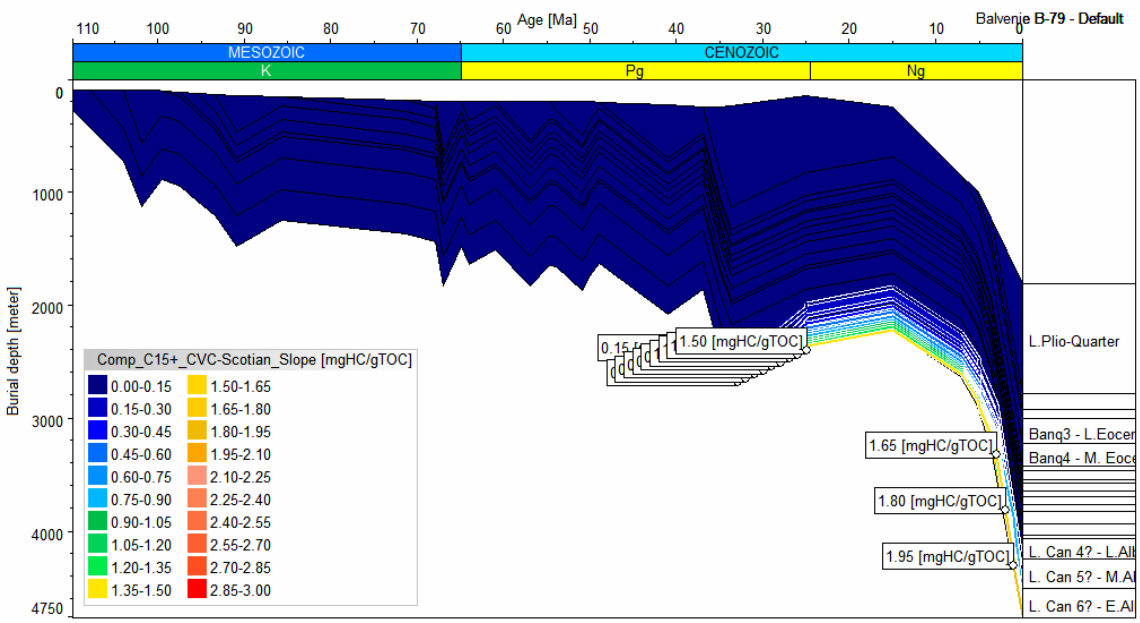

Figure 25e. Burial history of the Balvenie B-79 well with iso-oil generation lines and some values for the lowermost source

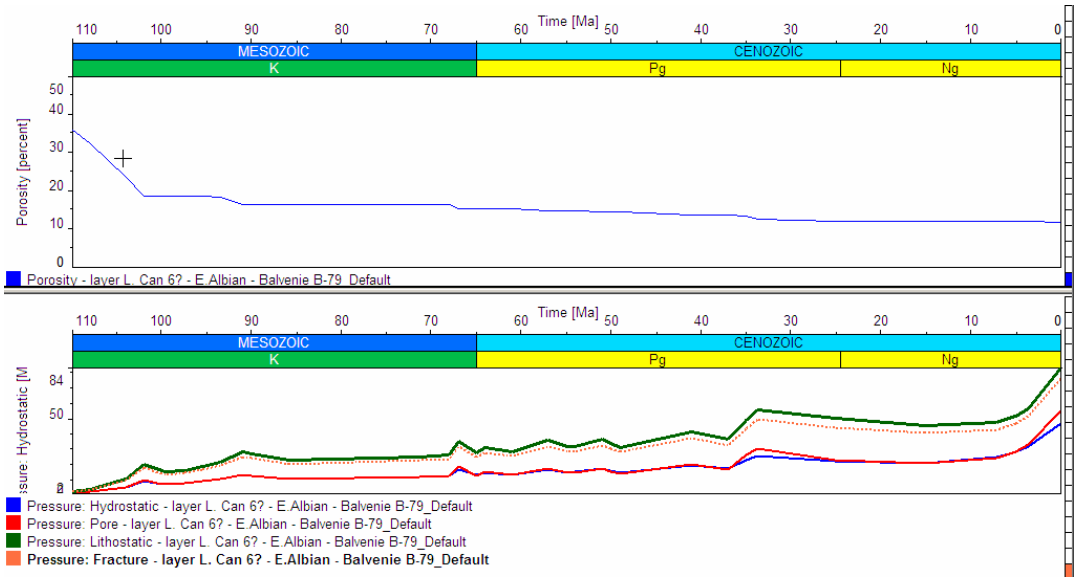

Figure 25f. Porosity and pressure versus geological time plots for Early Albian source rock

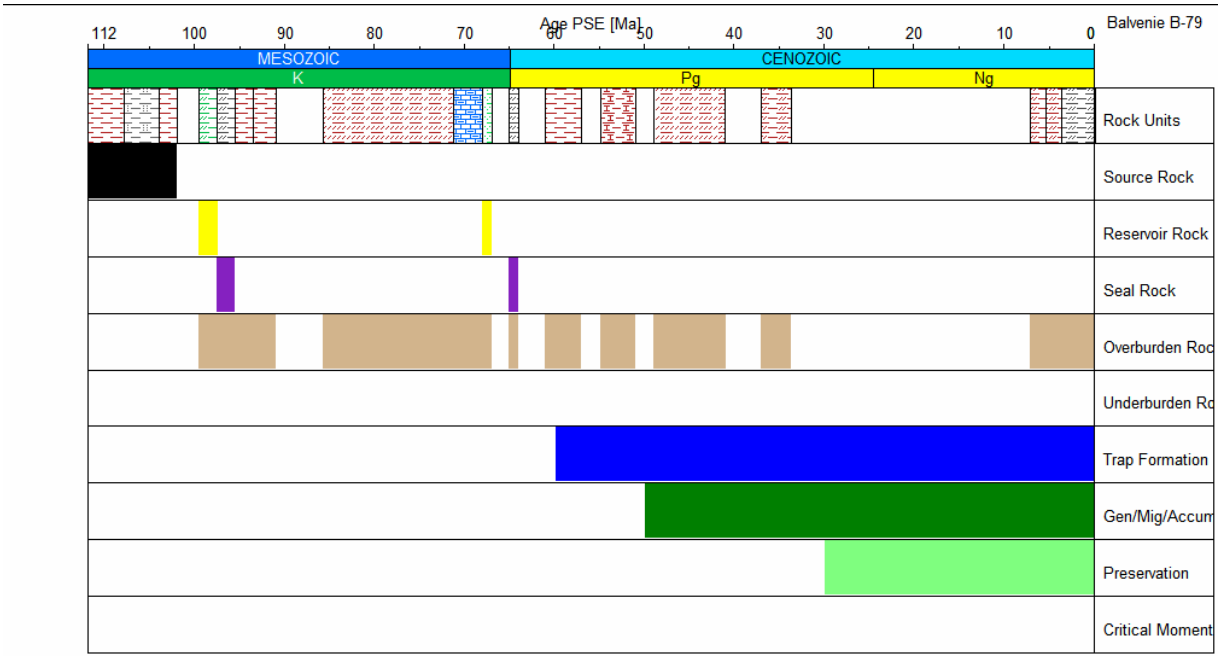

Figure 25g. Petroleum system events chart of the Balvenie B-79 well. Note that no threshold “Critical Moment” has been achieved within even for the lowermost source rock unit

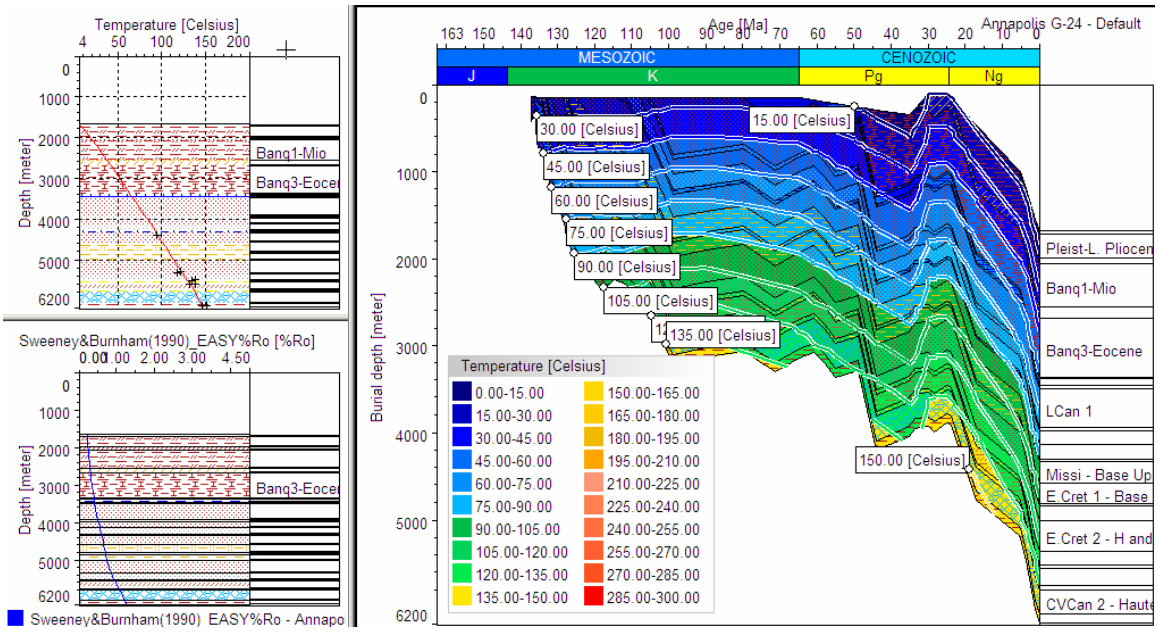

Figure 26a. Burial history of the Annapolis G-24 well with iso-temperature lines on the right and temperature or reflectance versus depth plots on the left

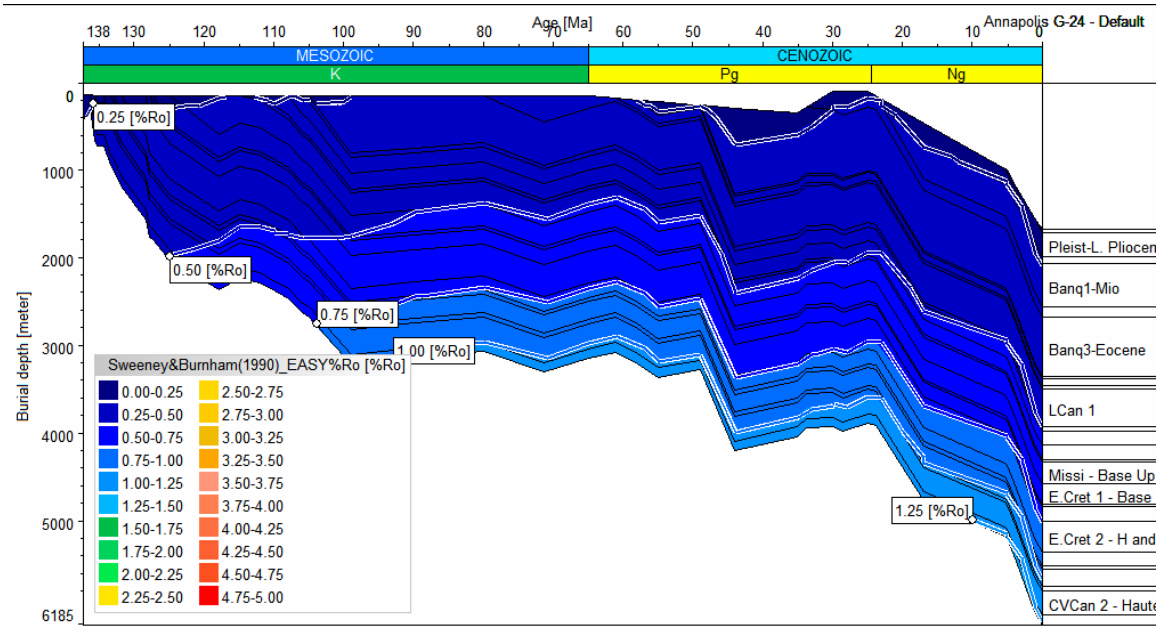

Figure 26b. Burial history of the Annapolis G-24 well with iso-reflectance lines

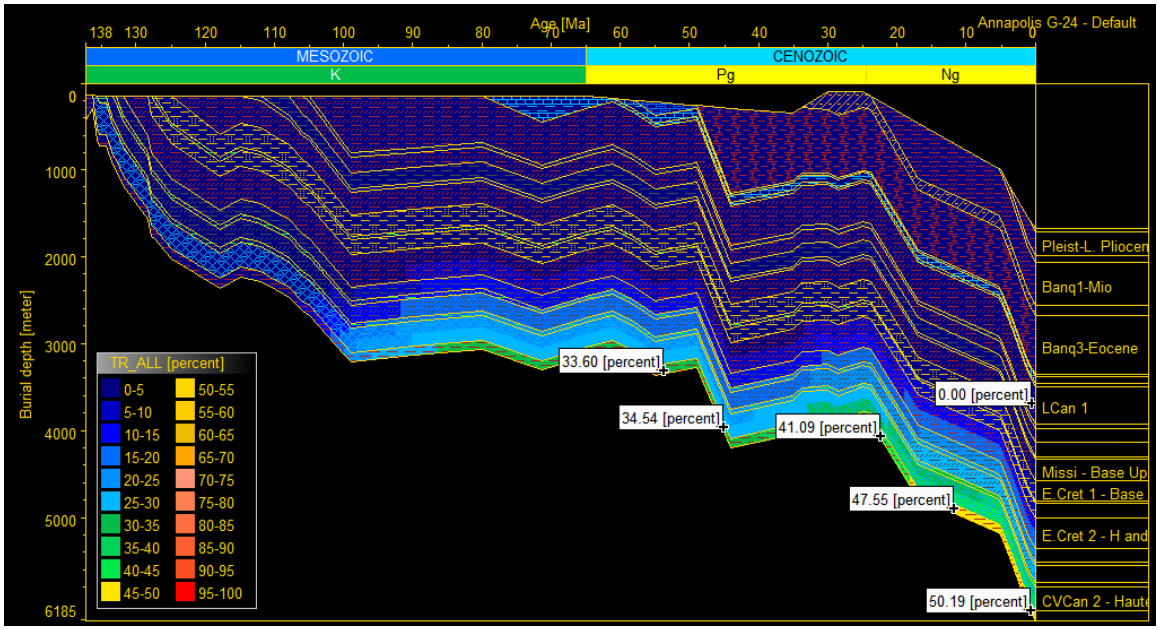

26c. Burial history of the Annapolis G-24 well with transformation ratio of various source rocks (especially the Cretaceous Verrill canyon source rock at different geological times)

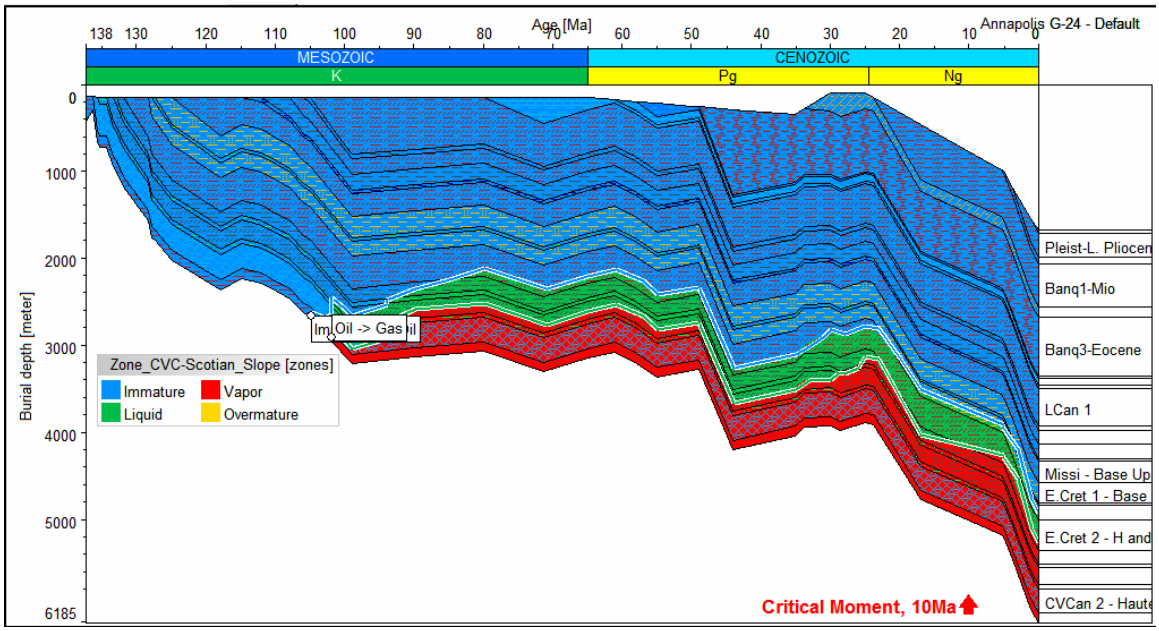

Figure 26d. Burial history of the Annapolis G-24 well with maturity zones (immature, liquid or oil, vapor or gas/condensate, and overmature gas)

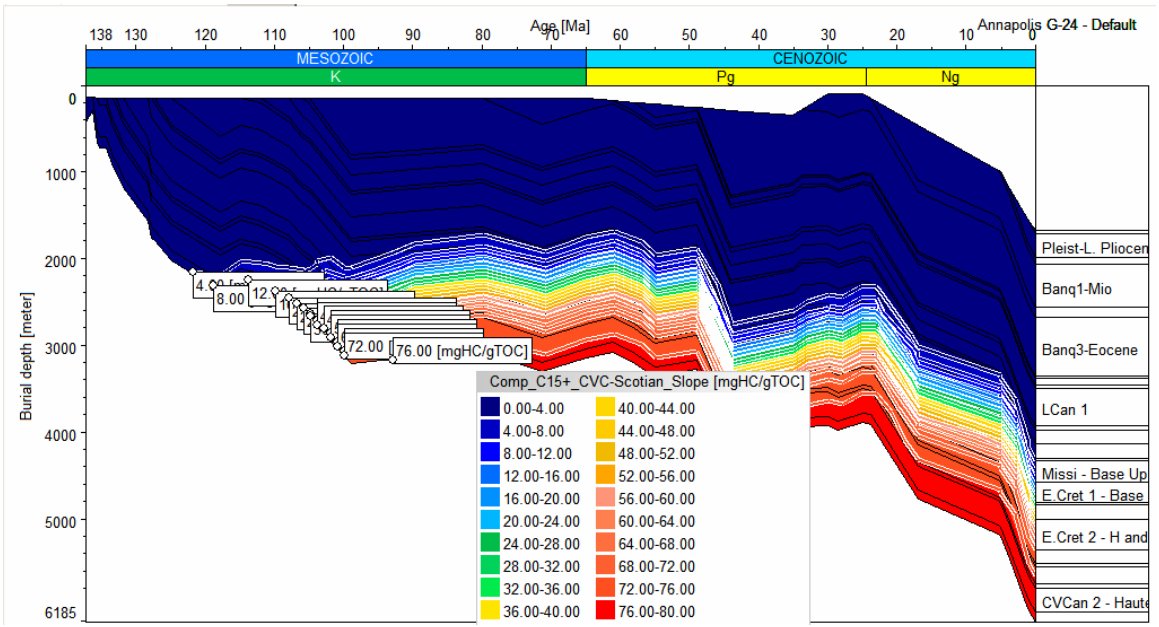

Figure 26e. Burial history of the Annapolis G-24 well with iso-oil (C15+) generation lines

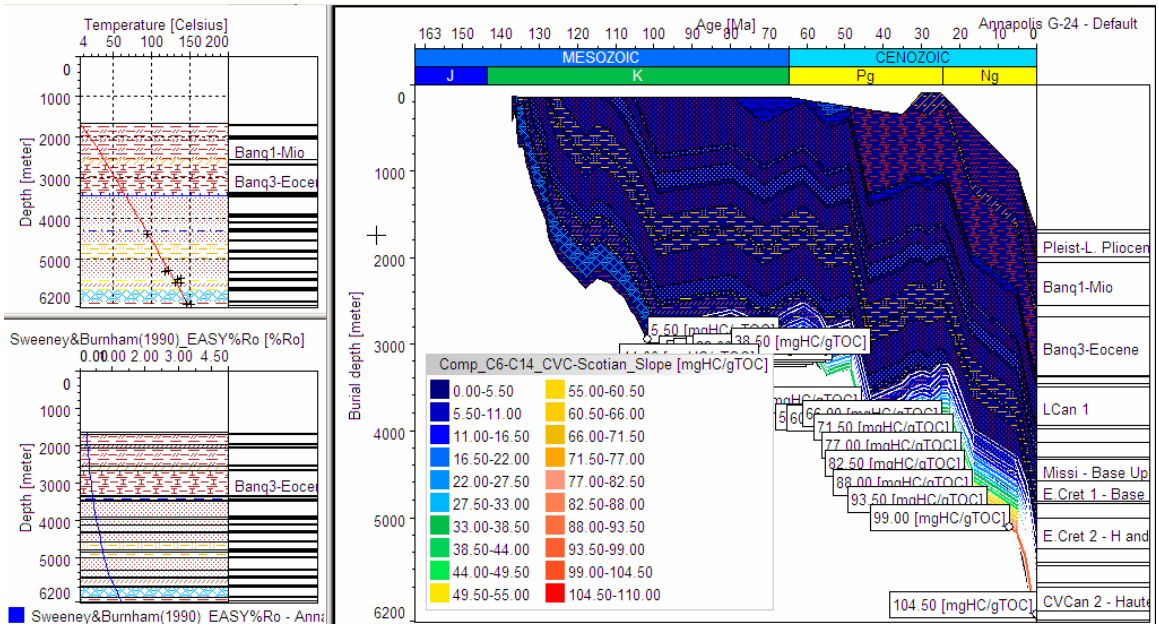

Figure 26f. Burial history of the Annapolis G-24 well with iso-light oil and condensate (C6-C14) generation lines; left hand figures are temperature and vitrinite reflectance depth plots.

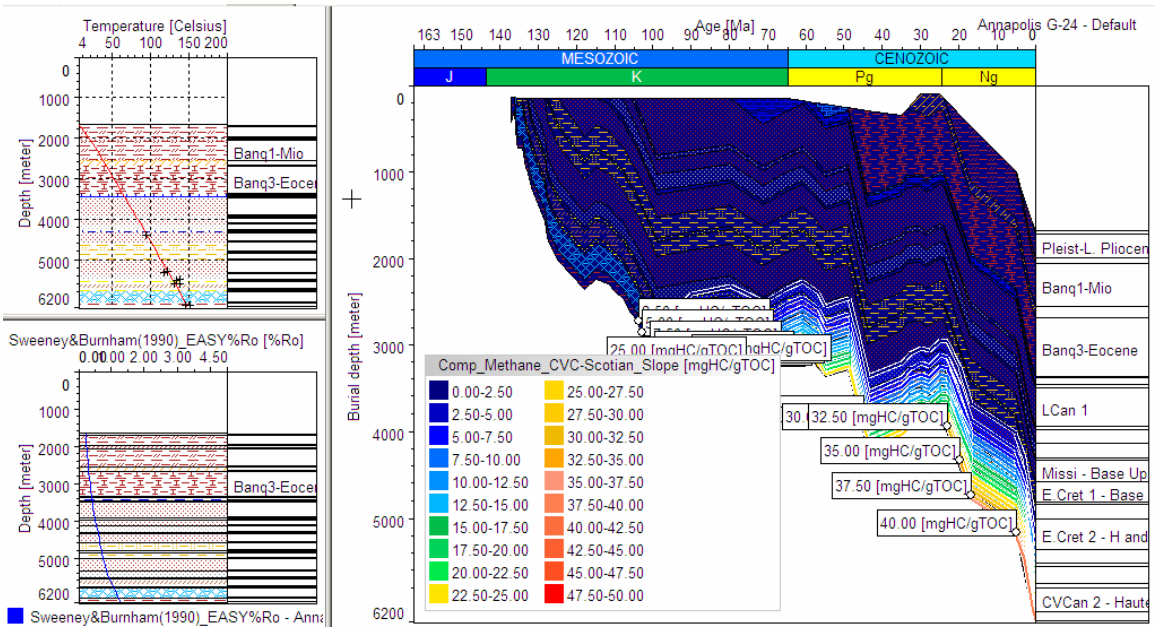

Figure 26g. Burial history of the Annapolis G-24 well with iso-primary methane-generation lines on the right; left hand figures are temperature and vitrinite reflectance depth plots.

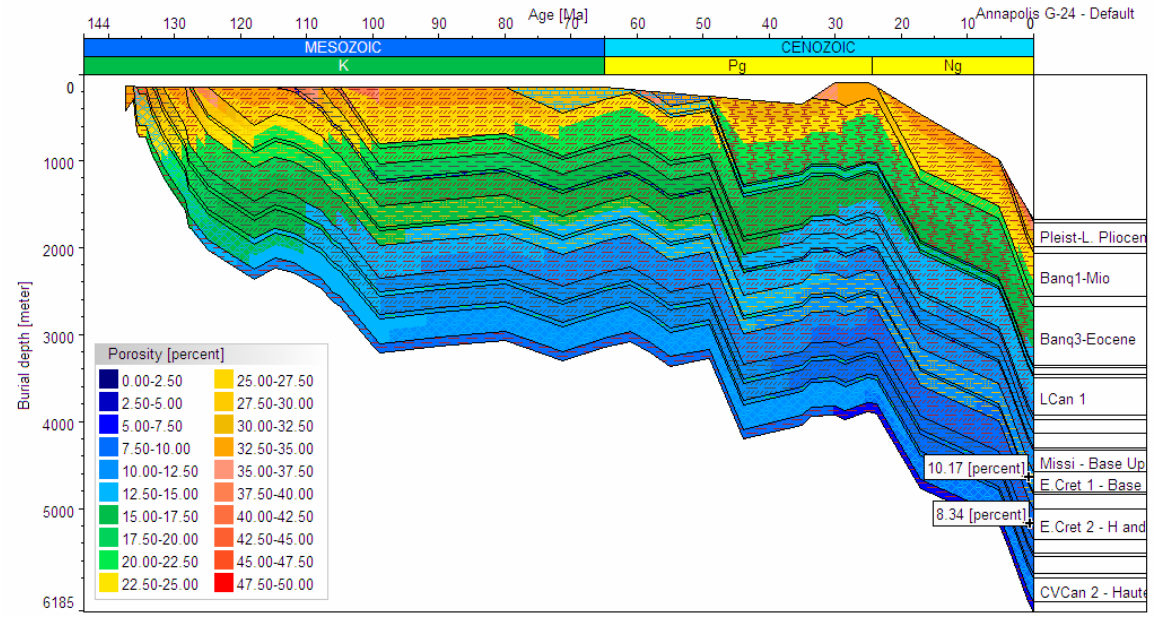

Figure 26h. Burial history of the Annapolis G-24 well with iso-porosity lines and a few modeled values

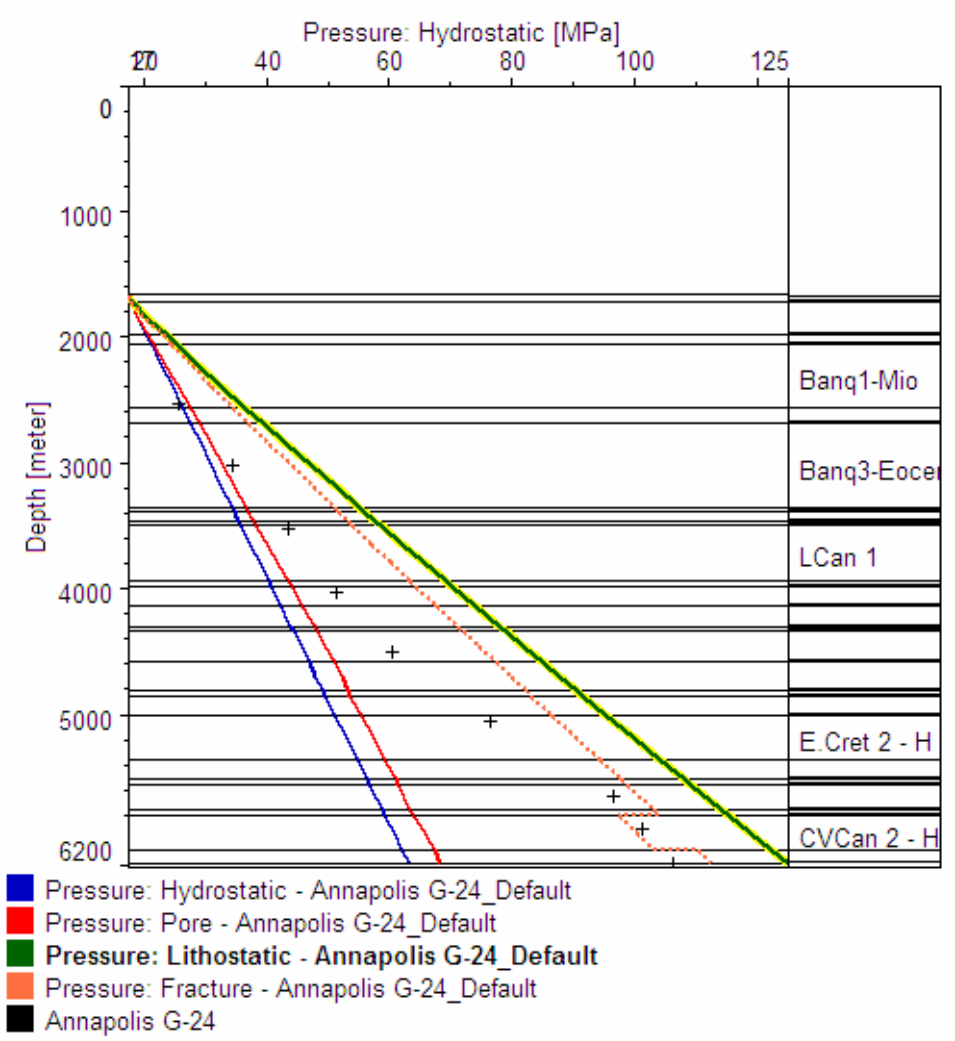

Figure 26i. Calculated and measured pressure data from the Annapolis G-24 well. Note the similarity of fracture pressure and well measured pressure data

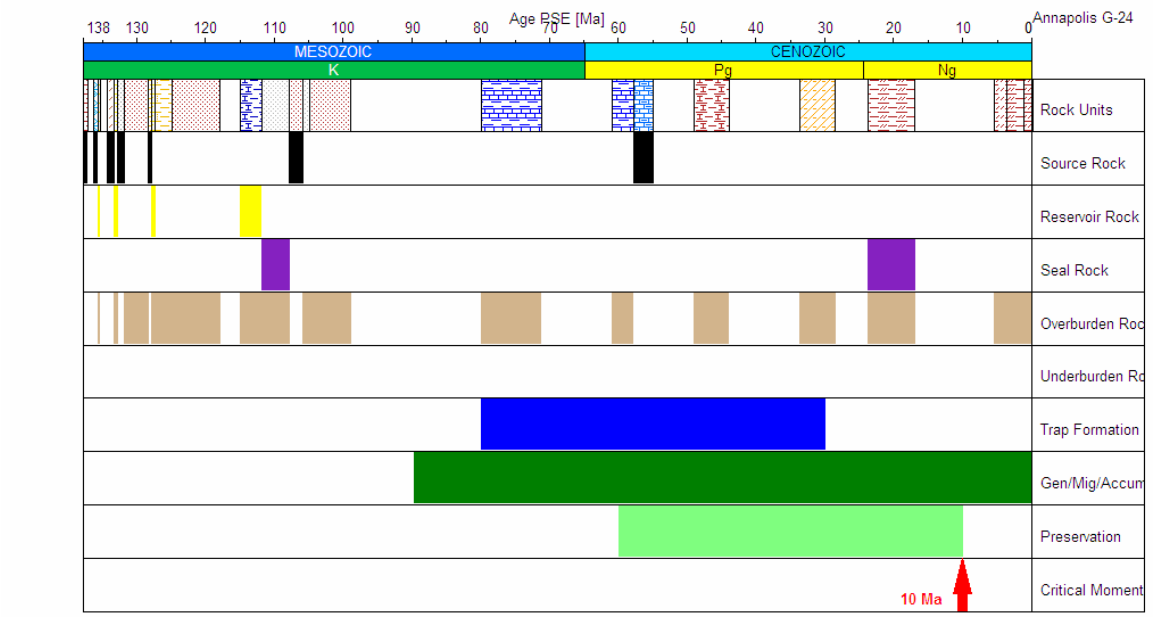

Figure 26j. Petroleum system events chart of the Annapolis G-24 well showing the "Critical Moment" of hydrocarbon emplacement.

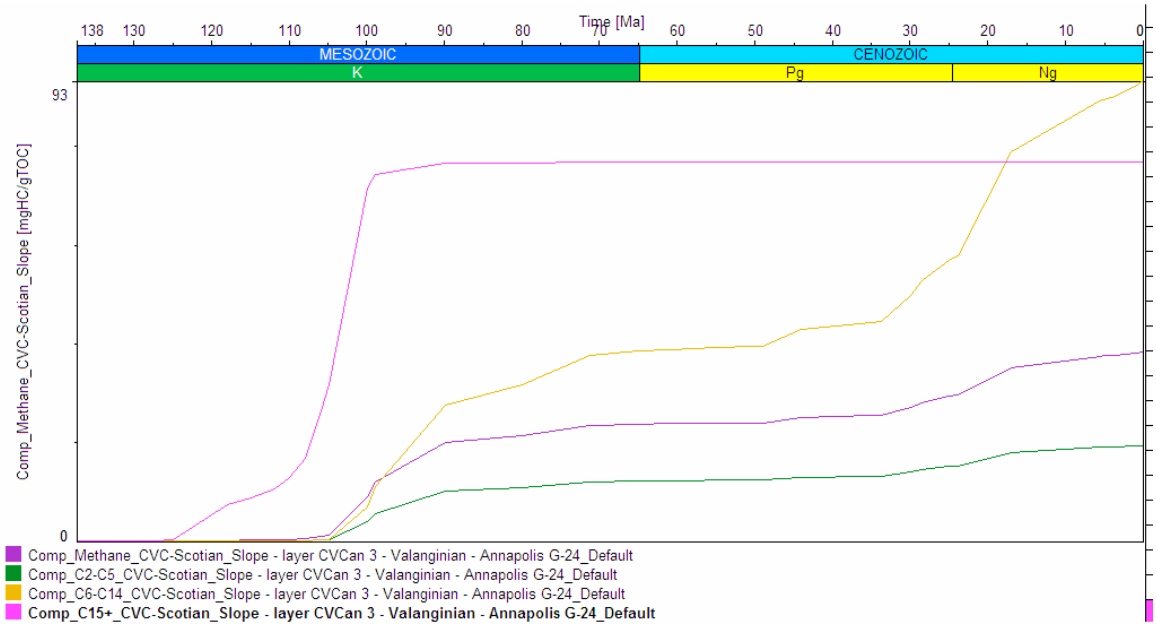

Figure 26k. Timing of multi-component hydrocarbon expulsion from the lowermost Cretaceous Verrill Canyon (layer 3) source rock

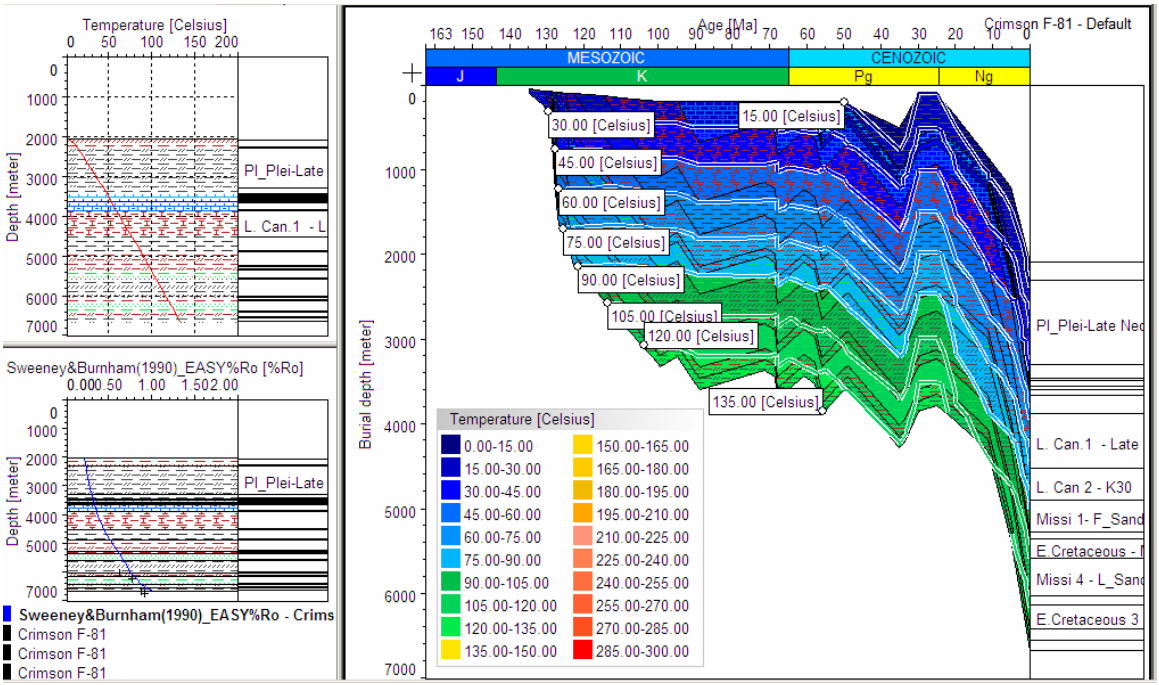

Figure 27a. Burial history of the Crimson F-81 well with iso-temperature lines on the right and temperature or reflectance versus depth plots on the left

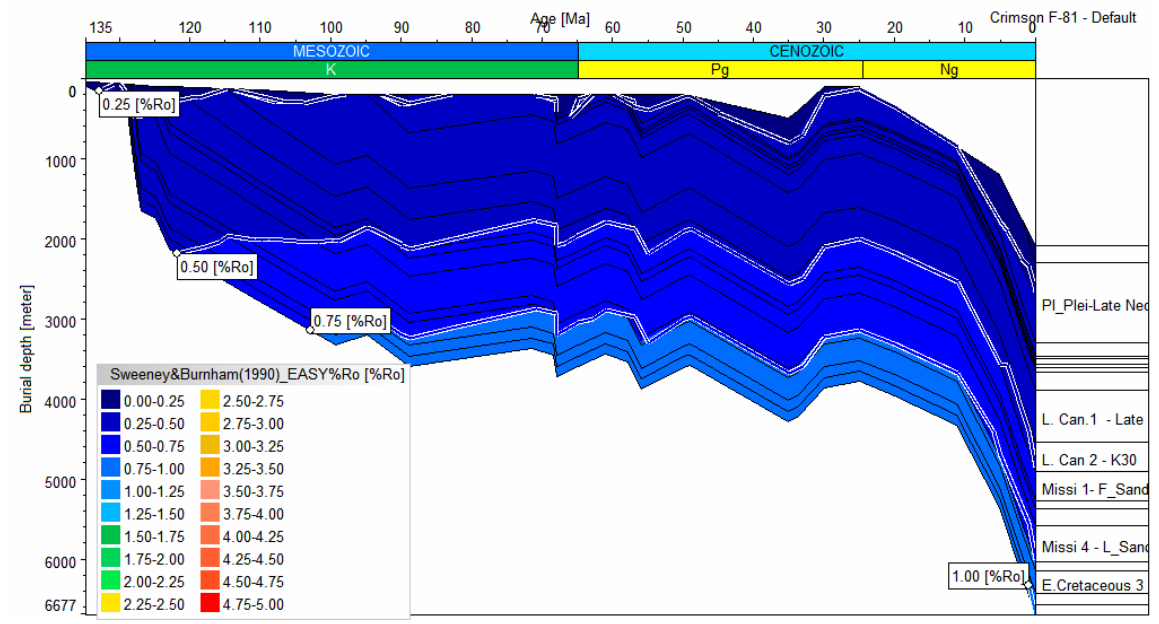

Figure 27b. Burial history of the Crimson F-81 well with iso-maturity lines

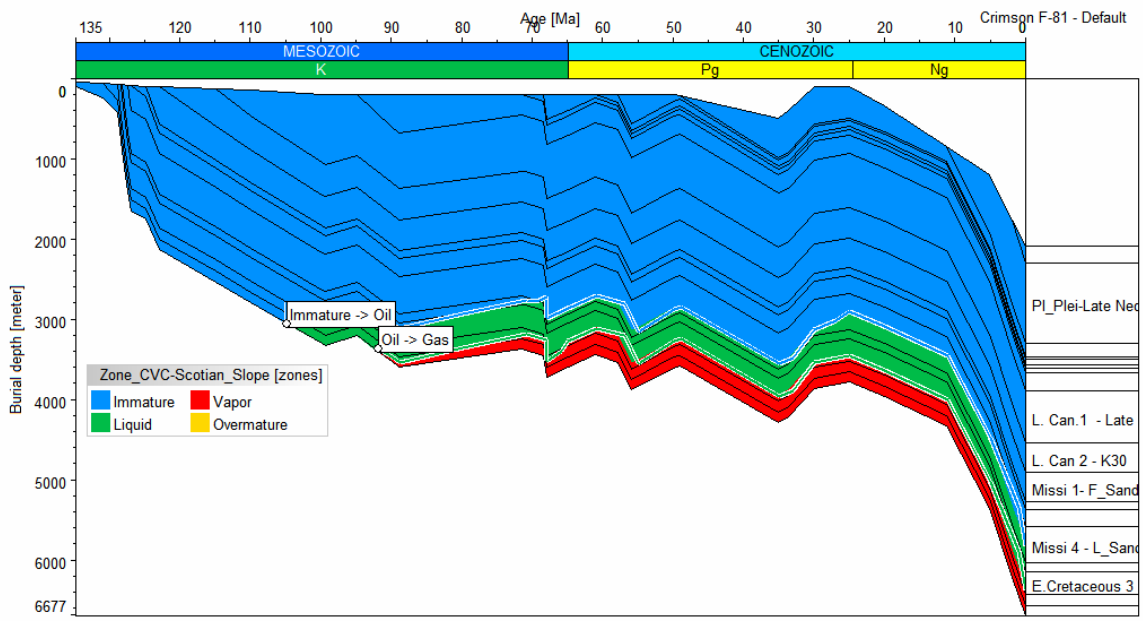

Figure 27c. Burial history of the Crimson F-81 well with iso-hydrocarbon maturity zones (immature, oil, vapour, and overmature)

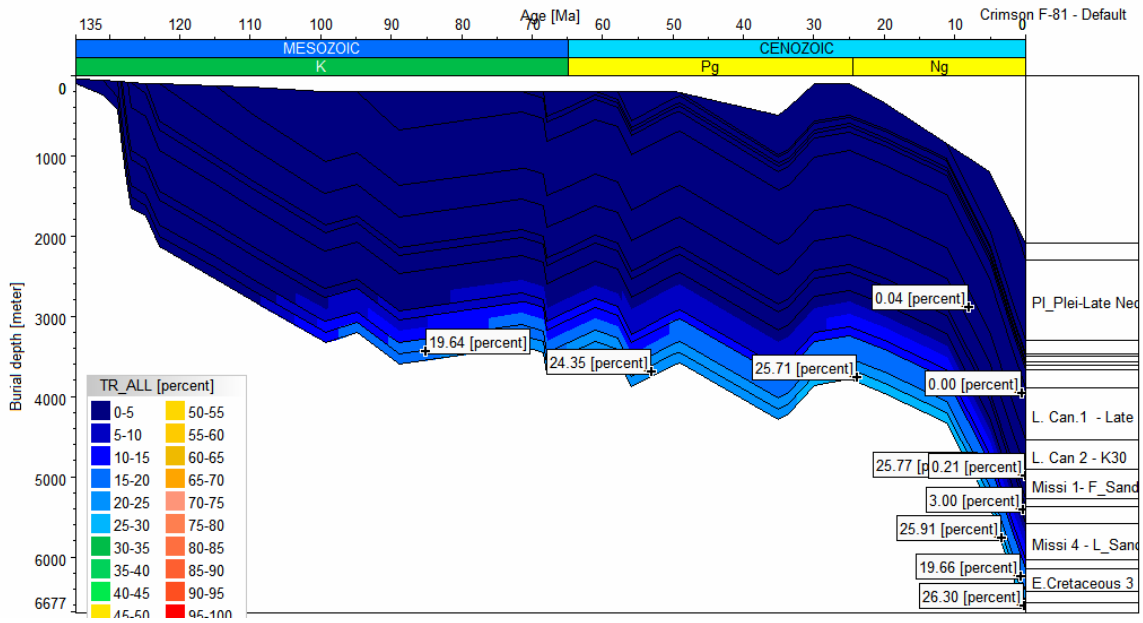

Figure 27d. Burial history of the Crimson F-81 well with iso-transformation ratio lines

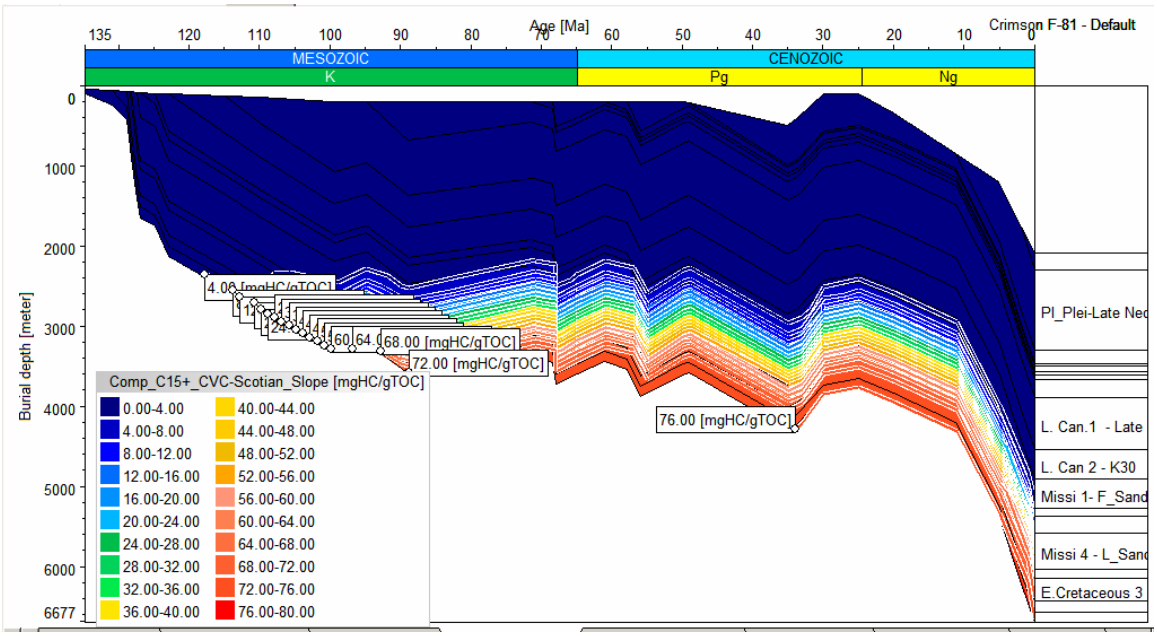

Figure 27e. Burial history of the Crimson F-81 well with iso-C15+ (oil) generation lines

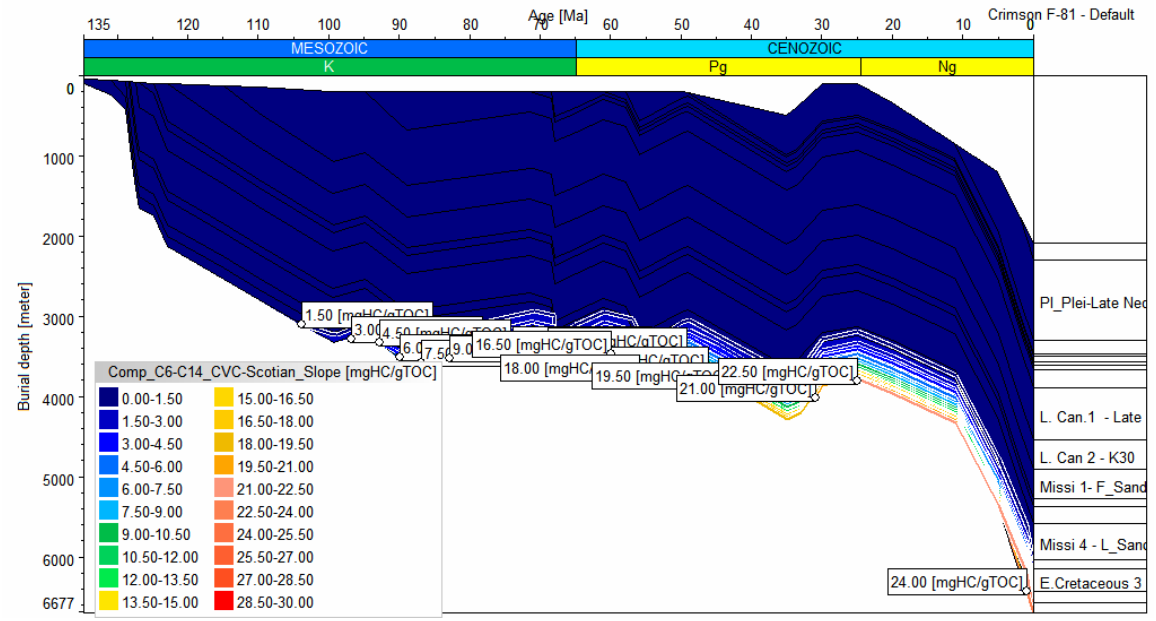

Figure 27f. Burial history of the Crimson F-81 well with iso-C6 to C14 (condensate and light oil) generation lines

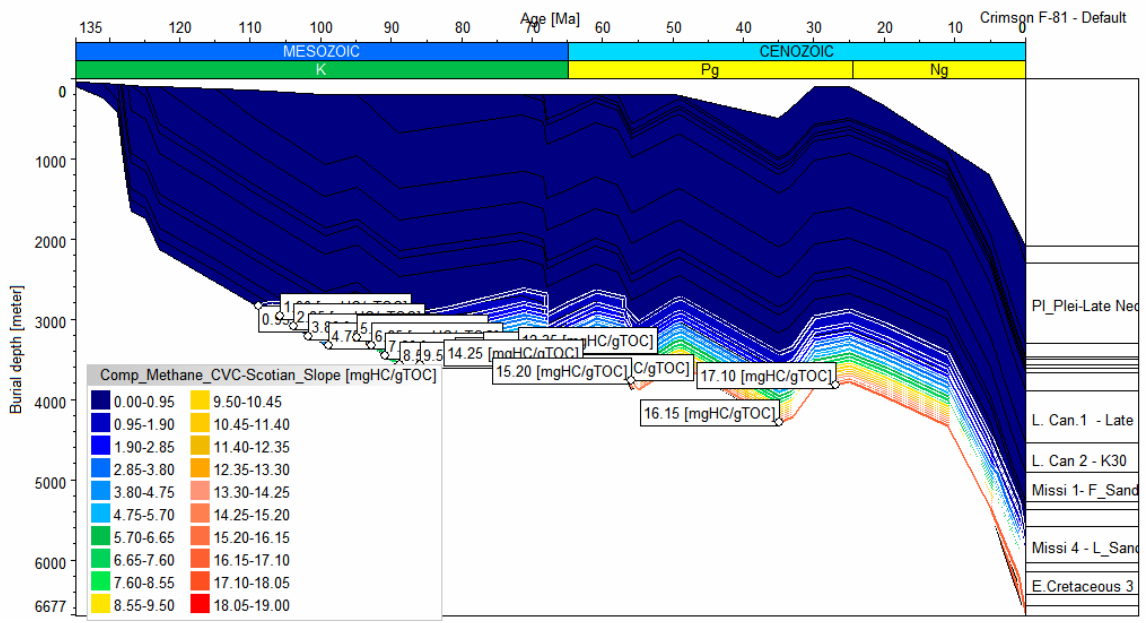

Figure 27g. Burial history of the Crimson F-81 well with iso-primary methane (dry gas) generation lines

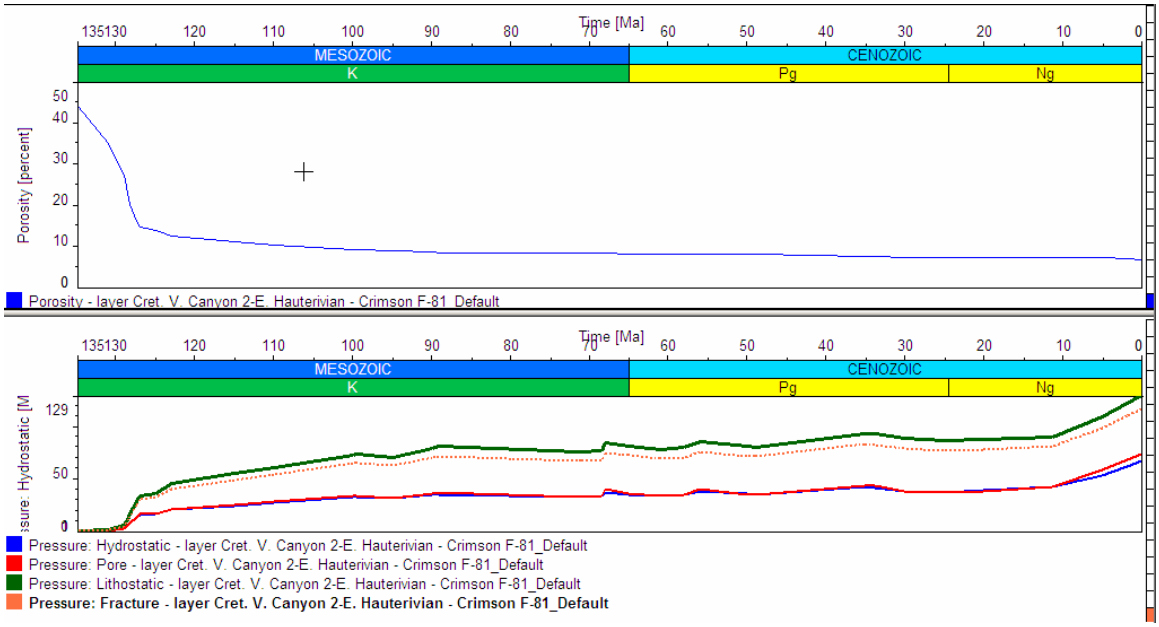

Figure 27h. Porosity and pressure versus geological time plots for the Crimson F-81 well

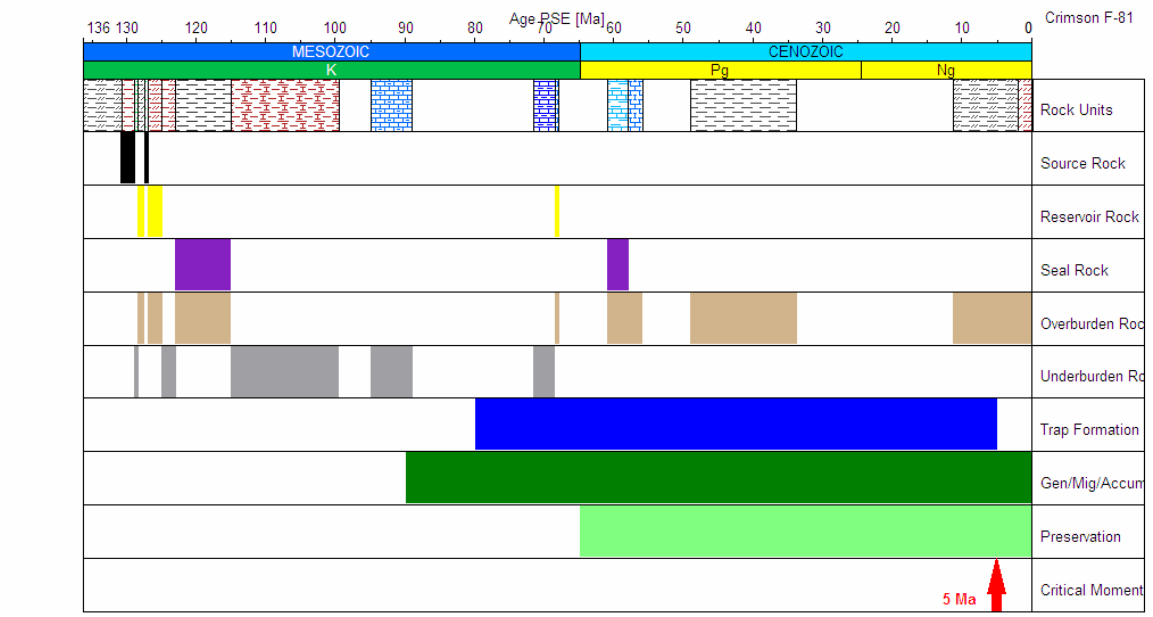

Figure 27i. Petroleum system events chart of the Crimson F-81 well with "Critical Moment" of hydrocarbon emplacement.

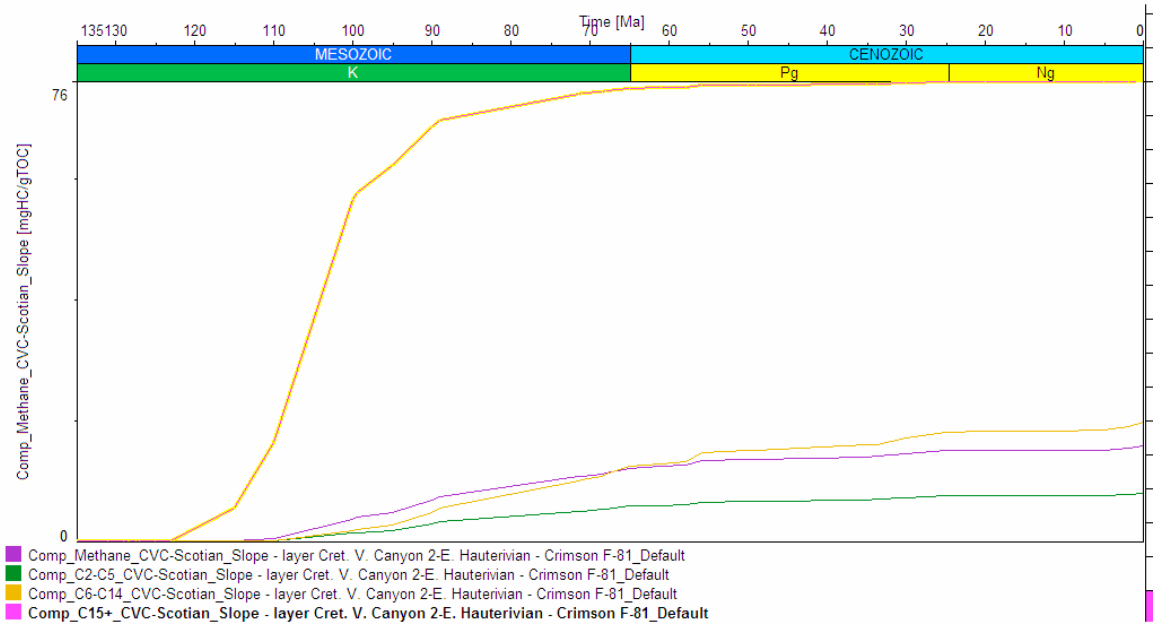

Figure 27j. Multi-component hydrocarbon expulsion versus time for the Cretaceous Verrill Canyon 2 layer for the Crimson F-81 well.

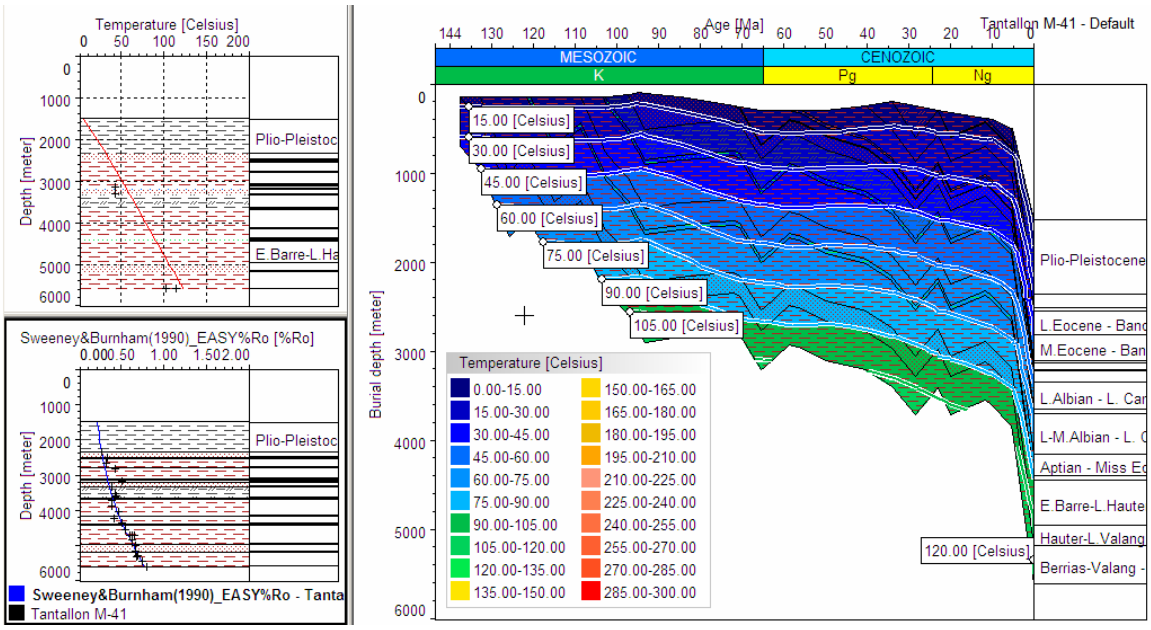

Figure 28a. Burial history of the Tantallon M-41 well with iso-temperature lines on the right and temperature or reflectance versus depth plots on the left

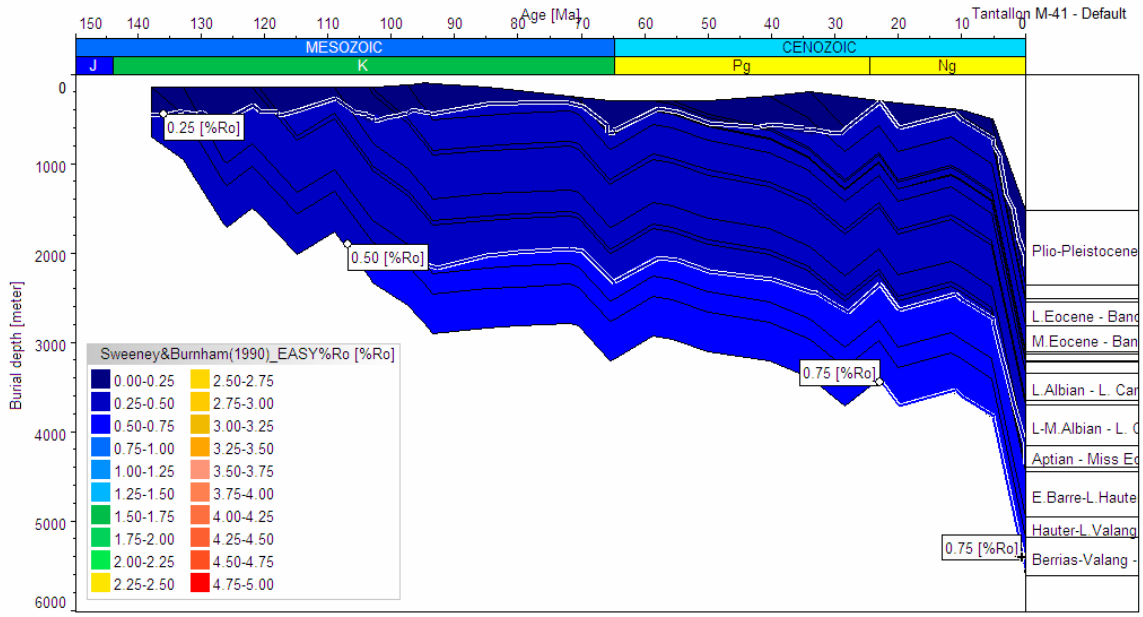

Figure 28b. Burial history of the Tantallon M-41 well with iso-reflectance line

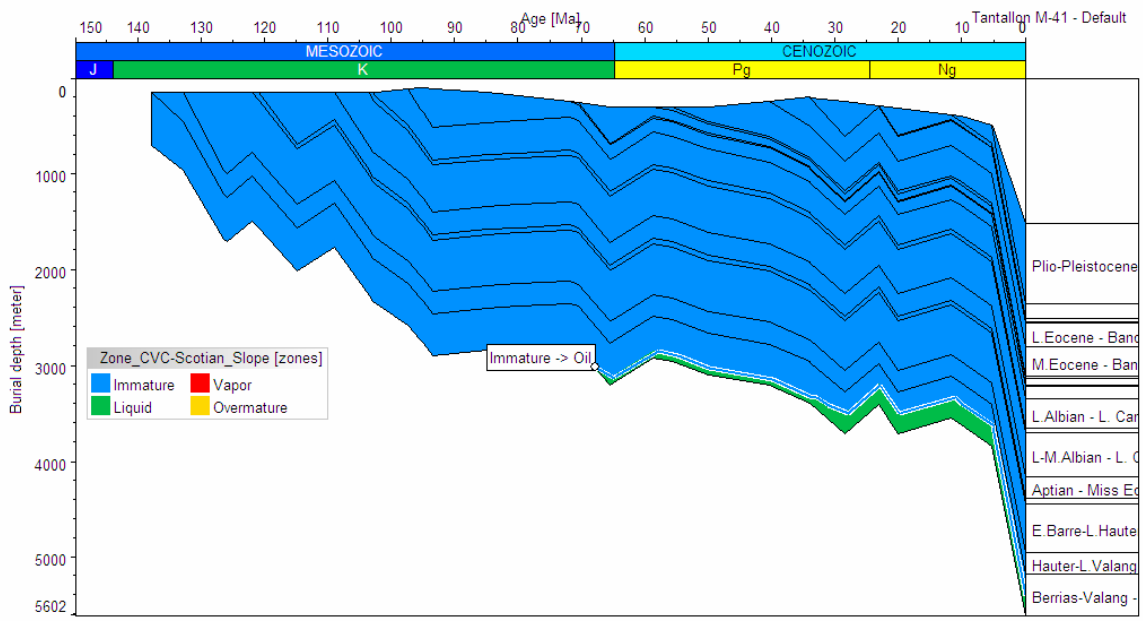

Figure 28c. Burial history of the Tantallon M-41 well with iso-hydrocarbon maturity zones (immature, oil, vapour, and overmature)

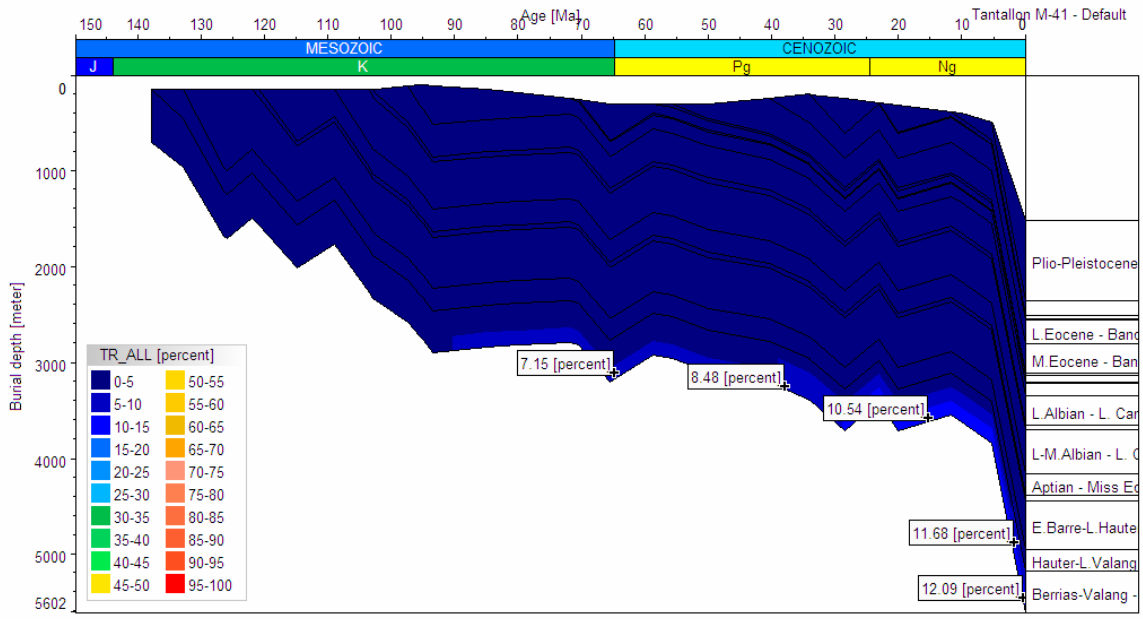

Figure 28d. Burial history of the Tantallon M-41 well with transformation ratios of Early Cretaceous source rock through geological time.

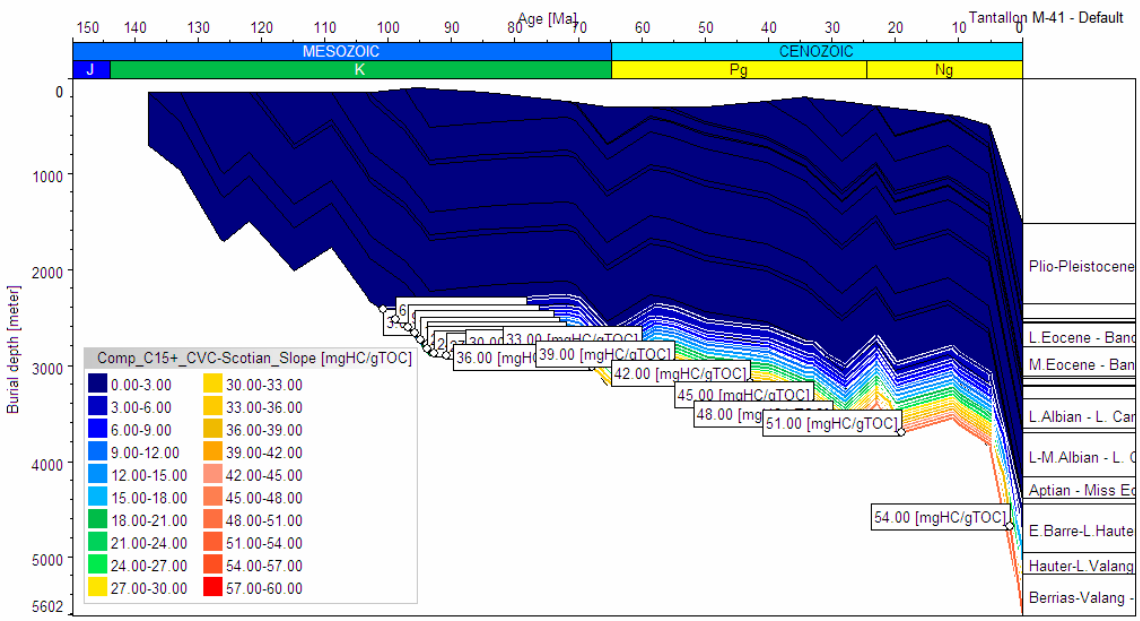

Figure 28e. Burial history of the Tantallon M-41 well with iso-C15+ (oil) generation lines

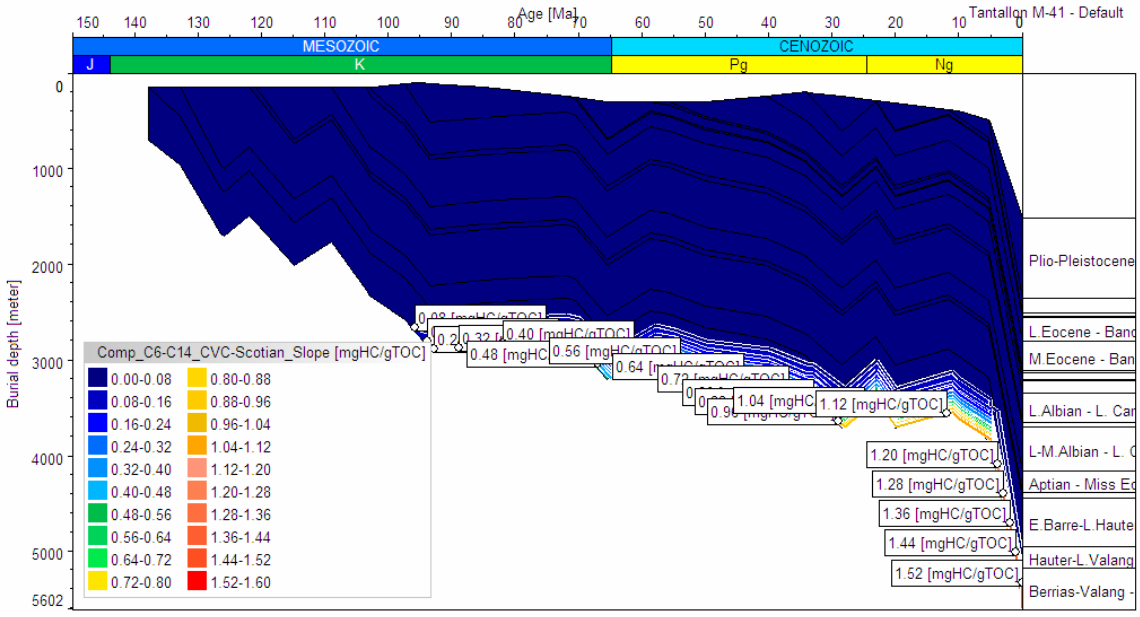

Figure 28f. Burial history of the Tantallon M-41 well with iso-C6 to C14 (condensate and light oil) generation lines

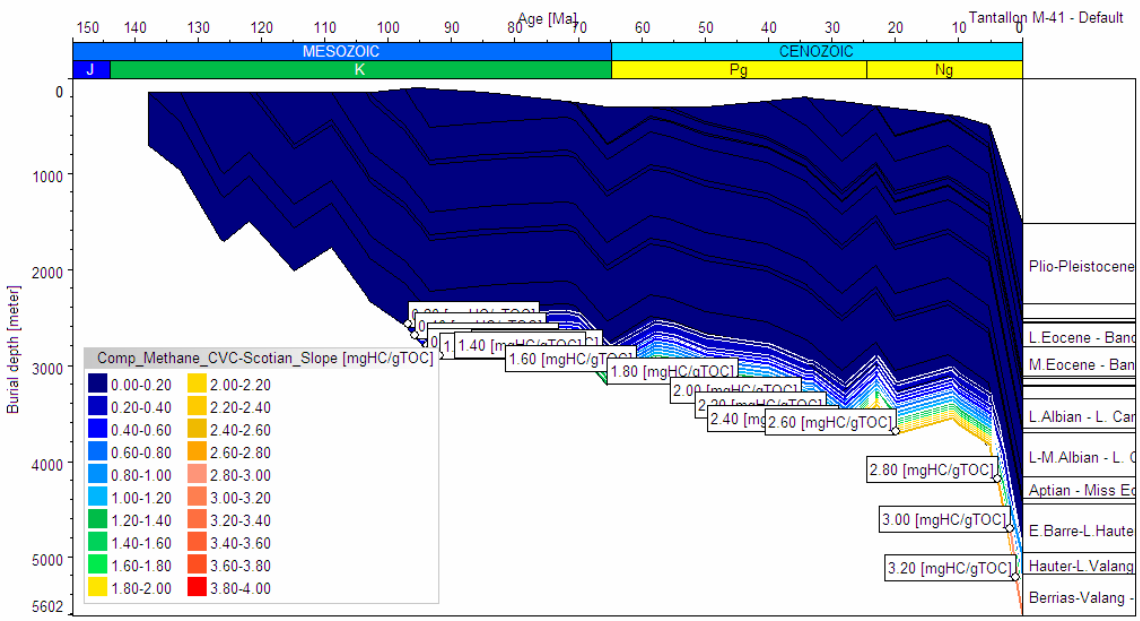

Figure 28g. Burial history of the Tantallon M-41 well with iso-methane (dry gas) generation lines (from primary cracking of kerogen)

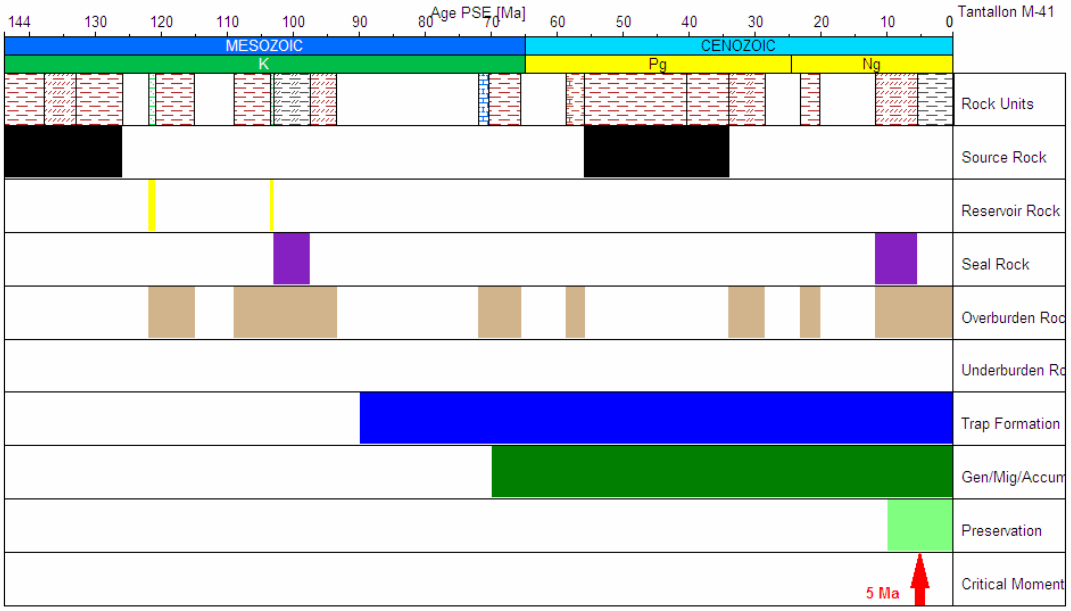

Figure 28h. Petroleum system events chart of the Tantallon M-41 well with “Critical Moment” of hydrocarbon emplacement.

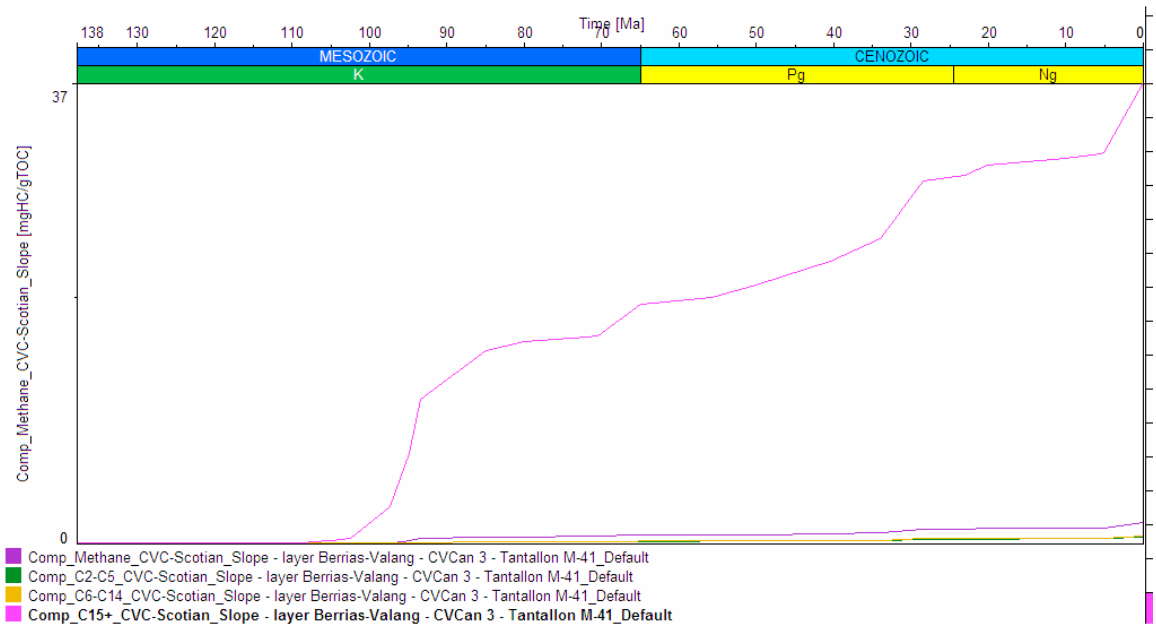

Figure 28i. Multi-component hydrocarbon expulsion versus time for the Cretaceous Verrill Canyon 3 layer from the Tantallon M-41 well.

Figures
(two dimensional petroleum system modeling)

Assigned Input Parameters in PetroBuilder and Simulation Interface

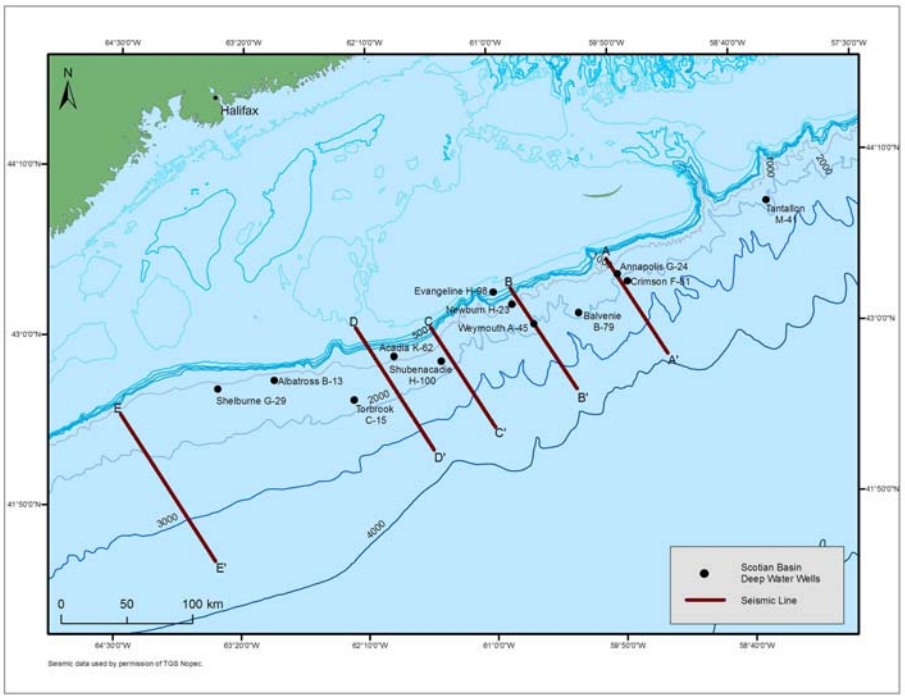

Figure 29. Location map of five seismic lines used for 2D petroleum system modeling

Modeling Input Parameters & Simulation

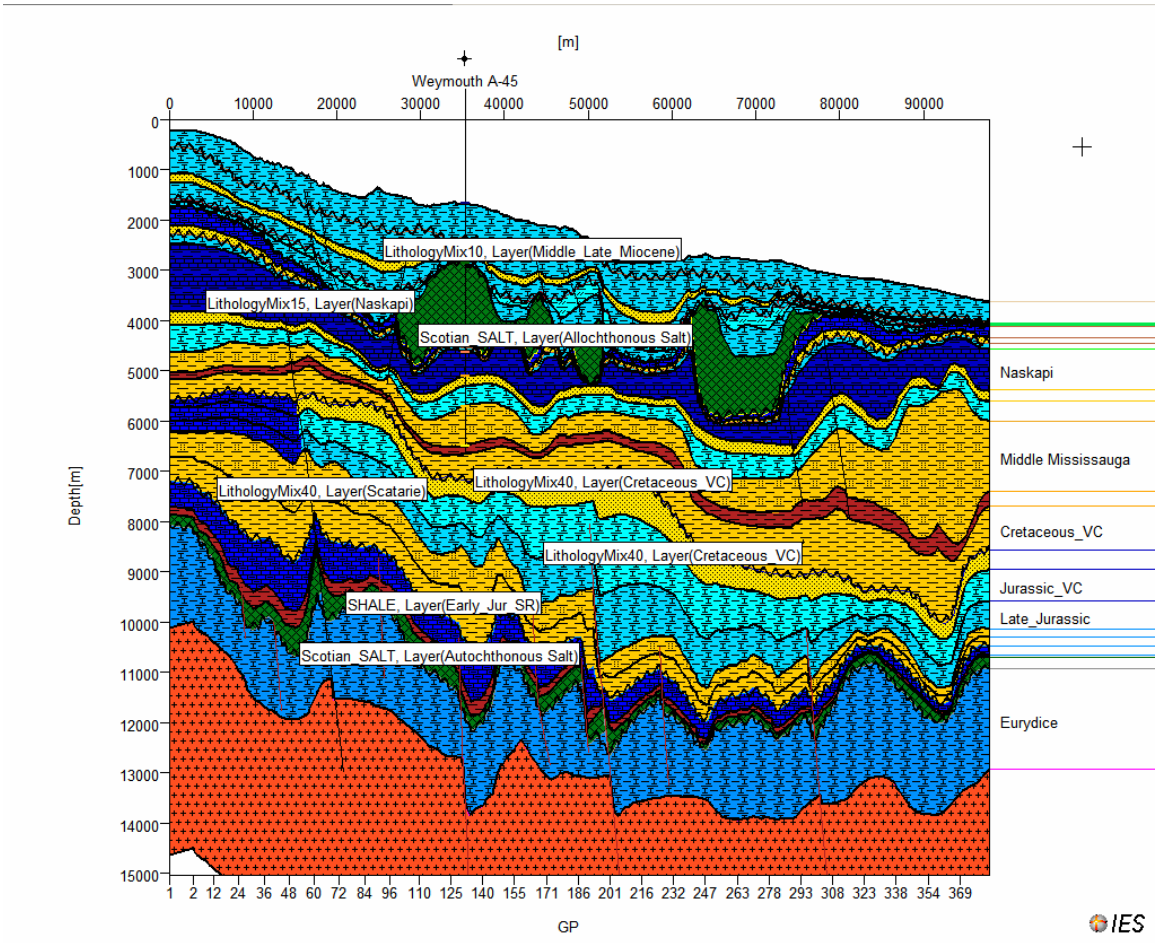

Figure 30a. Input Parameters - Assigned stratigraphic intervals, faults , and projected drilled well within the target line

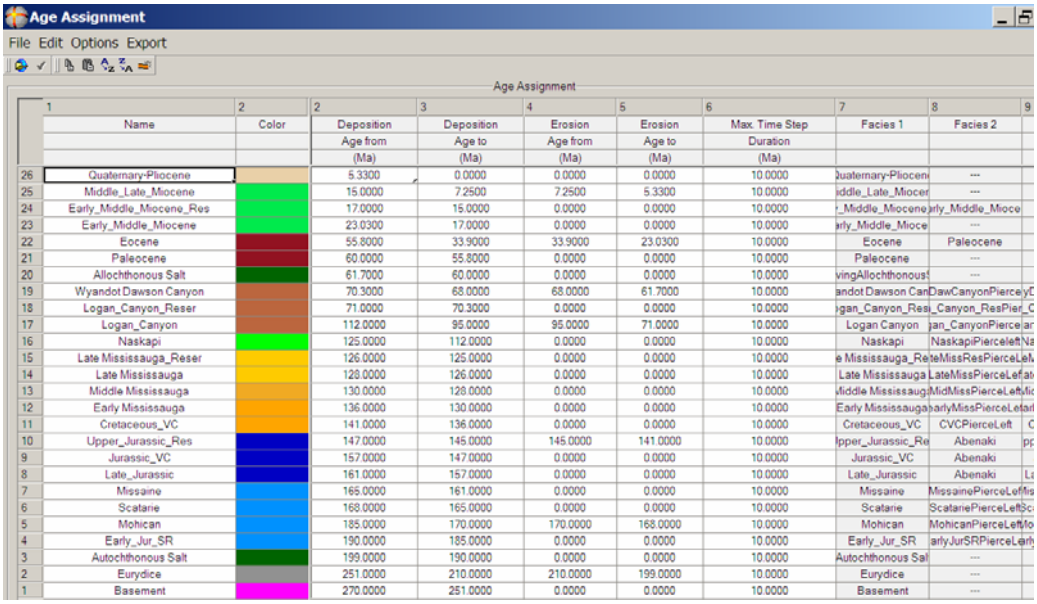

Age Assignment

File Edit Options Export

Age Assignment

	1	2	2	3	4	5	6	7	8	9
	Name	Color	Deposition Age from (Ma)	Deposition Age to (Ma)	Erosion Age from (Ma)	Erosion Age to (Ma)	Max. Time Step Duration (Ma)	Facies 1	Facies 2	
26	Quaternary-Pliocene		5.3300	0.0000	0.0000	0.0000	10.0000	uaternary-Pliocen	---	
25	Middle_Late_Miocene		15.0000	7.2500	7.2500	5.3300	10.0000	iddle_Late_Miocer	---	
24	Early_Middle_Miocene_Res		17.0000	15.0000	0.0000	0.0000	10.0000	_Middle_Miocene	rly_Middle_Mioce	
23	Early_Middle_Miocene		23.0300	17.0000	0.0000	0.0000	10.0000	rly_Middle_Mioce	---	
22	Eocene		55.8000	33.9000	33.9000	23.0300	10.0000	Eocene	Paleocene	
21	Paleocene		60.0000	55.8000	0.0000	0.0000	10.0000	Paleocene	---	
20	Allochthonous Salt		61.7000	60.0000	0.0000	0.0000	10.0000	vingAllochthonous	---	
19	Wyandot Dawson Canyon		70.3000	68.0000	68.0000	61.7000	10.0000	andot Dawson Can	DawCanyonPierce	yD
18	Logan_Canyon_Reser		71.0000	70.3000	0.0000	0.0000	10.0000	gan_Canyon_Resi	_Canyon_ResPier	C
17	Logan_Canyon		112.0000	95.0000	95.0000	71.0000	10.0000	Logan Canyon	an_CanyonPierce	ar
16	Naskapi		125.0000	112.0000	0.0000	0.0000	10.0000	Naskapi	NaskapiPierceLeft	Na
15	Late Mississauga_Reser		126.0000	125.0000	0.0000	0.0000	10.0000	e Mississauga_Re	teMissResPierceLe	M
14	Late Mississauga		128.0000	126.0000	0.0000	0.0000	10.0000	Late Mississauga	LateMissPierceLef	at
13	Middle Mississauga		130.0000	128.0000	0.0000	0.0000	10.0000	Middle Mississaug	MidMissPierceLeft	Mi
12	Early Mississauga		136.0000	130.0000	0.0000	0.0000	10.0000	Early Mississauga	arlyMissPierceLeft	ar
11	Cretaceous_VC		141.0000	136.0000	0.0000	0.0000	10.0000	Cretaceous_VC	CVCPierceLeft	C
10	Upper_Jurassic_Res		147.0000	145.0000	145.0000	141.0000	10.0000	pper_Jurassic_Re	Abenaki	pp
9	Jurassic_VC		157.0000	147.0000	0.0000	0.0000	10.0000	Jurassic_VC	Abenaki	
8	Late_Jurassic		161.0000	157.0000	0.0000	0.0000	10.0000	Late_Jurassic	Abenaki	La
7	Missaine		165.0000	161.0000	0.0000	0.0000	10.0000	Missaine	MissainePierceLef	Mis
6	Scatarie		168.0000	165.0000	0.0000	0.0000	10.0000	Scatarie	ScatariePierceLeft	Sc
5	Mohican		185.0000	170.0000	170.0000	168.0000	10.0000	Mohican	MohicanPierceLeft	Mo
4	Early_Jur_SR		190.0000	185.0000	0.0000	0.0000	10.0000	Early_Jur_SR	arlyJurSRPierceLe	ar
3	Autochthonous Salt		199.0000	190.0000	0.0000	0.0000	10.0000	Autochthonous Sal	---	
2	Eurydice		251.0000	210.0000	210.0000	199.0000	10.0000	Eurydice	---	
1	Basement		270.0000	251.0000	0.0000	0.0000	10.0000	Basement	---	

Figure 30b. Input Parameters- Assigned geological ages for each intervals

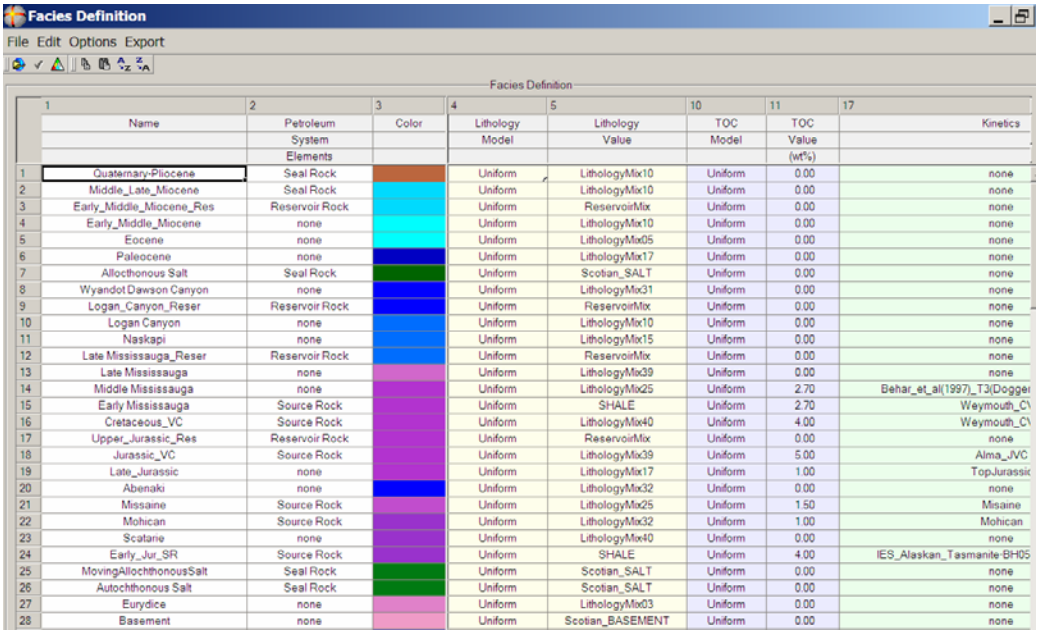

Facies Definition

File Edit Options Export

Facies Definition

	1	2	3	4	5	10	11	17
	Name	Petroleum System Elements	Color	Lithology Model	Lithology Value	TOC Model	TOC Value (wt%)	Kinetics
1	Quaternary-Pliocene	Seal Rock		Uniform	LithologyMix10	Uniform	0.00	none
2	Middle_Late_Miocene	Seal Rock		Uniform	LithologyMix10	Uniform	0.00	none
3	Early_Middle_Miocene_Res	Reservoir Rock		Uniform	ReservoirMix	Uniform	0.00	none
4	Early_Middle_Miocene	none		Uniform	LithologyMix10	Uniform	0.00	none
5	Eocene	none		Uniform	LithologyMix05	Uniform	0.00	none
6	Paleocene	none		Uniform	LithologyMix17	Uniform	0.00	none
7	Allocthonous Salt	Seal Rock		Uniform	Scotian_SALT	Uniform	0.00	none
8	Wyandot Dawson Canyon	none		Uniform	LithologyMix31	Uniform	0.00	none
9	Logan_Canyon_Reser	Reservoir Rock		Uniform	ReservoirMix	Uniform	0.00	none
10	Logan Canyon	none		Uniform	LithologyMix10	Uniform	0.00	none
11	Naskapi	none		Uniform	LithologyMix15	Uniform	0.00	none
12	Late Mississauga_Reser	Reservoir Rock		Uniform	ReservoirMix	Uniform	0.00	none
13	Late Mississauga	none		Uniform	LithologyMix39	Uniform	0.00	none
14	Middle Mississauga	none		Uniform	LithologyMix25	Uniform	2.70	Behar_et_al(1997)_T3(Dogger
15	Early Mississauga	Source Rock		Uniform	SHALE	Uniform	2.70	Weymouth_C
16	Cretaceous_VC	Source Rock		Uniform	LithologyMix40	Uniform	4.00	Weymouth_C
17	Upper_Jurassic_Res	Reservoir Rock		Uniform	ReservoirMix	Uniform	0.00	none
18	Jurassic_VC	Source Rock		Uniform	LithologyMix39	Uniform	5.00	Alma_JVC
19	Late_Jurassic	none		Uniform	LithologyMix17	Uniform	1.00	TopJurassic
20	Abenaki	none		Uniform	LithologyMix32	Uniform	0.00	none
21	Missaine	Source Rock		Uniform	LithologyMix25	Uniform	1.50	Misaine
22	Mohican	Source Rock		Uniform	LithologyMix32	Uniform	1.00	Mohican
23	Scatarie	none		Uniform	LithologyMix40	Uniform	0.00	none
24	Early_Jur_SR	Source Rock		Uniform	SHALE	Uniform	4.00	IES_Alaskan_Tasmanite-BH05
25	MovingAllochthonousSalt	Seal Rock		Uniform	Scotian_SALT	Uniform	0.00	none
26	Autochthonous Salt	Seal Rock		Uniform	Scotian_SALT	Uniform	0.00	none
27	Eurydice	none		Uniform	LithologyMix03	Uniform	0.00	none
28	Basement	none		Uniform	Scotian_BASEMENT	Uniform	0.00	none

Figure 30c(i): Input parameters - Petroleum system events structure along with the input lithology and kinetics

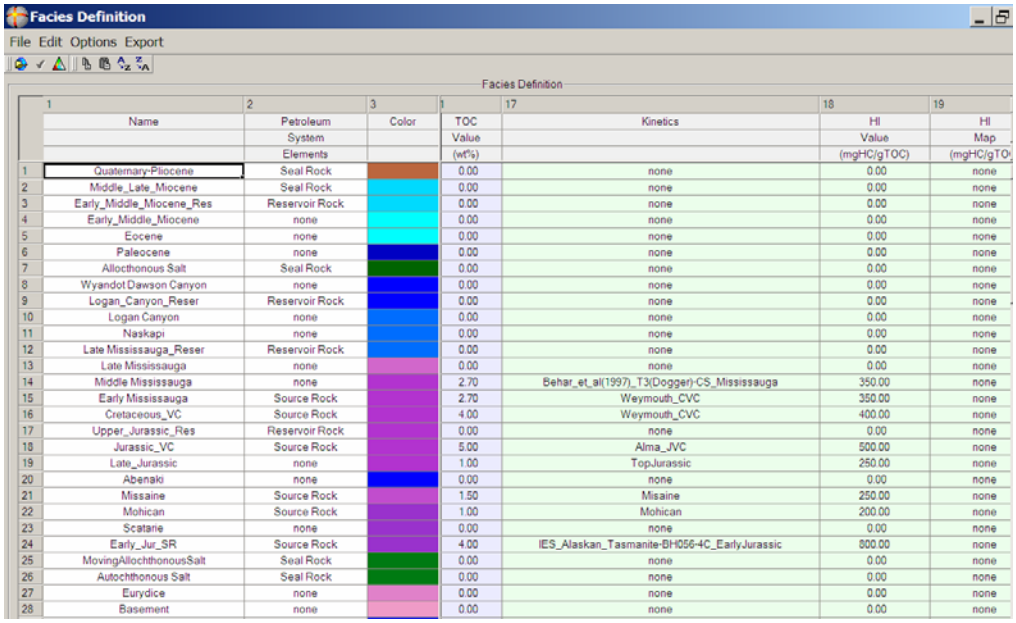

	1	2	3	1	17	18	19
	Name	Petroleum System Elements	Color	TOC Value (wt%)	Kinetics	HI Value (mgHC/gTOC)	HI Map (mgHC/gTO
1	Quaternary-Pliocene	Seal Rock		0.00	none	0.00	none
2	Middle_Late_Miocene	Seal Rock		0.00	none	0.00	none
3	Early_Middle_Miocene_Res	Reservoir Rock		0.00	none	0.00	none
4	Early_Middle_Miocene	none		0.00	none	0.00	none
5	Eocene	none		0.00	none	0.00	none
6	Paleocene	none		0.00	none	0.00	none
7	Allocthonous Salt	Seal Rock		0.00	none	0.00	none
8	Wyandot Dawson Canyon	none		0.00	none	0.00	none
9	Logan_Canyon_Reser	Reservoir Rock		0.00	none	0.00	none
10	Logan Canyon	none		0.00	none	0.00	none
11	Naskapi	none		0.00	none	0.00	none
12	Late Mississauga_Reser	Reservoir Rock		0.00	none	0.00	none
13	Late Mississauga	none		0.00	none	0.00	none
14	Middle Mississauga	none		2.70	Behar_et_al(1997)_T3(Dogger)-CS_Mississauga	350.00	none
15	Early Mississauga	Source Rock		2.70	Weymouth_CVC	350.00	none
16	Cretaceous_VC	Source Rock		4.00	Weymouth_CVC	400.00	none
17	Upper_Jurassic_Res	Reservoir Rock		0.00	none	0.00	none
18	Jurassic_VC	Source Rock		5.00	Alma_JVC	500.00	none
19	Late_Jurassic	none		1.00	TopJurassic	250.00	none
20	Abenaki	none		0.00	none	0.00	none
21	Missaine	Source Rock		1.50	Misaine	250.00	none
22	Mohican	Source Rock		1.00	Mohican	200.00	none
23	Scatarie	none		0.00	none	0.00	none
24	Early_Jur_SR	Source Rock		4.00	IES_Alaskan_Tasmanite-BH056-4C_EarlyJurassic	800.00	none
25	MovingAllochthonousSalt	Seal Rock		0.00	none	0.00	none
26	Autochthonous Salt	Seal Rock		0.00	none	0.00	none
27	Eurydice	none		0.00	none	0.00	none
28	Basement	none		0.00	none	0.00	none

Figure 30 c(ii): Input Parameters – Petroleum system events structure along with the input lithology, kinetics, and source rock properties

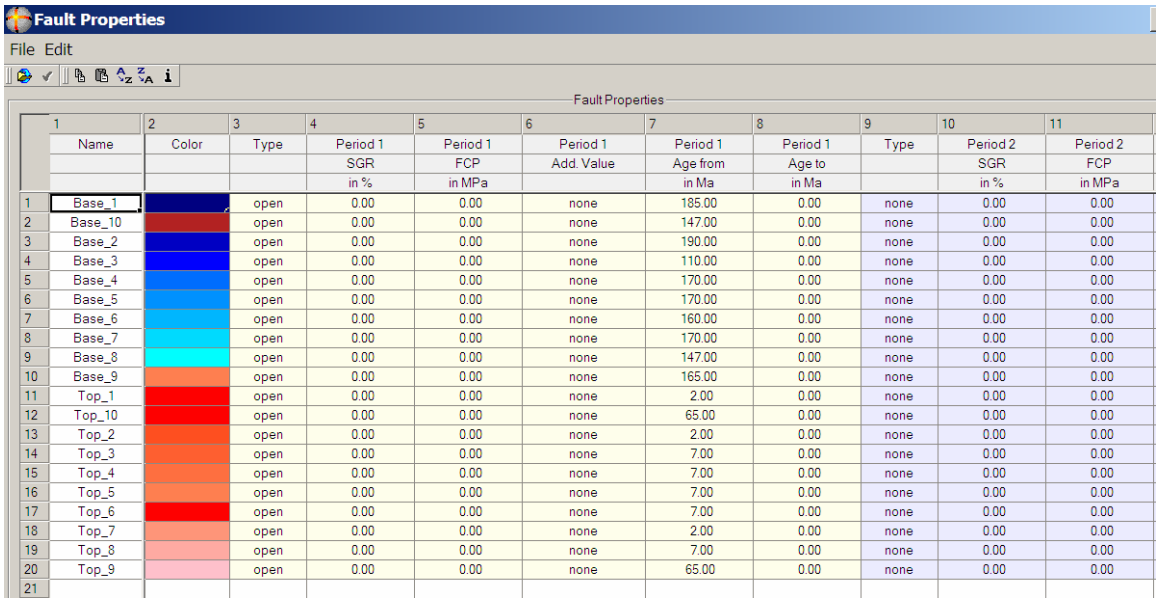

	1	2	3	4	5	6	7	8	9	10	11
	Name	Color	Type	Period 1 SGR in %	Period 1 FCP in MPa	Period 1 Add. Value	Period 1 Age from in Ma	Period 1 Age to in Ma	Type	Period 2 SGR in %	Period 2 FCP in MPa
1	Base_1		open	0.00	0.00	none	185.00	0.00	none	0.00	0.00
2	Base_10		open	0.00	0.00	none	147.00	0.00	none	0.00	0.00
3	Base_2		open	0.00	0.00	none	190.00	0.00	none	0.00	0.00
4	Base_3		open	0.00	0.00	none	110.00	0.00	none	0.00	0.00
5	Base_4		open	0.00	0.00	none	170.00	0.00	none	0.00	0.00
6	Base_5		open	0.00	0.00	none	170.00	0.00	none	0.00	0.00
7	Base_6		open	0.00	0.00	none	160.00	0.00	none	0.00	0.00
8	Base_7		open	0.00	0.00	none	170.00	0.00	none	0.00	0.00
9	Base_8		open	0.00	0.00	none	147.00	0.00	none	0.00	0.00
10	Base_9		open	0.00	0.00	none	165.00	0.00	none	0.00	0.00
11	Top_1		open	0.00	0.00	none	2.00	0.00	none	0.00	0.00
12	Top_10		open	0.00	0.00	none	65.00	0.00	none	0.00	0.00
13	Top_2		open	0.00	0.00	none	2.00	0.00	none	0.00	0.00
14	Top_3		open	0.00	0.00	none	7.00	0.00	none	0.00	0.00
15	Top_4		open	0.00	0.00	none	7.00	0.00	none	0.00	0.00
16	Top_5		open	0.00	0.00	none	7.00	0.00	none	0.00	0.00
17	Top_6		open	0.00	0.00	none	7.00	0.00	none	0.00	0.00
18	Top_7		open	0.00	0.00	none	2.00	0.00	none	0.00	0.00
19	Top_8		open	0.00	0.00	none	7.00	0.00	none	0.00	0.00
20	Top_9		open	0.00	0.00	none	65.00	0.00	none	0.00	0.00
21											

Figure 30d: Input Parameters – Assigned fault properties

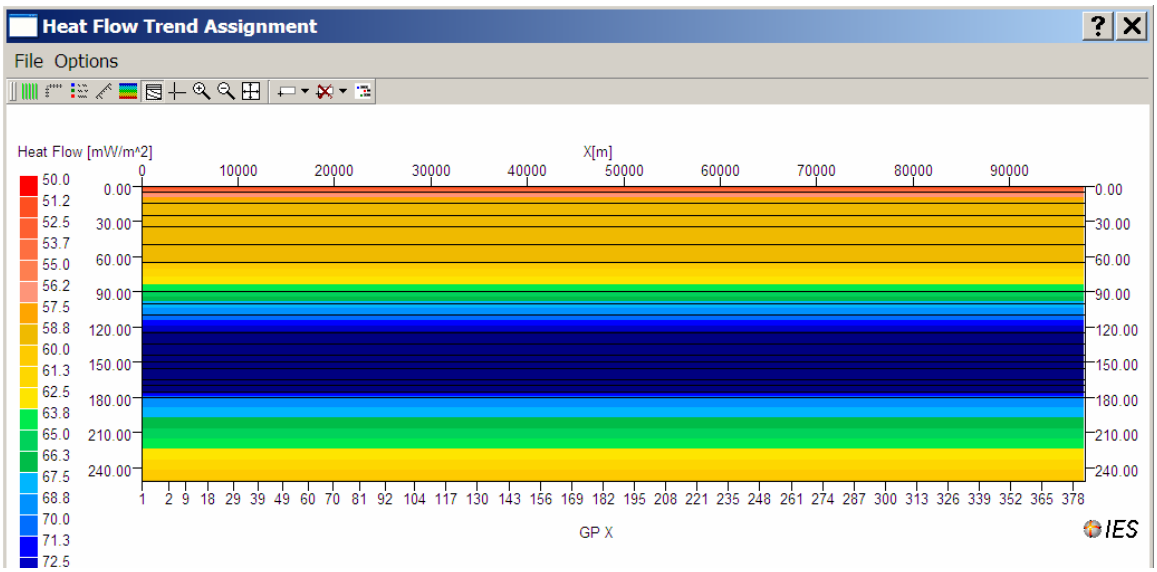

Figure 30e (i): Input Parameters – Assigned various paleo-trend surfaces (a) heat flow

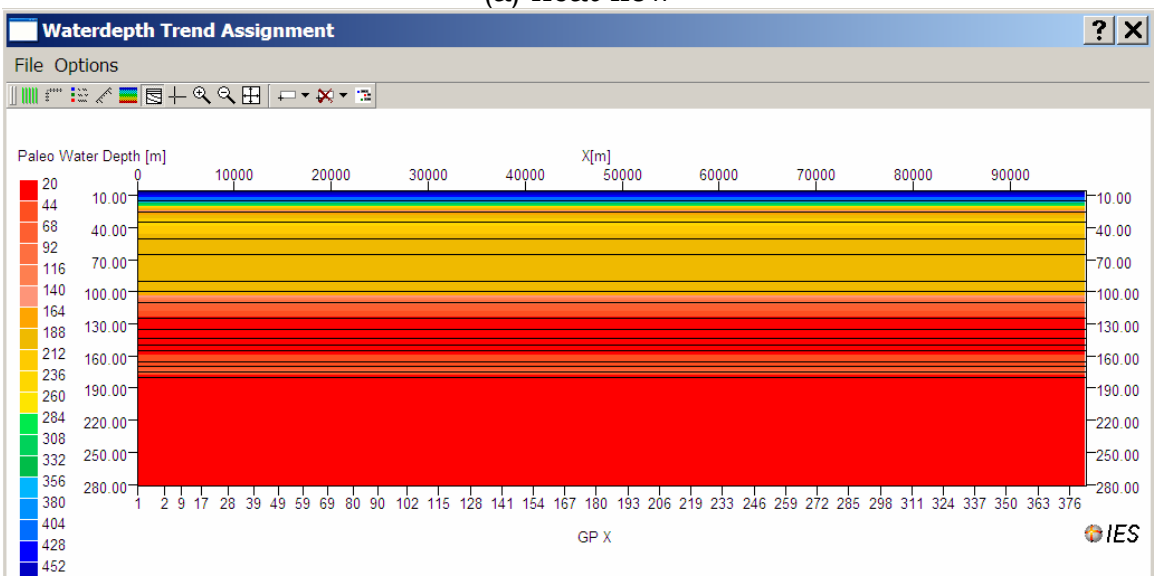

Figure 30e (ii): Input Parameters – Assigned various paleo-trend surfaces (b) water depth

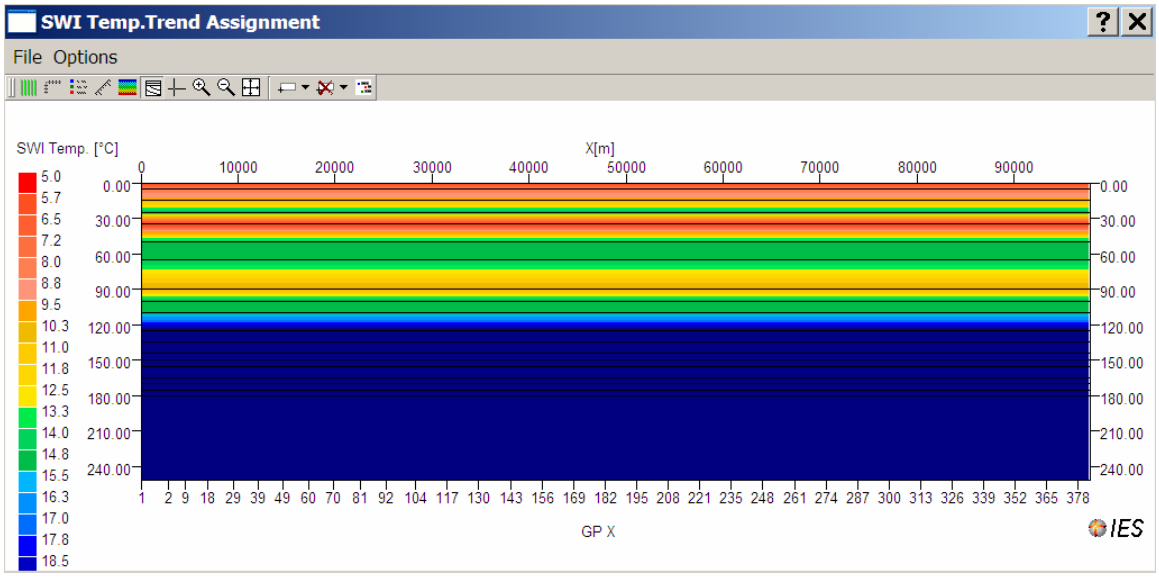

Figure 30e (iii): Input Parameters – Assigned various paleo-trend surfaces (c) temperature of sediment and water interface

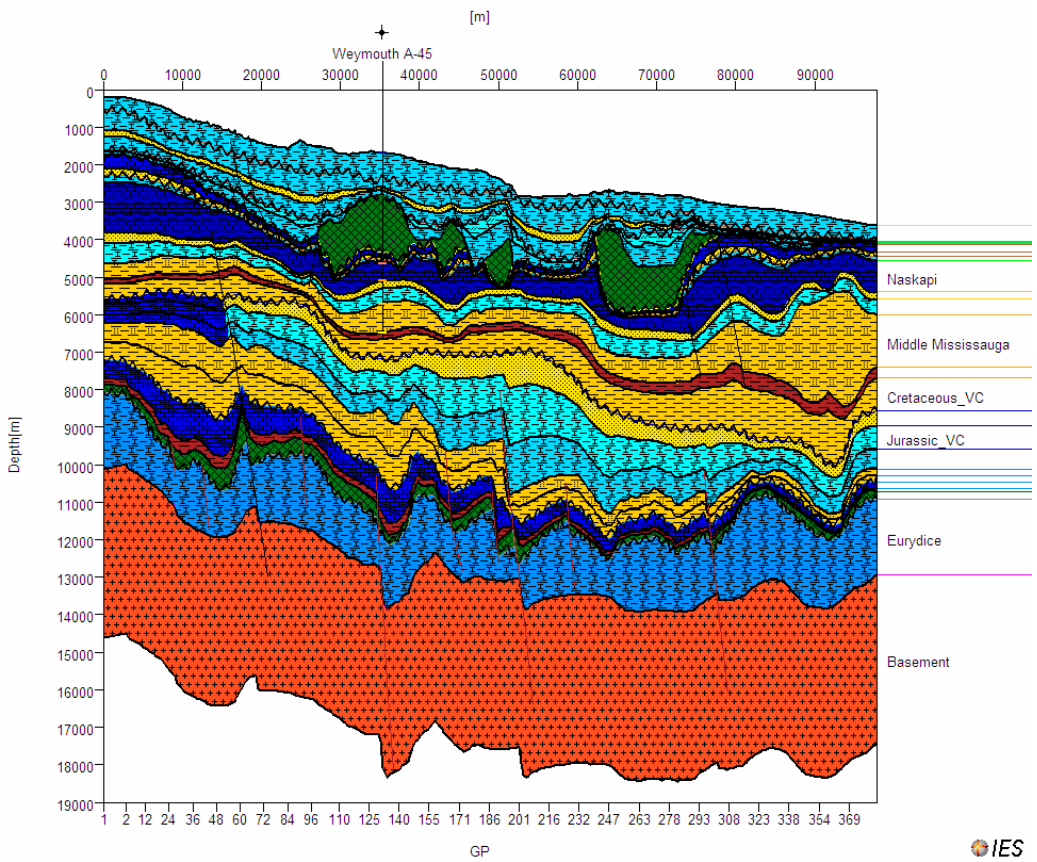

Figure 30f: Input Parameters – Assigned unconformities

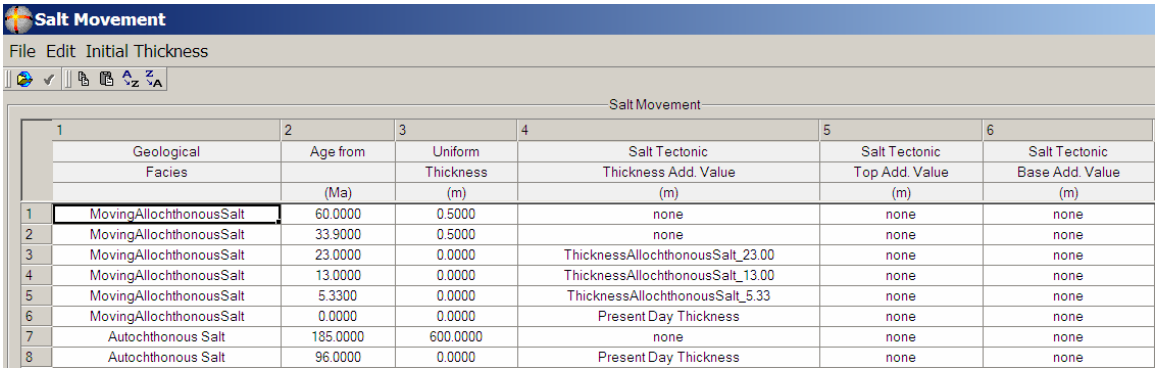

	1	2	3	4	5	6
	Geological Facies	Age from	Uniform Thickness	Salt Tectonic Thickness Add. Value	Salt Tectonic Top Add. Value	Salt Tectonic Base Add. Value
		(Ma)	(m)	(m)	(m)	(m)
1	MovingAllochthonousSalt	60.0000	0.5000	none	none	none
2	MovingAllochthonousSalt	33.9000	0.5000	none	none	none
3	MovingAllochthonousSalt	23.0000	0.0000	ThicknessAllochthonousSalt_23.00	none	none
4	MovingAllochthonousSalt	13.0000	0.0000	ThicknessAllochthonousSalt_13.00	none	none
5	MovingAllochthonousSalt	5.3300	0.0000	ThicknessAllochthonousSalt_5.33	none	none
6	MovingAllochthonousSalt	0.0000	0.0000	Present Day Thickness	none	none
7	Autochthonous Salt	185.0000	600.0000	none	none	none
8	Autochthonous Salt	96.0000	0.0000	Present Day Thickness	none	none

Figure 30g. Input Parameters - Assigned time periods for autochthonous salt movement and allochthonous salt piercement

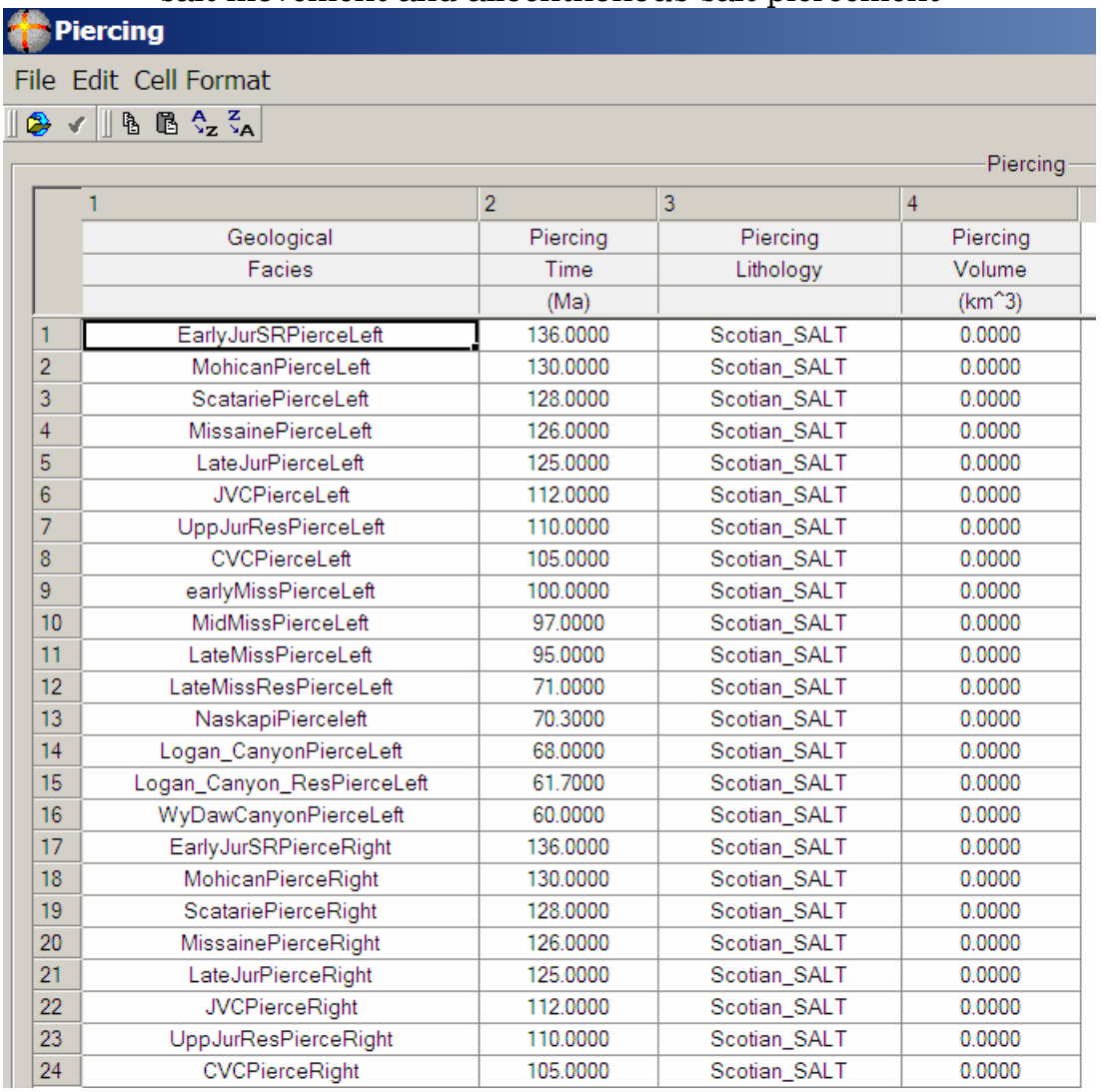

	1	2	3	4
	Geological Facies	Piercing Time	Piercing Lithology	Piercing Volume
		(Ma)		(km^3)
1	EarlyJurSRPierceLeft	136.0000	Scotian_SALT	0.0000
2	MohicanPierceLeft	130.0000	Scotian_SALT	0.0000
3	ScatariePierceLeft	128.0000	Scotian_SALT	0.0000
4	MissainePierceLeft	126.0000	Scotian_SALT	0.0000
5	LateJurPierceLeft	125.0000	Scotian_SALT	0.0000
6	JVCPierceLeft	112.0000	Scotian_SALT	0.0000
7	UppJurResPierceLeft	110.0000	Scotian_SALT	0.0000
8	CVCPierceLeft	105.0000	Scotian_SALT	0.0000
9	earlyMissPierceLeft	100.0000	Scotian_SALT	0.0000
10	MidMissPierceLeft	97.0000	Scotian_SALT	0.0000
11	LateMissPierceLeft	95.0000	Scotian_SALT	0.0000
12	LateMissResPierceLeft	71.0000	Scotian_SALT	0.0000
13	NaskapiPierceleft	70.3000	Scotian_SALT	0.0000
14	Logan_CanyonPierceLeft	68.0000	Scotian_SALT	0.0000
15	Logan_Canyon_ResPierceLeft	61.7000	Scotian_SALT	0.0000
16	WyDawCanyonPierceLeft	60.0000	Scotian_SALT	0.0000
17	EarlyJurSRPierceRight	136.0000	Scotian_SALT	0.0000
18	MohicanPierceRight	130.0000	Scotian_SALT	0.0000
19	ScatariePierceRight	128.0000	Scotian_SALT	0.0000
20	MissainePierceRight	126.0000	Scotian_SALT	0.0000
21	LateJurPierceRight	125.0000	Scotian_SALT	0.0000
22	JVCPierceRight	112.0000	Scotian_SALT	0.0000
23	UppJurResPierceRight	110.0000	Scotian_SALT	0.0000
24	CVCPierceRight	105.0000	Scotian_SALT	0.0000

Figure 30h. Input Parameters - Assigned allochthonous salt piercement time periods for the Weymouth A-45 well

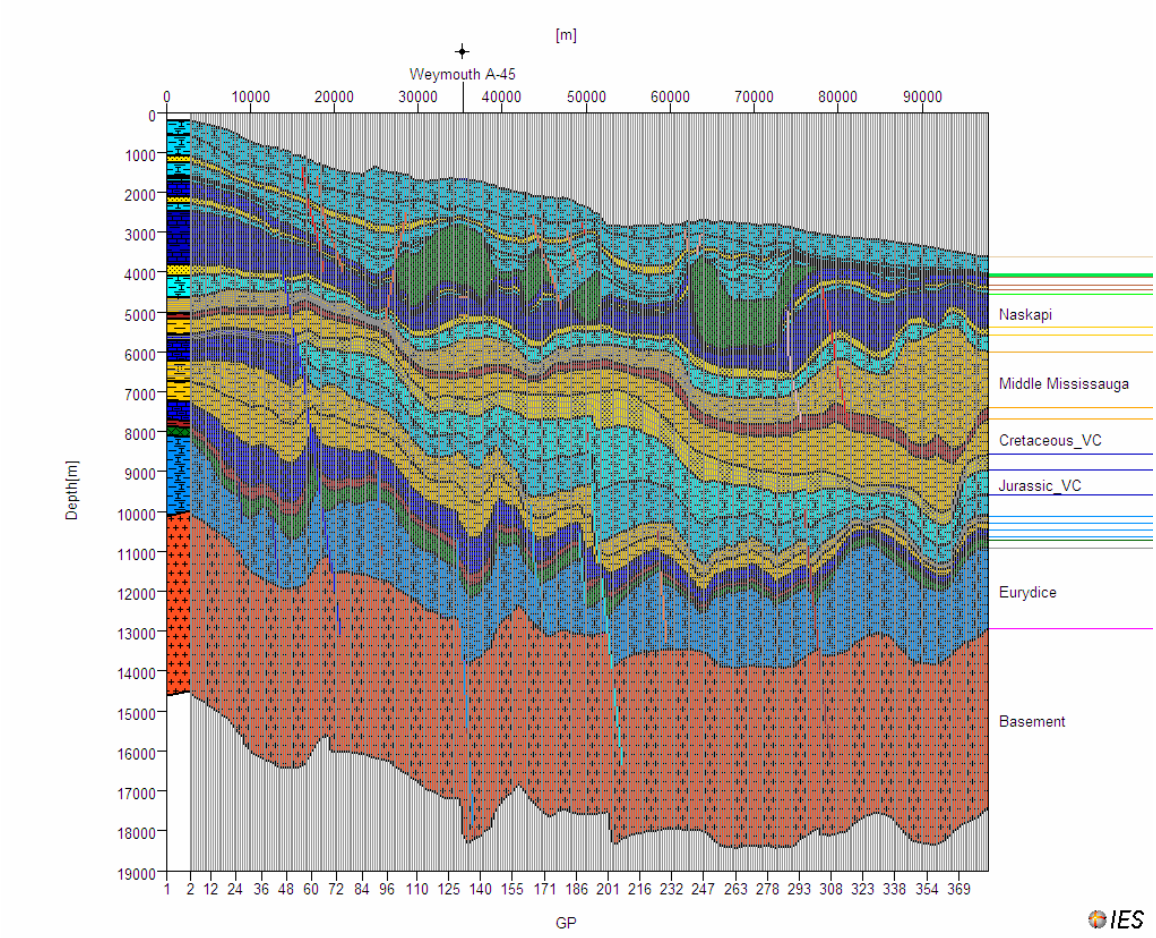

Figure 30i. Input Parameters - Assigned grid patterns forming the cell structures for the simulation of hydrocarbon migration

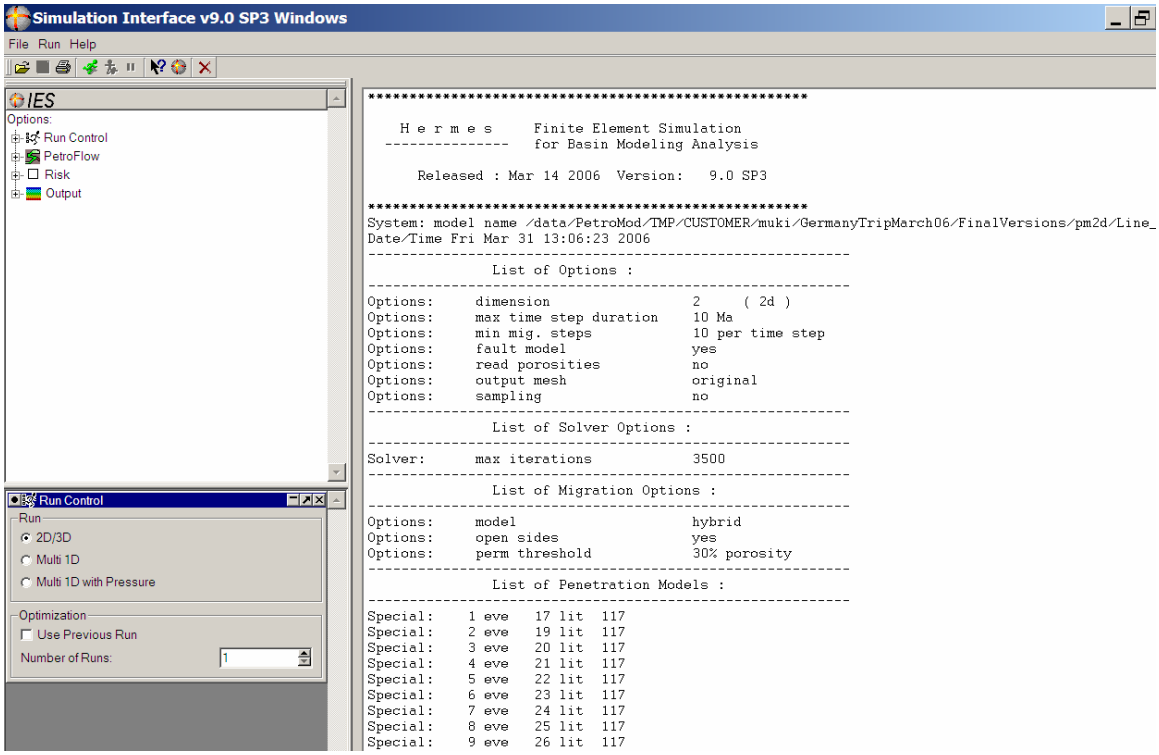

Figure 31. Simulation Interfaces for 2D petroleum system modeling

2D Modeling Output Results – Five Seismic Lines

Seismic Line E-E’

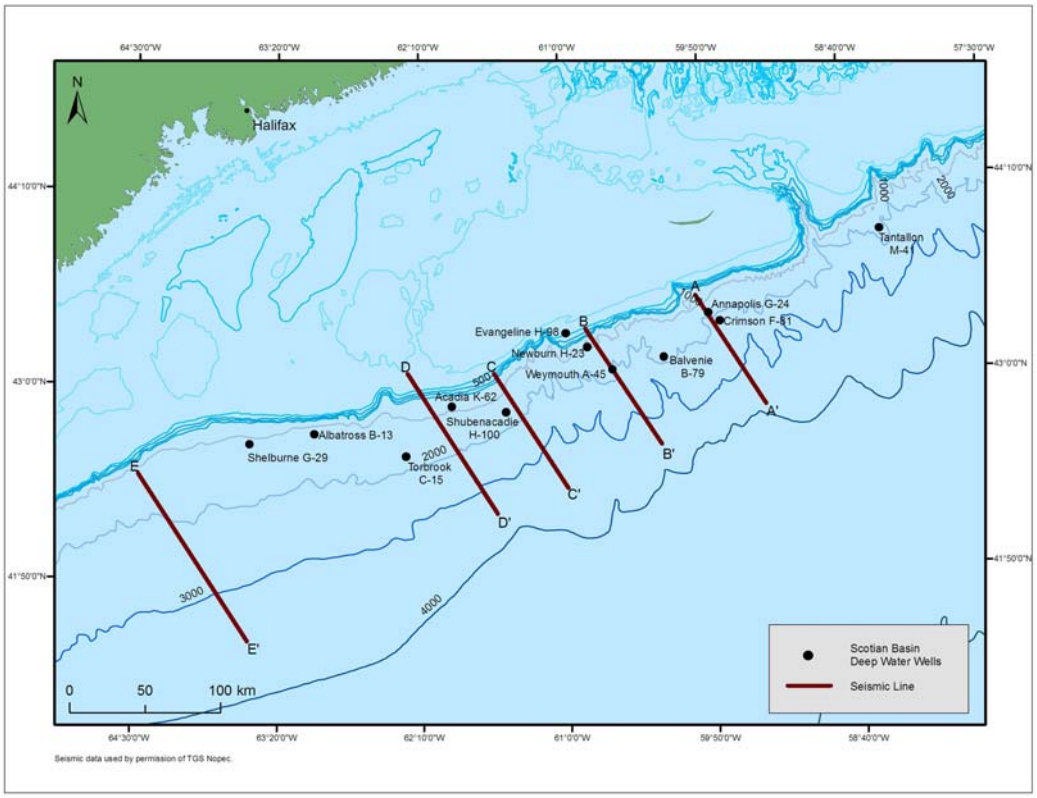

Figure 32a. Location map of the Seismic Line E-E’

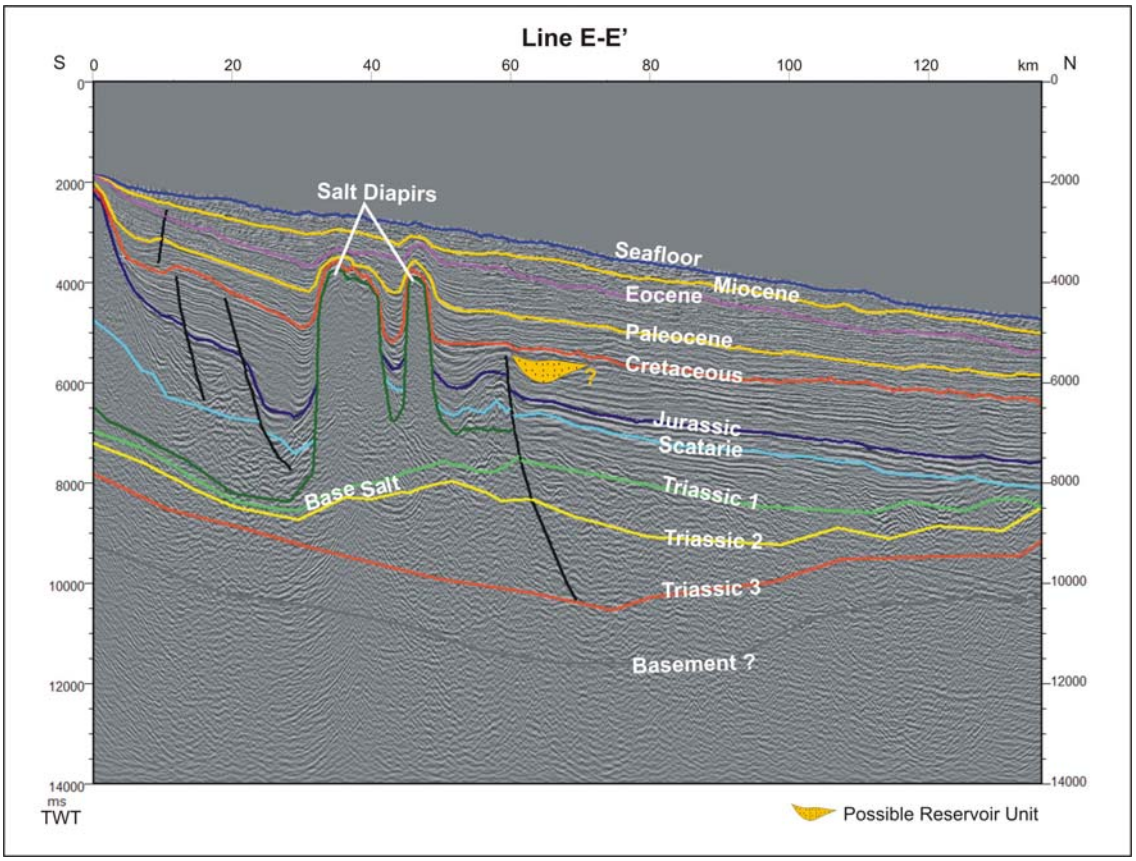

Figure 32b. Seismic line E-E (western Shelburne Subbasin) with selected formation boundaries, faults, salt diapirs, and a possible reservoir unit

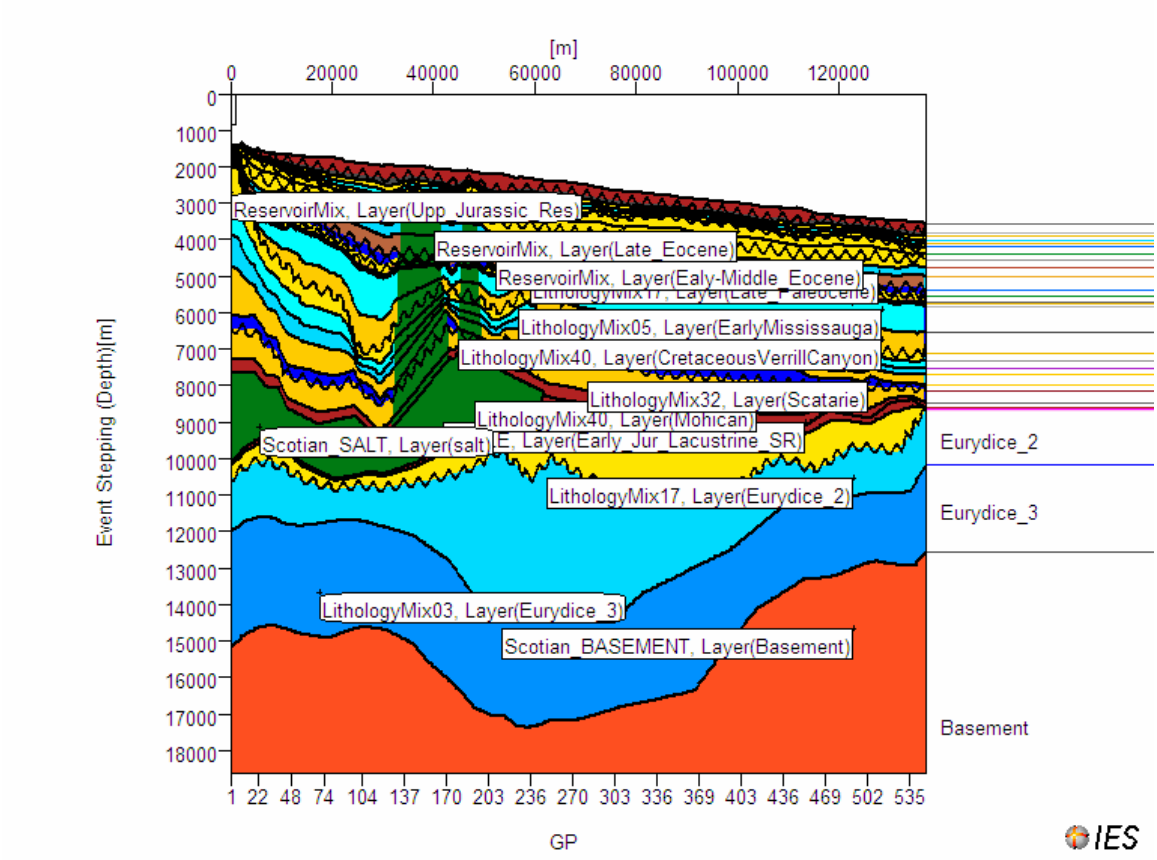

Figure 32c. line E-E' – formation boundaries, faults, and assigned lithology within PetroBuider after depth conversion

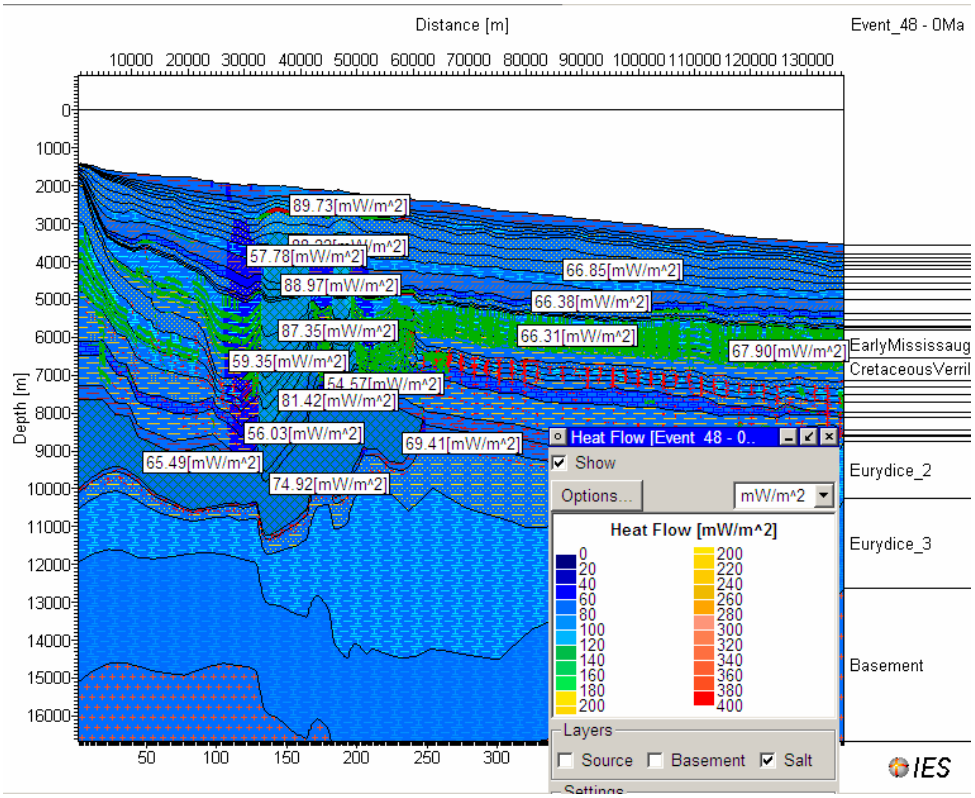

Figure 32d (i). Output data showing the distribution of heat flow and the trend of hydrocarbon flowpaths at the present time

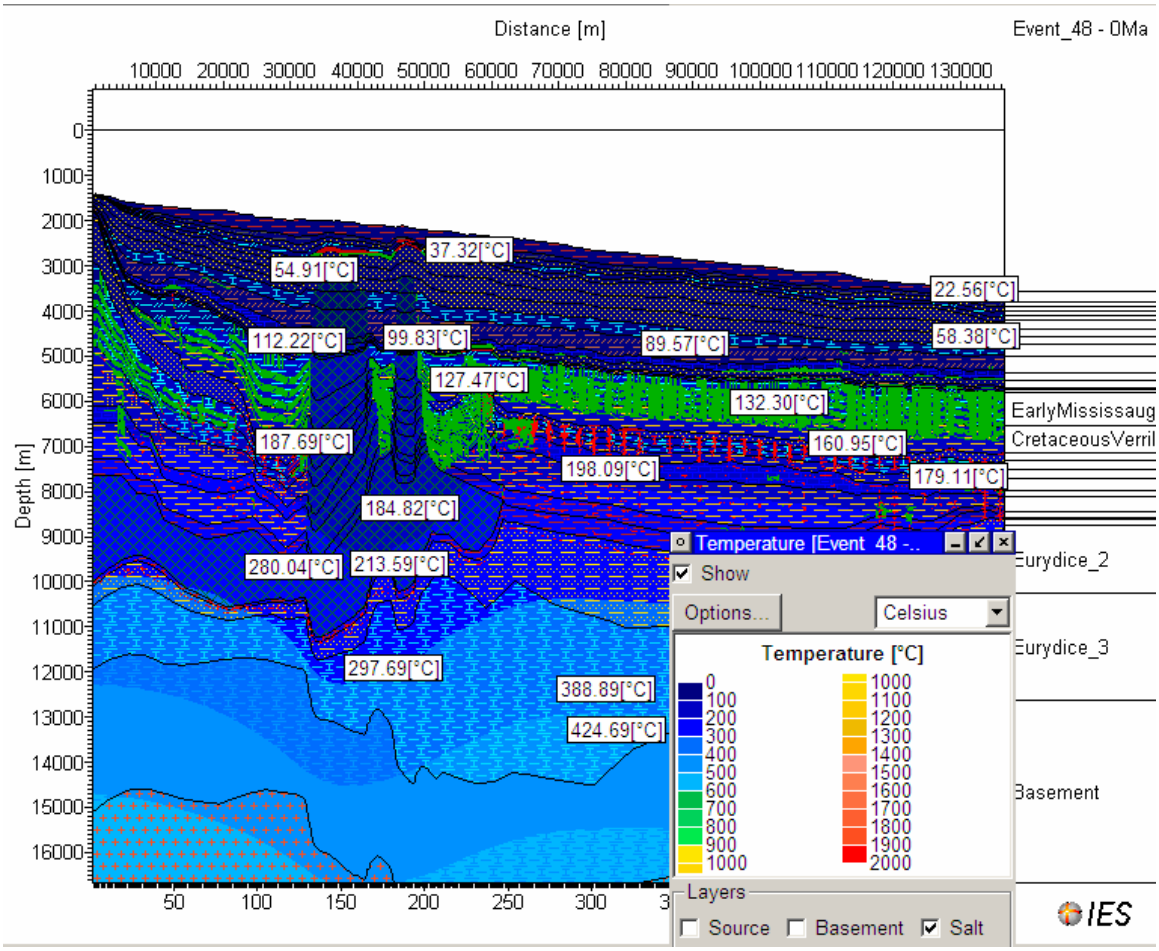

Figure 32d (ii). Line E-E' – Output data showing the distribution of temperatures and the trend of hydrocarbon flowpaths at the present time

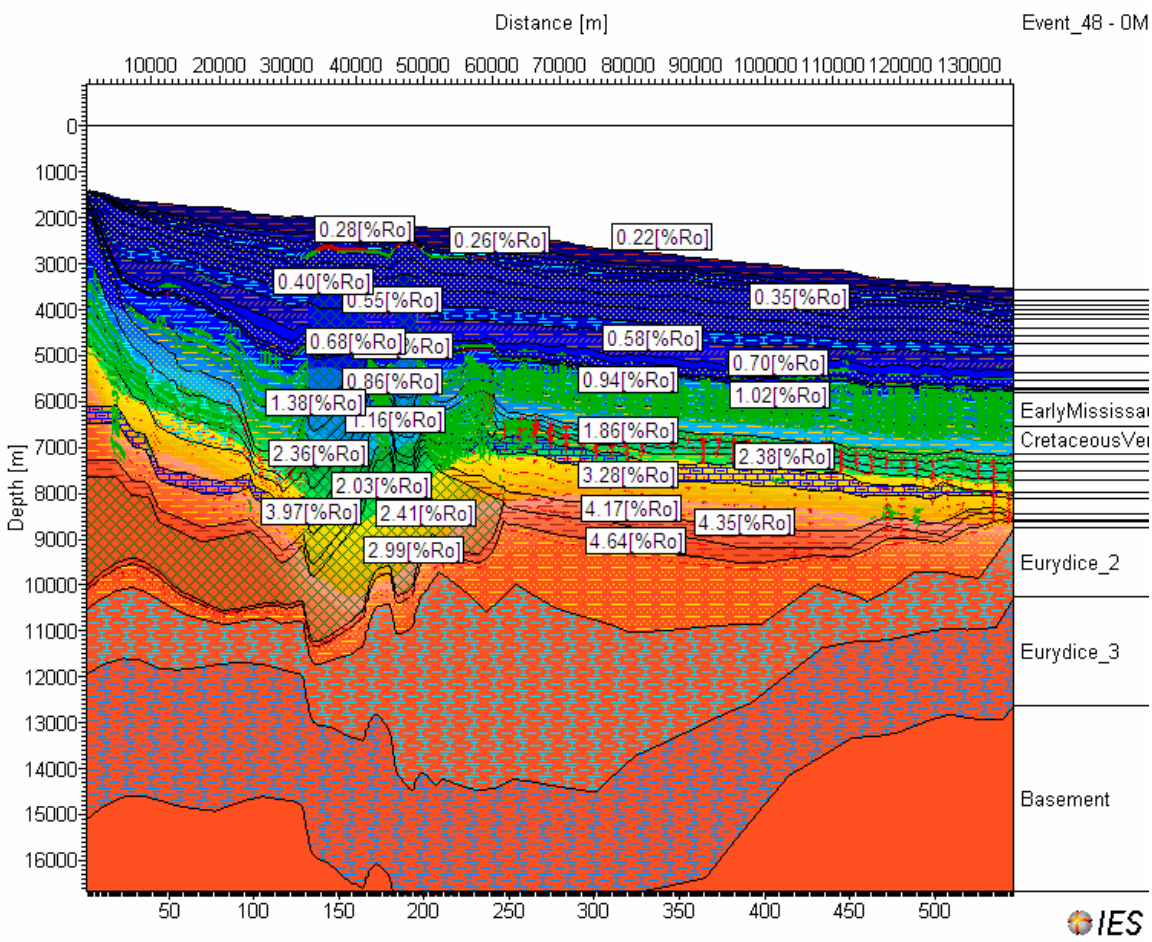

Figure 32d (iii). Line E-E' - Output data showing the distribution of the vitrinite reflectance values and the trend of hydrocarbon migration vectors at the present time

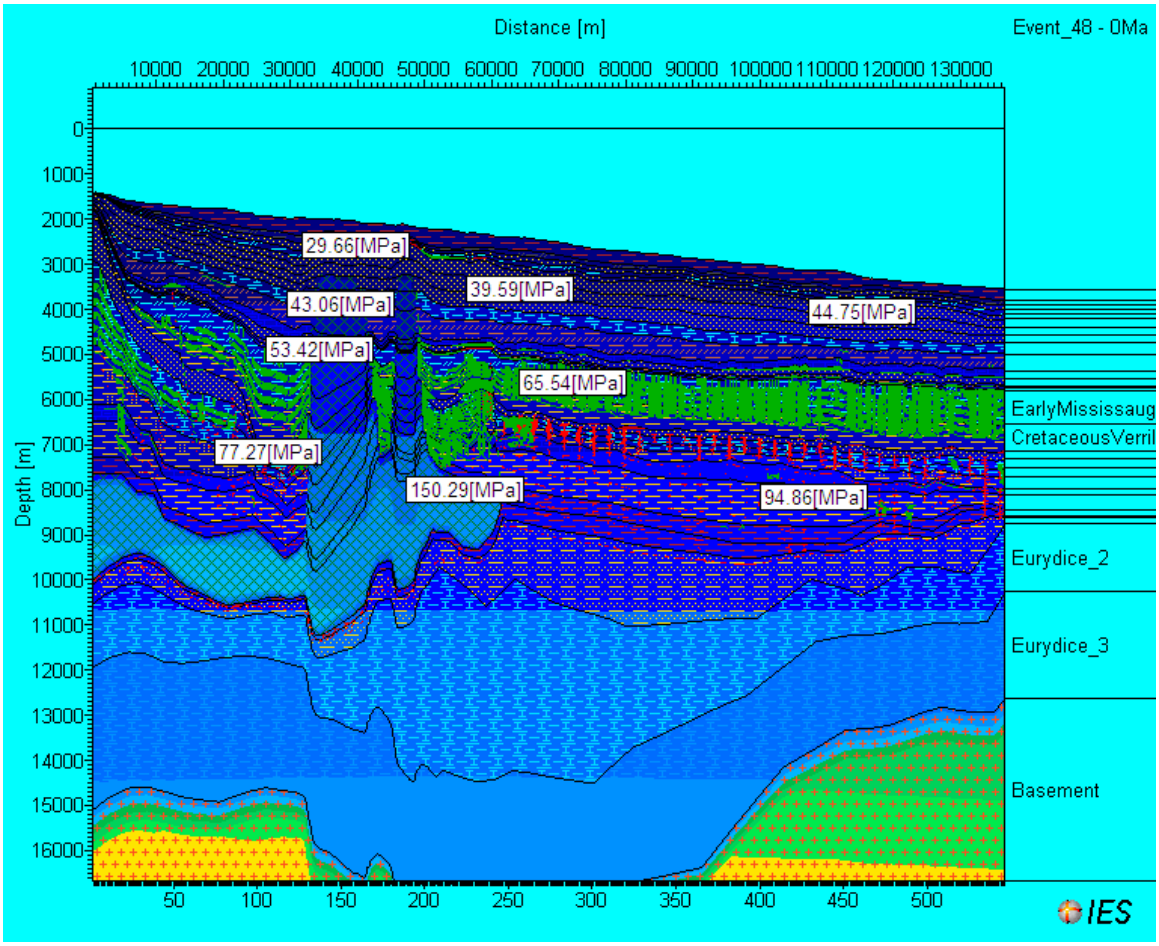

Figure 32e. Line E-E' – Output data showing the distribution of pore pressures and the trend of hydrocarbon flowpaths at the present time

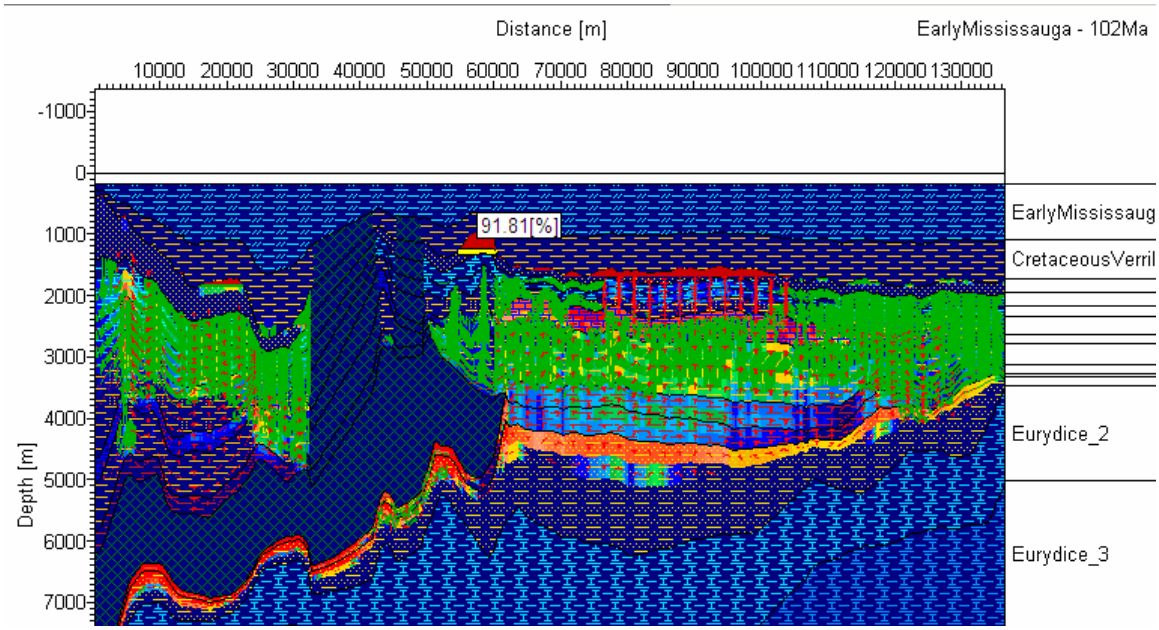

Figure 32f (i): petroleum saturation of various gas and condensate reservoirs in both liquid and vapor phases with and emphasis on the Early Cretaceous conceptual turbidite reservoir at 102 Ma

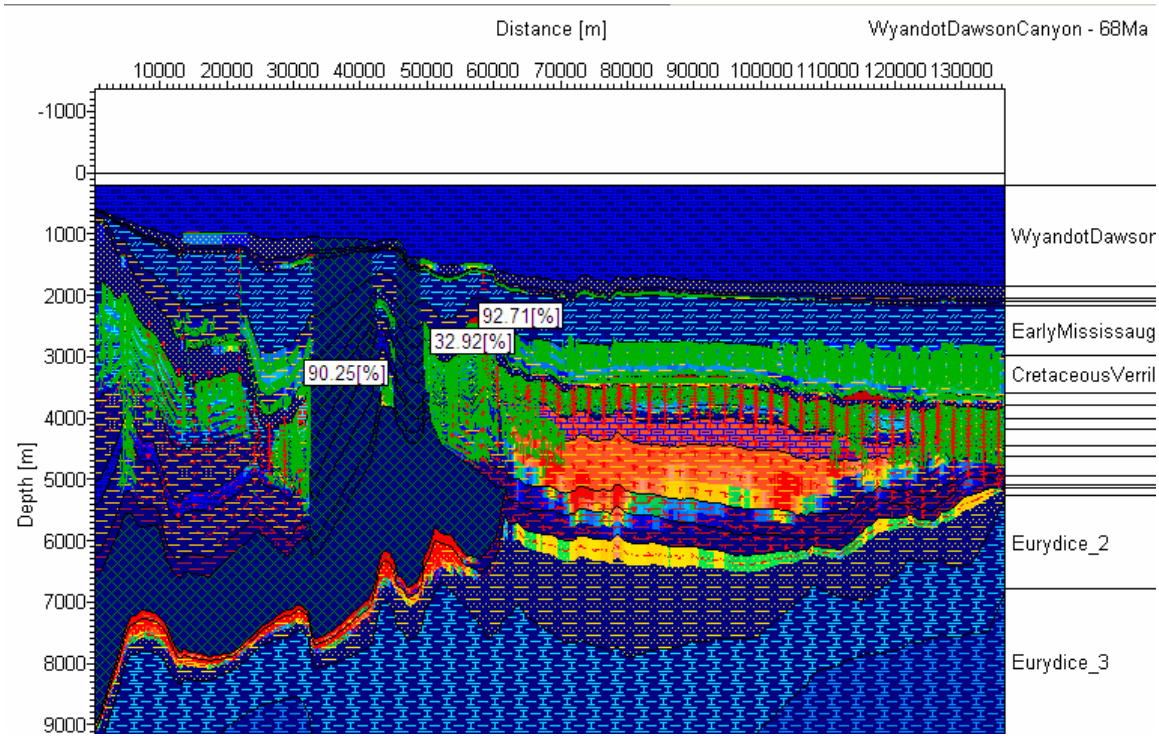

Figure 32f (ii): Line E-E' – petroleum saturation of various gas and condensate reservoirs in both liquid and vapor phases with an emphasis on the Early Cretaceous conceptual turbidite reservoir at 68 Ma

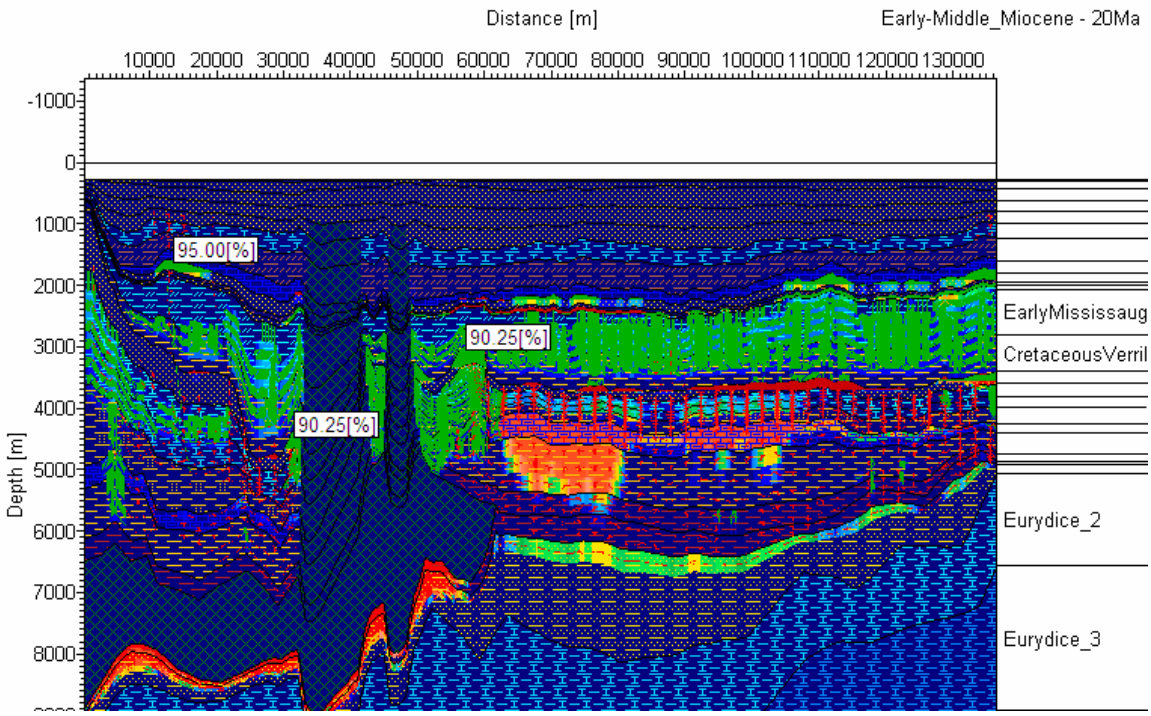

Figure 32f (iii): Line E-E' – petroleum saturation of various gas and condensate reservoirs in both liquid and vapor phases at 20 ma

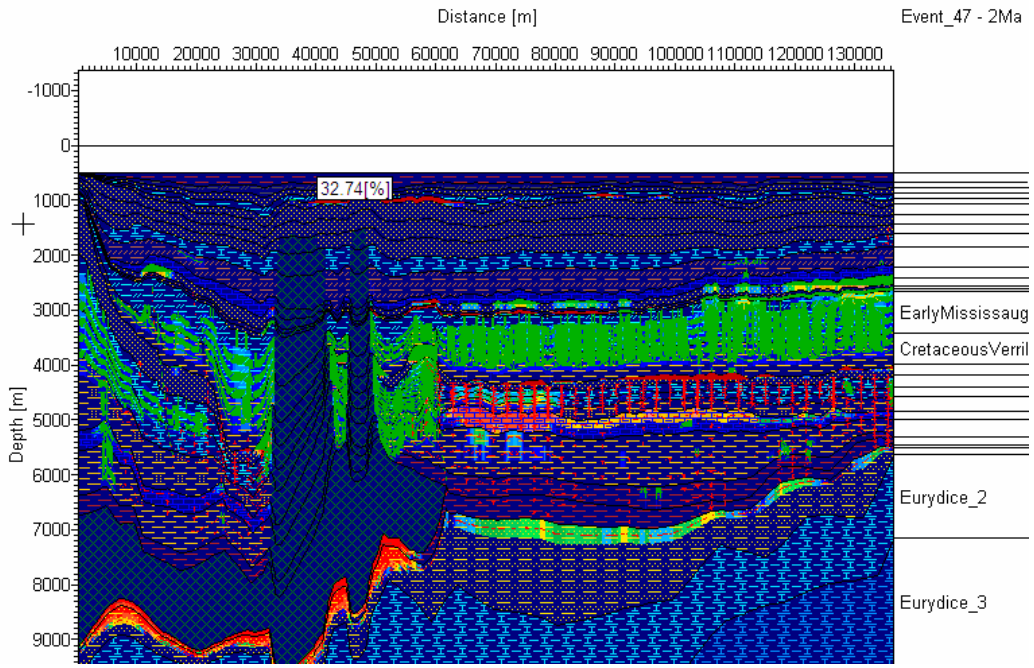

Figure 32f (iv): Line E-E' – petroleum saturation of various gas and condensate reservoirs in both liquid and vapor phases with an highlight on the early Miocene salt-top reservoirs at 2Ma

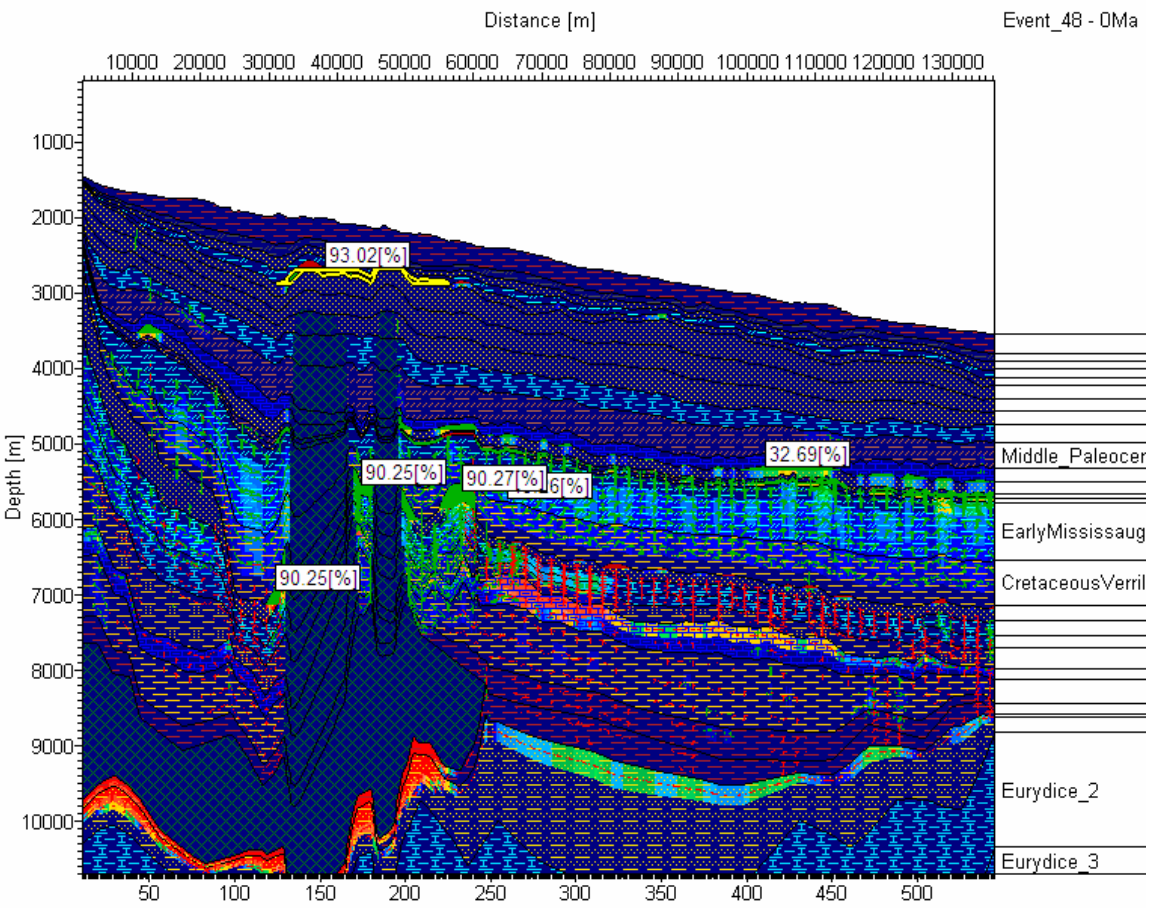

Figure 32f (v): Line E-E' – petroleum saturation of various gas and condensate reservoirs in both liquid and vapor phases with an highlight on the early Miocene salt-top reservoirs at the present day

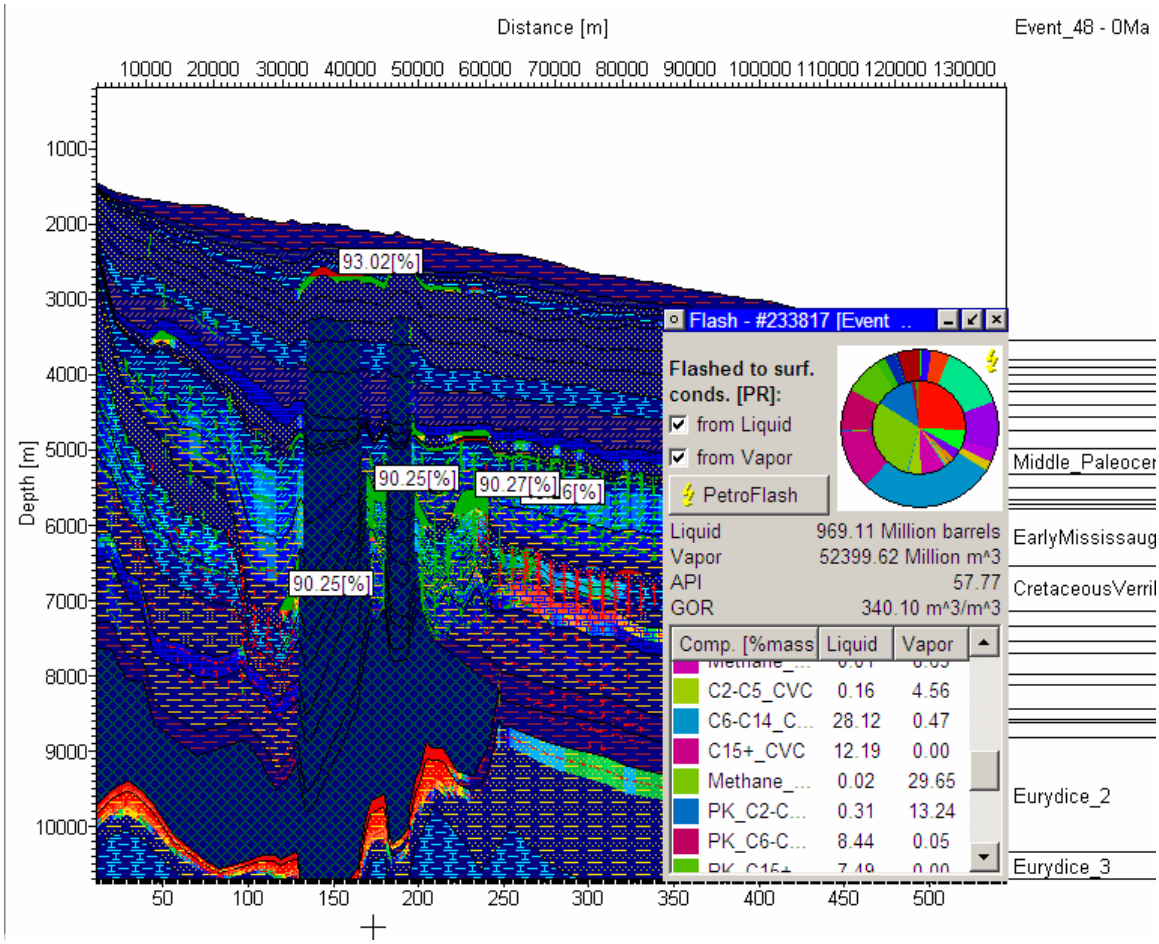

Figure 32g: Line E-E' – hydrocarbon saturation of Early Miocene reservoir showing the API gravity, GOR and other reservoir properties. The saturation of other reservoirs is also illustrated. Please disregard the volumes of reservoir hydrocarbons as the model is performed only on a two dimensional seismic line

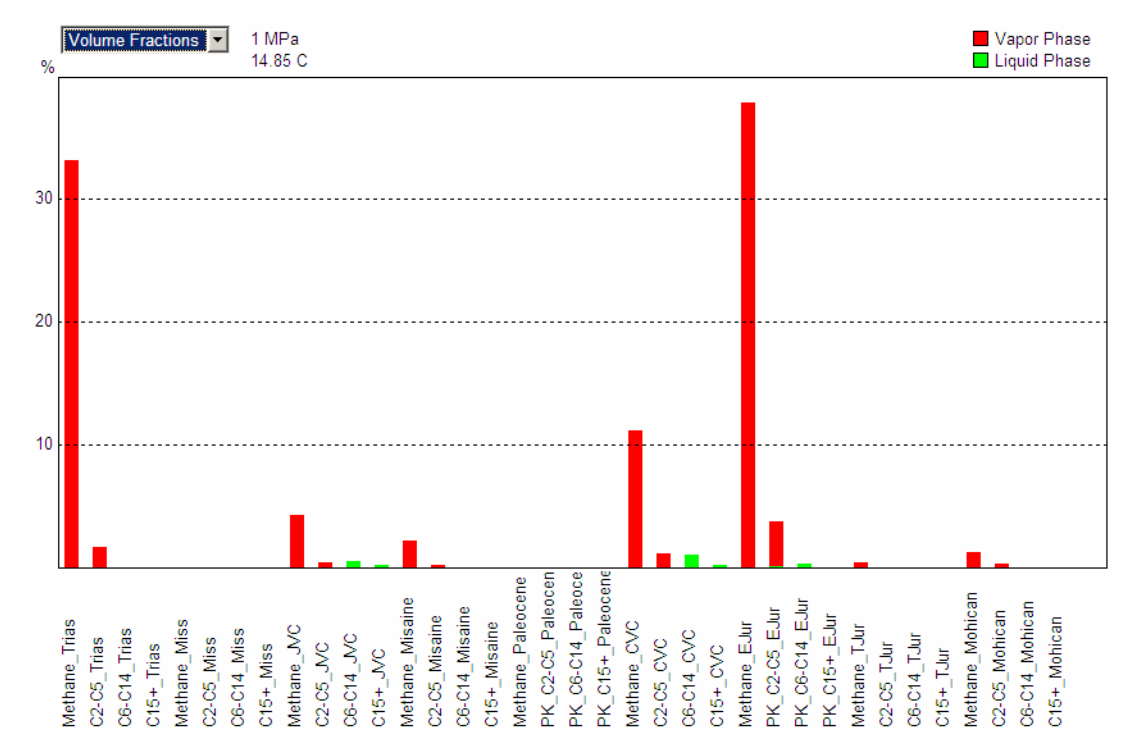

Figure 32h. Line E-E'. Tracking of various source rock components for the Early-Miocene salt-top reservoir. Please note that dry gas from Triassic lacustrine Type I, Early Jurassic lacustrine and Jurassic Verrill Canyon marine source rocks are the major hydrocarbon components for the Early Miocene reservoir

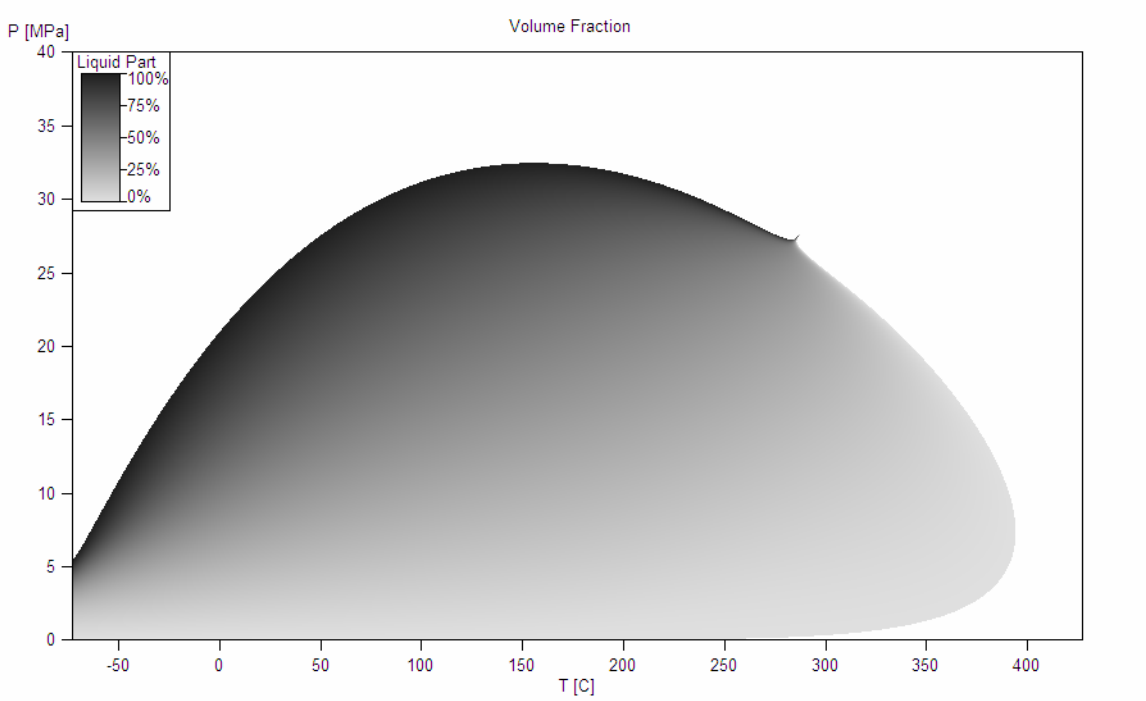

Figure 32i. Line E-E' - Bubble point curve of the Early Miocene salt-top reservoir showing the nature of the reservoir gaseous hydrocarbons in volume fraction

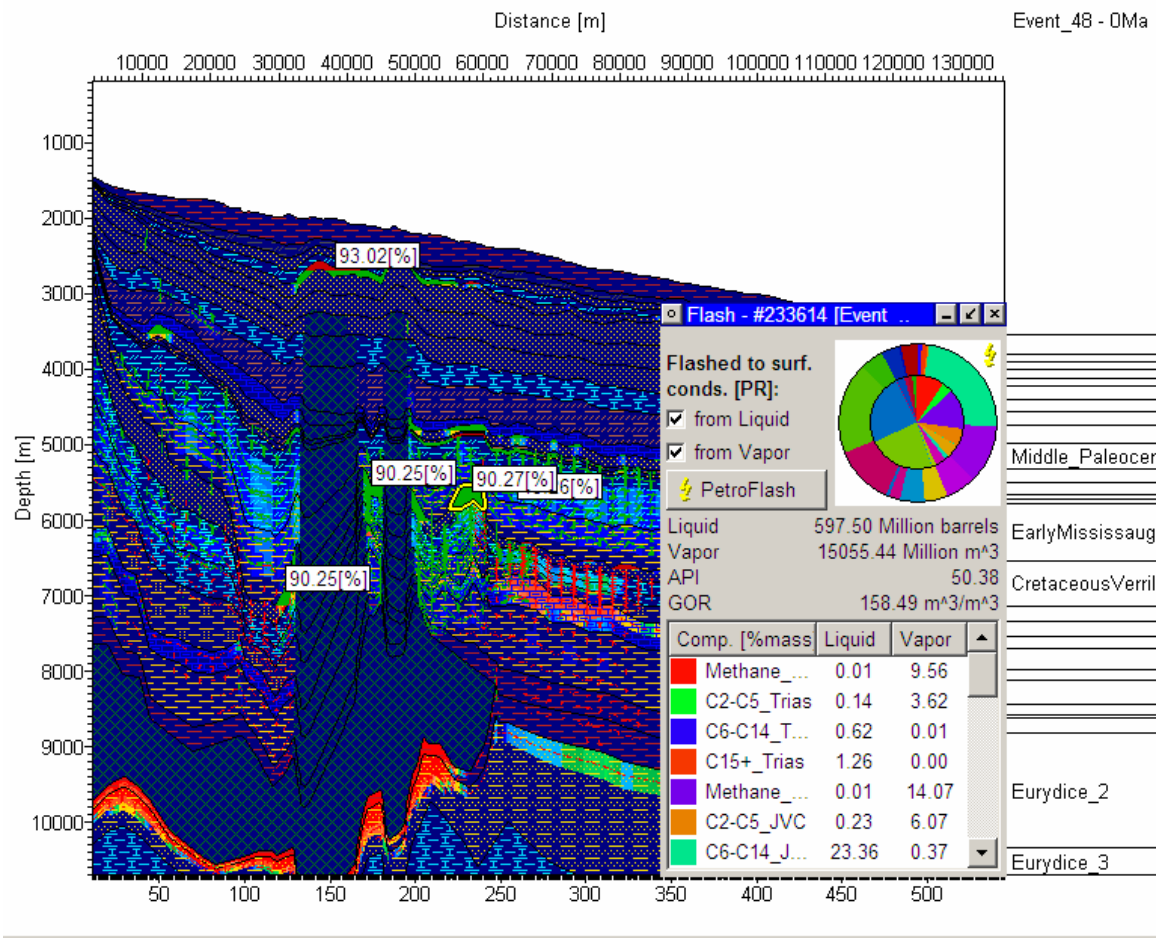

Figure 32j: Line E-E' – saturation of Early Missisauga turbidite sand reservoir showing the API gravity, GOR and other reservoir properties. Please disregard the volumes of reservoir hydrocarbons as the model is performed on a two dimensional seismic line

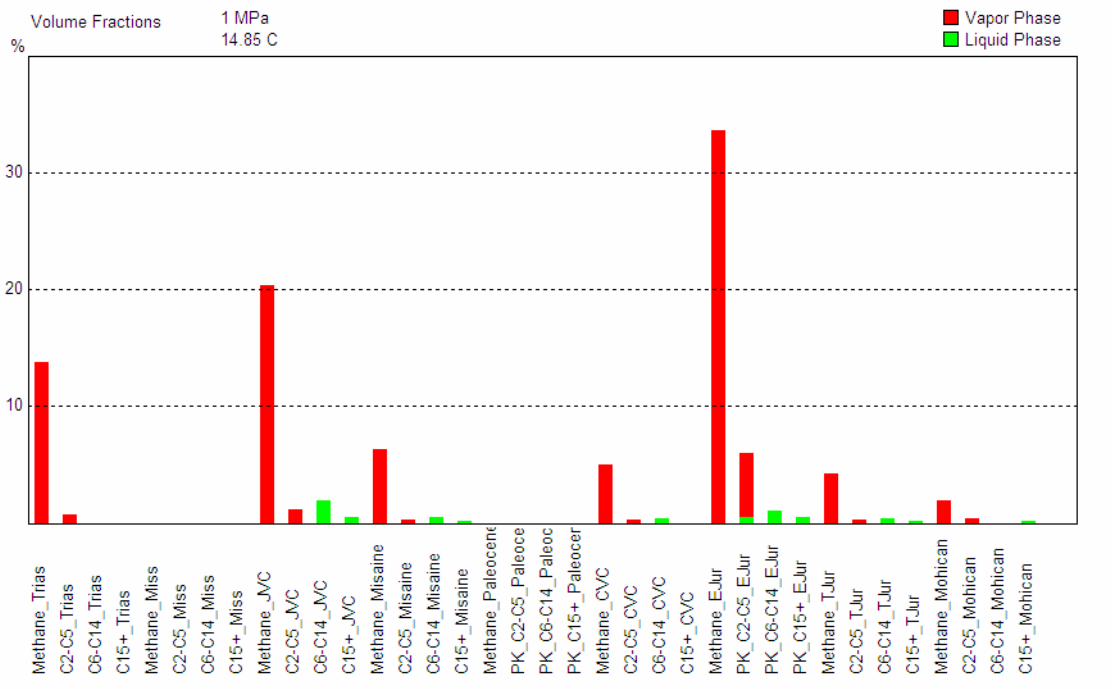

Figure 32k (i). Line E-E'. Tracking of multi-component hydrocarbon fractions from various source rock for the Early Missisauga turbidite sand reservoir (in volume %). Please note that dry gas from Triassic lacustrine Type I, Early Jurassic lacustrine Type II-III, and Jurassic Verrill Canyon marine source rocks are the major hydrocarbon components for the Early Missisauga turbidite reservoir

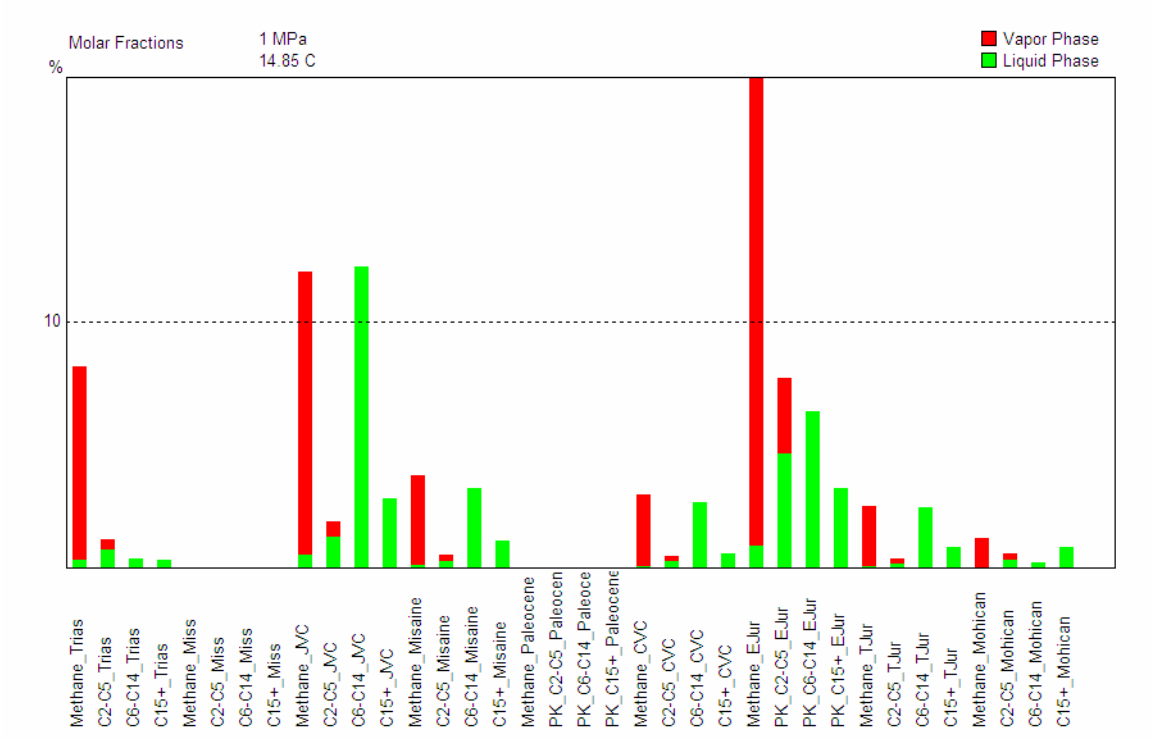

Figure 32k (ii). Line E-E'. Tracking of multi-component hydrocarbon fractions from various source rock for an early Missisauga turbidite sand reservoir (in Molar %). Please note that dry gas from Triassic lacustrine Type I and Early Jurassic lacustrine and light oil/condensate (C_6 to C_{14}) from Jurassic Verrill Canyon marine source rocks are the major hydrocarbon components for the Early Missisauga reservoir

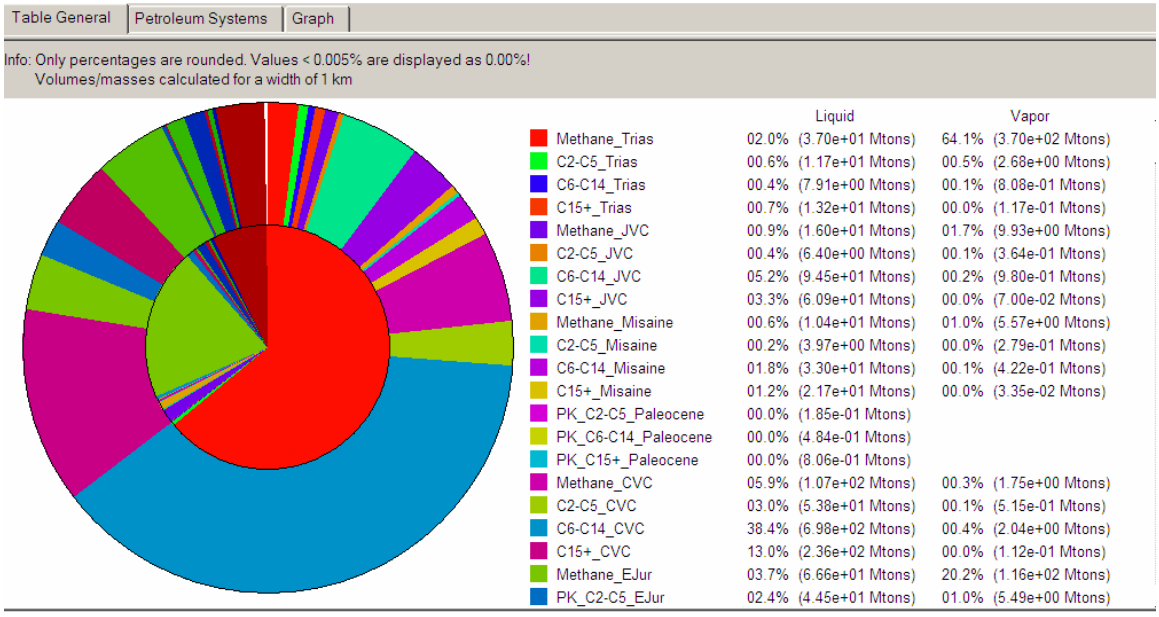

	Liquid	Vapor
Methane_Trias	02.0% (3.70e+01 Mtons)	64.1% (3.70e+02 Mtons)
C2-C5_Trias	00.6% (1.17e+01 Mtons)	00.5% (2.68e+00 Mtons)
C6-C14_Trias	00.4% (7.91e+00 Mtons)	00.1% (8.08e-01 Mtons)
C15+_Trias	00.7% (1.32e+01 Mtons)	00.0% (1.17e-01 Mtons)
Methane_JVC	00.9% (1.60e+01 Mtons)	01.7% (9.93e+00 Mtons)
C2-C5_JVC	00.4% (6.40e+00 Mtons)	00.1% (3.64e-01 Mtons)
C6-C14_JVC	05.2% (9.45e+01 Mtons)	00.2% (9.80e-01 Mtons)
C15+_JVC	03.3% (6.09e+01 Mtons)	00.0% (7.00e-02 Mtons)
Methane_Misaine	00.6% (1.04e+01 Mtons)	01.0% (5.57e+00 Mtons)
C2-C5_Misaine	00.2% (3.97e+00 Mtons)	00.0% (2.79e-01 Mtons)
C6-C14_Misaine	01.8% (3.30e+01 Mtons)	00.1% (4.22e-01 Mtons)
C15+_Misaine	01.2% (2.17e+01 Mtons)	00.0% (3.35e-02 Mtons)
PK_C2-C5_Paleocene	00.0% (1.85e-01 Mtons)	
PK_C6-C14_Paleocene	00.0% (4.84e-01 Mtons)	
PK_C15+_Paleocene	00.0% (8.06e-01 Mtons)	
Methane_CVC	05.9% (1.07e+02 Mtons)	00.3% (1.75e+00 Mtons)
C2-C5_CVC	03.0% (5.38e+01 Mtons)	00.1% (5.15e-01 Mtons)
C6-C14_CVC	38.4% (6.98e+02 Mtons)	00.4% (2.04e+00 Mtons)
C15+_CVC	13.0% (2.36e+02 Mtons)	00.0% (1.12e-01 Mtons)
Methane_EJur	03.7% (6.66e+01 Mtons)	20.2% (1.16e+02 Mtons)
PK_C2-C5_EJur	02.4% (4.45e+01 Mtons)	01.0% (5.49e+00 Mtons)

Figure 321.Cummulative masses of multi-component hydrocarbons expelled from various source rocks (masses calculated Within a kilometer radius)

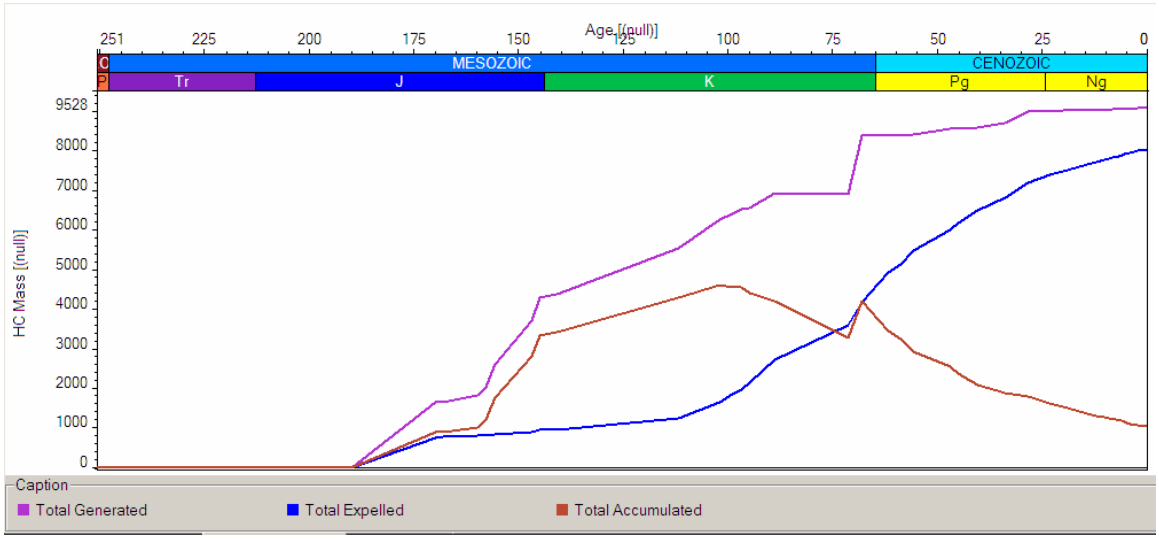

Figure 33m.Line C-C' – Timing of total generated, total expelled, and total accumulated cummulative hydrocarbon mass from various source rocks (masses calculated for a width of 1 km)

Seismic Line D-D’

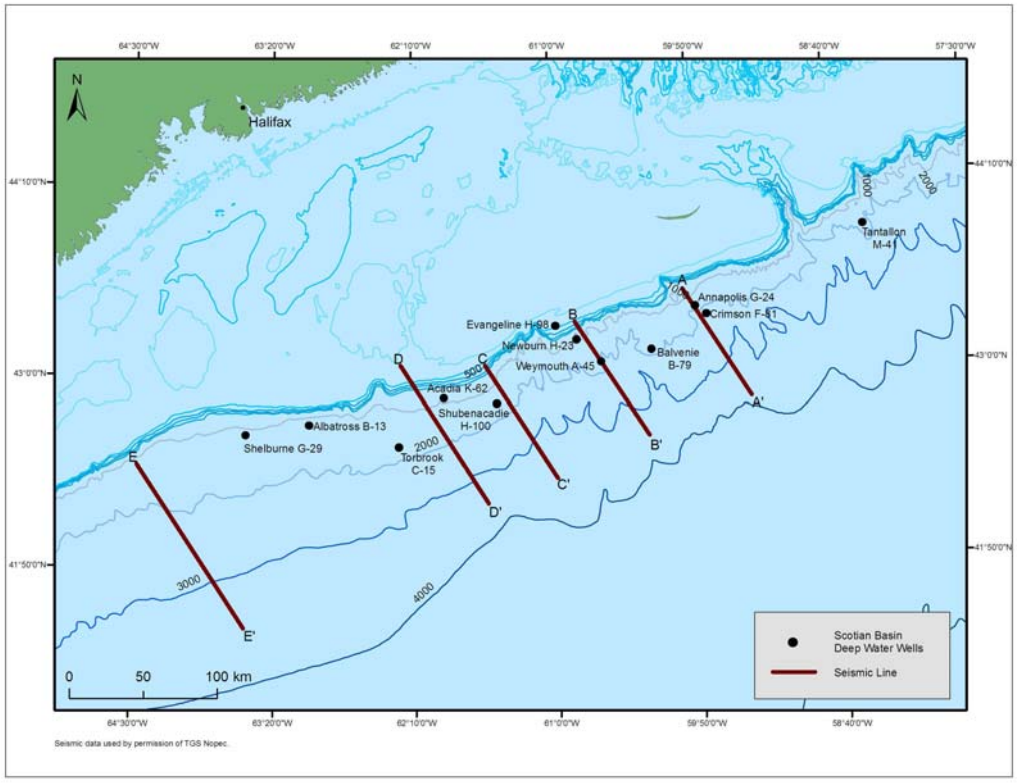

Figure 33a. Location map of the seismic line D-D’

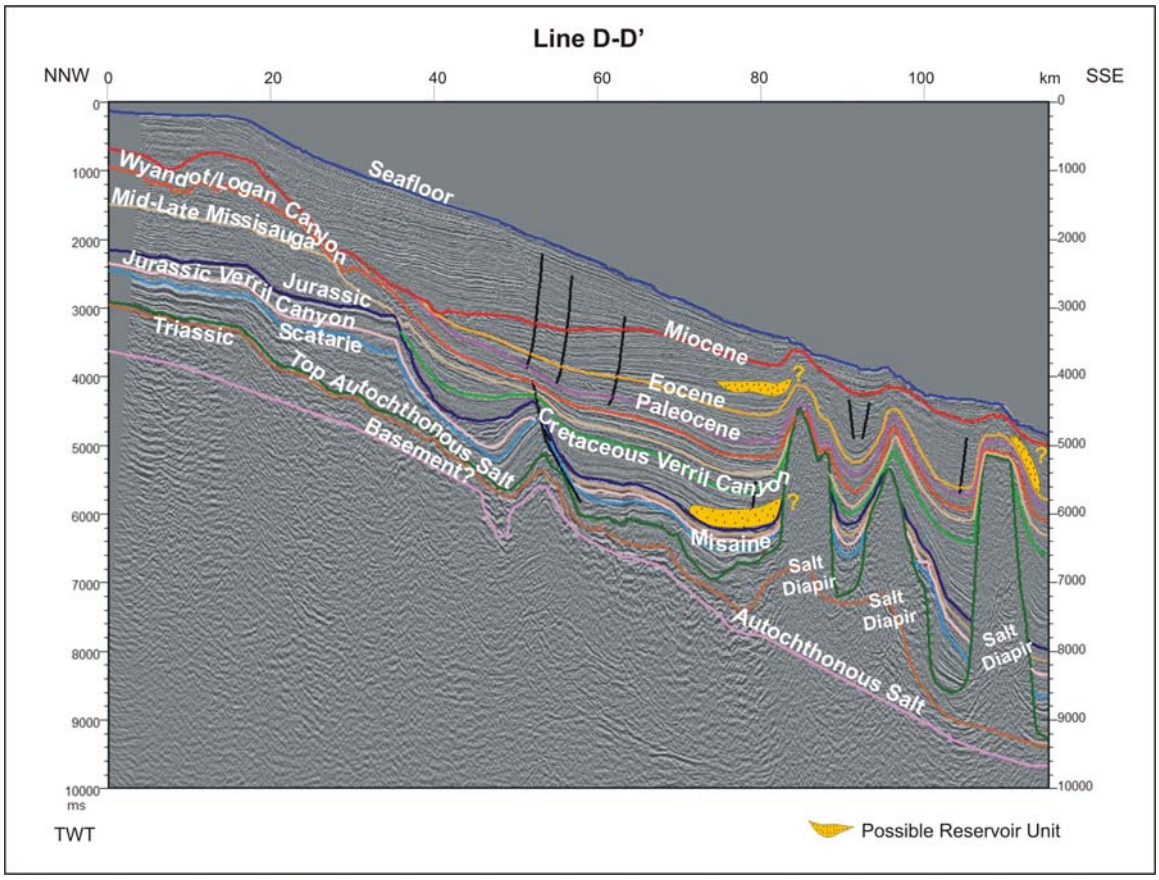

Figure 33b. Seismic line D-D' with selected formation boundaries, faults, salt diapirs, and possible reservoir units

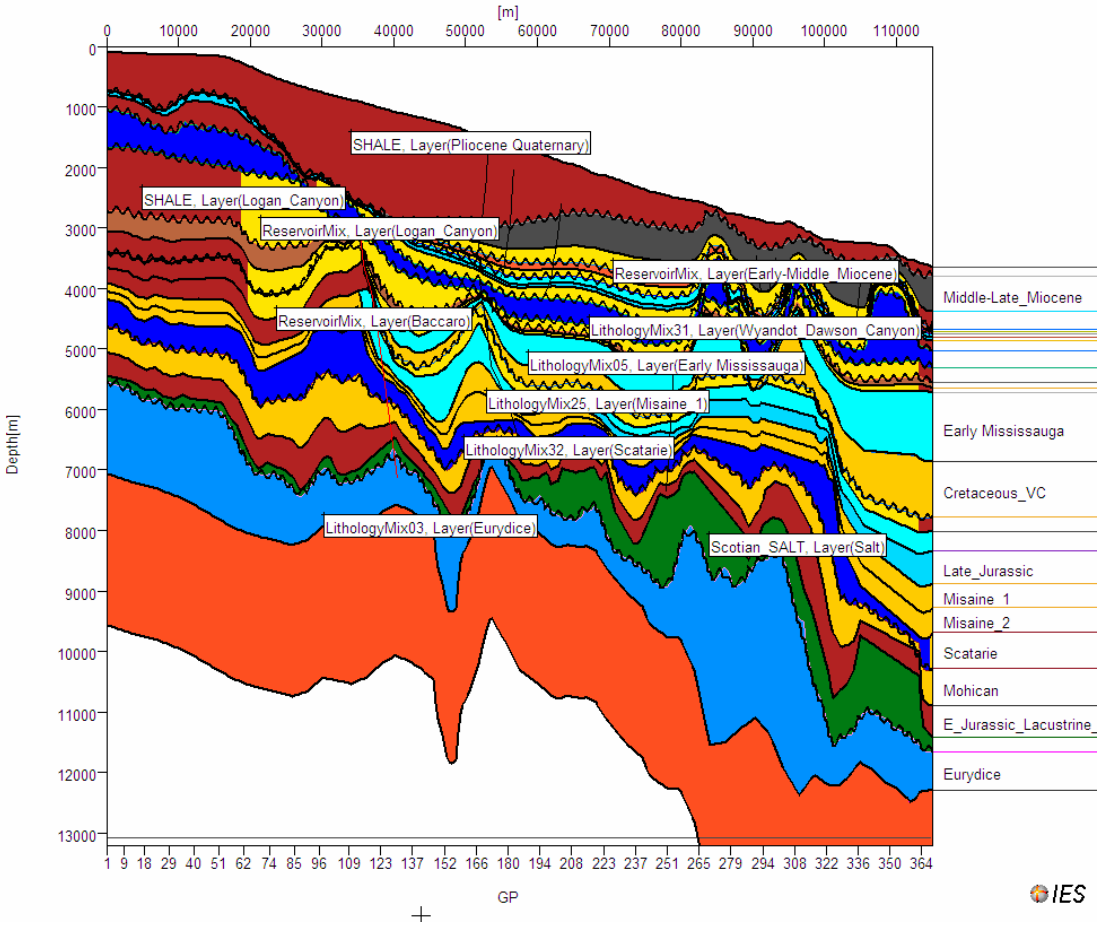

Figure 33c. Line D-D' - Input parameters – formation boundaries, lithology, and unconformities

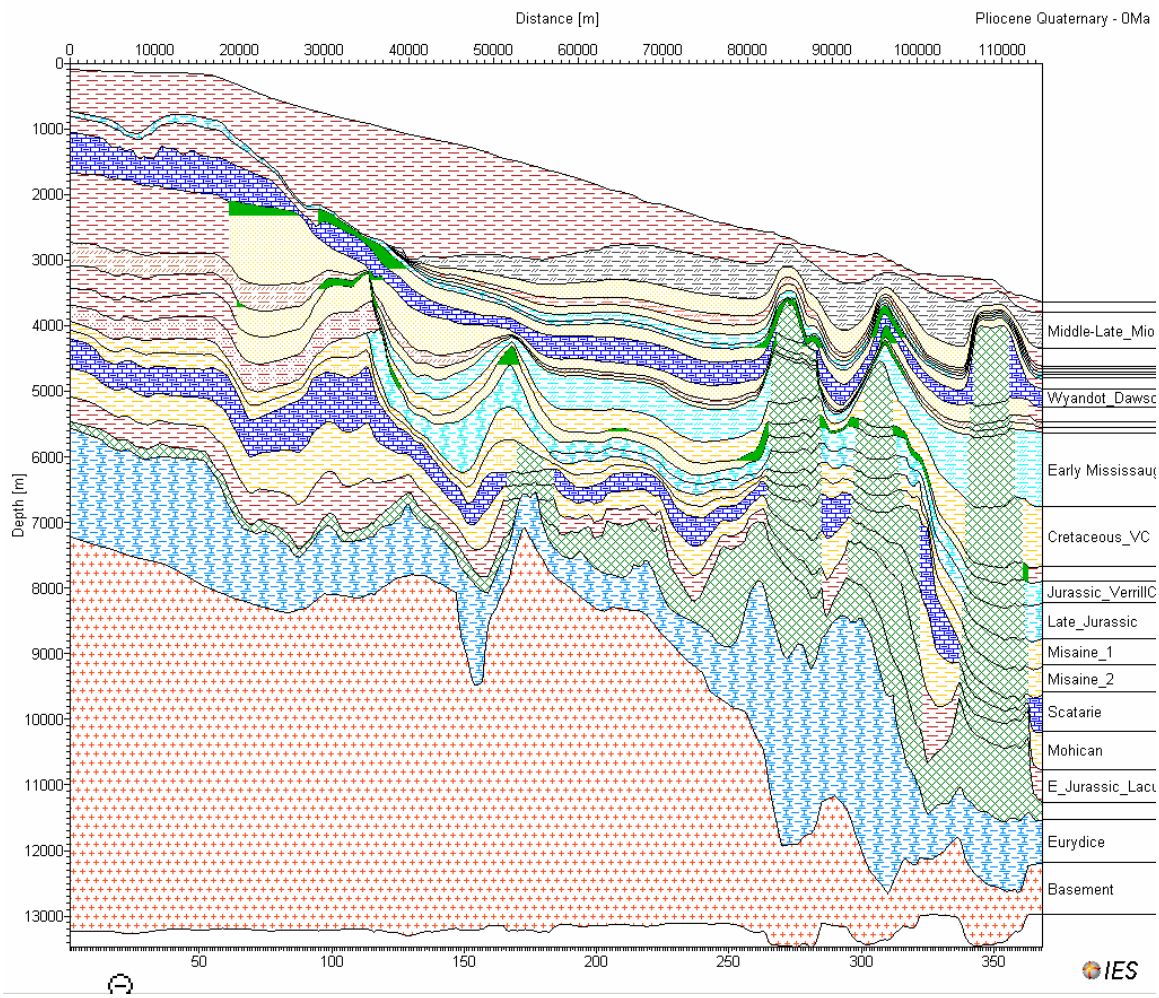

Figure 33d. Line D-D' – Output Parameters showing hydrocarbon-saturated reservoirs with lithology patterns and diapiric salt structures. Color of various lithology pattern indicates the usual legend color of various lithologies (eg. Blue – major carbonate, etc.)

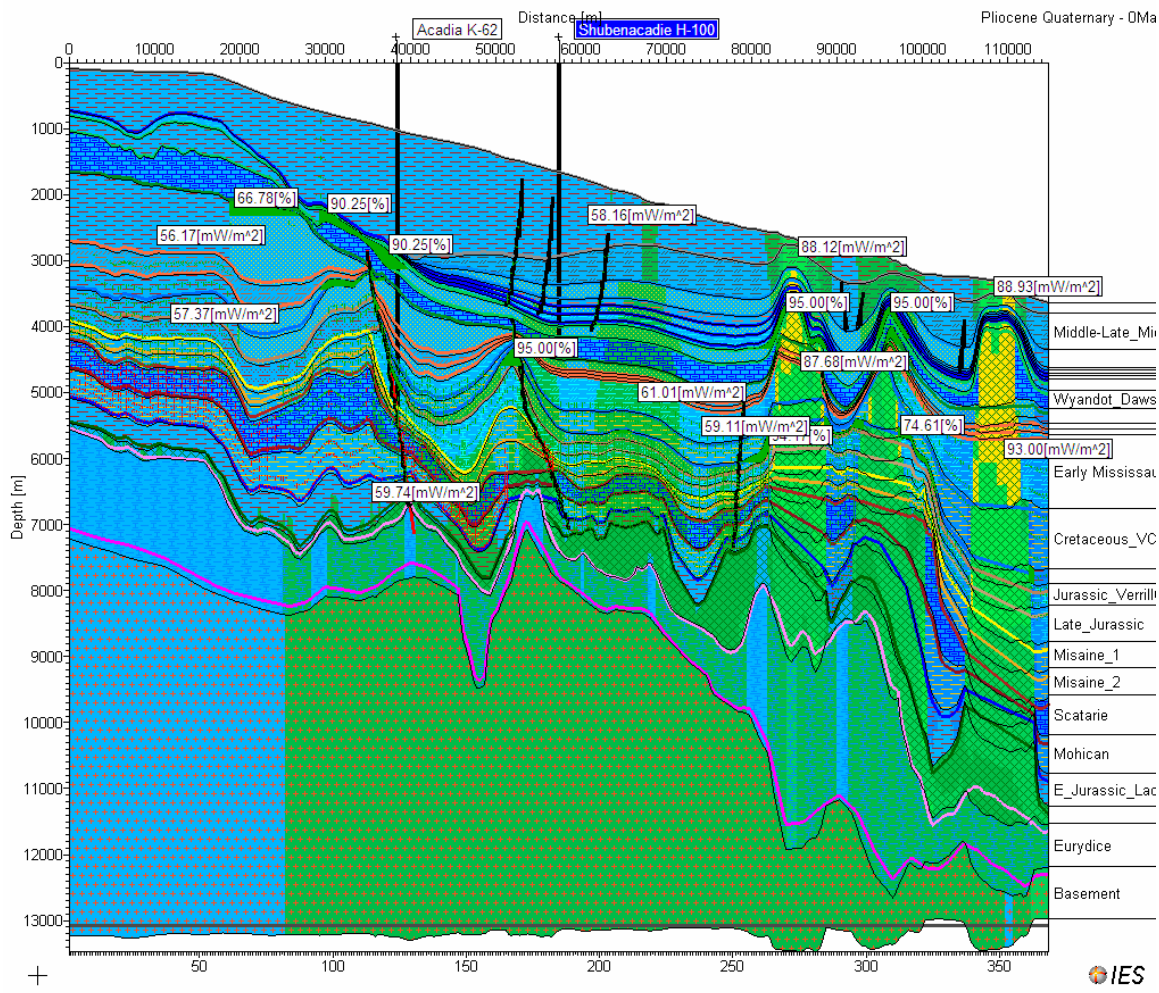

Figure 33e. Heat flow variability of various salt-related areas at the present time

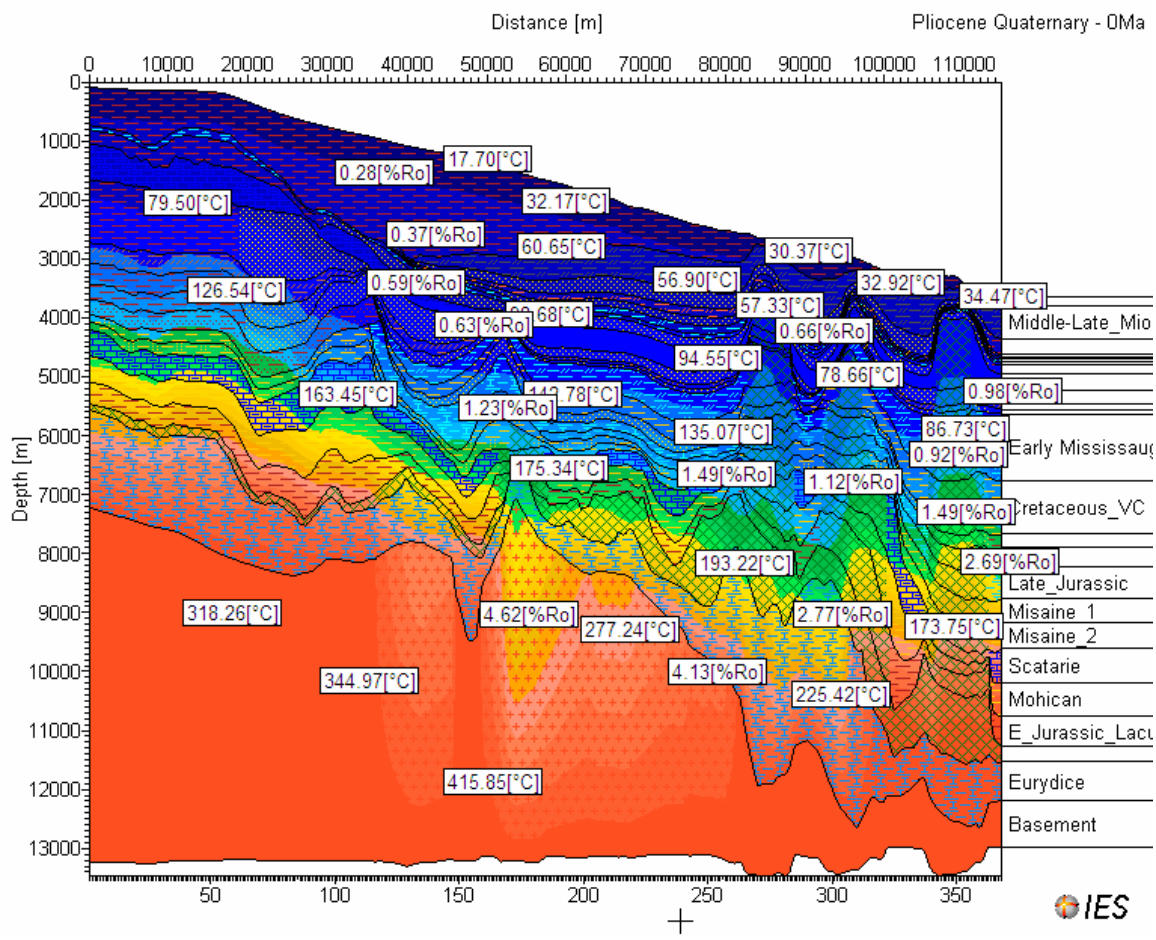

Figure 33f (i). Line D-D' – Present day maturity in relation to temperature and hydrocarbon saturation of various reservoirs and showing hydrocarbon vectors or flow path

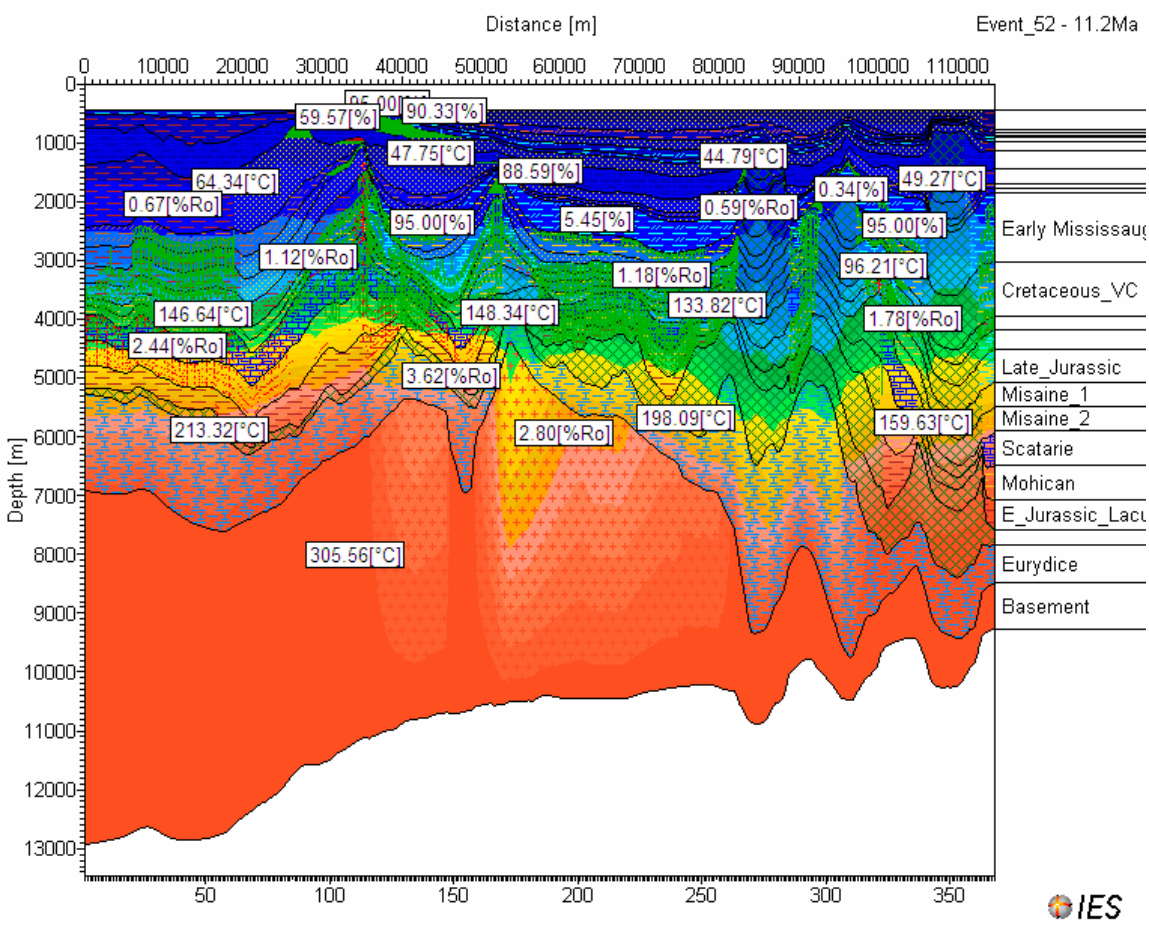

Figure 33f (ii). Line D-D' – The temperature and maturity of various horizons at 11.2 Ma. The figures also shows the hydrocarbon saturation in various reservoirs and hydrocarbon vectors or flow path of hydrocarbons

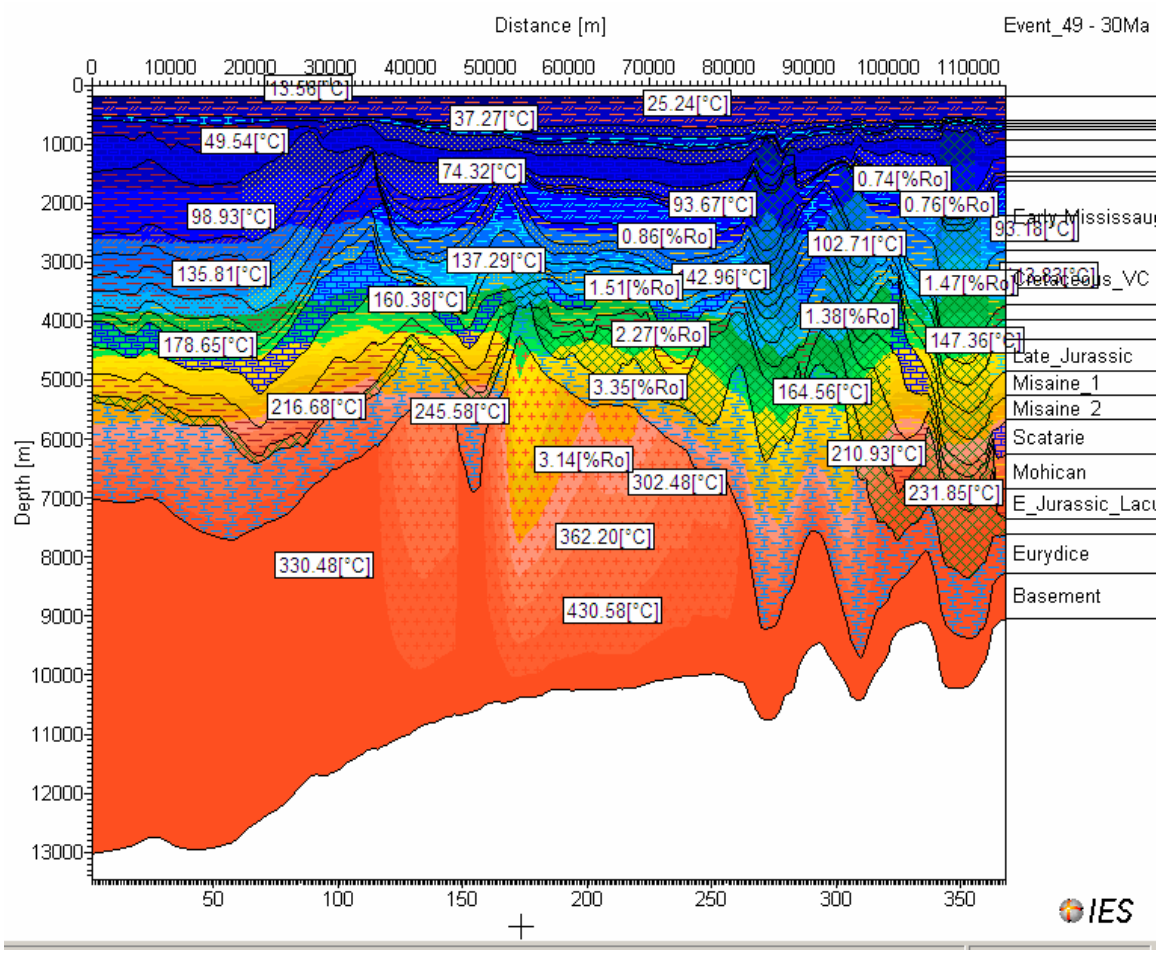

Figure 33f (iii). Line D-D' – The maturity and temperature of various horizons at 30 Ma.

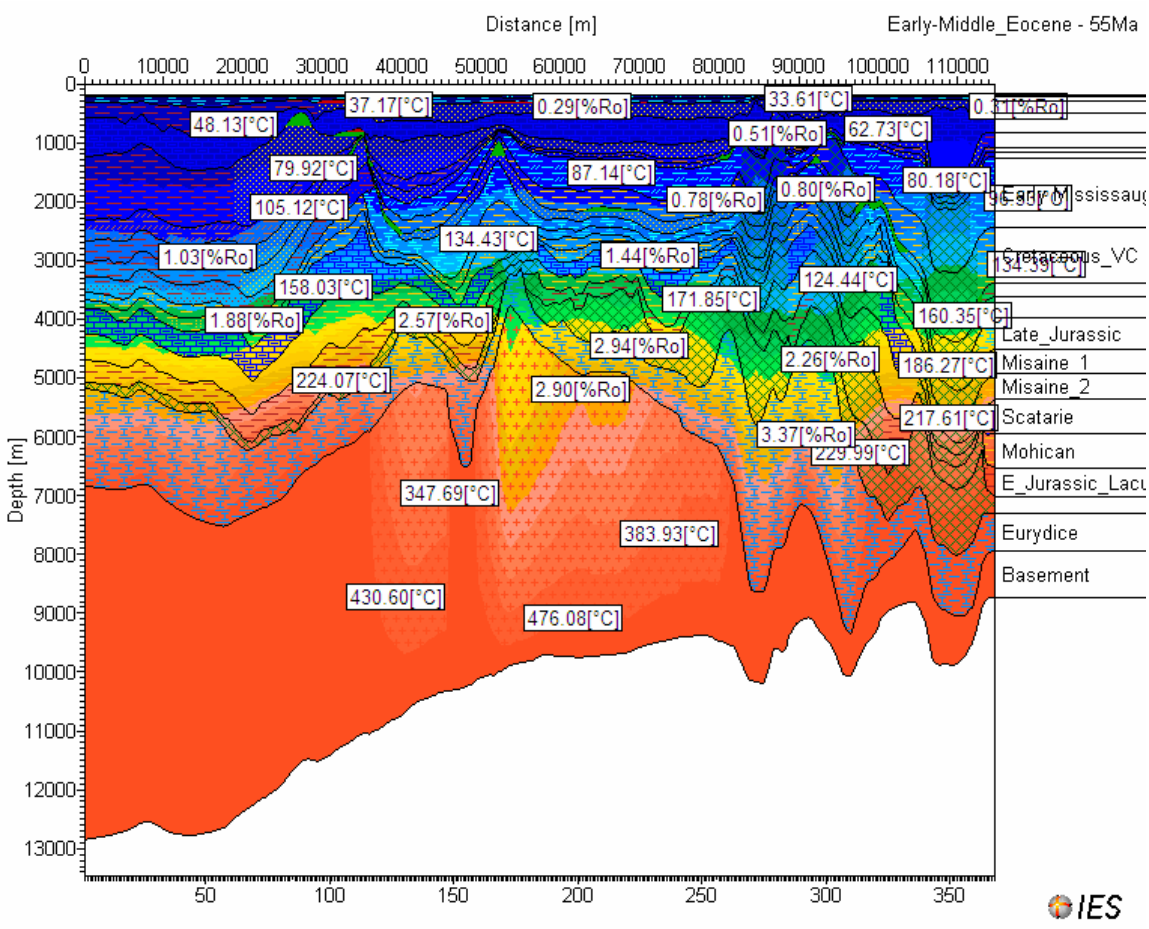

Figure 33f (iv). Line D-D' – The maturity and temperature of various horizons at 55 Ma.

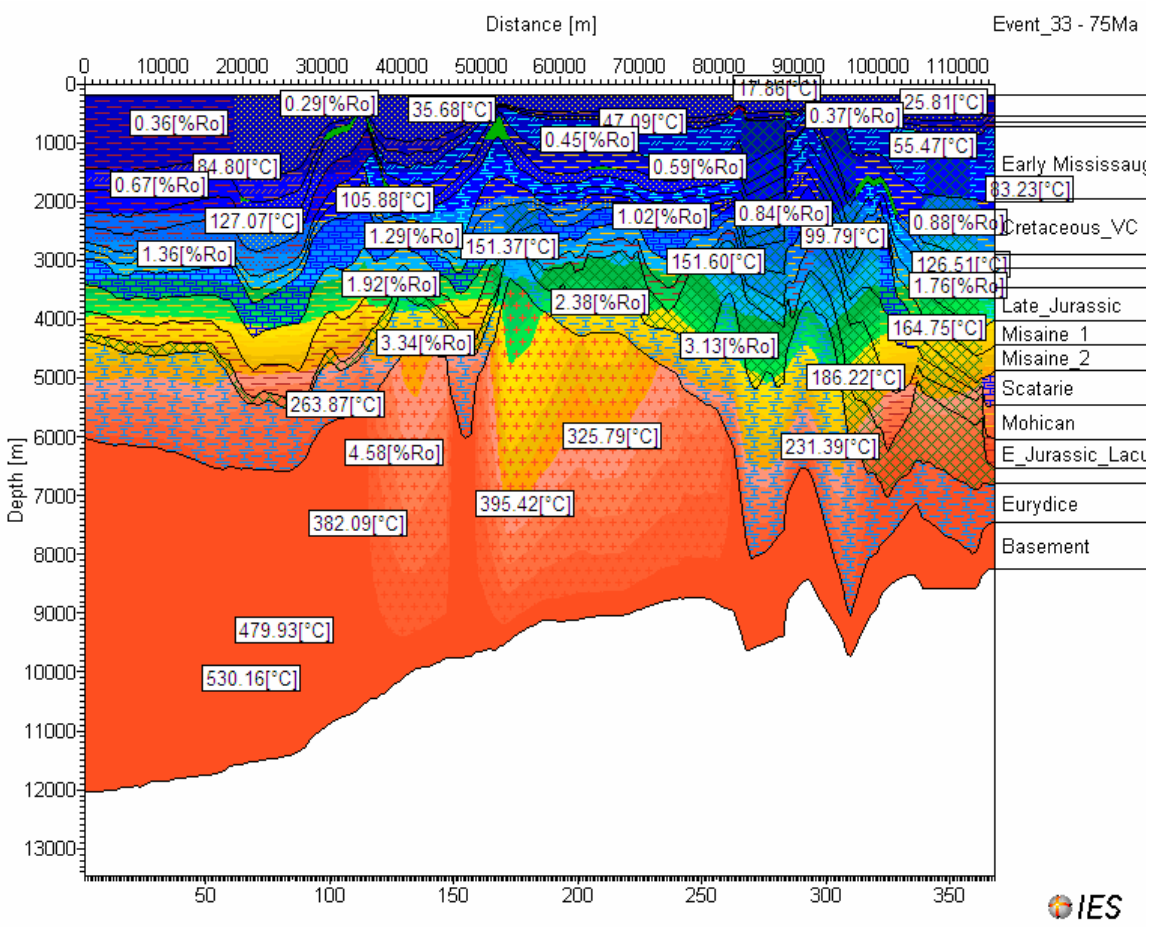

Figure 33f (v). Line D-D' – The maturity and temperature of various horizons at 75 Ma.

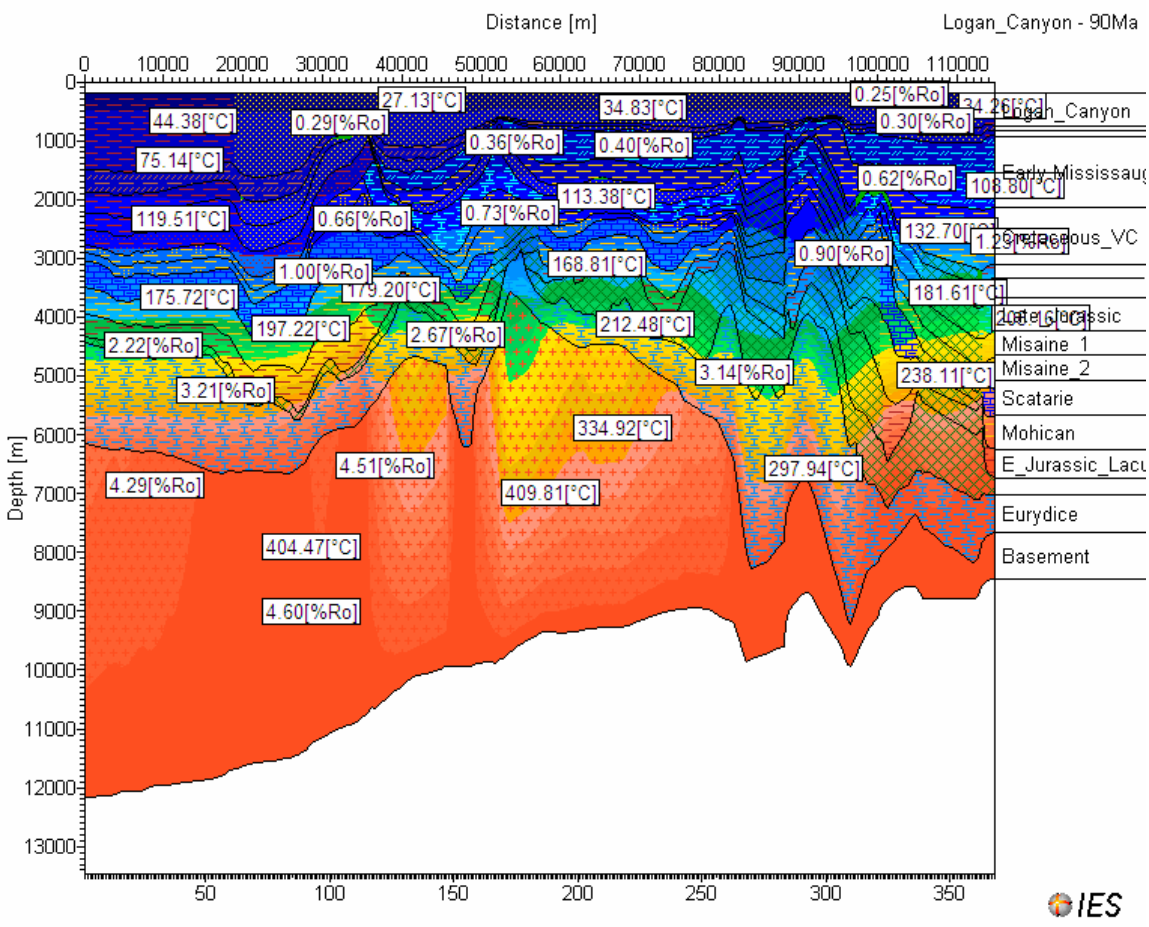

Figure 33f (vi). Line D-D' – The maturity and temperature of various horizons at 90 Ma.

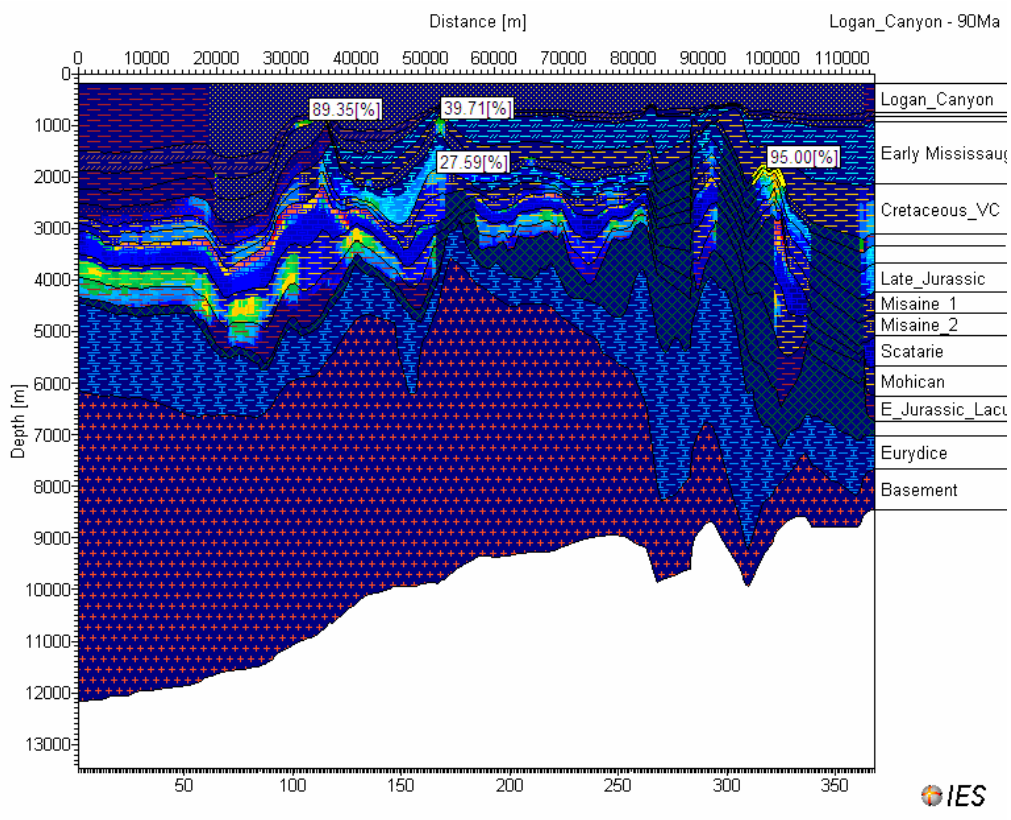

Figure 33g (i). Line D-D' - Hydrocarbon saturation of various reservoirs at 90 Ma.

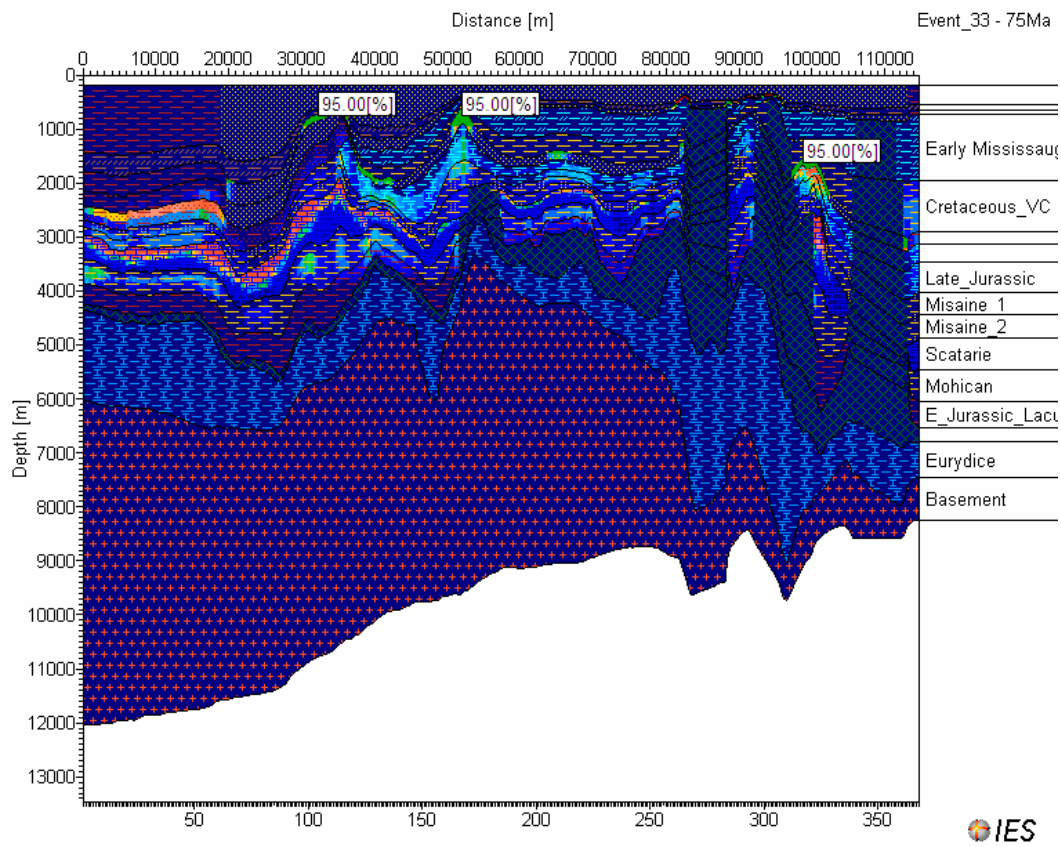

Figure 33g (ii). Line D-D' - Hydrocarbon saturation of various reservoirs at 75 Ma.

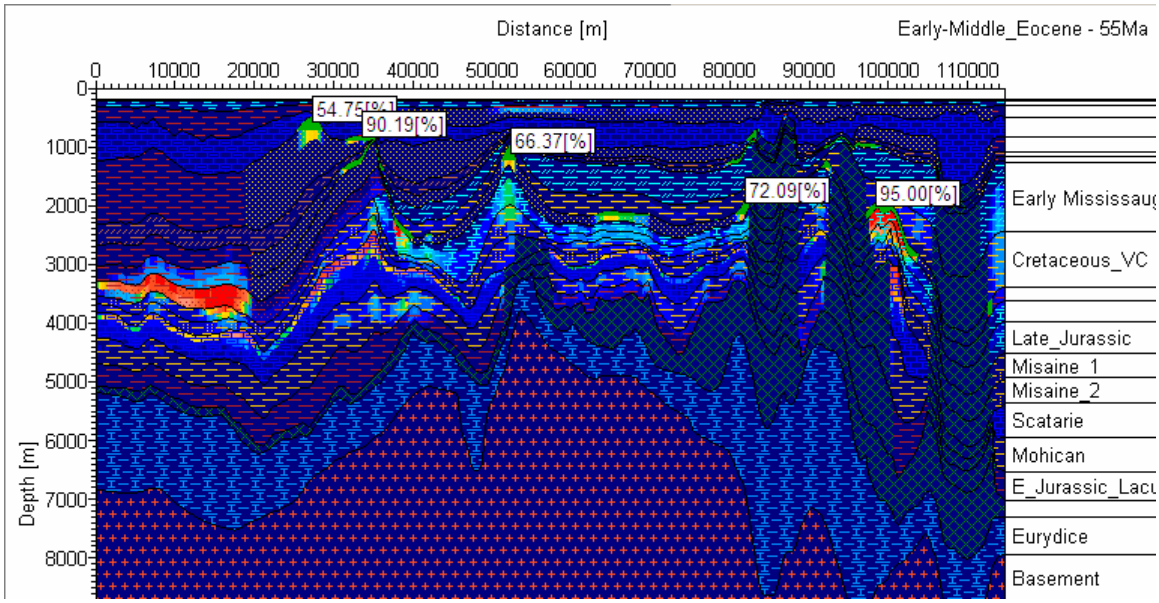

Figure 33g (iii). Line D-D'. Hydrocarbon saturation of various reservoirs at 55 Ma

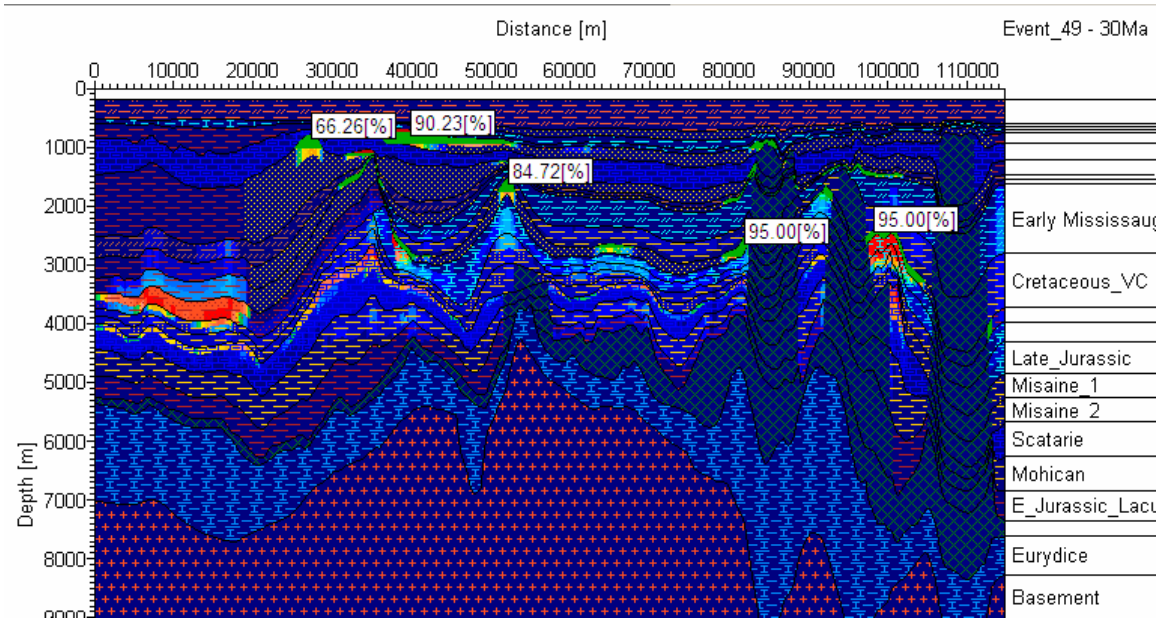

Figure 33g (iv). Line D-D' - Hydrocarbon saturation of various reservoirs at 30 Ma

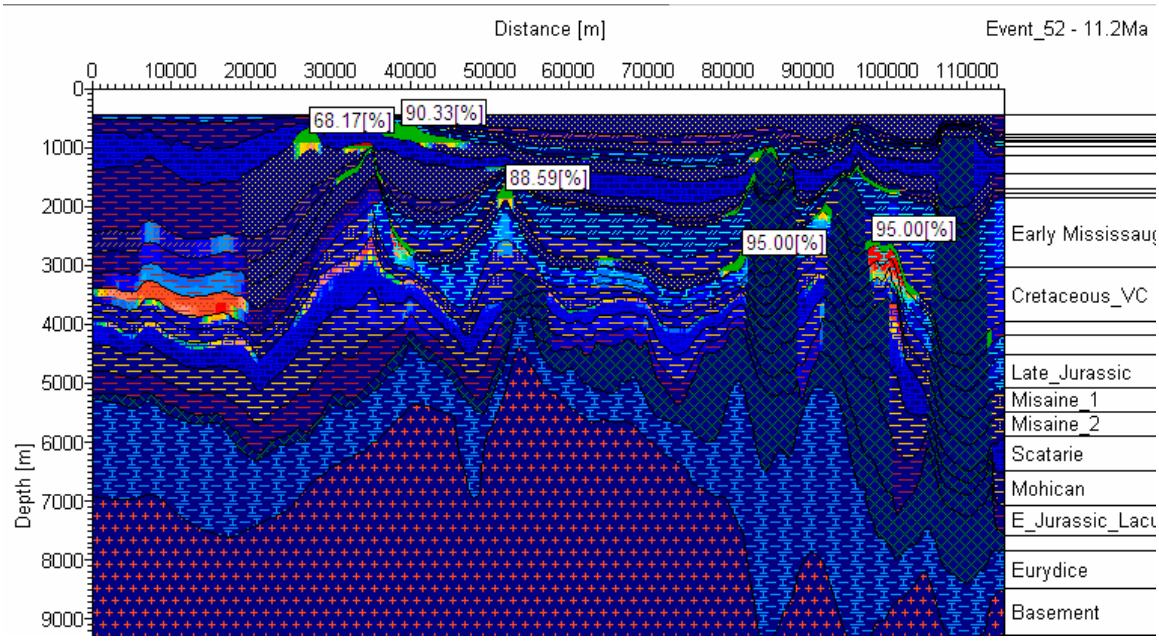

Figure 33g (v). Line D-D' - Hydrocarbon saturation at 11.2 Ma

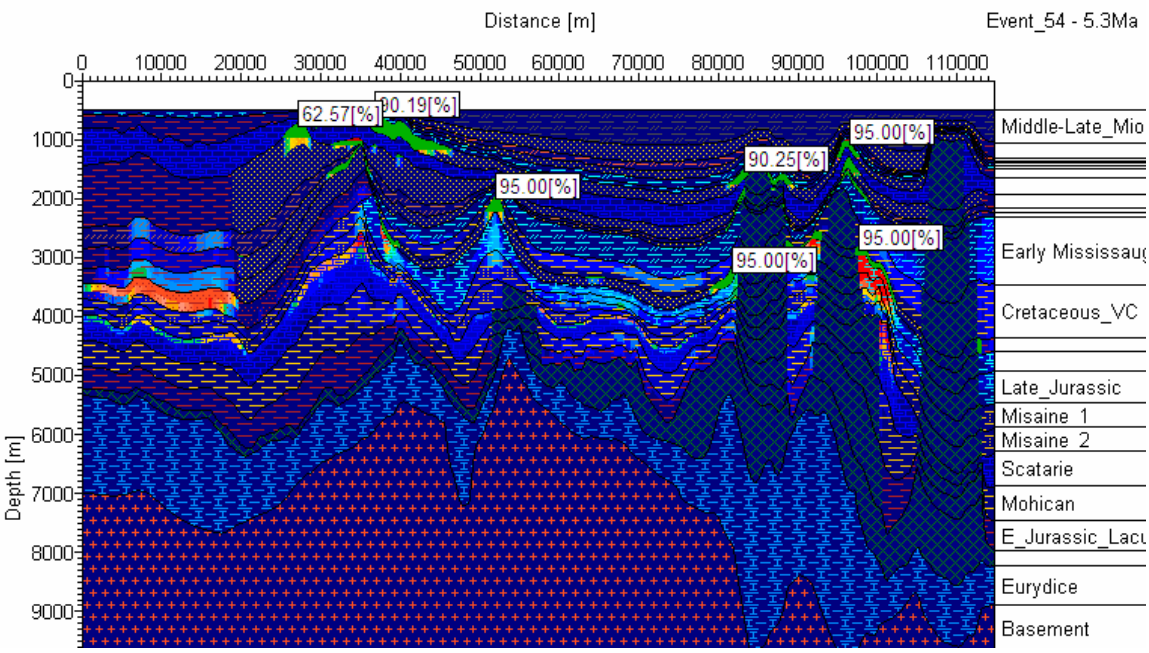

Figure 33g (vi). Line D-D' - Hydrocarbon saturation at 5.3 Ma

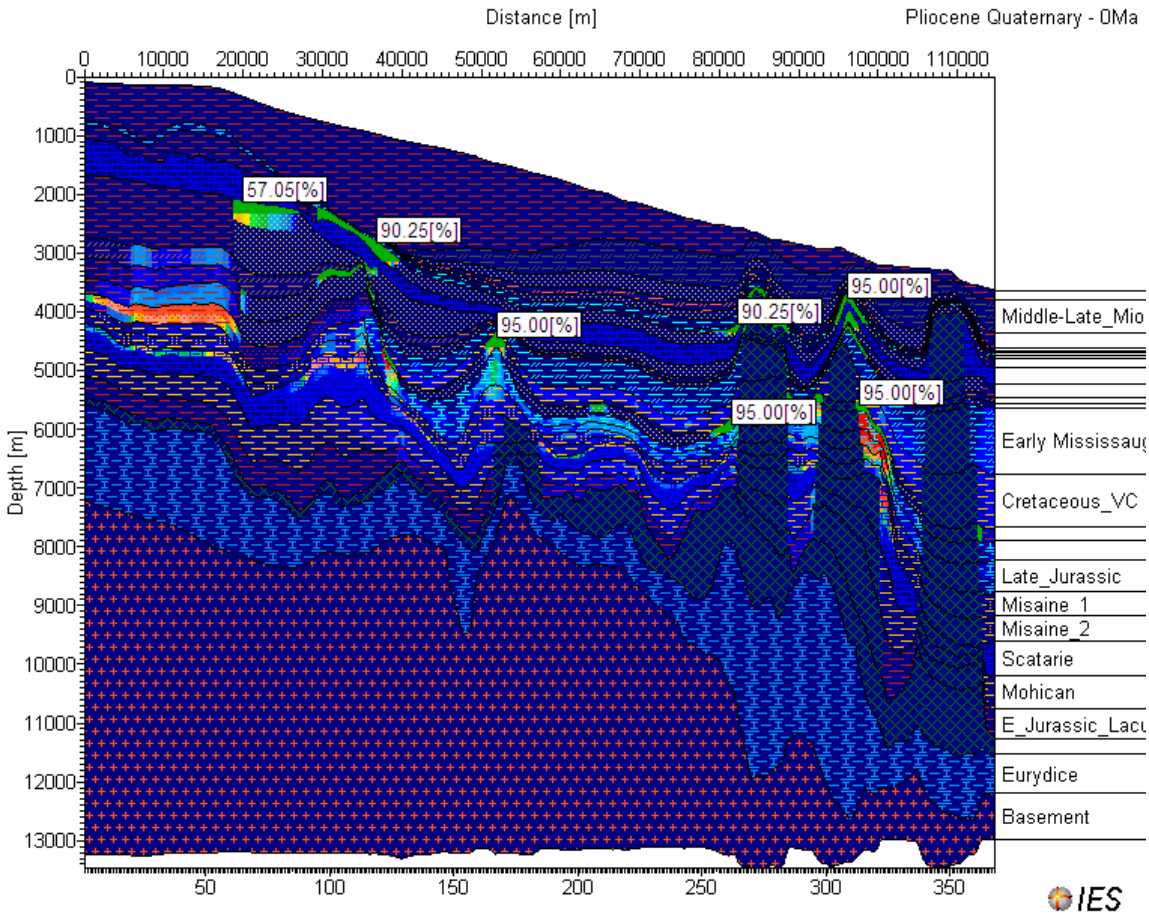

Figure 33g (vii). Line D-D' - Hydrocarbon saturation at the present time

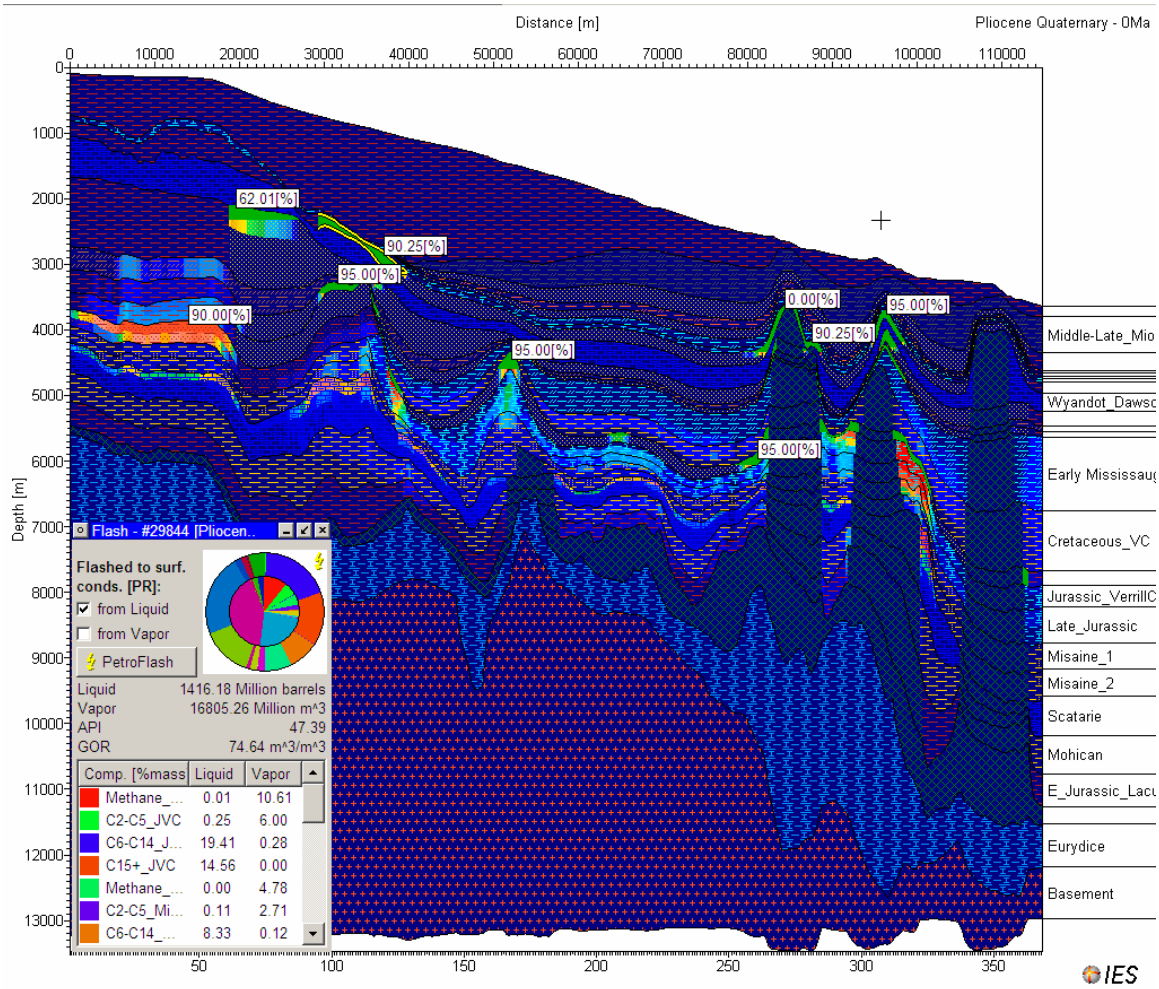

Figure 33h (i). Line D-D' – Saturation of various reservoirs with API gravity and possible GOR of Mid-Paleocene Turbidite Reservoir. Please disregard the volumes of reservoir hydrocarbons as the model is performed on a two dimensional seismic line

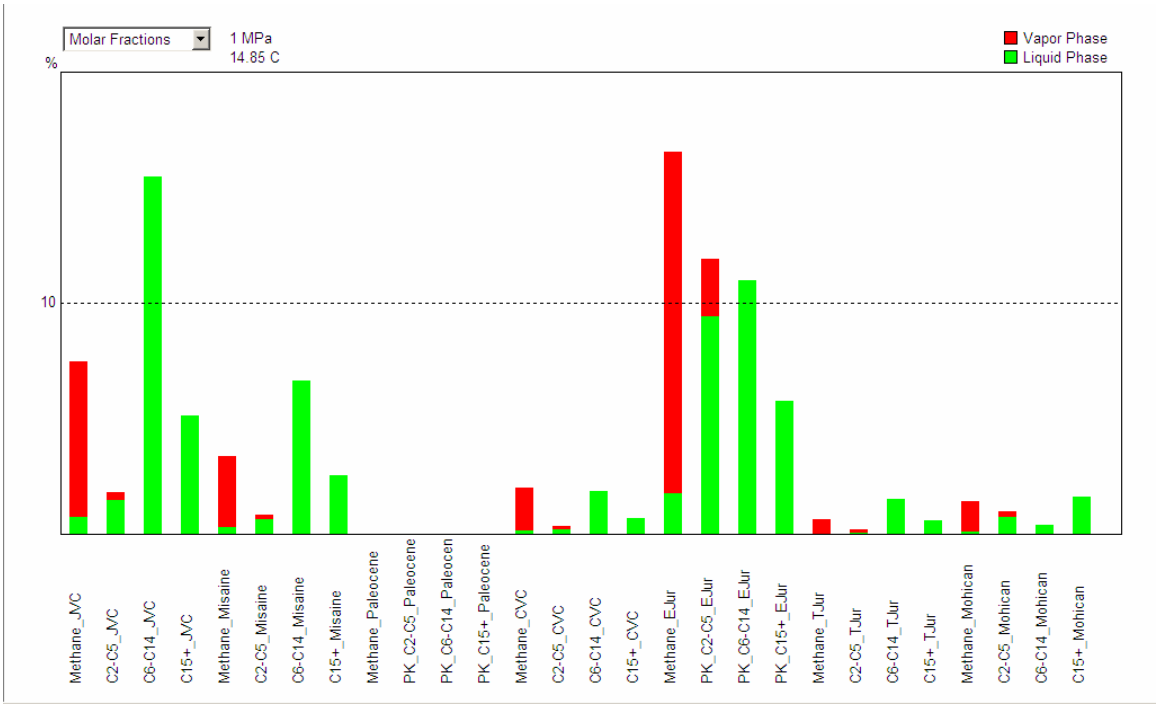

Figure 33h(ii). Line D-D' – Hydrocarbon component tracking of the Middle Paleocene Turbidite reservoir showing the molar percentages of various hydrocarbons from source rocks

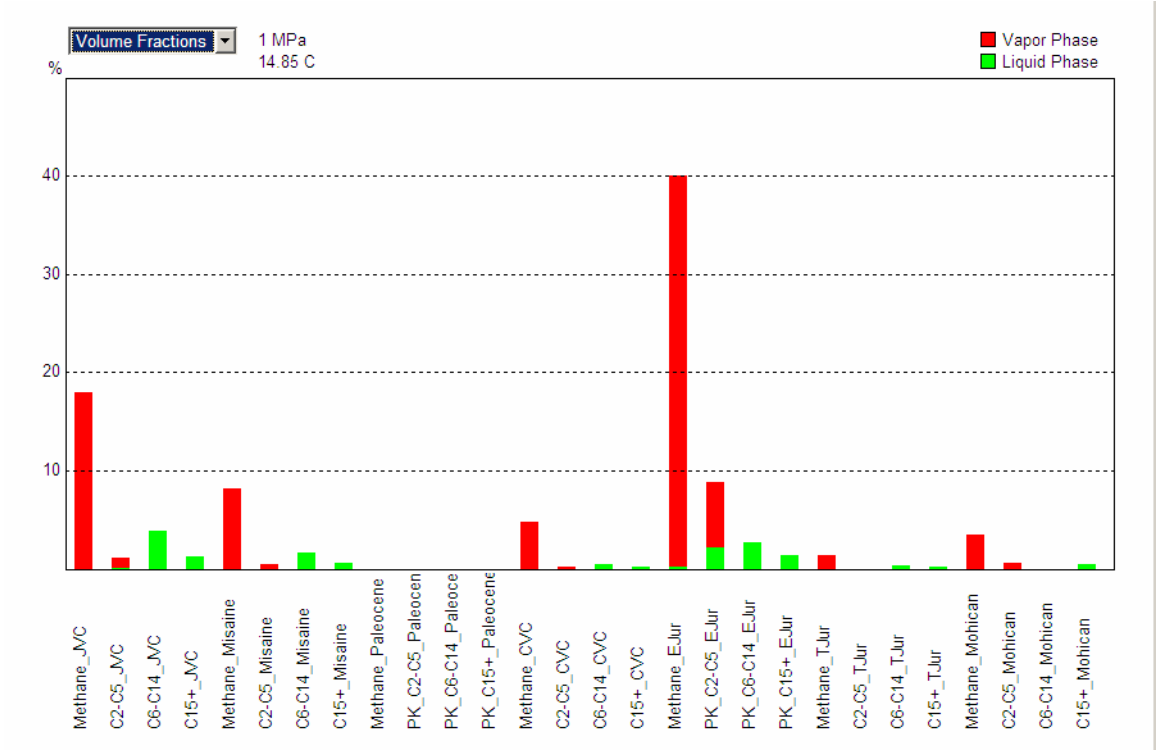

Figure 33h(iii). Line D-D' – Hydrocarbon component tracking of the Middle Paleocene Turbidite reservoir showing the volume percentages of various hydrocarbons from source rocks

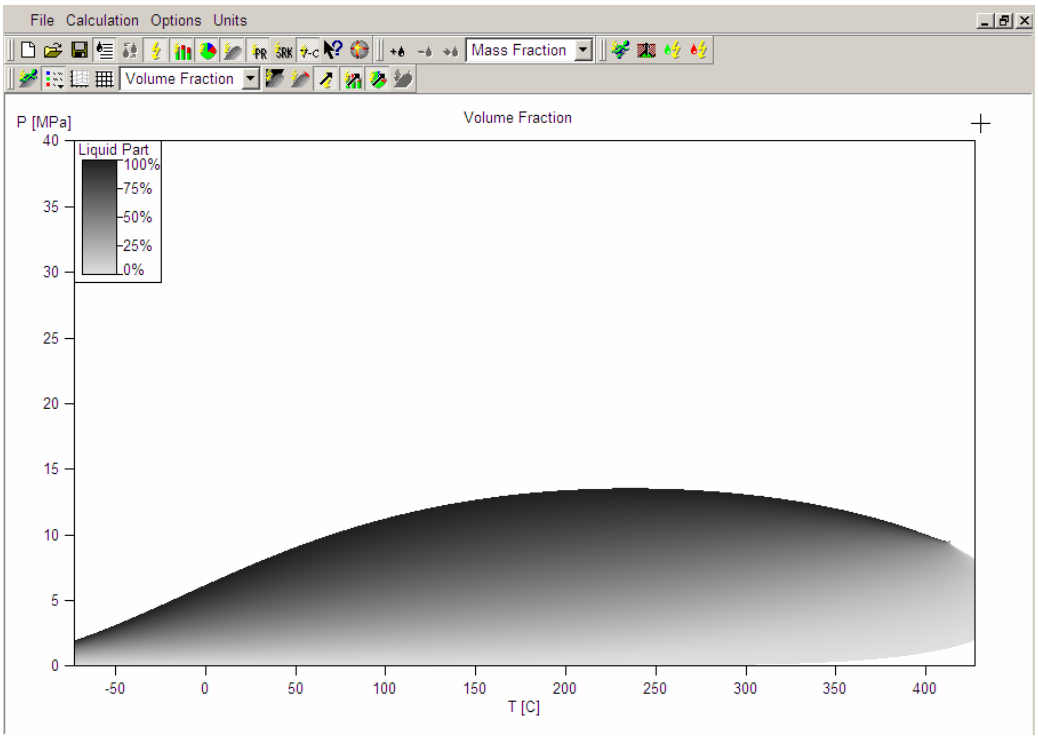

Figure 33h (iv). Line D-D' – Bubble Point Curve of the hydrocarbon components in volume fraction for the Mid-Paleocene Turbidite Reservoir from Line B-B'

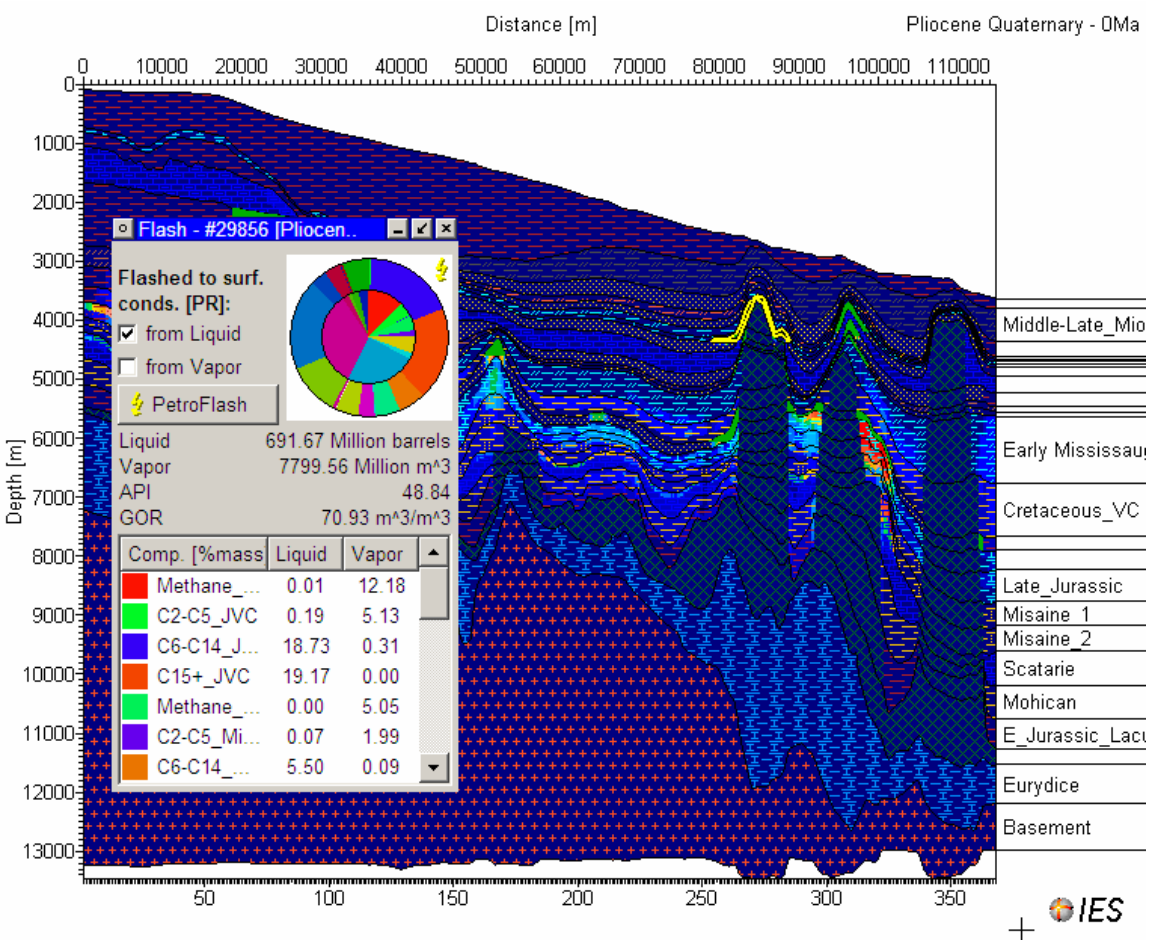

Figure 33i (i). Line D-D' – Saturation of various reservoirs with API gravity and possible GOR of Mid-Paleocene Salt-flank Reservoir. Please disregard the volumes of reservoir hydrocarbons as the model is performed on a two dimensional seismic line

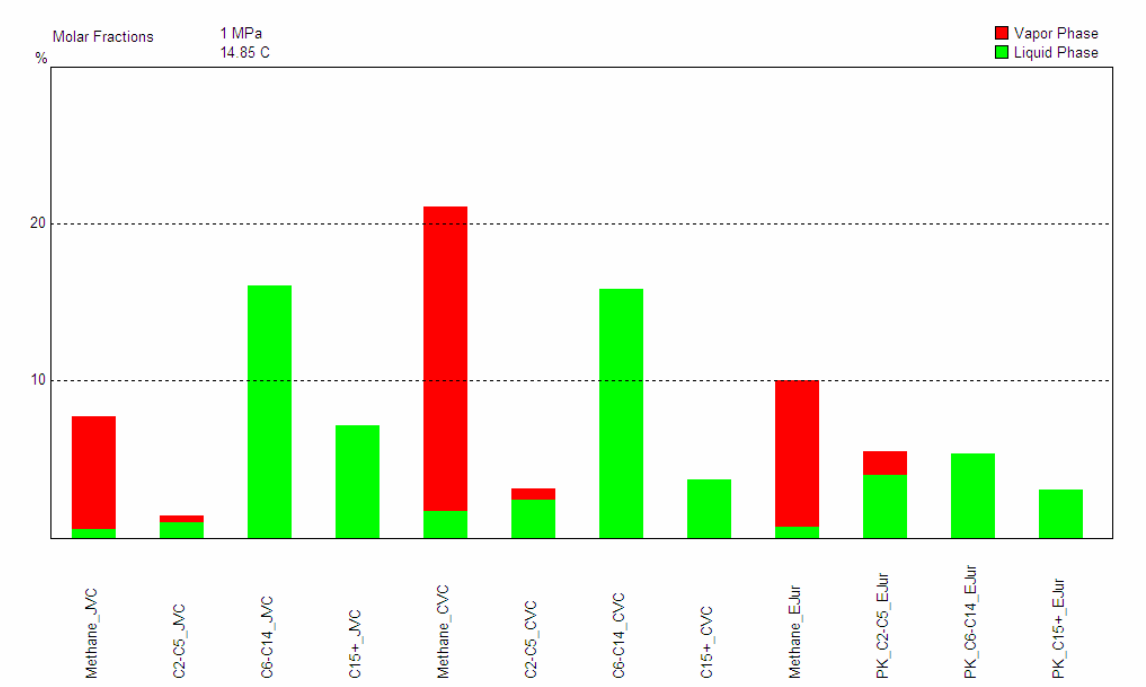

Figure 33i(ii). Hydrocarbon component tracking of the Middle Paleocene salt-flank reservoir showing the volume percentages of various hydrocarbons from source rocks. Note that Methane from the Early Jurassic, Jurassic and Cretaceous Verrill Canyon source rocks and light oil/condensate from Jurassic and Cretaceous Verrill Canyon source rocks are the main components

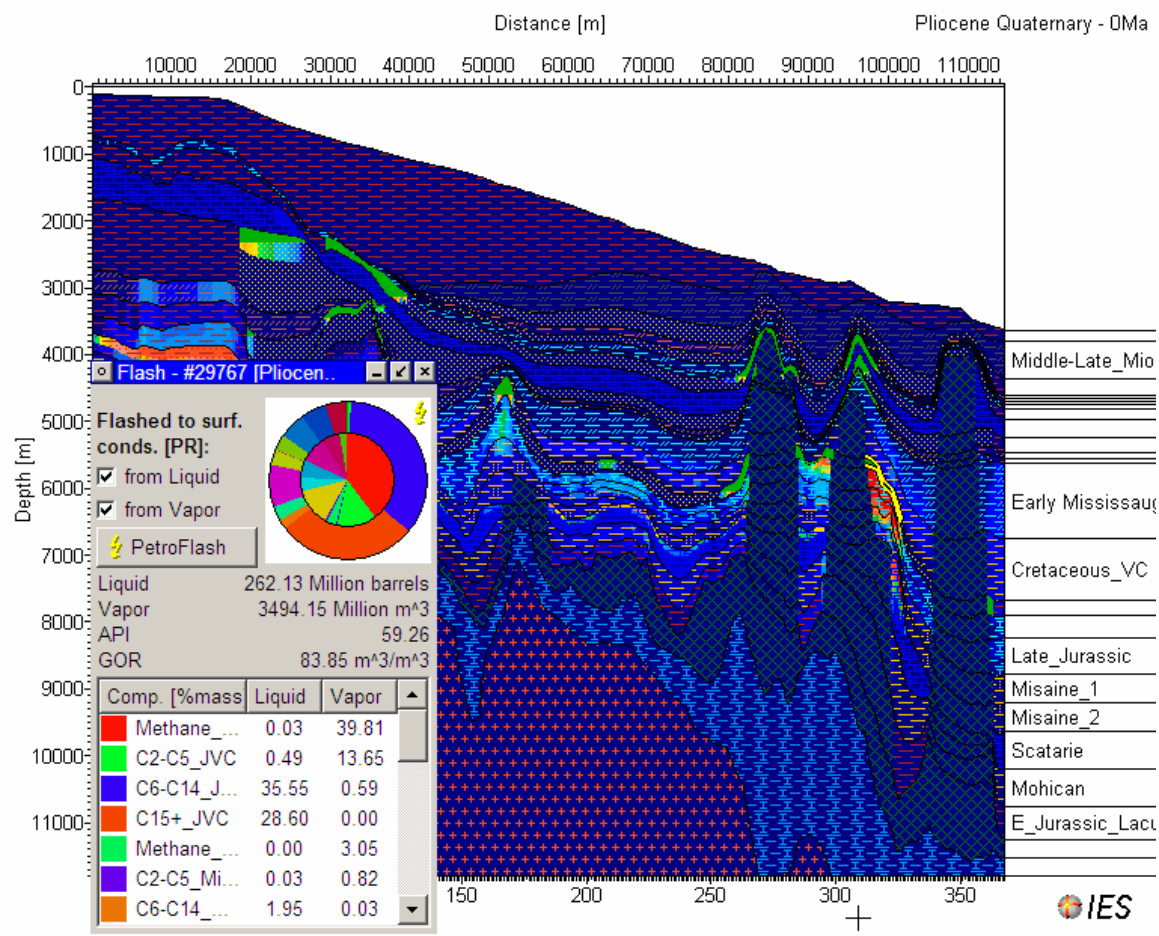

Figure 33j (i). Line D-D' – Saturation of various reservoirs with API gravity and possible GOR of Late Jurassic salt-flank Reservoir (see highlight [yellow boundary on the right side of the line) for the conceptual reservoir position). Please disregard the volumes of reservoir hydrocarbons as the model is performed on a two dimensional seismic line

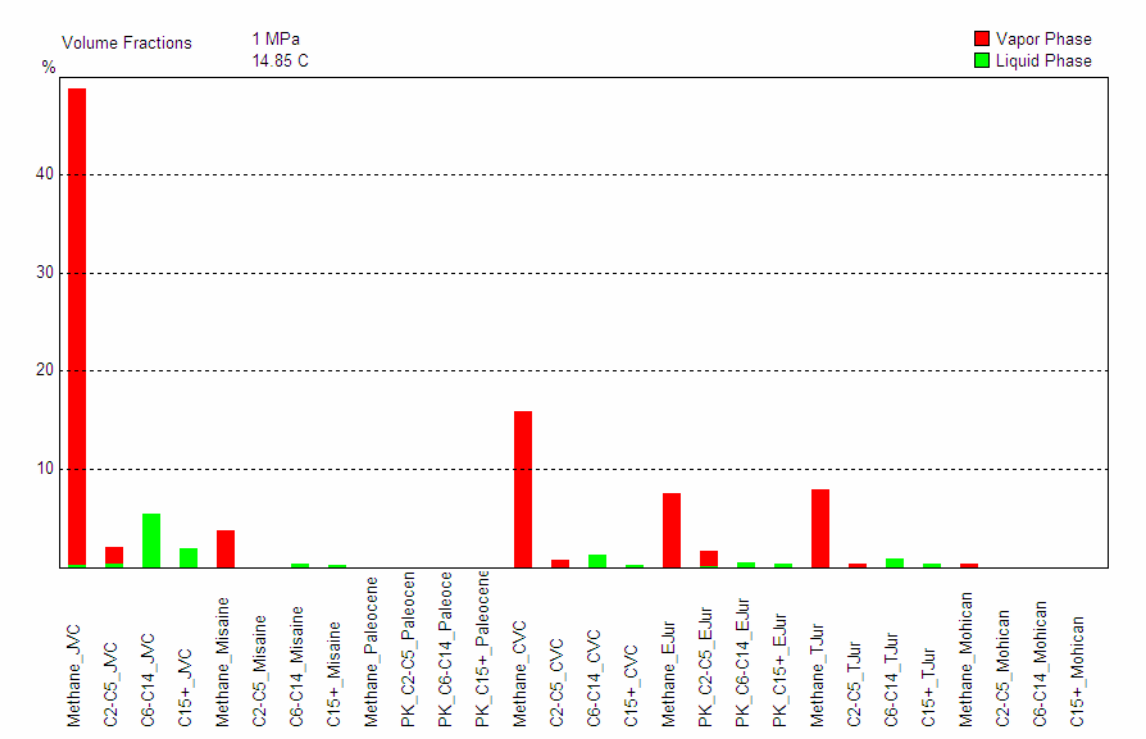

Figure 33j (ii). Line D-D' – Hydrocarbon component tracking of the Late Jurassic (see the highlight for the reservoir identification) reservoir showing the volume percentages of various hydrocarbons from source rocks

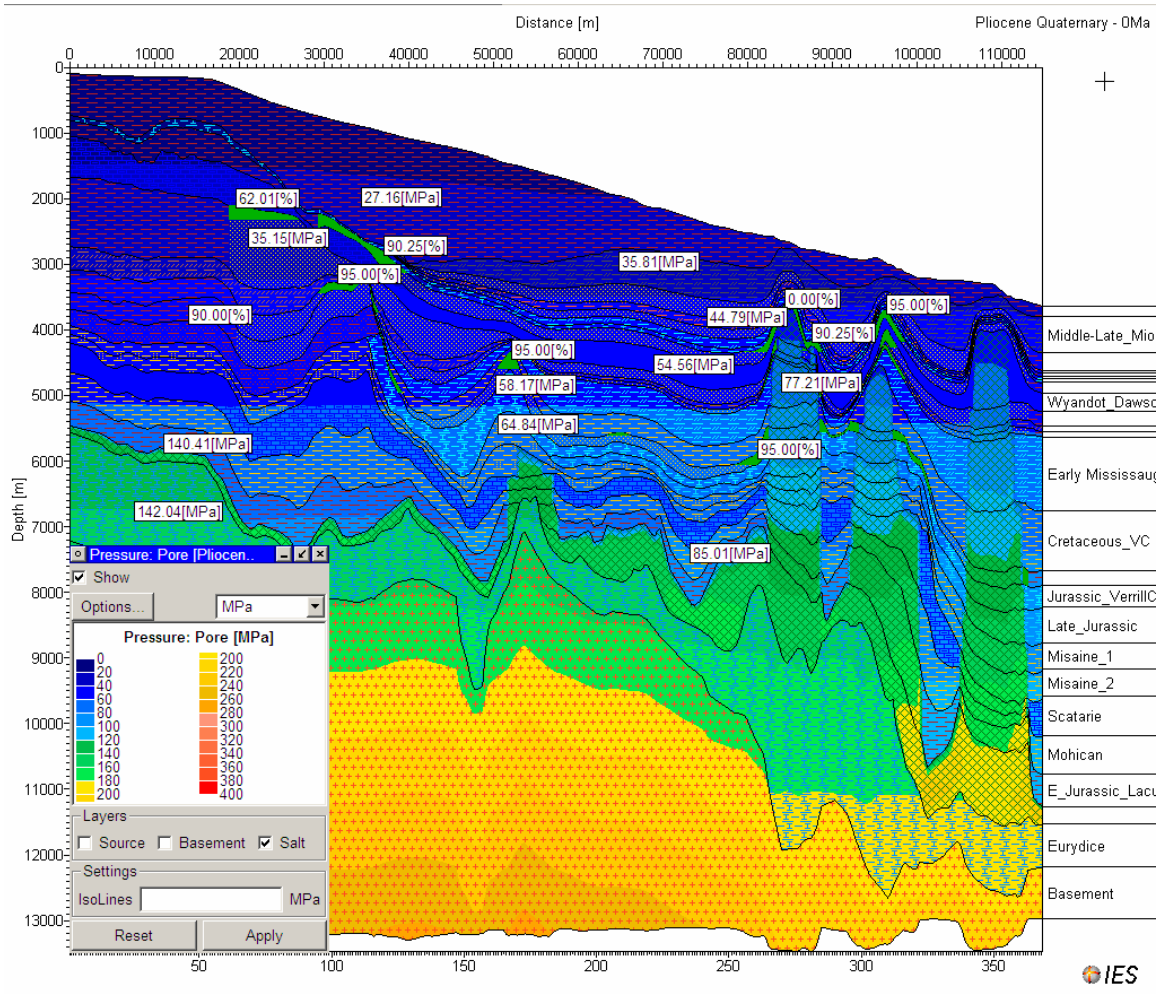

Figure 33k. Line D-D' – Pore pressure distributions of various stratigraphic units.

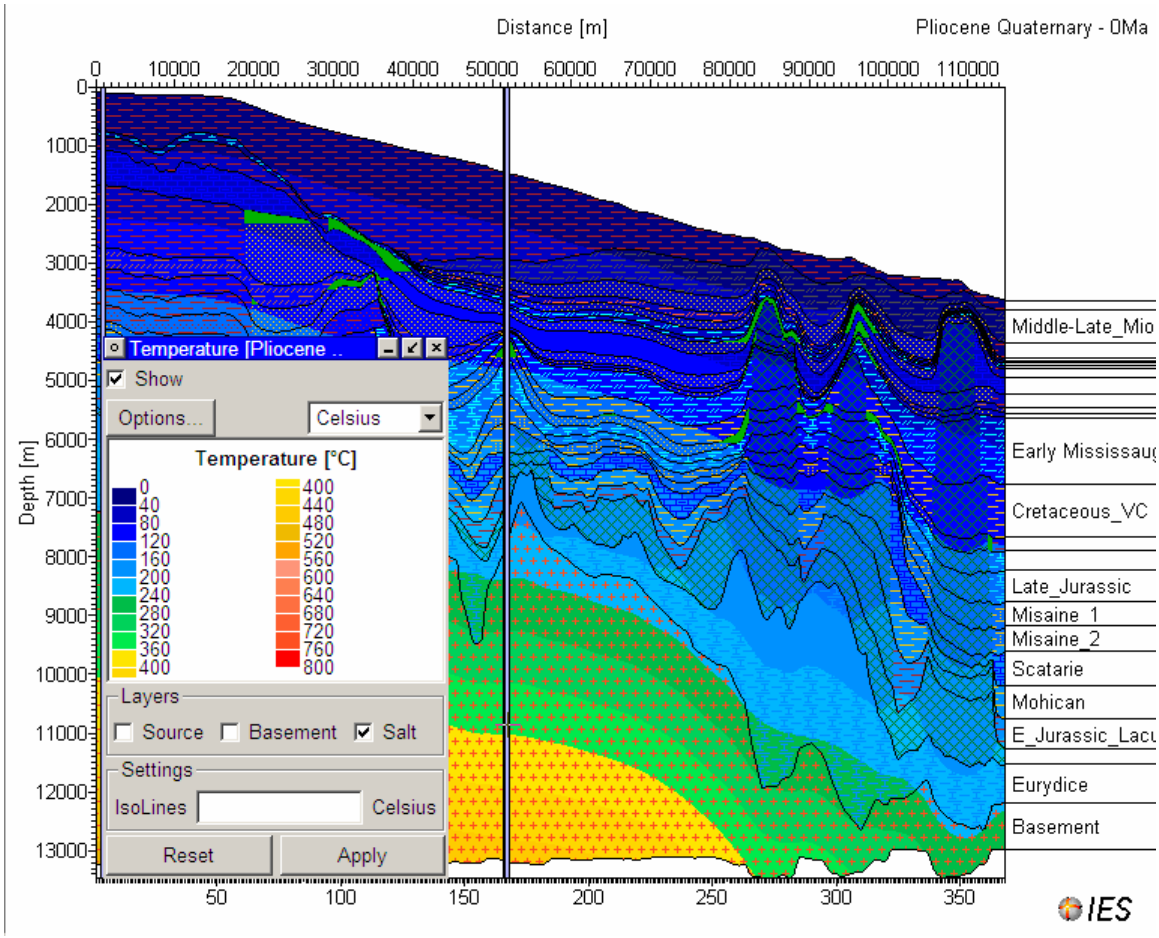

Figure 33m (i). Line D-D'. 1D extraction on top of Jurassic hydrocarbon reservoir

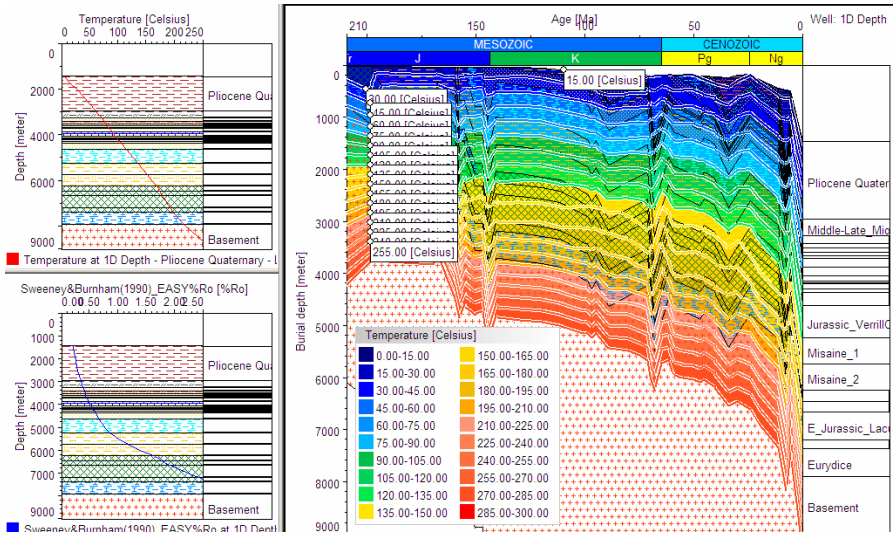

Figure 33m (ii). Line D-D'. 1D extraction on top of Jurassic hydrocarbon reservoir – Burial history with iso-temperature line

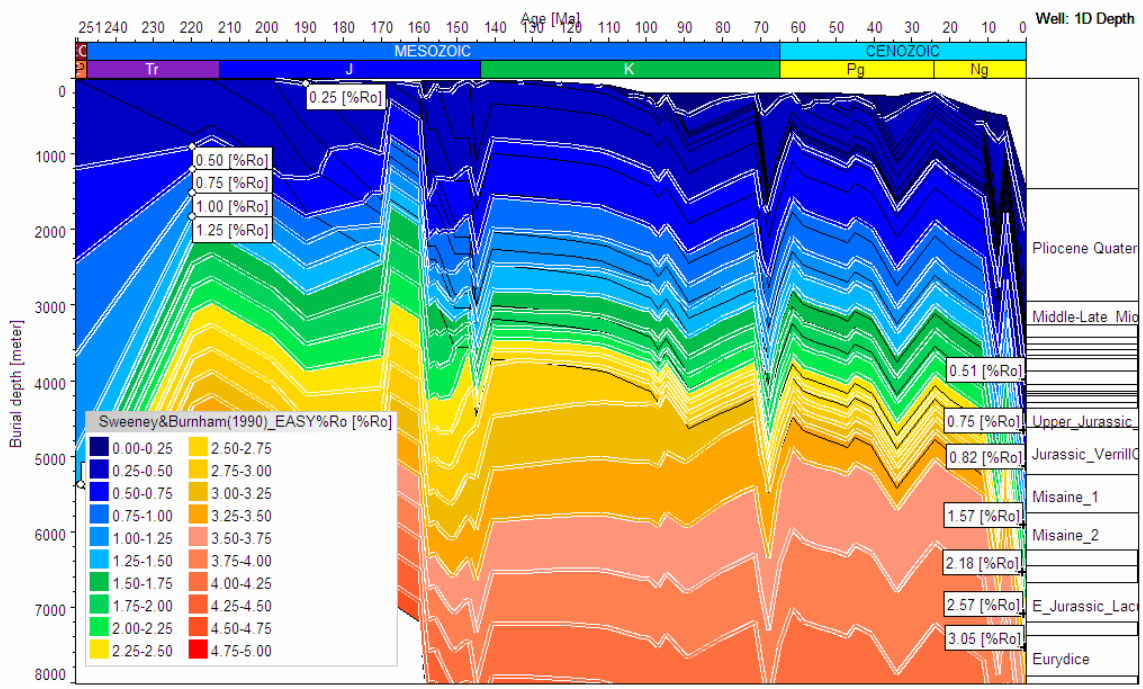

Figure 33m (iii). Line D-D' - 1D extraction on top of Jurassic hydrocarbon reservoir – iso-maturation histories

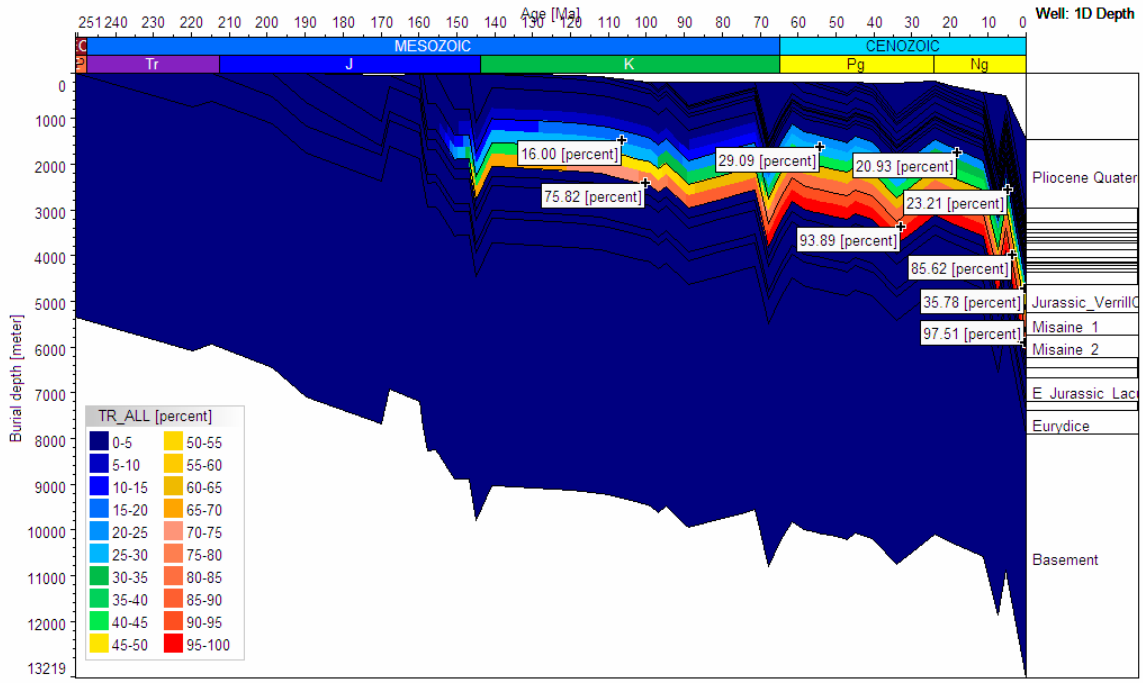

Figure 33m (iv). Line D-D' - Burial history of the 1D extraction line with the total amount of expelled hydrocarbons from various source rocks.

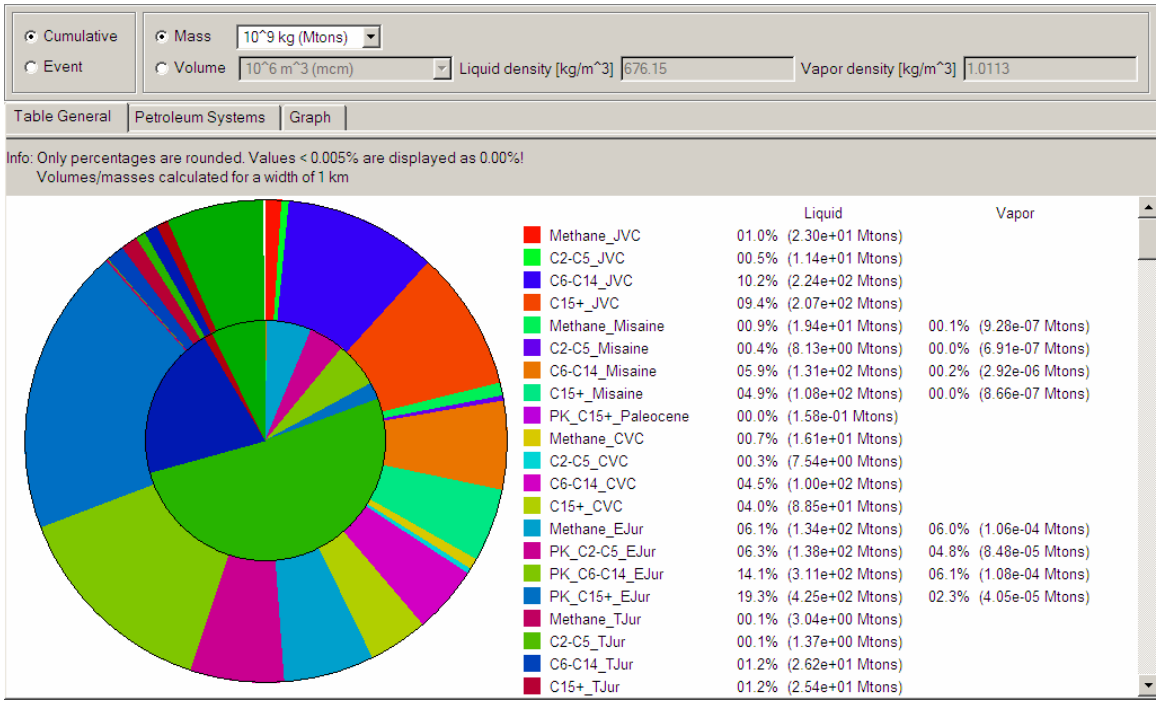

Figure 33n.Cummulative masses of multi-component hydrocarbons expelled from various source rocks (masses calculated for a kilometer radius of an area)

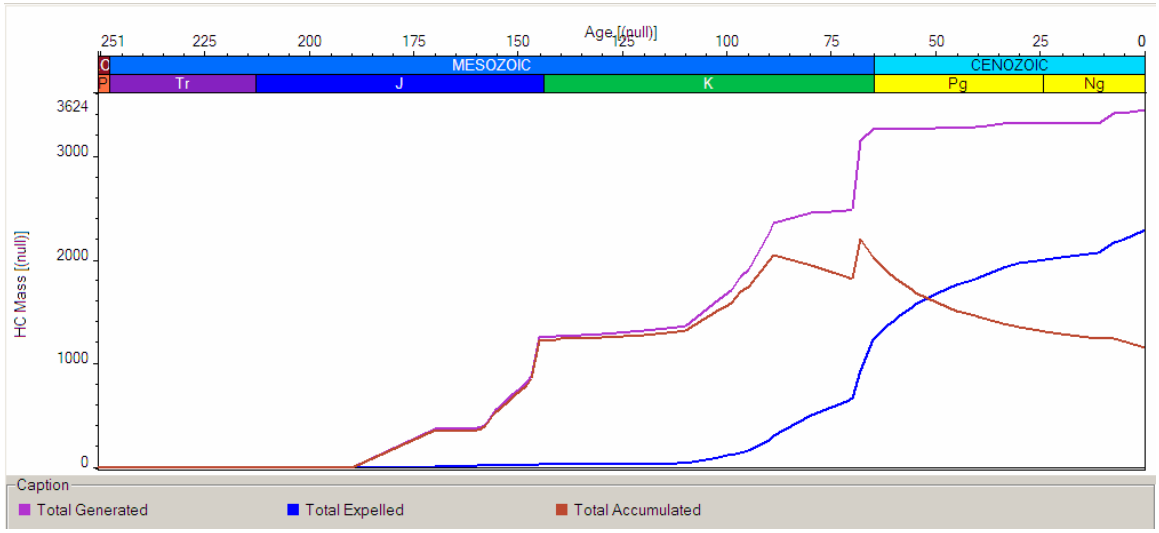

Figure 33p.Line C-C' – Timing of total generated, total expelled, and total accumulated cummulative hydrocarbon mass from various source rocks (masses calculated for a width of 1 km)

Seismic Line C-C’

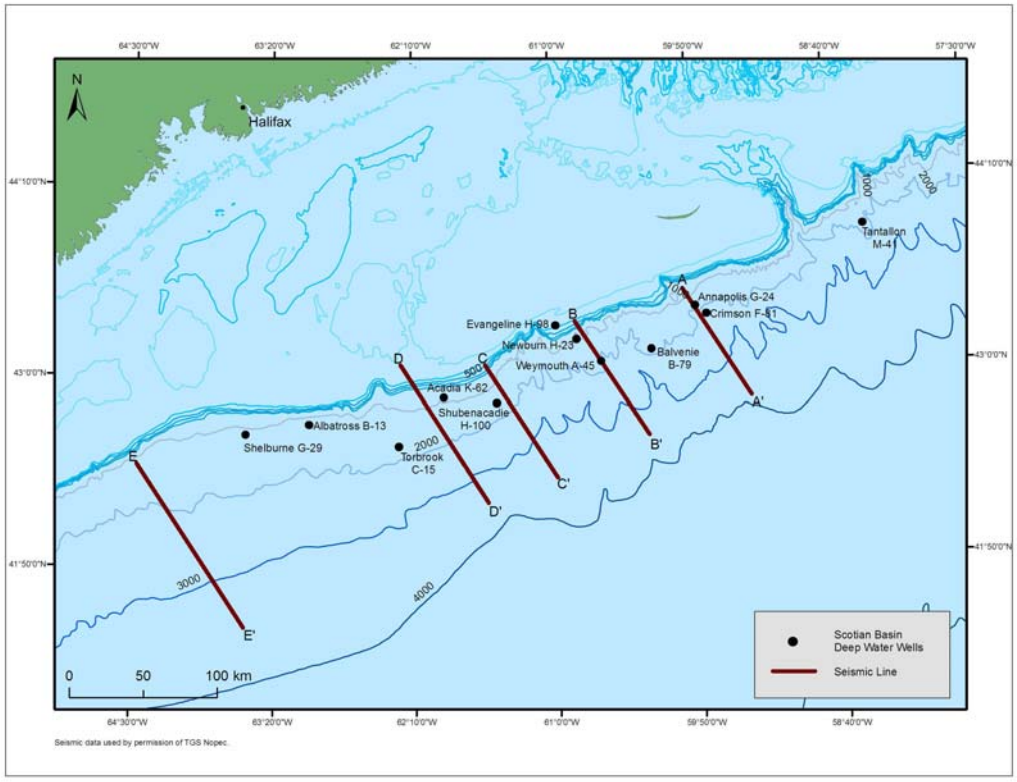

Figure 34a. Location map of seismic line C-C’

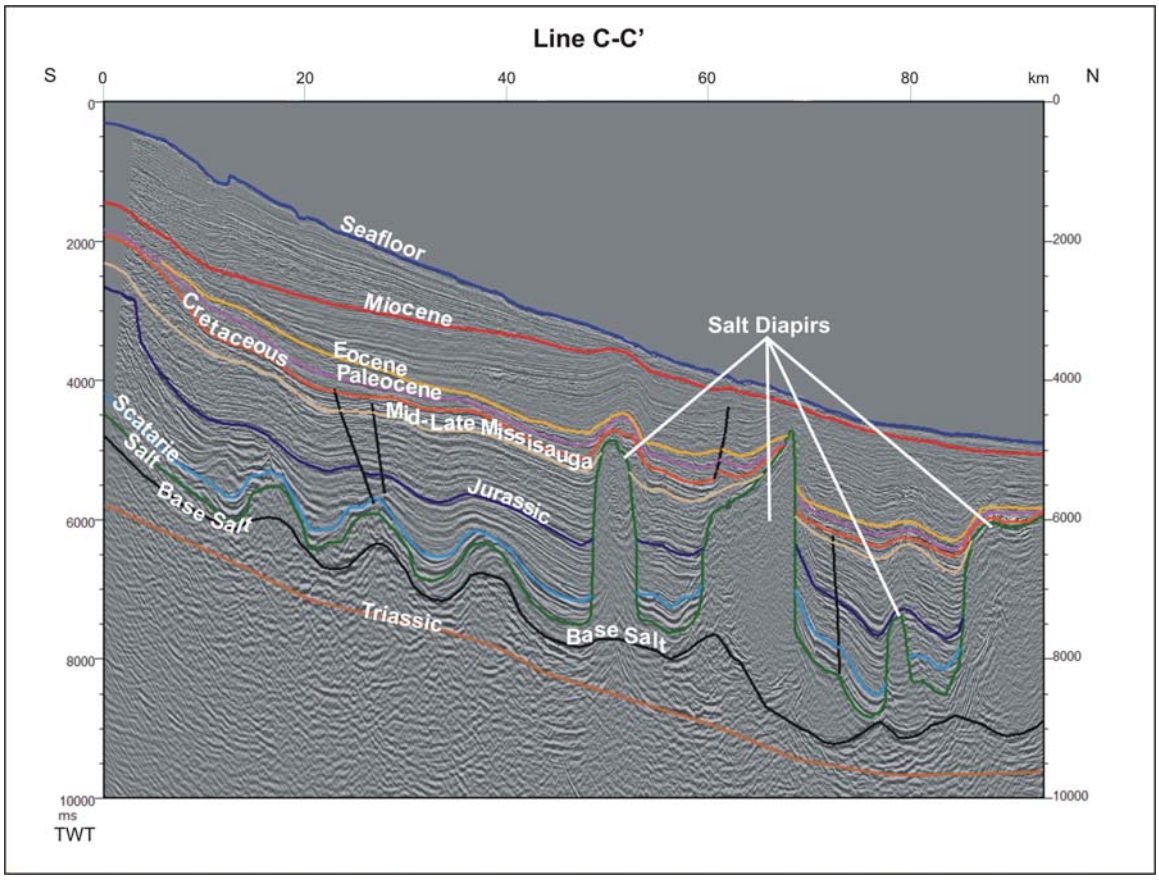

34b. Seismic line line C-C' with selected formation boundaries, faults, and salt diapirs

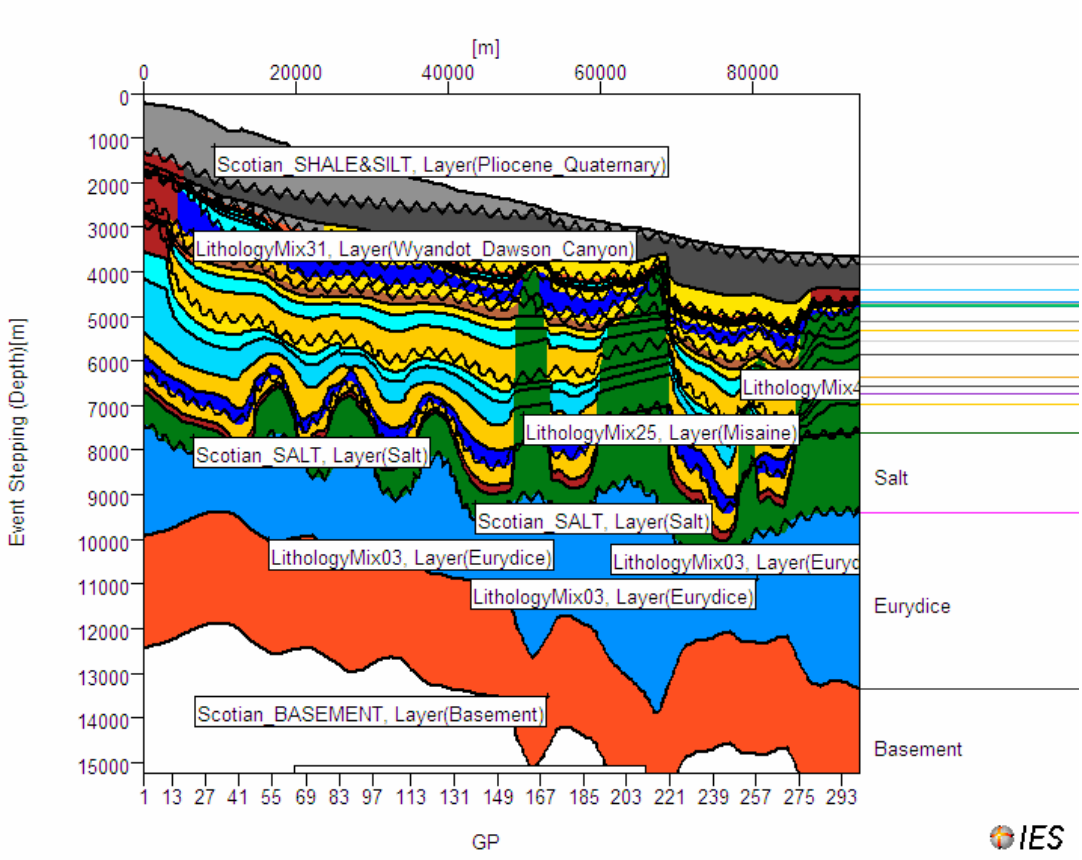

Figure 34c. Line C-C' – PetroBuilder input data before simulation showing the lithology mix with various stratigraphic units and the position of salt piercement structures

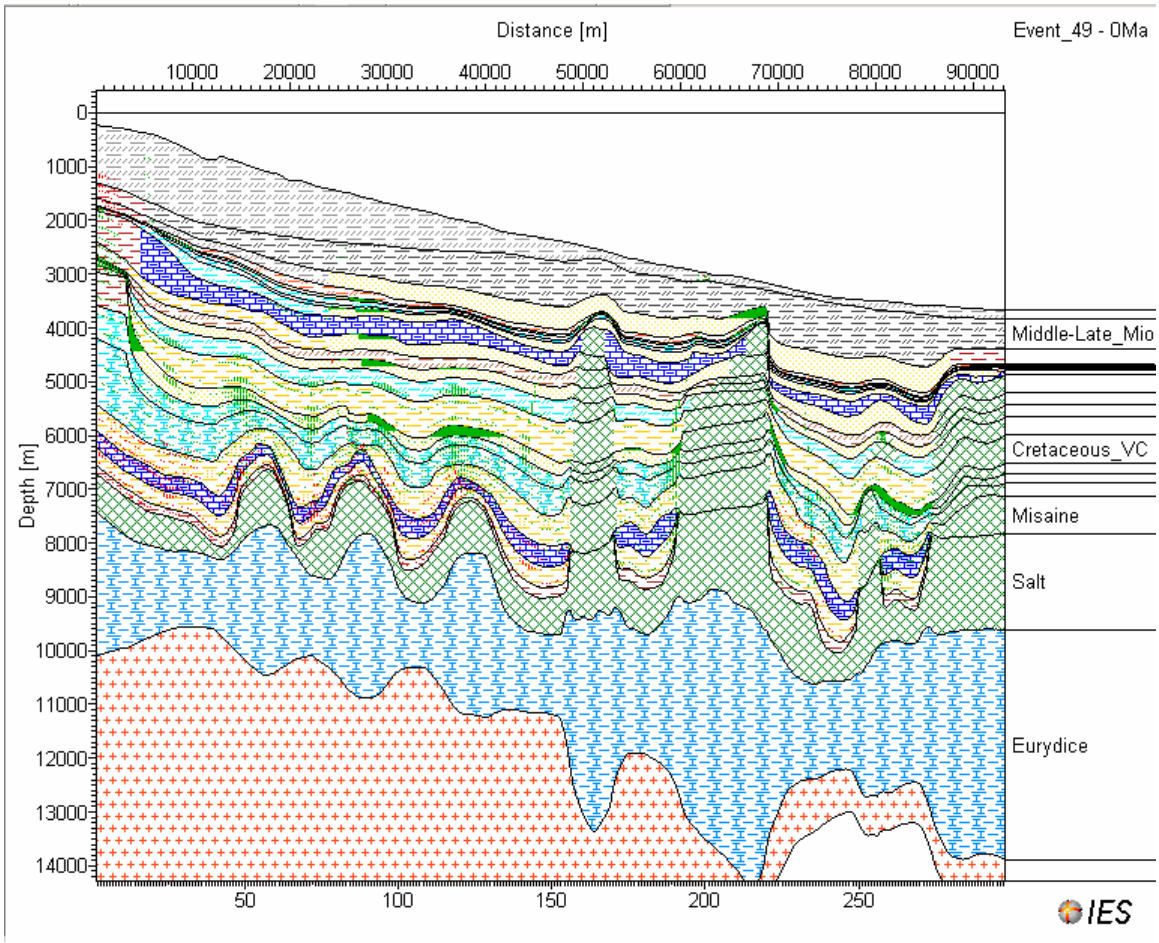

Figure 34d. Line C-C' – Output data: conceptual reservoir saturation with hydrocarbon vectors

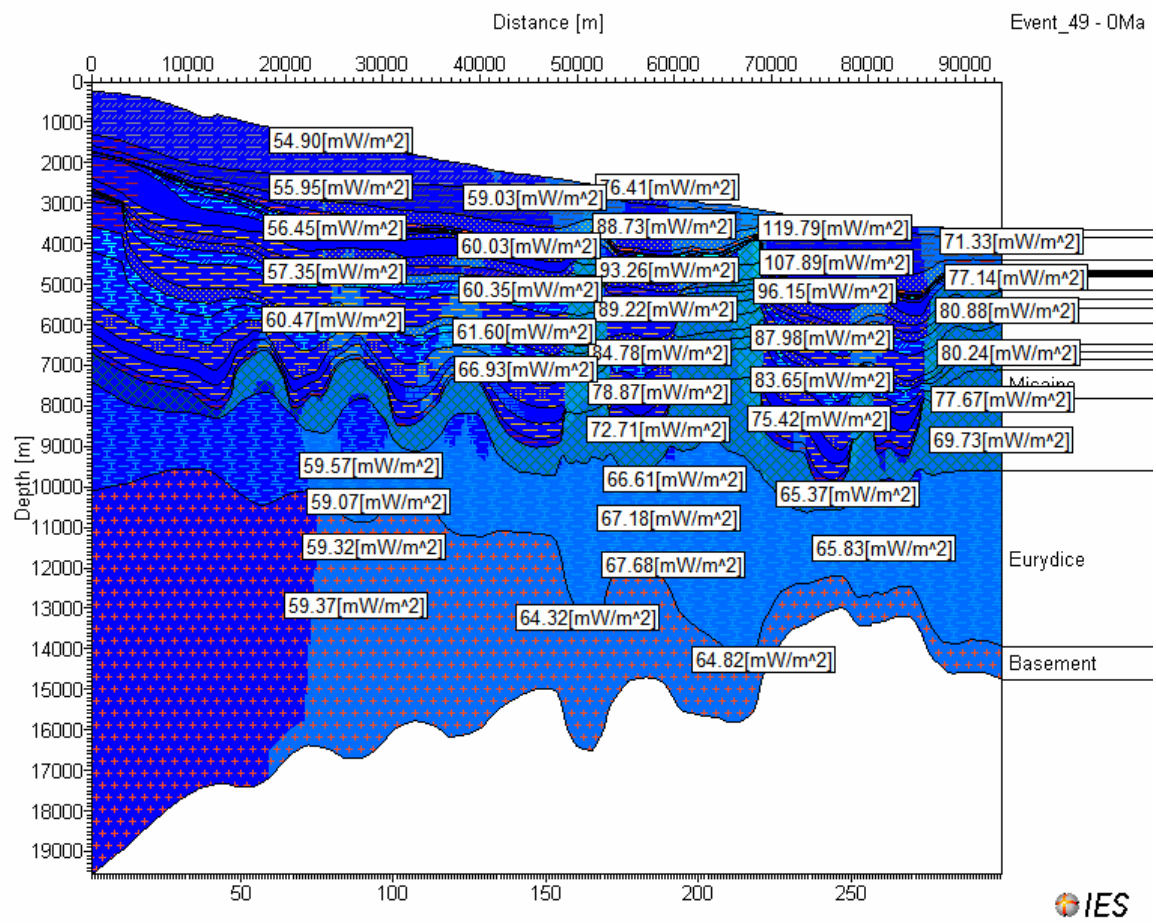

Figure 34e (i). Line C-C' – Heat flow variation within various sediments at the present time

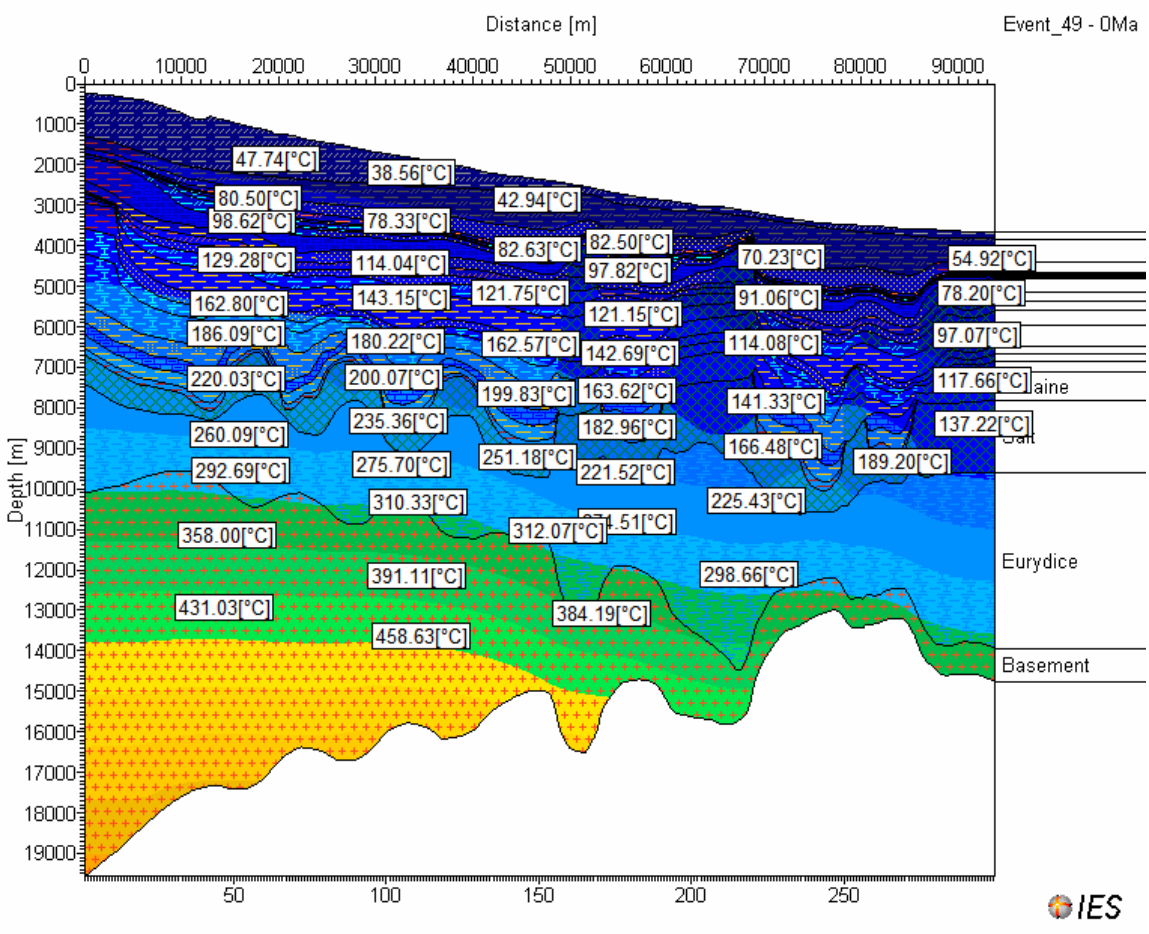

Figure 34e (ii). Line C-C' – present day temperature at various stratigraphic units. It also shows the reservoir saturation

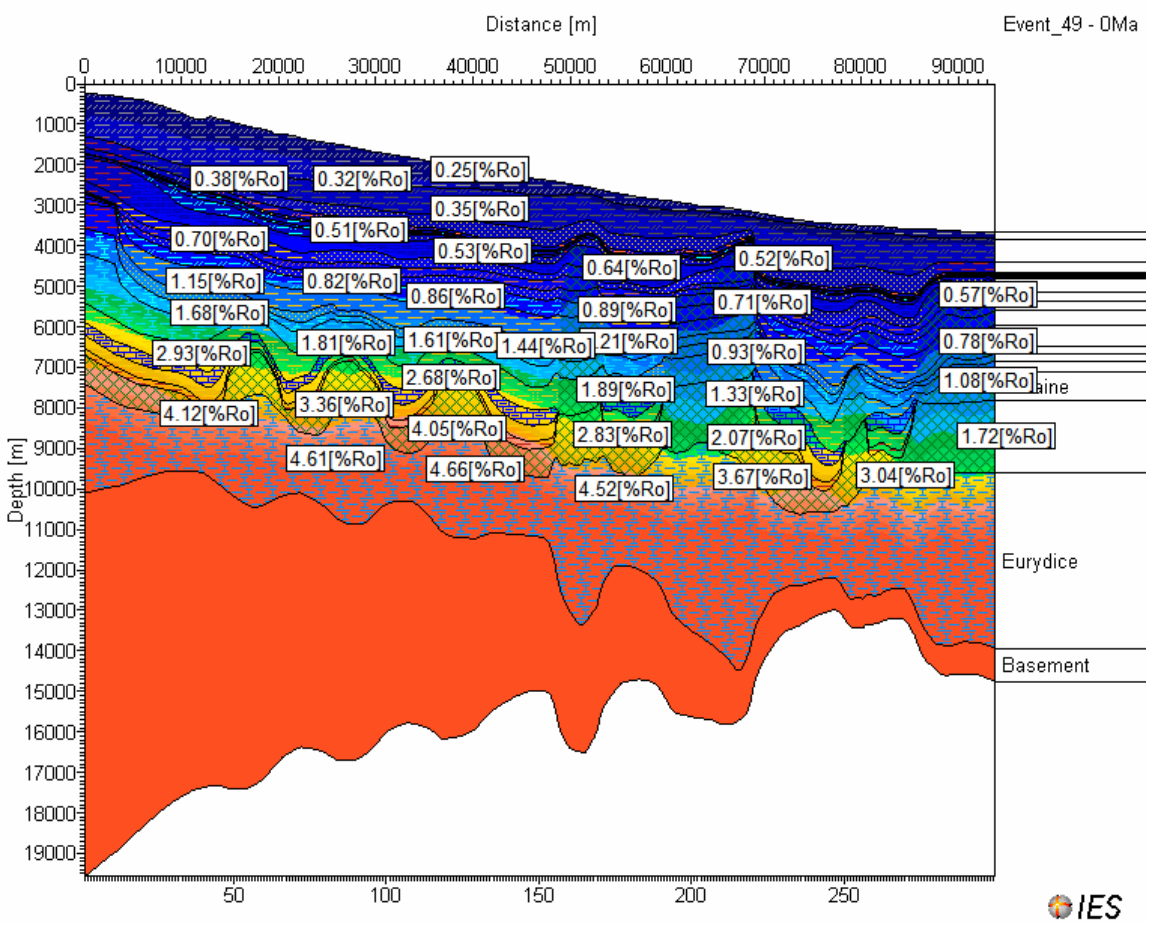

Figure 34e (iii). Line C-C' – present day maturity at various stratigraphic intervals

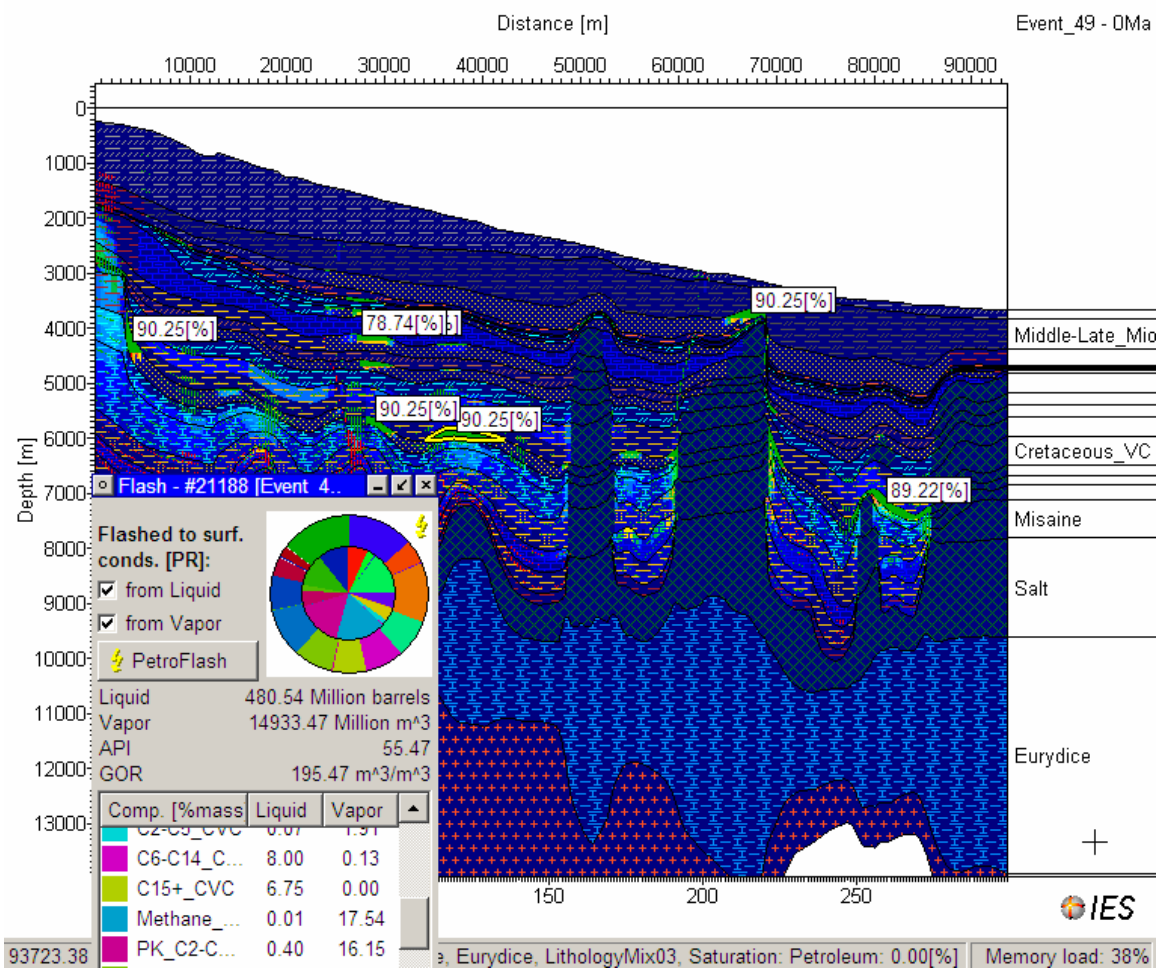

Figure 34f (i). Line C-C' - Saturation of various reservoirs with API gravity and possible GOR of Late Jurassic Reservoir. Please disregard the volumes of reservoir hydrocarbons as the model is performed on a two dimensional seismic line

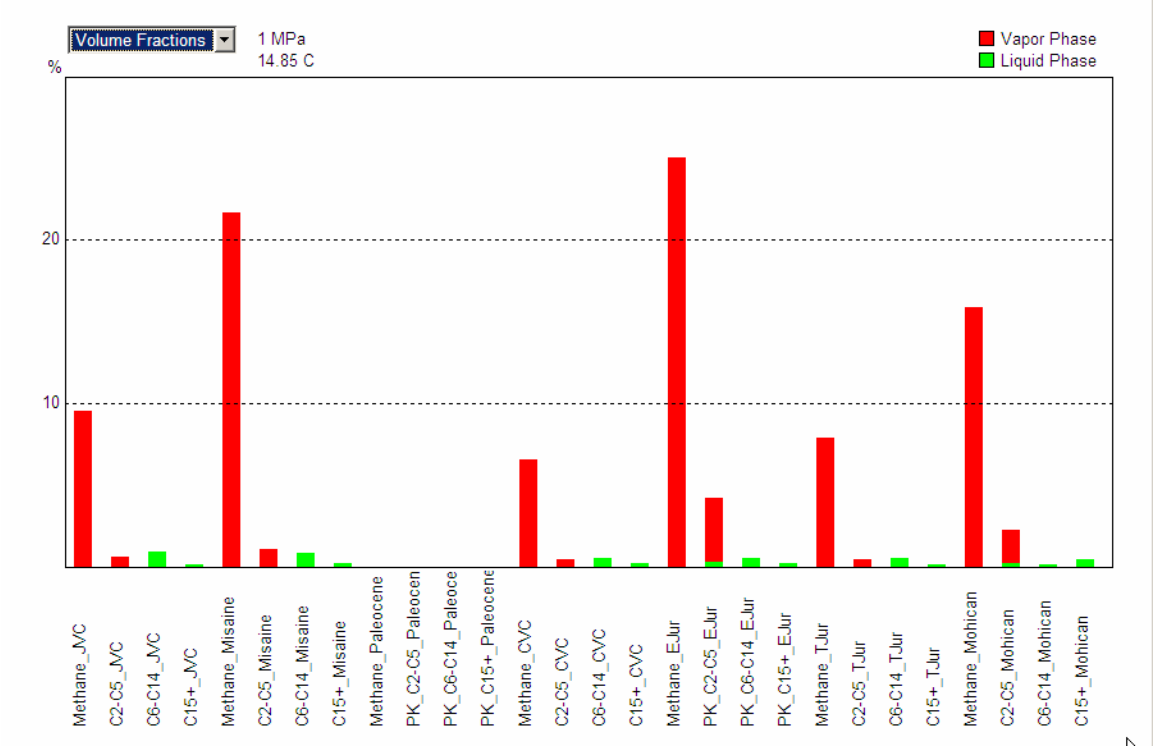

Figure 34f (ii). Line C-C' - Hydrocarbon component tracking of the Late Jurassic reservoir showing the volume percentages of various hydrocarbons from source rocks

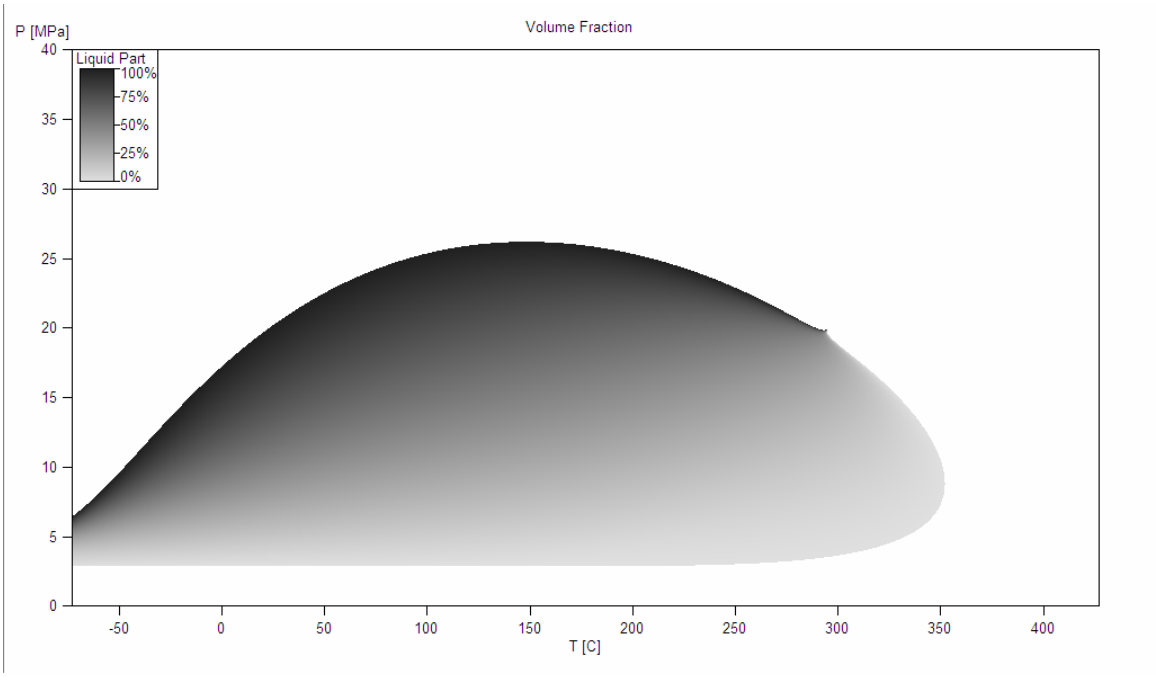

Figure 34f (iii). Line C-C' – Bubble point curve of Late Jurassic reservoir hydrocarbons

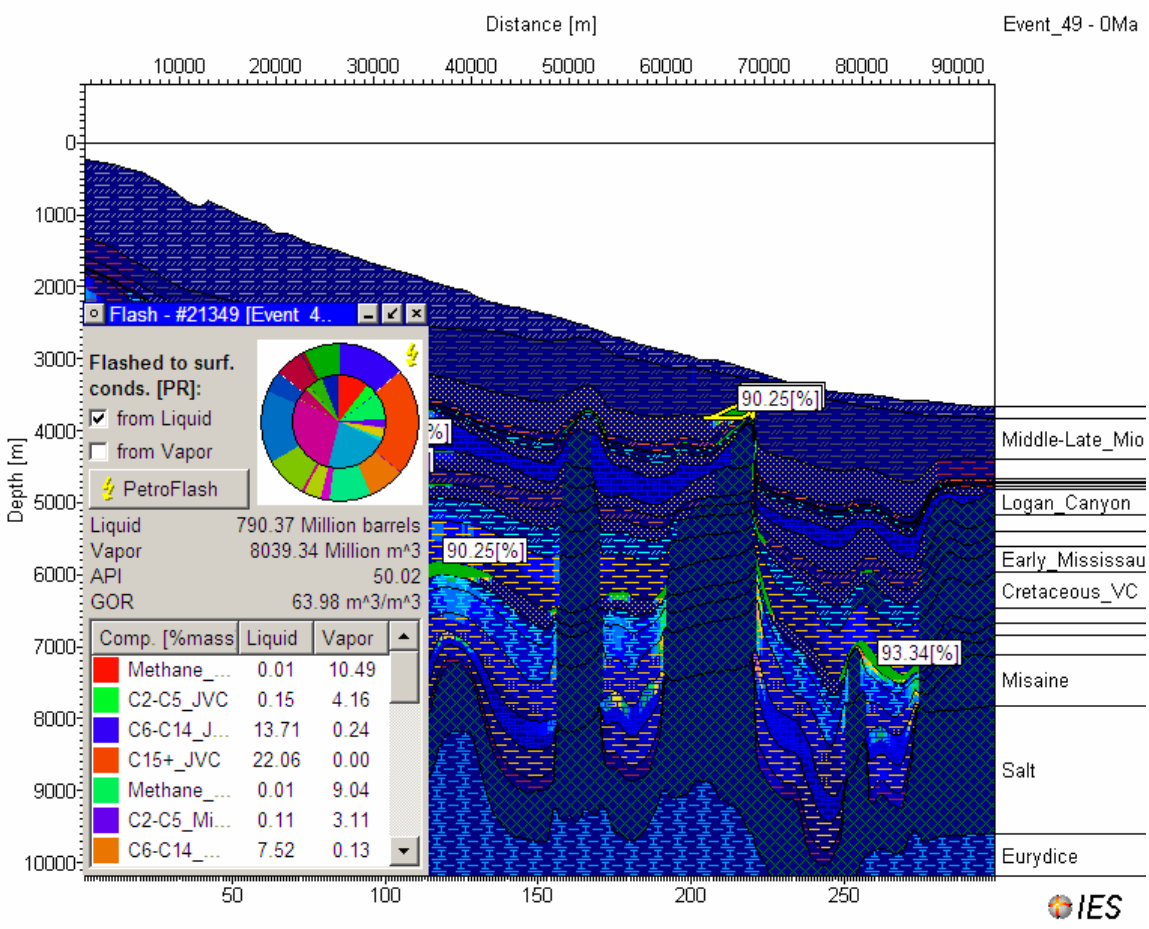

Figure 34g (i). Line C-C' - Saturation of various reservoirs with API gravity and possible GOR of Late to Middle Miocene Reservoir. Please disregard the volumes of reservoir hydrocarbons as the model is performed on a two dimensional seismic line

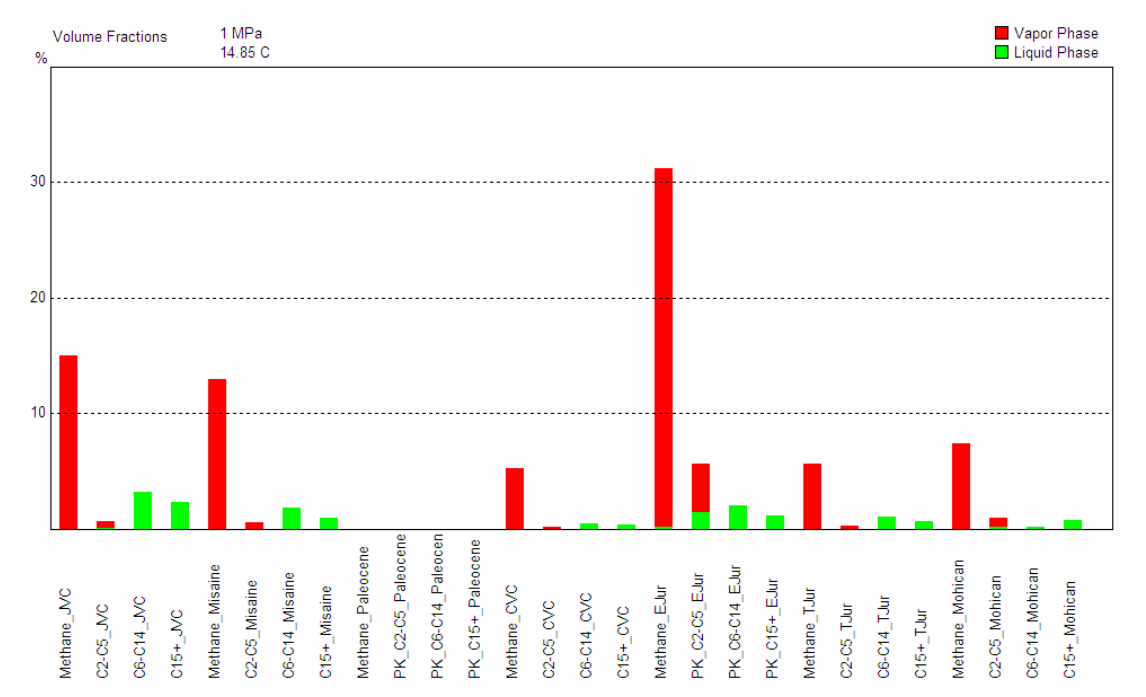

Figure 34g (ii). Line C-C' - Hydrocarbon component tracking of the Late to Middle Miocene reservoir showing the volume percentages of various hydrocarbons from source rocks

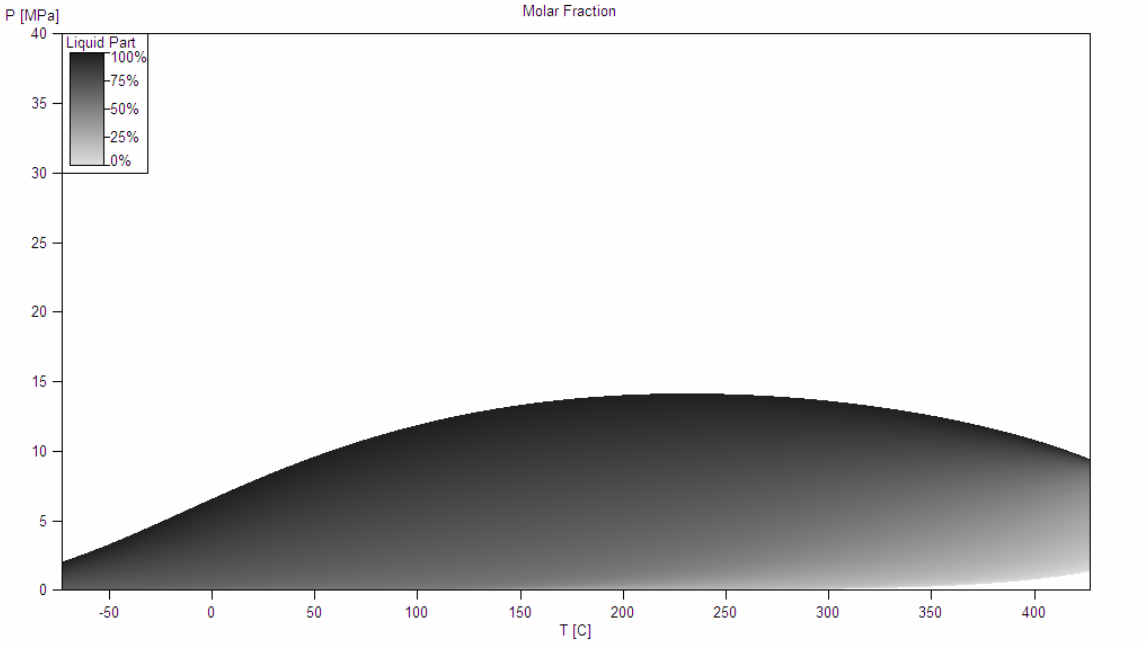

Figure 34g (iii): Bubble point curve of Middle Miocene reservoir hydrocarbons

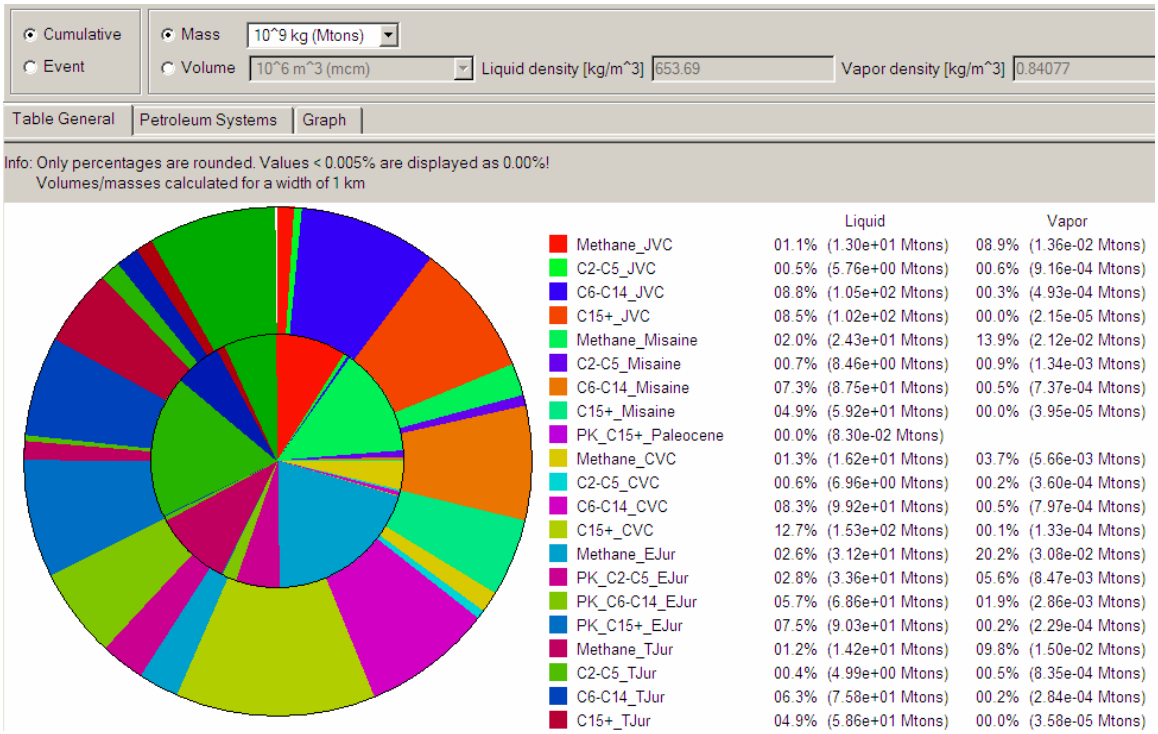

Figure 34h.Line C-C' - Cummulative masses of multi-component hydrocarbons expelled from various source rocks (masses calculated for a kilometer radius area)

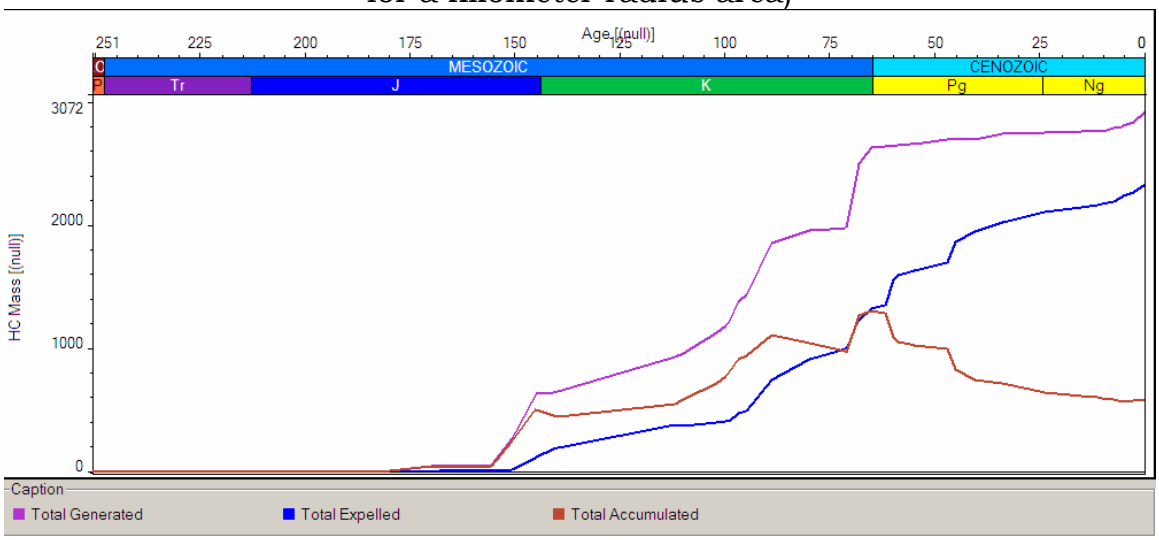

Figure 34i.Line C-C' – Timing of total generated, total expelled, and total accumulated cumulative hydrocarbon mass from various source rocks (masses calculated for a width of 1 km)

Seismic Line B-B’

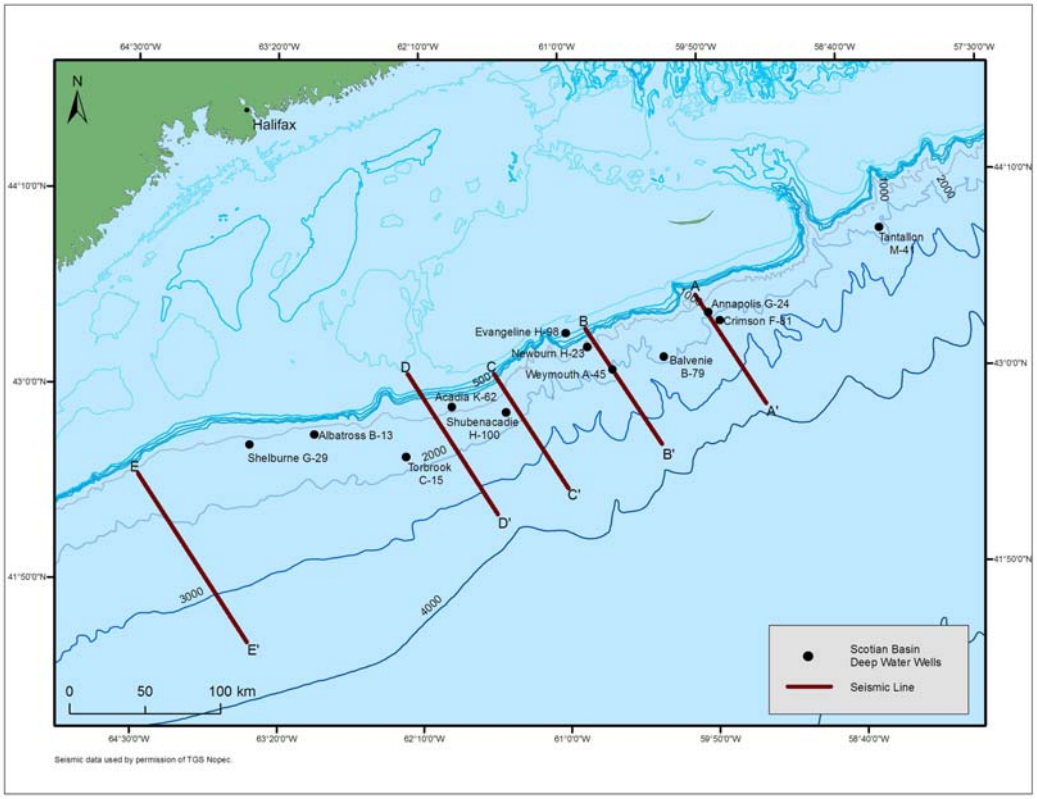

Figure 35a. Location map of the seismic line B-B’

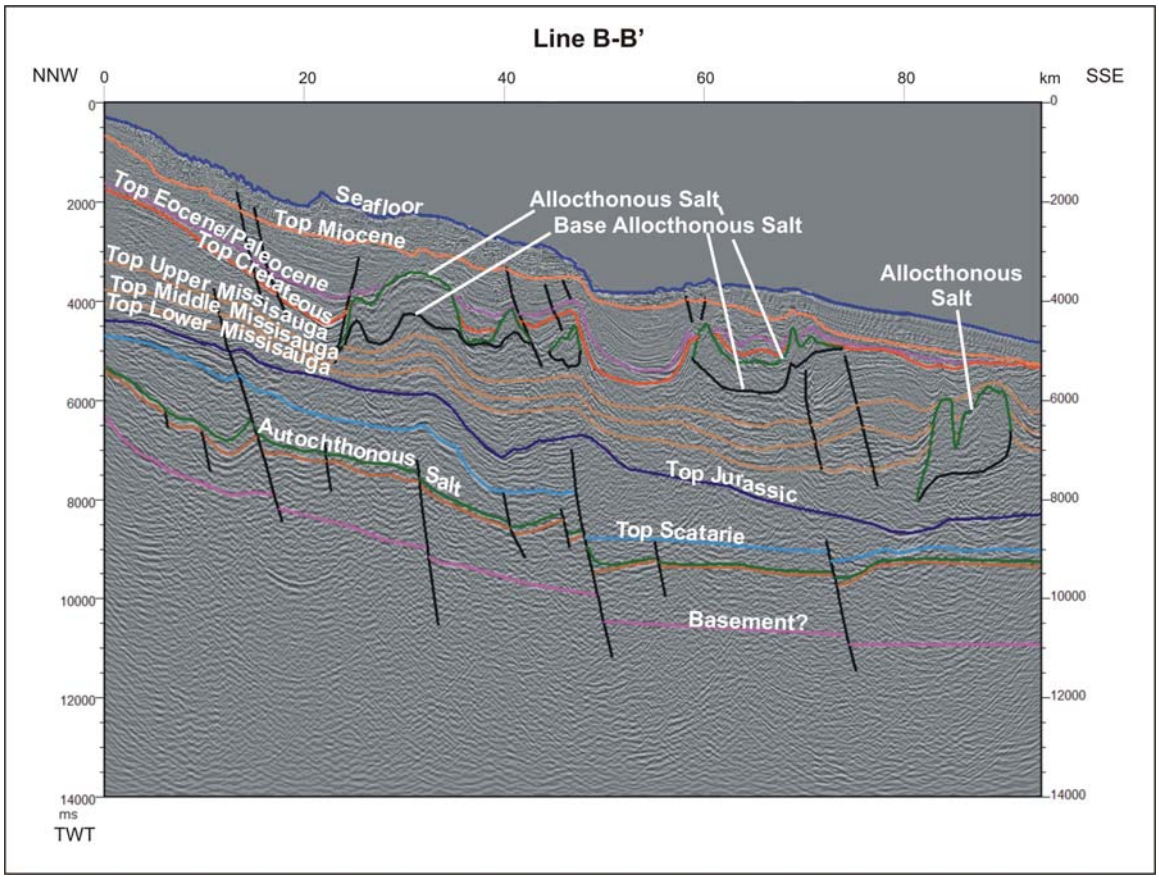

Figure 35b. Seismic line B-B'(Sable Subbasin) with selected formation boundaries, faults, and both allochthonous and autochthonous salt bodies (depth in ms)

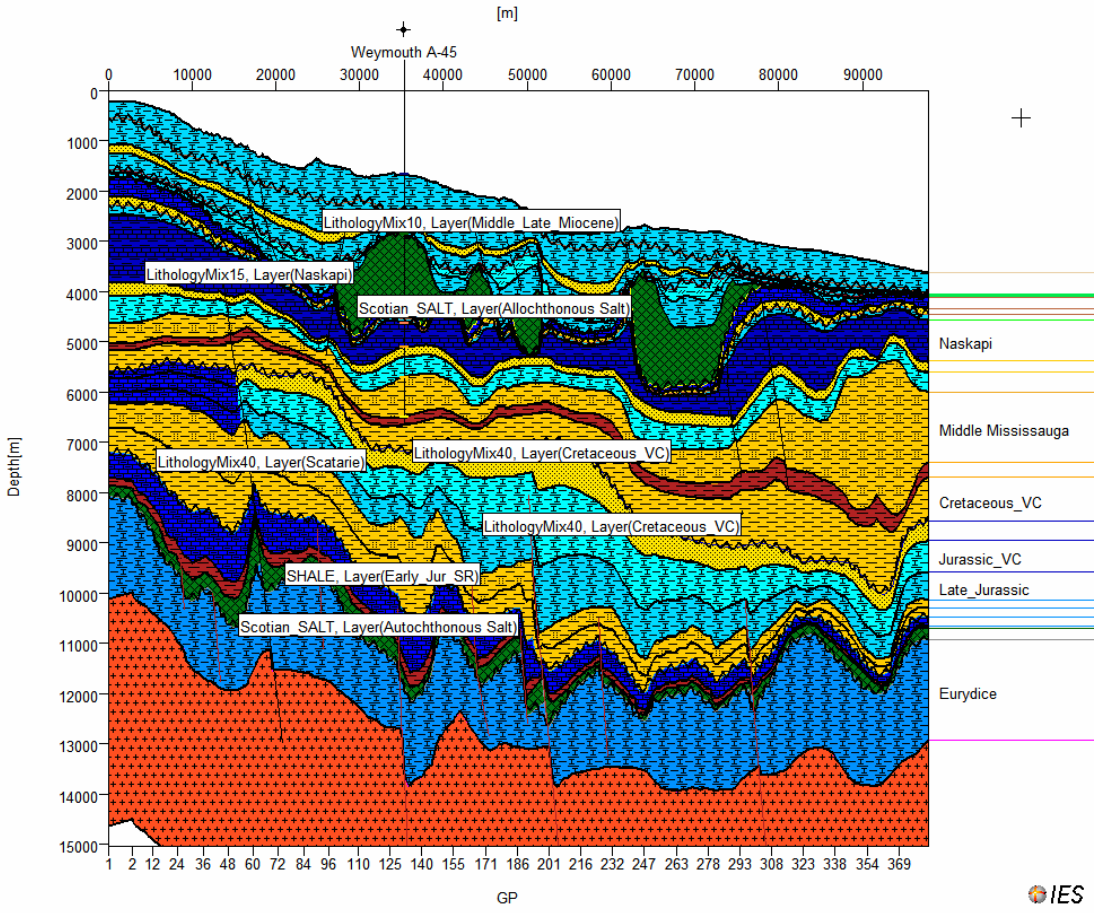

Figure 35c. Line B-B' – Input Parameters in Petrobuilder with unconformity, horizons etc.

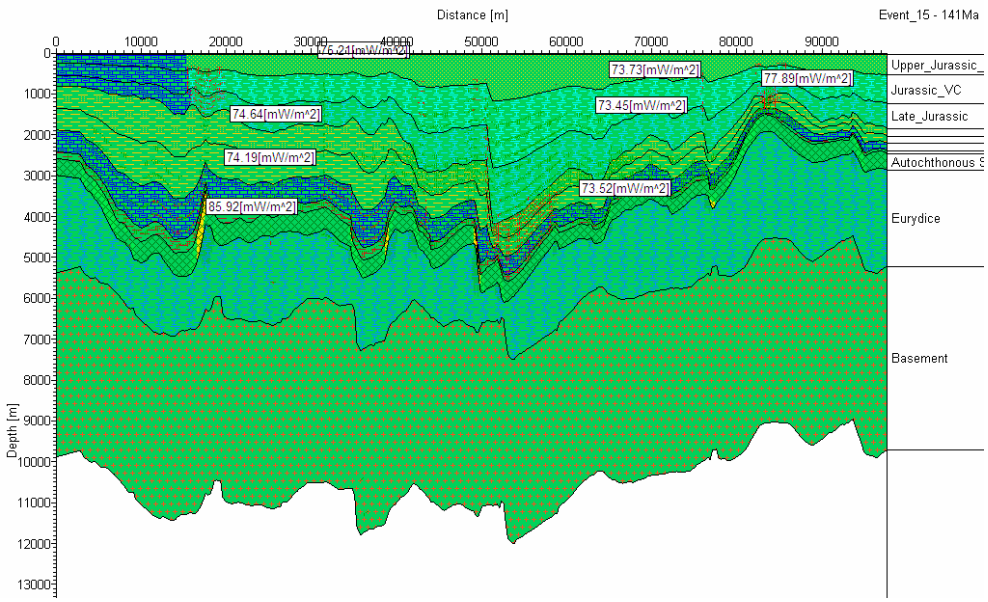

Figure 35d (i). Line B-B': Output Data - Heat Flow profile at 141 Ma.

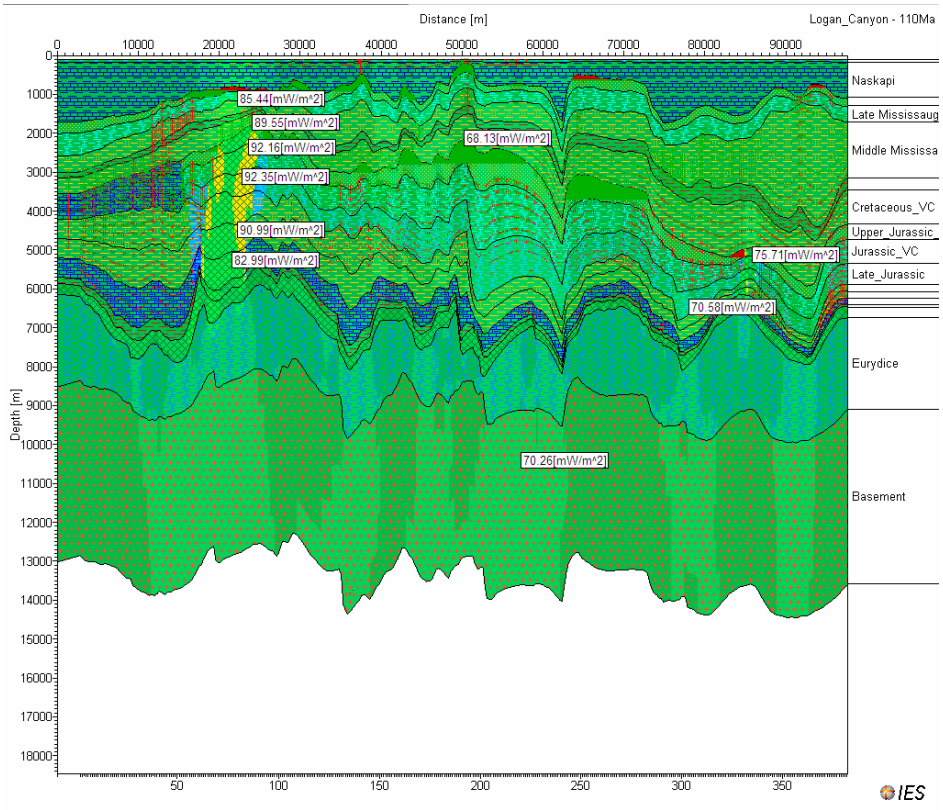

Figure 35d (ii). Line B-B': Output Data Heat Flow at 110 Ma

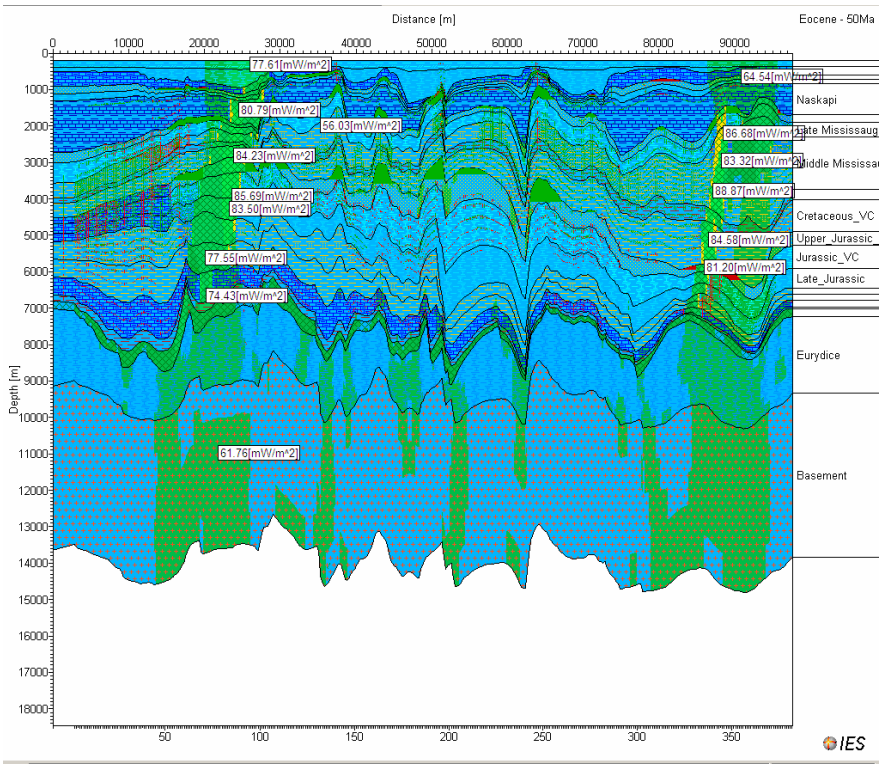

Figure 35d (iii). Line B-B': Output Data Heat Flow at 50 Ma

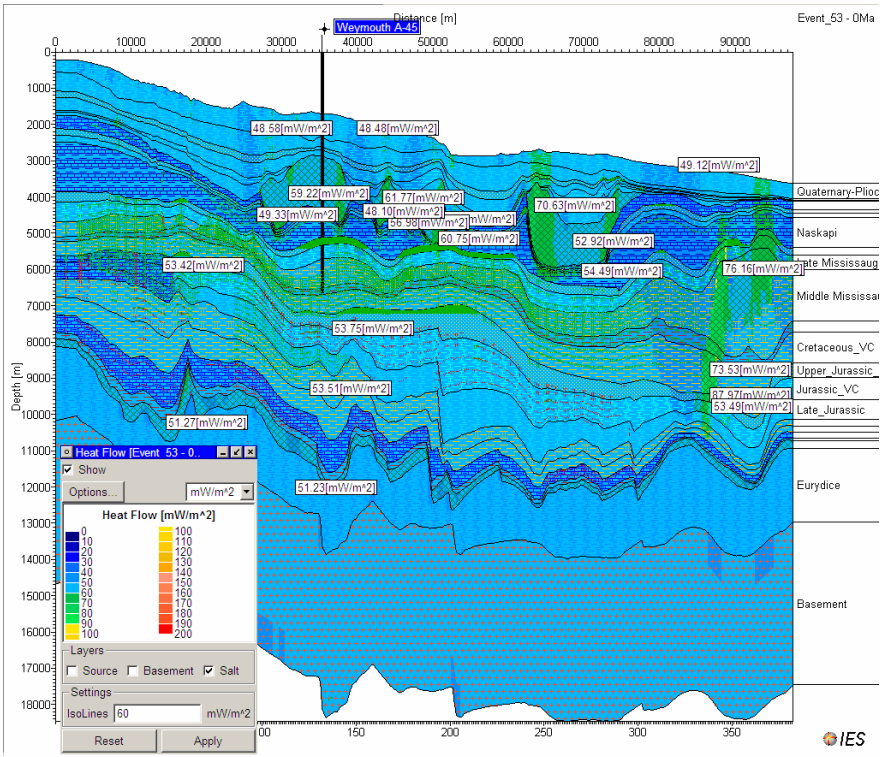

Figure 35d (iv). Line B-B': Output Data – Heat flow data of various sedimentary units at the present time

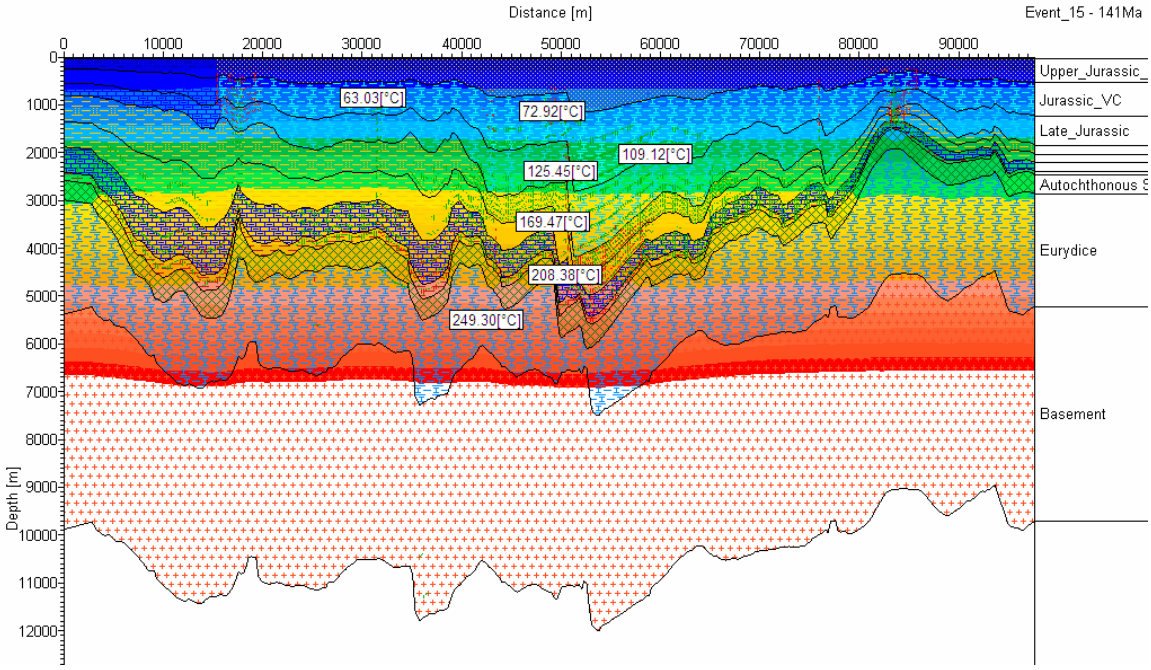

Figure 35e (i). Line B-B' – temperature profile of various sedimentary units at 141 Ma

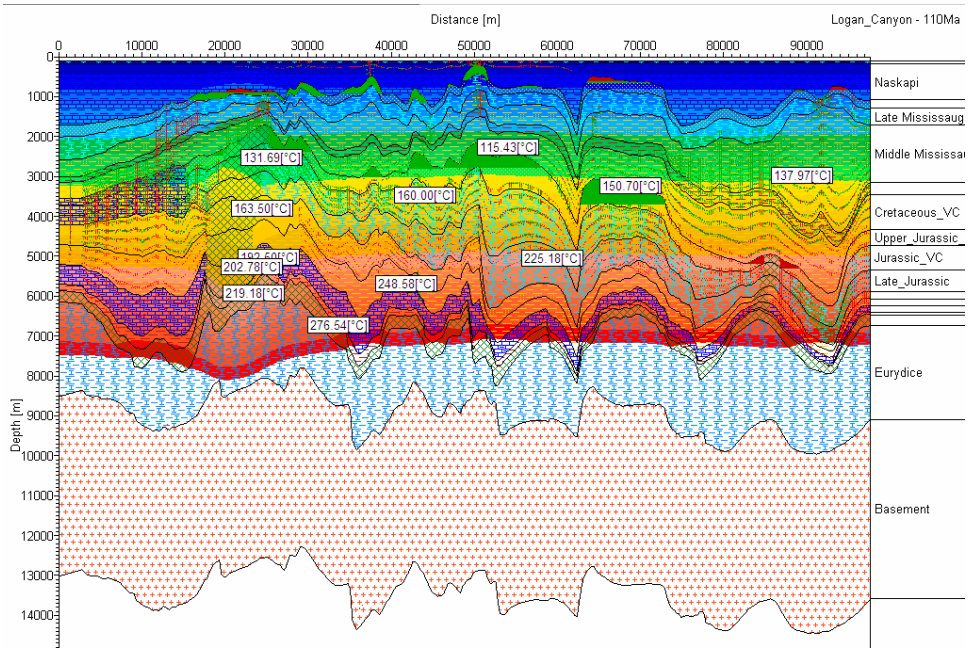

Figure 35e (ii). Line B-B' –Temperature profile of various sedimentary units at 110 Ma.

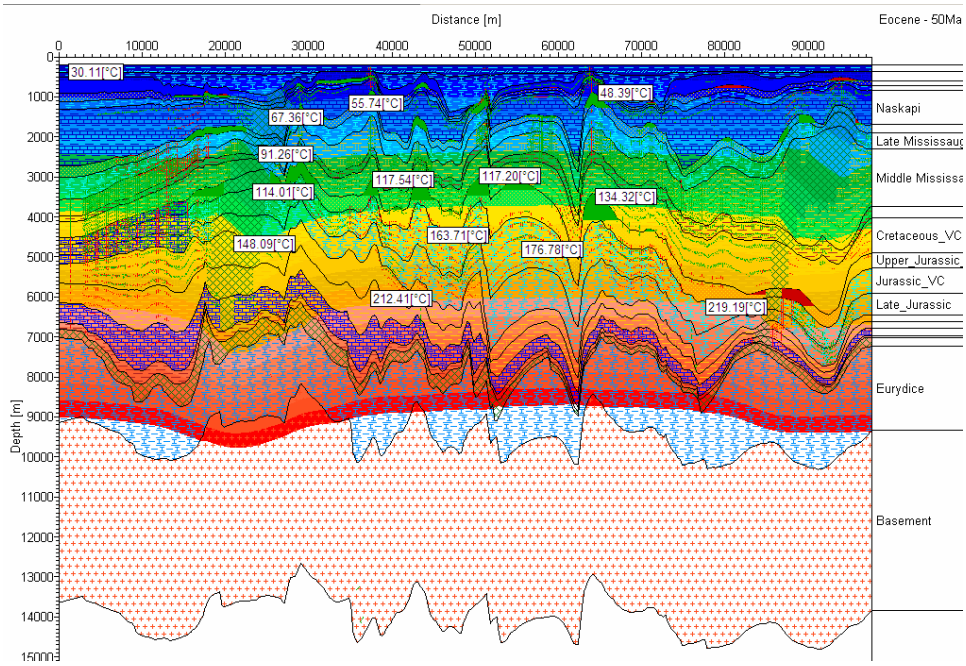

Figure 35e (iii). Line B-B' – Temperature profile of various sedimentary units
at 50 Ma

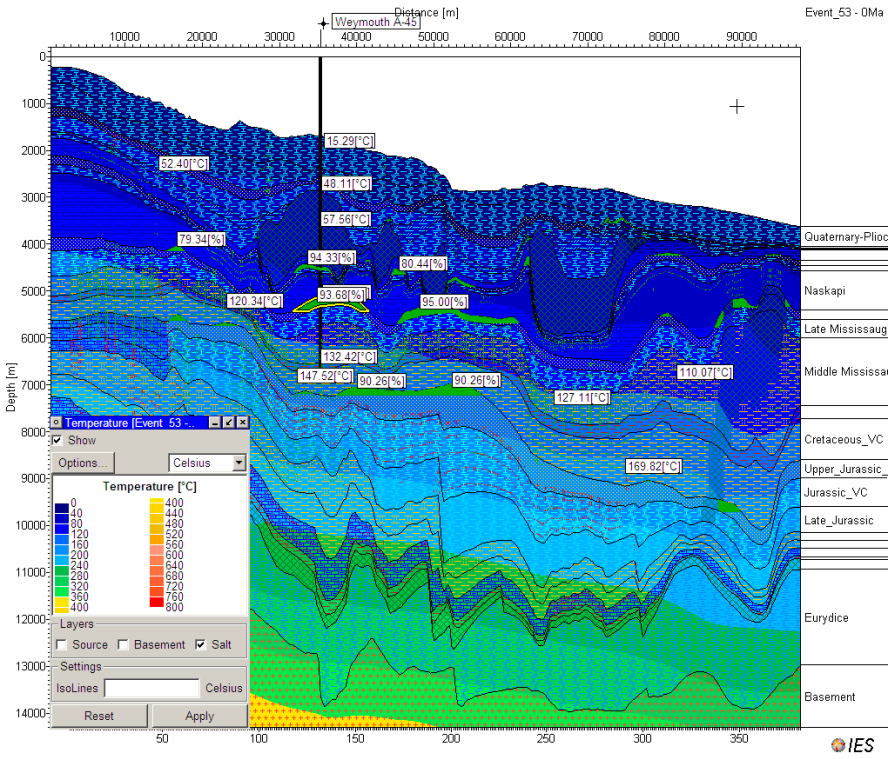

Figure 35e (iv). Line B-B' –Temperature Profile of various sedimentary units at the present time

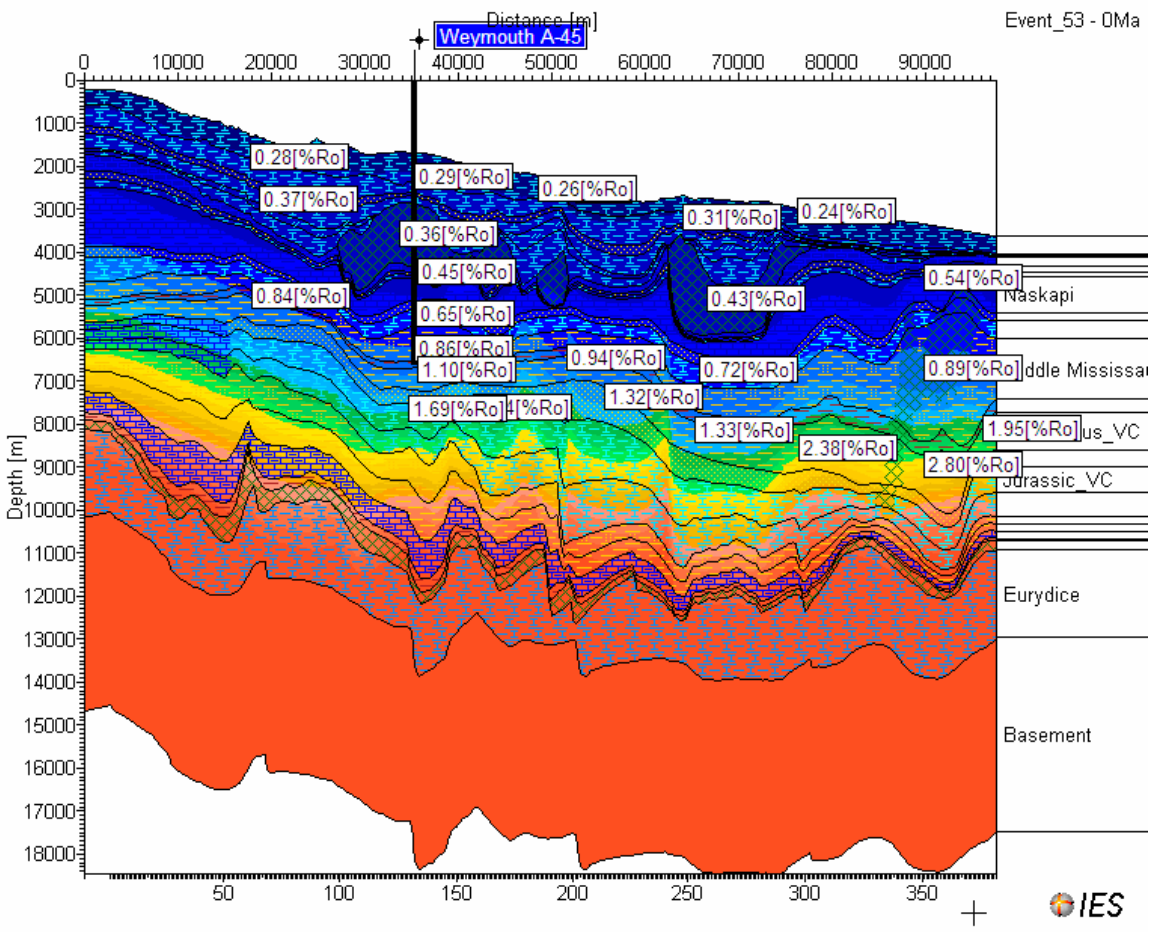

Figure 35f. Line B-B': Output Data – Maturity profile of various sedimentary units at the present time

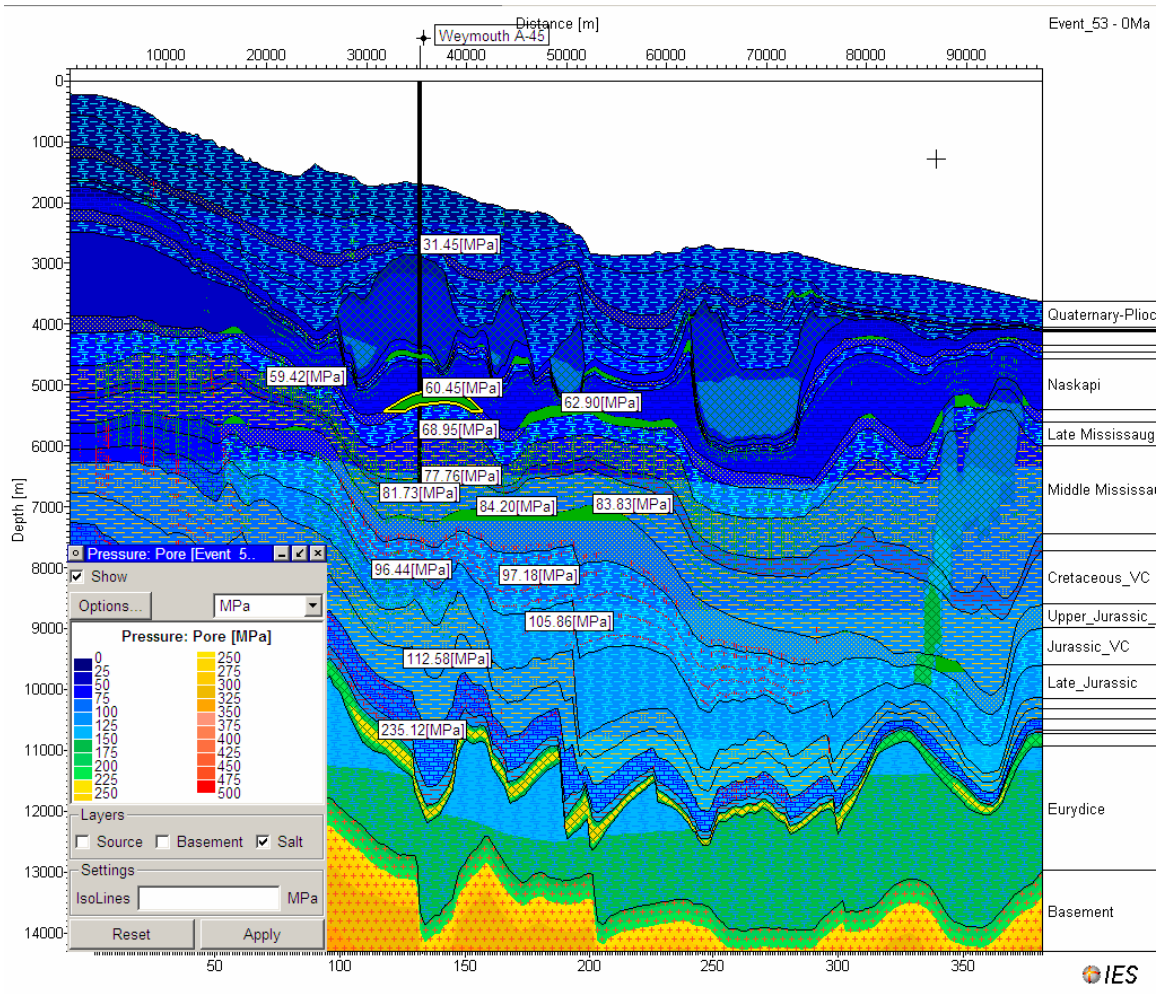

Figure 35g. Pore pressure at the present day

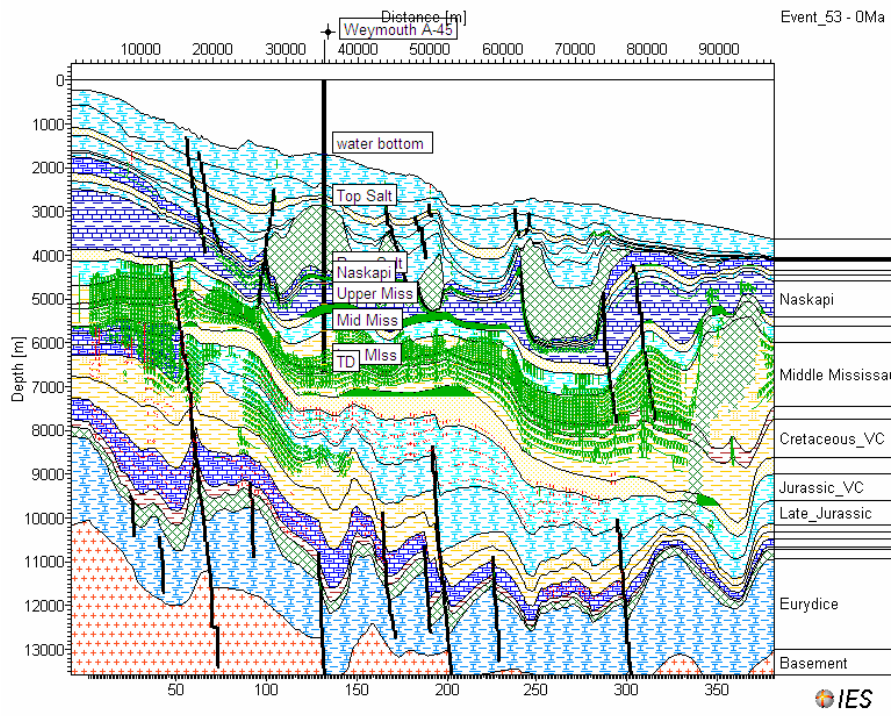

Figure 35h (i). Line B-B': Output data - Present time possible reservoirs with hydrocarbon flow paths. It also shows the projection of the Weymouth A-45 well with picks of various stratigraphic intervals.

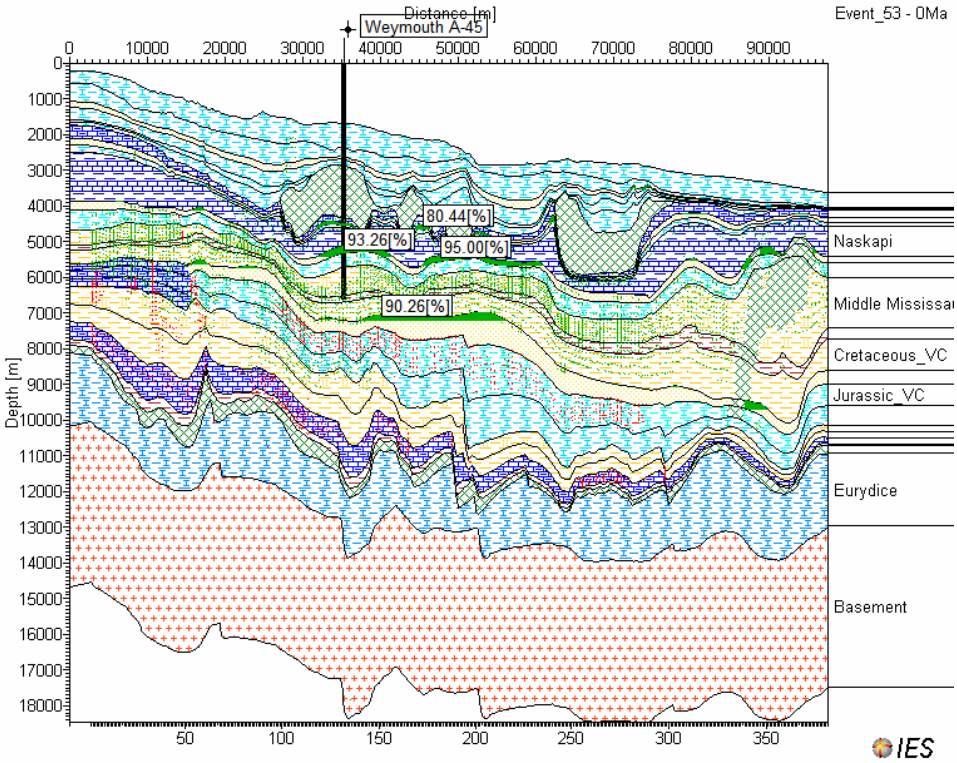

Figure 35h (ii). Line B-B': Output data - Present time possible saturation of reservoirs with hydrocarbon vectors. It also shows the projection of the Weymouth A-45 well.

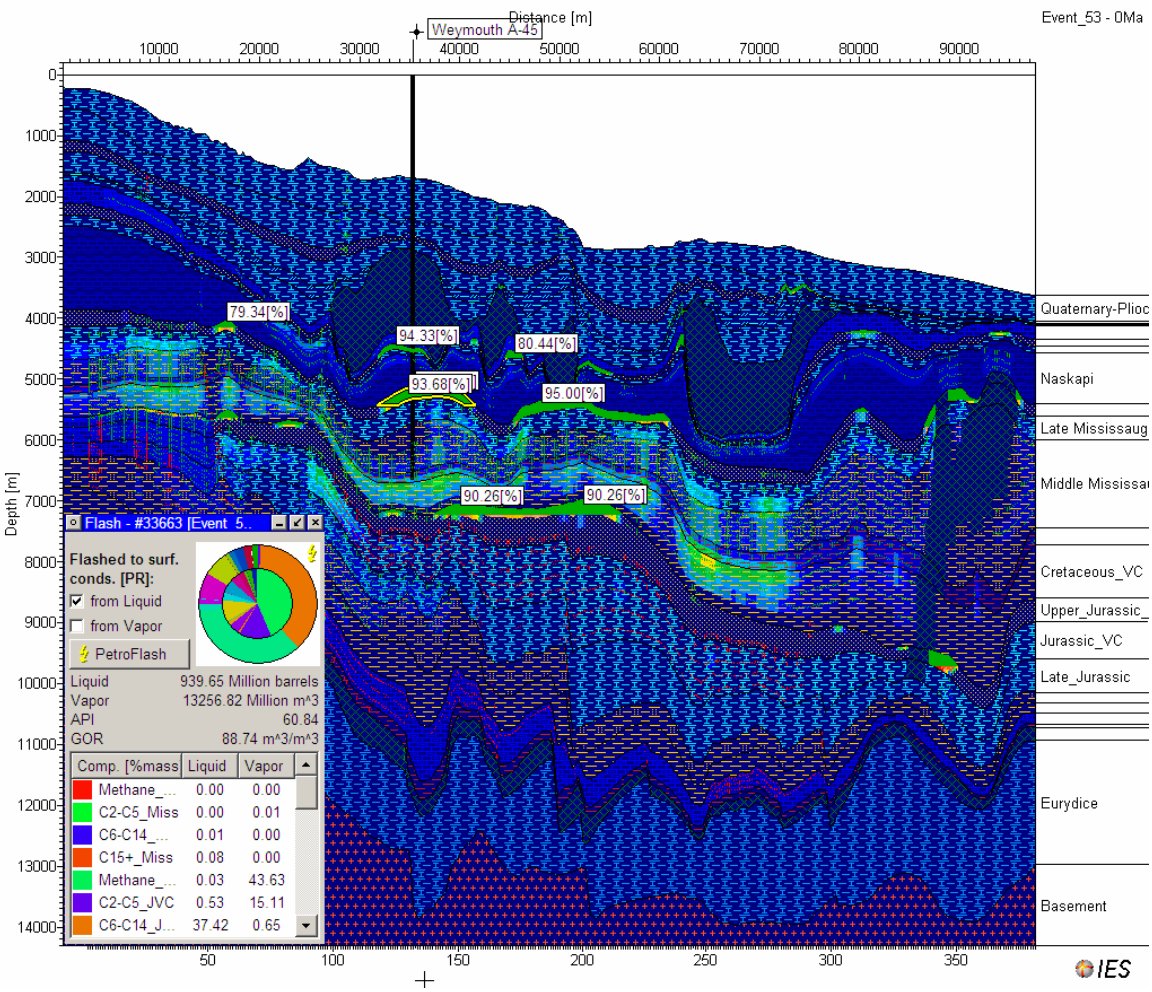

Figure 35i (i). Line B-B': saturation hydrocarbons within various reservoirs and API or GOR of the Sub-salt Middle Missisauga reservoir. Please disregard the volume of hydrocarbons as it is a 2D modeling

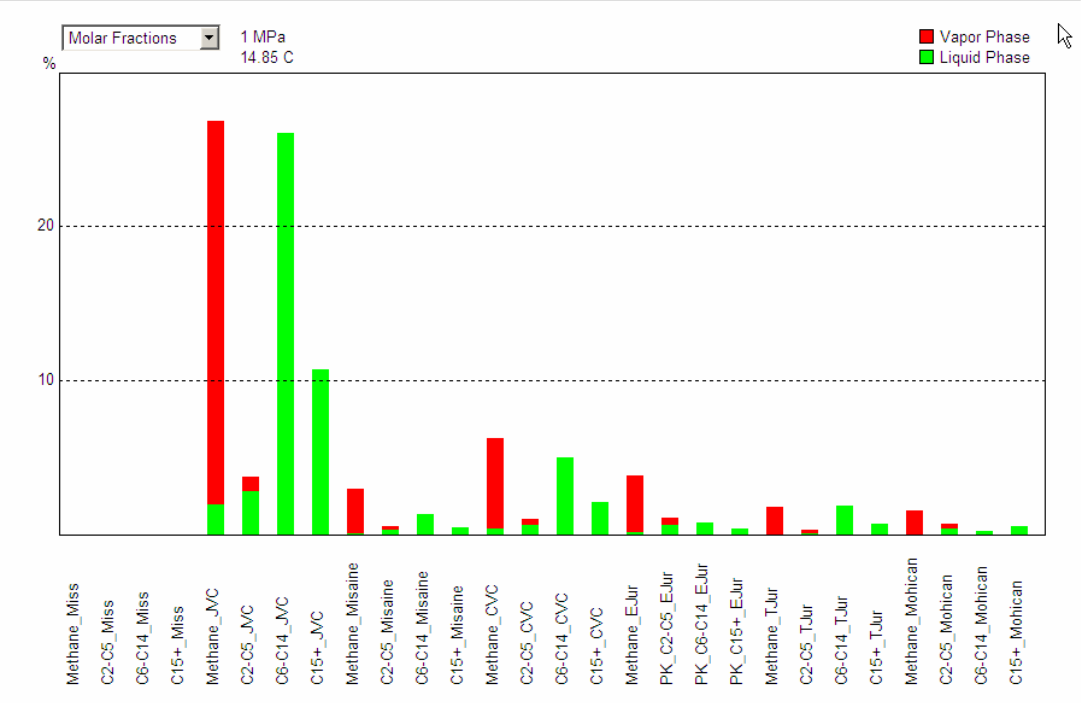

Figure 35i (ii). Hydrocarbon component tracking of the Middle Missisauga Reservoir (in molar fraction), which shows the volume % of various hydrocarbon components from individual source rocks

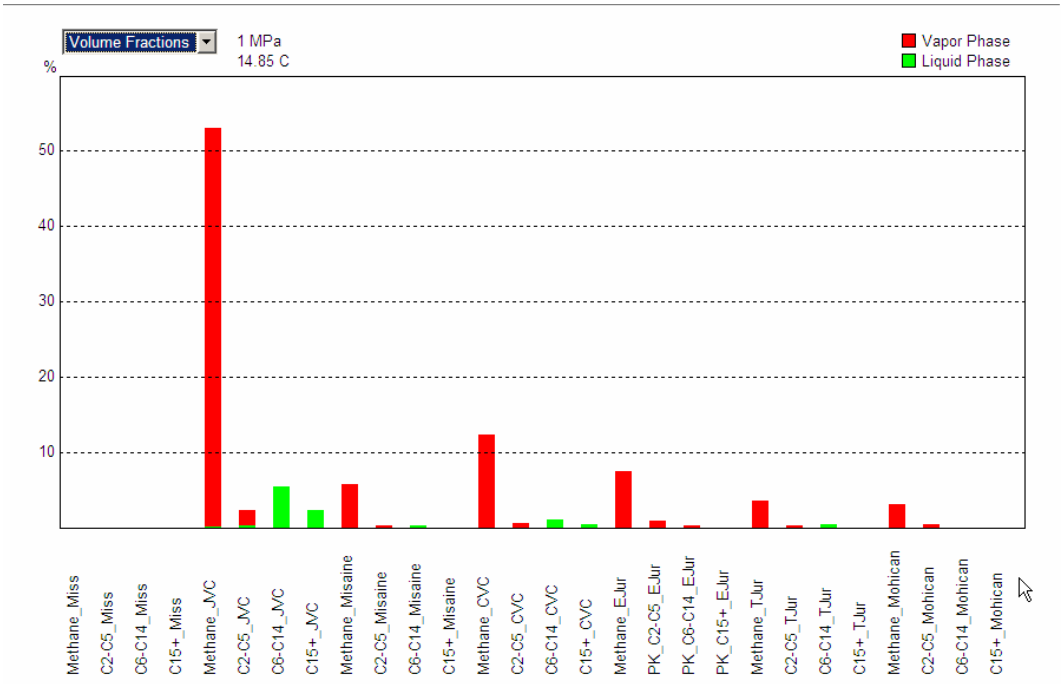

Figure 35i (iii). Line B-B' - Hydrocarbon component tracking of the Middle Missisauga Reservoir (in volume fraction), which shows tracking of volume percentages of various hydrocarbon components from individual source rocks

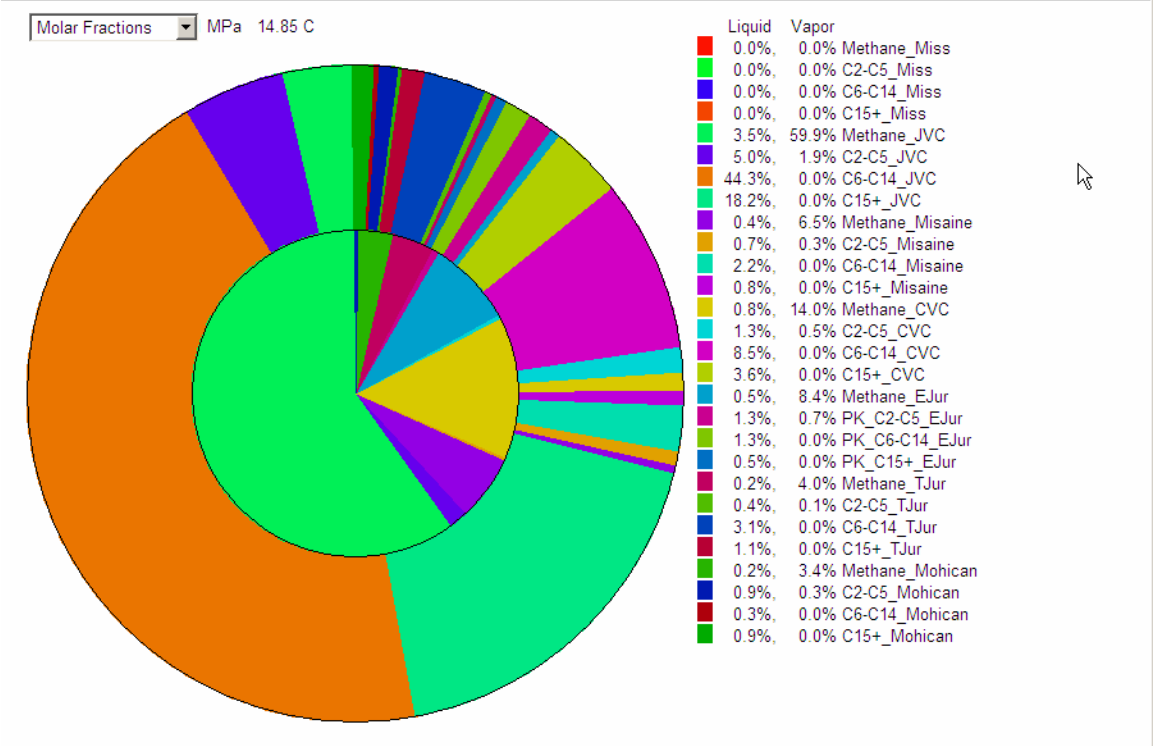

Figure 35i (iv). Line B-B' - Phase Composition of Middle Missisauga Reservoir hydrocarbons

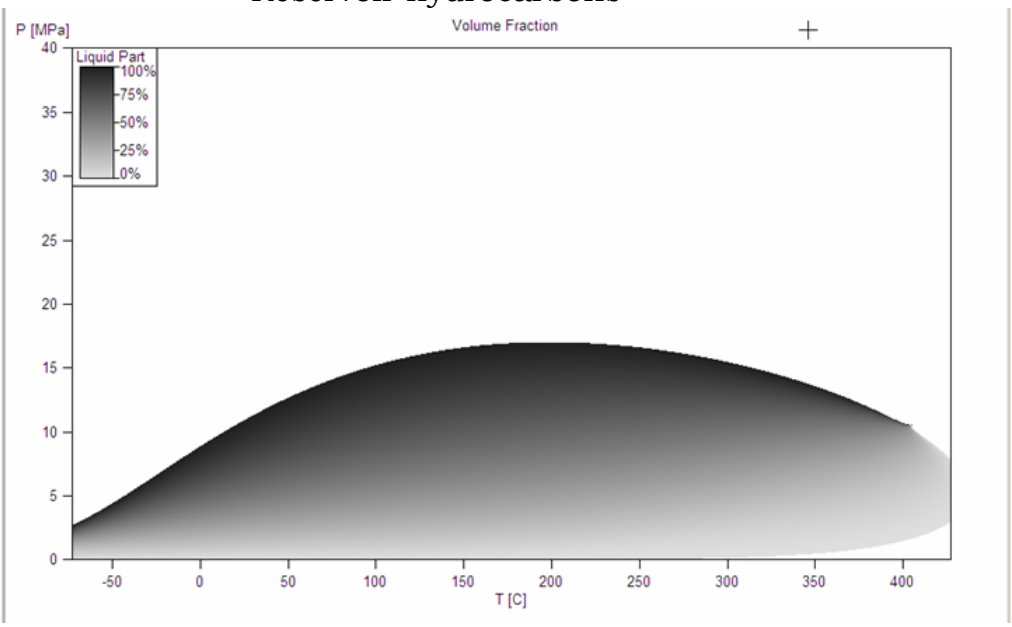

Figure 35i (v). Line B-B' - Bubble Point Curve of Middle Missisauga reservoir

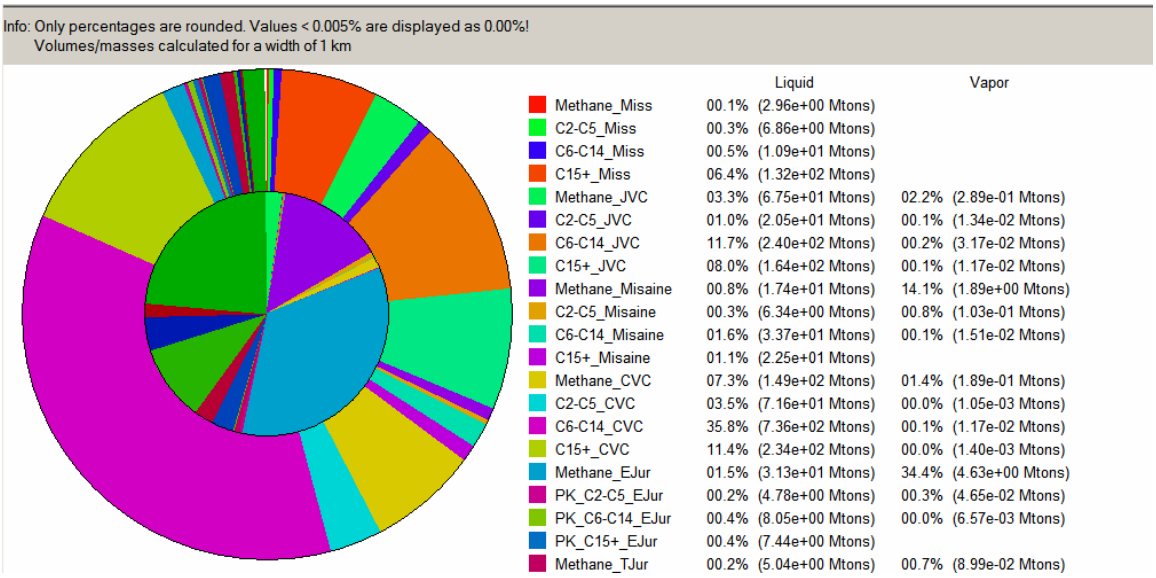

Figure 35j. Line B-B' - Cummulative masses of multi-component hydrocarbons expelled from various source rocks (masses calculated for a kilometer radius area)

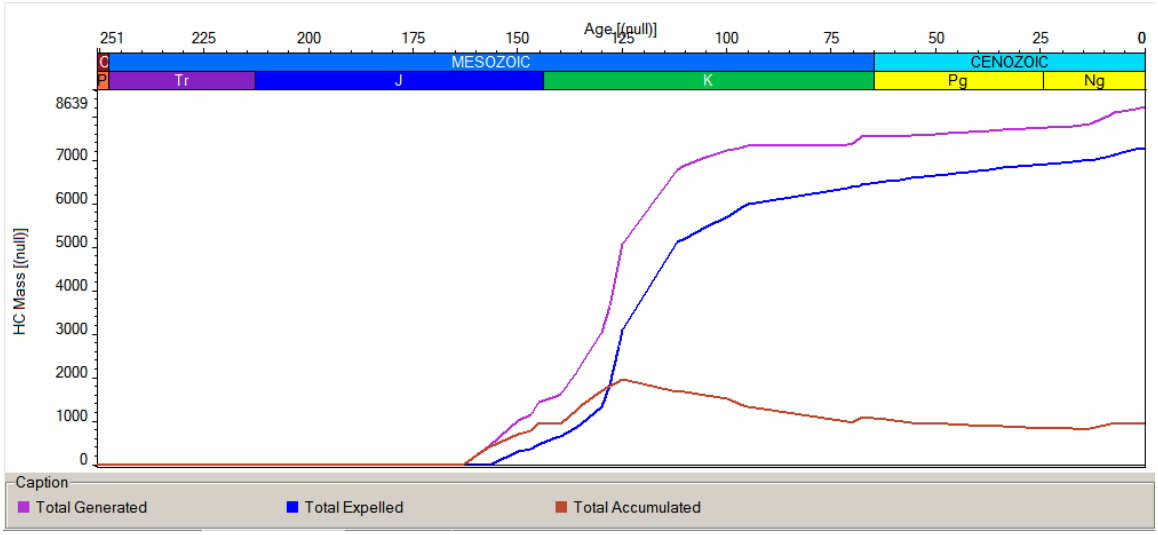

Figure 35k. Line B-B' - Timing of total generated, total expelled, and total accumulated cummulative hydrocarbon mass from various source rocks (masses calculated for a width of 1 km)

Seismic Line A-A’

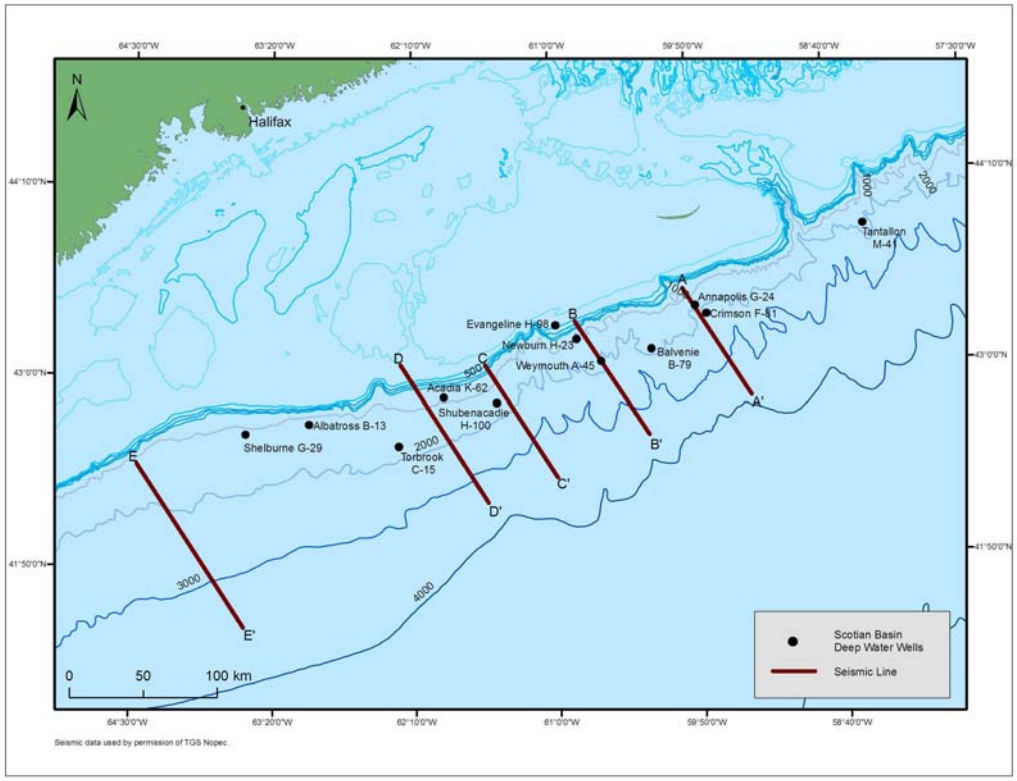

36a. Location map of seismic line A-A’

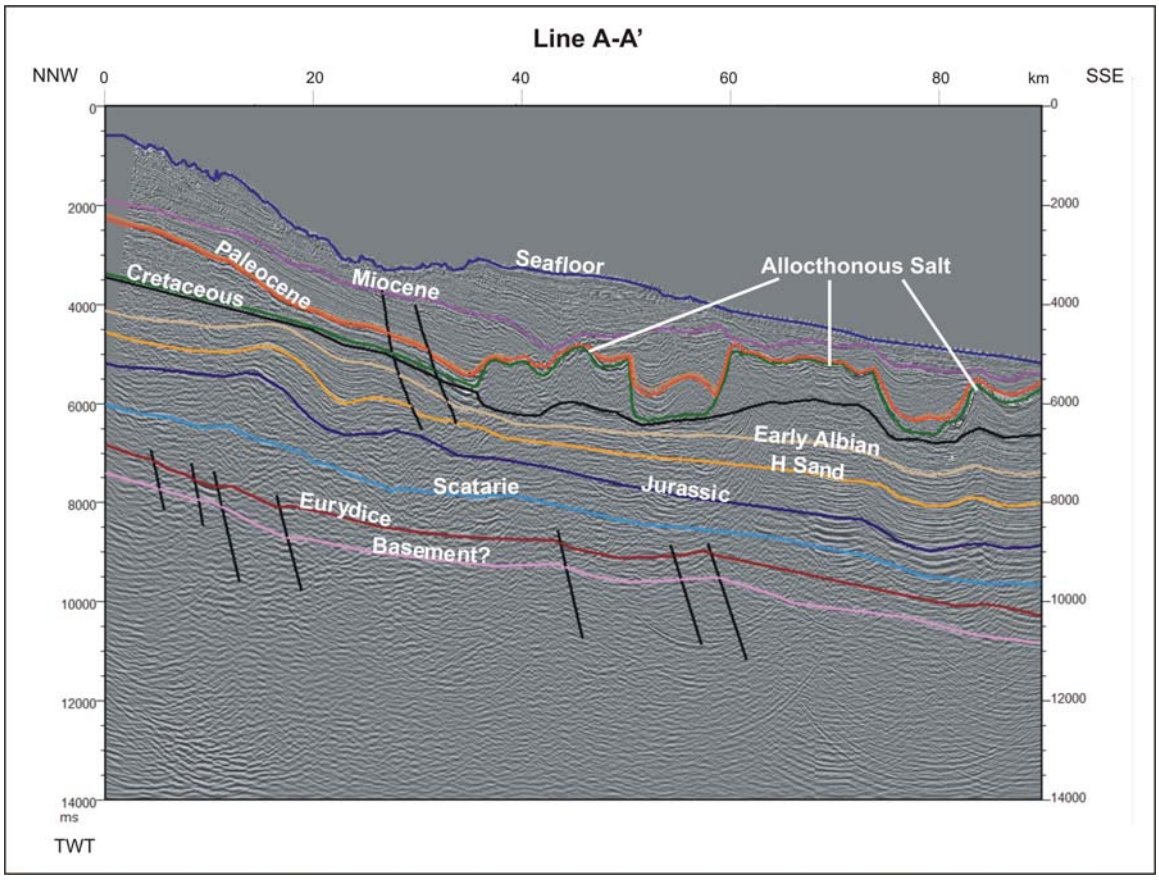

36b. Seismic line A-A' (Sable Subbasin) with selected formation boundaries, faults, and both allochthonous salt bodies (depth in ms)

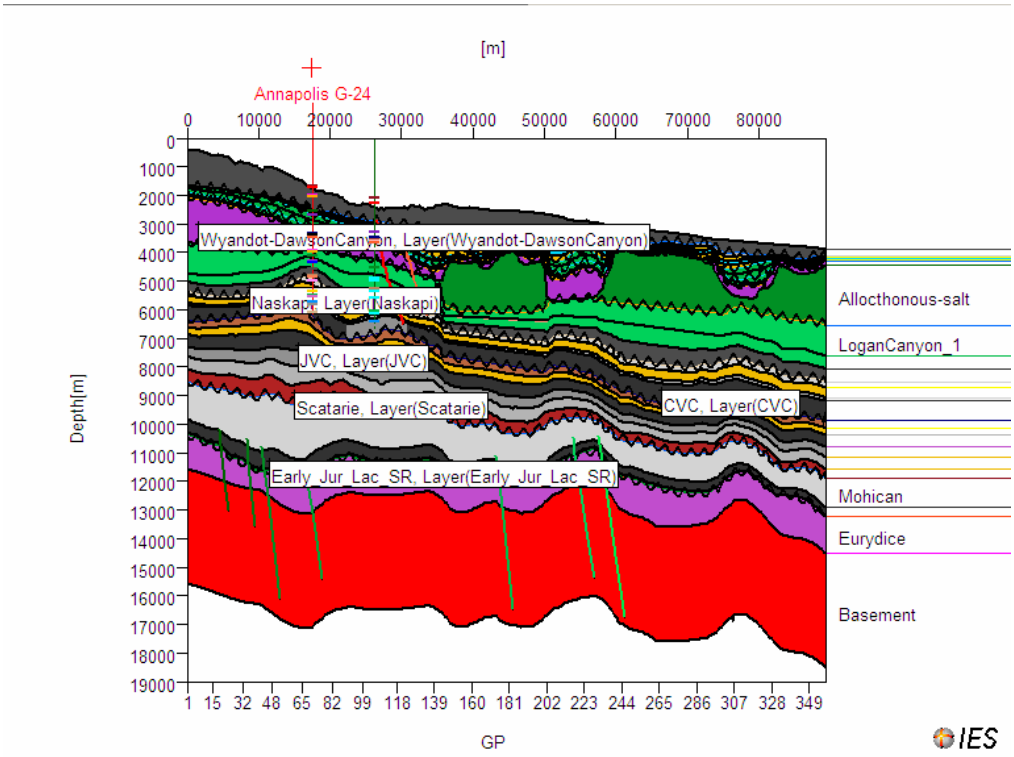

Figure 36c (i). Line A-A' with horizons, unconformities, and faults as seen within PetroBuilder input parameters

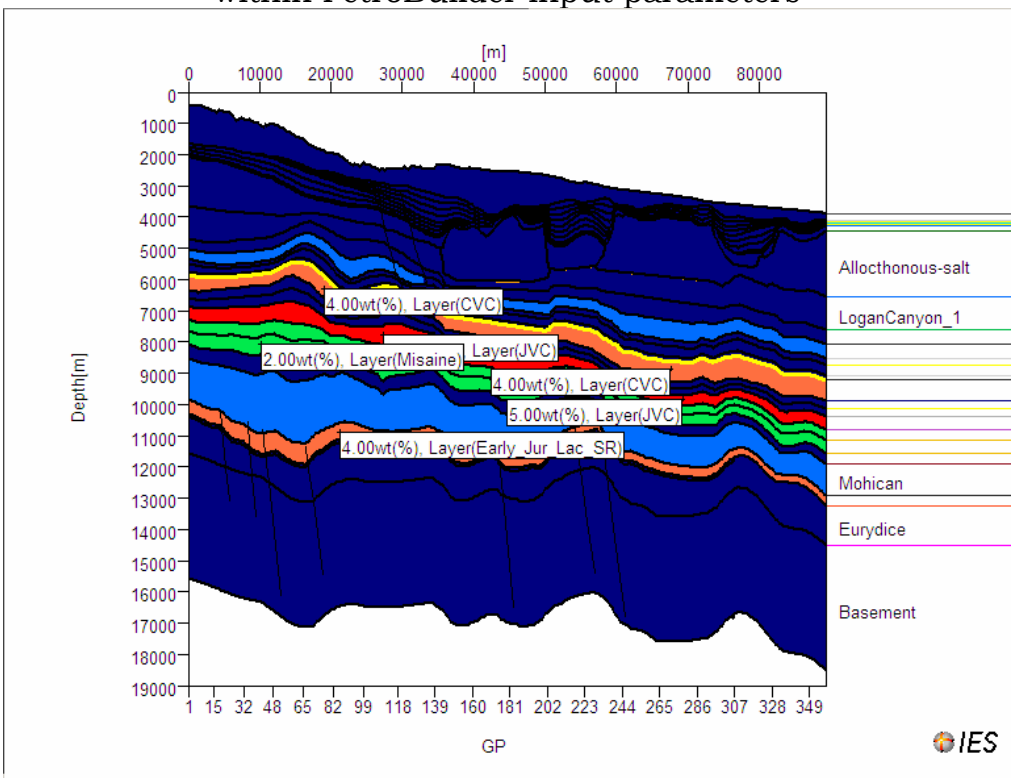

Figure 36c (ii). Line A-A' – PetroBuilder Input with source rock properties (TOC)

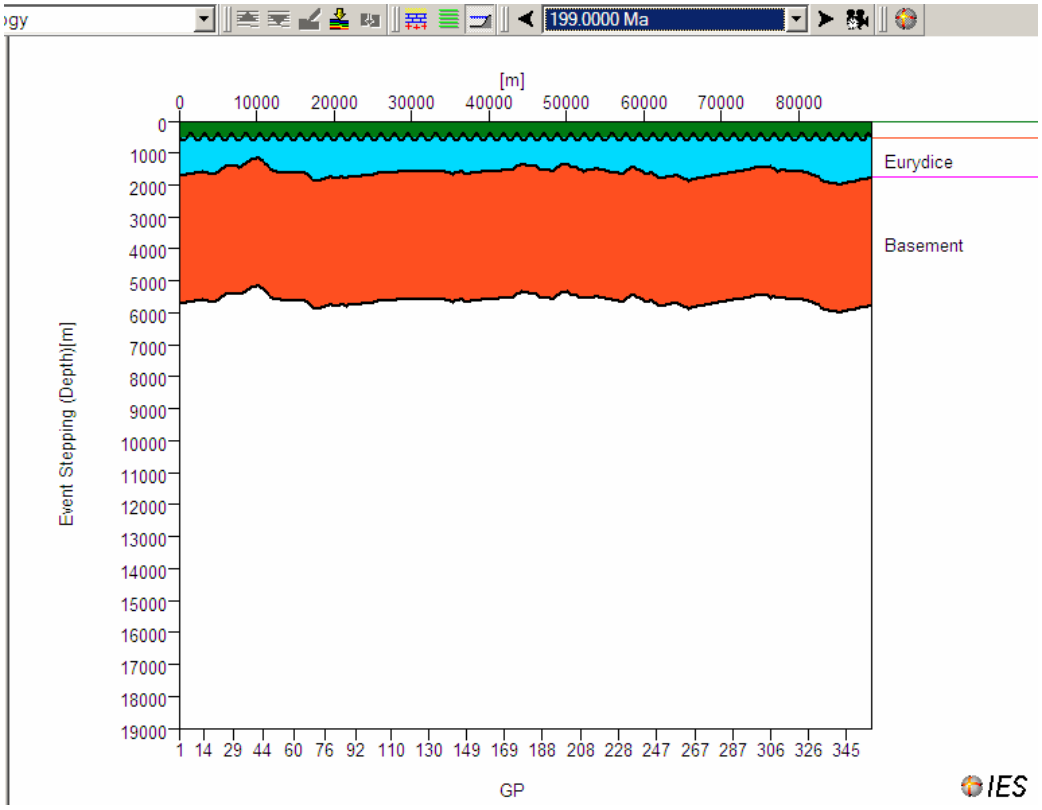

Figure 36d (i). Conceptual movement of the Early Jurassic Argo Salt using Event Stepping method within PetroBuilder (at199 Ma).

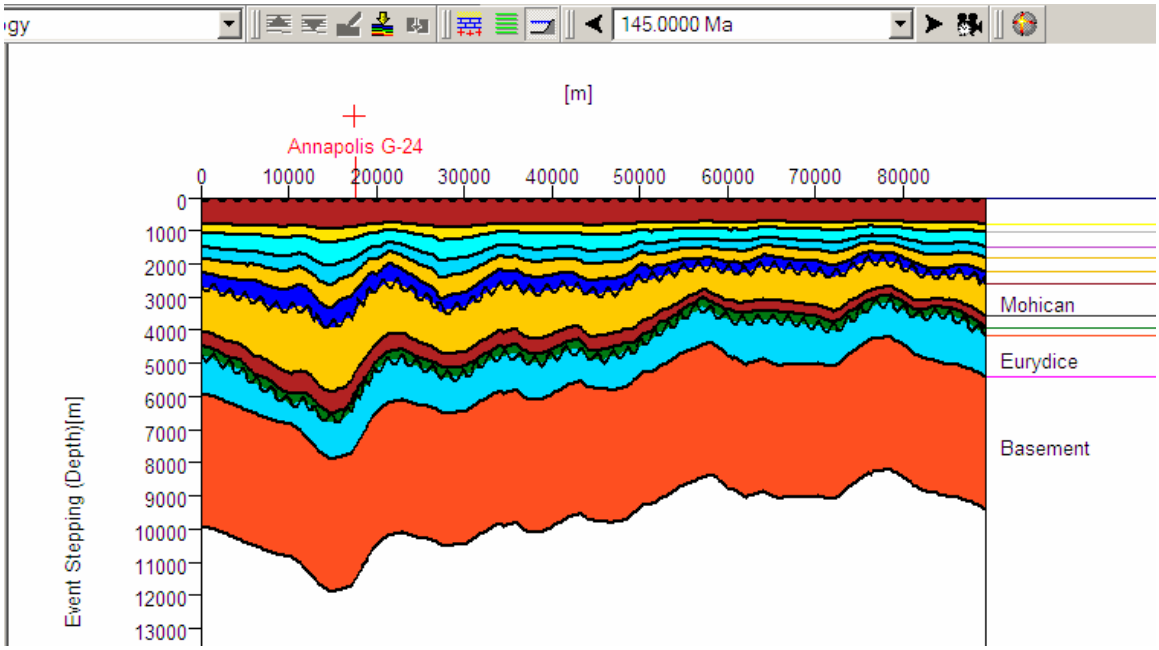

Figure 36d (ii). Conceptual buildup of Argo Salt using Event Stepping method within PetroBuilder (at145 Ma)

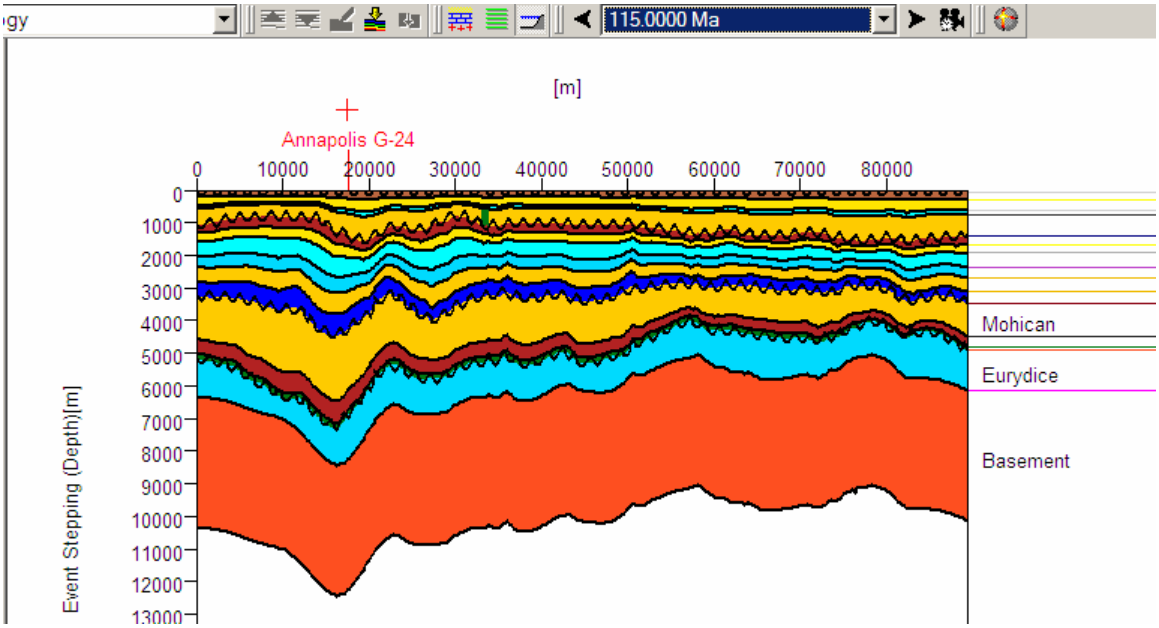

Figure 36d (iii). Conceptual buildup of Argo Salt using Event Stepping method within PetroBuilder (at 115 Ma).

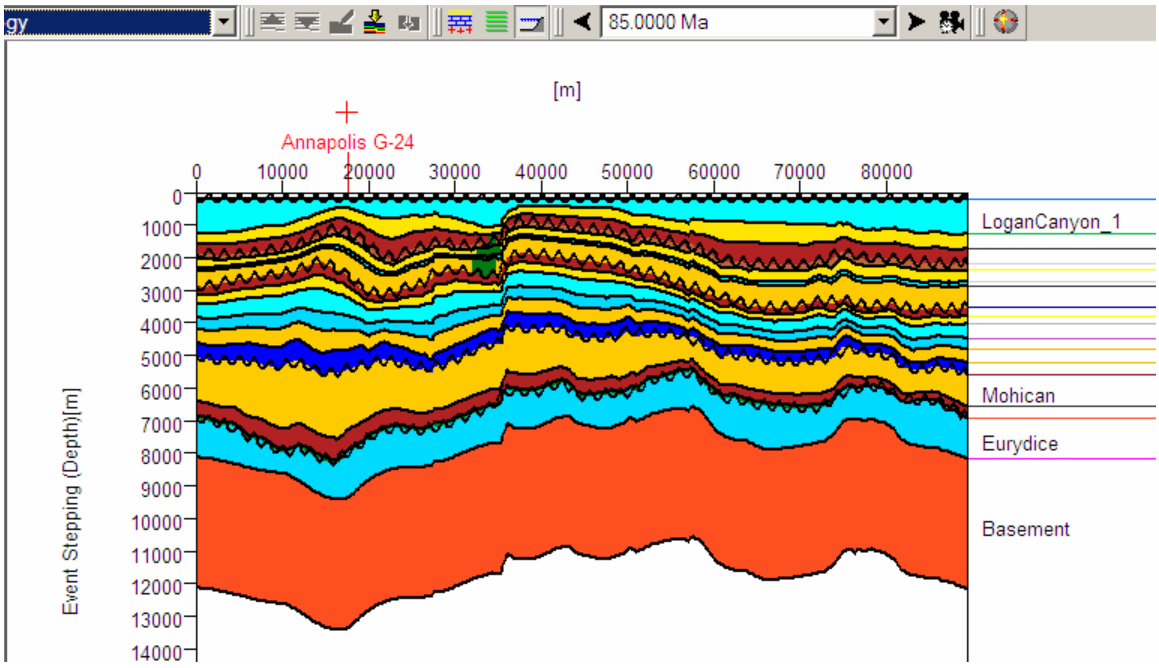

Figure 36d (iv). Conceptual buildup of Argo Salt using Event Stepping method within PetroBuilder (at 85 Ma).

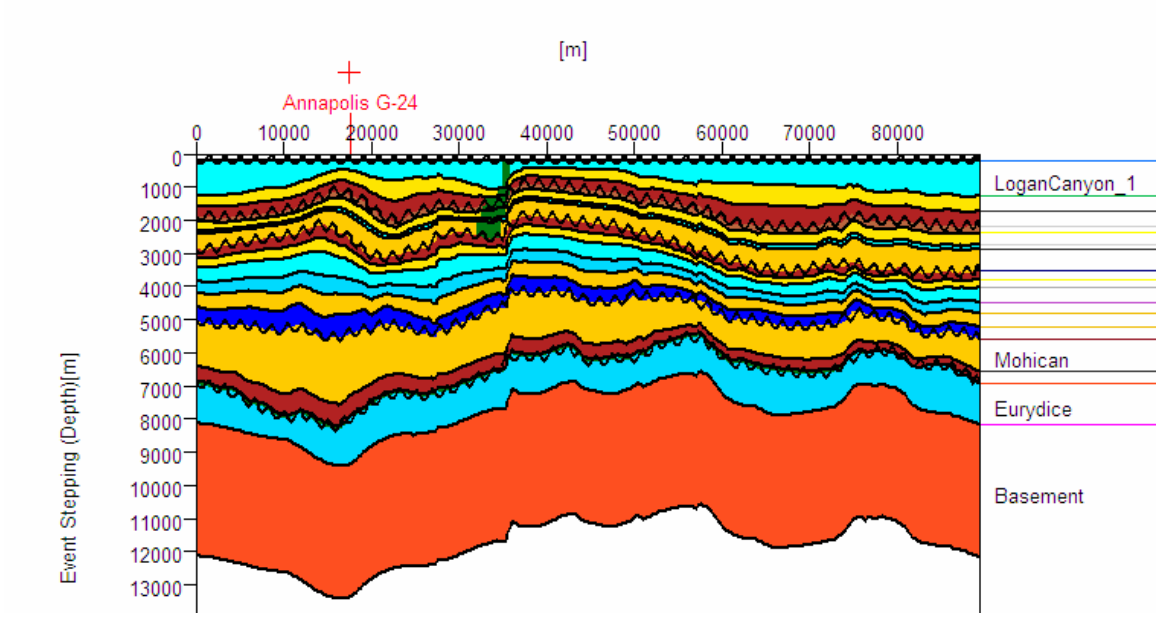

Figure 36d (v). Conceptual buildup of Argo Salt using Event Stepping method within PetroBuilder (at 75Ma).

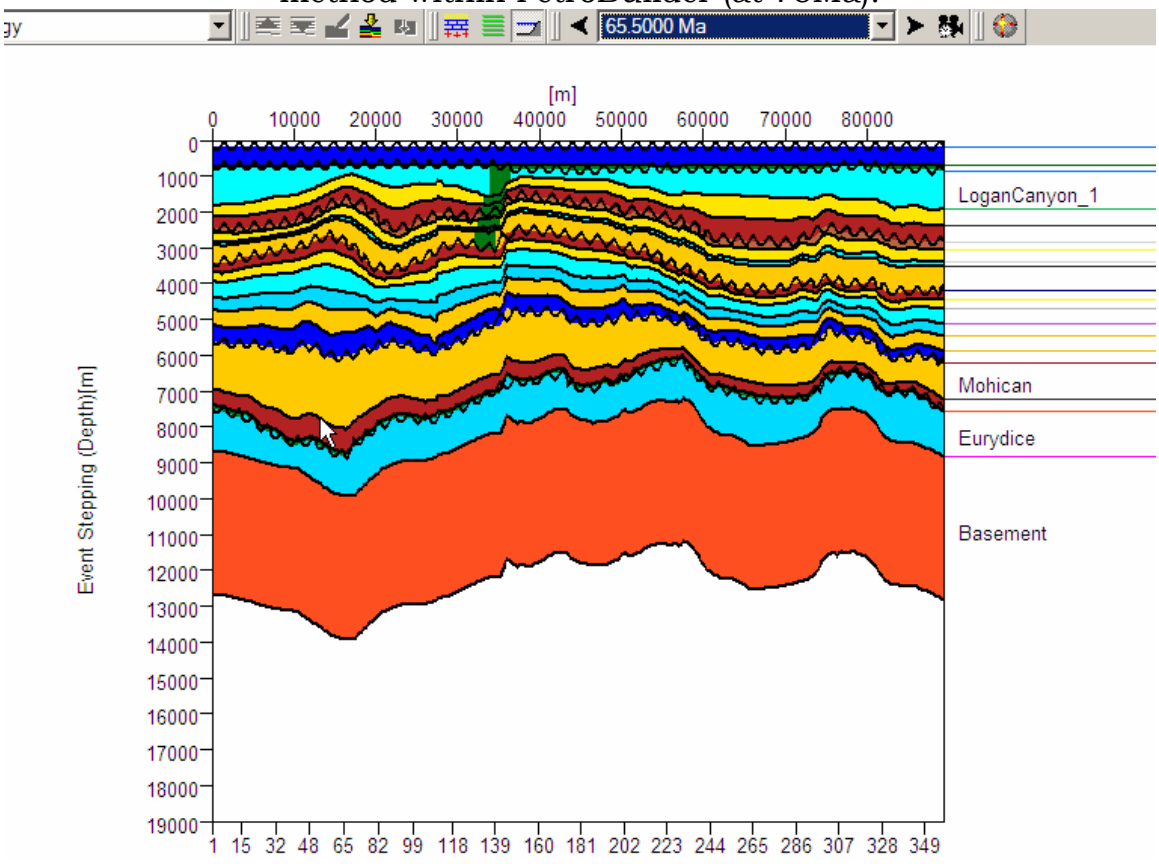

Figure 36d (vi). Conceptual buildup of Argo Salt using Event Stepping method within PetroBuilder (at 65 Ma).

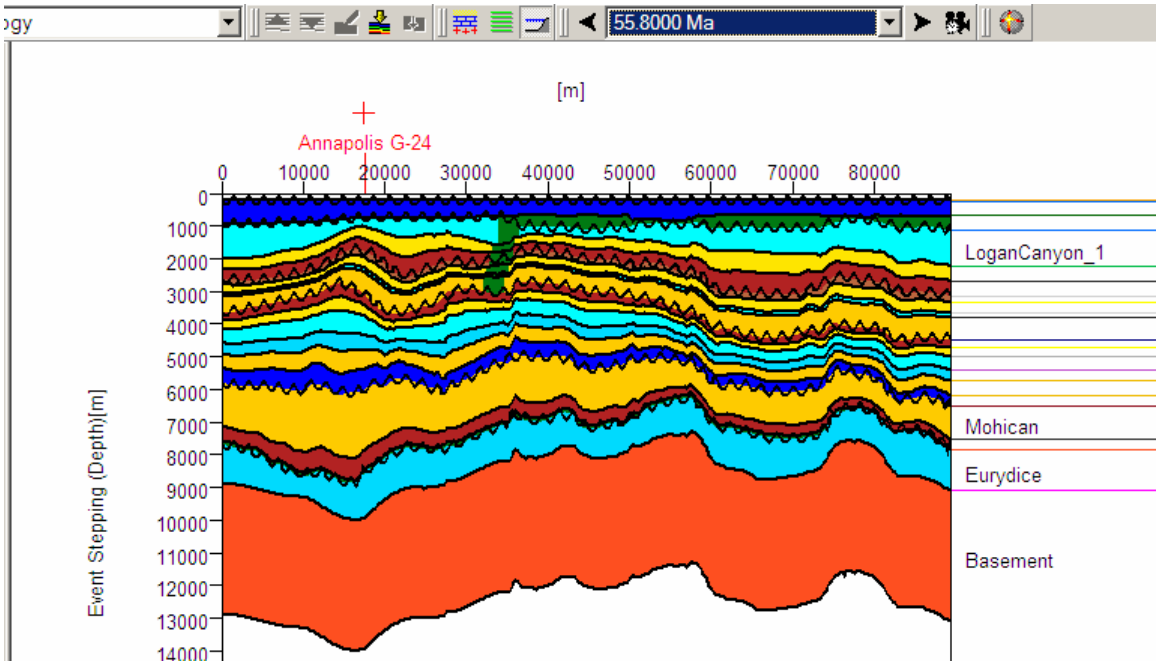

Figure 36d (vii). Conceptual buildup of Argo Salt using Event Stepping method within PetroBuilder (at 55.8 Ma).

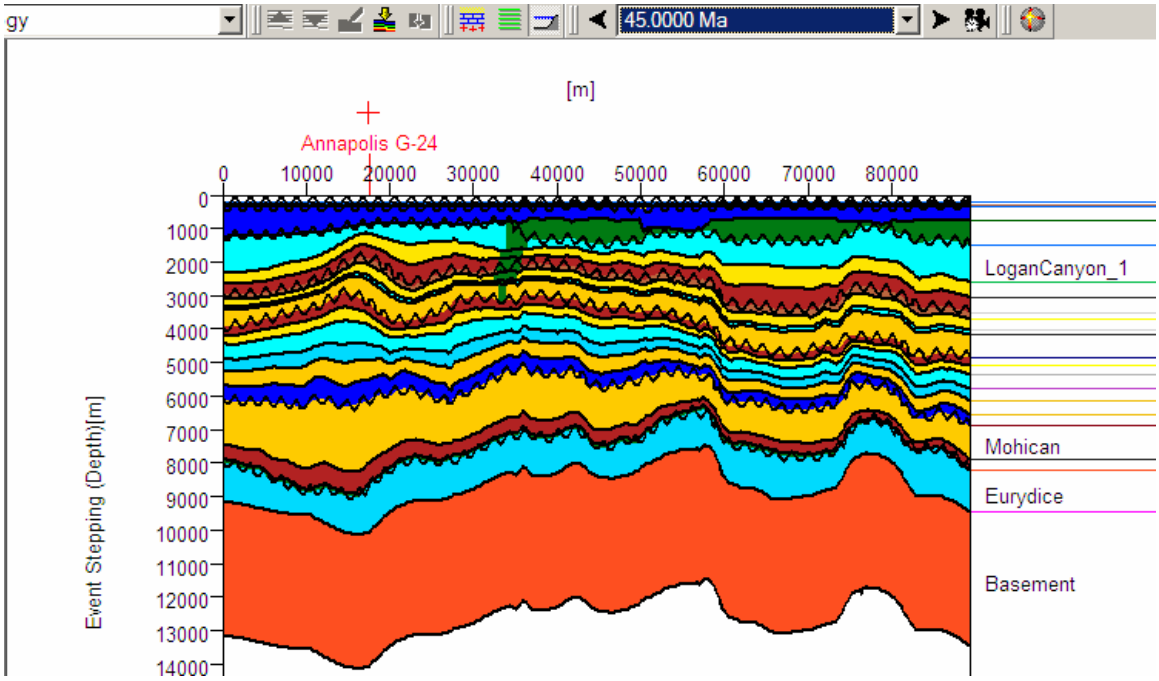

Figure 36d (viii). Conceptual buildup of Argo Salt using Event Stepping method within PetroBuilder (at 45 Ma).

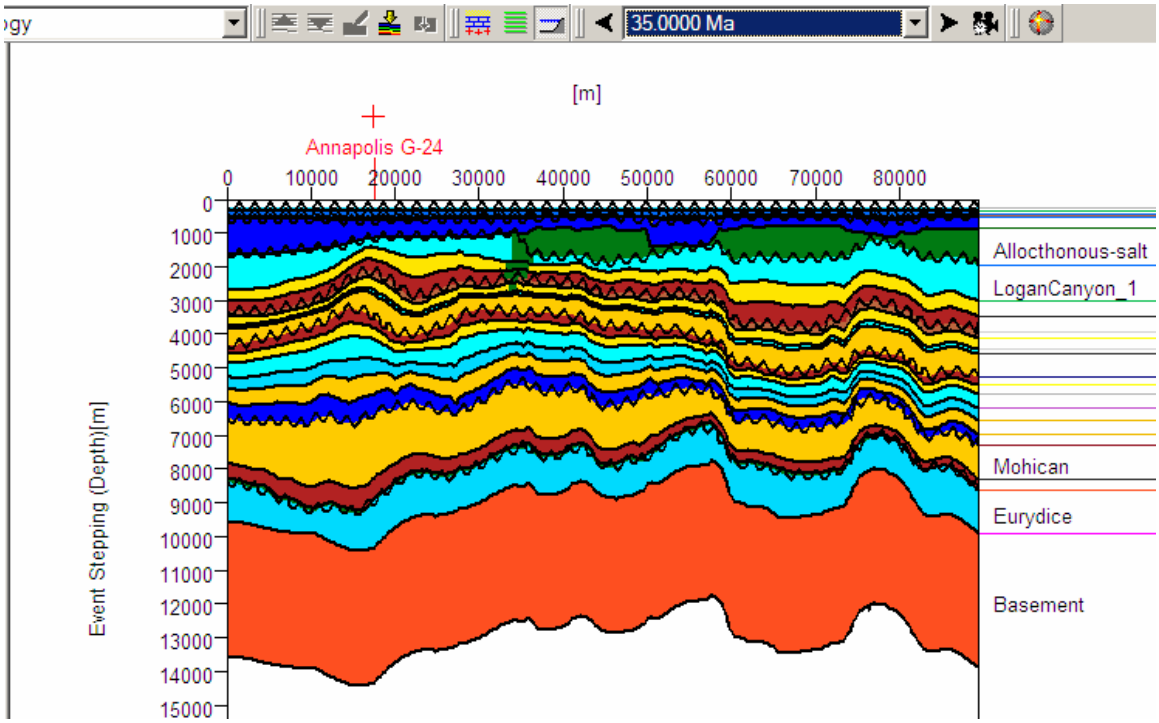

Figure 36d (ix). Conceptual buildup of Argo Salt using Event Stepping method within PetroBuilder (at 35 Ma).

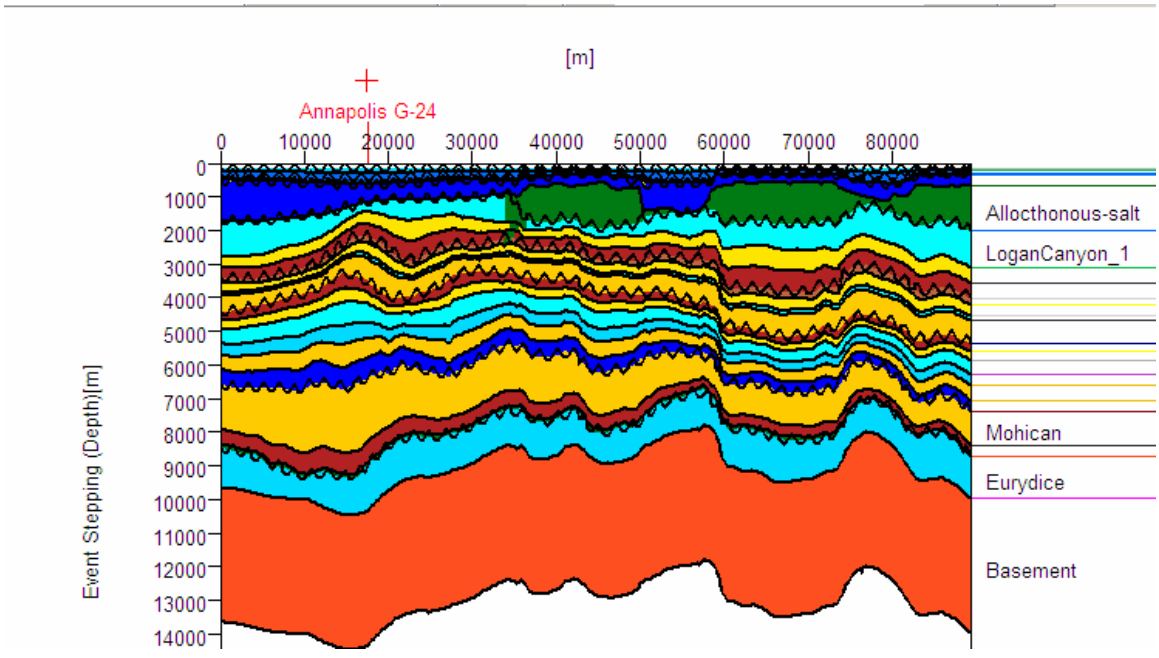

Figure 36d (x). Conceptual buildup of Argo Salt using Event Stepping method within PetroBuilder (at 25 Ma).

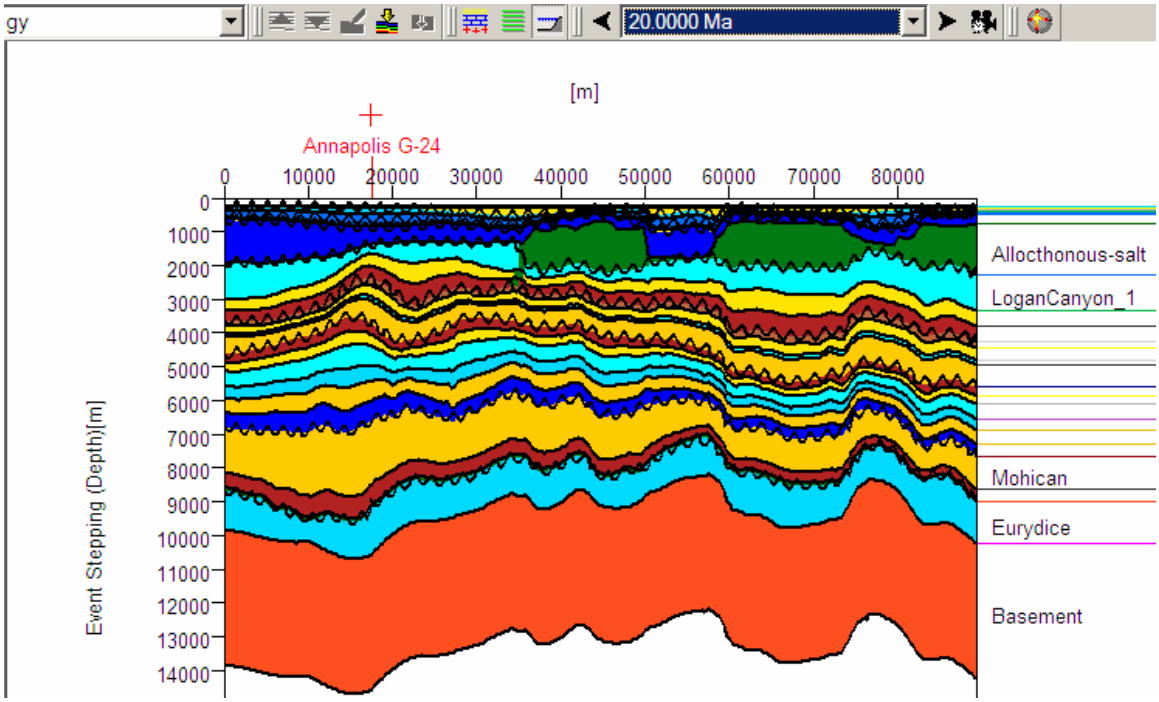

Figure 36d (xi). Conceptual buildup of Argo Salt using Event Stepping method within PetroBuilder (at 20 Ma).

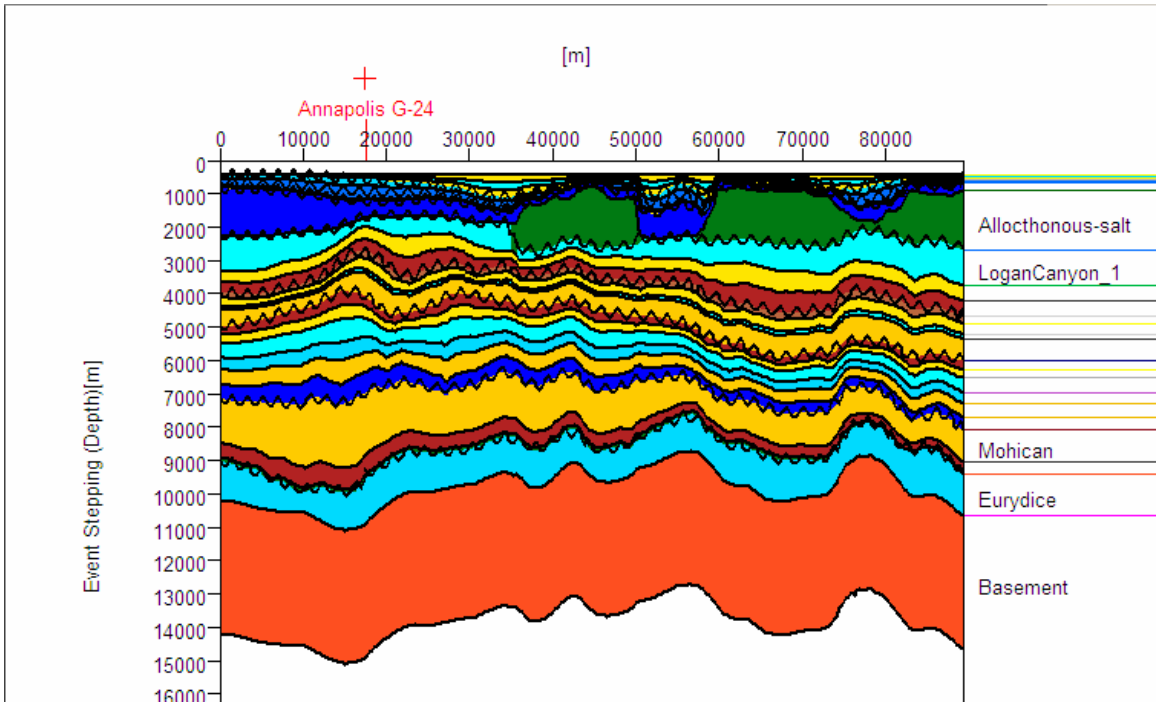

Figure 36d (xii). Conceptual buildup of Argo Salt using Event Stepping method within PetroBuilder (at 10 Ma).

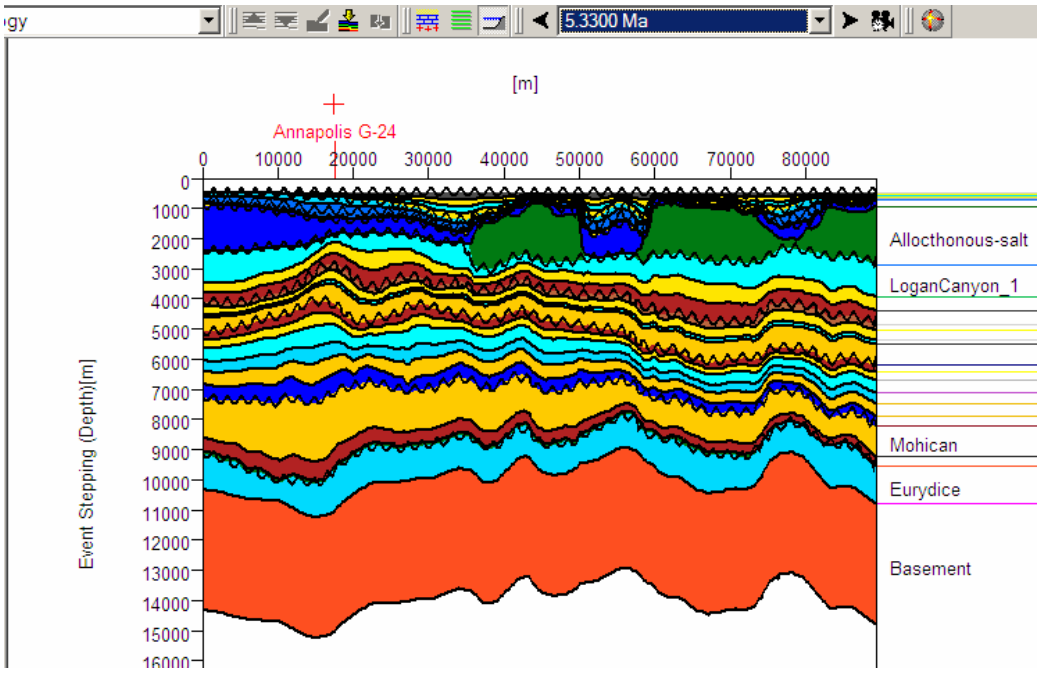

Figure 36d (xiii). Conceptual buildup of Argo Salt using Event Stepping method within PetroBuilder at 5.33 Ma

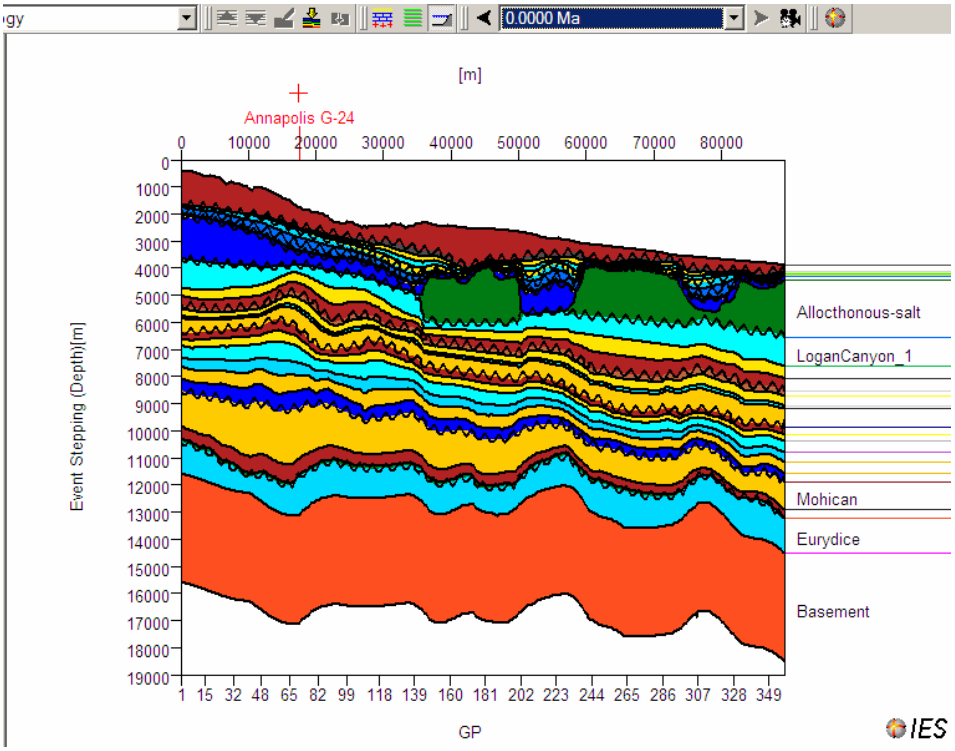

Figure 36d (xiv). Conceptual buildup of Argo Salt using Event Stepping method within PetroBuilder (at the Present day)

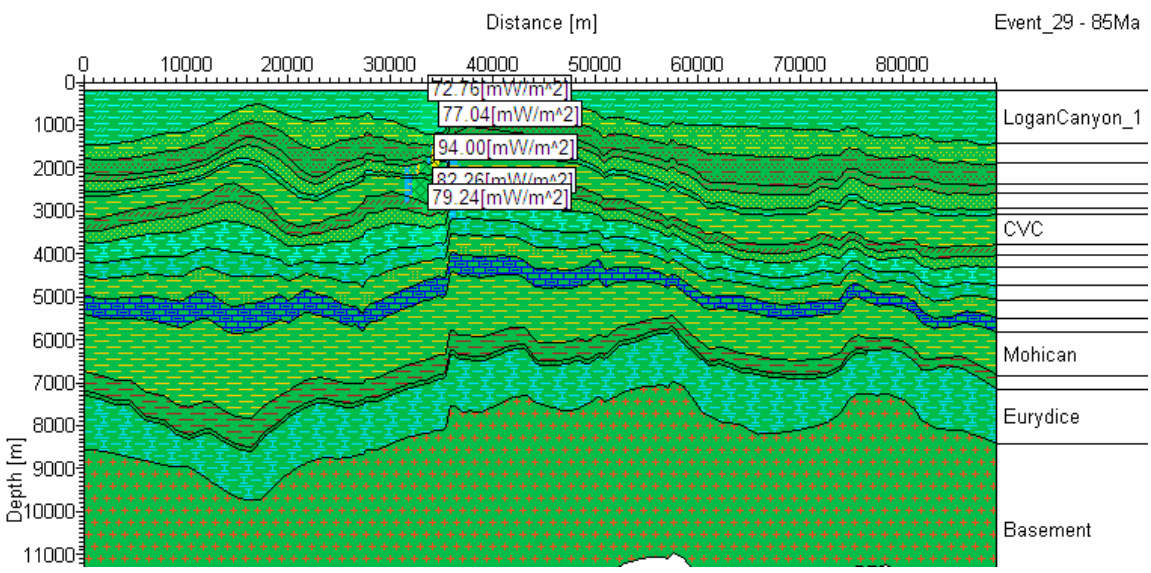

Figure 36e (i). Line A-A' - Heat flow profile at 85 Ma

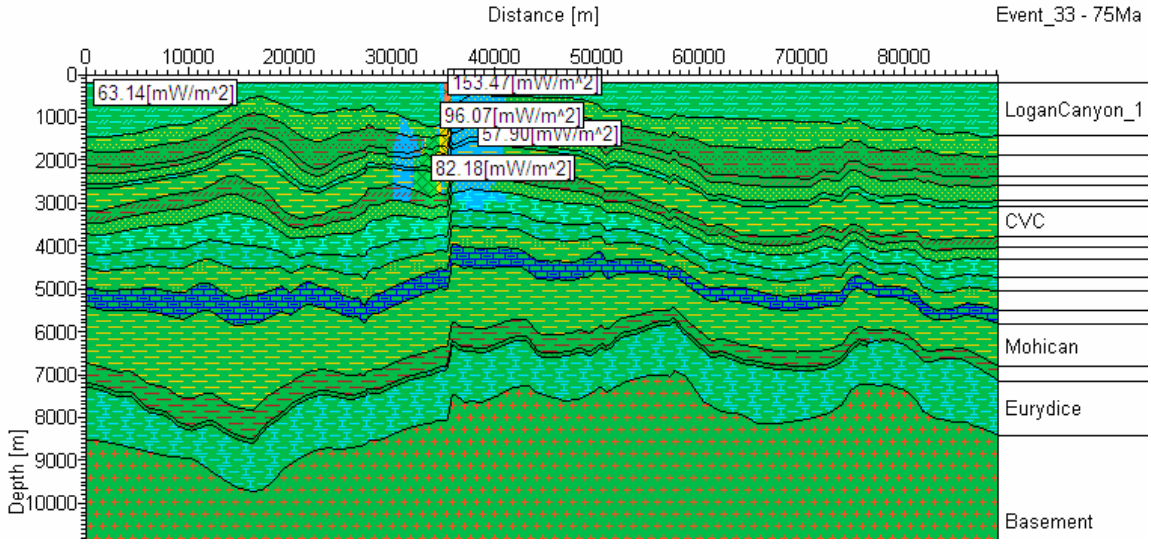

Figure 36e (ii). Line A-A' - Heat flow profile at 75 Ma

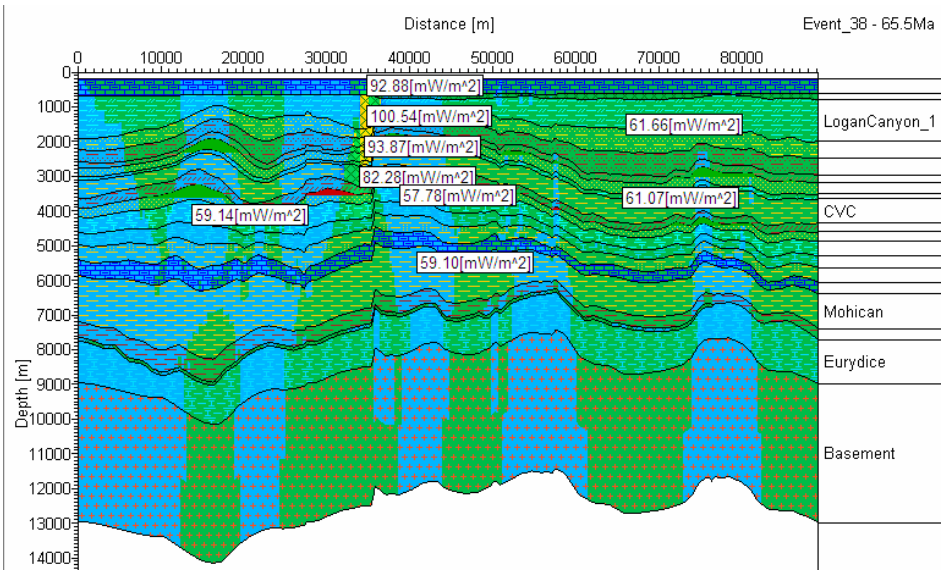

Figure 36e (iii). Line A-A' - Heat flow profile at 65 Ma.

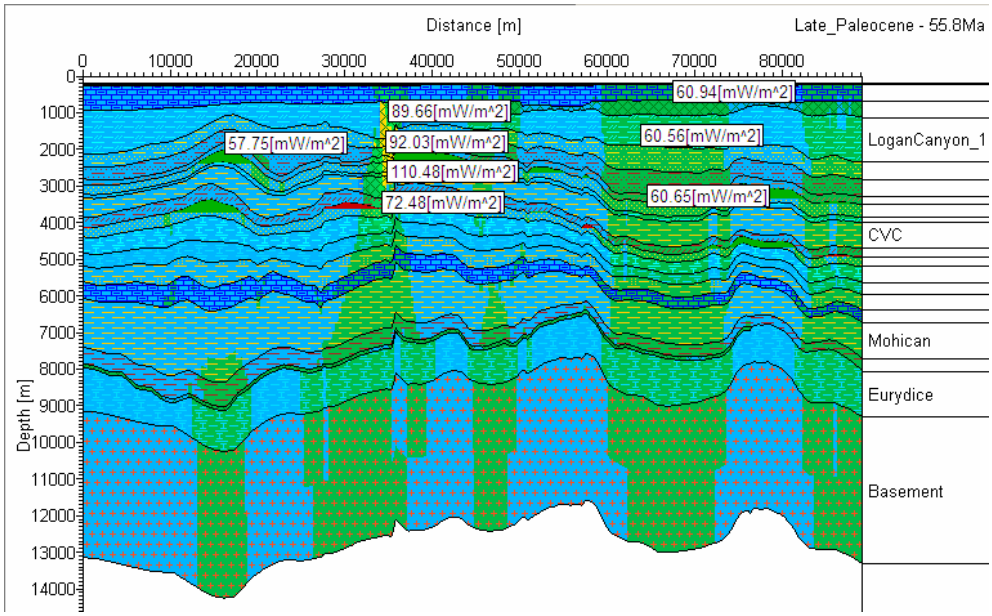

Figure 36e (iv). Line A-A' - Heat flow profile at 55 Ma

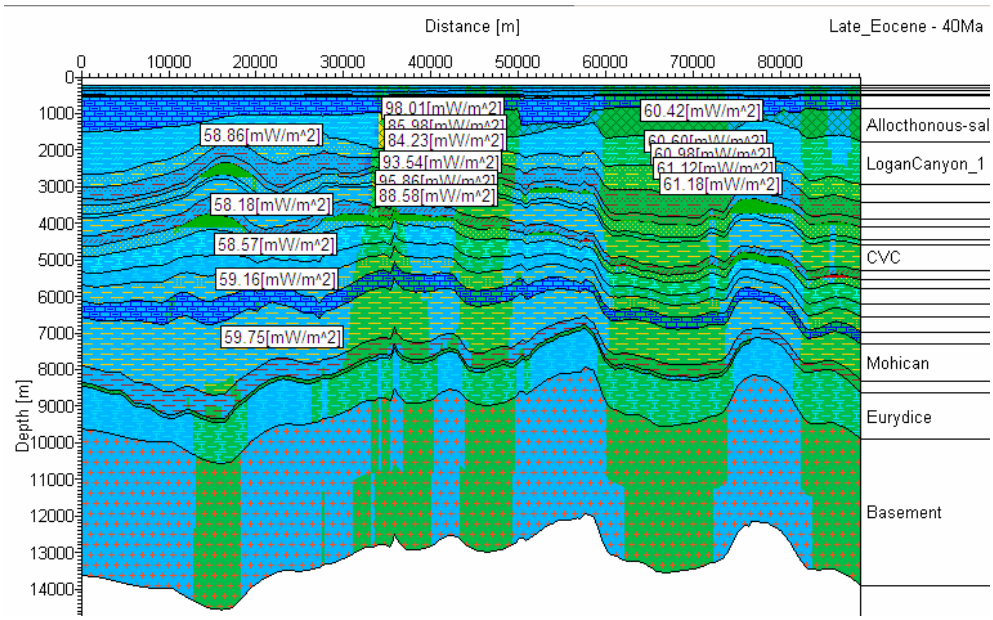

Figure 36e (v). Line A-A' - Heat flow profile at 40 Ma

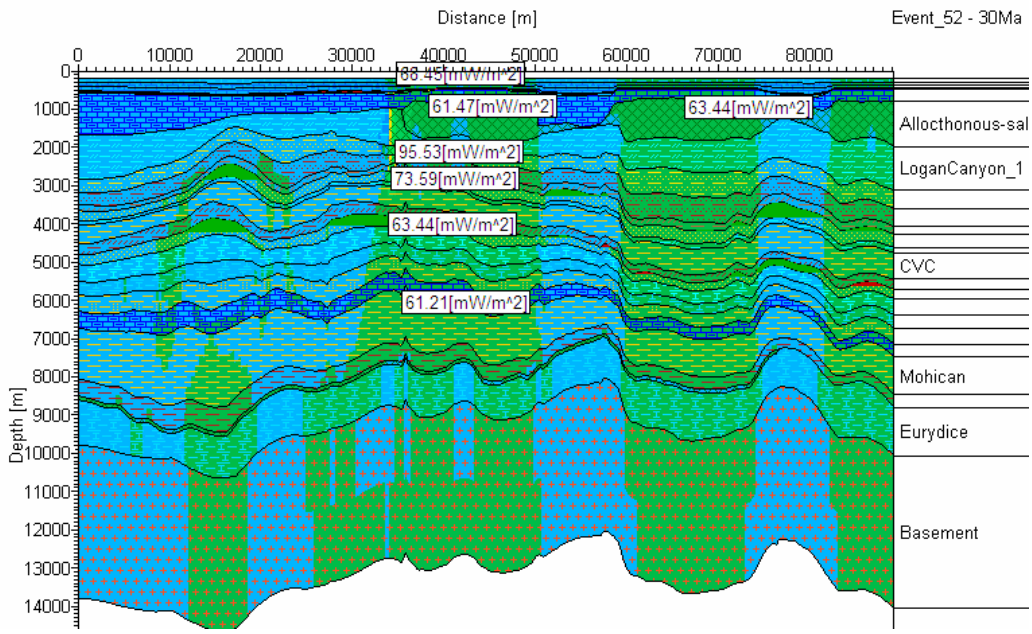

Figure 36e (vi). Line A-A' - Heat flow profile at 30 Ma

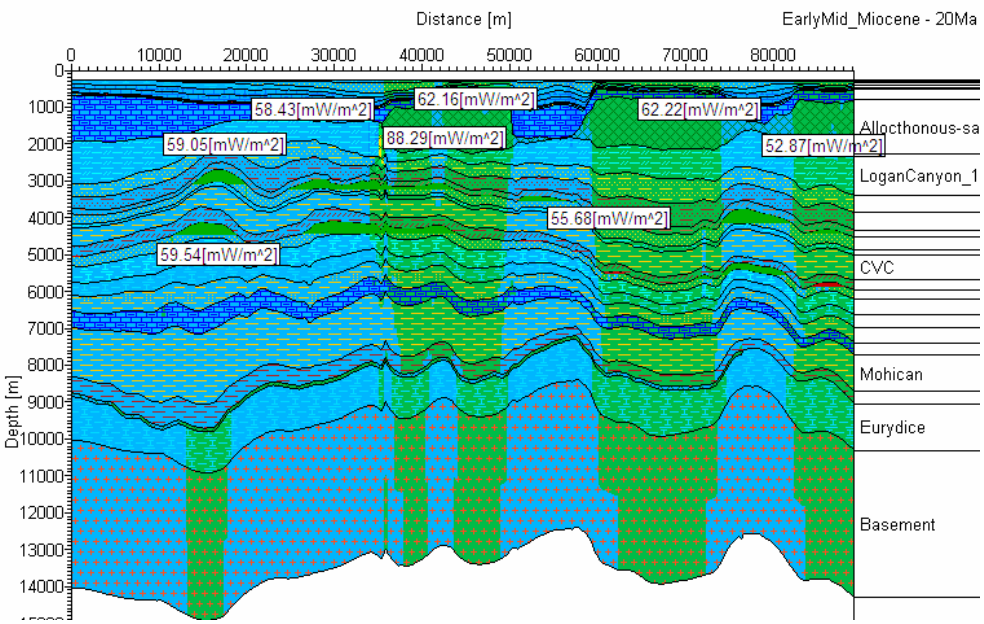

Figure 36e (vii). Line A-A' - Heat flow profile at 20 Ma

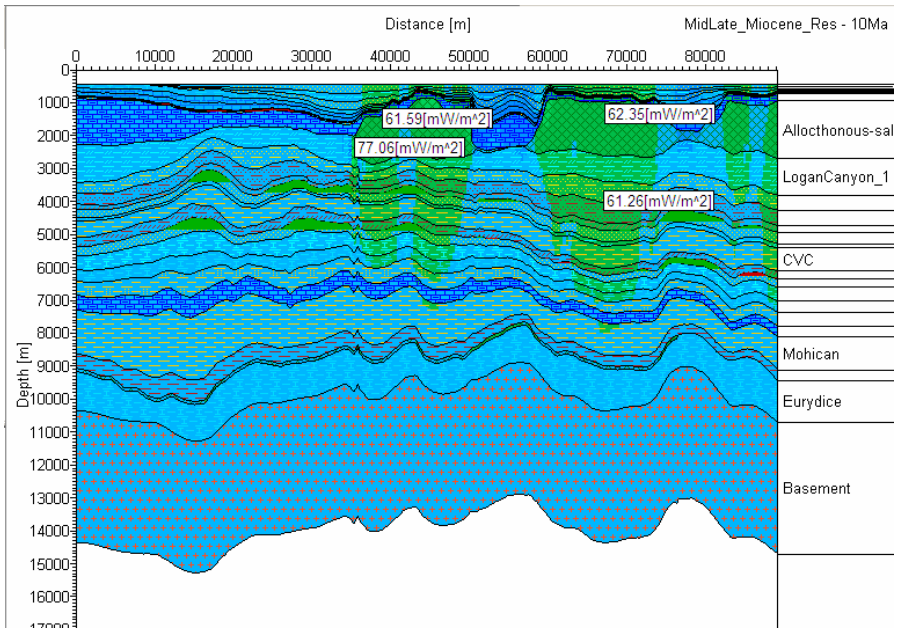

Figure 36e (viii). Line A-A' - Heat flow profile at 10 Ma

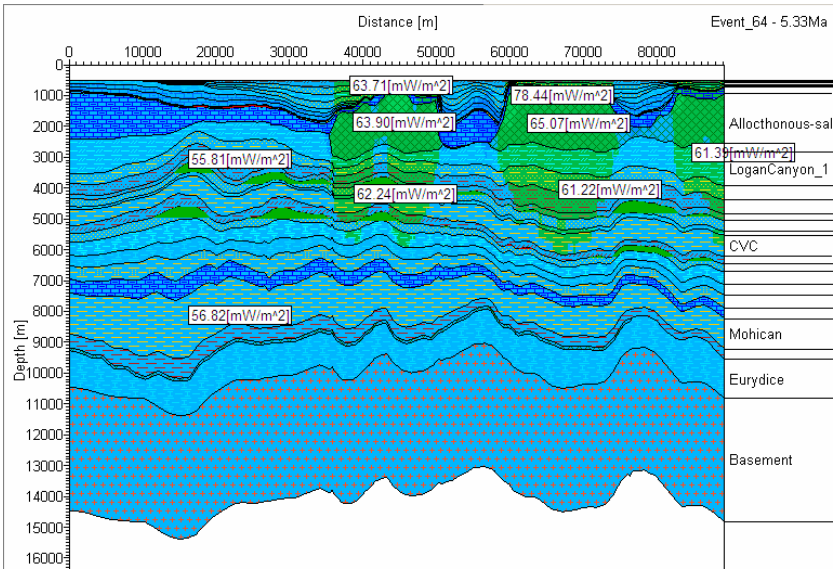

Figure 36e (ix). Line A-A' - Heat flow profile at 5.3 Ma

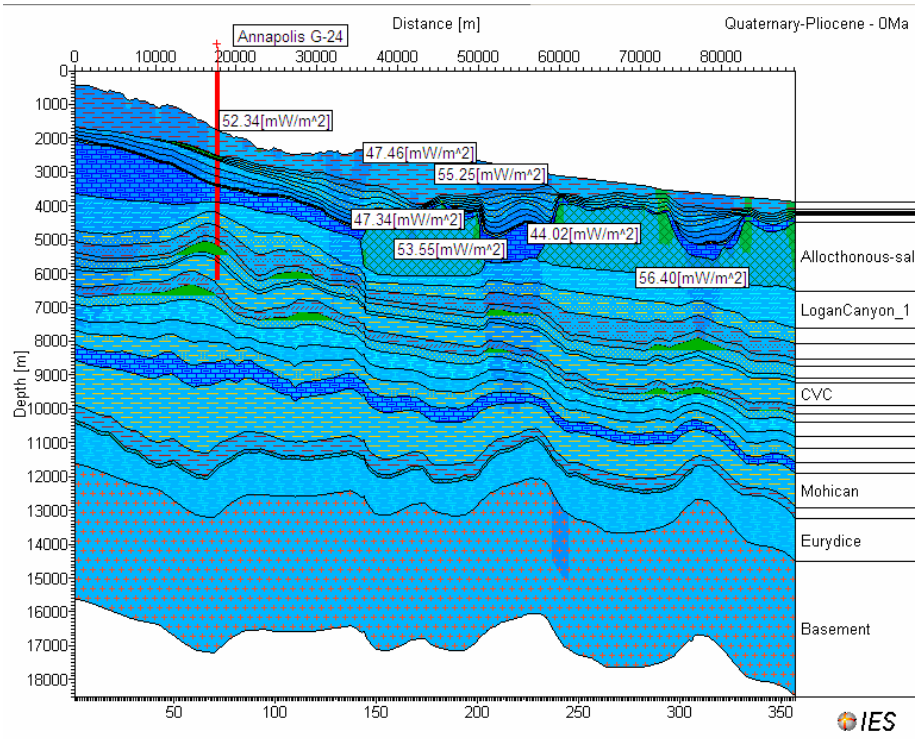

Figure 36e (x). Line A-A' - Heat flow profile at Present day

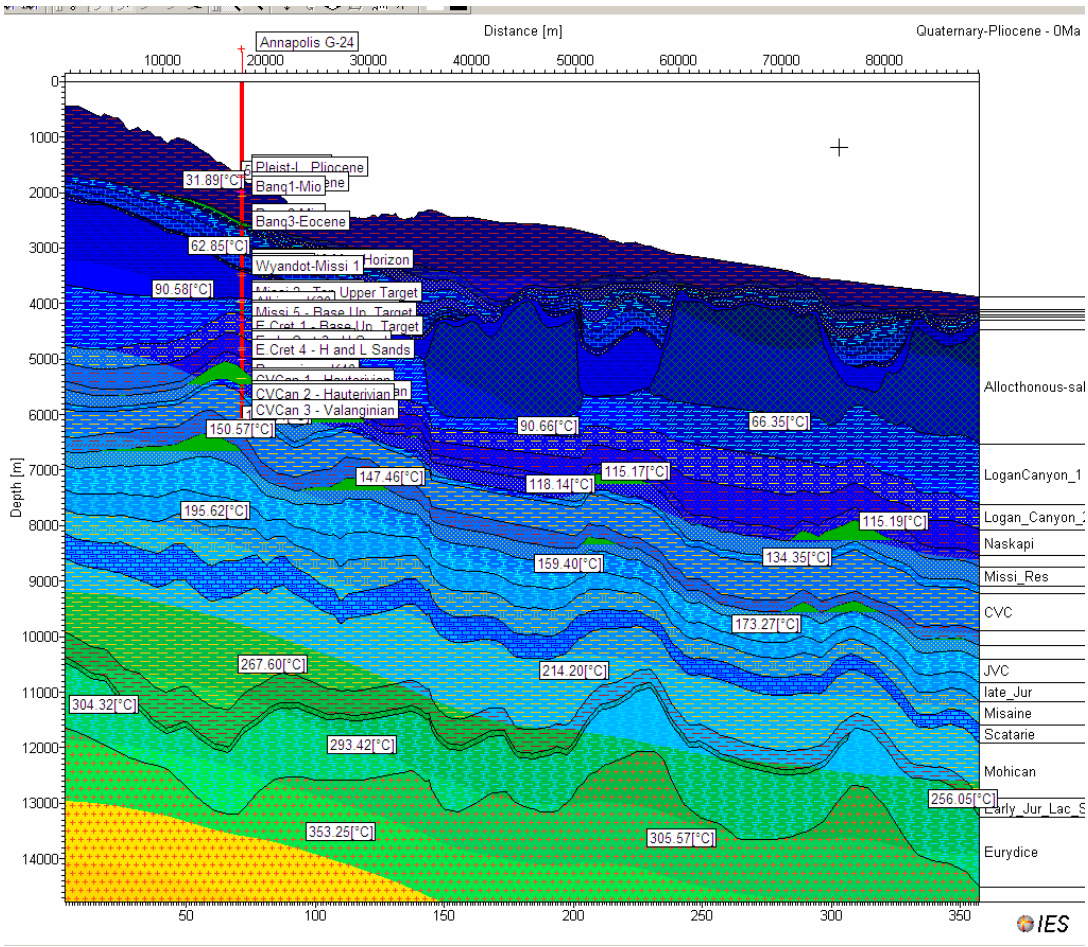

Figure 36f. Line A-A' – Temperature profile (at the present time) within various stratigraphic units and showing different stratigrapic picks of the Annapolis G-24 well

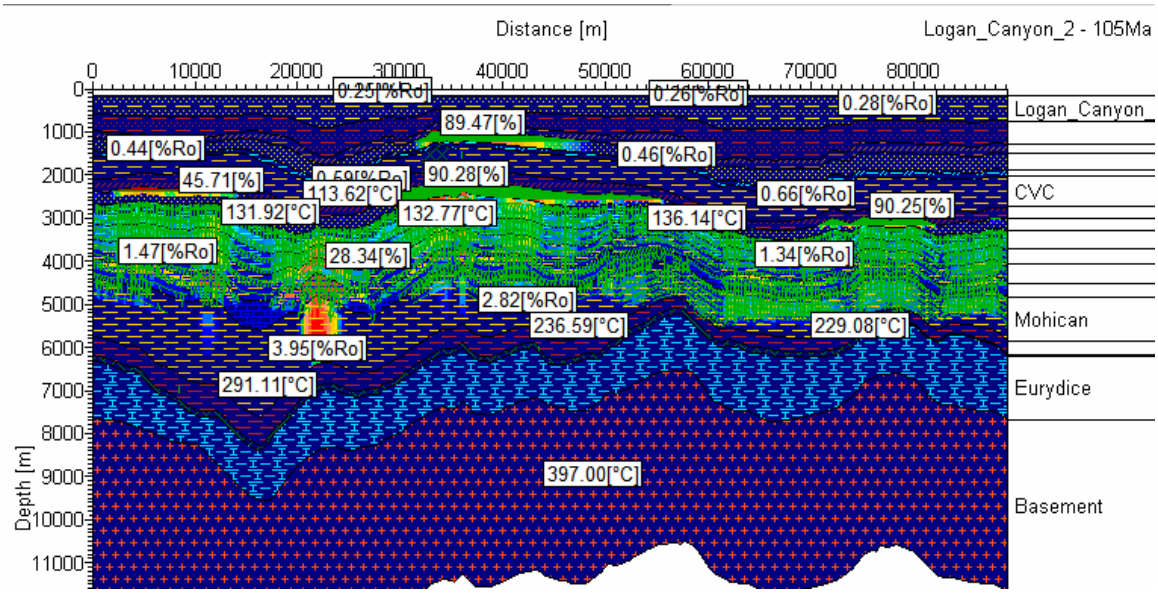

Figure 36g (i). Line A-A' – Relation between reservoir hydrocarbon saturation, temperature, and maturity with flowpath direction at 105 Ma

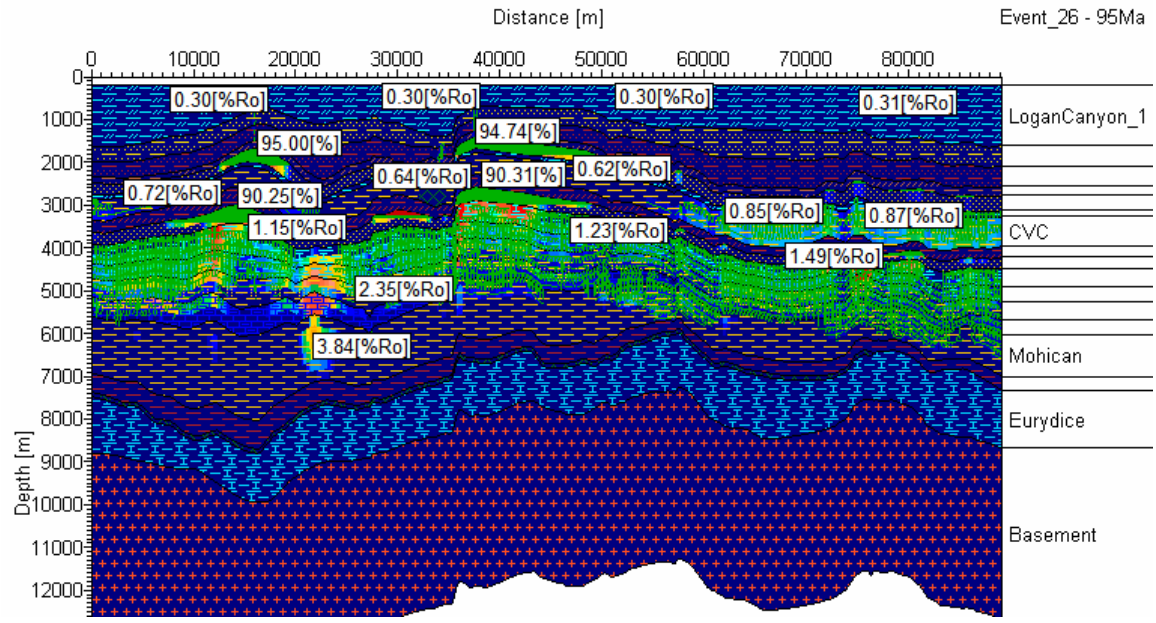

Figure 36g (ii). Line A-A' – Relation between reservoir hydrocarbon saturation and maturity with flowpath direction at 95 Ma

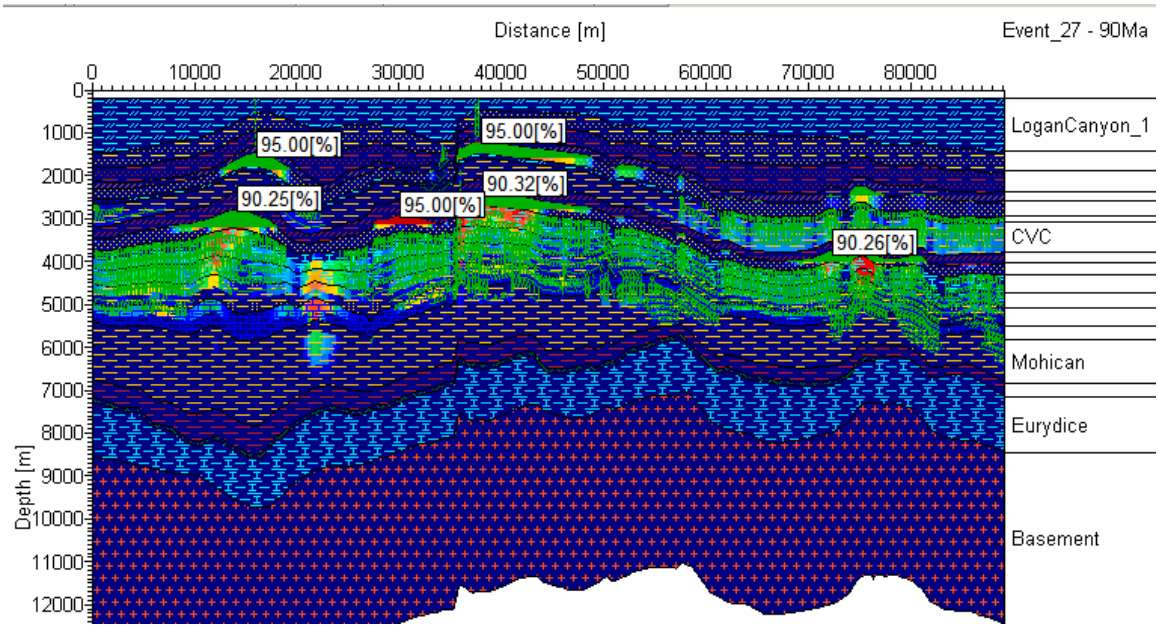

Figure 36g (iii). Line A-A' – Relation between reservoir hydrocarbon saturation and maturity with flowpath direction at 90 Ma

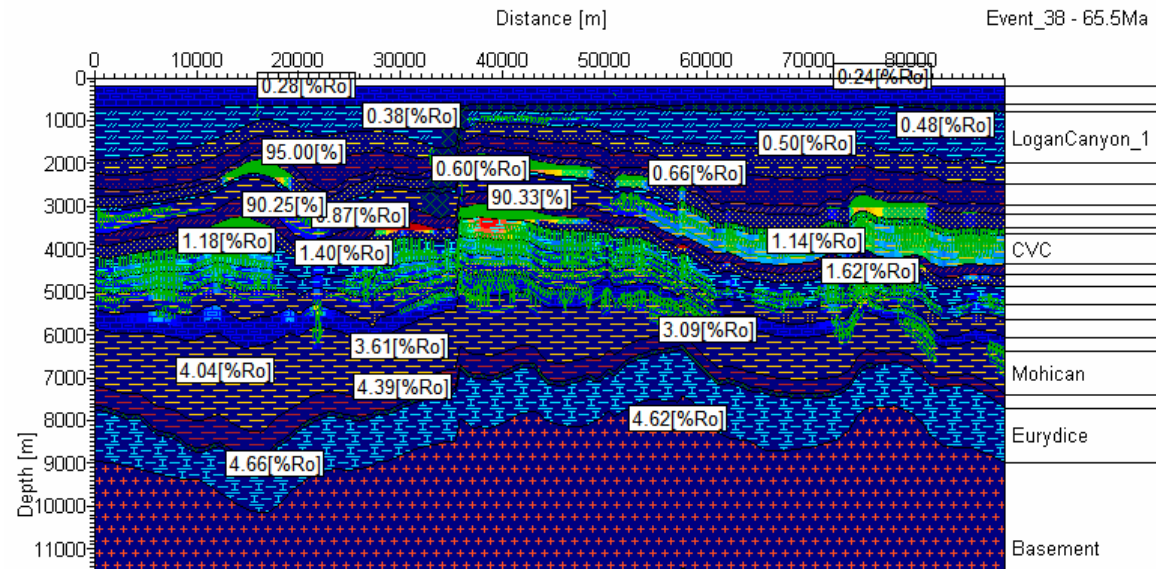

Figure 36g (iv). Line A-A' – Relation between reservoir hydrocarbon saturation and maturity with flowpath direction at 65.5 Ma

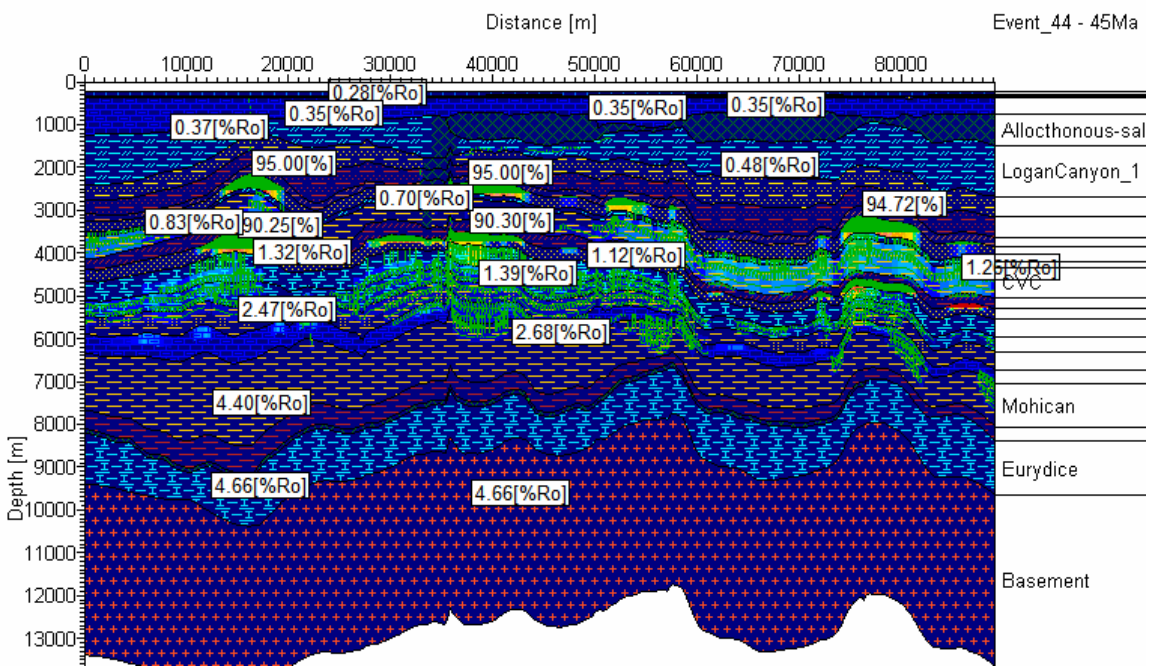

Figure 36g (v). Line A-A' – Relation between reservoir hydrocarbon saturation and maturity with flowpath direction at 45 Ma

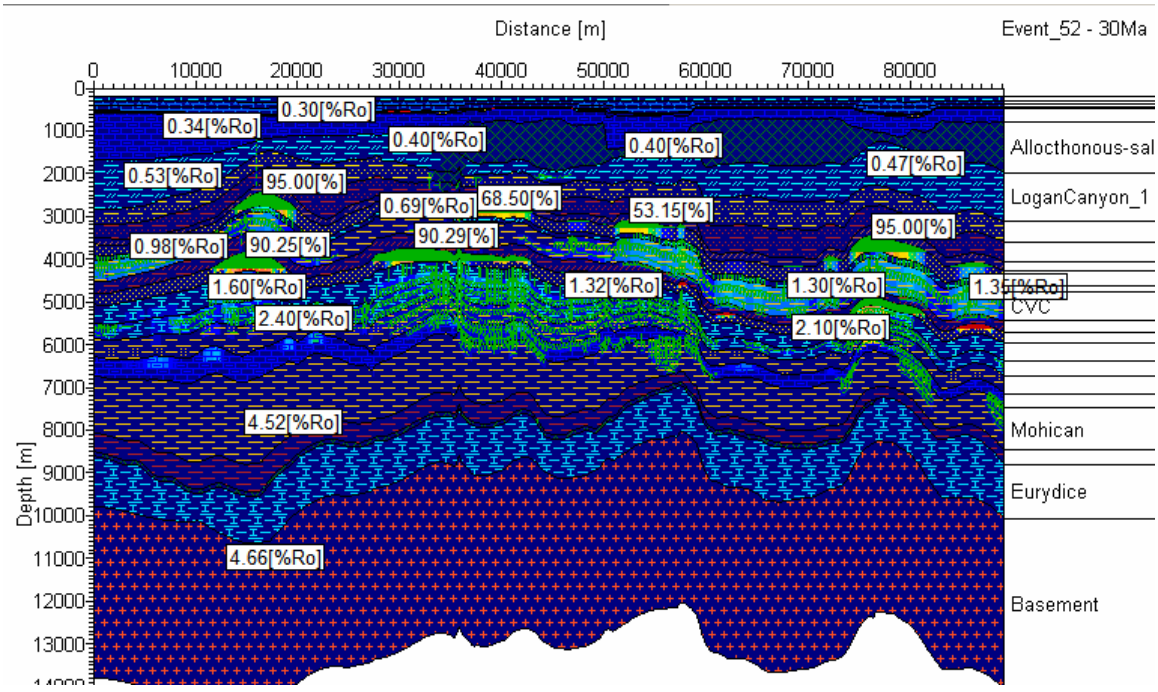

Figure 36g (vi). Line A-A' – Relation between reservoir hydrocarbon saturation and maturity with flowpath direction at 30 Ma

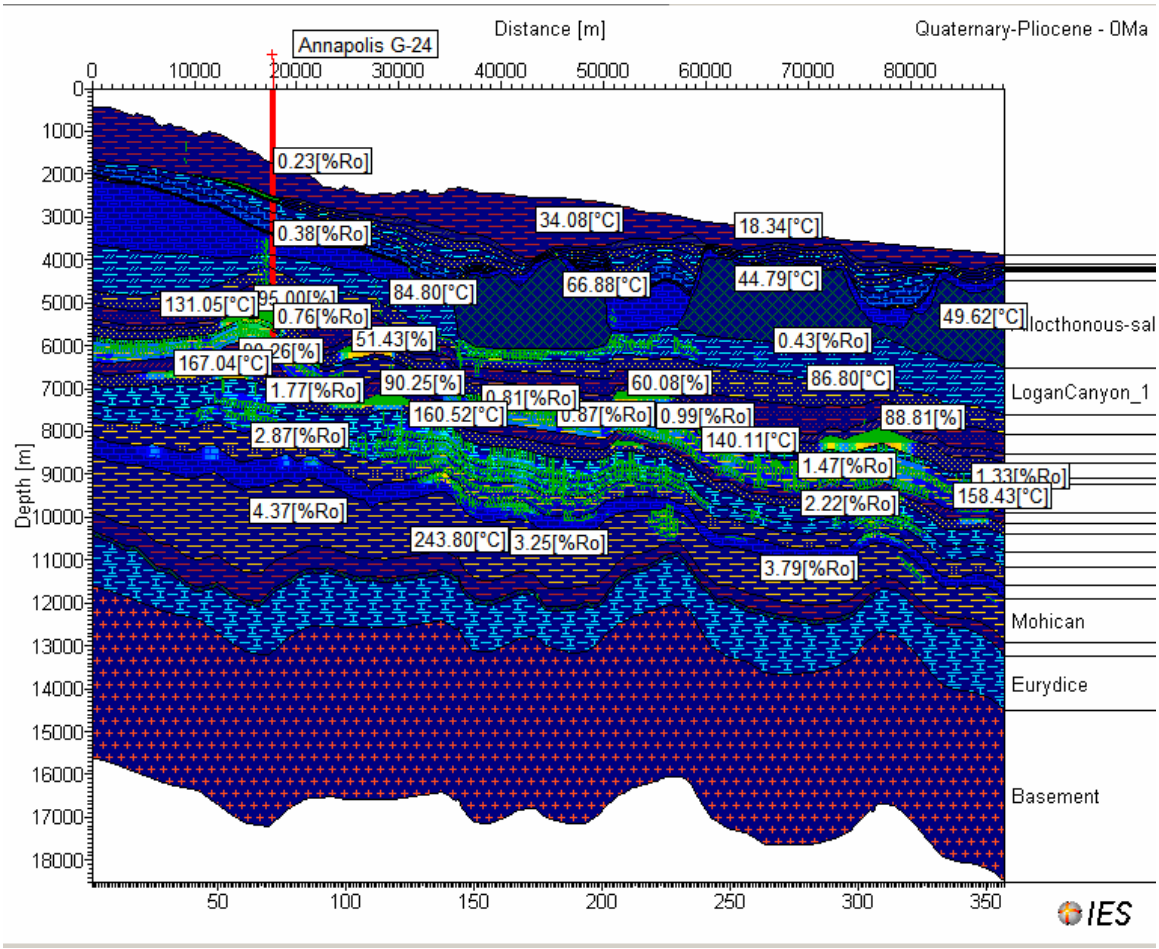

Figure 36g (vii). Line A-A' – Relation between reservoir hydrocarbon saturation and maturity with flowpath direction at the present time

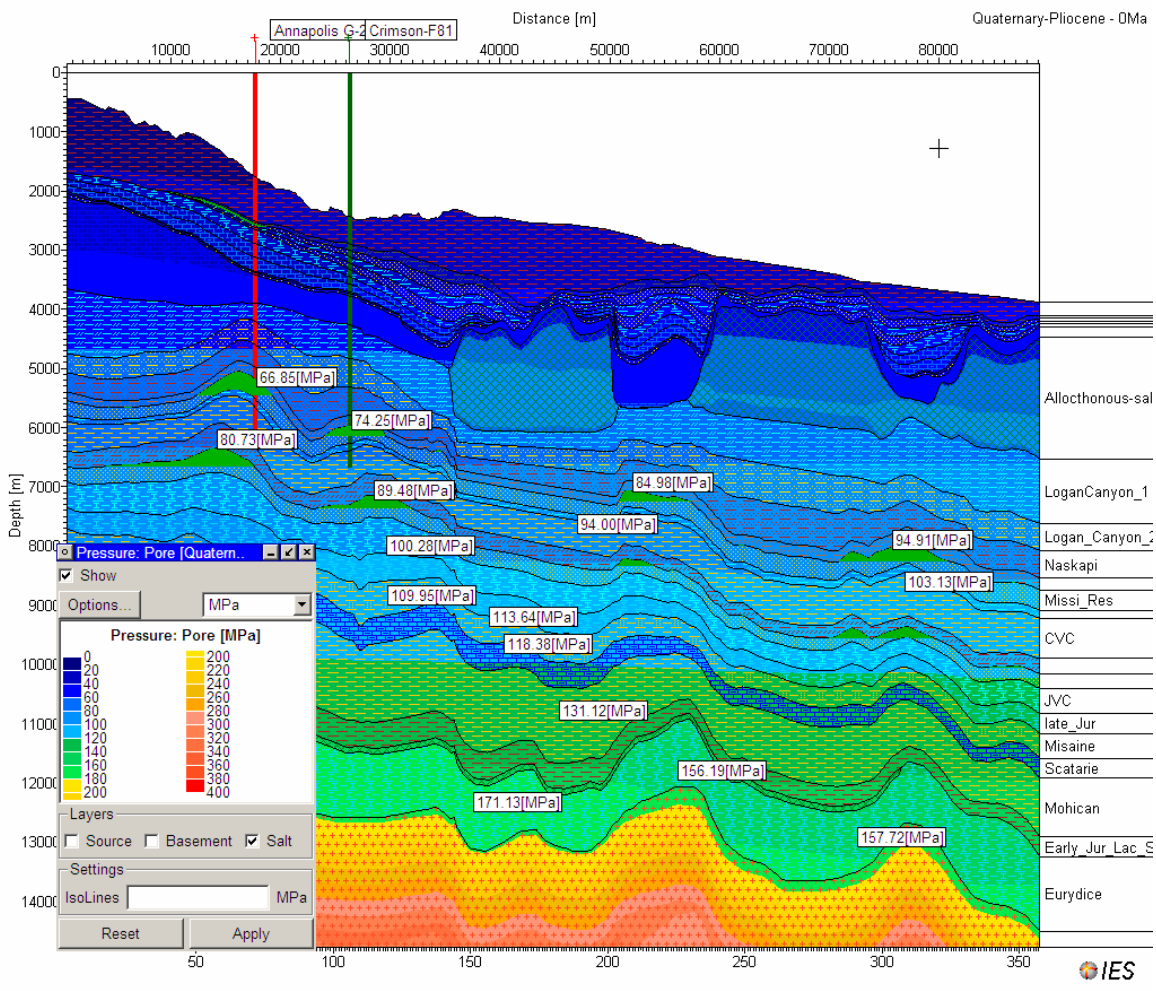

Figure 36h. Line A-A' – Pore Pressure profile at the present day

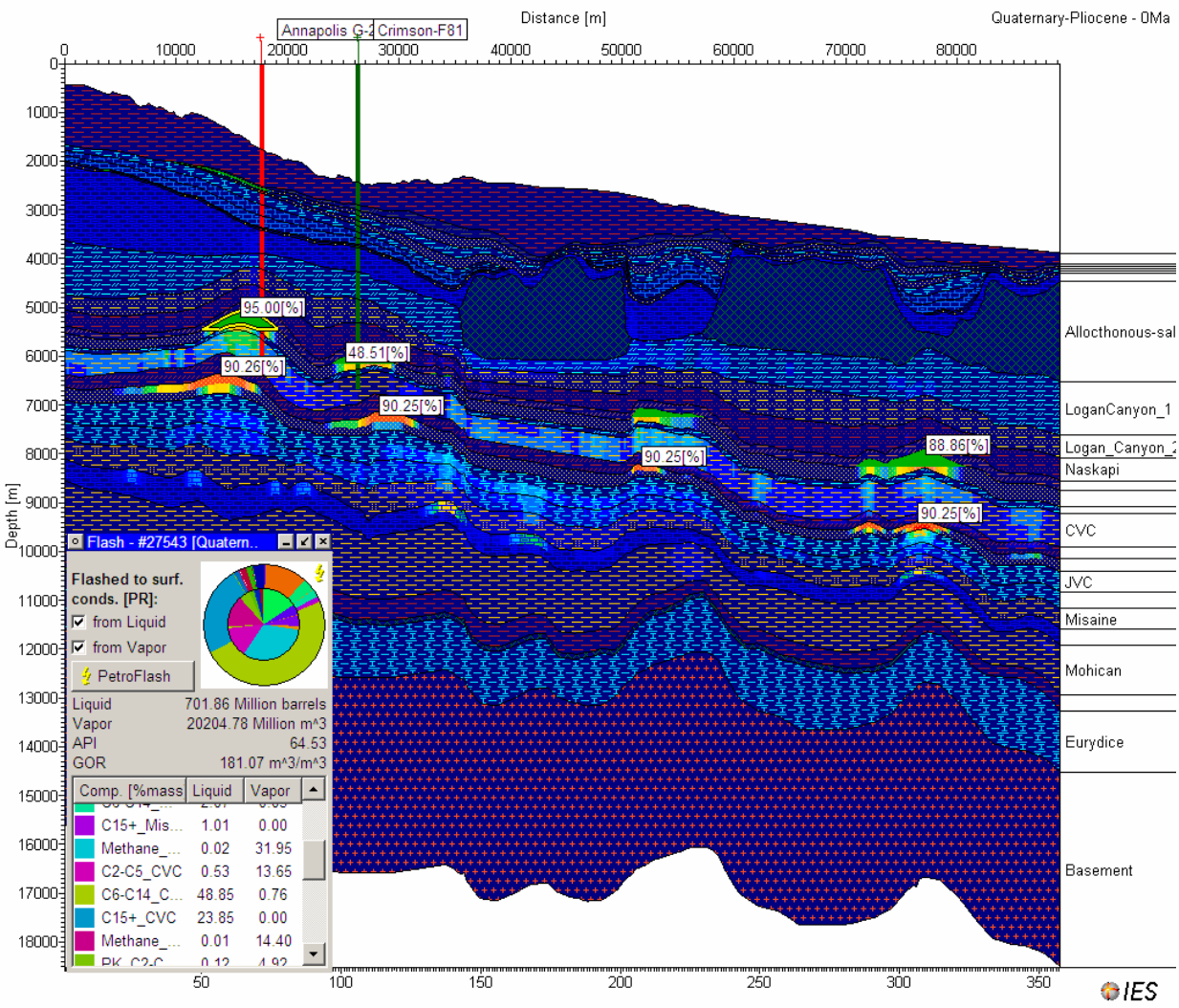

Figure 36i (i). Hydrocarbon saturation of various reservoirs with projected 90% saturation of Early Cretaceous reservoir of the Annapolis G-24 well along with API and GOR of that hydrocarbon composition. It also shows that Crimson F-81 did not have enough saturation of hydrocarbons even if good reservoir would have been present

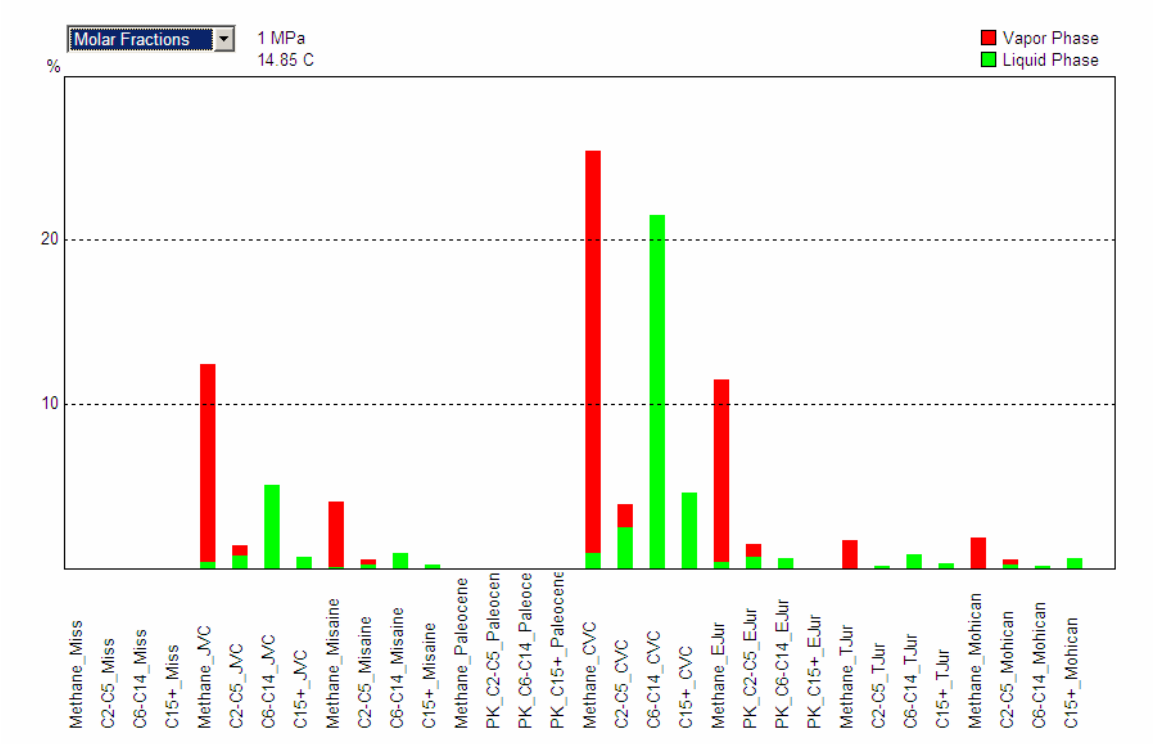

Figure 36i (ii). Hydrocarbon component tracking of Early Cretaceous reservoir of the Annapolis G-24 well (in molar fraction), which shows tracking of volume percentages of various hydrocarbon components from individual source rocks

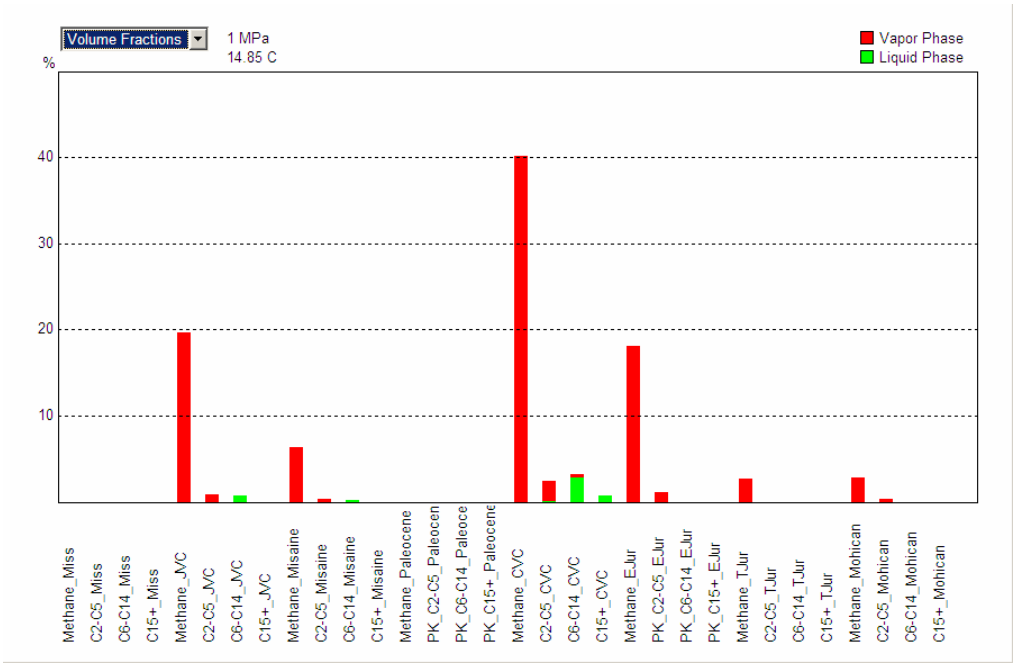

Figure 36i (iii). Hydrocarbon component tracking of Early Cretaceous reservoir of the Annapolis G-24 well (in volume fraction), which shows tracking of volume percentages of various hydrocarbon components from individual source rocks

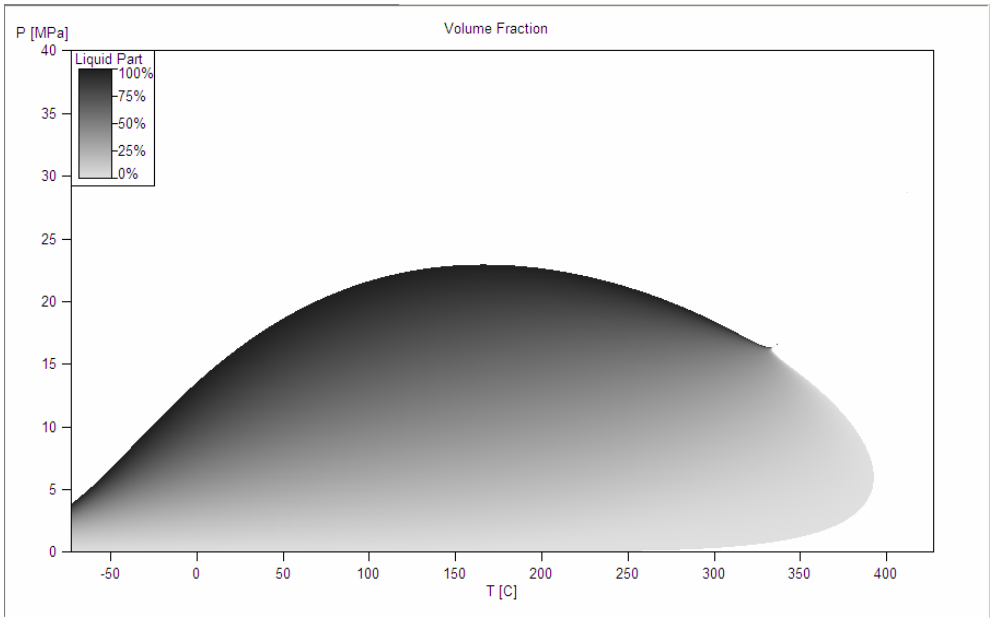

Figure 36i (iv). Modeled Bubble Point Curve of the Early Cretaceous reservoir hydrocarbons of the Annapolis G-24 well (in volume fraction)

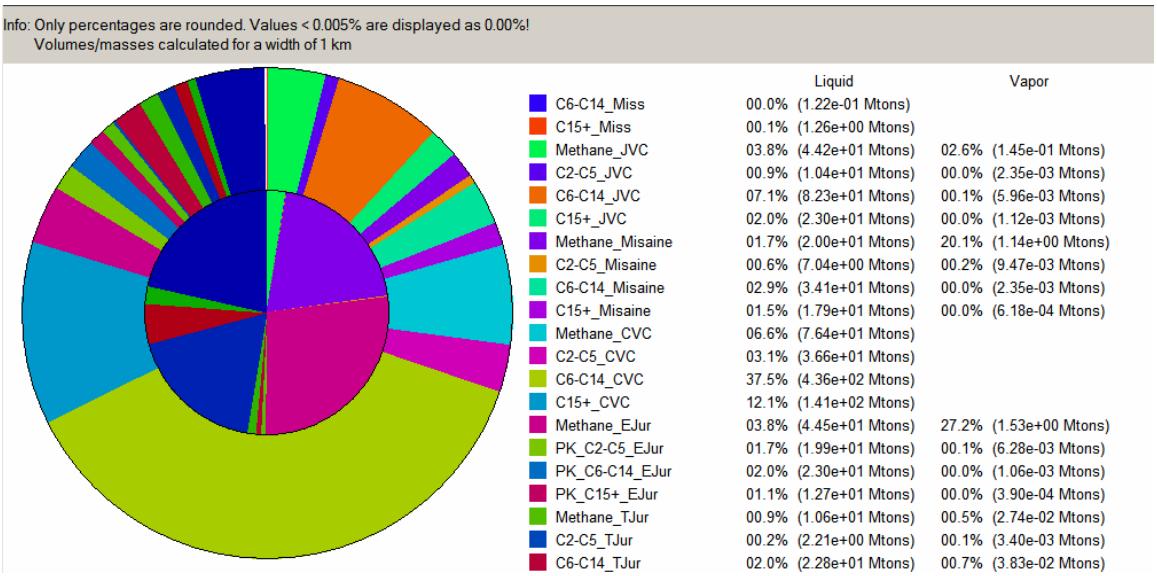

Figure 36j. Line A-A' - Cummulative masses of multi-component hydrocarbons expelled from various source rocks (masses calculated for a kilometer radius area)

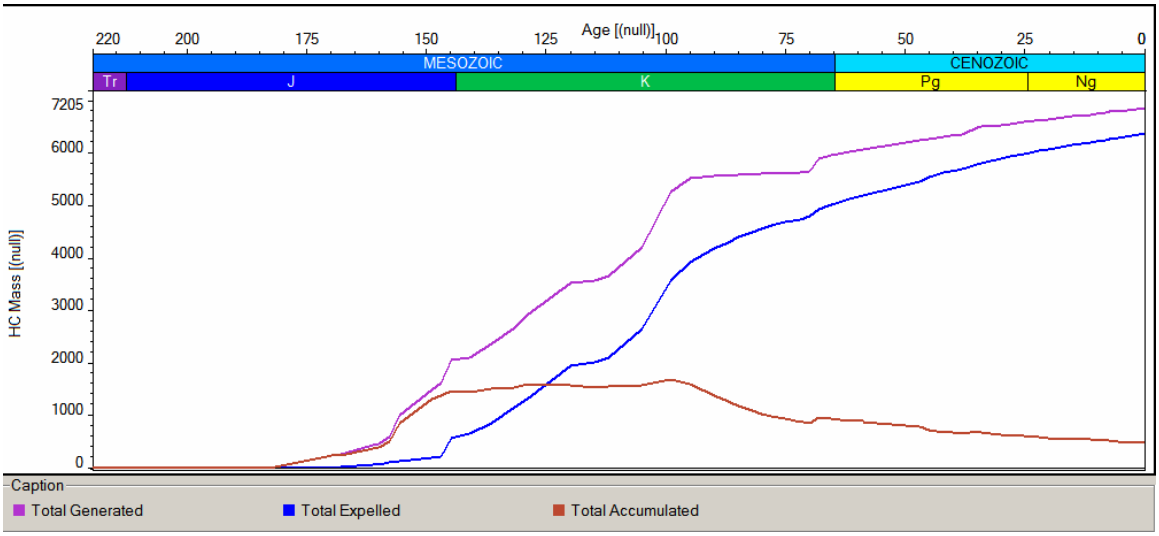

Figure 36k. Line A-A' - Timing of total generated, total expelled, and total accumulated cummulative hydrocarbon mass from various source rocks (masses calculated for a width of 1 km)

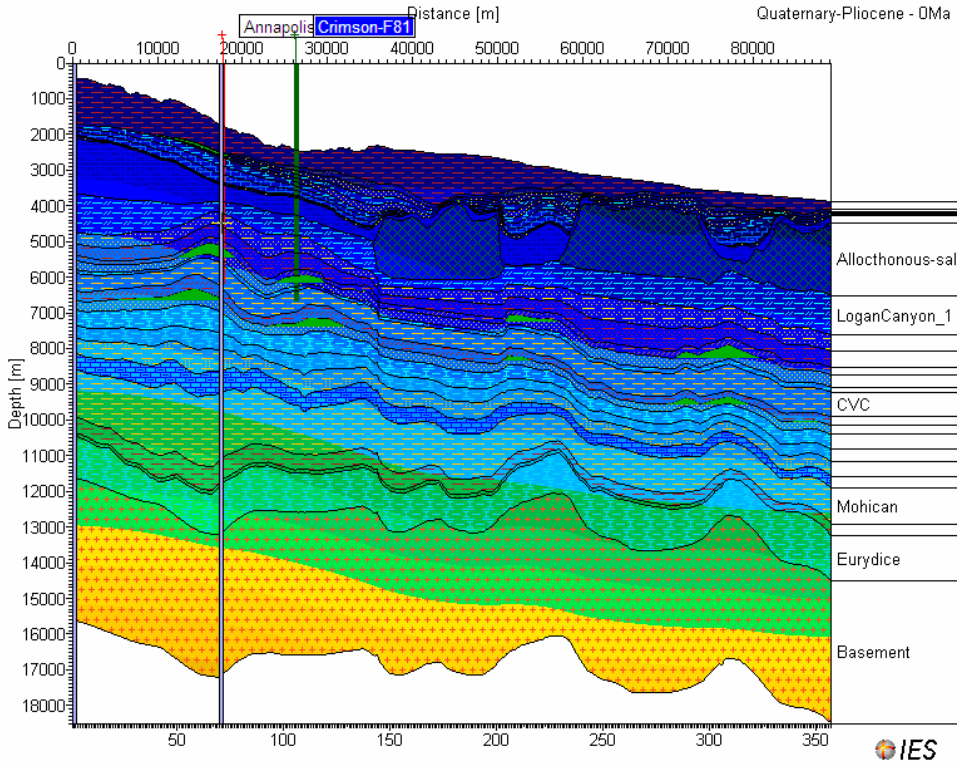

Figure 36l (i). Line A-A' – 1D Extraction of various parameters for the Annapolis G-24 well

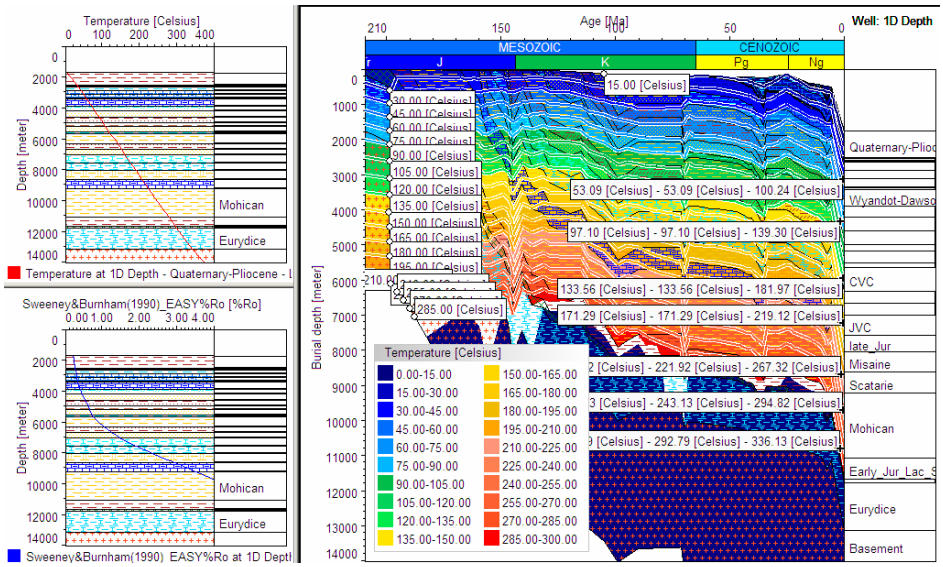

Figure 36l (ii). Line A-A' - One dimensional extraction of Annapolis G-24 well with burial history and iso-temperature lines on the right and depth versus temperature and reflectance plots

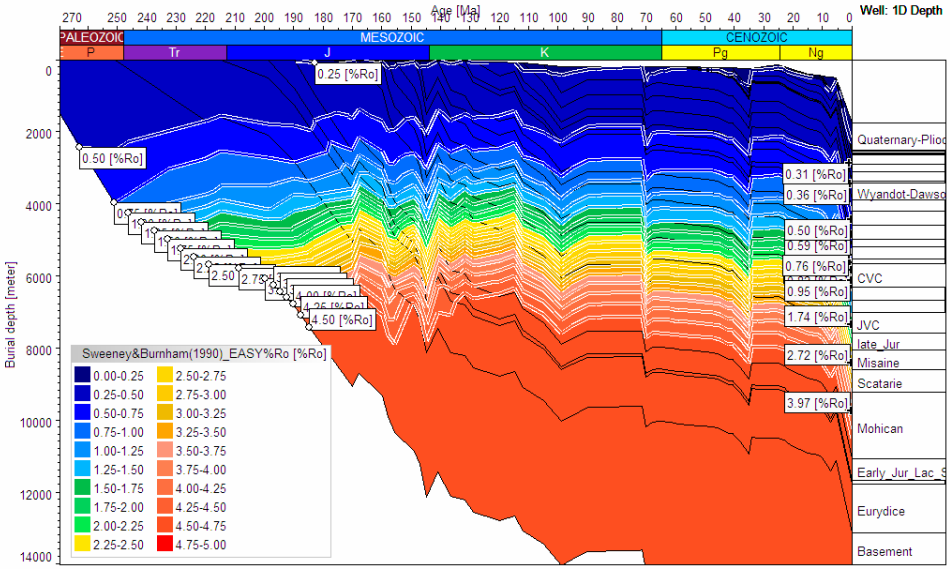

Figure 36l (iii). Line A-A' -One dimensional extraction of Annapolis G-24 well with burial history and iso-maturation line

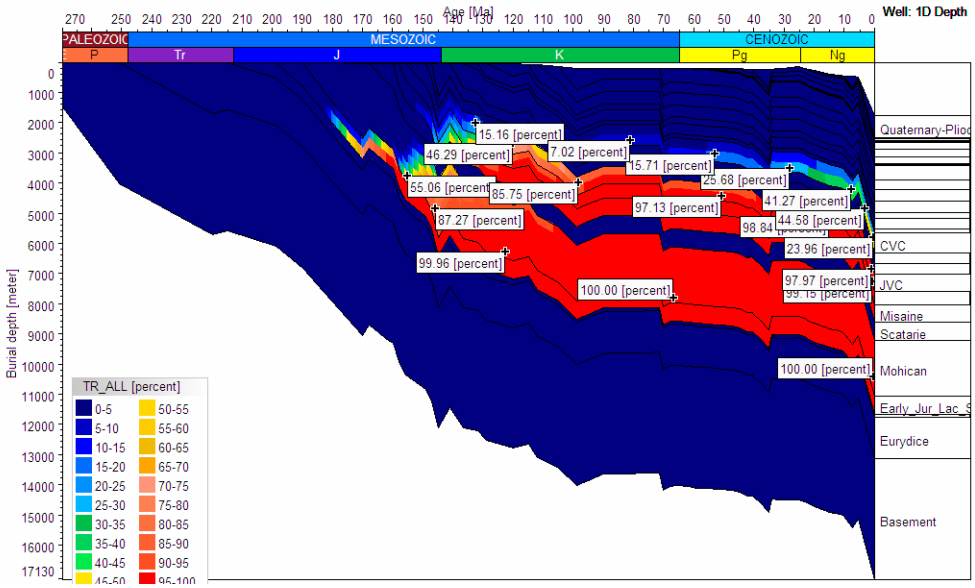

Figure 36l (iv). Line A-A' -One dimensional extraction of Annapolis G-24 well with burial history and transformation ratios of various source rocks through time

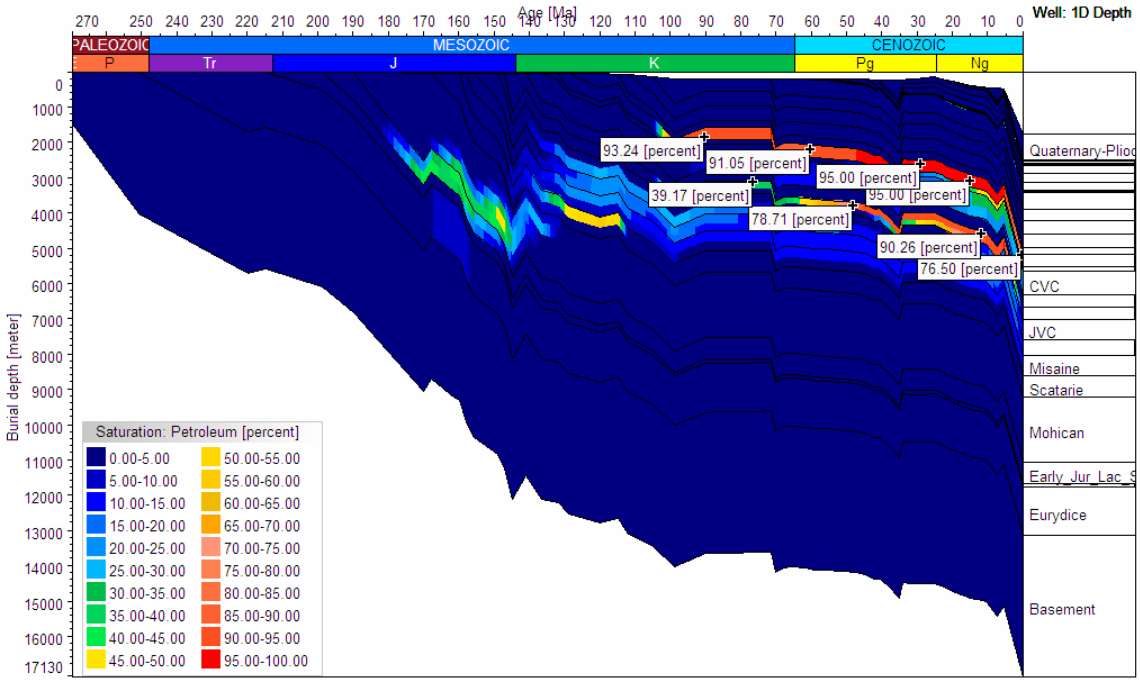

Figure 36l (v). Line A-A' -One dimensional extraction of Annapolis G-24 well with burial history and saturation of various reservoir facies

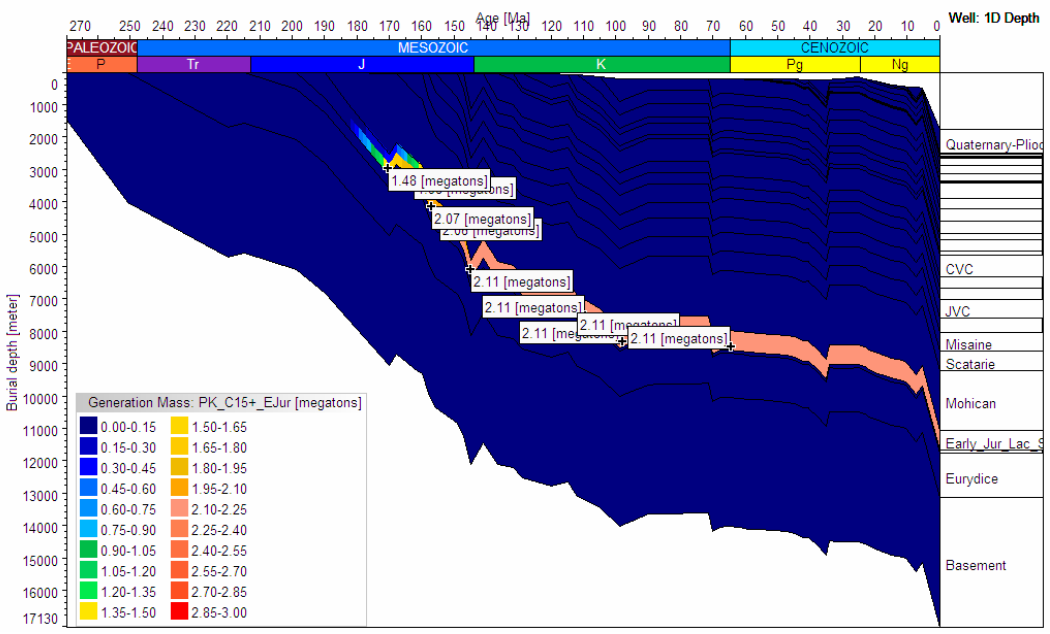

Figure 36l (vi). Line A-A' -One dimensional extraction of Annapolis G-24 well with burial history and mass (megatons) generation of C15+ hydrocarbons from the Early Jurassic source rock

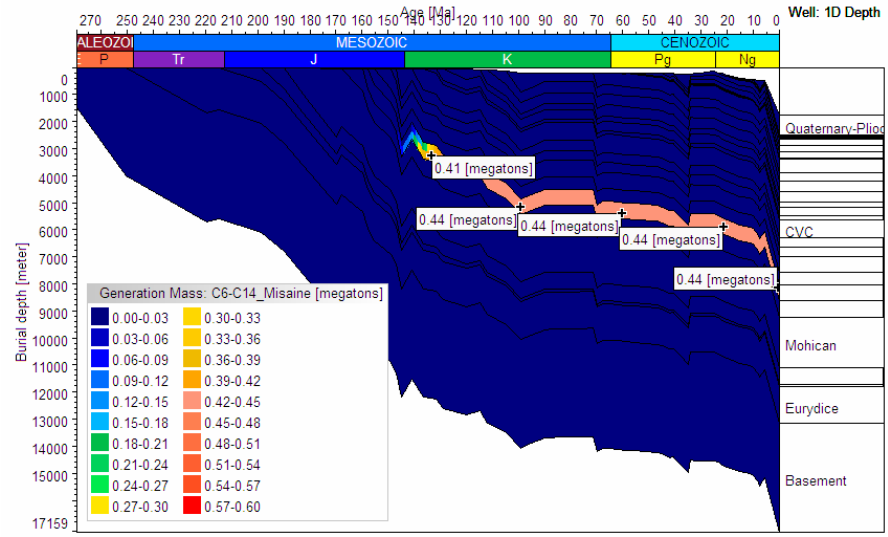

Figure 36l (vii). Line A-A' -One dimensional extraction of Annapolis G-24 well with burial history and mass (megatons) generation of C6-C14 hydrocarbons from the Misaine source rock

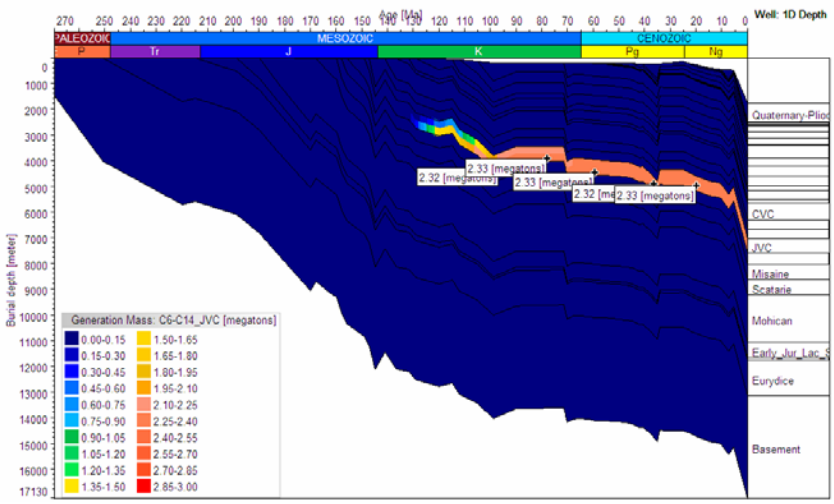

Figure 36l (viii). Line A-A' -One dimensional extraction of Annapolis G-24 well with burial history and mass (megatons) generation of C6-C14 hydrocarbons from the Jurassic Verrill Canyon source rock

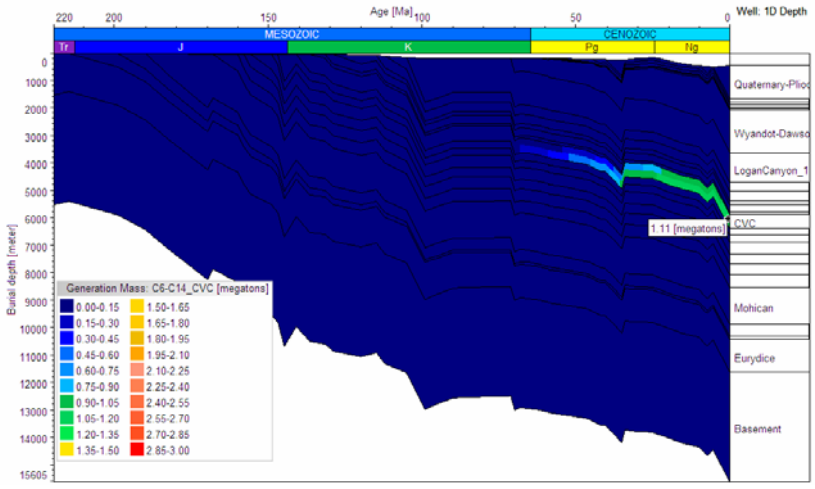

Figure 36l (ix). Line A-A' -One dimensional extraction of Annapolis G-24 well with burial history and mass (megatons) generation of C6-C14 hydrocarbon generation from the Cretaceous Verrill Canyon source rock

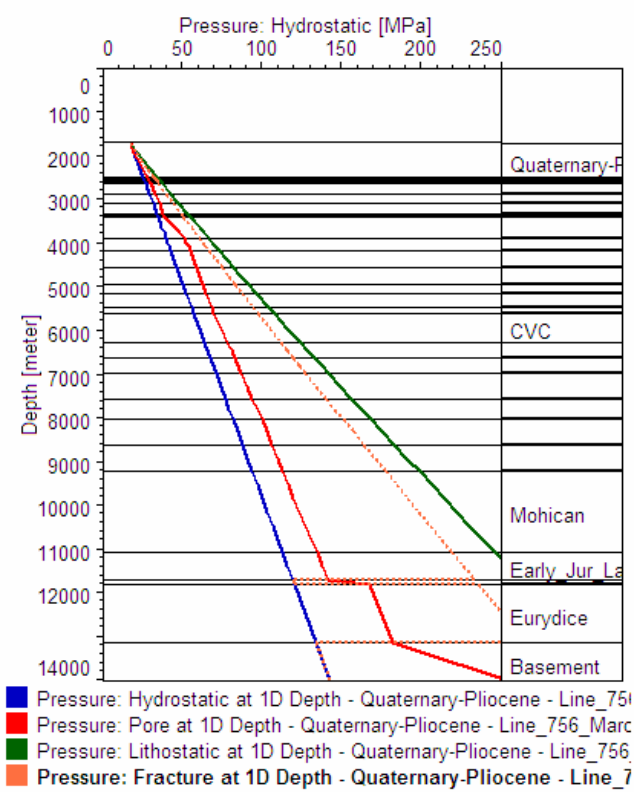

Figure 36l (x). Line A-A' -One dimensional extraction of Annapolis G-24 well with various modeling pressure data

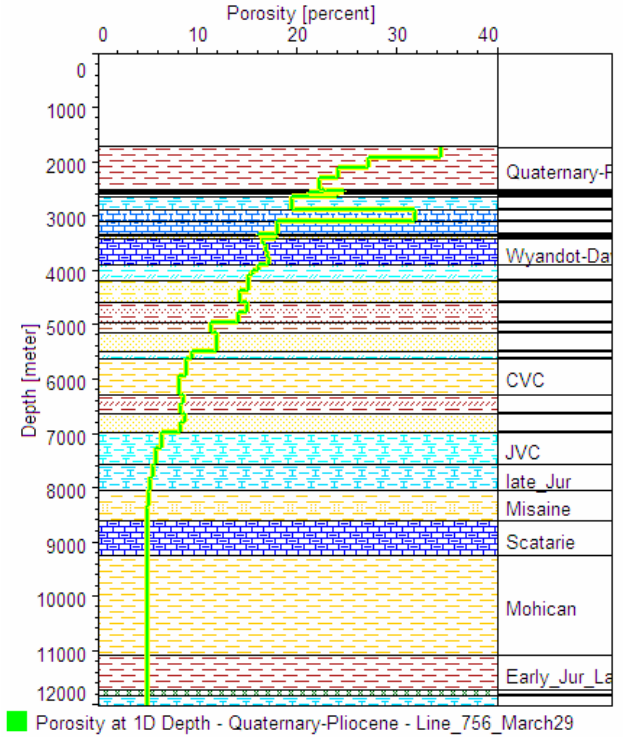

Figure 36l (xi). Line A-A' -One dimensional extraction of Annapolis G-24 well with modeled porosity versus depth

Appendices

Appendix A

(Analytical Methods)

(A-1: sample cleaning, TOC/Rock-Eval, and Vitrinite Reflectance)

(A-2: Multi-component Kinetics)

APPENDIX A-1 AND A-2: ANALYTICAL METHODS

Appendix A-1: Geochemical Screening Methods

Appendix A-1.1. Cleaning of Samples from Synthetic Oil Base Mud

As all four deepwater wells (Annapolis G-24, Crimson F-81, Torbrook C-15, and Weymouth A-45) were drilled with synthetic oil base mud, all thirty samples have been thoroughly cleaned before any analysis was performed. The dried samples that have been cleaned first by *Sunlight Detergent* and water have been placed in a soxhlet thimble and extracted for 12-16 hours using a solvent mixture of 90% *dichloromethane* and 10% *methanol*. The solvent has eventually been poured off and each sample has been rinsed twice more with *toluene* to eradicate any trace amount of synthetic base oil.

Appendix A-1.2. Total Organic Carbon Determination by Leco Carbon Analyzer

Total organic carbon (TOC) is best determined by direct combustion. Approximately 0.2 grams of sample were carefully weighed, treated with concentrated HCl to remove carbonates, and vacuum filtered on glass fiber paper. The residue and paper were placed in a ceramic crucible, dried, combusted with pure oxygen in a LECO EC-12 carbon analyzer at about 1000^{o}C. A laboratory standard is run every five minutes. 'Total Carbonate' can be determined from differences in weight of the original sample and residue that remained after acid treatment or by LECO combustion TOC differences before and after the acid digestion. For organic carbon determination, all thirty samples have been analyzed (Tables 1A, 1B, and 1C).

Appendix A-1.3. Rock-Eval Pyrolysis

Rock-Eval II pyrolysis was used to determine kerogen type (S_2 and HI [hydrogen index, mg HC/g TOC]), kerogen maturity [T_{max} (^{o}C)], amount of free hydrocarbons (S_1 and PI [production index; S_1/S_1+S_2]), and oxygen concentration (S_3 or mg CO_2/g TOC) of the kerogen. About 0.1 gm of the same ground sample used for LECO TOC is carefully weighed in a pyrolysis crucible and then heated to 300^{o}C to determine the amount of free hydrocarbons, S_1, which is thermally distilled. The amount of pyrolyzable hydrocarbons, S_2, is measured when the sample is heated in an inert atmosphere between 300^{o} to 550^{o} C using a heating rate of 25^{o}C/minute. S_1 and S_2 are reported in mg HC/g of sample. T_{max}, a maturity indicator, is the temperature of maximum S_2 generation. The S_2 values less than 0.2 mg HC/g sample has poor definition of the S_2-maximum. Accordingly, the T_{max} cannot be determined reliably (Peters, 1986). Carbon dioxide is also being generated during kerogen pyrolysis. The resulting peak S_3 is an indicator of original oxidation during sediment deposition. It is collected up to a temperature of 390^{o}C and reported as S_3 in units of mg CO_2/g sample. A laboratory standard is run every 10 samples. Both the Hydrogen Index (HI = S_2 * 100/TOC) and Oxygen Index (OI = S_3 *100/TOC) values are used as pseudo-van Krevelen-Type diagram. For details of the Rock-Eval pyrolysis, see Espitalie et al. (1985), Peters (1986), and Hunt (1995). Tables 1-A, 1-B, and 1-C illustrate all the Rock-Eval data of 30 samples from four wells (Alma K-85, Annapolis G-24, Torbrook C-15, and Weymouth A-45)

Appendix A-1.4. Vitrinite Reflectance Measurement

For vitrinite reflectance measurementa, all selected thirty whole rock samples (wells: Annapolis G-24, Alma K-85, Crimson F-81, Newburn H-23, Torbrook C-15, Weymouth A-45) were subjected to kerogen isolation by acid (HCl and HF) treatment and heavy liquid separation. The other sample from Newburn H-23 well has been polished as a whole rock plug. For details of kerogen isolation procedures, please review previous works (Durand,

1980; Mukhopadhyay, 1992). Two types of sample preparation were made from isolated kerogen: polished plug and smear slide. Although the contract did not include visual kerogen analysis, the report will include some interpretations on visual kerogen analysis. Vitrinite reflectance was determined using a ZEISS Axioskop Incident Light Microscope and standard procedures (ASTM, 1991; Stach et al., 1982; Mukhopadhyay, 1992). The reflectance was measured with an oil immersion objective (40X). The reflectance measurement was calibrated with three glass standards of 0.94%, 1.01% and 1.69% R_o acquired from Leitz and Zeiss Canada. Usually 50 vitrinite grains were measured for each sample. For this work, random vitrinite reflectance was measured. For more details about the vitrinite reflectance procedures and interpretation of vitrinite reflectance measurement, see Dow (1977), Mukhopadhyay (1992, 1994).

Tables 2 and 3 illustrate the TOC/Rock-Eval and vitrinite reflectance (both measured and calculated) of all analyzed samples from five wells of Scotian Shelf and Slope (Alma K-85, Annapolis G-24, Crimson F-81, Torbrook C-15, and Weymouth A-45). Appendix A-3 illustrates the reflectance histograms of 30 samples from three wells (Crimson F-81, Torbrook C-15, and Weymouth A-45).

Appendix A-2. Compositional Kinetics of Source Rocks – Analytical Method

The goal of this study was to assess the rates of kerogen decomposition into primary oil and gas and to measure those yields. Measurement of the kinetics of primary kerogen cracking requires decoupling of primary from secondary cracking reactions. Determination of primary cracking parameters in a laboratory setting is a function of the analytical approach, e.g., open or closed system pyrolysis, nonisothermal or isothermal heating. In open system pyrolysis, cracked products are swept away immediately in an inert carrier gas. Thus, minimal secondary cracking of formed products occurs when relatively fast heating rates are used. Closed system pyrolysis, depending on the conditions utilized, will yield products derived from both primary and secondary cracking and it becomes very difficult to decouple these two processes. Pyrolysis experiments completed using either nonisothermal or isothermal experiments are necessarily completed at high heating rates or temperatures relative to geological conditions. Both yield primary products. Thus, either nonisothermal or isothermal open system pyrolysis provides reasonable data for measuring primary kinetic parameters. In this study primary cracking was assessed using nonisothermal, open-system pyrolysis.

Measurement of gas and oil yields is complicated by the inability to trap and resolve light gases (C_1, C_2, and C_3) from open-system pyrolysis experiments. This is further complicated by the need to reproducibly release higher molecular weight hydrocarbons to about C_{40}. Development of analytical technology to accomplish these two goals was achieved prior to initiation of this study and was used to measure primary oil and gas generation and total hydrocarbon yields that are reported in this study. Generation rate curves for specific compounds or compound classes were determined by thermal slicing of pyrolyzates into these newly developed traps. Using this new technology, the compound and compound classes on which primary kinetic assessments were completed included the following 4-components:

- C_1 (dry gas)
- C_2-C_4 (wet gas)
- C_5-C_{14} (light oil)
- C_{15}+ (normal oil)

The experimental yields of these primary products were also measured and recorded from these experiments. Thus, a detailed assessment of primary cracking of kerogen to oil and gas was completed and reported in this study.

Appendix A-2.1. Analytical Background

Samples were first extracted using a binary azeotrope of chloroform-methanol and their bulk kinetic parameters were determined using Humble Instrument's SR Analyzer. Bulk kinetic parameters are determined by measuring the total petroleum hydrocarbon yield by pyrolyzing rock samples directly into a flame ionization detector (FID) without separation of any compounds. Bulk kinetic parameters describe the rate at which kerogen decomposes into hydrocarbons, whereas compositional kinetics describes the rate at which kerogen decomposes into specific hydrocarbons or hydrocarbon groups.

Compositional kinetic parameters were computed from generation rate profiles measured from nonisothermal pyrolysis experiments using Humble Instruments' pyrolysis-multiple automatic cryogenic trapping- gas chromatography system (P-MACT10-GC). These experiments were completed on extracted rock samples using 2-3 different heating rates of 3, 10, and 30°C/minute. The pyrolyzates were "sliced" into 9 different traps, each of which is subsequently desorbed into a gas chromatograph (GC) for separation and detection of specific compounds by FID. Bulk kinetic parameters were used to determine how the "slice" the pyrolyzate since pyrolysis profiles can be very broad or very narrow depending on the organic matter composition or kerogen type. Thus, temperature slices were variable depending on the bulk kinetic results. Slices were typically taken over 24°C intervals around peak generation temperatures for that heating rate.

Humble Instruments' P-MACT10-GC is based on the work of Tang and Stauffer (1994a-b) with a technology enhancement in the ability to trap gaseous hydrocarbons. Their approach consisted of a pyrolysis oven connected to an automatically sequencing 24 port valve connected to 10 traps (Figure 3). Each trap is completely immersed in liquid nitrogen and the temperature reaches about –190°C in the trap. However, even at these

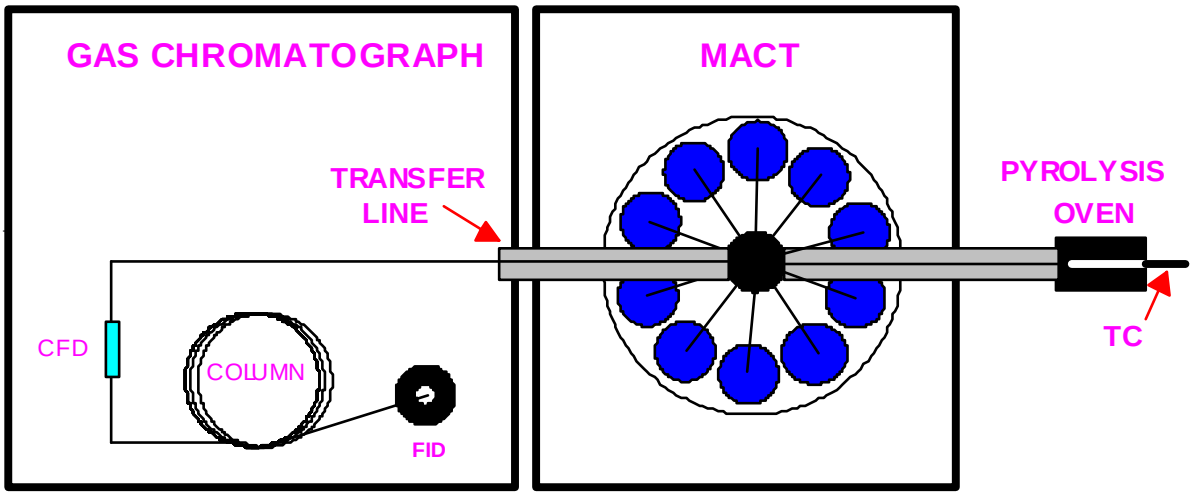

Schematic of Pyrolysis-Multiple Automatic Cryogenic Trapping (MACT10)-GC system.

temperatures the lightest gases are not retained in the trap. Humble Instruments devised a gradient trap, now referred to as Gas Trapper (patent pending by Humble

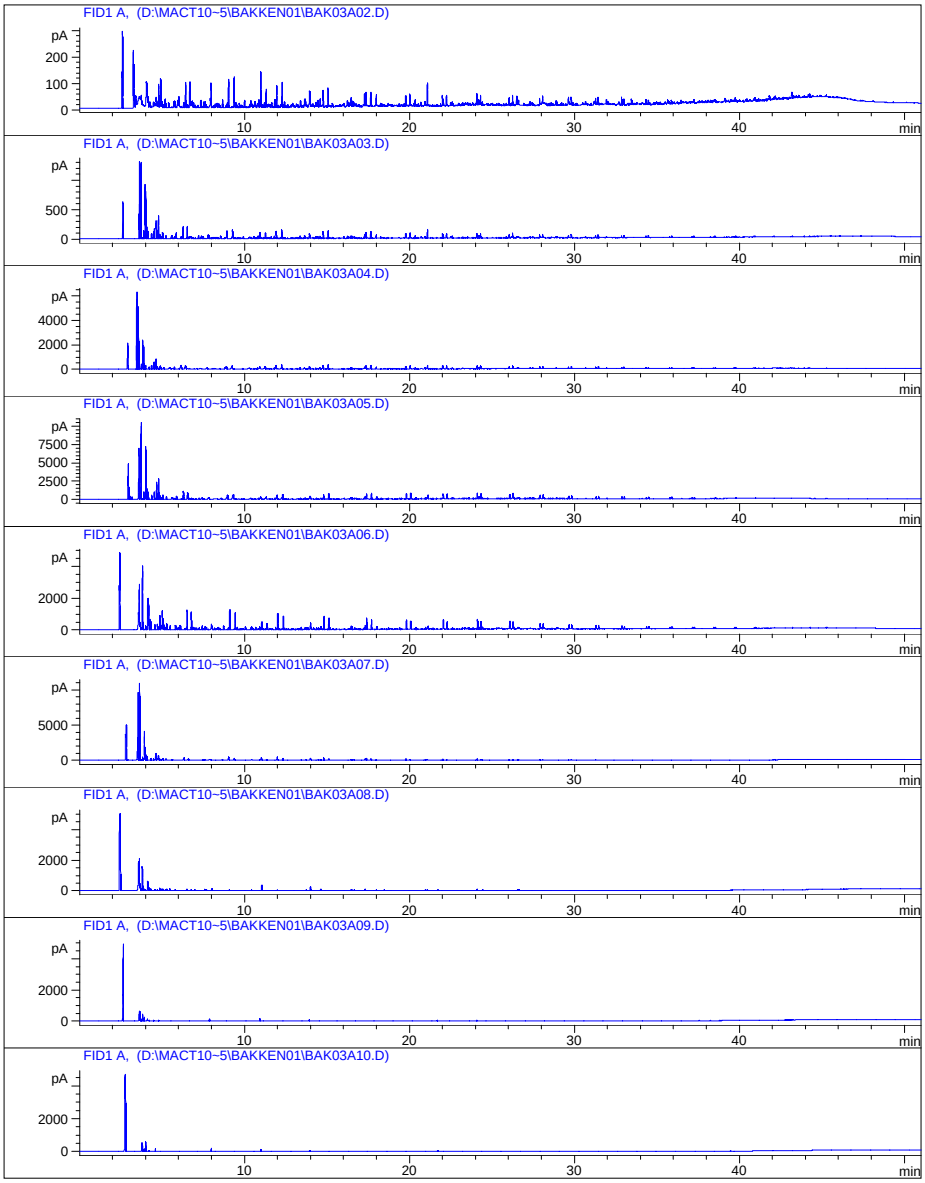

Instruments and Services, Humble, Texas), which traps and holds all hydrocarbons during lengthy pyrolysis experiments and also reproducibly releases higher molecular weight hydrocarbons.

The trapping of methane, ethane, and propane evolved into a research project unto itself and the results are reported in part in Appendix 1. The data provided in Appendix demonstrates the resolution, trapping, and reproducibility results from the MACT10.

Thermal slices of pyrolyzate from low temperature pyrolysis products to high temperature products (primarily methane) at bottom. Kinetic parameters were determined from generation rate curves measured from the experimental pyrolysis gas chromatographic fingerprints at the various heating rates. Rate curves were constructed from the yields of a range of resolved components in these fingerprints. A typical suite of 9 pyrolysis GC (PGC) fingerprints is shown in Figure 4. Note the change from a complex fingerprint in the first 2-3 PGC fingerprints, to fingerprints consisting primarily of a homologous series of alkene-alkane doublets, and finally to primarily methane. The yield of various compound or compound classes were calculated from

these fingerprints at each heating rate utilized. The compound and compound classes on which kinetic assessments were completed included the following 4-components:

- C_1 (dry gas)
- C_2-C_4 (wet gas)
- C_5-C_{14} (light oil)
- C_{15}+ (normal oil)

Similarly, yields were determined for these same fractions at 100% conversion of kerogen. These yields were used to compute fractional kinetic distributions, i.e., the percentage of each fraction governed by the compound or compound class kinetic assignments.

A-2.2. Mathematical Model

Data from pyrolysis experiments are used to compute kinetic parameters. From nonisothermal open system pyrolysis experiments data files are constructed using time, true temperature, and rates. Rates are from the flame ionization detector (FID) response, either the total response as in bulk kinetics or from various hydrocarbons or hydrocarbon ranges in the case of compositional kinetics.

One limitation of the P-MACT10-GC data is the small number of data points. For example, utilization of 9 traps provides only 9 data points for a given rate profile. This was mathematically evaluated to insure that such small data sets could accurately processed for kinetic parameters. This was verified by mathematical processing of simulated data sets using the Kinetics2000™ program (Jarvie *et al.*, 1998; Jarvie and Braun, 1998). Appendix 2 provides the data and results of the simulation. This simulation shows that the mathematical model is sufficiently rigorous using simulated data to accurately predict kinetic parameters on small data sets. However, simulated data do not have the noise of experimental data. The reliability of experimental data was tested by summing all the fractions into a total fraction, i.e., a file comparable to that derived from bulk kinetic experiments. Generally, the results were very similar and substantiated the P-MACT10-GC data. The proof itself is only for the reliability of the data not the results themselves as the argument is circular in that both approaches use nonisothermal open system pyrolysis. However, this is one criterion for assessment of the compatibility and reliability of P-MACT-GC data.

Various mathematical may be used to compute kinetic parameters (Burnham and Braun, 1999). The most common model is the discrete model, which takes into account both the shift-in-Tmax as well as peak shape in a rigorous, nested linear and nonlinear regression calculation. It is sensitive to the selection of the spacing of the activation energy as about 1000 cal/mole is the minimum range (Sundararaman, 1992). Fitting of the peak shape is cited as providing the principal mathematical advantage of the discrete model. On the other hand, a Gaussian model provides activation energies distributed in a normal (bell-shape) manner around the central (principal) activation energy. The rigorous mathematical solution provides a distribution of activation energies and an Arrhenius constant (A), hereafter referred to as a probability factor using a linear regression calculation. Although peak shape is not directly accounted for, the Gaussian distribution parameter does take into account the full width at half height (FWHH) of the pyrolysis curve. This results in a range of Gaussian distributions depending on the width of the pyrolysis curve, e.g., broad peaks will have large distribution parameters, whereas narrow peaks will have very small distribution parameters. This results in excellent fitting of the pyrolysis profiles comparable to the discrete model. Demonstration of this comparable fitting result was shown by

comparing kinetic results from these two models to transformation ratios measured from closed system pyrolysis (Jarvie and Wavrek, 1996). In fact the Gaussian model more accurately predicted the early and late generation of hydrocarbons than did the discrete model, both of which slightly underestimated low temperature conversion of kerogen. An overlay of the Gaussian and discrete model showed slight variability, but excellent agreement (Jarvie and Wavrek, 1996).

Further, Burnham *et al.* (1996) demonstrated that a Gaussian or a nucleation model provided the best fit to narrow pyrolysis profiles found in algal (Type I) kerogens. Thus, the Gaussian model provides excellent peak fitting results despite being a normal distribution and better fits narrow pyrolysis profiles as found in Type I kerogens. The fitting of the methane generation rate curves was attempted with both discrete and Gaussian models. Because of the broad distribution of methane, which begins with generation of the first pyrolysis products to very high temperatures, the discrete model could not accurately model the generation rate. The activation energies were broadly, but unevenly distributed resulting in start-stop, start-stop, methane generation (Figure 5). While this can be speculated to reflect the release of methane from different reaction mechanisms, e.g., demethylation of aromatics, it is entirely inconsistent with the experimental data that shows continuous methane generation. On the other hand, the Gaussian model accurately models methane generation from the start of oil generation to the end of pyrolysis. In addition because of its broad distribution and incomplete formation by the end of pyrolysis (650^{o}C), it even reasonably models high temperature non-associated methane generation. This is a function of the Gaussian distribution parameter, which is large for such a broad generation profile. Additional discussion of ethane generation is provided under the heading "*Limitation of results"*.

A-2.3. Secondary cracking of oil to light hydrocarbons and gas

Remember that the models provided in this report only describe primary cracking of kerogen to oil and gas. Current models for secondary cracking of oil to gas generally use

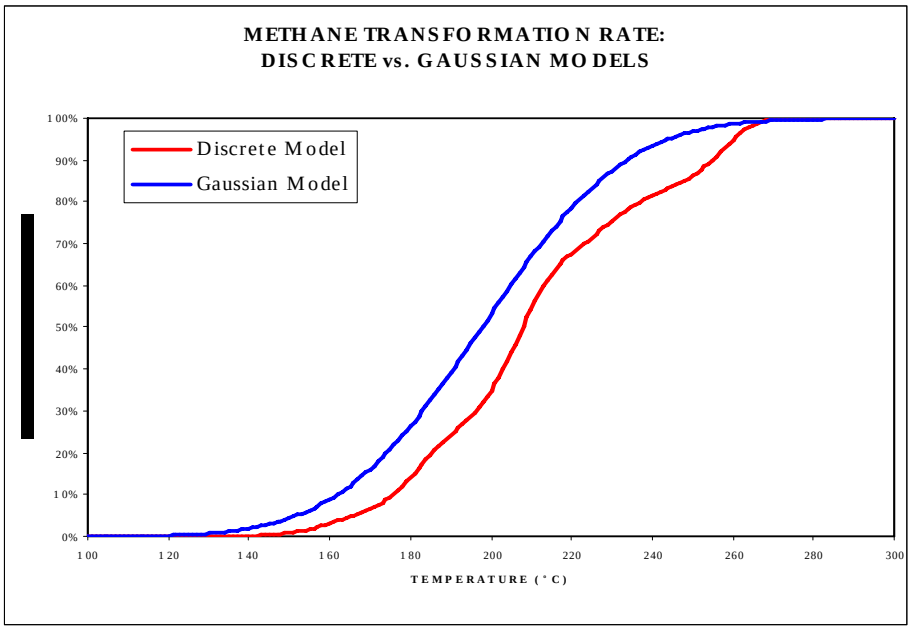

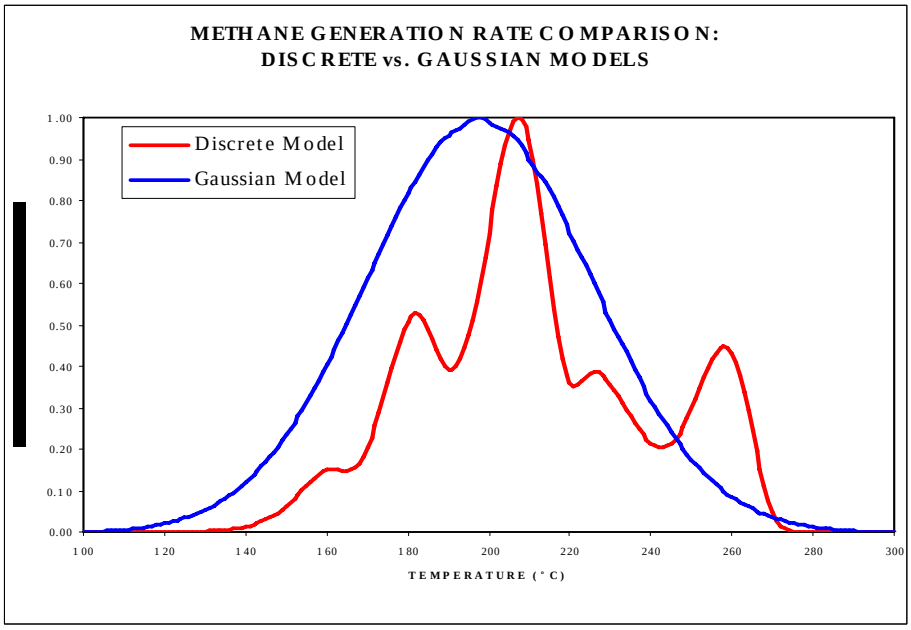

Comparison of models of methane generation using the discrete and Gaussian mathematical models. Top – kerogen to methane transformation rate curves are shifted by *ca.* 10-20°C between the 2 models. Bottom – the methane generation rate curve from the discrete model shows a "start-stop" sequence, which is not seen in the experimental data; this is not evident in the Gaussian or bell-shaped distribution for methane generation.

a single or very narrow distribution of activation energies with a single A factor for this reaction. Results from primary cracking experiments suggest a more complicated process and likely broader range of activation energies, perhaps governed by more than a single A factor.

Waples (2000) has published a distributed Gaussian kinetic model for secondary cracking of oil to gas based on empirical and experimental evidence. However, it may overlap primary generation of gas from kerogen in certain cases. An 11 component model is shown in Table 1.

Gaussian Kinetic Parameters for secondary cracking of oil to gas		
A = 1.78E+14/sec		
Reactant	**Percent of Reaction**	**Activation Energy (cal/mole)**
1	0.2661	54580
2	1.3448	55460
3	4.7408	56350
4	11.6606	57230
5	20.0097	58120
6	23.9559	59000
7	20.0097	59890
8	11.6606	60770
9	4.7408	61660
10	1.3448	62540
11	0.2661	63430
Gaussian distribution parameter 880 cal/mole		

Gaussian kinetic parameters for secondary cracking of oil to gas (Waples, 2000).

These data predict that 10% conversion of oil to methane occurs at about 157-164°C (*ca.* 1.22%Ro), peak oil to gas at 175-183°C (*ca.* 1.57%Ro), and 90% conversion at 192-200°C (*ca.* 2.00%Ro) using a 3.3°C/my constant heating rate calculation.

A-2.4. Yields

The yields from each heating rate were measured and recorded. However, these yields include only resolved hydrocarbon or nonhydrocarbon components. Any unresolved material eluting as an unresolved complex mixture (UCM) under the pyrolysis gas chromatographic fingerprint was not measured. The reason for this was the inability to accurately measure the UCM. It was felt that this measurement included an artistic component as it is difficult to discern UCM from column bleed at high temperatures. There was very little UCM in most samples as can be seen in the pyrolysis GC fingerprints of these samples.

Thus, the yields reported as uncorrected yields are strictly resolved compounds. However, a corrected yield was calculated based on the experimental results of Behar *et al.* (1997). In their study various kerogen types were found to yield a certain percentage of saturate, aromatic, and NSO compounds from a preparative open system pyrolysis process described in their paper. Basically, their results show percentages of resolved (saturate and aromatic hydrocarbons) and unresolved components (NSO compounds), which varied depending on kerogen type. These results were used to correct the yields from the P-MACT10-GC yields by assuming that the resolved components were measured in the P-MACT10-GC yields and that the unresolved compounds were not measured. Thus, the yields correction factor (Ycf) would be as shown in Table 4.

Yields Correction Factor
based on Behar et al. (1997)

	Saturate plus aromatics	**NSOs**	**Average Yields Correction Factor**
	Percent of C_{15}+	**Percent of C_{15}+**	**Percent of C_{15}+**
Type I	59	41	0.59
Type II	35	65	0.35
Type II-S	44	56	0.44
Type III	27	73	0.27

Average correction factor for C15+ yields derived from P-MACT10-GC data.

The yields were very consistent between or among the 2-3 heating rates employed on most samples. In most samples the variation was less than 1% among the various runs for any given fraction.

A-2.5. Interpretation of Results

With new analytical data it is difficult to assess the reliability of such unconstrained data. However, it appears that there are two basic constraints that can be used to assess these data. First, if the totals from the fractions are comparable to the bulk kinetic parameters, the data are experimentally consistent. From a scientific viewpoint this argument is circular as one could not use open system pyrolysis data to prove another set of open system pyrolysis data. However, the fact that these experiments provide comparable data is evidence of consistency in manipulation of the pyrolysis GC data generated from the P-MACT10-GC instrument. We have found that we can reasonably predict isothermal, closed system pyrolysis conversion of kerogen from these nonisothermal, open system pyrolysis data, while the inverse is not true (*unpublished data*).

Second, the calculation of kinetic parameters for the total fraction versus the individual components is independent calculations even though they may not be perceived as such. The total fraction is dependent upon the sum of the fractions, but the calculation itself is independent. The individual kinetic parameters consisting of both activation energies and A factor must underlie the total fraction with its single A factor and related distribution of activation energies. If they do not, there is a mathematical problem with

the calculation of the kinetic parameters. We have found this to occur and samples having those characteristics were eliminated from the study. The fact that other calculations do not have this difficulty *per se* indicates the reliability of the solution for most samples. The C_{15}+ fraction is generally the most problematic fraction as the number of data points is often very small across this fraction. Because the C_{15}+ fraction generally elutes in the lower temperature regimes of the pyrolysis process, there are fewer traps containing moderate levels of C_{15}+ hydrocarbons. For example, if the C_{15}+ elutes primarily over a 48°C temperature range only 2-4 traps would contain between 0-80% of the released products. The remainder would be in the 80-100% conversion temperatures that do not enhance resolution of the main phase of C_{15}+ oil generation. However, it was found that it was relatively easy to infill data points between measured intervals and this infilling did not alter the calculation. Thus, the curve fitting results for each fraction and how they fit under the independently calculated total fraction are an indication of the reliability of the fractional calculations. If data fits under the total curve, it is reasonably reliable; if it does not, it is not reliable.

The methane generation profile does not fit under the total generation curve, which suggests unreliable data. However, this is not correct. Methane generation occurs across the entire phase of oil generation as has been shown for many years. The fact that it occurs from the start of pyrolysis to the end of pyrolysis suggests a very broad generation profile and, concomitantly, a very broad distribution of activation energies. In all samples methane generation was incomplete at the final pyrolysis temperature of 650°C. High temperature pyrolysis experiments showed that methane generation extends to about 850°C as also have been previously reported. In fact high temperature pyrolysis experiments were completed on the P-MACT10-GC system. The problem for these experiments is the fact that only 9 traps are available to trap products that evolve between about 350°C and 850°C thereby requiring a very broad temperature interval for each trap of 55°C. This would not be compatible with measurement of the C_2-C_{15}+ fractions. To measure the high temperature methane a set of experiments were completed, where the pyrolysis products from 300-650°C were placed into the first trap; subsequent traps were filled with methane from slicing the pyrolyzate from 650°C to 850°C. This demonstrated methane yield from even Type I kerogens that was modeled accurately by the Gaussian distribution for methane. In addition even though the experimental conditions stop at 650°C, the extrapolation of methane generation to higher temperatures is consistent with high temperature experimental data. The discrete model does not predict this high temperature generation of methane. Thus, the Gaussian model reasonably predicts nonassociated methane generation.

Appendix B

(Vitrinite Reflectance Histograms)

(Crimson F-81, Torbrook C-15 and Weymouth A-45 wells)

For: Nova Scotia Department of Energy

Vitrinite Reflectance Histograms: Crimson F-81 well, Scotian Slope

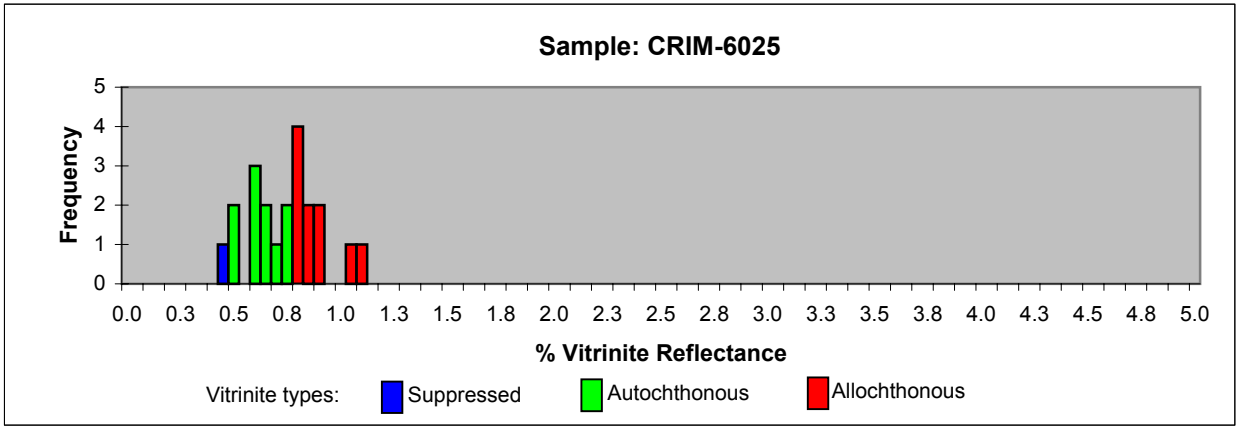

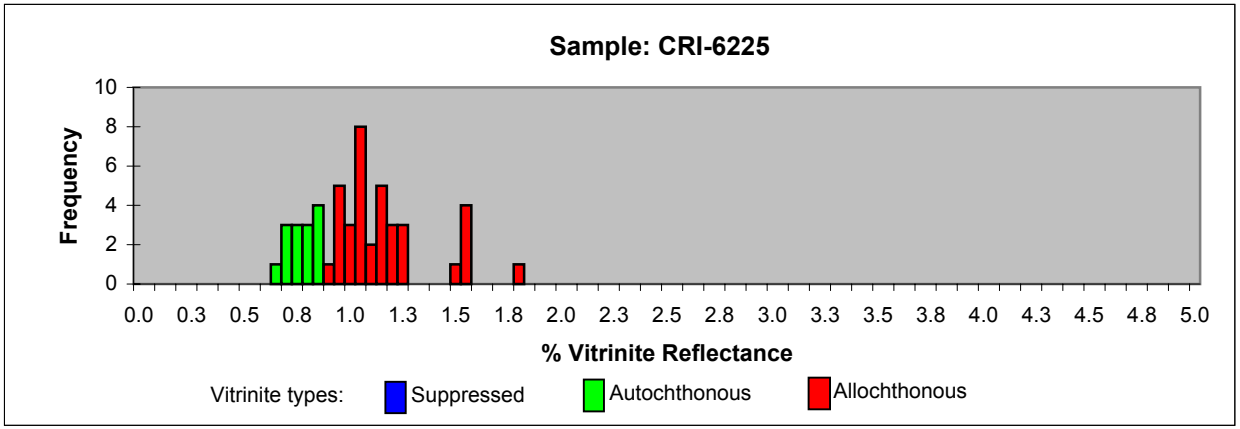

For: Nova Scotia Department of Energy

Vitrinite Reflectance Histograms: Crimson F-81 well, Scotian Slope

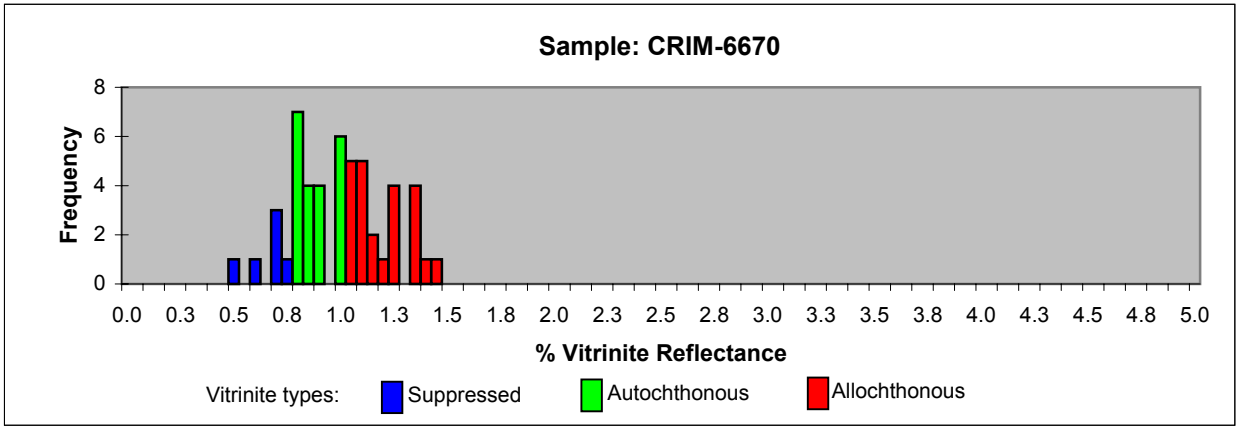

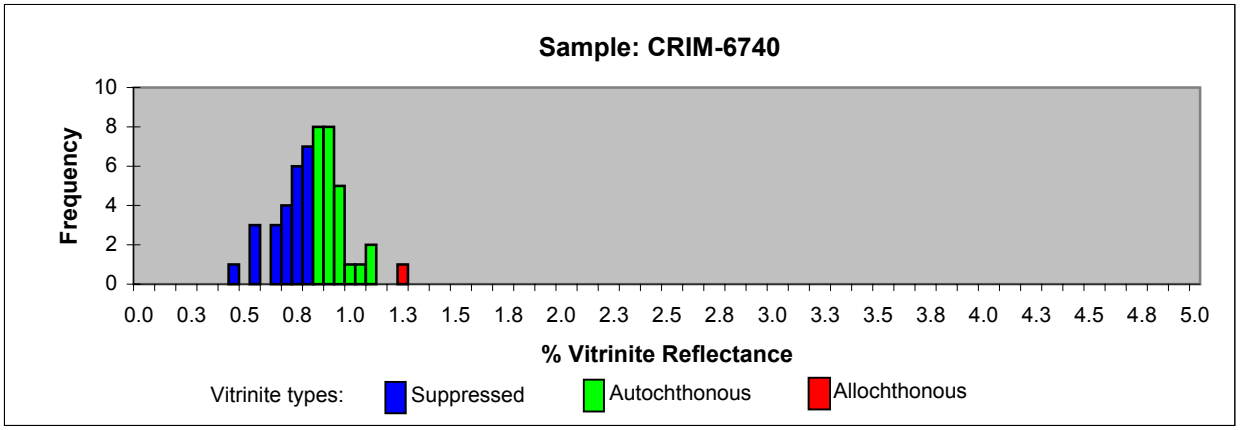

Vitrinite Reflectance Histograms: Torbrook C-15 well, Scotian Slope

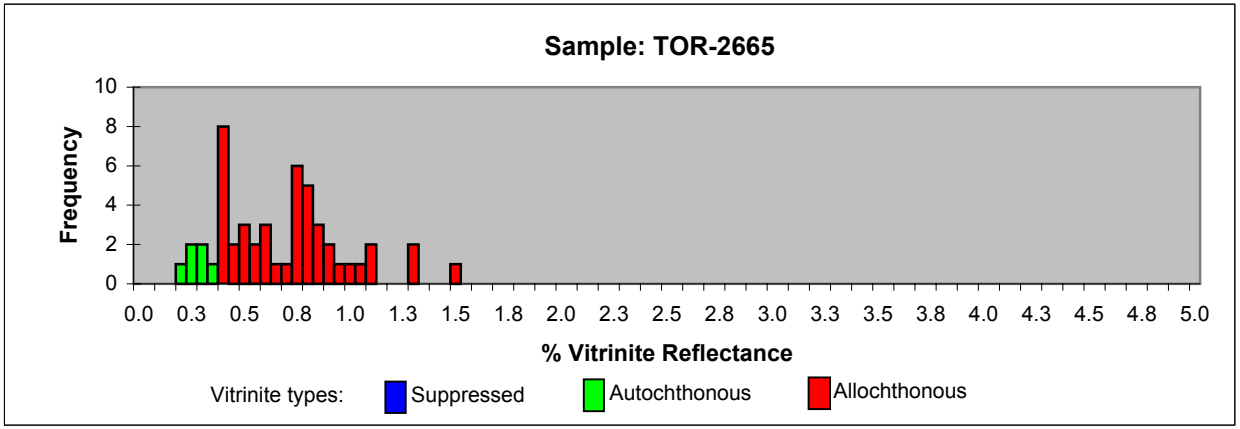

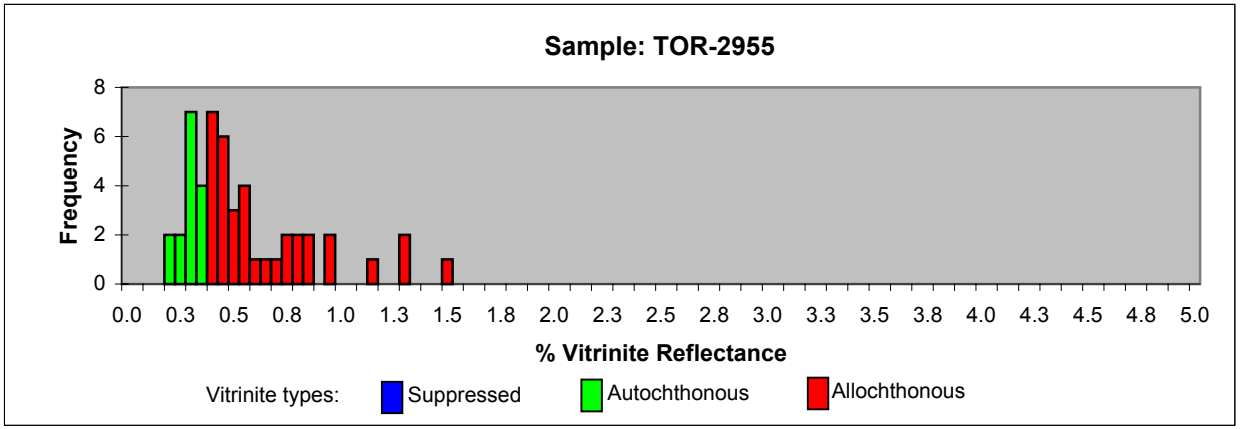

Vitrinite Reflectance Histograms: Torbrook C-15 well, Scotian Slope

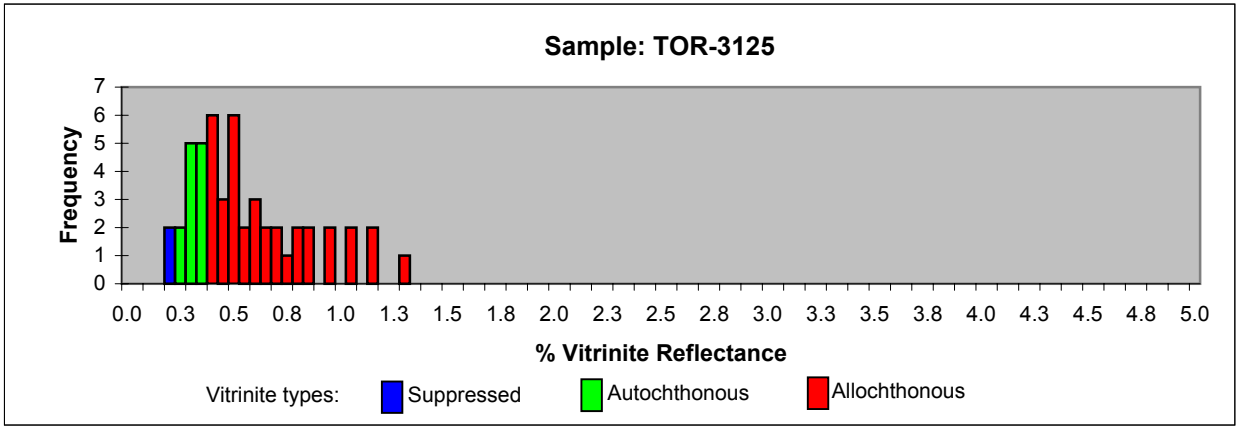

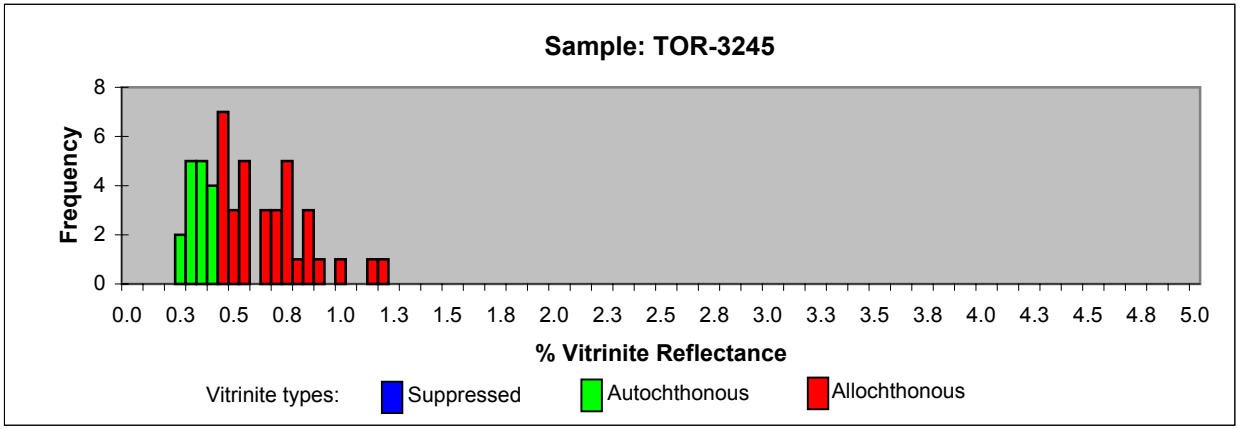

Vitrinite Reflectance Histograms: Torbrook C-15 well, Scotian Slope

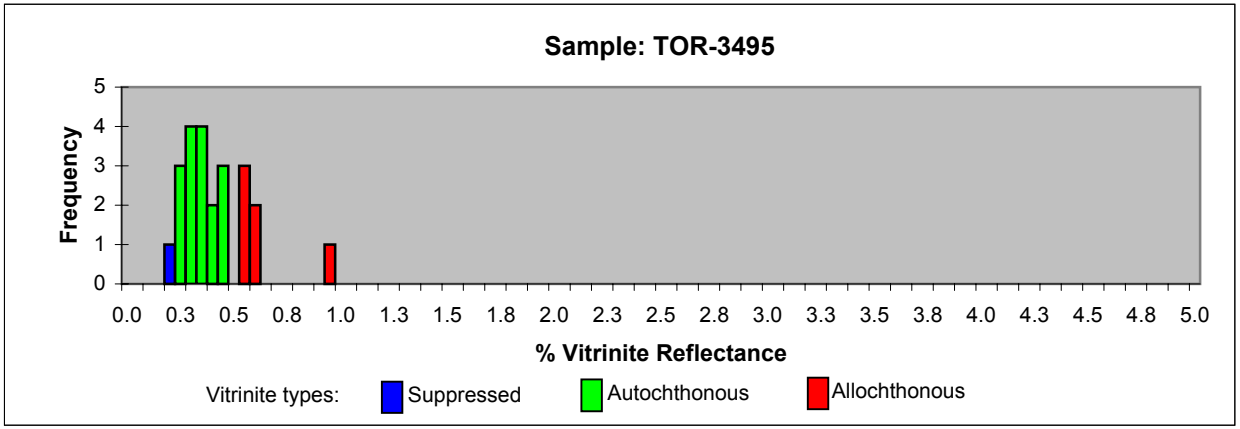

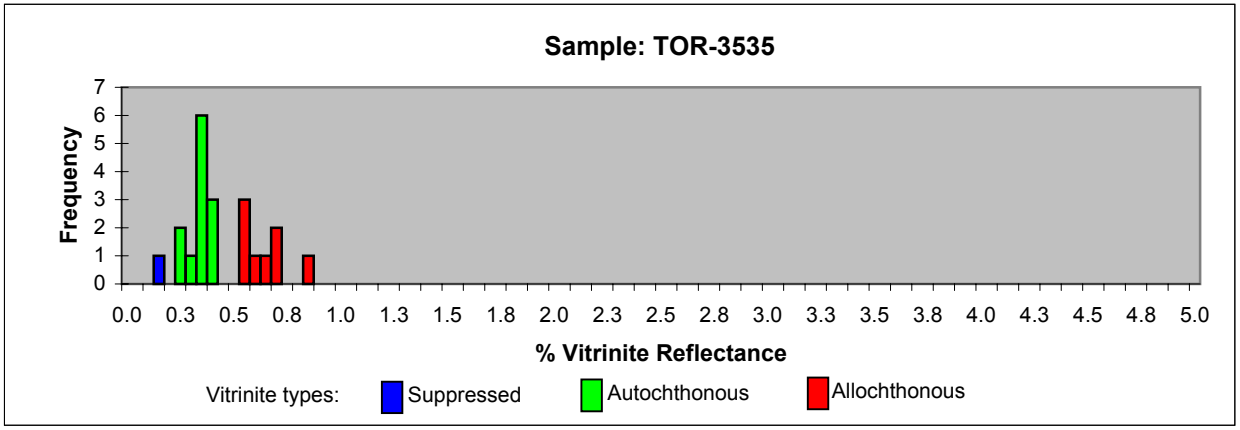

Vitrinite Reflectance Histograms: Torbrook C-15 well, Scotian Slope

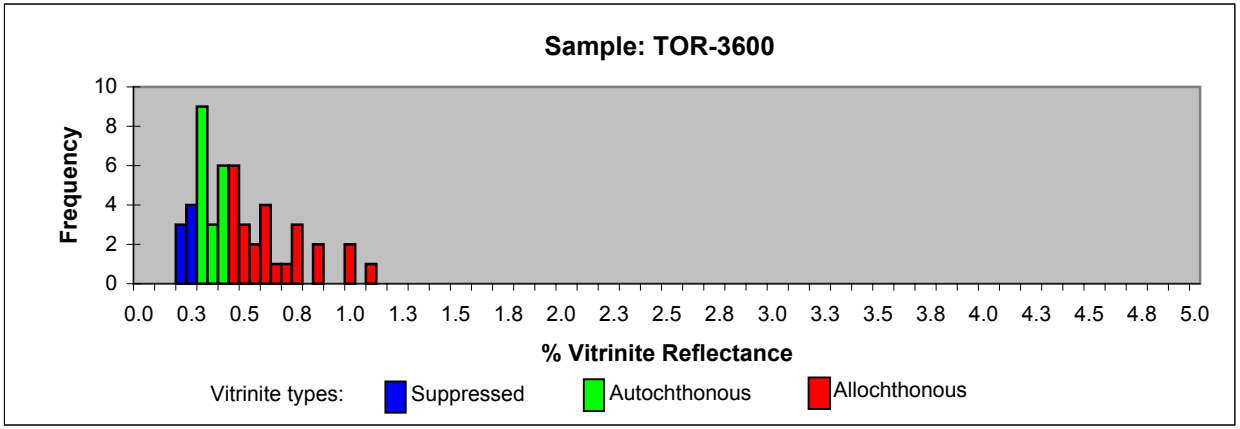

Vitrinite Reflectance Histograms: Weymouth A-15 well, Scotian Slope

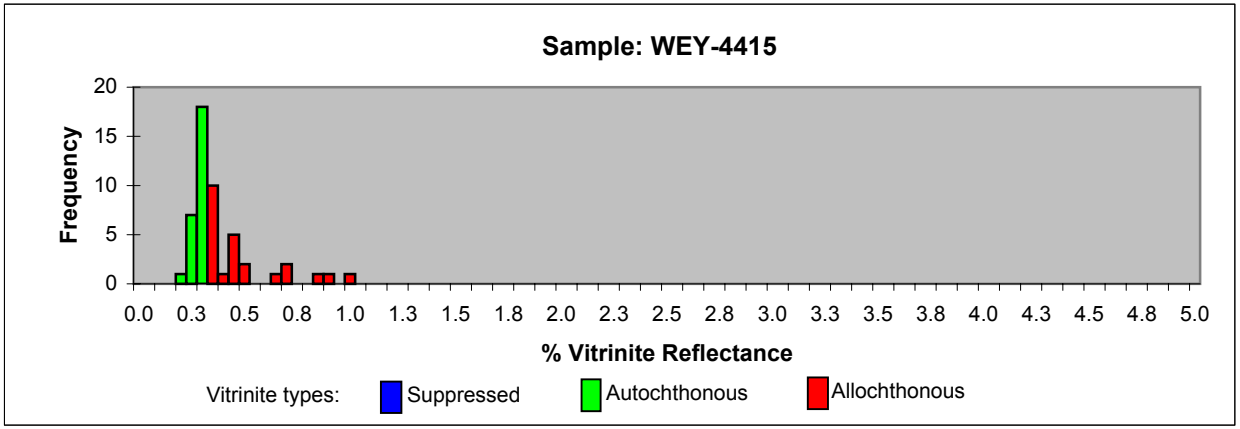

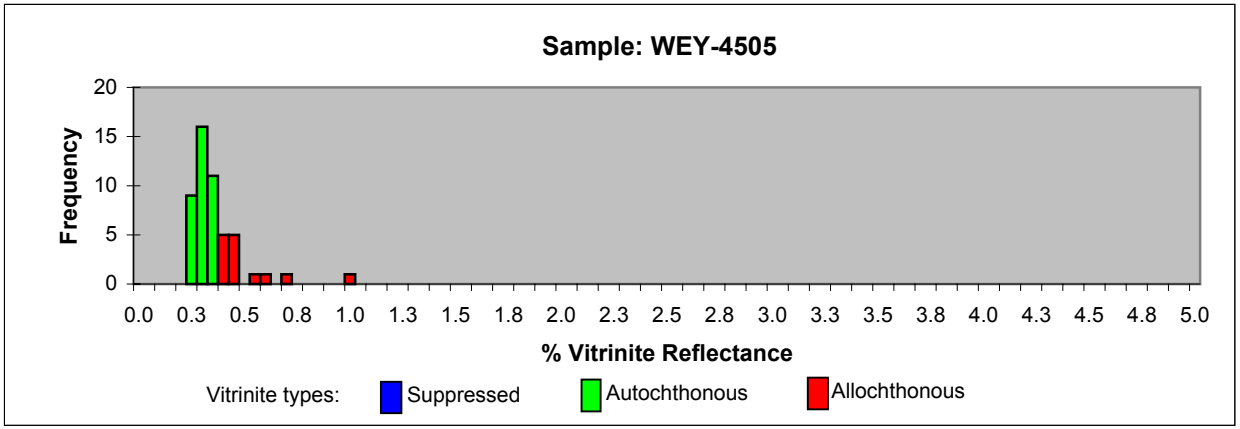

Vitrinite Reflectance Histograms: Weymouth A-15 well, Scotian Slope

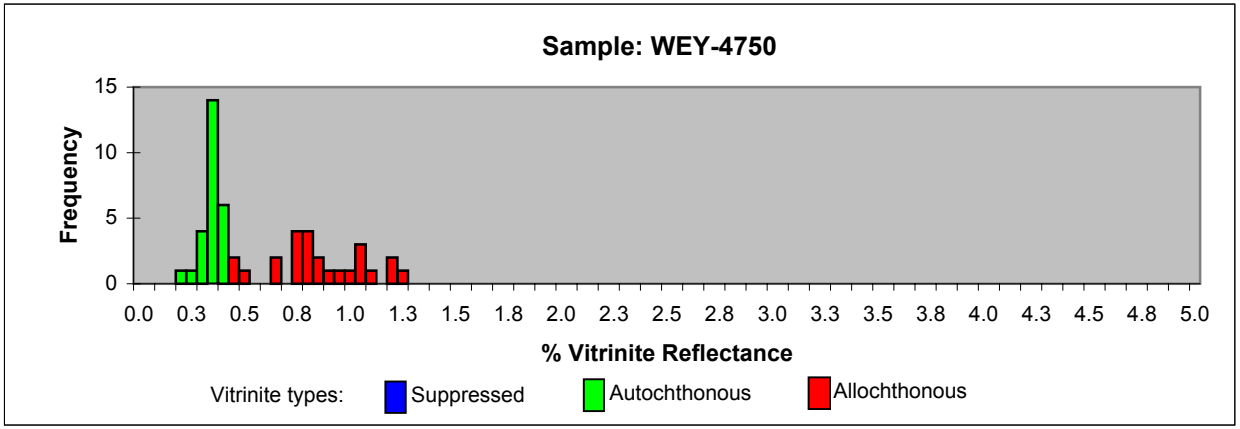

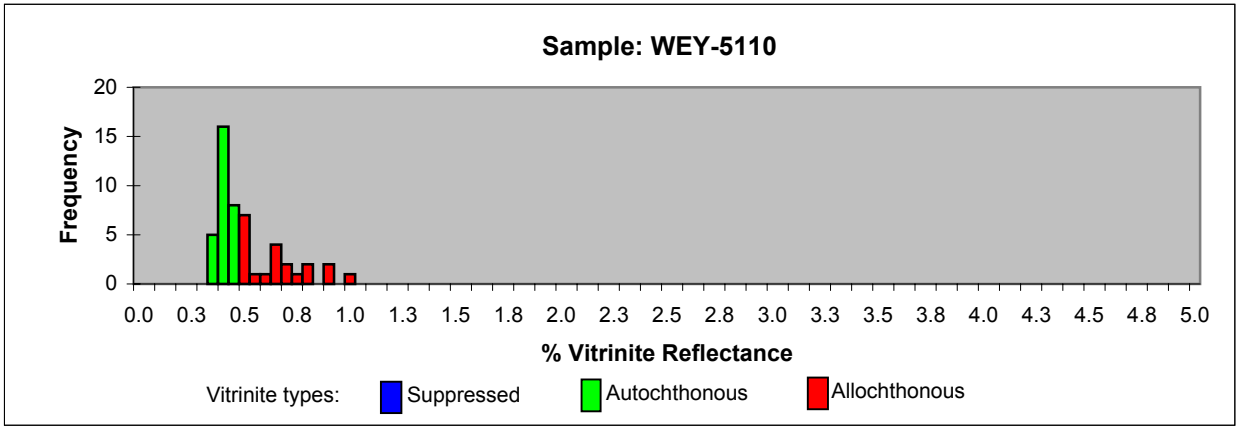

Vitrinite Reflectance Histograms: Weymouth A-15 well, Scotian Slope

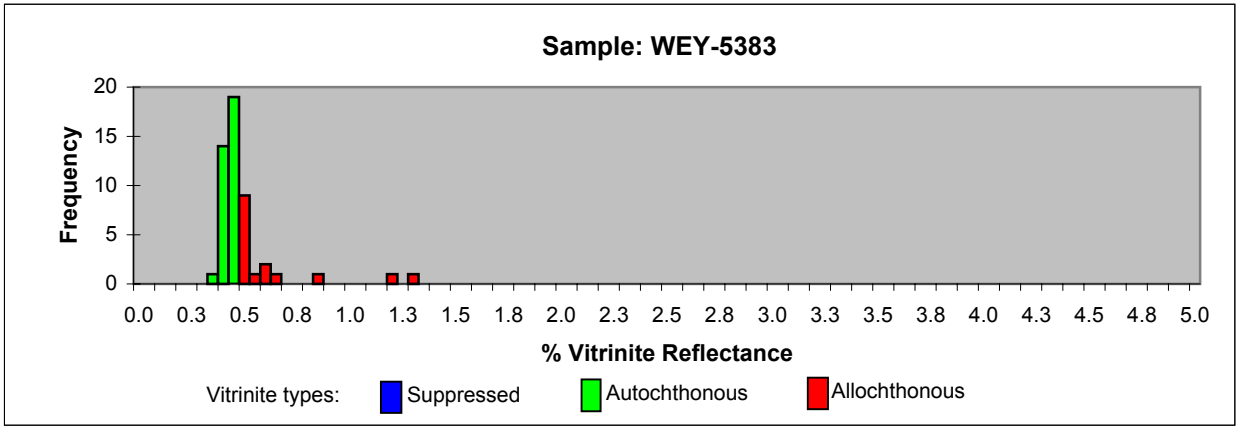

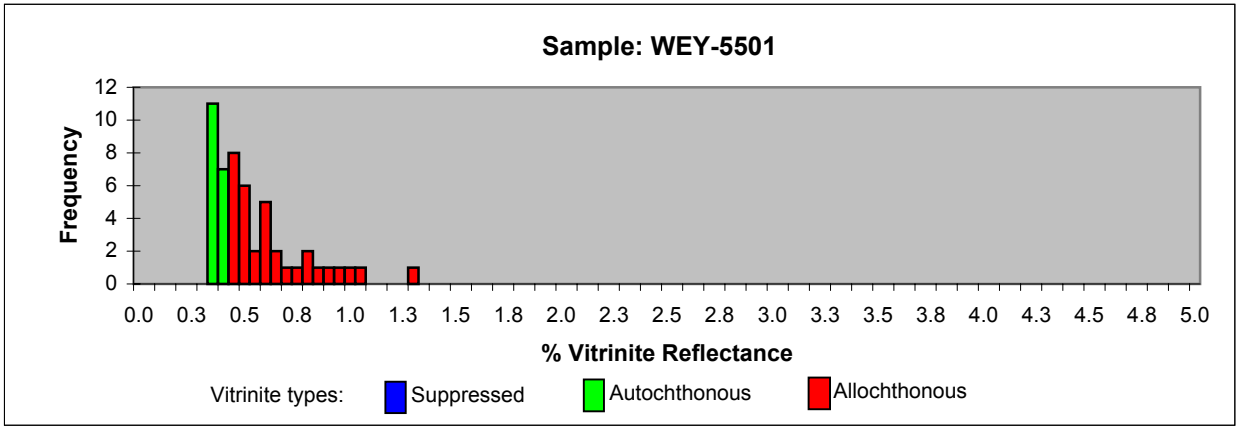

Vitrinite Reflectance Histograms: Weymouth A-15 well, Scotian Slope

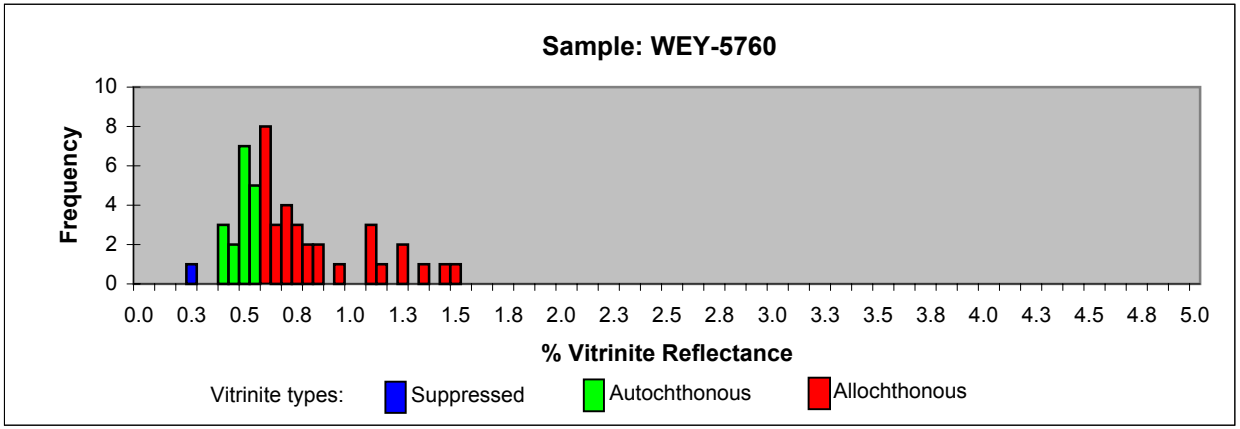

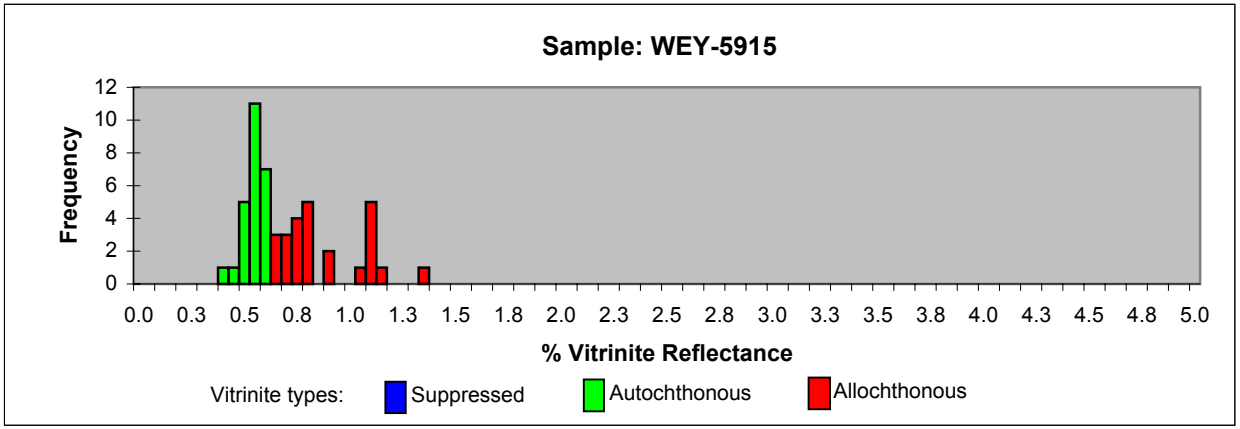

Vitrinite Reflectance Histograms: Weymouth A-15 well, Scotian Slope

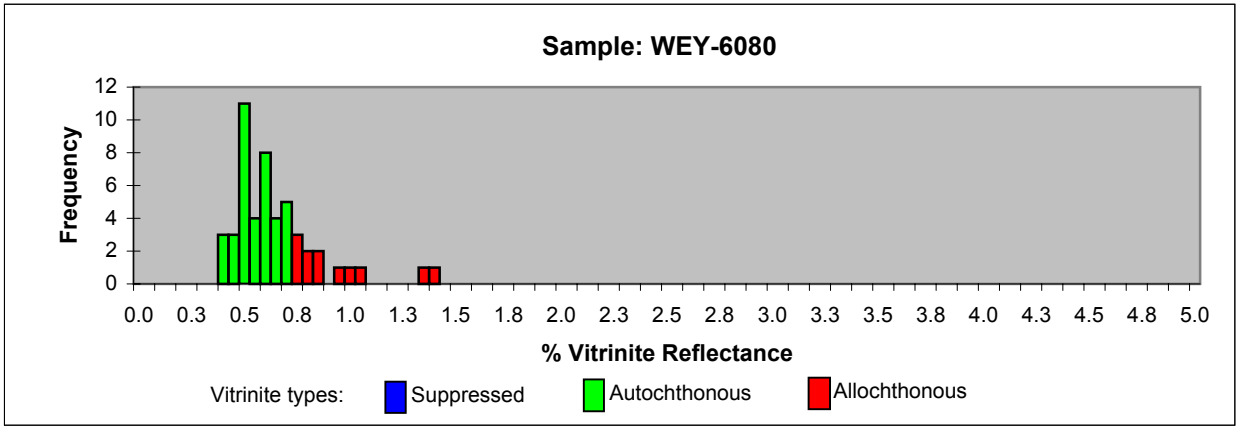

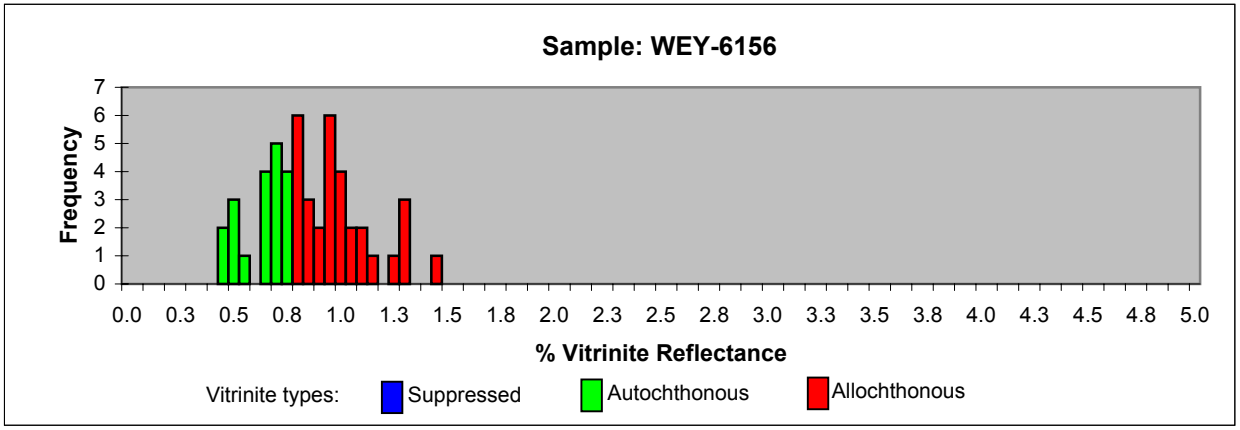

Vitrinite Reflectance Histograms: Weymouth A-15 well, Scotian Slope

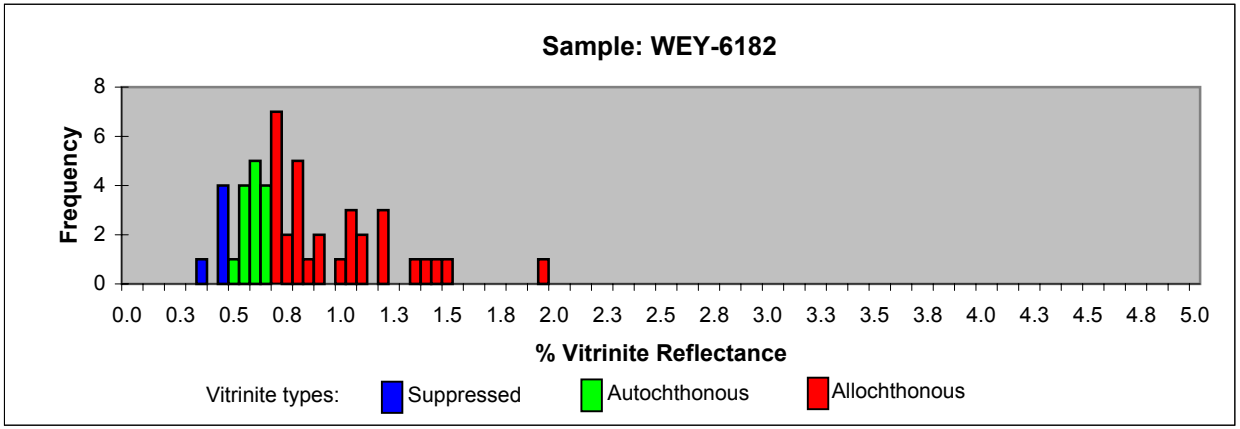

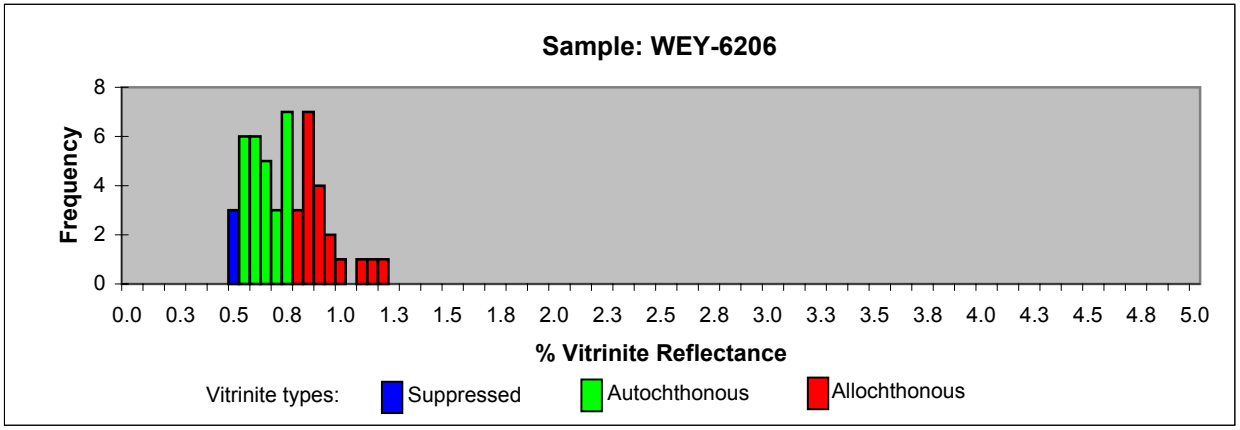

Vitrinite Reflectance Histograms: Weymouth A-15 well, Scotian Slope

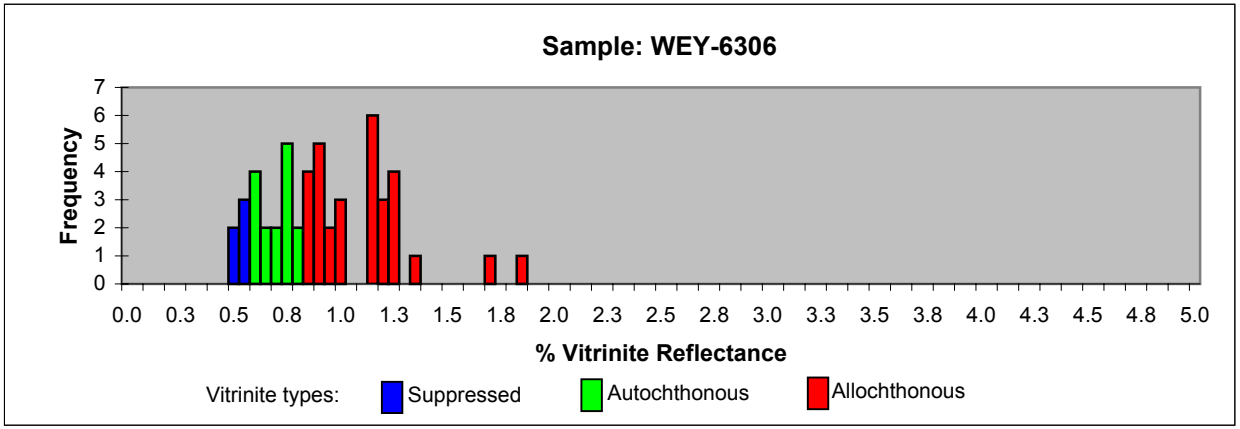

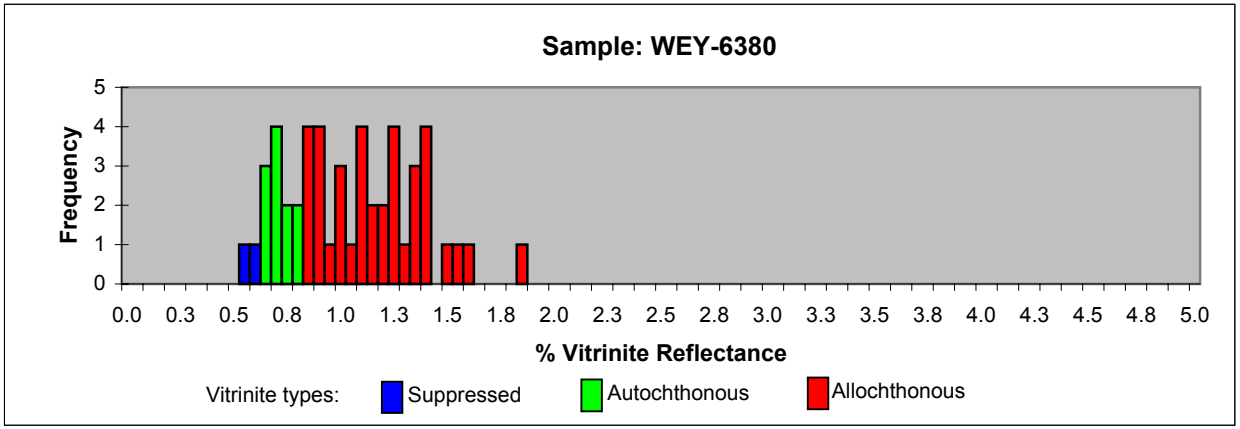

Vitrinite Reflectance Histograms: Weymouth A-15 well, Scotian Slope

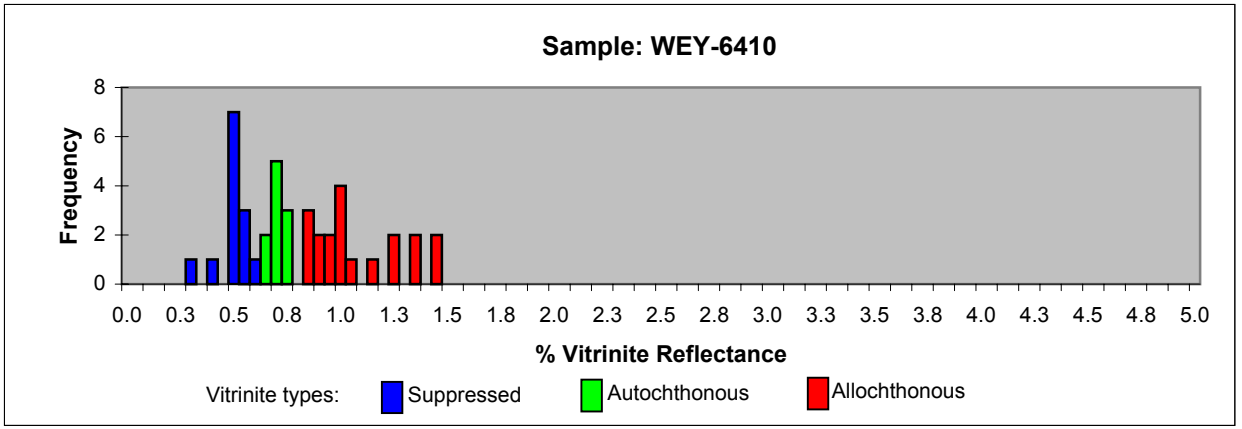

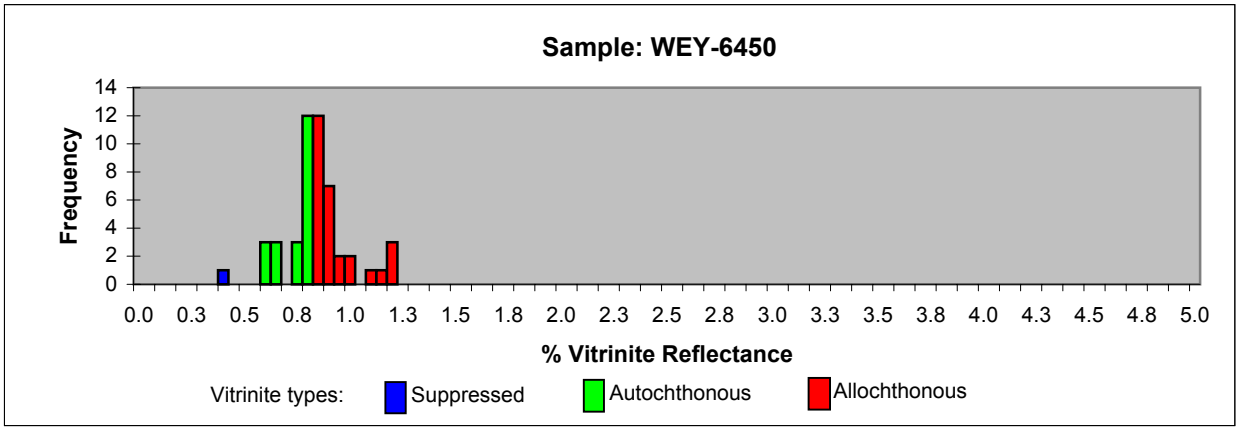

Vitrinite Reflectance Histograms: Weymouth A-15 well, Scotian Slope

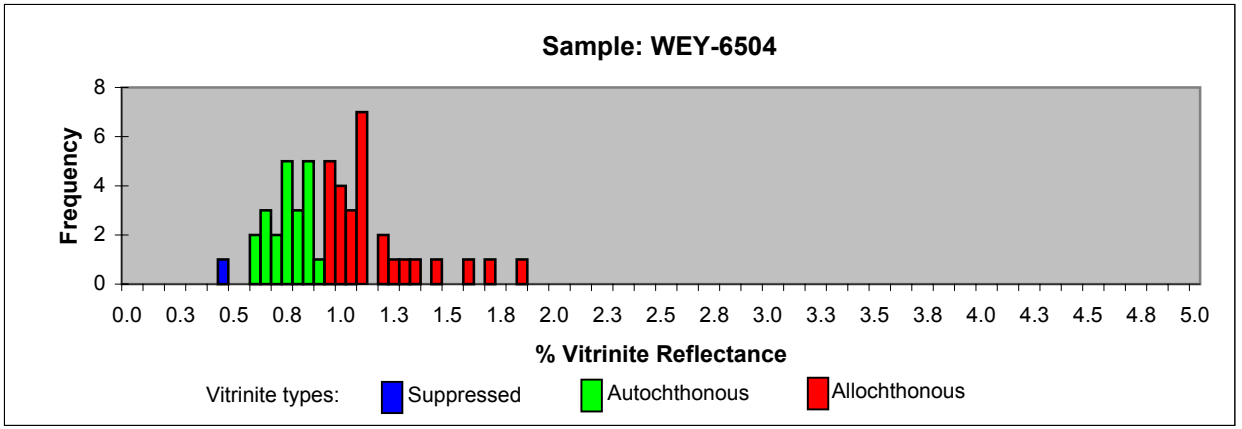

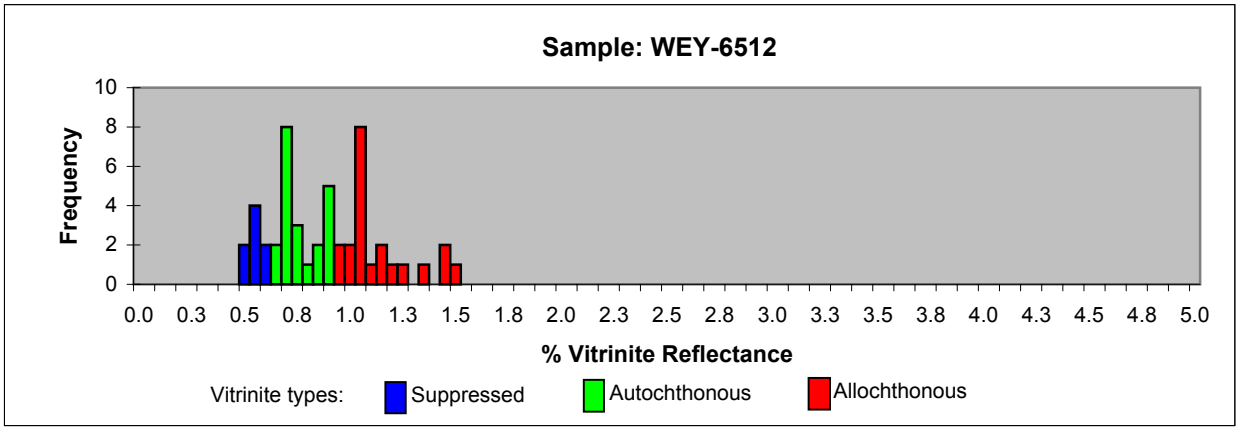

Vitrinite Reflectance Histograms: Weymouth A-15 well, Scotian Slope

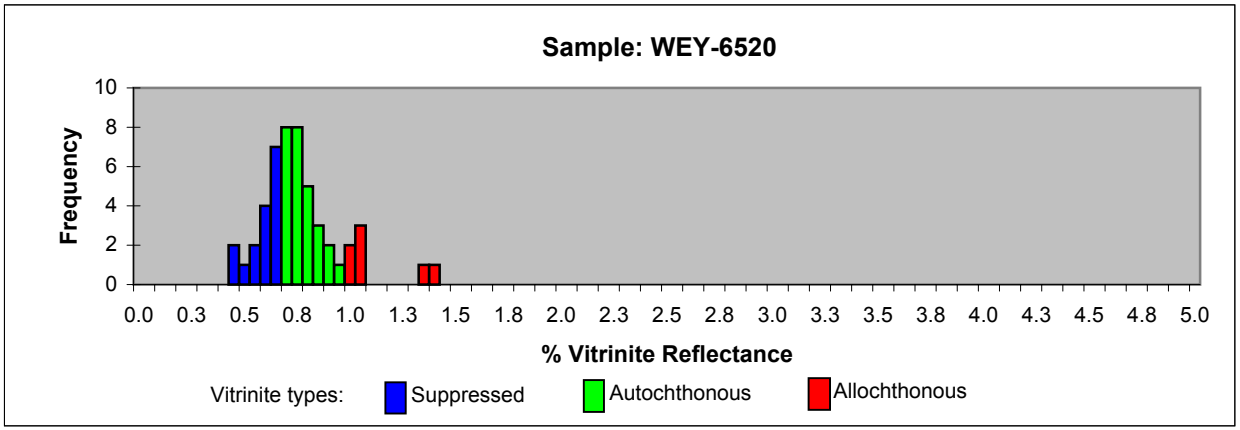

Appendix C

(Salient Features of the
1D and 2D Petroleum System Modeling)

Appendix C-1: Petroleum Systems Modeling: Objectives

Use the data!

- ... by providing a **framework** for regional scale geological data management
- ... to improve **communications** and multi-disciplinary work.

Understand

- ... the presently known distribution of hydrocarbons and their **properties** and **phases** by integrating the controlling factors and **simulating** the processes.

Predict

- ... hydrocarbons and their **properties** and **phases**, e.g. in new exploration targets or in satellite structures in existing production areas.
- **...** the **risks** and **rank** prospects and their controlling factors.
- ... **volumetrics estimates** to assess exploration **potential** and **reserves**

Appendix C-2: Petroleum Systems Modeling: Historical Background

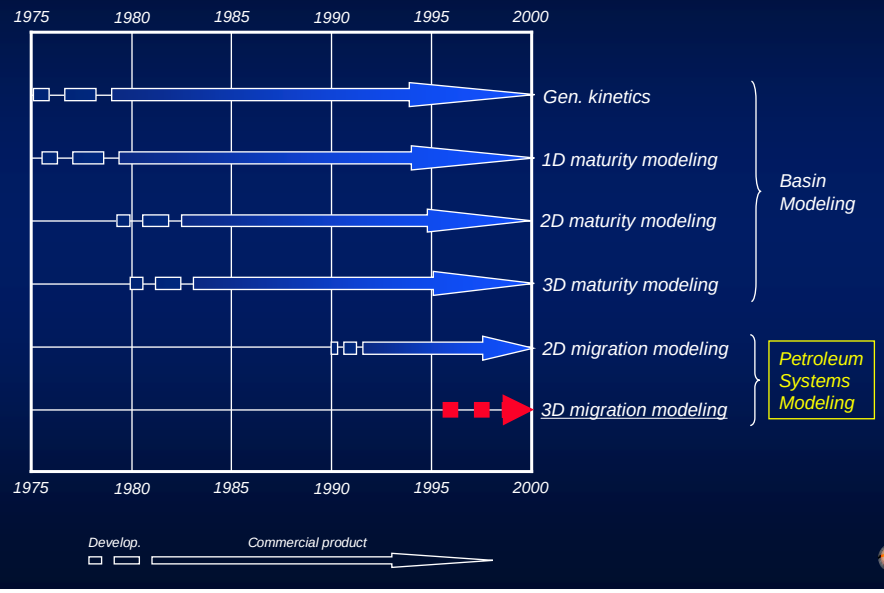

Appendix C-3: PetroMod: Comparison of 1D and 2D Modelling

1D/2D well / section based	PetroMod 1D Express	PetroMod 1D	PetroMod 2D	PetroMod 2D
	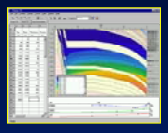	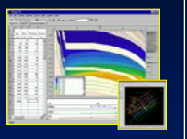	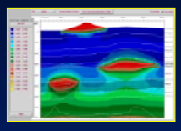	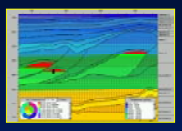
	Essential 1D modeling tool; fully compatible with IES' 2D and 3D modeling system; freeware!	1D thermal, hydrocarbon maturation and pressure modeling; special tools to model effects of salt movements, igneous intrusions, etc.	2D thermal, hydrocarbon maturation and pressure modeling; tools to model the effects of faults, salt movements, igneous intrusions, etc.	2D n-component, 3-phase migration modeling with Darcy and hybrid simulators; includes all PetroGen 2D functions

Appendix C-4: Petroleum Migration Modeling: Modelling Sequences

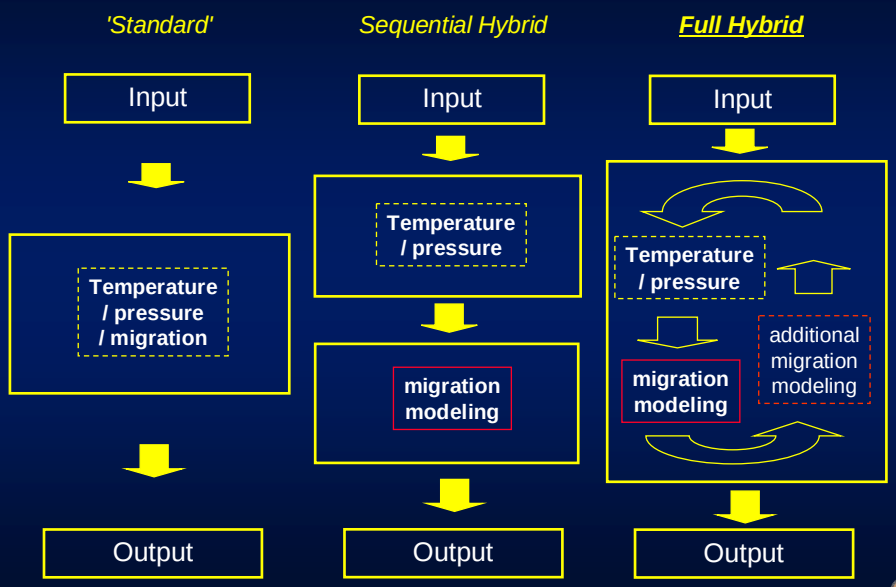

Appendix C-5: PetroMod 2D/3D: Workflow Patterns

2D

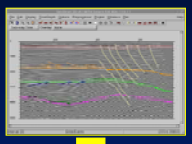

SeisStrat 2D (not always necessary)
Interpretation (graphical), depth conversion, property assignment
Data loading from SeisWorks, OpenWorks, IESX, Charisma, GeoFrame, SEGY, ascii

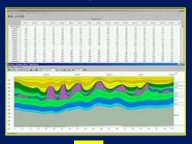

Input 2D: PetroBuilder 2D
2D model editing of gridded model with table and section viewers
Data loading from structural models

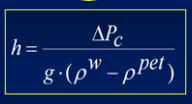

Simulation 2D
Select simulation method (Flowpath, Darcy or Hybrid Darcy/Flowpath); control and run simulation

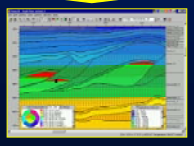

Output 2D
Display, analyse and plot all simulation results; includes 1D and burial history viewers

3D

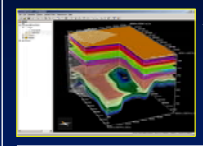

SeisStrat 3D (not always necessary)
3D data Quality Control; regridding
Data Loading from ZMap, CPS, proprietary grid formats, etc.

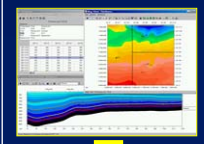

Input 3D
3D model building and editing of grids with table, map and section viewers
Data loading from ZMap, CPS, proprietary grid formats, etc.

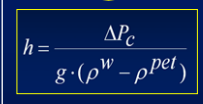

Simulation 3D
Select simulation method (Flowpath, Darcy or Hybrid Darcy/Flowpath); control and run simulation

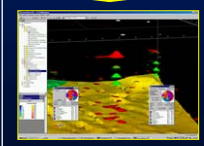

Output 3D
Display, analyse and plot all simulation results; includes 1D, 2D, burial history and map viewers

Appendix C-6: Migration Modeling Phases

Different simulation methods (Darcy, Flowpath) can be used to handle different processes in the petroleum system:

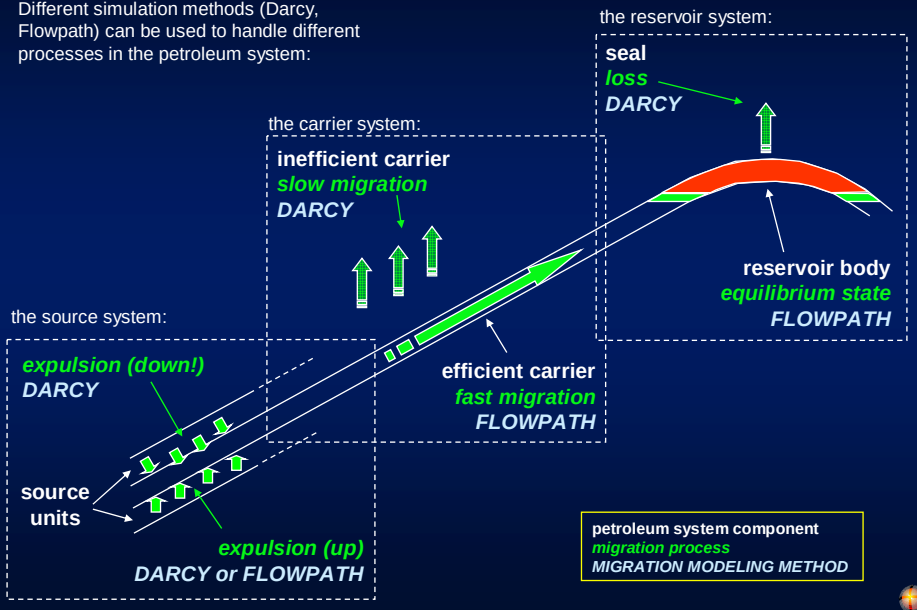

Appendix C-7: The Reservoir Components

Problem:
Reservoirs can play a crucial role in controlling HC distributions and properties in a petroleum system.

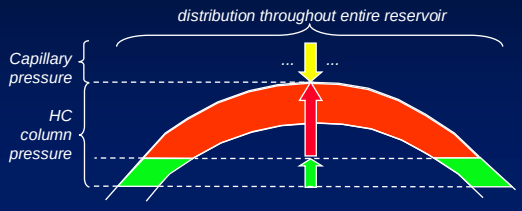

Solution: *the hybrid simulator can perform the following processing tasks during each time loop:*

	Processing task	Modeling Method
1	***Migration into reservoir***	***Flowpath and Darcy***
2	***Initial reservoir body calculation***	***Flowpath*** *(reservoir geometry functions)*
3	***PVT control and correction***	***Darcy***
4	***Reservoir body calculation***	***Flowpath*** *(reservoir geometry functions)*
5	***Seal efficiency control***	***Darcy and Flowpath*** *(reservoir geometry functions)*

Appendix C-8: Suitability of Darcy and Flowpath Migration Modelling

	Darcy	*Flowpath*
3D Modeling Requirements:		
dynamics	++	-
scaling	-	+
process. speed	--	+
data availability	+	+
Petroleum System Components:		
source and expulsion	+	-
migration – low perm. units	+	--
migration – high perm. carriers	-	++
reservoir bodies	--	++

Conclusion: ... there is no method that provides an acceptable solution for 3D modeling if used on its own!

Appendix C-9: Parameters for Multicomponent pvT-Analysis

HC Components

Component	Mol%	Mass%
CO2	0.91	0.43
N2	0.16	0.05
C1	36.47	6.24
C2	9.67	3.10
C3	6.95	3.27
iC4	1.44	0.89
nC4	3.93	2.44
iC5	1.44	1.11
nC5	1.41	1.09
C6	4.33	3.97
C7+	33.29	44.71

HC Phases

p
T
?

Liquid

Vapour

Volume
Liquid, Vapour, (Water) Phase

Composition
Liquid, Vapour, (Water) Phase

Density
Liquid, Vapour, (Water) Phase

Viscosity
Liquid, Vapour, (Water) Phase

p, T Separator → GOR, API Density

Appendix C-10: Phase Components

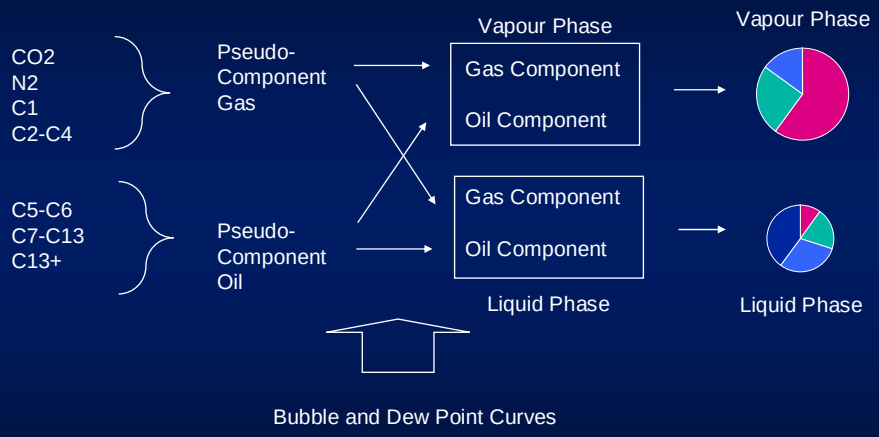

Appendix C-11: The Role of Darcy and Flowpath modeling in Hybrid Flow Modeling

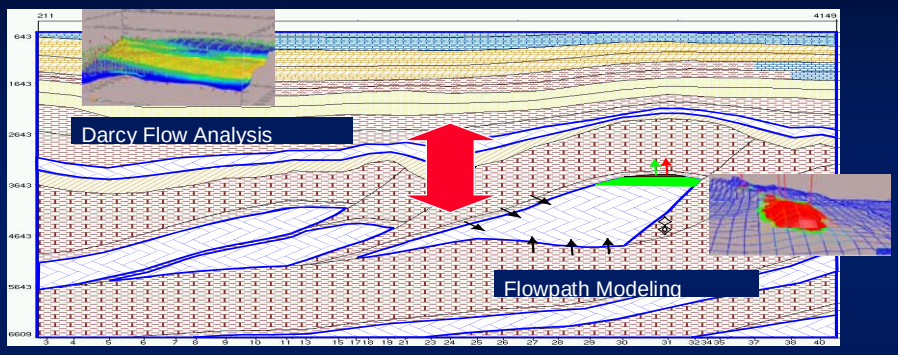

Challenges :

- Testing the Injection of Break-Through Amounts
- Reinjection of Break-Through Amounts for Nonequilibrium Accumulations
- Different Grid Resolutions

Appendix C-12: hybrid, n-component, phase migration modeling

Hybrid, n-component migration modeling *during the entire migration process can be performed in both 2D and 3D. Flash calculations, symmetrical black oil and other phase composition models can be used for component/phase handling.*

Gas (red) and oil (green) accumulations are shown as well-defined reservoir bodies.

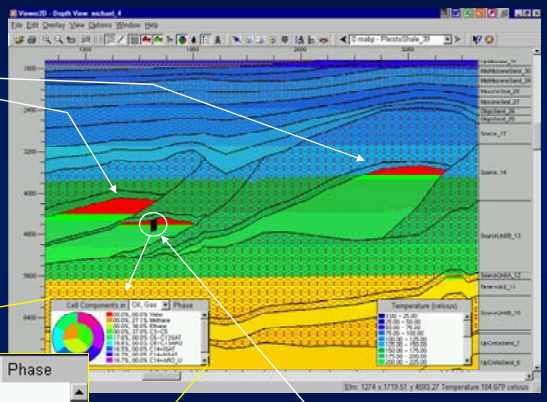

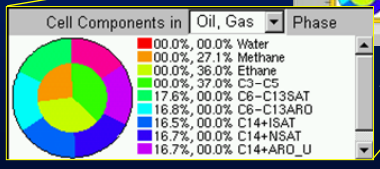

oil and gas component display

Hydrocarbon components in each phase can be shown for a selected cell or reservoir in a pie chart (gas in the inside, oil in the outside circle) and as values in a table.